pISSN 1598-2998
eISSN 2005-9256

https://www.e-crt.org

CANCER RESEARCH AND TREATMENT

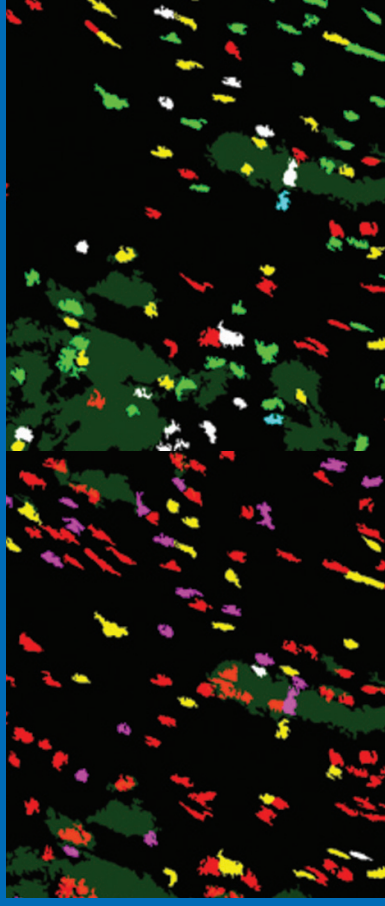

VOLUME 52
NUMBER 4
OCTOBER 2020

The Korean Cancer Association

Korean Society of Medical Oncology

Korean Association for Lung Cancer

CANCER RESEARCH *AND* TREATMENT

pISSN 1598-2998
eISSN 2005-9256
https://www.e-crt.org

It is indexed in Science Citation Index Expanded SCIE, PubMed, PubMed Central, Medline, Scopus, KoreaMed, KoreaMed Synapse, KoMCI, WPRIM, Worldwidescience.org, DOI/CrossRef and Google Scholar.

It has been published since 1966 with a title of The Journal of Korean Cancer Association.
Its title was changed from the year of 2001 as Cancer Research and Treatment.

Aims and Scope

Cancer Research and Treatment is a peer-reviewed open access publication of the Korean Cancer Association. It is published quarterly, one volume per year. Abbreviated title is *Cancer Res Treat*. It accepts manuscripts relevant to experimental and clinical cancer research. Subjects include carcinogenesis, tumor biology, molecular oncology, cancer genetics, tumor immunology, epidemiology, predictive markers and cancer prevention, pathology, cancer diagnosis, screening and therapies including chemotherapy, surgery, radiation therapy, immunotherapy, gene therapy, multimodality treatment and palliative care.

Volume 52, No. 4
October 2020

Printed on October 10, 2020
Published on October 15, 2020

Published by Korean Cancer Association
Room 1824, Gwanghwamun Officia,
92 Saemunan-ro, Jongno-gu,
Seoul 03186, Korea
Tel: 82-2-792-1486
Fax: 82-2-792-1410
E-mail: cancer@kams.or.kr
Homepage: http://www.cancer.or.kr

Edited by Korean Cancer Association
E-mail: journal@cancer.or.kr

Printed by ONBEST Inc.
17, World Cup-ro 12-gil, Mapo-gu,
Seoul 04004, Korea
Tel: 82-2-322-4020
E-mail: onbest2@gmail.com

This journal was supported by the Korean Federation of Science and Technology Societies Grant funded by the Korean Government (Ministry of Education).

CANCER
RESEARCH *AND*
TREATMENT

Volume 52, No. 4, October 2020

pISSN 1598-2998
eISSN 2005-9256
https://www.e-crt.org

Original Articles

CANCER
RESEARCH *AND*
TREATMENT

Volume 52, No. 4, October 2020

pISSN 1598-2998
eISSN 2005-9256
https://www.e-crt.org

pISSN 1598-2998, eISSN 2005-9256

Cancer Res Treat. 2020;52(4):993-1001

https://doi.org/10.4143/crt.2020.285

Original Article

Open Access

The Fear of Cancer from the Standpoint of Oneself, the Opposite Sex and the Fear of Side Effects of Cancer Treatment

Keeho Park, MD, PhD[1,2]
Youngae Kim, PhD[1]
Hyung Kook Yang, MD, MPH[1]
Hye Sook Min, MD, PhD[1]

[1]*National Cancer Control Institute, National Cancer Center, Goyang,* [2]*Department of Cancer Control and Population Health, Graduate School of Cancer Science and Policy, National Cancer Center, Goyang, Korea*

Correspondence: Keeho Park, MD, PhD
Department of Cancer Control and Population Health, Graduate School of Cancer Science and Policy, National Cancer Center, 323 Ilsan-ro, Ilsandong-gu, Goyang 10408, Korea
Tel: 82-31-920-2160
Fax: 82-31-920-2929
E-mail: park.keeho@gmail.com

Received April 7, 2020
Accepted June 23, 2020
Published Online June 24, 2020

Purpose

It is important to understand the differences between men and women when it comes to attitudes and risk perception toward disease. This study aimed to explore the fear of cancer from the standpoint of themselves and the opposite sex by cancer type.

Materials and Methods

A cross-sectional survey with a representative sample was conducted.

Results

The least and the most feared cancers in men were thyroid cancer and lung cancer, respectively. When men assumed the perspective of women, the least and the most feared cancer were thyroid cancer and stomach cancer, respectively. The least and the most feared cancers in women were thyroid cancer and stomach cancer, respectively. When women assumed the perspective of men, the least and the most feared cancer were prostate cancer and lung cancer, respectively. When both men and women assume the perspective of the opposite sex, the fear of sex-specific cancer was relatively low compared to the actual responses of both men and women. The top six of the most feared side effects of cancer treatment were pain, psychological problems, general weakness, digestive dysfunction, fatigue, and appearance change. These were the same between men and women.

Conclusion

Health care providers and caregivers in the family should provide care with more attention to the differences in thoughts about cancer between men and women. Health care providers should provide care with more attention to the differences in these problems between men and women.

Key words

Cancer, Fear, Complication, Sex, Difference

Introduction

Fear is the body's natural, survival-oriented response for protecting itself from danger or threats [1]. However, fear for health has both positive and negative aspects [2]. Fear may serve as a motivation for preventive action [3,4] or a hindrance to disease control [5]. In a broad sense, risk perception of people involved with the disease is important not only for the prevention of the disease, but also for their management [6].

Cancer is one of the most feared diseases [7]. Cancer is more frightening because the treatment process is painful and its aftereffects significantly reduce the quality of life [8,9]. The physical, mental, social, and economic problems caused by cancer have a significant impact on not only the patient but also on the caregiver's family [10]. Cancer is not a single disease and different types of cancer can be considered as different diseases [11]. Thus, fear of cancer and other psychological reactions to cancer may be different according to various cancer types.

The problem is that the diversity of these cancers is complicated more by the sex factor. Sex factor does not simply mean two biologically distinct groups, because the various aspects of suffering through a disease can be different between men and women [10,12,13]. Effects of sex factor can be seen in the research findings that show that there is a difference between the care, attitude, or behavior towards cancer patients in male and female spouses [14,15]. In addition, the problems that arise due to insufficient consideration of the difference in risk perception between men and women in performing health

communication have increased [16,17].

A person's health behavior can be affected by both their own as well as their family members' risk perception [18-20]. In cancer patients, risk perception of the patient and his or her family may affect the care of the patient [20,21]. In addition, there are reports of better outcomes when considering not only individual patients but also families in patient care [22]. In this context, it is important to understand the differences between men and women's attitudes and risk perception towards diseases. Although studies comparing risk perceptions of cancer fears between men and women exist [23,24], few studies have examined how they think from the perspective of the opposite sex. Moreover, knowledge of how men and women are guessing the thoughts of the opposite sex may allow us to understand how men and women understand differences between sexes. In this study, we explored the fear of cancer from the standpoint of themselves and the opposite sex by cancer type, and those fears were compared between men and women. We also investigated the fear of side effects of cancer treatment and compared it between men and women.

Materials and Methods

1. Study population

A cross-sectional survey was conducted in May 2017. The survey used a proportional quota random sampling design to select a representative sample of non-institutionalized Koreans who had no experience of cancer for themselves or their family members. With stratification by age and sex in each 17-administrative district based on the 2016 census of Korea, a probability proportional to size method was used to sample. Of the randomly selected 1,460 responders who were consecutively telephoned, 460 responders were excluded because of absence and refusal to participate for several reasons, or because the responder was a cancer patient or had a family member with cancer. A total of 1,000 participants were finally chosen and a face-to-face interview was conducted by professional interviewers of research firm Metrix Corporation (Seoul, Korea). The interview process was carefully reviewed and monitored by the researchers.

2. Assessment

Sociodemographic variables such as age, marital status, education level, income level, and economic activity were included. The variables were categorized as follows: age (20-29, 30-39, 40-49, 50-59, 60-69, and 70 years and older), marital status (married, widowed, divorced/separated, or single), education level (middle school or lower, high school, and college graduate or higher), average monthly individual income (≤ 0.99, 1-1.99, 2-2.99, 3-3.99, 4-4.99, ≥ 5.0 million KRW/mo), and economic activity (employed, housewife, student, or not employed).

The following questions were asked about the least feared cancer and the most feared cancer; "If you had cancer, which of the following would you fear less? Please check the 1st, 2nd and 3rd ranks of the less feared cancers. And in the case of men, assume that you're a female, and in the case of women, assume that you're a male." "If you had cancer, which of the following would you fear most? Please check the 1st, 2nd, and 3rd ranks of the most feared cancers. And in the case of men, assume that you're a female, and in the case of women, assume that you're a male." Cancers of choice were stomach cancer, colon cancer, lung cancer, liver cancer, thyroid cancer, prostate cancer, bladder cancer, renal cancer, pancreatic cancer, cancer of bile duct and gallbladder, leukemia, breast cancer, cervical cancer, uterine cancer, and ovarian cancer.

The following questions were asked about the fear of side effects of cancer treatment. "What is the most feared side effects of cancer treatment? Please check the 1st, 2nd, and 3rd ranks of the most feared side effects of cancer treatment." Side effects of cancer treatment of choice were pain, fatigue, general weakness, digestive dysfunction, sexual dysfunction, psychological problems, urological dysfunction, motor dysfunction, sensory dysfunction, appearance change, lymphedema, and infertility. The questionnaire used in this study can be found in the Supplementary Material.

3. Statistical methods

To compare the status of sociodemographic variables between men and women, chi-square analysis was used as a univariate analysis. For the questions about cancer fear and fear of the side effects of cancer treatment, 3 points were given for the 1st rank, 2 points for the 2nd rank, and 1 point for the 3rd rank, and the points were summed as rank scores for each type of cancer. Then each type of cancer was ranked by scores for each category such as least feared cancer or most feared cancer, and the fear of side effects of cancer treatment was ranked by the rank scores. Each type of cancer was also ranked by 5-year relative survival rate, and the ranks were used to compare the fatalness of cancer (5-year relative survival rate) to the fear ranks mentioned above. Rank difference was calculated to show the gaps between 5-year relative survival rate and each fear rank, and between the fear rank of men or women and the fear rank generated from the opposite sex. Rank difference was also calculated to show the gaps in the fear of side effects of cancer treatment between men and women. Student's t test was used to compare the thoughts of men and women about cancer fears and the fear of side effects of cancer treatment in both men and women. The analysis was performed using SPSS ver. 16 (SPSS Inc., Chicago, IL).

4. Ethical statement

The present study was approved by the Korean National

Table 1. General characteristic of the study population

Characteristic	Total (n=1,000)	Men (n=501, 50.1%)	Women (n=499, 49.9%)	p-value[a]
Age (yr)				
20-29	167 (16.7)	89 (17.8)	78 (15.6)	0.840
30-39	188 (18.8)	95 (19.0)	93 (18.6)	
40-49	216 (21.6)	110 (22.0)	106 (21.2)	
50-59	209 (20.9)	105 (21.0)	104 (20.8)	
60-69	206 (20.6)	95 (19.0)	111 (22.2)	
≥ 70	14 (1.4)	7 (1.4)	7 (1.4)	
Marital status				
Married	704 (70.4)	333 (66.5)	371 (74.3)	< 0.001
Widowed	32 (3.2)	8 (1.6)	24 (4.8)	
Divorced/Separated	34 (3.4)	18 (3.6)	16 (3.2)	
Single	230 (23.0)	142 (28.3)	88 (17.6)	
Education				
Middle school or lower	88 (8.8)	30 (6.0)	58 (11.6)	0.002
High school	422 (42.2)	206 (41.1)	216 (43.3)	
College or higher	490 (49.0)	265 (52.9)	225 (45.1)	
Income (million KRW/mo)				
≤ 0.99	119 (11.9)	36 (7.2)	83 (16.6)	< 0.001
1-1.99	147 (14.7)	36 (7.2)	111 (22.2)	
2-2.99	229 (22.9)	126 (25.1)	103 (20.6)	
3-3.99	241 (24.1)	148 (29.5)	93 (18.6)	
4-4.99	150 (15.0)	91 (18.2)	59 (11.8)	
≥ 5	114 (11.4)	64 (12.8)	50 (10.0)	
Economic activity				
Employed	751 (75.1)	455 (90.8)	296 (59.3)	< 0.001
Housewife	180 (18.0)	0	180 (36.1)	
Student	39 (3.9)	26 (5.2)	13 (2.6)	
Not employed	30 (3.0)	20 (4.0)	10 (2.0)	

Values are presented as number (%). [a]Chi-square test was used.

Cancer Center Institutional Review Board (NCC 2017-0137). All participants provided written informed consent for the survey.

Results

As a matter of course due to sampling methods, there was no significant difference in age distribution between men and women (Table 1).

The least and the most feared cancers in men were thyroid and lung cancer, respectively (Table 2). When men assumed the perspective of women, the least and the most feared cancers were thyroid and stomach cancer, respectively. Rank difference between 5-year relative survival rate and the least feared cancer showed that the most optimistic view was of stomach cancer, followed by cancer of bile duct and gallbladder in men. The least and the most feared cancers in women were thyroid and stomach cancer, respectively.

In terms of the least feared cancer, the men's guess was in line with the women's response for stomach cancer, lung cancer, thyroid cancer, pancreatic cancer, cancer of bile duct and gallbladder, breast cancer, and cervical cancer. In the case of ovarian cancer, liver cancer, and uterine cancer, men were less afraid of those cancers than women.

For the most feared cancer, the men's guess was in line with the women's response for stomach cancer, liver cancer, bladder cancer, cancer of bile duct and gallbladder, and leukemia. In the case of ovarian cancer, breast cancer, cervical cancer, and uterine cancer, men were more afraid of those cancers than women. The women's guess was in line with the men's response for colon cancer, lung cancer, renal cancer, cancer of bile duct and gallbladder, leukemia, and breast cancer.

When the fear rank scores for the least fearful cancer in men were compared between responses of men and guesses by women, men feared stomach cancer and thyroid cancer less than women's guesses (Table 3). When women assumed the perspective of men, women feared prostate cancer, renal

Table 2. Awareness of the least fearful cancer and the most fearful cancer among men and women

Cancer type	Men					Women					Rank difference					
	5-Year relative survival rate (rank) (A)	Least fearful cancer (rank)		Most fearful cancer (rank)		5-Year relative survival rate (rank) (F)	Least fearful cancer (rank)		Most fearful cancer (rank)							
		Me (B)	Assuming I am a woman (C)	Me (D)	Assuming I am a woman (E)		Me (G)	Assuming I am a man (H)	Me (I)	Assuming I am a man (J)	B-A	G-F	C-G	E-I	H-B	J-D
Stomach	7	2	2	5	1	6	2	3	1	6	–5	–4	0	0	1	1
Colon	6	5	12	4	9	7	9	7	6	4	–1	2	3	3	2	0
Lung	11	9	10	1	7	11	10	9	3	1	–2	–1	0	4	0	0
Liver	9	8	11	3	10	12	13	8	10	2	–1	1	–2	0	0	–1
Thyroid	1	1	1	10	12	1	1	2	13	11	0	0	0	–1	1	1
Prostate	2	3	-	6	-	-	-	1	-	5	1	-	-	-	–2	–1
Bladder	5	4	6	11	14	8	5	4	14	10	–1	–3	1	0	0	–1
Renal	4	7	7	9	13	4	6	6	12	9	3	2	1	1	–1	0
Pancreatic	12	11	14	2	6	14	14	11	2	3	–1	0	0	4	0	1
Bile duct and gallbladder (tie)	10	6	8 (tie)	8	11	13	8	5	11	8	–4	–5	0	0	–1	0
Leukemia	8	10	13	7	8	10	12	10	8	7	2	2	1	0	0	0
Breast	3	12	3	12	2	2	3	12	4	12	9	1	0	–2	0	0
Cervical	-	-	4	-	5	5	4	-	7	-	-	–1	0	–2	-	-
Uterine (endometrial)	-	-	5	-	3	3	7	-	5	-	-	4	–2	–2	-	-
Ovarian	-	-	8 (tie)	-	4	9	11	-	9	-	-	2	–3	–5	-	-

Table 3. Comparison of cancer fear between men and women

Cancer type	Men						Women					
	Least fearful cancer			Most fearful cancer			Least fearful cancer			Most fearful cancer		
	Men's response	Women's response	p-value[a)]	Men's response	Women's response	p-value	Women's response	Men's response	p-value	Women's response	Men's response	p-value
Stomach	1.24±1.23	0.92±1.16	< 0.001	0.45±0.97	0.37±0.83	0.160	0.97±1.16	0.94±1.14	0.743	0.83±1.15	0.93±1.15	0.185
Colon	0.46±0.93	0.36±0.83	0.084	0.82±1.08	0.80±1.07	0.760	0.24±0.69	0.13±0.53	0.005	0.53±0.97	0.42±0.89	0.045
Lung	0.21±0.67	0.26±0.71	0.245	1.43±1.27	1.41±1.26	0.877	0.16±0.59	0.14±0.54	0.724	0.82±1.14	0.54±0.99	< 0.001
Liver	0.26±0.70	0.29±0.71	0.573	1.02±1.13	0.98±1.10	0.609	0.10±0.43	0.13±0.55	0.228	0.41±0.84	0.35±0.77	0.279
Thyroid	1.32±1.25	1.09±1.24	0.004	0.07±0.39	0.05±0.38	0.367	1.98±1.17	1.45±1.31	< 0.001	0.06±0.34	0.16±0.61	0.002
Prostate	1.09±1.16	1.26±1.27	0.028	0.37±0.86	0.38±0.91	0.782	-	-	-	-	-	-
Bladder	0.46±0.87	0.51±0.94	0.405	0.05±0.30	0.07±0.42	0.336	0.34±0.76	0.36±0.78	0.704	0.05±0.34	0.08±0.39	0.228
Renal	0.28±0.71	0.40±0.84	0.014	0.13±0.51	0.17±0.58	0.216	0.32±0.79	0.27±0.66	0.200	0.08±0.34	0.14±0.53	0.017
Pancreatic	0.10±0.43	0.18±0.61	0.011	1.04±1.17	0.94±1.18	0.170	0.08±0.37	0.06±0.33	0.366	0.83±1.17	0.57±0.94	< 0.001
Bile duct and gallbladder	0.35±0.78	0.46±0.84	0.025	0.17±0.56	0.22±0.66	0.193	0.25±0.65	0.26±0.71	0.799	0.11±0.44	0.20±0.66	0.010
Leukemia	0.17±0.62	0.19±0.63	0.710	0.29±0.77	0.34±0.85	0.318	0.13±0.53	0.13±0.55	0.965	0.44±0.92	0.46±0.96	0.760
Breast	0.03±0.24	0.05±0.32	0.214	0.20±0.22	0.44±0.34	0.186	0.57±0.94	0.85±1.13	< 0.001	0.66±1.07	0.82±1.20	0.024
Cervical	-	-	-	-	-	-	0.52±0.93	0.81±1.12	< 0.001	0.49±0.97	0.57±1.03	0.207
Uterine (endometrial)	-	-	-	-	-	-	0.29±0.71	0.40±0.82	0.020	0.59±1.01	0.64±1.04	0.503
Ovarian	-	-	-	-	-	-	0.13±0.49	0.26±0.69	0.001	0.44±0.91	0.63±1.05	0.002

Values are presented as mean±standard deviation. [a)]Student's t test was used.

Table 4. Awareness of the most fearful side effects of cancer treatment among men and women

Side effect	Total (rank)	Men (rank)	Women (rank)	Rank difference (men-women)
Pain	1	1	1	0
Fatigue	5	5	5	0
General weakness	3	3	3	0
Digestive dysfunction	4	4	4	0
Sexual dysfunction	9	8	11	–3
Psychological problems	2	2	2	0
Urological dysfunction	10	9	10	–1
Motor dysfunction	11	11	9	2
Sensory dysfunction	7	10	7	3
Appearance change	6	6	6	0
Lymphedema	8	7	8	–1
Infertility	12	12	12	0

Table 5. Comparison of fear of side effects of cancer treatment between men and women

Side effect	Men	Women	p-value[a)]
Pain	2.07±1.20	2.10±1.14	0.703
Fatigue	0.49±0.90	0.57±0.99	0.169
General weakness	0.66±0.93	0.82±1.01	0.011
Digestive dysfunction	0.58±0.91	0.65±0.95	0.259
Sexual dysfunction	0.23±0.64	0.08±0.40	< 0.001
Psychological problems	0.83±1.08	0.85±1.07	0.776
Urological dysfunction	0.21±0.66	0.09±0.39	0.001
Motor dysfunction	0.10±0.44	0.09±0.42	0.780
Sensory dysfunction	0.16±0.53	0.19±0.62	0.500
Appearance change	0.41±0.82	0.44±0.86	0.525
Lymphedema	0.24±0.73	0.11±0.45	0.001
Infertility	0.01±0.16	0.02±0.17	0.842

Values are presented as mean±standard deviation. [a)]Student's t test was used.

cancer, pancreatic cancer, and cancer of bile duct and gallbladder less than men. No statistically significant difference was found in case of the most feared cancer.

When the fear rank scores for the least fearful cancer in women were compared between responses of women and guesses by men, women feared colon cancer and thyroid cancer less than men's guesses. When men assumed the perspective of women, men feared breast cancer, cervical cancer, uterine cancer, and ovarian cancer less than women. In case of the most fearful cancer, women feared colon cancer, lung cancer, and pancreatic cancer more than men's guesses. When men assumed the perspective of women, men feared thyroid cancer, renal cancer, cancer of bile duct and gallbladder, breast cancer, and ovarian cancer more than women. Interestingly, in the case of breast and ovarian cancer, when asked about the least feared cancers, men rated those cancers less fearful than women, and men rated them more fearful than women when asked about the most feared cancer.

The most feared side effect of cancer treatment was pain, and the top six of the most feared side effects were identical for men and women (pain, psychological problems, general weakness, digestive dysfunction, fatigue, and appearance change) (Table 4). Sexual dysfunction, urinary disorders, and lymphedema were more feared side effects in men than in women. On the other hand, sensory dysfunction and motor dysfunction were more feared side effects in women than in men. When comparing fear rank scores for those side effects, general weakness was feared more in females, and sexual dysfunction, urological dysfunction, and lymphedema were feared more in males (Table 5).

Discussion

In this study, we found that there was an optimistic view of stomach cancer in both men and women. We believe this

is because early detection of stomach cancer has been highly emphasized in Korea with the message that the rate of cure is very high if detected early [25]. With a gastric cancer screening rate of only 61.6% in 2018 [26], this optimistic view of stomach cancer may not help increase the screening rate. On the other hand, the reason for having a relatively optimistic fear perception for cancer of the bile duct and gallbladder is thought to be because the cancer is not well known for its subsistence despite the very poor survival rate. Cancer of the bile duct and gallbladder is not so prevalent, which ranks 9th in incidence respectively in males and females [27].

If both men and women assume that they are the opposite sex, the fear of sex-specific cancer was relatively lower compared to the actual responses of both men and women: prostate cancer in men, breast cancer, cervical cancer, uterine cancer, and ovarian cancer in women. This difference in thinking between men and women can affect mutual understanding in health problems related to cancer occurring in opposite sex, and also affect the behavior of health professionals [28].

Contrary to reports that most men fear prostate cancer because of fear of losing their masculinity [29], this study did not show much fear of prostate cancer. As a reason for this, it is presumed that unlike the West, especially in the United States, where the incidence of prostate cancer is low, there is limited opportunity to observe the side effects associated with prostate cancer treatment, such as the loss of masculinity.

It is interesting that the top six of the most feared side effects of cancer treatment were identical for men and women (pain, psychological problems, general weakness, digestive dysfunction, fatigue, and appearance change). In one study using a convenience sample of patients recently diagnosed with cancer, the rankings of the most feared side effects of cancer were different in men and women [30]. For women, it was hair loss, vomiting, infection, nausea, weight loss, shortness of breath (co-5th place), and fatigue. On the other hand, for men it was vomiting, infection, fatigue, weight loss, hair loss, and shortness of breath (co-5th place), followed by nausea. Because the respondents of this study consisted of people who had no experience of cancer for themselves or their family members, it is understandable that the responses of this survey may differ from the patients and their families. The fact that men fear more about urological and sexual dysfunction seems to have been rarely investigated in other studies, and further research is needed.

This study has the following strengths. Although it is not a large sample, it is a study conducted by a national survey by random probability allocation. In addition, by excluding cancer patients or families of cancer patients from the survey, experience-based responses could be eliminated as much as possible. It was difficult to find previous studies in which men and women responded assuming the perspective of the opposite sex as well as their own sex. This design allowed us to examine the idea of the opposite sex. However, the study has the following limitations. First of all, 1,460 respondents were contacted to enroll 1,000 respondents for this study, and the survey participation rate was 68.5%. Although this participation rate is not low, the probability that some bias was involved in the representativeness of this sample cannot be excluded. In this study, when investigating the fear of cancer and side effects, a ranking score method was used to add up to the third place rather than just the frequency corresponding to the first place. In this case, even though statistical analysis can be diversified, and there are advantages to more inclusive analysis of the items answered in the top-level rankings, the differentiation between ranks may be weakened. With various judgments among respondents, more than 10 choices seem to have contributed to a widening of response variance. However, because cancer can be viewed as a collection of diseases rather than a single disease, expansion of options was inevitable. If more diverse questionnaires are constructed and qualitative studies are added to these variations, a more precise survey could be available.

Finally, since this study was conducted as a descriptive profiling study which summarized the differences in fear profiles between men and women, multivariate analysis was not used. Few studies have analyzed the fear of cancer types and side effects by sex to provide such cancer fear profile to health professionals. In this situation, we found it meaningful to present the results of this study to meet these needs. However, it can be said that there are limitations as a study for examining sex-specific effects by excluding the effects of other variables. Despite these limitations, while there are few studies comparing fears of cancer and side effects of cancer treatment between men and women, there are very few studies comparing those fears between men and women on the assumption of opposite sex, and this study has contributed to the accumulation of research literature.

In addition to the characteristics of the health problems caused by various types of cancer and the side effects of various types of cancer treatment, health care providers should provide care in response to the differences in these problems between men and women. Doctors can adequately and directly deal with the patient's emotional distress by verbally expressing understanding, empathy, support, and justification of emotion, which in turn leads to improvement in physical symptoms and the negative effects of insufficient social support [31]. The problem of communication in the medical field due to the difference in sex between health professionals such as doctors and patients due to changes in the sex ratio of medical service providers may also be an important issue in the future [32]. In order to prepare for this, it is necessary to educate the sex difference in the curriculum of health care professionals such as medical schools and nursing colleges. This will require understanding not only the biological aspects of sex, but also psychological and sociological aspects

as well as training in communication skills.

In addition, family care givers, including spouses, will be able to provide more patient-friendly care if they communicate with each other, paying attention to the fact that there is a difference in the thought processes about cancer between men and women.

The least and the most feared cancers in men were thyroid and lung cancer, respectively. When men assumed the perspective of women, the least and the most feared cancers were thyroid and stomach cancer, respectively. The least and the most feared cancers in women were thyroid and stomach cancer, respectively. When women assumed the perspective of men, the least and the most feared cancers were prostate cancer and lung cancer, respectively. If both men and women assume that they are the opposite sex, the fear of sex-specific cancer was relatively lower compared to the actual responses of both men and women: prostate cancer in men, breast cancer, cervical cancer, uterine cancer and ovarian cancer in women. The most feared side effect of cancer treatment was pain, and the top six of the most feared side effects were identical for men and women (pain, psychological problems, general weakness, digestive dysfunction, fatigue, and appearance change). The fact that men fear more about urological and sexual dysfunction seems to have been rarely investigated in other studies, and further research is needed. Our findings highlight the importance of understanding the differences between men and women's attitudes and risk perception towards cancer.

Electronic Supplementary Material

Supplementary materials are available at Cancer Research and Treatment website (https://www.e-crt.org).

Conflicts of Interest

Conflicts of interest relevant to this article was not reported.

References

1. Mobbs D, Hagan CC, Dalgleish T, Silston B, Prevost C. The ecology of human fear: survival optimization and the nervous system. Front Neurosci. 2015;9:55.
2. Ropeik D. The consequences of fear. EMBO Rep. 2004;5(Suppl 1):S56-60.
3. Aral SO, Douglas JM, Lipshutz JA. Behavioral interventions for prevention and control of sexually transmitted diseases. Boston, MA: Springer; 2007.
4. Rogers RW. Cognitive and psychological processes in fear appeals and attitude change: a revised theory of protection motivation. In: Cacioppo JT, Petty RE, editors. Social psychophysiology: a sourcebook. New York: The Guilford Press; 1983. p. 153-76.
5. Consedine NS, Magai C, Krivoshekova YS, Ryzewicz L, Neugut AI. Fear, anxiety, worry, and breast cancer screening behavior: a critical review. Cancer Epidemiol Biomarkers Prev. 2004;13:501-10.
6. Ferrer R, Klein WM. Risk perceptions and health behavior. Curr Opin Psychol. 2015;5:85-9.
7. Hong WK, Bas RC Jr, Hait WN, Kufe DW, Pollock RE. Holland-Frei cancer medicine 8th ed. Shelton, CT: People's Medical Publishing House-USA; 2010.
8. Polanski J, Jankowska-Polanska B, Rosinczuk J, Chabowski M, Szymanska-Chabowska A. Quality of life of patients with lung cancer. Onco Targets Ther. 2016;9:1023-8.
9. Schulman-Green D, Ercolano E, Dowd M, Schwartz P, McCorkle R. Quality of life among women after surgery for ovarian cancer. Palliat Support Care. 2008;6:239-47.
10. Committee on Psychosocial Services to Cancer Patients/Families in a Community Setting; Adler NE, Page AE. Cancer care for the whole patient: meeting psychosocial health needs. Washington, DC: National Academies Press; 2008.
11. Benz EJ Jr. The Jeremiah Metzger lecture cancer in the twenty-first century: an inside view from an outsider. Trans Am Clin Climatol Assoc. 2017;128:275-97.
12. Hernandez LM, Blazer DG, Committee on Assessing Interactions among Social, Behavioral, and Genetic Factors in Health. Genes, behavior, and the social environment: moving beyond the nature/nurture debate. Washington, DC: National Acade-mies Press; 2006.
13. Committee on Understanding the Biology of Sex and Gender Differences, Pardue ML, Wizemann TM. Exploring the biological contributions to human health: does sex matter? Washington, DC: National Academies Press; 2001.
14. Li QP, Mak YW, Loke AY. Spouses' experience of caregiving for cancer patients: a literature review. Int Nurs Rev. 2013;60:178-87.
15. Ketcher D, Trettevik R, Vadaparampil ST, Heyman RE, Ellington L, Reblin M. Caring for a spouse with advanced cancer: similarities and differences for male and female caregivers. J Behav Med. 2020;43:817-28.
16. Hugman B. Perspectives on risk communication and gender issues. In: Harrison-Woolrych M, editor. Medicines for women. Cham: Adis; 2015. p. 531-83.
17. de Jonge ET, Vlasselaer J, Van de Putte G, Schobbens JC. The construct of breast cancer risk perception: need for a better risk communication? Facts Views Vis Obgyn. 2009;1:122-9.
18. Kim SE, Perez-Stable EJ, Wong S, Gregorich S, Sawaya GF, Walsh JM, et al. Association between cancer risk perception and screening behavior among diverse women. Arch Intern Med. 2008;168:728-34.
19. Vernon SW. Risk perception and risk communication for cancer screening behaviors: a review. J Natl Cancer Inst Monogr. 1999;1999:101-19.
20. Pellmar TC, Brandt EN Jr, Baird MA. Health and behavior: the interplay of biological, behavioral, and social influences: sum-

mary of an Institute of Medicine report. Am J Health Promot. 2002;16:206-19.
21. Fawcett TN, McQueen A. Perspectives on cancer care. Chichester: Wiley-Blackwell; 2010.
22. Committee on the Learning Health Care System in America, Smith M, Saunders R, Stuckhardt L, McGinnis JM. Best care at lower cost: the path to continuously learning health care in America. Washington, DC: National Academies Press; 2013.
23. McQueen A, Vernon SW, Meissner HI, Rakowski W. Risk perceptions and worry about cancer: does gender make a difference? J Health Commun. 2008;13:56-79.
24. Shiloh S, Wade CH, Roberts JS, Alford SH, Biesecker BB. Associations between risk perceptions and worry about common diseases: a between- and within-subjects examination. Psychol Health. 2013;28:434-49.
25. Lee SY, Lee EE. Cancer screening in Koreans: a focus group approach. BMC Public Health. 2018;18:254.
26. National Health Insurance Service. 2018 National health screening statistics yearbook. Wonju: National Health Insurance Service; 2019.
27. Jung KW, Won YJ, Kong HJ, Lee ES. Prediction of cancer incidence and mortality in Korea, 2019. Cancer Res Treat. 2019;51:431-7.
28. Celik H, Lagro-Janssen TA, Widdershoven GG, Abma TA. Bringing gender sensitivity into healthcare practice: a systematic review. Patient Educ Couns. 2011;84:143-9.
29. Kedrowski KM, Sarow MS. Cancer activism: gender, media, and public policy. Chicago, IL: University of Illinois Press; 2007.
30. Passik SD, Kirsh KL, Rosenfeld B, McDonald MV, Theobald DE. The changeable nature of patients' fears regarding chemotherapy: implications for palliative care. J Pain Symptom Manage. 2001;21:113-20.
31. Epstein RM, Street RL Jr. Patient-centered communication in cancer care: promoting healing and reducing suffering. Bethesda, MD: National Institutes of Health; 2007.
32. van den Brink-Muinen A. The role of gender in healthcare communication. Patient Educ Couns. 2002;48:199-200.

pISSN 1598-2998, eISSN 2005-9256

Cancer Res Treat. 2020;52(4):1002-1009 https://doi.org/10.4143/crt.2020.190

Original Article Open Access

Perspectives on Professional Burnout and Occupational Stress among Medical Oncologists: A Cross-sectional Survey by Korean Society for Medical Oncology (KSMO)

Yun-Gyoo Lee, MD, PhD[1]
Chi Hoon Maeng, MD, PhD[2]
Do Yeun Kim, MD, PhD[3]
Bong-Seog Kim, MD, PhD[4]

[1]*Department of Internal Medicine, Kangbuk Samsung Hospital, Sungkyunkwan University School of Medicine, Seoul,* [2]*Department of Internal Medicine, Kyung Hee University Hospital, Kyung Hee University College of Medicine, Seoul,* [3]*Department of Internal Medicine, Dongguk University Ilsan Hospital, Goyang,* [4]*Department of Internal Medicine, Veterans Health Service Medical Center, Seoul, Korea*

Correspondence: Do Yeun Kim, MD, PhD
Department of Internal Medicine, Dongguk University Ilsan Hospital, 27 Dongguk-ro, Ilsandong-gu, Goyang 10326, Korea
Tel: 82-31-961-7143
Fax: 82-31-961-7141
E-mail: kkamgdog@gmail.com

Co-correspondence: Bong-Seog Kim, MD, PhD
Department of Internal Medicine, Veterans Health Service Medical Center, 53 61-gil, Jinhwangdo-ro, Gangdong-gu, Seoul 05368, Korea
Tel: 82-2-2225-1319
Fax: 82-2-740-4160
E-mail: seog9270@gmail.com

Received January 30, 2020
Accepted July 9, 2020
Published Online July 10, 2020

*Yun-Gyoo Lee and Chi Hoon Maeng contributed equally to this work.

Purpose
This study aimed to investigate the prevalence and risk factors of burnout and occupational stress among medical oncologists in Korea.

Materials and Methods
A survey was conducted of medical oncologists who were members of Korean Society for Medical Oncology (KSMO) using the Korean Occupational Stress Scale, the validated Maslach Burnout Inventory (MBI) and supplemental questions about work and lifestyle factors.

Results
Among 220 active KSMO members, 111 responses were collected. The median age was 42 years (range, 32 to 63 years). Two-thirds of responders worked 6 days per week and half of them worked a total of 60-80 hours per week. Each medical oncologist treated a median of 90-120 patients per week in outpatient clinics and 20-30 patients per week in patient practices. MBI subscales indicated a high level of emotional exhaustion in 74%, a high level of depersonalization in 86%, and a low level of personal accomplishment in 65%: 68% had professional burnout according to high emotional exhaustion and high depersonalization scores. The risk of burnout was higher for medical oncologists aged from 30-39 than 40-49 years, and unmarried than married. Considering personal accomplishment, females had a higher risk of burnout. The median score of occupational stress was 63 (range, 43 to 88). Having night-duty call was the strongest risk factor on more stress. A higher stress score was associated with a higher prevalence of burnout.

Conclusion
Burnout and occupational stress are quite common amongst Korean medical oncologists. Achieving a healthy work-life balance, ensuring balanced workload distribution, and engaging in proper stress relief solutions are necessary.

Key words
Burnout, Occupational stress, Medical oncologists

Introduction

A career in medical oncology is exceedingly rewarding. Fast-moving advances in research and therapeutics, intriguing dynamics in practice environments, and opportunities to provide critical support to patients are professionally appealing and satisfying [1]. Still, all of these characteristics place medical oncologists at high risk for stress. Therefore, medical oncologists have been the focus of concerns regarding stress.

Burnout is a psychosocial syndrome that involves prolonged response to chronic emotional and interpersonal stressors on the job [2]. Burnout is characterized by emotional exhaustion (EE), feelings of depersonalization (DP), and reduced personal accomplishment (PA) [2]. Physicians commonly suf-

fer from distress due to burnout, with studies suggesting a prevalence of 32% among medical oncologists [3]. High mortality rates among patients with advanced cancer, increasing numbers of cancer patients, as well as changing practice migrating to more comprehensive care management solutions can trigger burnout in medical oncologists [4].

Since such stress and burnout can cause negative consequences related to professional satisfaction and personal life, as well as quality of patient care, this issue deserves attention [5]. Burnout and occupational stress have been extensively studied among oncologists in the United States and Europe [6,7]. However, little is known about the situation among Korean medical oncologists. Therefore, we conducted a nationwide survey to investigate the prevalence of professional burnout and occupational stress among Korean medical oncologists. Then we identified work and lifestyle factors that affect burnout and occupational stress.

Materials and Methods

1. Participants

Between May 2018 and June 2018, a cross-sectional, web-based survey of 220 medical oncologists who were active in the field was conducted through the Korean Society for Medical Oncology (KSMO). All responders were invited via an e-mail that included a link to the survey and fully informed of the overall purpose of our survey prior to participation. SurveyMonkey (https://ko.surveymonkey.com) was used to build the web-based online survey. All authors as the committee members of the KSMO Insurance and Policy Committee supervised the entire investigation, ensured the reliability of the data and analyzed the results.

2. Study measures

The survey consisted of three parts with a total of 73 questions: personal and professional characteristics (27 questions), occupational stress (24 questions), and burnout (22 questions). The initial 26 questions consisted of two questions regarding demographics, 12 regarding occupational environment, and 13 regarding a pattern of living. Among 13 questions for lifestyle, the respondents were asked to rate their job satisfaction on a scale of 100 and asked if they were balanced in their work and life.

Occupational stress was assessed by the Korean Occupational Stress Scale (KOSS) [8]. Job stress should be investigated in the local and cultural context of each worker, and KOSS is a validated self-reported questionnaire that examines job stress and reflects the organizational culture of Korea. The KOSS short-form (KOSS-SF), which was used in this study, is an abbreviated survey designed to be used at work place settings [9]. It consists of seven subscales (24 items total): job demand (4 items), insufficient job control (4 items), interpersonal conflict (3 items), job insecurity (2 items), occupational system (4 items), lack of reward (3 items), and organizational climate (4 items).

Burnout was estimated using the validated Maslach Burnout Inventory–Human Service Survey (MBI-HSS) [10]. The MBI-HSS consists of 22 questions to evaluate three domains of burnout: EE (9 questions), feelings of DP (5 questions), and reduced PA (8 questions). Each question was scored on a 7-point frequency rating from '0' (never) to '6' (every day). The sum of raw scores was assessed for the presence of burnout: a score of 27 or higher on the EE subscale, 10 or higher on the DP subscale, or lower than 33 on the PA subscale was considered to indicate a high level of burnout [2,11]. In this study, MBI-HSS which was translated into Korean and validated for university hospital workers in Korea was used. The cutoff values in three domains in burnout were also verified [12]. To define burnout in a conventional approach, medical oncologists with high DP and EE, and low PA subscale scores were considered to have professional burnout [13]. The next predominant definition of burnout (high DP and EE) was also used.

3. Statistical analysis

The questionnaires completed by June 2018 were included for further analyses. To compare the characteristics of the study participants between the groups, we used independent t tests for continuous variables and Fisher exact tests or chi-square tests for categorical variables. To analyze the risk factors for professional burnout, multivariate logistic regression analyses were performed. To analyze the relationship between risk factor and occupational stress, linear regression analyses were performed. All statistical analyses were performed by STATA ver. 13.0 software (StataCorp LP, College Station, TX).

4. Ethical statement

This study complied with the Declaration of Helsinki and was conducted under Institutional Review Board (IRB) approval at the Veterans Health Service Medical Center (IRB No. 2108-04-033). Participation in this survey was regarded as agreeing to the study, so written informed or verbal consent requirements from respondents were waived. All data were de-identified.

Results

1. Personal and professional characteristics

An e-mail invitation was sent to 220 active medical oncologists and 175 responses (80%) were received. There were 64 incomplete questionnaires, and complete responses from 111 participant (51%) were included in the final analysis.

Personal and professional characteristics of participants

Table 1. Personal and professional characteristics of participating medical oncologists (n=111)

Characteristic	No. (%)
Sex	
Male	62 (55.8)
Female	49 (44.1)
Age (yr)	
Median (range)	42 (32-63)
≤ 39	38 (34.2)
40-49	58 (52.2)
≥ 50	15 (13.5)
Relationship status	
Married	92 (82.9)
Single	19 (17.1)
Religious: yes vs. no	
Yes	64 (57.7)
No	47 (42.3)
Drinking habit	
≤ 1 drink per month	40 (36.0)
2-4 drinks per month	55 (49.5)
≥ 2-3 drinks per week	16 (14.4)
Exercise per week	
Never	49 (44.1)
1-2 days	43 (38.7)
3-5 days	17 (15.3)
Every day	2 (1.8)
Type of hospital	
Superior general hospital	68 (61.3)
General hospital	37 (33.3)
Public hospital	6 (5.4)
Faculties in medical oncology, number	
Median (range)	5 (1-16)
In-house hospitalists (yes)	36 (32.4)
Daytime primary on-call (yes)	30 (27.0)
Nights on-call (yes)	16 (14.4)
Saturday duty (yes)	73 (65.8)
For outpatient clinic	12 (10.8)
For inpatient rounding	45 (40.5)
For outpatient and inpatient	16 (14.4)
Work hours per week (includes patient care, administrative work, research, and teaching)	
< 40	1 (0.9)
40-60	35 (31.5)
60-80	45 (40.5)
80-100	18 (16.2)
> 100	12 (10.8)
Outpatients seen in clinic every week	
30-60	20 (18.0)
60-90	26 (23.4)
90-120	25 (22.5)
120-150	16 (14.4)
> 150	24 (21.6)
Inpatients seen in hospital every week	
< 10	11 (9.9)
10-20	53 (47.7)
20-30	26 (23.4)
> 30	21 (18.9)
Overall job satisfaction (0-100 scale)	
Mean±SD	54.8±21.8
Median (range)	50 (0-100)

Table 2. Prevalence of burnout and occupational stress among medical oncologists (n=111)

Characteristic	Score
Burnout indices	
Emotional exhaustion (EE)	
Mean±SD	33.3±9.7
Median (range)	34 (8-54)
High degree of burnout, sum ≥ 27, n (%)	82 (73.9)
Depersonalization (DP)	
Mean±SD	15.2±5.9
Median (range)	14 (0-27)
High degree of burnout, sum ≥ 10, n (%)	96 (86.5)
Personal accomplishment (PA)	
Mean±SD	31.3±5.4
Median (range)	30 (19-42)
High degree of burnout, sum ≤ 33, n (%)	72 (64.9)
Overall professional burnout, n (%)	
High EE and DP scores	76 (68.4)
High EE and DP, and low PA	54 (48.6)
Occupational stress	
Mean±SD	61.7±7.8
Median (range)	63 (43-88)

are summarized in Table 1. Men were 56% of participants. A median age of participants was 42 years old. Of the responders, 83% were married and 58% practiced a religion. As for drinking habits, 34% of participants reported they rarely drink (less than one drink a month), 50% reported that they drink sometimes (two-four drinks a month), the others (14%) reported they drink frequently (more than two-three drinks a week). As for exercise habits, approximately 44% of participants responded that they never exercise at all and only 2% responded that they exercise every day.

Most participants were working in tertiary care hospitals (61%) and general hospitals (33%). The median number of accompanying faculty in medical oncology was five persons. Roughly one-third of participants (32%) were working in institutions with in-house hospitalists. Only 11% of participants were in a single-organ specialty practice, and the others served in multi-organ specialty practice. Participants

Table 3. The relationship between professional burnout, occupational stress, and job satisfaction

Burnout	Occupational stress		Job satisfaction	
	Score	p-value[a]	Score	p-value[a]
High EE and DP scores				
No burnout	56.9±7.4	< 0.001	66.3±2.1	< 0.001
Burnout	63.9±6.9		49.5±2.0	
High EE and DP, and low PA				
No burnout	59.0±7.3	< 0.001	63.9±2.0	< 0.001
Burnout	64.5±7.2		45.2±1.9	

Values are presented as mean±standard deviation. EE, emotional exhaustion; DP, depersonalization; PA, personal accomplishment.
[a]p-value was derived from independent t test to compare mean values between two groups.

treated a median of three types of cancer. About one-quarter of participants had daytime primary call, and 14.0% received night emergency calls instead of residents. Two-thirds of participants responded that they work 6 days a week, including Saturday. Participants spent an average of 60 to 80 hours each week devoted to professional activities, including patient care, administrative work, research, and teaching. On average, participants cared for 90 to 120 patients in the outpatient setting each week and 20 to 30 patients in the inpatient setting. The mean overall job satisfaction score was 54.8.

2. Prevalence of burnout, and its relationship with occupational stress and job satisfaction

The prevalence of burnout and occupational stress among participating medical oncologists is presented in Table 2. In all, 74% of participants experienced a high degree of EE, 87% experienced a high level of DP, and 65% had a low sense of PA. In aggregate, 76 (68%) medical oncologists had professional burnout according to high EE and high DP scores. On a more conservative basis (high EE and high DP, and low PA), about half (49%) of medical oncologists were found to have burnout.

The mean occupational stress score was 61.7 (range 43 to 88). We investigated the relationship between professional burnout and occupational stress, and job satisfaction (Table 3). The participants with burnout showed a higher occupational stress score than those without burnout ($p < 0.001$). The participants with burnout showed a lower job satisfaction score than those without burnout ($p < 0.001$). Only 27% of medical oncologists reported that they maintained work-life balance well.

Predictors that were significantly associated with burnout or occupational stress on multivariate analysis are listed in Tables 4 and 5. The risk of burnout was higher for medical oncologists aged from 30 to 39 years than those aged 40 to 49 years. Unmarried persons had a higher risk of burnout than married persons. After consideration of PA score, females had a higher risk of burnout than males.

For risk factors on occupational stress, there was a strong relationship between having night-duty call and high occupational stress score (p=0.001).

In this survey, multiple answer choices were accepted for the question related to causes of stress. In all, 78% of participants stated that the biggest cause of burnout or occupational stress was the enforcement of the Act for the Improvement of Training Conditions and Status of Medical Residents, which limits maximum weekly hours of work for residents to 80. Other major causes of burnout or occupational stress included a lack of residents in the department of internal medicine (52%), increased administrative and clinical workloads required by the Life-Sustaining Treatment Decision-Making Act (44%), and responsibilities of daytime primary call (23%).

Discussion

The phenomenon of burnout is caused by frequent exposure to chronic occupational stress and is characterized by a 3-dimensional syndrome comprised of EE, DP (also known as cynicism), and reduced PA [12]. Physician's burnout is particularly dangerous and should be avoided, since it can increase medical errors and reduce quality of care for patients [13-15]. The nature of practicing oncology is changing. An increment of workload by expansion in patient volume, burdensomeness of administrative tasks, and complexity of innovative oncology place medical oncologists at increasing risk of stress and subsequent burnout [16]. Burnout can be overcome by investigating work environments and identifying underlying problems [17].

In line with these environments, we conducted the first large-scale nationwide study of Korean medical oncologists using standardized instruments to evaluate burnout and occupational stress. Overall, 68% of Korean medical oncologists were burned out according to the high EE and DP domains at the time of the survey, which was higher than the 44.7% of U.S. oncologists and the 51% of Chinese oncologists reported in previous studies [18,19]. Our result was similar to the 71% burnout rate reported by study in European countries

Table 4. Multivariate analysis for burnout related to personal and professional factors

Characteristic	Odds ratio (p-value)							
	Burnout (high EE and DP)				Burnout (high EE and DP, and low PA)			
	Univariate	p-value	Multivariate	p-value	Univariate	p-value	Multivariate	p-value
Sex								
Male	1		-		1		1	
Female	2.63	0.027	-	-	2.92	0.007	2.87	0.011
Age group (yr)								
≤ 39	1		1		1		1	
40-49	0.38	0.069	0.20	0.012	0.54	0.154	0.13	0.012
≥ 50	0.09	0.001	-	-	0.09	0.004	-	-
Relationship status								
Single	1		1		1		-	
Married	0.09	0.025	0.10	0.030	0.37	0.064	-	-
Religion								
No	1		-		1		-	
Yes	0.61	0.246	-	-	0.85	0.663	-	-
Drinking habit								
≤ 1 per month	1		-		1		-	
2-4 per month	1.13	0.784	-	-	1.16	0.724	-	-
≥ 2-3 per week	1.56	0.506	-	-	1.16	0.804	-	-
Exercise								
Never	1		-		1		-	
1-2 days per week	1.02	0.969	-	-	0.55	0.152	-	-
3-7 days per week	0.76	0.623	-	-	0.32	0.046	-	-
Type of hospital								
Superior general	1		-		1		-	
General	0.57	0.190	-	-	0.81	0.604	-	-
Public	1.94	0.557	-	-	5.30	0.137	-	-
Daytime on-call								
No	1		-		1		-	
Yes	1.74	0.261	-	-	1.08	0.862	-	-
Nights on-call								
No	1		1		1		-	
Yes	8.36	0.044	8.46	0.049	1.43	0.512	-	-
Saturday duty								
No	1		-		1		-	
Yes	1.21	0.661	-	-	1.49	0.321	-	-
Work hours per week								
< 60	1		-		1		-	
60-80	1.76	0.232	-	-	0.875	0.765	-	-
80-100	1.43	0.555	-	-	1	> 0.99	-	-
> 100	7.86	0.060	-	-	1	> 0.99	-	-

EE, emotional exhaustion; DP, depersonalization; PA, personal accomplishment.

that focused on young (≤ 40 years old) oncologists. Among personal characteristics, younger age (30-39 years vs. 40-49 years), being unmarried, and working night duty were independently associated with a high risk of professional burnout. Younger age, as well as being early in their careers, are well-known demographic risk factors for burnout of physicians in many medical departments [17]. In general, young people often take on a variety of administrative tasks in addition to clinical workloads. Additionally, physicians who are in early career stages must spend time not only on patient care but also on research and education.

Interestingly, when we consider more conservative definition of burnout including low PA (high EE and DP, and low PA), female gender was significantly associated with a high

Table 5. Multivariate analysis for occupational stress related to personal and professional factors

Characteristic	Occupational stress			
	Univariate		Multivariate	
	Coefficient	p-value	Coefficient	p-value
Sex				
Male	1		-	
Female	2.44	0.099	-	-
Age group (yr)				
≤ 39	1		-	
40-49	–1.48	0.161	-	-
≥ 50	–3.68	0.122	-	-
Relationship status				
Single	1		-	
Married	–2.11	0.283	-	-
Religion				
No	1		-	
Yes	–2.11	0.157	-	-
Drinking habit				
≤ 1 per month	1		-	
2-4 per month	–1.25	0.438	-	-
≥ 2-3 per week	–3.11	0.177	-	-
Exercise				
Never	1		-	
1-2 days per week	–0.22	0.894	-	-
3-7 days per week	–2.00	0.345	-	-
Type of hospital				
Superior general	1		-	
General	–2.37	0.136	-	-
Public	2.33	0.480	-	-
Daytime on-call				
No	1		-	
Yes	2.32	0.163	-	-
Nights on-call				
No	1		1	
Yes	6.44	0.002	6.44	0.001
Saturday duty				
No	1		-	
Yes	0.23	0.884	-	-
Work hours per week				
< 60	1		-	
60-80	–1.72	0.318	-	-
80-100	0.75	0.735	-	-
> 100	4.11	0.110	-	-

risk of burnout. Analysis that female gender was a risk factor of burnout has been reported in previous studies [20-22]. Rath et al. [21] reported a large study on burnout for gynecologic oncologists that female gender was also identified as risk factor for burnout. In another study for surgeons, more women than men surgeons had burnout and depressive symptoms [22]. In that study, work-home conflicts accounted for a major contributor to surgeon burnout, especially to female surgeon. Although we did not measure work-home conflicts in our survey, our results could be interpreted that women medical oncologists are under more pressure in terms of personal achievement probably from work-home conflicts.

Yeob et al. [20] conducted a similar nationwide survey recruiting a total of 130 medical, surgical, and radiation oncologists from 13 cancer centers in Korea. That study found that

female gender and long working hours were associated with increased risks of burnout, which was consistent finding of our study. To evaluate burnout, unlike our study, they used Professional Quality of Life scale, which was developed to measure the quality of life of health care professionals [23]. Although burnout is a domain of the Professional Quality of Life Scale described above, MBI-HSS is appreciated a more reliable and valid measure of burnout [24].

One of the biggest reasons for burnout or occupational stress reported in our survey—chosen by 78% of participants—was the enforcement of the Act for the Improvement of Training Conditions and Status of Medical Residents, which limits residents to a maximum of 80 work hours per week. Although the working time of residents has been substantially reduced due to the enactment of the law, many hospitals were not equipped with alternative personnel such as a hospitalist (only 32% of participants were working with in-house hospitalists). It caused a significant increase in faculty's workload.

Our study showed that medical oncologists who felt burnout had a high level of occupational stress and a low level of job satisfaction (Table 3). According to a recent global survey of job satisfaction among medical oncologists [25], younger age and fewer years in clinical practice were associated with low job satisfaction. Interestingly, that study showed that medical oncologists with low job satisfaction tended to have fewer conversations with patients about disease prognosis, suggesting that low job satisfaction is also associated with low quality of patient care. In other words, burnout, low job satisfaction, and low quality of patient care correlate with each other, and one may be the cause and/or effect of the other.

There have been many reports of interventions to decrease physician burnout. Interventions that focus on individual physicians include intensive face-to-face workshops [26], communication skills training [27], stress management skills training [28], and mindfulness-based stress reduction programs [5]. Such interventions have been reported to help relieve stress, but these programs are not readily applicable or available to each oncologist. Even without formal programs, one of the easiest things is exercise. In our study, only half of the participants exercised. Exercise is known to have the potential to be effective for burnout prevention, so even in harsh clinical works, it is recommended to encourage medical oncologists to engage in regular exercise programs [29]. One study suggested the idea that enhancing professionalism can lower burnout [30]. Professionalism is often used to describe behavioral and value standards of performance that any professional is expected to achieve in their work, and knowledge that professionals need to perform their job efficiently. It is necessary to improve professionalism by reinforcement of expertise and applied rewards.

Still, one report suggested that organizational or system-level interventions are much more effective for controlling burnout than individual efforts [31]. Organization-directed strategies are mostly related to changes in work shift schedules, but oncologist-specific system-level methods have not been studied [31]. Therefore, the system-level strategies for management of Korean medical oncologists are warranted [32].

Our study has some limitations. First, there is considerable variation across studies regarding cutoff scores for burnout among healthcare professionals [33]. According to Maslach guidelines, more conservative definitions (the combination of high EE, high DP, and low PA) have been widely used [2,33]. However, this definition risks underestimating the burnout rate. In our study, we followed the recent consensus that defined burnout as high EE and high DP [11,18,34]. Based on our further analyses (Tables 3 and 4), the difference between the two definitions did not show a significant difference in the results except for prevalence. Second, our study participants were younger than those in previous surveys. Additionally, only 51% of potential participants (active medical oncologists) responded to this survey. These factors may have resulted in selection and response bias. However, our study is the first large-scale national study only for Korean medical oncologists registered to a major association (i.e., KSMO). Therefore, the results of our study are representative of a major population of medical oncology professionals in Korea. Third, our survey did not recruit other experts from different disciplines such as surgical and radiation oncologists. Because multidisciplinary team approach is essential in the management of advanced cancer, a follow-up study including all key professionals is warranted to make this burnout study more practical.

A considerable number of medical oncologists in Korea are burning out with a high level of occupational stress and lower job satisfaction. In order to provide the high quality of cancer care to cancer patients, further efforts should be conducted to find out the way to relieve the burnout and occupational stress of Korean medical oncologists from point of view of system-level management plan as well as individual effort.

Conflicts of Interest

Conflicts of interest relevant to this article was not reported.

Acknowledgments

This study was supported for administrative assistance by KSMO.

References

1. Shanafelt T, Dyrbye L. Oncologist burnout: causes, consequences, and responses. J Clin Oncol. 2012;30:1235-41.
2. Maslach C, Schaufeli WB, Leiter MP. Job burnout. Annu Rev Psychol. 2001;52:397-422.
3. Medisauskaite A, Kamau C. Prevalence of oncologists in distress: systematic review and meta-analysis. Psychooncology. 2017;26:1732-40.
4. Jung KW, Won YJ, Kong HJ, Lee ES. Prediction of cancer incidence and mortality in Korea, 2018. Cancer Res Treat. 2018;50:317-23.
5. Amutio A, Martinez-Taboada C, Delgado LC, Hermosilla D, Mozaz MJ. Acceptability and effectiveness of a long-term educational intervention to reduce physicians' stress-related conditions. J Contin Educ Health Prof. 2015;35:255-60.
6. Shanafelt TD, Raymond M, Kosty M, Satele D, Horn L, Pippen J, et al. Satisfaction with work-life balance and the career and retirement plans of US oncologists. J Clin Oncol. 2014;32:1127-35.
7. Banerjee S, Califano R, Corral J, de Azambuja E, De Mattos-Arruda L, Guarneri V, et al. Professional burnout in European young oncologists: results of the European Society for Medical Oncology (ESMO) Young Oncologists Committee Burnout Survey. Ann Oncol. 2017;28:1590-6.
8. Shin HC. Measuring stress with questionnaires. J Korean Med Assoc. 2013;56:485-95.
9. Park SG, Min KB, Chang SJ, Kim HC, Min JY. Job stress and depressive symptoms among Korean employees: the effects of culture on work. Int Arch Occup Environ Health. 2009;82:397-405.
10. Maslach C, Jackson SE, Leiter MP. Maslach burnout inventory manual. Palo Alto, CA: Consulting Psychologists Press; 1996.
11. Shanafelt TD, Boone S, Tan L, Dyrbye LN, Sotile W, Satele D, et al. Burnout and satisfaction with work-life balance among US physicians relative to the general US population. Arch Intern Med. 2012;172:1377-85.
12. Bianchi R, Schonfeld IS, Laurent E. Burnout-depression overlap: a review. Clin Psychol Rev. 2015;36:28-41.
13. Wallace JE, Lemaire JB, Ghali WA. Physician wellness: a missing quality indicator. Lancet. 2009;374:1714-21.
14. Fahrenkopf AM, Sectish TC, Barger LK, Sharek PJ, Lewin D, Chiang VW, et al. Rates of medication errors among depressed and burnt out residents: prospective cohort study. BMJ. 2008;336:488-91.
15. Shanafelt TD, Balch CM, Bechamps G, Russell T, Dyrbye L, Satele D, et al. Burnout and medical errors among American surgeons. Ann Surg. 2010;251:995-1000.
16. Genentech. The 2018 Genentech oncology trend report. 10th ed. South San Francisco, CA: Genentech; 2018.
17. Murali K, Makker V, Lynch J, Banerjee S. From burnout to resilience: an update for oncologists. Am Soc Clin Oncol Educ Book. 2018;38:862-72.
18. Shanafelt TD, Gradishar WJ, Kosty M, Satele D, Chew H, Horn L, et al. Burnout and career satisfaction among US oncologists. J Clin Oncol. 2014;32:678-86.
19. Ma S, Huang Y, Yang Y, Ma Y, Zhou T, Zhao H, et al. Prevalence of burnout and career satisfaction among oncologists in China: a national survey. Oncologist. 2019;24:e480-9.
20. Yeob KE, Kim SY, Park BR, Shin DW, Yang HK, Park K, et al. Burnout among oncologists in the Republic of Korea: a nationwide survey. Curr Probl Cancer. 2020;44:100535.
21. Rath KS, Huffman LB, Phillips GS, Carpenter KM, Fowler JM. Burnout and associated factors among members of the Society of Gynecologic Oncology. Am J Obstet Gynecol. 2015;213:824.
22. Dyrbye LN, Shanafelt TD, Balch CM, Satele D, Sloan J, Freischlag J. Relationship between work-home conflicts and burnout among American surgeons: a comparison by sex. Arch Surg. 2011;146:211-7.
23. Stamm BH. The concise ProQOL manual. Pocatello, ID: ProQOL; 2010.
24. Newell JM, MacNeil GA. A comparative analysis of burnout and professional quality of life in clinical mental health providers and health care administrators. J Workplace Behav Health. 2011;26:25-43.
25. Raphael MJ, Fundytus A, Hopman WM, Vanderpuye V, Seruga B, Lopes G, et al. Medical oncology job satisfaction: results of a global survey. Semin Oncol. 2019;46:73-82.
26. Butow P, Cockburn J, Girgis A, Bowman D, Schofield P, D'Este C, et al. Increasing oncologists' skills in eliciting and responding to emotional cues: evaluation of a communication skills training program. Psychooncology. 2008;17:209-18.
27. Bragard I, Etienne AM, Merckaert I, Libert Y, Razavi D. Efficacy of a communication and stress management training on medical residents' self-efficacy, stress to communicate and burnout: a randomized controlled study. J Health Psychol. 2010;15:1075-81.
28. Gunasingam N, Burns K, Edwards J, Dinh M, Walton M. Reducing stress and burnout in junior doctors: the impact of debriefing sessions. Postgrad Med J. 2015;91:182-7.
29. Bretland RJ, Thorsteinsson EB. Reducing workplace burnout: the relative benefits of cardiovascular and resistance exercise. PeerJ. 2015;3:e891.
30. Jang I, Kim Y, Kim K. Professionalism and professional quality of life for oncology nurses. J Clin Nurs. 2016;25:2835-45.
31. Panagioti M, Panagopoulou E, Bower P, Lewith G, Kontopantelis E, Chew-Graham C, et al. Controlled interventions to reduce burnout in physicians: a systematic review and meta-analysis. JAMA Intern Med. 2017;177:195-205.
32. Unger JP. Physicians' burnout (and that of psychologists, nurses, magistrates, researchers, and professors) for a control program. Int J Health Serv. 2020;50:73-81.
33. Doulougeri K, Georganta K, Montgomery A. "Diagnosing" burnout among healthcare professionals: can we find consensus? Cogent Med. 2016;3:1.
34. Shanafelt TD, Hasan O, Dyrbye LN, Sinsky C, Satele D, Sloan J, et al. Changes in burnout and satisfaction with work-life balance in physicians and the general US working population between 2011 and 2014. Mayo Clin Proc. 2015;90:1600-13.

pISSN 1598-2998, eISSN 2005-9256

Cancer Res Treat. 2020;52(4):1010-1018

https://doi.org/10.4143/crt.2020.254

Original Article

Open Access

Nomogram for Predicting Central Lymph Node Metastasis in Papillary Thyroid Cancer: A Retrospective Cohort Study of Two Clinical Centers

Zheyu Yang, MD[1]
Yu Heng, MS[2]
Jianwei Lin, MS[1]
Chenghao Lu, MS[1]
Dingye Yu, MS[1]
Lei Tao, PhD[2]
Wei Cai, PhD[1]

[1]*Department of General Surgery, Shanghai Jiaotong University School of Medicine Affiliated Ruijin Hospital, Shanghai,* [2]*ENT Institute and Department of Otorhinolaryngology, Eye & ENT Hospital, Fudan University, Shanghai, China*

Correspondence: Wei Cai, PhD
Department of General Surgery, Shanghai Jiaotong University School of Medicine Affiliated Ruijin Hospital, 197 Ruijin 2nd Road, Shanghai 200031, China
Tel: 86-18917762028
Fax: 86-021-64333548
E-mail: caiwei@shsmu.edu.cn

Co-correspondence: Lei Tao, PhD
ENT Institute and Department of Otorhinolaryngology, Eye & ENT Hospital, Fudan University, 83 Fenyang Road, Shanghai 200031, China
Tel: 86-13916944810
Fax: 86-021-64377134-962
E-mail: doctortaolei@163.com

Received March 26, 2019
Accepted June 8, 2020
Published Online June 9, 2020

*Zheyu Yang and Yu Heng contributed equally to this work.

Purpose
Central lymph node metastasis (CNM) are highly prevalent but hard to detect preoperatively in papillary thyroid carcinoma (PTC) patients, while the significance of prophylactic compartment central lymph node dissection (CLND) remains controversial as a treatment option. We aim to establish a nomogram assessing risks of CNM in PTC patients, and explore whether prophylactic CLND should be recommended.

Materials and Methods
One thousand four hundred thirty-eight patients from two clinical centers that underwent thyroidectomy with CLND for PTC within the period 2016-2019 were retrospectively analyzed. Univariate and multivariate analysis were performed to examine risk factors associated with CNM. A nomogram for predicting CNM was established, thereafter internally and externally validated.

Results
Seven variables were found to be significantly associated with CNM and were used to construct the model. These were as follows: thyroid capsular invasion, multifocality, creatinine > 70 μmol/L, age < 40, tumor size > 1 cm, body mass index < 22, and carcinoembryonic antigen > 1 ng/mL. The nomogram had good discrimination with a concordance index of 0.854 (95% confidence interval [CI], 0.843 to 0.867), supported by an external validation point estimate of 0.825 (95% CI, 0.793 to 0.857). A decision curve analysis was made to evaluate nomogram and ultrasonography for predicting CNM.

Conclusion
A validated nomogram utilizing readily available preoperative variables was developed to predict the probability of central lymph node metastases in patients presenting with PTC. This nomogram may help surgeons make appropriate surgical decisions in the management of PTC, especially in terms of whether prophylactic CLND is warranted.

Key words
Nomograms, Central lymph node metastasis, Papillary thyroid cancer, Risk factors

Introduction

More than 90% of all thyroid carcinoma are differentiated thyroid cancer (DTC) [1]. Papillary thyroid carcinoma (PTC), a lymphotropic tumor that tends to metastasize to cervical lymph nodes, is the most common type of DTC. Among these lymph nodes, the central neck compartment has the highest risk of metastasis [2]. Although detection techniques such as high-resolution ultrasonography (US) and US-guided fine-needle aspiration (FNA) biopsy greatly improve diagnosis of PTC [3], the sensitivity of US in assessing deep anatomical spaces of the central neck compartment is low [4]. Thus, a considerable number of PTC patients were found to have level VI metastatic lymph nodes when already under sur-

gery or histopathological examinations [5]. In our research, the rate of central lymph node (level VI) metastasis (CNM) whose preoperative examinations showed no lymph nodes metastasis was as high as 36.1% (601/1,663).

Thyroidectomy with central compartment lymph node dissection (CLND) is recommended for PTC patients with CNM. Yet, due to poor reliability of preoperative examinations, prophylactic CLND is not routinely recommended in clinical or radiological node-negative PTC patients, as per American Thyroid Association guidelines. Thus, a tool that helps to quantify the risk of nodal metastasis may facilitate preoperative decision-making [6].

With this objective in mind, our retrospective analysis from two centers was designed using nomogram as the evaluation system, for it excels in user-friendliness and convenience in formulating personalized treatments for a variety of cancers [7,8]. In this study, we covered several factors that could help predict CNM in PTC patients that were absent in the other studies, such as body mass index (BMI), carcinoembryonic antigen (CEA), and creatinine (Cr). Our comprehensive nomogram may aid clinicians in selecting the most appropriate operative strategies to achieve optimal outcome.

Table 1. Demographics and clinical characteristics of the cohort

Variable	Value
Age (yr)	
Mean	43.1
BMI (kg/m²)	
Mean	23.81
Sex	
Male	447 (35.7)
Female	805 (64.3)
Size of largest lesion (US)	
Mean	0.86
Medium	0.7
Thyroid capsule invasion (US)	495 (39.5)
Multifocality (US)	373 (29.8)
Bilateral disease	243 (19.4)
Serum index (mean)	
CEA	1.42
Creatinine	64
CNM	618 (49.4)
Central lymph node	
Mean harvested	7.1
Mean positive	4.3
LLNM	158 (12.6)

Vaues are presented as number (%) unless otherwise indicated. BMI, body mass index. US, ultrasonography; CEA, carcinoembryonic antigen; CNM, central lymph node metastasis; LLNM, lateral lymph node metastasis.

Materials and Methods

1. Patient recruitment

Patients who underwent the first-time thyroidectomy to treat thyroid carcinoma at Department of General Surgery, Ruijin Hospital, Shanghai Jiao Tong University School of Medicine (Shanghai, China), and Department of Otorhinolaryngology, Head and Neck Surgery, at the Eye, Ear, Nose, and Throat (EENT) Hospital of Fudan University (Shanghai, China) from June 2016 to June 2019 were studied. A total of 1,731 patients were enrolled (1,294 patients from Ruijin Hospital and 437 from EENT Hospital). The exclusion criteria were as follows: (1) no histologically proven PTC (n=81), (2) no lymph nodes removed (n=68) and had inadequate preoperative blood test report (n=95), (3) pathologically confirmed skip metastasis (n=43), and (4) history or coexistence of other head and neck cancer (n=6). After exclusion, 1,438 patients that had pathological PTC, and received thyroidectomy along with CLND were studied. Among the 1,438 recruits, 1,252 patients (December 2016-May 2019) from both clinical centers were used to make the original model, while 186 patients (June 2019-October 2019) from Ruijin Hospital only were used for external validation.

2. Preoperative examination, surgical strategy, and pathological examination

Preoperative examination including serum index, FNA, and US were performed at Shanghai Ruijin Hospital or Shanghai EENT Hospital. Preoperative US included the following features: type of the surrounding thyroid tissues (normal, Hashimoto thyroiditis, or nodular goiter), tumor size (longest length of the largest lesion), multifocality (more than one nodule scoring higher than Thyroid Imaging Reporting and Data System (TI-RADS) 4A in unilateral thyroid lobe), thyroid capsular invasion (TCI) and suspicious lymph node detected (central lymph node or lateral lymph node).

According to 2010 TNM staging system of the American Joint Committee on Cancer (AJCC) [9], all patients enrolled were identified as $T_{0\text{-}4}N_{0\text{-}1}M_0$. These patients also received total thyroidectomy or thyroid lobectomy with therapeutic or prophylactic CLND.

All acquired specimens were examined by two or more board-certified pathologists from Shanghai Ruijin Hospital and Shanghai EENT Hospital. Pathological features analyzed were pathological type of tumor, type of the surrounding thyroid tissues, tumor size, multifocality (more than one lesion in unilateral thyroid lobe), and lymph node metastasis.

3. Statistical analysis

We used logistic univariate and multivariate regression analyses to screen risk factors that were significantly associated with CNM using the SPSS ver. 24.0 package (IBM Corp.,

Armonk, NY). Variables of which the p-value < 0.05 from the univariate logistic regression were then used for multivariate logistic regression to construct a risk prediction model – Nomogram, in R software (ver. 3.5.1, R Development Core Team). The method of decision curve analysis (DCA) was used to evaluate the nomogram model and the US model for prediction of CNM. The decision analytic technique is available in the R statistical package and a step-by-step tutorial is available online [10]. All statistical tests were performed using the R statistical package. The discrimination and consensus degree of our newly-established predictive model were tested through the receiver operating characteristic (ROC) curve, the calibration curve, and the area under the ROC curve (AUC) which is also known as the concordance index (C-index). The likelihood of CNM were quantified as risk scores according to our nomogram, and each patient was stratified into different subgroups by their calculated CNM risk scores.

4. Ethical statement

Consent has been obtained from each patient or subject after full explanation of the purpose and nature of all procedures used. All procedures performed in studies involving human participants were in accordance with the ethical standards of the Institutional Ethics Committee of the Eye and ENT Hospital of Fudan University and the Ruijin Hospital of Shanghai Jiao Tong University School of Medicine, and with the 1964 Helsinki declaration and its later amendments

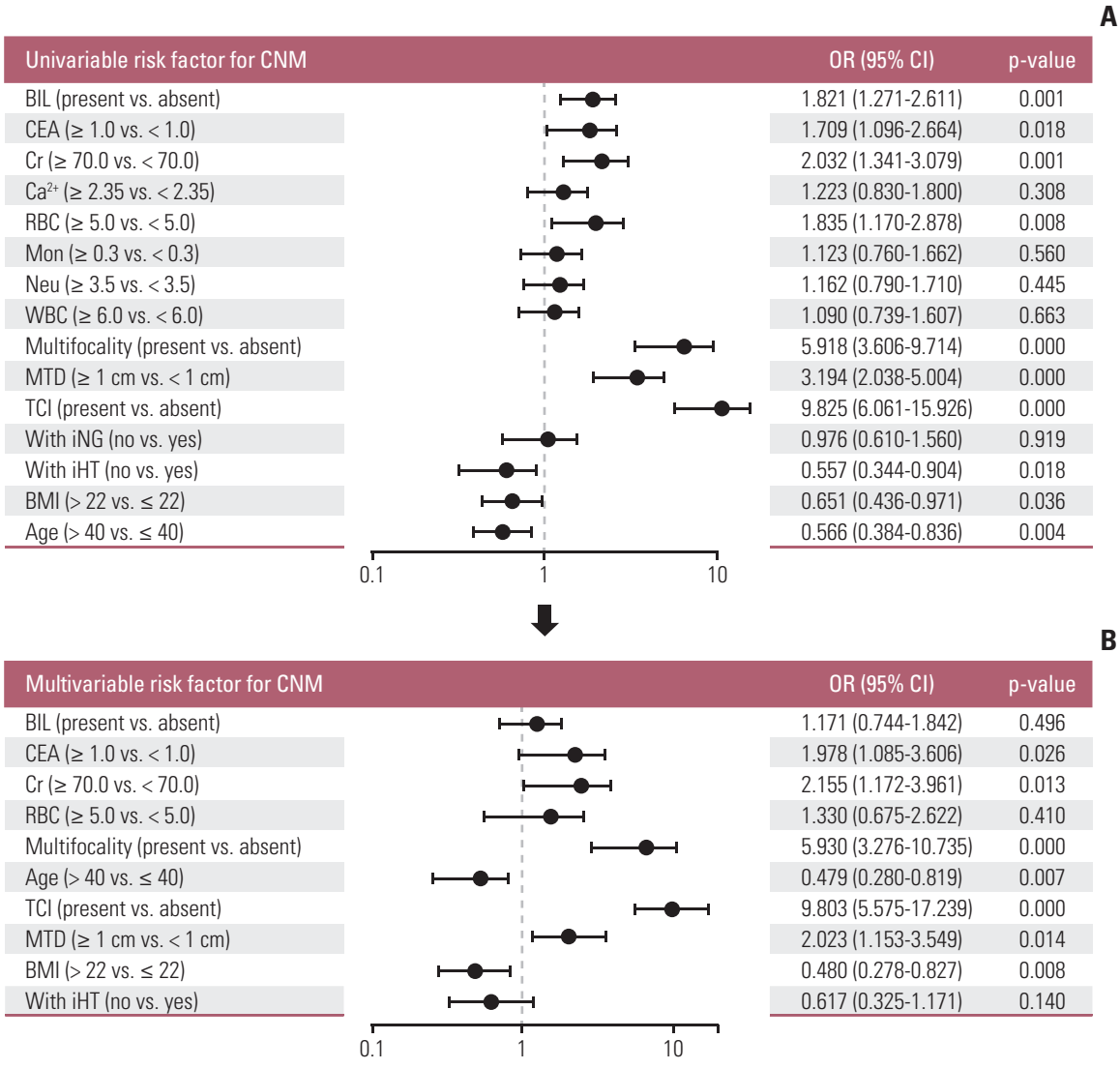

Fig. 1. Univariate (A) and multivariate (B) logistic regression of factors associated with central lymph node metastasis (CNM). BIL, bilirubin; CEA, carcinoembryonic antigen; Cr, creatinine; RBC, red blood cell; Mon, monocyte; Neu, neutrophil; WBC, white blood cell; MTD, maximum tumor diameter; TCI, thyroid capsular invasion; iNG, ipsilateral Nodular Goiter; iHT, ipsilateral Hashimoto thyroiditis; BMI, body mass index.

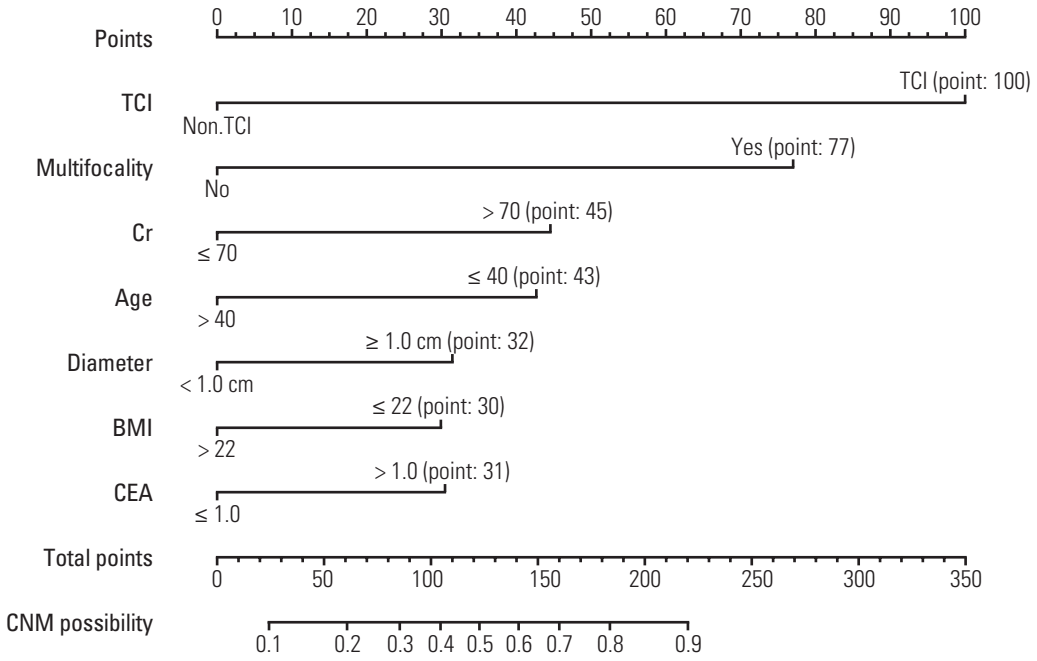

Fig. 2. The nomogram for predicting risk of possible central lymph node metastasis (CNM) in papillary thyroid carcinoma patients. TCI, thyroid capsular invasion; Cr, creatinine; BMI, body mass index; CEA, carcinoembryonic antigen.

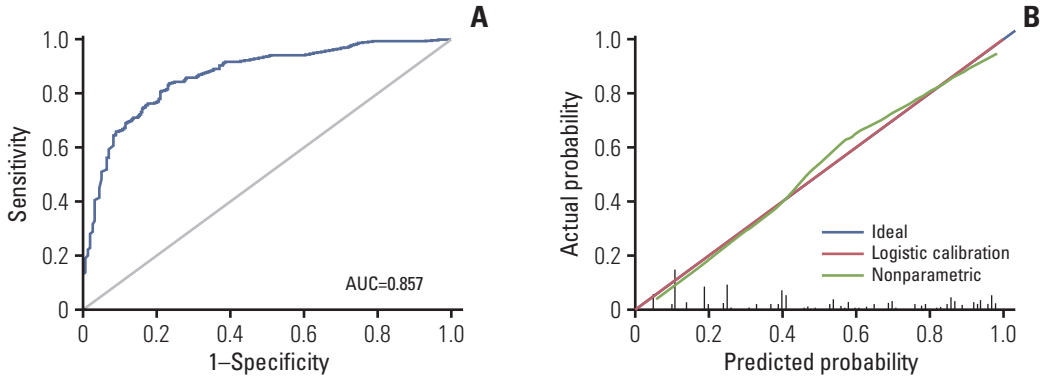

Fig. 3. Evaluation and Validation of the nomogram. (A) The receiver operating characteristics (ROC) curve and area under the ROC curve (AUC) of the nomogram. (B) The calibration curve of the nomogram for predicting possible central lymph node metastasis. Actual probability is plotted on the y-axis, and nomogram predicted probability on the x-axis.

or comparable ethical standards.

Results

1. Demographics and clinical characteristics in original model

A total of 1,252 PTC patients including 447 males (35.7%) and 805 females (64.3%) underwent thyroidectomy with CLND in our institution. Mean age was 43.1 years with a range of 14-78 years, and mean BMI was 23.81 with a range of 16.67-43.56. Two serum indexes were included, CEA medium was 1.42 while the Cr medium was 64. Through preoperative US detection, the mean size of tumor size was 0.86 cm with a range of 0.05-6.5 cm. Four hundred ninety-five (39.5%) were diagnosed with thyroid capsule invasion, 373 patients (29.8%) were found to have more than one lesion higher than TI-RADS 4A in the same lobe (multifocality). Among the surgical specimens, 243 (19.4%) were confirmed to have bilateral PTC, 618 (49.4%) were ultimately confirmed to have CNM. The mean harvested central lymph nodes was 7.1, mean positive nodes was 4.3, and 158 patients (12.6%) were pathologically confirmed to have lateral lymph node metastasis (LLNM) (Table 1).

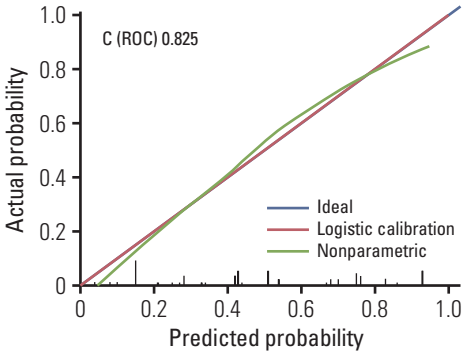

Fig. 4. The calibration curve of the nomogram for external validation set. ROC, receiver operating characteristics.

2. Univariate and multivariate analysis of CNM variables

In the univariate analysis, bilaterality ($p < 0.001$), CEA (p=0.018), Cr ($p < 0.001$), red blood cell (p=0.008), multifocality (US) ($p < 0.001$), maximum tumor diameter (MTD, US) ($p < 0.001$), TCI (US) ($p < 0.001$), ipsilateral Hashimoto thyroiditis (p=0.018), BMI (p=0.018), and age (p=0.004) have association with CNM (Fig. 1A). Multivariate logistic regression modeling was further conducted to screen for significant variables associated with CNM. Results were as follows: CEA > 1 ng/mL, Cr > 70 μmol/L, multifocality, age < 40 years, TCI, MTD > 1 cm, BMI < 22 (Fig. 1B).

3. Nomogram for predicting likelihood of CNM in PTC patients

Based on the independent factors screened through multivariate analysis, a nomogram was established for predicting individual risk of CNM. The risk of each factor including CEA, Cr, multifocality, age, TCI, and BMI was quantified in our predicting model (score of each factor was shown in Fig. 2) to predict the presence of CNM in PTC patients.

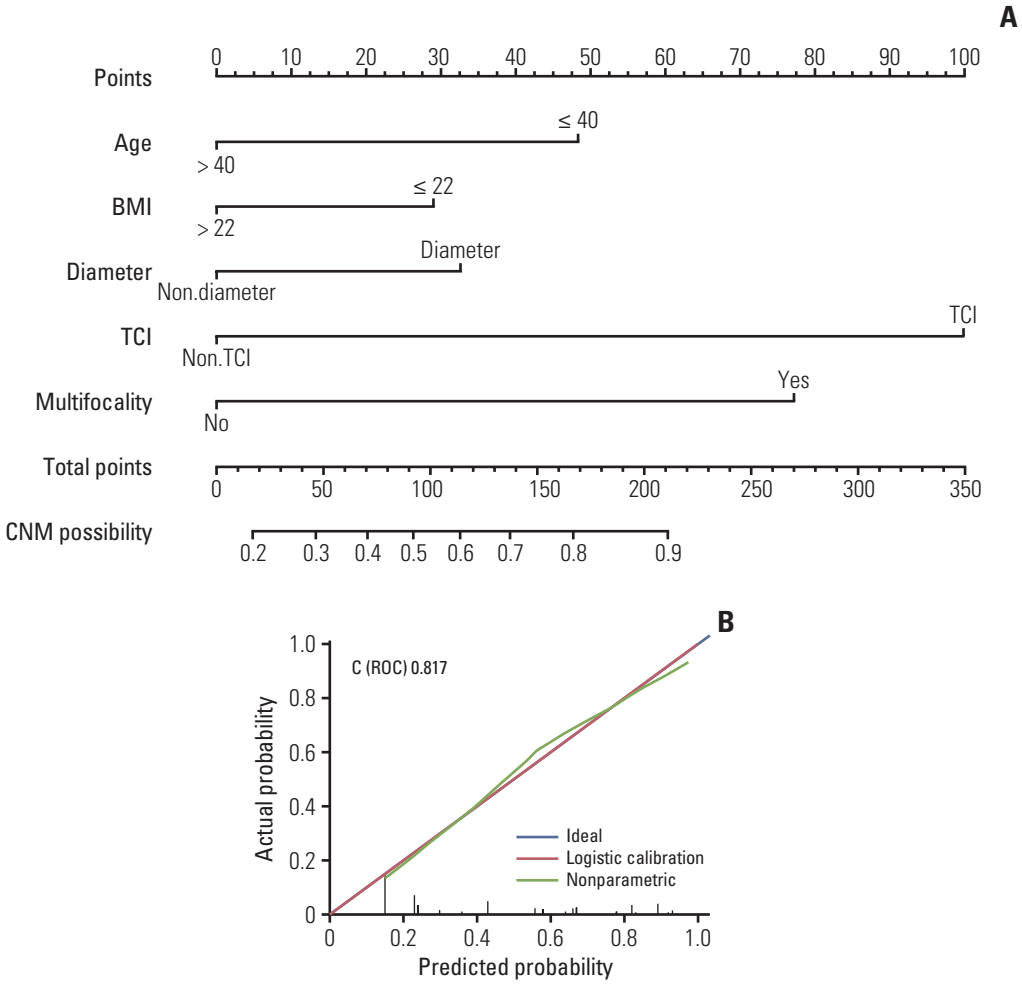

Fig. 5. (A) Nomogram without serum index for predicting central lymph node metastasis (CNM) in papillary thyroid carcinoma (PTC) patients. (B) The calibration curve of the nomogram excluding serum index. BMI, body mass index; TCI, thyroid capsular invasion; ROC, receiver operating characteristics.

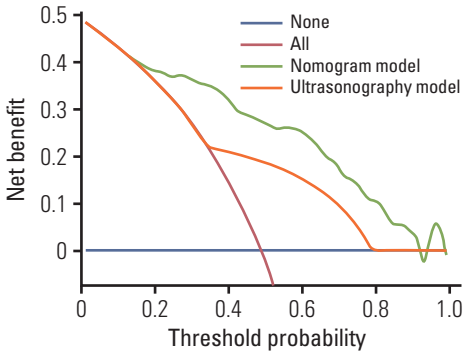

Fig. 6. Decision curve analysis for comparing our nomogram and ultrasonography in predicting central lymph node metastasis in papillary thyroid carcinoma patients.

4. Internal and external validation of the nomogram

To evaluate our nomogram's ability to predict CNM in PTC patients, we conducted an internal validation using 1,000 bootstrap resamples. A C-index of 0.857 (95% CI, 0.821 to 0.894) was achieved, and a similar C-index 0.854 (95% CI, 0.843 to 0.867) was acquired after 1,000 bootstrapping, confirming its satisfactory accuracy in predicting central lymph nodes involvement. ROC curve and AUC are presented in Fig. 3A. Furthermore, we also conducted a calibration plot for our newly-established model, and a favorable agreement was shown between the actual and estimated probability of CNM (Fig. 3B). The external validation population comprised of 186 patients (122 females) with a 53% overall rate of nodal metastases. The mean age was 41.8 years with a range of 19-72 years. When applied to the original model, the external validation data set produced a C-index of 0.825 (95% CI, 0.793 to 0.857) (Fig. 4).

5. Validation of the predictive effect of serum factors

In order to evaluate the effect of serum indicators (CEA and Cr) we included in this prediction model, we excluded two serum indicators and reproduced a contrast nomogram (Fig. 5A), with a C-index of 0.817 (Fig. 5B), proving that these two factors we included were significant and could improve our nomogram's ability to predict CNM.

6. Comparing two models in predicting CNM based upon a decision curve analysis

A DCA was performed to compare the predictive ability between our nomogram and the US model. The US model used the data from the preoperative ultrasonographic diagnosis of CNM in our patient cohort (n=1,252). The DCA showed that the prediction ability of our nomogram is superior to US in detecting CNM for PTC patients (Fig. 6).

7. Novel risk stratification according to the scores obtained by the nomogram

Every variable included in our nomogram had its corresponding risk point and total risk scores calculated for all patients to quantitatively predict their individual risk of CNM. To stratify patients according to their risk scores, four cut-off values were selected. Five subgroups were thus established: (1) extreme low-risk group (patients with a CNM score of ≤ 50, n=137), (2) low-risk group (50 < risk score ≤ 100, n=311), (3) moderate-risk group (100 < risk score ≤ 150, n=305), (4) high-risk group (150 < risk score ≤ 200, n=184), and (5) extreme high-risk group (patients with a CNM score of > 200, n=315).

The rates of CNM for extreme low, low, moderate, high, extreme high-risk groups were 8.8%, 17.7%, 41.3%, 77.2%, and 89.8%, respectively. Differences were significant between these subgroups ($p < 0.001$) (Table 2).

Discussion

Increasing incidence of thyroid cancer has been reported over recent years, and surgical resection is generally accepted to be the most effective treatment for PTC [11], yet the role of prophylactic CLND in PTC continues to be debated. Advocates point that prophylactic CLND in cN0 patient reduces local recurrence which contributes to less hazardous

Table 2. CNM risk stratification of PTC patients based on the model database

Nomogram		ELR	LR	MR	HR	HER	Total
		0-50	50-100	100-150	150-200	> 200	
No CNM	Value	125	256	179	42	32	634
	%	91.2	82.3	58.7	22.8	10.2	50.6
CNM	Value	12	55	126	142	283	618
	%	8.8	17.7	41.3	77.2	89.8	49.4
Total	Value	137	311	305	184	315	1,252
	%	100	100	100	100	100	100

CNM, central lymph node metastasis; PTC, papillary thyroid carcinoma; ELR, extreme low risk; LR, low risk; MR, moderated risk; HR, high risk; HER, extreme high risk.

reoperative surgery [6,12,13]. In our country, given the combination of higher CNM risks in Asian patients and unreliability of preoperative examinations in detecting CNM [14], most institutions prefer thyroidectomy with prophylactic CLND. In this study, the rate of patients who received prophylactic CLND was 96.1% (1,663/1,731).

Although there is increasing support for prophylactic CLND given its benefits for recurrence and survival, many clinicians worldwide still opt for therapeutic CLND only, due to potential risks of prophylactic CLND. These could include permanent hypoparathyroidism, recurrent laryngeal nerve injury, and other postoperative complications [15-17]. Furthermore, in the American Thyroid Association guidelines (2015), "less is more" seemed to be the theme running throughout the consensus, recommending less extensive surgeries, less radioactive iodine and less surveillance testing [9,18]. In addition, the importance of regional lymph nodes for cancer survival is stressed in immunotherapy [19], as preservation of normal lymph nodes in meaningful for follow-up treatments. Thus, accurately assessing risks of CNM may play an important role in surgical options, for it is the deciding factor in whether prophylactic CLND should be performed.

Our study aimed to develop a nomogram to predict the likelihood of CNM in PTC patients. A CNM rate of 49.4% was identified, which is in accordance with figures of 40-58% reported by other similar works [20,21]. Among these patients, 158 patients (25.6%) were observed to have LLNM, while 43 patients (3.4%) had skip metastasis (i.e., had LLNM without CNM) which is similar to the observation made by Thompson et al. [6,22]. Given the low prevalence of skip metastasis, most LLNM will be accompanied by CNM, and a routine CLND will be performed; thus, we question the significance of including LLNM as a risk factor for CNM suggested by Wang et al. [23]. However, their results match our finding where there is a significant association between CNM and LLNM, and we will report this clinical research in our following work.

Referencing similar works on predicting CNM, our research confirms their results and takes it a step further. The nomogram developed by Thompson et al. [6] was based on 914 patients and had good discrimination with a C-index of 0.764, while only four variables were considered. The nomograms established by Wang et al. [23] and Kim et al. [24] enrolled larger patient cohorts, yet their discrimination presented a C-index of 0.711 to 0.721, which was weaker than this study. In addition, the equal split of the variables (age and tumor size) in Kim et al.'s work [24] is also quite puzzling given the nonlinear relationship between the variable and CNM according to Thompson's article [6], which raised further questions about the representative of their nomogram for the general population.

There were a few references on the association between BMI and CNM [25,26], yet our results were quite different to previous findings. Wu et al. [25] found that increased BMI was associated with lymph node metastasis by analyzing a cohort of 796 PTC patients, while we observed that BMI less than 22 kg/m^2 was the risk factor for CNM of PTC patients. This difference may be caused by disparate ways of BMI grouping or and the diagnose distinction of lymph node metastasis. However, we believe our nomogram showed a better predictive accuracy (AUC, 0.854) based on greater amount of samples of 1,252 PTC patients.

In this study, we took TCI diagnosed by preoperative US as variable instead of pathological TCI due to the lack of pathologically uniform standard (whether TCI or extrathyroidal extension [ETE]) in our institutions. This stems from a lack of definite definition for TCI or ETE in thyroid pathology [27]. Preoperative US TCI was identified in 39.5% cases, while other studies reported that pathological TCI was present in around 30%-53% cases [6,28,29]. Interestingly, we observed TCI to be the most sensitive characteristic in our nomogram. Several works have proven the connections between TCI or ETE and CNM [23,24] and Thompson et al. [6] found wider spread ETE had a higher likelihood of lymph node metastasis compared to mere capsular invasion.

Multifocality and large tumor size have frequently been shown to promote CNM of PTC patients [2,6,12,20,23,24]. In our research, we obtained similar findings to previous studies, shown in our nomogram (Fig. 2), in which multifocality and tumor size larger than 1 cm both played an important role.

Preoperative serum index is available in most institutions, yet their association with CNM of PTC patients seems to be overlooked. We gathered all the pre-operation clinical serum index including blood routine examination, serum hepatorenal function, serum electrolyte, serum thyroid function, parathyroid hormone and CEA. Interestingly, we found serum Cr and CEA did contribute to our nomogram, suggesting PTC patients with Cr over 70 μmol/L or CEA over 1 ng/mL might suffer a higher risk of CNM.

Above all, this nomogram made it possible to score the likelihood of CNM in PTC patients before operation, which showed a significant advantage over preoperative US (Fig. 6). By gathering readily available clinical characteristics, we divided PTC patients into five quantified risk stratification in our nomogram (Table 2) so that it is easier to use clinically. Using this risk stratification table, clinicians may be better informed in their assessment of the risk factors.

There are several limitations of this study which we hope to address in our following research. Although we gathered patient cohort from two institutions, our sample was not as large as the two recent researches [23,24]. In addition, only 523 patients' *BRAF* mutation reports were available and fewer patients received a postoperative immunohistochemical examinations. Future predictive models may incorporate

microRNA and PTC subtypes, as well as immunohistochemical biopsy and genotype of FNA samples, which are not available at present. Furthermore, we were able to incorporate several new variables that are significant for prediction of CNM. This implies that there may be potential variables waiting to be discovered that could make the nomogram more complete.

Using available pre-operative variables, we were able to construct a nomogram that stratify PTC patients into five groups that possess different CNM risk levels. This provides guidance for whether a patient should receive CLND on a case by case basis, and promotes balanced approach between avoiding CLND complications and maximizing survival/lowering recurrence rates.

Conflicts of Interest

Conflicts of interest relevant to this article was not reported.

Acknowledgments

This research was supported by the Shanghai Municipal Science and Technology Commission(19441905400); Shanghai Jiaotong University(YG2019ZDA15).

References

1. Maino F, Forleo R, Pacini F. Prognostic indicators for papillary thyroid carcinoma. Expert Rev Endocrinol Metab. 2017;12:101-8.
2. Al Afif A, Williams BA, Rigby MH, Bullock MJ, Taylor SM, Trites J, et al. Multifocal papillary thyroid cancer increases the risk of central lymph node metastasis. Thyroid. 2015;25:1008-12.
3. Bernet V. Approach to the patient with incidental papillary microcarcinoma. J Clin Endocrinol Metab. 2010;95:3586-92.
4. Stulak JM, Grant CS, Farley DR, Thompson GB, van Heerden JA, Hay ID, et al. Value of preoperative ultrasonography in the surgical management of initial and reoperative papillary thyroid cancer. Arch Surg. 2006;141:489-94.
5. Kim SK, Woo JW, Lee JH, Park I, Choe JH, Kim JH, et al. Prophylactic central neck dissection might not be necessary in papillary thyroid carcinoma: analysis of 11,569 cases from a single institution. J Am Coll Surg. 2016;222:853-64.
6. Thompson AM, Turner RM, Hayen A, Aniss A, Jalaty S, Learoyd DL, et al. A preoperative nomogram for the prediction of ipsilateral central compartment lymph node metastases in papillary thyroid cancer. Thyroid. 2014;24:675-82.
7. Egelmeer AG, Velazquez ER, de Jong JM, Oberije C, Geussens Y, Nuyts S, et al. Development and validation of a nomogram for prediction of survival and local control in laryngeal carcinoma patients treated with radiotherapy alone: a cohort study based on 994 patients. Radiother Oncol. 2011;100:108-15.
8. Wan G, Gao F, Chen J, Li Y, Geng M, Sun L, et al. Nomogram prediction of individual prognosis of patients with hepatocellular carcinoma. BMC Cancer. 2017;17:91.
9. Tuttle RM, Haugen B, Perrier ND. Updated American Joint Committee on Cancer/tumor-node-metastasis staging system for differentiated and anaplastic thyroid cancer (eighth edition): what changed and why? Thyroid. 2017;27:751-6.
10. Mo S, Dai W, Xiang W, Li Q, Wang R, Cai G. Predictive factors of synchronous colorectal peritoneal metastases: Development of a nomogram and study of its utilities using decision curve analysis. Int J Surg. 2018;54(Pt A):149-55.
11. Pellegriti G, Frasca F, Regalbuto C, Squatrito S, Vigneri R. Worldwide increasing incidence of thyroid cancer: update on epidemiology and risk factors. J Cancer Epidemiol. 2013;2013:965212.
12. Perrino M, Vannucchi G, Vicentini L, Cantoni G, Dazzi D, Colombo C, et al. Outcome predictors and impact of central node dissection and radiometabolic treatments in papillary thyroid cancers < or =2 cm. Endocr Relat Cancer. 2009;16:201-10.
13. Popadich A, Levin O, Lee JC, Smooke-Praw S, Ro K, Fazel M, et al. A multicenter cohort study of total thyroidectomy and routine central lymph node dissection for cN0 papillary thyroid cancer. Surgery. 2011;150:1048-57.
14. Goropoulos A, Karamoshos K, Christodoulou A, Ntitsias T, Paulou K, Samaras A, et al. Value of the cervical compartments in the surgical treatment of papillary thyroid carcinoma. World J Surg. 2004;28:1275-81.
15. Lee YS, Kim SW, Kim SW, Kim SK, Kang HS, Lee ES, et al. Extent of routine central lymph node dissection with small papillary thyroid carcinoma. World J Surg. 2007;31:1954-9.
16. Moo TA, McGill J, Allendorf J, Lee J, Fahey T 3rd, Zarnegar R. Impact of prophylactic central neck lymph node dissection on early recurrence in papillary thyroid carcinoma. World J Surg. 2010;34:1187-91.
17. Sancho JJ, Lennard TW, Paunovic I, Triponez F, Sitges-Serra A. Prophylactic central neck disection in papillary thyroid cancer: a consensus report of the European Society of Endocrine Surgeons (ESES). Langenbecks Arch Surg. 2014;399:155-63.
18. Kim BW, Yousman W, Wong WX, Cheng C, McAninch EA. Less is more: comparing the 2015 and 2009 American Thyroid Association guidelines for thyroid nodules and cancer. Thyroid. 2016;26:759-64.
19. Thomas SN, Rohner NA, Edwards EE. Implications of lymphatic transport to lymph nodes in immunity and immunotherapy. Annu Rev Biomed Eng. 2016;18:207-33.
20. Lee YS, Lim YS, Woo CG, Lee JC, Wang SG, Lee KD, et al. PP049: growth pattern of micropapillary thyroid cancer without extrathyroidal extension predicts central lymph node metastasis. Oral Oncol. 2013;49(Suppl 1):S110.
21. Usluogullari CA, Onal ED, Ozdemir E, Ucler R, Kiyak G, Ersoy PE, et al. A retrospective analysis of prognostic factors predictive of lymph-node metastasis and recurrence in thyroid papillary microcarcinoma. Minerva Endocrinol. 2015;40:15-22.
22. Grebe SK, Hay ID. Thyroid cancer nodal metastases: biologic significance and therapeutic considerations. Surg Oncol Clin N Am. 1996;5:43-63.

23. Wang Y, Guan Q, Xiang J. Nomogram for predicting central lymph node metastasis in papillary thyroid microcarcinoma: a retrospective cohort study of 8668 patients. Int J Surg. 2018;55:98-102.
24. Kim SK, Chai YJ, Park I, Woo JW, Lee JH, Lee KE, et al. Nomogram for predicting central node metastasis in papillary thyroid carcinoma. J Surg Oncol. 2017;115:266-72.
25. Wu C, Wang L, Chen W, Zou S, Yang A. Associations between body mass index and lymph node metastases of patients with papillary thyroid cancer: a retrospective study. Medicine (Baltimore). 2017;96:e6202.
26. Dieringer P, Klass EM, Caine B, Smith-Gagen J. Associations between body mass and papillary thyroid cancer stage and tumor size: a population-based study. J Cancer Res Clin Oncol. 2015;141:93-8.
27. Mete O, Rotstein L, Asa SL. Controversies in thyroid pathology: thyroid capsule invasion and extrathyroidal extension. Ann Surg Oncol. 2010;17:386-91.
28. Kim ES, Lim DJ, Lee K, Jung CK, Bae JS, Jung SL, et al. Absence of galectin-3 immunostaining in fine-needle aspiration cytology specimens from papillary thyroid carcinoma is associated with favorable pathological indices. Thyroid. 2012;22:1244-50.
29. Furlan JC, Bedard YC, Rosen IB. Significance of tumor capsular invasion in well-differentiated thyroid carcinomas. Am Surg. 2007;73:484-91.

pISSN 1598-2998, eISSN 2005-9256

Cancer Res Treat. 2020;52(4):1019-1030 https://doi.org/10.4143/crt.2020.012

Original Article Open Access

Protective Effects of N-Acetylcysteine against Radiation-Induced Oral Mucositis *In Vitro* and *In Vivo*

Haeng Jun Kim, MS[1]
Sung Un Kang, PhD[2]
Yun Sang Lee, PhD[2]
Jeon Yeob Jang, MD, PhD[2]
Hami Kang[3]
Chul-Ho Kim, MD, PhD[2]

[1]*Department of Molecular Science and Technology, Ajou University, Suwon,* [2]*Department of Otolaryngology, Ajou University School of Medicine, Suwon, Korea,* [3]*Program of Public Health Studies, Johns Hopkins University, Baltimore, MD, USA*

Correspondence: Chul-Ho Kim, MD, PhD
Department of Otolaryngology,
Ajou University School of Medicine,
206 World cup-ro, Yeongtong-gu,
Suwon 16499, Korea
Tel: 82-31-219-5269
Fax: 82-31-219-5264
E-mail: ostium@ajou.ac.kr

Received January 6, 2020
Accepted June 18, 2020
Published Online June 18, 2020

*Haeng Jun Kim and Sung Un Kang contributed equally to this work.

Purpose

Radiation-induced oral mucositis limits delivery of high-dose radiation to targeted cancers. Therefore, it is necessary to develop a treatment strategy to alleviate radiation-induced oral mucositis during radiation therapy. We previously reported that inhibiting reactive oxygen species (ROS) generation suppresses autophagy. Irradiation induces autophagy, suggesting that antioxidant treatment may be used to inhibit radiation-induced oral mucositis.

Materials and Methods

We determined whether treatment with N-acetyl cysteine (NAC) could attenuate radiation-induced buccal mucosa damage *in vitro* and *in vivo*. The protective effects of NAC against oral mucositis were confirmed by transmission electron microscopy and immunocytochemistry. mRNA and protein levels of DNA damage and autophagy-related genes were measured by quantitative real-time polymerase chain reaction and western blot analysis, respectively.

Results

Rats manifesting radiation-induced oral mucositis showed decreased oral intake, loss of body weight, and low survival rate. NAC intake slightly increased oral intake, body weight, and the survival rate without statistical significance. However, histopathologic characteristics were markedly restored in NAC-treated irradiated rats. LC3B staining of rat buccal mucosa revealed that NAC treatment significantly decreased the number of radiation-induced autophagic cells. Further, NAC inhibited radiation-induced ROS generation and autophagy signaling. *In vitro*, NAC treatment significantly reduced the expression of NRF2, LC3B, p62, and Beclin-1 in keratinocytes compared with that after radiation treatment.

Conclusion

NAC treatment significantly inhibited radiation-induced autophagy in keratinocytes and rat buccal mucosa and may be a potentially safe and effective option for the prevention of radiation-induced buccal mucosa damage.

Key words

Radiation, Oral mucositis, N-acetylcysteine (NAC), Autophagy, Nuclear factor erythroid 2-related factor 2 (NRF2)

Introduction

Radiotherapy is a commonly used cancer treatment that entails lethal doses of radiation against cancer cells [1]. However, exposure of normal tissue to radiation can cause both acute and chronic toxicity, including dermatitis, oral mucositis, altered taste, pain, dry mouth, decreased appetite, and even ulceration [2].

Oral mucositis is one of the most common complications of cancer therapy, chemotherapy, and radiation therapy. In patients with granulocytopenia, it often leads to systemic infections and nutritional deficiencies due to the intake of a restricted diet [3].

Despite technological advances, a successful method for the prevention of radiation-induced oral mucositis and normal cell toxicity has yet to be developed [4]. Although many recent studies have shown the potential of radiation in protection against chemicals and small molecules, most of them have yet to reach the preclinical stage due to their toxicity and side effects, and the unknown mechanisms involved in radia-

tion protection. Radiation-induced oral mucositis is caused by a variety of mechanisms, including but not limited to the release of free radicals, modified proteins, and proinflammatory cytokines, including interleukin-1β, prostaglandins, and tumor necrosis factor by irradiated epithelial, endothelial, and connective tissue cells in the buccal mucosa [5].

Previous studies have reported an increase in intracellular reactive oxygen species (ROS) levels during radiation-induced oral mucositis. Scavengers such as vitamin E, amifostine, and N-acetylcysteine (NAC) are known to inhibit oral mucositis, indicating a role for ROS in radiation-induced oral mucositis [6].

Although the radioprotective effects of scavengers are unknown, ROS scavenger supplements are seen to partially protect against sublethal damage induced by ionizing radiations. Therefore, we elucidated the relationship between autophagy and the antioxidant signal transduction mechanism.

NAC is a free radical scavenging antioxidant [7]. Several studies have reported on its efficacy in reducing inflammation of the mucous membranes, improving the elimination and excretion of sputum in inflammatory diseases of the respiratory system, and inhibiting the secretion of cytokines [8].

Nuclear factor erythroid 2-related factor 2 (NRF2), an antioxidant, is regulated by upstream signal transduction factors such as mitogen-activated protein kinases, extracellular signal-regulated kinase, c-Jun N-terminal kinase, and phosphatidylinositol 3-kinase [9]. Under oxidative stress, NRF2 is not degraded and translocates to the nucleus where it binds to the promoter regions of antioxidant genes, such as glutathione transferases, UDP-glucuronosyltransferases, γ-glutamylcysteine synthetase, glutathione peroxidase, heme oxygenase-1, catalase, and NAD(P)H:quinone oxidoreductase-1, to upregulate their transcription [10].

The mechanism for the radioprotective effect of NRF2 is unknown. However, it is known to depend on radiation-induced ROS generation that leads to cell and DNA damage. Interestingly, recent reports have shown that the NRF2 pathway correlates with autophagic signaling and contributes to antioxidant-mediated protection of the cells by eliminating oxidatively damaged organelles and proteins [11].

In this study, we investigated the protective effect of NAC against radiation-induced oral mucositis in animal studies and keratinocytes. The associated signaling mechanisms, specifically those involving the autophagic signaling pathway, were also studied.

Materials and Methods

1. Animal study

Six-week-old female Sprague-Dawley rats were purchased from Orient Bio Co. Ltd. (Seongnam, Korea).

The animals were randomly assigned to either an irradiation group (n=20) or a non-irradiation group (n=20) for 3 weeks. Each group was divided into two groups. One group was treated with NAC (Mucomyst, Boryung Pharm, Ansan, Korea) (n=10), and the other group was treated with saline (n=10).

A single 30 Gy dose was delivered by opposing photon beams at a rate of 2 Gy/min bilaterally at a distance of 100 cm from the source to the axis using the 6 MV LINAC (21EX, Varian Medical Systems, Palo Alto, CA). Radiation dose and evaluation were previously described [12].

Rats were treated with NAC (Mucomyst, Boryung Pharm) from the day after irradiation. Rats were placed in an acryl box (30×20×20 cm), and a nebulizer was used to administer NAC (air flow, 10.01 L/min) for 5 minutes and stabilized for 5 minutes. The control groups were administered saline. Treatment was conducted twice every day for 3 weeks (9 am and 6 pm).

2. Cell culture and radiation conditions

The human immortalized keratinocytes, HaCaT cells, were obtained from the American Type Culture Collection (ATCC, Manassas, VA). HaCaT cells were maintained in high glucose Dulbecco's modified Eagle's medium (Gibco, Grand Island, NY), supplemented with 10% fetal bovine serum and 100 U/mL penicillin-streptomycin (Gibco, Paisley, PA) at 37°C with 5% CO_2 under humidified conditions.

Cells were pre-treated with 10 mM of NAC for a 1 hour before radiation and were irradiated for 10 minutes with 6 MV LINAC (21EX, Varian Medical Systems) at a fixed dose rate of 2 Gy/min. A radiation of 20 Gy was selected to induce DNA damage [12,13].

3. Terminal deoxynucleotidyl transferase dUTP nick end labeling assay

Apoptotic cells in the buccal mucosa were assessed by DNA fragmentation within cells using the *In Situ* Cell Death Detection Kit, POD (Roche Molecular Biochemicals, Indianapolis, IN), according to the manufacturer's protocol. Nuclei were counterstained with Hoechst 33342.

4. Cell cycle analysis and measurement of ROS production

HaCaT cells were harvested by trypsinization and washed with phosphate buffered saline (PBS). Cold 70% ethanol was slowly added to the cells while vortexing, and were fixed overnight at –20°C. The cells were washed with PBS twice, centrifuged at 1,300 rpm for 3 minutes, and resuspended in 200 μL PBS. Subsequently, they were incubated with 300 μg/mL RNase (Intron Biotechnology, Seongnam, Korea) for 30 minutes at 37°C, and 500 μL propidium iodide (10 μg/mL, Invitrogen, Carlsbad, CA) for another 30 minutes at 4°C in a dark room. Cell cycle distribution was calculated in 10,000 cells using a BD FACS Aria III instrument (BD Biosciences, Bedford, MA).

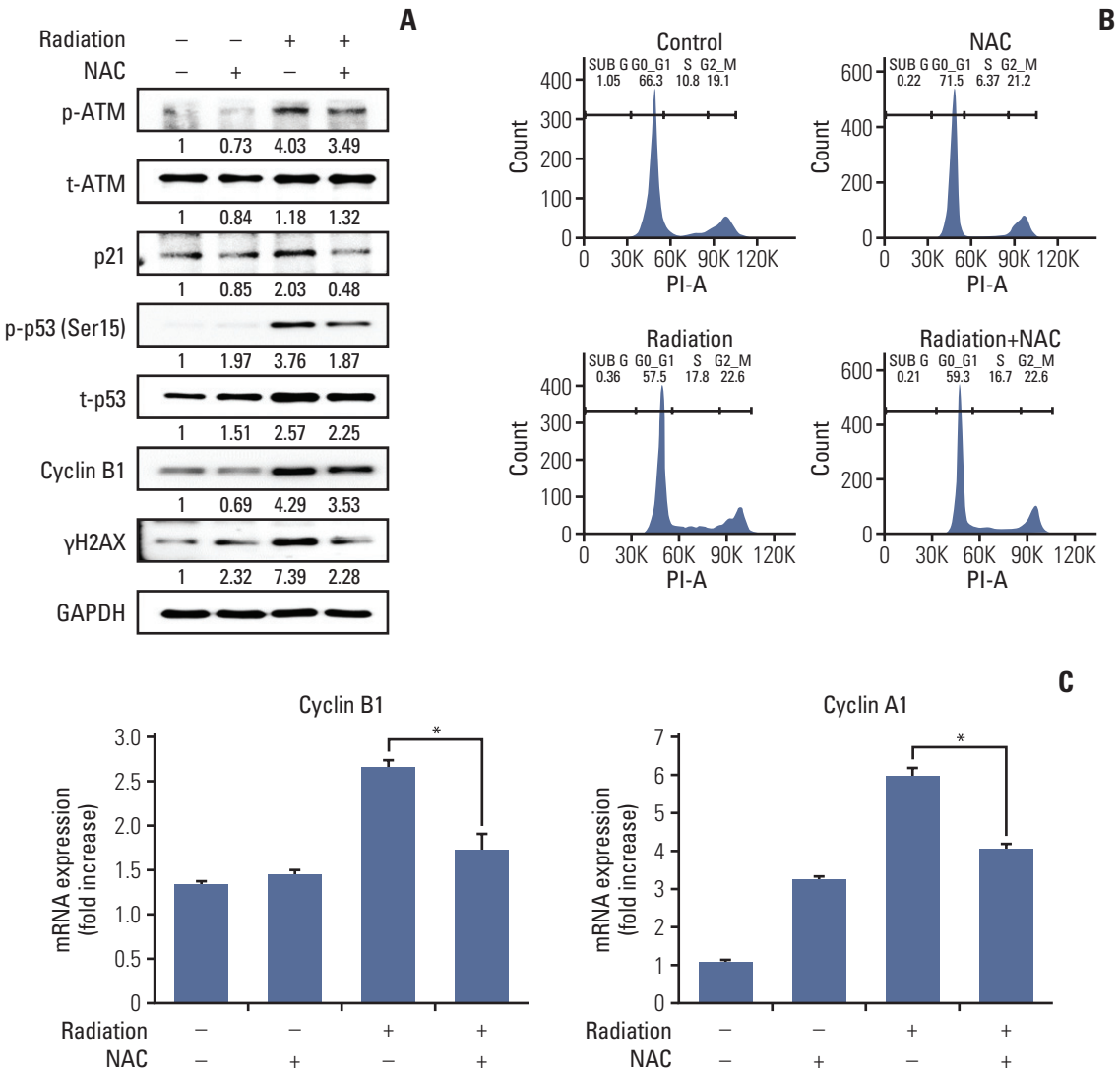

Fig. 1. Effect of N-acetylcysteine (NAC) on DNA damage in the HaCaT cells after radiation treatment. (A) Western blot analysis of signals mediating cell cycle checkpoint and DNA damage. Cell lysates were collected 24 hours after irradiation and NAC treatment, followed by gel electrophoresis, and the levels of p-ATM (Ser1981), total ATM (t-ATM), p21, p-p53 (Ser15), total p53 (t-p53) cyclin B1, γH2AX, and alpha-tubulin were measured. A representative of three experiments is shown in triplicate. (B) Cell cycle analysis by flow cytometry. The distribution of each HaCaT cell line in various stages of the cell cycle was analyzed by propidium iodide staining after radiation and NAC treatment. (C) Cyclin A/cyclin B1 mRNA level was measured using real-time polymerase chain reaction. Asterisks indicate statistically significant differences. *$p < 0.05$. *(Continued to the next page)*

The cellular ROS production was measured by treating HaCaT cells with 10 μM hydroethidine (Molecular Probes, Eugene, OR) for 30 minutes at 37°C. Fluorescence-stained cells were then analyzed with BD FACS Aria III (BD Biosciences).

5. Western blot analysis

Cells were lysed in RIPA buffer (Sigma-Aldrich, St. Louis, MO) containing 50 mM Tris (pH 8.0), complete EDTA-free protease inhibitor, and PhoSTOP (Roche Molecular Biochemicals, Basel, Switzerland), as described previously. The cell lysates were mixed with 5× sodium dodecyl sulfate sample buffer and run on a 10%-12% sodium dodecyl sulfate polyacrylamide gel electrophoresis gel, followed by electrophoretic transfer to PVDF membrane. Targeted proteins were immunoblotted with specific antibodies. The following primary antibodies were used: p21, p27, phospho-p53 (Ser15), p53, cyclin B1, γH2AX, mammalian target of rapamycin (mTOR), phospho-mTOR, ATG3, ATG5, P62, LC3B, and glyceraldehyde 3-phosphate dehydrogenase (1:1,000, Cell Signaling Technology, Danvers, MA). Secondary antibodies (1:4,000, anti-rabbit IgG or anti-mouse IgG) were purchased

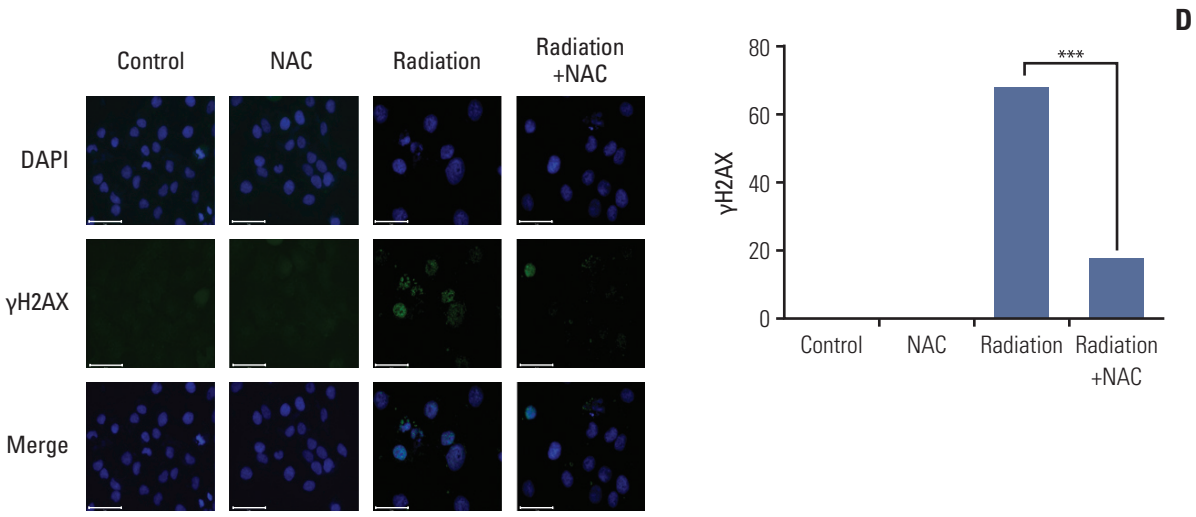

Fig. 1. *(Continued from the previous page)* (D) Immunofluorescence of γH2AX (green spot). Cells were exposed to a single dose of radiation (20 Gy), NAC (10 mM) or radiation+NAC. After 24-hour incubation, immunocytochemistry was performed with an antibody targeting γH2AX, indicative of the cellular response to DNA damage. This experiment was independently repeated at least three times. Scale bars=75 μm. ***$p < 0.001$.

from Cell Signaling Technology.

6. Cell proliferation assay (BrdU assay)

Cell proliferation was measured using a BrdU assay kit (Roche Diagnostics, Penzberg, Germany), according to the manufacturer's protocol (BD Biosciences) as described previously [12]. Absorbance was measured at a wavelength of 370 nm using an enzyme-linked immunosorbent assay reader (Bio-Tek, Winooski, VT). The rate of cell proliferation was expressed as a percentage of untreated cells.

7. Transmission electron microscopy

The cells were fixed in 2% glutaraldehyde after treatment with vehicle or NAC (10 mM, Sigma-Aldrich) only, radiation alone (20 Gy), or radiation (20 Gy) plus NAC (10 mM), as previously described [14]. All thin sections were observed with an electron microscope (JEM-1011, Jeol, Tokyo, Japan) at an acceleration voltage of 80 kV, and the images were analyzed with the Camera-Megaview III Soft imaging system.

8. Quantitative real-time polymerase chain reaction

Total RNAs from HaCaT cells treated with vehicle or NAC (10 mM, Sigma-Aldrich) only, radiation only (20 Gy), or radiation (20 Gy) plus NAC were isolated using TRIzol reagent (Gibco-BRL, Grand Island, NY). The cDNA synthesis was performed as described previously [15]. We quantified the targeted gene expression via one-step real-time PCR using Step One Plus TM (Applied Biosystems, Foster City, CA). All primers were purchased from Qiagen (Hilden, Germany) and resuspended in 100 μM stock solutions in TE buffer (pH 8.0, Teknova, Hollister, CA).

9. Immunohistochemistry

Immunohistochemistry was performed using paraffin-embedded tissue sections collected on poly L-lysine–coated slides. The specimens were briefly incubated in a blocking solution with anti-LC3B (1:200), NRF2 (1:200) antibody overnight at 4°C. The sections were thoroughly rinsed in PBS and incubated for 2 hours at room temperature with SPlink HRP Detection Kit (GBI Labs, Mukilteo, WA). Immunolabeling was performed after three washes in PBS and stained with Liquid DAB+ Substrate Kit (GBI Labs).

10. Immunocytochemistry

HaCaT cells were cultured on microscope coverslips (Thermo Fisher Scientific, Rochester, NY) and treated with vehicle or NAC (10 mM, Sigma-Aldrich) only, radiation only (20 Gy), or radiation (20 Gy) plus NAC. After 24 hours, the slides were washed with PBS, fixed for 20 minutes in 3.7% formaldehyde, and rehydrated in PBS. Immunocytochemistry assays were performed as described previously [16]. The slides were washed and mounted with Vectashield (Vector Laboratories, Inc., Burlingame, CA). Cells were imaged using a fluorescence microscope (EVOS, Seattle, WA) [17].

11. Isolation of nuclear and cellular extracts

Nuclear and cellular extracts were isolated from cells treated with vehicle or NAC (10 mM, Sigma-Aldrich) only, radiation only (20 Gy), or radiation (20 Gy) plus NAC (10 mM) for 24 hours using the NE-PER Nuclear and Cytoplasmic Extraction Reagent kit (Pierce Biotechnology, Rockford, IL), following the manufacturer's protocol.

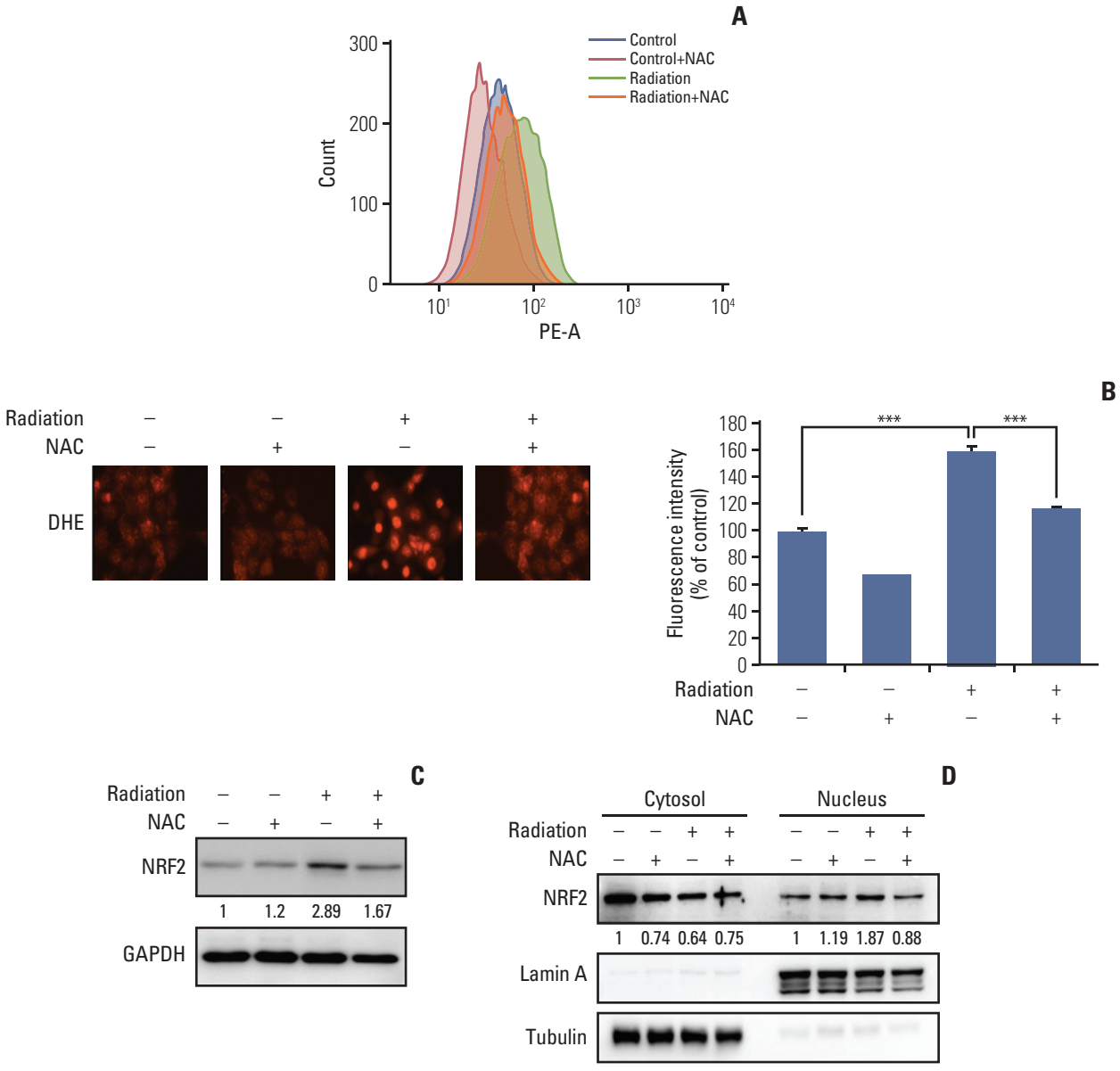

Fig. 2. Effect of N-acetyl cysteine (NAC) on radiation-induced intracellular reactive oxygen species (ROS) generation in HaCaT cells. (A) Intracellular ROS generation was measured in HaCaT cells treated with 20 Gy of radiation in the presence or absence of NAC (10 mM). The level of intracellular ROS was measured by flow cytometry using the peroxide-sensitive fluorescent probe, dihydroethidium (DHE). (B) Intracellular ROS generation was evaluated by DHE fluorescence staining for 30 minutes at 37°C. Values are presented as the mean±SD of three experiments in triplicate and was calculated as a percentage of the control. ***$p < 0.001$. (C) NAC downregulates radiation-induced nuclear factor erythroid 2-related factor 2 (NRF2) protein expression. Western blots were performed using NRF2 and glyceraldehyde 3-phosphate dehydrogenase (GAPDH) antibodies. (D) Protein levels of NRF2 in fractionated nuclear or cytosolic lysates treated with 20 Gy of radiation in the presence or absence of NAC (10 mM) were determined by western blot analysis. *(Continued to the next page)*

12. Statistical analysis

Data from at least three independent experiments were expressed as mean±SD. Comparisons of the means of different groups were performed using one-way analysis of variance (ANOVA). We conducted one-way ANOVA based on the Mann-Whitney U test using SPSS ver. 20.0 statistical software (IBM Corp., Armonk, NY). p-values < 0.05 were considered statistically significant.

13. Ethical statement

This study was approved by the Committee for Ethics in Animal Experiments, Ajou University School of Medicine (IACUC number: 2016-0031).

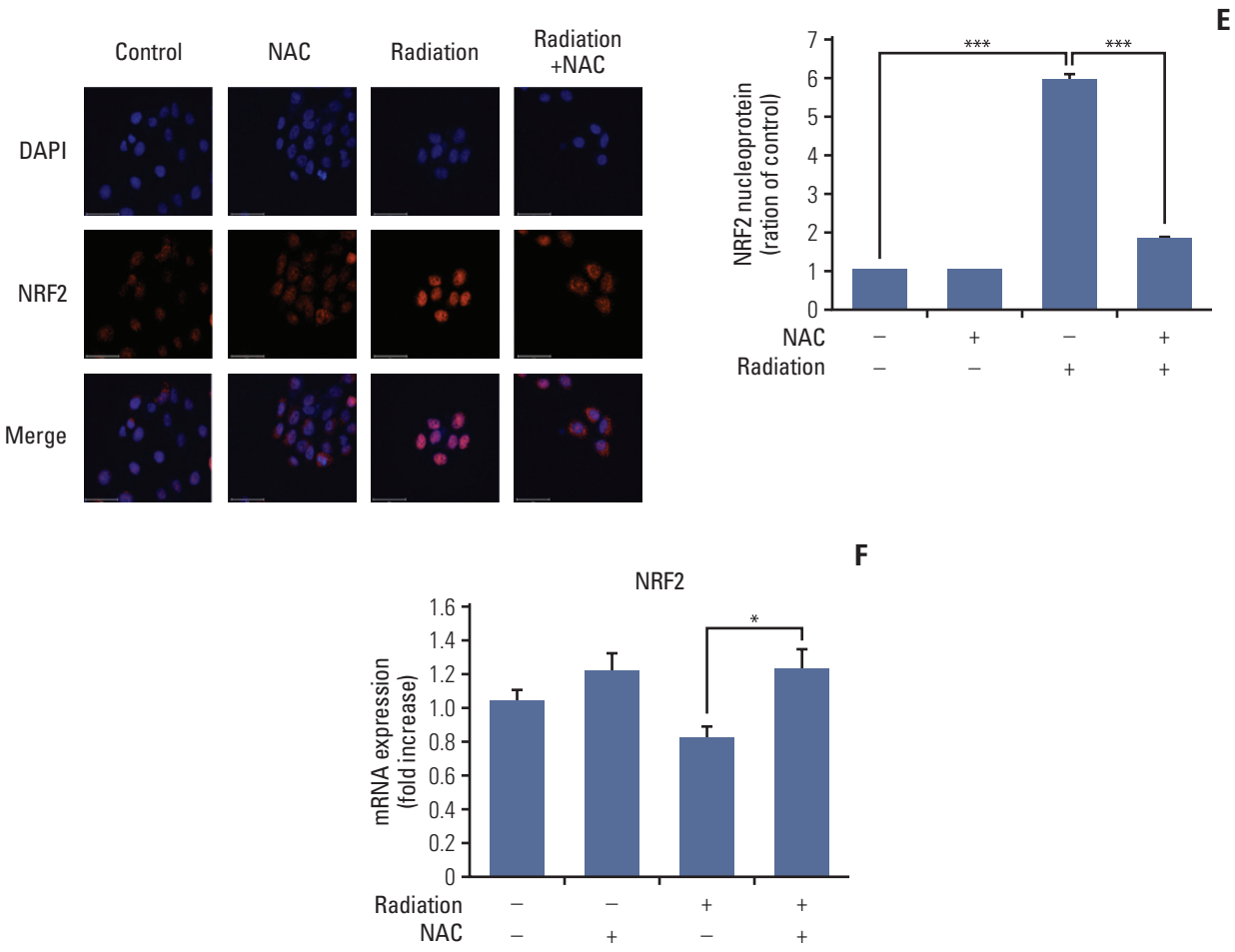

Fig. 2. *(Continued from the previous page)* (E) NRF2 protein levels were detected by immunocytochemistry. Cells were exposed to a single dose of radiation (20 Gy), NAC (10 mM) or radiation+NAC. After 24-hour incubation, immunocytochemistry was performed with an NRF2 antibody. (F) NRF2 mRNA level was measured using real-time polymerase chain reaction. Asterisks indicate statistically significant differences. *$p < 0.05$.

Results

1. Pre-treatment with NAC protects irradiated HaCaT cells against DNA damage

Radiation induces HaCaT cell death by inducing DNA damage [18]. Therefore, DNA damage markers were measured, and cell cycle analysis was performed to determine whether 10 mM NAC pre-treatment could prevent DNA damage.

We analyzed protein-related DNA damage for p-ATM, ATM, p21, p53, cyclin B1, and γH2AX to determine whether NAC could block the ATM pathway and DNA damage mediating the cell cycle arrest observed. Increased protein levels or phosphorylation of p-ATM, p-p53 (Ser15), p21, cyclin B1, and γH2AX after irradiation and treatment with NAC reduced the phosphorylation of p-ATM, p-p53 (Ser15), and the protein levels of p21, cyclin B1, and γH2AX, which were increased by radiation treatment (Fig. 1A).

Interestingly, the length of the S phase of the cell cycle increased during radiation treatment and decreased after NAC treatment (Fig. 1B).

As shown in Fig. 1C, the mRNA levels of cyclin A and B were significantly lower in the NAC-treated group than in the radiation only group. These results were consistent with those of the western blot analysis.

In addition, to analyze DNA damage related to cell cycle arrest, we evaluated the expression of γH2AX, which plays an essential role in the cellular DNA damage response. NAC significantly inhibited the expression of γH2AX induced by irradiation (Fig. 1D). These results suggested that the protective mechanism of action of NAC and decreased DNA damage correlate with reduced phosphorylation of ATM and p53.

2. NAC inhibits radiation-induced intracellular ROS production via regulation of NRF2 expression in HaCaT cells

Radiation has been shown to increase ROS-induced oxida-

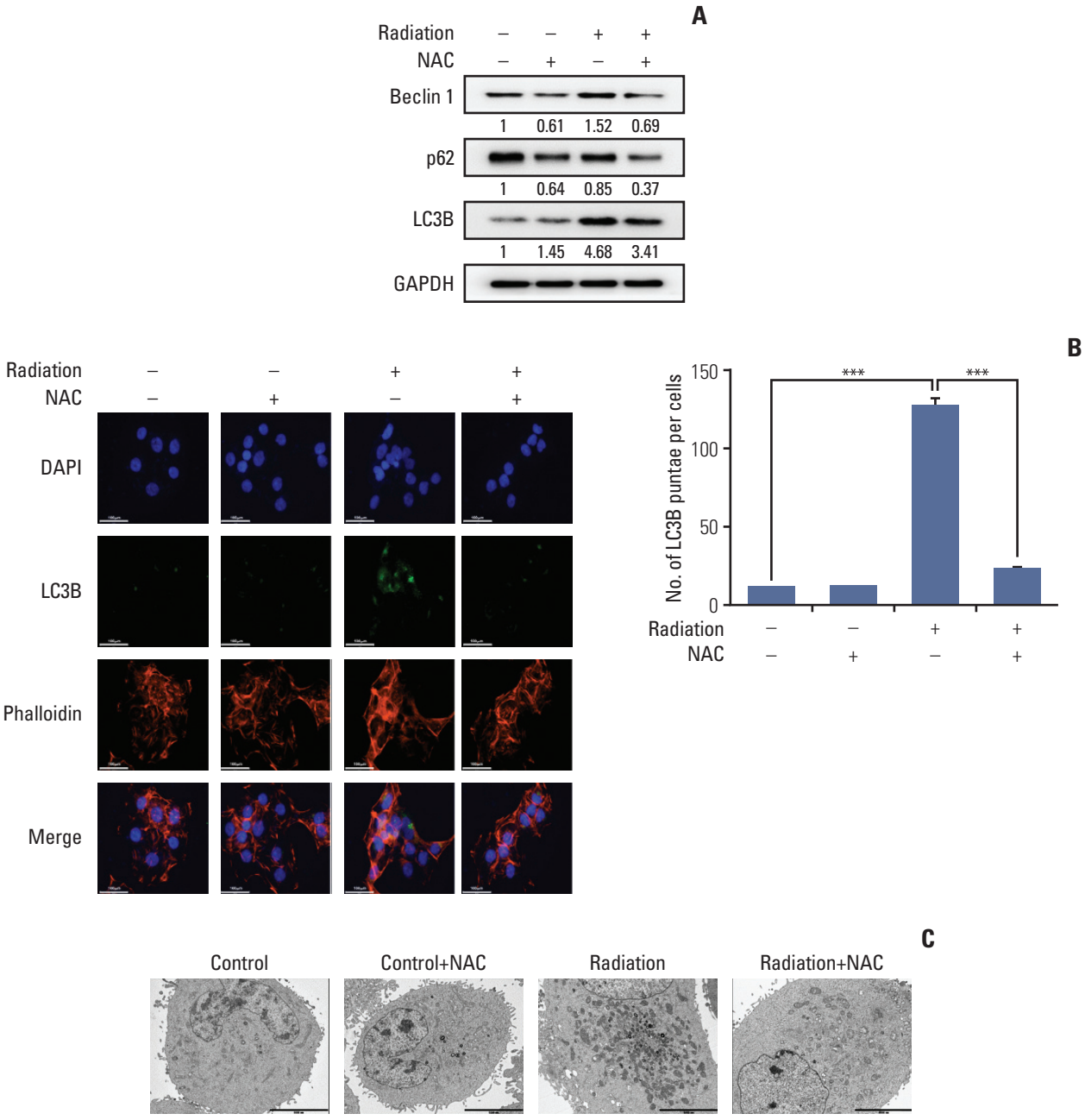

Fig. 3. Protective effect of N-acetyl cysteine (NAC) against radiation-induced autophagy in the HaCaT cells. (A) Western blot analysis with antibodies against Beclin-1, p62, and LC3B. (B) Immunocytochemistry staining of LC3B (green), F-actin (red), and nucleus (blue) in cells exposed to a single dose of radiation (20 Gy), NAC (10 mM) or radiation+NAC for 24 hours. LC3B puncta-positive cells were counted in five random fields (n=3). Scale bars=100 μm. Values are presented as mean±standard deviation (SD). ***$p < 0.001$. (C) Transmission electron microscopy analysis of morphological changes in autophagic vesicles in HaCaT cells. Scale bars=5,000 nm. *(Continued to the next page)*

tive stress in cells [19]. Therefore, we investigated ROS levels after irradiation to identify the mechanism by which NAC inhibits ROS production. First, the generation of ROS was quantified using dihydroethidium (DHE). As shown in Fig. 2A, the significant increase in ROS generation induced by irradiation was inhibited significantly by NAC. To confirm these results, we used DHE fluorescence staining. As shown in Fig. 2B, the radiation-induced increase in fluorescence intensity was inhibited significantly by NAC.

To elucidate the mechanism underlying the activity of radiation and NAC, we evaluated the effects of radiation and NAC-induced changes on gene expression. Radiation has been reported to increase NRF2 expression in human lymphocytes. Given the role of NRF2-Keap1 signaling in stress res-

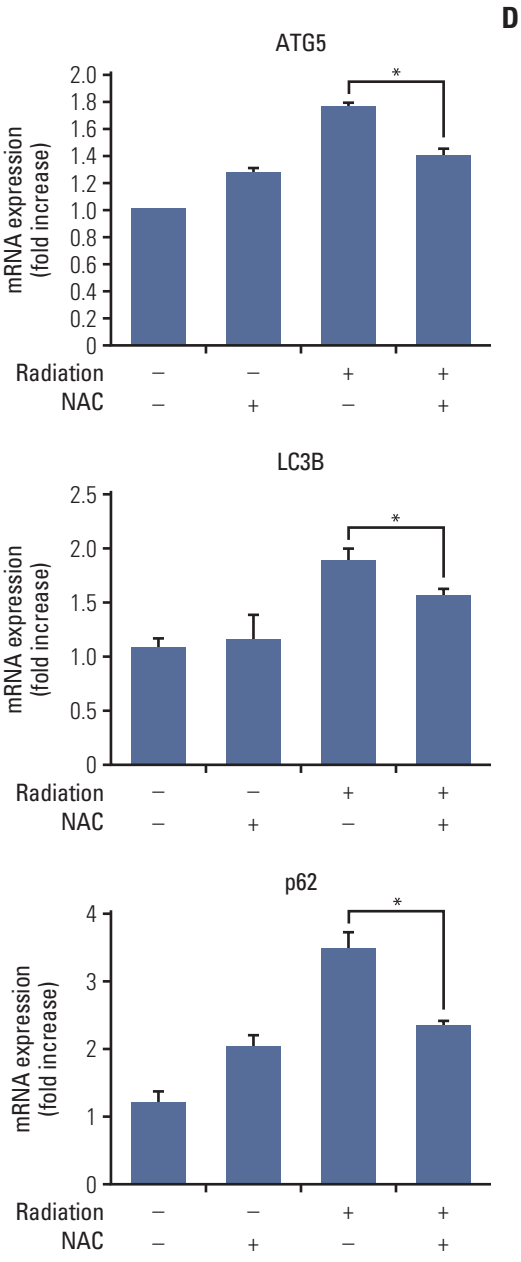

Fig. 3. *(Continued from the previous page)* (D) Quantitative real-time polymerase chain reaction was used to quantify the effect of NAC on radiation-induced autophagy-related genes, ATG5, LC3B, and p62. Results are presented as mean±SD of three independent experiments. *$p < 0.05$.

ponse, the NRF2 signaling mechanism protects cells by activating antioxidant-related genes [20].

To identify the relationship between radiation-induced ROS and NRF2 expression, HaCaT cells were irradiated, and the protein levels of NRF2 were measured by western blotting. A representative western blot is shown in Fig. 2C. The results confirmed the increased expression of NRF2 after radiation treatment and showed that NAC treatment reduced the expression of NRF2.

As shown in Fig. 2D, NAC treatment attenuated the protein level of NRF2 increased by radiation treatment in both the nuclear and cytoplasmic fractions.

To confirm our findings regarding NRF2 expression, the nuclear translocation of each molecule was analyzed using immunocytochemistry. These results were consistent with those of western blot analysis.

3. NAC inhibits radiation-induced autophagy in HaCaT cells

Recent reports have shown that autophagy is closely related to radiation [21]. Therefore, to identify the relationship between radiation-induced ROS generation and DNA damage and the inhibitory effect of NAC, autophagy-related proteins were quantified by western blotting. As shown in Fig. 3A, radiation treatment increased the expression of autophagy-related proteins such as Beclin-1, LC3B, and p62. However, NAC treatment reduced the expression of Beclin-1, LC3B, and p62, which had increased after radiation treatment. Furthermore, LC3 puncta were visualized using a laser scanning fluorescent confocal microscope. As shown in Fig. 3B, radiation treatment enhanced the accumulation of LC3 puncta in HaCaT cells, which was effectively suppressed by NAC.

To confirm these results, transmission electron microscopy was performed to visualize autophagic structures in HaCaT cells. As shown in Fig. 3C, untreated cells showed normal nuclei, mitochondria, and other organelles and no autophagic vacuoles were detected. In contrast, autophagic vacuoles were observed in irradiated cells, suggesting that radiation treatment induced autophagy in HaCaT cells. In addition, NAC treatment significantly decreased the number of autophagic vacuoles compared with radiation treatment.

In summary, NAC can effectively inhibit the transcription of LC3B, ATG5, and p62 in HaCaT cells (Fig. 3D).

4. NAC protected against radiation-induced histopathological changes in injured rat buccal mucosa

To determine the protective effects of NAC against radiation *in vivo*, we exposed rats to 30 Gy of radiation plus NAC. Thereafter, we investigated the morphological changes caused by the treatment and the effect on survival up to 3 weeks of development. All animals were examined after death during the experiment or euthanized after 3 weeks.

The food intake between the experimental groups was not significantly different until day 5, when the irradiation group and the radiation+NAC-treated group showed a significant decrease in food intake. Therefore, there was no statistically significant difference in the average food intake of the radiation+NAC group and the irradiation group (S1A Fig.). The weights of the irradiated rats were also not significantly different from those of the radiation+NAC group (S1B Fig.).

Inflammation and survival rate, however, were inhibited in

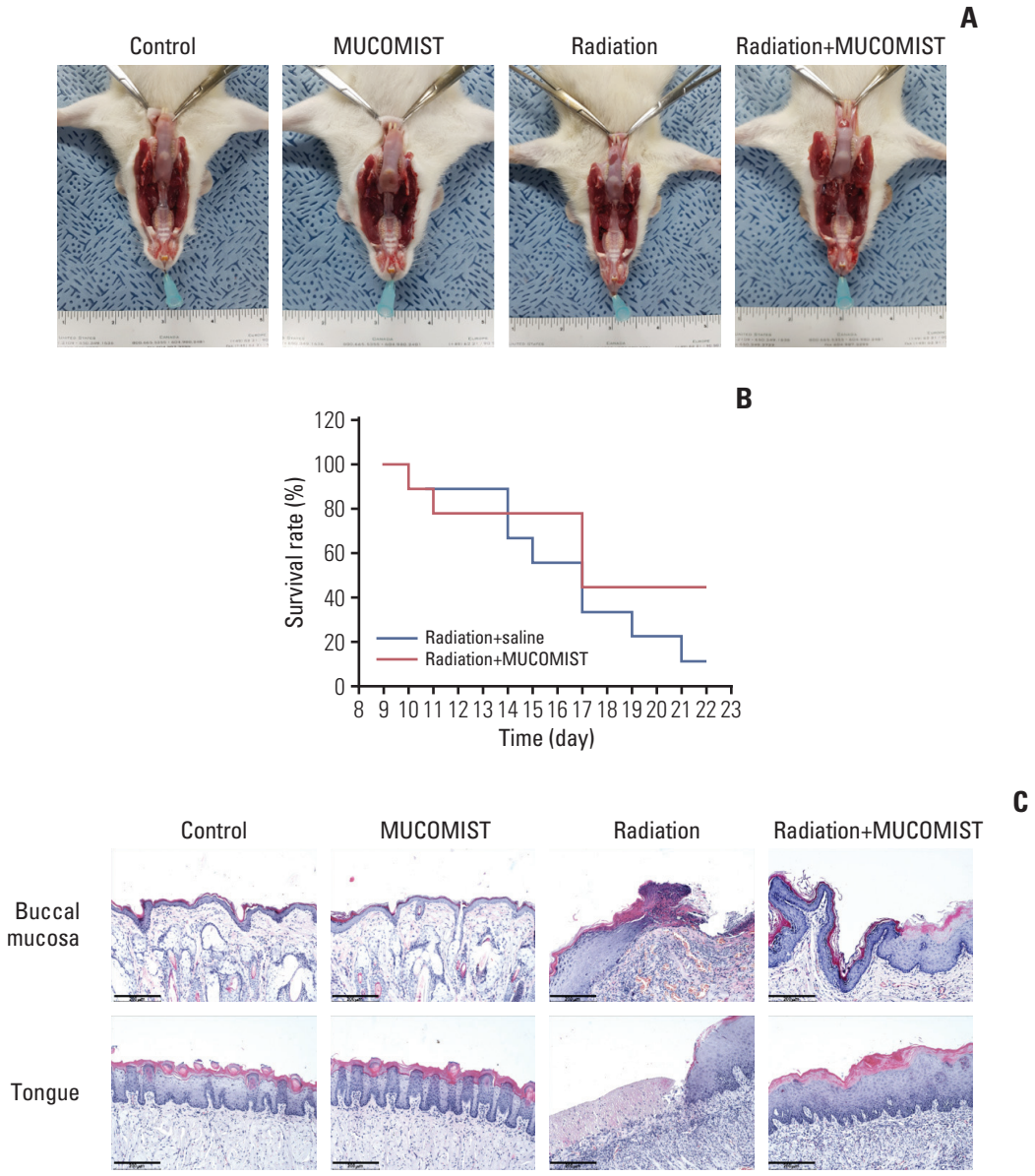

Fig. 4. Protective effect of N-acetyl cysteine (NAC) against histopathologic effects in irradiated rats. (A) Photographic images of buccal mucosa on day 23 after irradiation. Rats in the radiation group were found to have more tongue mucositis (the tip of the tongue is not fully healed). However, the MUCOMIST(NAC) treatment group is clean except for the tip of the tongue. (B) Survival rate and time of death. There was no statistical significance between the treatment and non-treatment groups. (C) Histopathologic images (H&E staining, ×400) of buccal mucosa and tongue on day 23 after irradiation. Scale bars=200 μm.

the radiation+NAC group compared with that in the radiation treatment group (Fig. 4B)

Histopathologically, the buccal mucosa of the irradiation group was severely ulcerated with necrotic inflammatory exudates. However, after 3 weeks of irradiation, the tongue and buccal mucosa in the radiation+NAC group recovered similar to those in the control group (Fig. 4A). Mucosal recovery was also observed in hematoxylin-eosin stained tissue (Fig. 4C).

5. NAC prevents radiation-induced autophagy and NRF2 expression in rat buccal mucosa

To determine whether NAC treatment had similar effects *in vivo*, we confirmed the expression of NRF2 and LC3B in the rat tongue. The expression levels of LC3B and NRF2 were elevated in the group exposed to radiation, compared with those in the group treated with radiation+NAC (Fig. 5A).

We also conducted western blotting for NRF2 and LC3B in the rat tongue. NRF2 and LC3B protein levels increased in the radiation treatment group. In the radiation+NAC group,

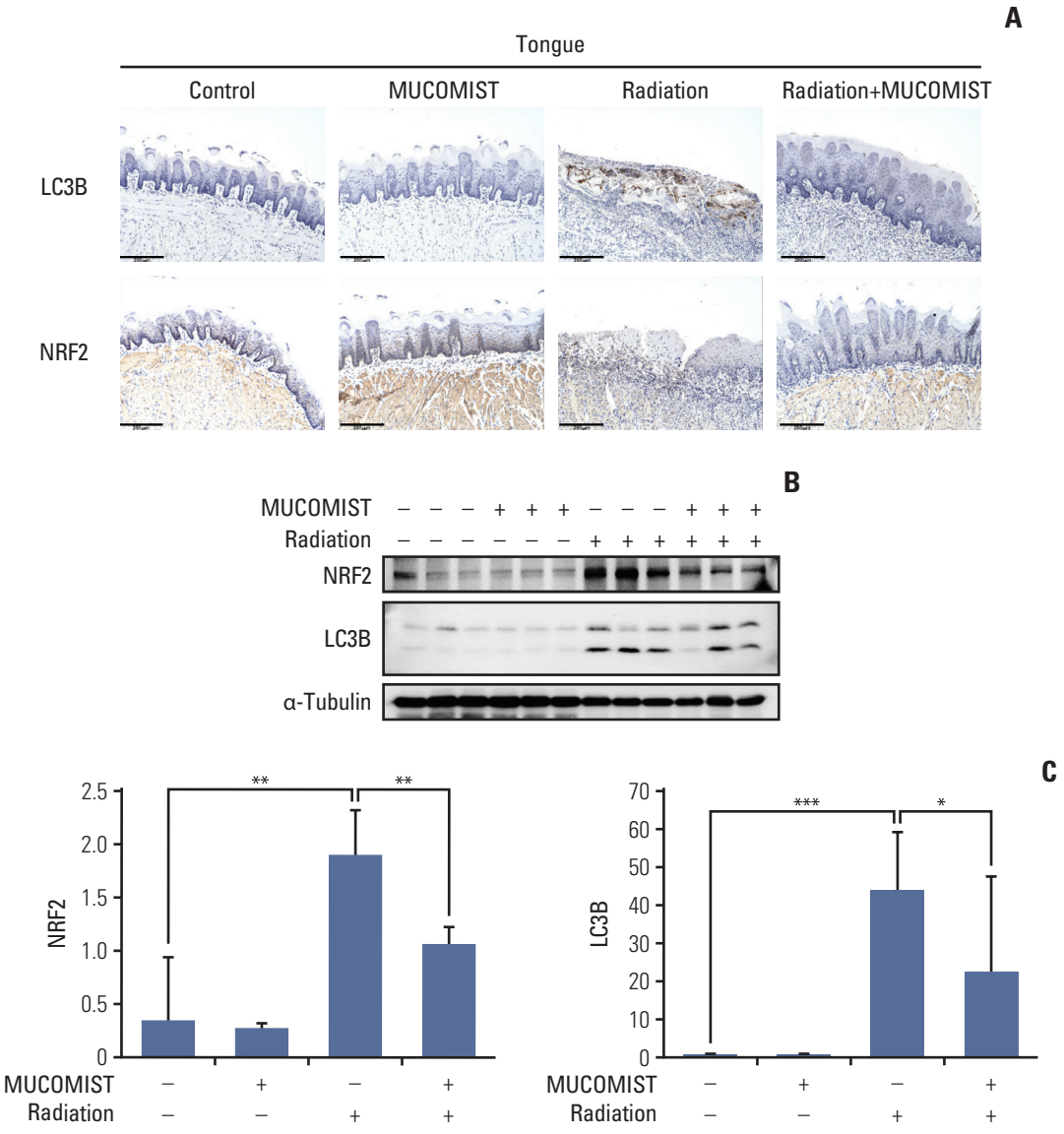

Fig. 5. Protective effect of N-acetyl cysteine (NAC) against irradiation of rat tongue. (A) Immunohistochemical analysis. Rat tongue sections from each experimental group (control, MUCOMIST, radiation, radiation+MUCOMIST) were stained with LC3B and NRF2 antibody. Scale bars=200 μm. (B) NRF2 and LC3B expression was detected by western blot. All the western blotting experiments were performed under the same conditions. (C) Relative expression levels of mRNA of NRF2 and LC3B were determined by real-time polymerase chain reaction analysis. *p < 0.05, **p < 0.01, ***p < 0.001.

however, there was a marked decrease in NRF2 and LC3B expression (Fig. 5B and C), indicating that NAC treatment was effective *in vivo* as well as *in vitro*.

Discussion

The mechanism of radiation-induced oral mucositis is not fully understood. However, radiation therapy is essential for tumor treatment and is commonly used despite its side effects, such as skin damage and oral mucositis [22].

Radiotherapy and chemotherapy are known to induce ROS generation that activates various signaling pathways that have recently been reported to interact via autophagy-inducing factors [23]. These activated pathways inhibit cell regeneration and induce apoptosis and ulceration. DNA damage is also known to be induced directly by radiation; indirectly, S-phase arrest is induced by ROS [19]. Our results showed that NAC secured the progression of the S-phase by suppressing ROS-mediated DNA damage. In addition, another previous report demonstrated that NAC protected the cell cycle against UV damage; our results also showed

its protective effect on the cell cycle against radiation damage [24]. Thus, we hypothesized that the antioxidant NAC is a possible protective agent against radiation-induced oral mucositis.

Previous studies have identified the preventive effect of NAC on radiation through 3D cell culture [25]. However, our experiments were performed *in vivo* to confirm the effect of NAC. In addition, the report did not observe the effect of NAC single treatment. Apoptosis was reduced when QYD (Qingre Liyan decoction) was used with NAC. In our study, cell damage was caused by ROS, which is increased upon irradiation, thereby resulting in increased autophagy. However, NAC treatment inhibited ROS production, and consequently, prevented cell death.

In our previous report, we demonstrated that the protective effect of NAC against radiation and cisplatin is mediated via the reduction of ROS generation [26]. Natural antioxidants play a role in autophagy and cell death induction. Therefore, we investigated the protective effect of NAC against radiation-induced cellular damage in HaCaT cells and in a rat model [27]. We concluded that NAC treatment prevents radiation-induced mucositis by decreasing NRF2-dependent ROS synthesis. Recent studies have shown that a low-dose radiation of 2.5 Gy increased the nuclear accumulation of NFR2 in the mouse macrophage cell line RAW 264.7 [28]. In our study, we also found nuclear accumulation of NRF2 induced by exposure to radiation.

The activation mechanism of NRF2 is mediated via direct interaction between p62 and SQSTM1, as well as the antioxidant response. Given that the accumulation of p62 and SQSTM1 is a hallmark of autophagy response, we investigated the association between autophagy and the NRF2 pathway.

Autophagy is activated by ROS. Under oxidative stress, autophagy has a protective effect against cardiovascular, renal, and neurological disorders and obesity [29,30]. Therefore, it is an important regulator of cell survival following damage and exposure to increased ROS levels or starvation. Autophagy eliminates ROS within the cell, which is similar to the role of the antioxidant-signaling pathway.

In our study, radiation-induced autophagy promoted the expression of NRF2 and induced the expression of p62. These results suggested that autophagy may play a regulatory or synergistic role in antioxidant-signaling pathways. However, the role of autophagy in radiation-induced early and delayed toxicity is unclear, and studies investigating the toxicity and death in autophagy are still ongoing.

However, regarding the mechanism involved, autophagy was activated and NRF2 production was promoted in irradiated cells by ROS. In our study, we found that NAC prevented both autophagy and NRF2 production by inhibiting the synthesis of radiation-induced ROS in cells and an animal model, thus demonstrating the ability of NAC to protect against radiation-induced DNA damage, including oral mucositis. We observed the protective effect of NAC against radiation-induced cellular damage via its function in inhibiting ROS production.

Although the relevance of autophagy requires further elucidation to confirm the effectiveness of NAC, our results suggest that NAC may inhibit oral mucositis, which is the most common complication of chemotherapy.

Even though our animal experiments showed that treatment with NAC is not effective with respect to oral intake and body weight, histological analysis results confirmed that NAC treatment improved tissue healing rate and quality. Therefore, it seems that NAC can treat radiation-induced oral mucositis, although NAC treatment did not affect oral intake or body weight. Therefore, more experiments are required to find a more effective way of NAC treatment, such as oral intake and body weight, to improve clinical parameters.

In this study, we demonstrated that NAC significantly inhibited radiation-induced autophagy in keratinocytes and rat buccal mucosa. These results suggest that NAC may be a safe and effective therapeutic candidate for the inhibition of radiation-induced buccal mucosa damage.

Electronic Supplementary Material

Supplementary materials are available at Cancer Research and Treatment website (https://www.e-crt.org).

Conflicts of Interest

Conflicts of interest relevant to this article was not reported.

Acknowledgments

This study was financially supported by the Boryung Pharmaceutical Co., Ltd and National Research Foundation of Korea grant awarded by the Korean government (MSIP) (2017M3A9F7079339 to CH Kim), and Basic Science Research Program via the National Research Foundation of Korea (NRF) funded by the Ministry of Science, ICT, and Future Planning (2018R1A2B3009008 awarded to CH Kim).

References

1. Sankaranarayanan R, Masuyer E, Swaminathan R, Ferlay J, Whelan S. Head and neck cancer: a global perspective on epidemiology and prognosis. Anticancer Res. 1998;18:4779-86.
2. Epstein JB, Gorsky M, Guglietta A, Le N, Sonis ST. The correlation between epidermal growth factor levels in saliva and the severity of oral mucositis during oropharyngeal radiation therapy. Cancer. 2000;89:2258-65.
3. Leborgne JH, Leborgne F, Zubizarreta E, Ortega B, Mezzera J. Corticosteroids and radiation mucositis in head and neck cancer: a double-blind placebo-controlled randomized trial. Radiother Oncol. 1998;47:145-8.
4. Rosenthal DI, Trotti A. Strategies for managing radiation-induced mucositis in head and neck cancer. Semin Radiat Oncol. 2009;19:29-34.
5. Hille A, Rave-Frank M, Pradier O, Damm C, Dorr W, Jackel MC, et al. Effect of keratinocyte growth factor on the proliferation, clonogenic capacity and colony size of human epithelial tumour cells in vitro. Int J Radiat Biol. 2003;79:119-28.
6. Klaunig JE, Wang Z, Pu X, Zhou S. Oxidative stress and oxidative damage in chemical carcinogenesis. Toxicol Appl Pharmacol. 2011;254:86-99.
7. Zafarullah M, Li WQ, Sylvester J, Ahmad M. Molecular mechanisms of N-acetylcysteine actions. Cell Mol Life Sci. 2003;60:6-20.
8. Sheng-Tanner X, Bump EA, Hedley DW. An oxidative stress-mediated death pathway in irradiated human leukemia cells mapped using multilaser flow cytometry. Radiat Res. 1998;150:636-47.
9. Ishii T, Itoh K, Yamamoto M. Roles of Nrf2 in activation of antioxidant enzyme genes via antioxidant responsive elements. Methods Enzymol. 2002;348:182-90.
10. Chan K, Lu R, Chang JC, Kan YW. NRF2, a member of the NFE2 family of transcription factors, is not essential for murine erythropoiesis, growth, and development. Proc Natl Acad Sci USA. 1996;93:13943-8.
11. Zhang J. Teaching the basics of autophagy and mitophagy to redox biologists: mechanisms and experimental approaches. Redox Biol. 2015;4:242-59.
12. Shin YS, Shin HA, Kang SU, Kim JH, Oh YT, Park KH, et al. Effect of epicatechin against radiation-induced oral mucositis: in vitro and in vivo study. PLoS One. 2013;8:e69151.
13. Zhu W, Xu J, Ge Y, Cao H, Ge X, Luo J, et al. Epigallocatechin-3-gallate (EGCG) protects skin cells from ionizing radiation via heme oxygenase-1 (HO-1) overexpression. J Radiat Res. 2014;55:1056-65.
14. Koike M, Shiomi T, Koike A. Identification of skin injury-related genes induced by ionizing radiation in human keratinocytes using cDNA microarray. J Radiat Res. 2005;46:173-84.
15. Won HR, Kang SU, Kim HJ, Jang JY, Shin YS, Kim CH. Non-thermal plasma treated solution with potential as a novel therapeutic agent for nasal mucosa regeneration. Sci Rep. 2018;8:13754.
16. Cha HY, Lee BS, Chang JW, Park JK, Han JH, Kim YS, et al. Downregulation of Nrf2 by the combination of TRAIL and valproic acid induces apoptotic cell death of TRAIL-resistant papillary thyroid cancer cells via suppression of Bcl-xL. Cancer Lett. 2016;372:65-74.
17. Li XY, Zhao Y, Sun MG, Shi JF, Ju RJ, Zhang CX, et al. Multifunctional liposomes loaded with paclitaxel and artemether for treatment of invasive brain glioma. Biomaterials. 2014;35:5591-604.
18. Lomax ME, Folkes LK, O'Neill P. Biological consequences of radiation-induced DNA damage: relevance to radiotherapy. Clin Oncol (R Coll Radiol). 2013;25:578-85.
19. Yamamori T, Yasui H, Yamazumi M, Wada Y, Nakamura Y, Nakamura H, et al. Ionizing radiation induces mitochondrial reactive oxygen species production accompanied by upregulation of mitochondrial electron transport chain function and mitochondrial content under control of the cell cycle checkpoint. Free Radic Biol Med. 2012;53:260-70.
20. McDonald JT, Kim K, Norris AJ, Vlashi E, Phillips TM, Lagadec C, et al. Ionizing radiation activates the Nrf2 antioxidant response. Cancer Res. 2010;70:8886-95.
21. Yang Y, Yang Y, Yang X, Zhu H, Guo Q, Chen X, et al. Autophagy and its function in radiosensitivity. Tumour Biol. 2015;36:4079-87.
22. Erwin-Toth P. Skin changes from radiation therapy. J Wound Ostomy Continence Nurs. 2007;34:546.
23. Sonis ST. The biologic role for nuclear factor-kappaB in disease and its potential involvement in mucosal injury associated with anti-neoplastic therapy. Crit Rev Oral Biol Med. 2002;13:380-9.
24. Renzing J, Hansen S, Lane DP. Oxidative stress is involved in the UV activation of p53. J Cell Sci. 1996;109(Pt 5):1105-12.
25. Lambros MP, Kondapalli L, Parsa C, Mulamalla HC, Orlando R, Pon D, et al. Molecular signatures in the prevention of radiation damage by the synergistic effect of N-acetyl cysteine and qingre liyan decoction, a traditional chinese medicine, using a 3-dimensional cell culture model of oral mucositis. Evid Based Complement Alternat Med. 2015;2015:425760.
26. Kim CH, Kang SU, Pyun J, Lee MH, Hwang HS, Lee H. Epicatechin protects auditory cells against cisplatin-induced death. Apoptosis. 2008;13:1184-94.
27. Shin YS, Cha HY, Lee BS, Kang SU, Hwang HS, Kwon HC, et al. Anti-cancer effect of luminacin, a marine microbial rxtract, in head and neck dquamous cell carcinoma progression via autophagic cell death. Cancer Res Treat. 2016;48:738-52.
28. Tsukimoto M, Tamaishi N, Homma T, Kojima S. Low-dose gamma-ray irradiation induces translocation of Nrf2 into nuclear in mouse macrophage RAW264.7 cells. J Radiat Res. 2010;51:349-53.
29. Muriach M, Flores-Bellver M, Romero FJ, Barcia JM. Diabetes and the brain: oxidative stress, inflammation, and autophagy. Oxid Med Cell Longev. 2014;2014:102158.
30. Fang C, Gu L, Smerin D, Mao S, Xiong X. The Interrelation between reactive oxygen apecies and autophagy in neurological disorders. Oxid Med Cell Longev. 2017;2017:8495160.

pISSN 1598-2998, eISSN 2005-9256

Cancer Res Treat. 2020;52(4):1031-1040

https://doi.org/10.4143/crt.2020.310

Original Article

Open Access

Intensity-Modulated Radiotherapy-Based Reirradiation for Head and Neck Cancer: A Multi-institutional Study by Korean Radiation Oncology Group (KROG 1707)

Jeongshim Lee, MD[1]
Tae Hyung Kim, MD[2]
Yeon-Sil Kim, MD, PhD[3]
Myungsoo Kim, MD, PhD[4]
Jae Won Park, MD, PhD[5]
Sung Hyun Kim, MD[6]
Hyun Ju Kim, MD[7]
Chang Geol Lee, MD, PhD[2]

[1]Department of Radiation Oncology, Inha University Hospital, Inha University College of Medicine, Incheon, [2]Department of Radiation Oncology, Yonsei University College of Medicine, Seoul, [3]Department of Radiation Oncology, St. Mary's Hospital, College of Medicine, The Catholic University of Korea, Seoul, [4]Department of Radiation Oncology, Incheon St. Mary's Hospital, College of Medicine, The Catholic University of Korea, Seoul, [5]Department of Radiation Oncology, Yeungnam University Medical Center, Yeungnam University College of Medicine, Daegu, [6]Department of Radiation Oncology, Wonju Severance Christian Hospital, Yonsei University Wonju College of Medicine, Wonju, [7]Department of Radiation Oncology, Gachon University Gil Medical Center, Incheon, Korea

Correspondence: Chang Geol Lee, MD, PhD
Department of Radiation Oncology,
Yonsei University College of Medicine,
50 Yonsei-ro, Seodaemun-gu, Seoul 03722, Korea
Tel: 82-2-2228-8114
Fax: 82-2-312-9033
E-mail: cglee1023@yuhs.ac

Received April 14, 2020
Accepted July 6, 2020
Published Online July 7, 2020

Purpose
The benefits of reirradiation for head and neck cancer (HNC) have not been determined. This study evaluated the efficacy of reirradiation using intensity-modulated radiotherapy (IMRT) for recurrent or second primary HNC (RSPHNC) and identified subgroups for whom reirradiation for RSPHNC is beneficial.

Materials and Methods
A total of 118 patients from seven Korean institutions with RSPHNC who underwent IMRT-based reirradiation between 2006 and 2015 were evaluated through retrospective review of medical records. We assessed overall survival (OS) and local control (LC) within the radiotherapy (RT) field following IMRT-based reirradiation. Additionally, the OS curve according to the recursive partitioning analysis (RPA) suggested by the Multi-Institution Reirradiation (MIRI) Collaborative was determined.

Results
At a median follow-up period of 18.5 months, OS at 2 years was 43.1%. In multivariate analysis, primary subsite, recurrent tumor size, interval between RT courses, and salvage surgery were associated with OS. With regard to the MIRI RPA model, the class I subgroup had a significantly higher OS than class II or III subgroups. LC at 2 years was 53.5%. Multivariate analyses revealed that both intervals between RT courses and salvage surgery were prognostic factors affecting LC. Grade 3 or more toxicity and grade 5 toxicity rates were 8.5% and 0.8%, respectively.

Conclusion
IMRT-based reirradiation was an effective therapeutic option for patients with RSPHNC, especially those with resectable tumors and a long interval between RT courses. Further, our patients' population validated the MIRI RPA classification by showing the difference of OS according to MIRI RPA class.

Key words
Head and neck neoplasm, Recurrence, Reirradiation, Intensity modulated radiotherapy

Introduction

Despite aggressive multidisciplinary management including radiotherapy (RT), up to half of patients with locally advanced head and neck cancer (HNC) experience locoregional recurrence [1-3]. Although surgery was the best salvage therapy option for such patients, only a few patients could be candidates for surgical resection due to unresectability or inoperability associated with poor performance functions and their comorbidities [4,5]. Thus, for these patients, reirradiation has been considered as a salvage therapy to improve outcomes, although the concern of severe toxicity

following reirradiation has remained [6].

With the widespread adoption of conformal RT techniques such as intensity-modulated RT (IMRT) and volume-modulated arc therapy, the therapeutic ratio of reirradiation may have increased owing to the advanced technique using multiple small beamlets, which have an accurate target system for irregularly shaped tumors while simultaneously avoiding normal tissue [7,8]. Therefore, reirradiation in the modern advanced RT era has led to the expectation that the efficacy after reirradiation would be improved [9], and it has contributed to the frequent application of reirradiation using IMRT in clinical practice [10-12].

However, the efficacy of reirradiation in the IMRT era still remains unclear. In particular, difficulties associated with the selection of patients who would benefit from reirradiation and the potential for lethal toxicity following reirradiation are barriers to performing reirradiation. Therefore, we conducted a multi-institutional study to describe the efficacy of IMRT-based reirradiation for recurrent or second primary HNC (RSPHNC) and to identify prognostic factors for which the benefit of reirradiation appears favorable. We also sought to externally validate the recursive partitioning analysis (RPA) published by the Multi-Institution Reirradiation (MIRI) Collaborative [13].

Materials and Methods

1. Study design

We performed a multicenter, retrospective cohort study to assess the efficacy of IMRT-based reirradiation for HNC. The eligibility criteria were as follows: (1) adult patients (≥ 18 years) who had locoregional RSPHNC without distant metastasis (M0) based on histologic and/or radiographic evidence of progression of the disease treated with IMRT-based reirradiation from January 1, 2006, to December 31, 2015; (2) availability of a medical record related to the initial radiation dose; and (3) patients who previously received ≥ 40 Gy RT at the reirradiation site. Information on the patients' clinicodemographic characteristics, tumor characteristics, and administered treatments was collected from their medical records. All institutions decided on re-irradiation for patients with RSPHNC through each institution's multidisciplinary discussion during a head and neck tumor conference, in which an otolaryngologist, radiation oncologist, medical oncologist, and radiologist participated. Finally, 118 patients from seven institutions with recurrent (n=109) or second primary (n=9) HNC who underwent IMRT-based reirradiation were analyzed.

2. Treatment outcomes and prognostic variables

The primary endpoint was 2-year overall survival (OS) rate, and the secondary endpoint was local control (LC) rate. OS period was calculated from the time of reirradiation for recurrence to the date of death from any cause, and freedom from local progression was defined as an absence of disease on histologic and radiographic evaluation from the reirradiation. The prognostic factors associated with OS and LC were as follows: age, sex, Karnofsky performance status, initial subsite, initial histology, surgery at recurrence, tumor size at recurrence, interval between RT courses, and organ dysfunction at reirradiation. In addition, we divided patients into prognostic subgroups using the RPA according to the interval between RT courses, resectability, and organ dysfunction defined by the MIRI Collaborative [13] and assessed OS by class. Additionally, the late toxicity following reirradiation was assessed by reviewing medical charts.

3. Statistical analysis

Actuarial estimates for OS and LC were calculated using the Kaplan-Meier methods. Log-rank test was used to compare risk factors affecting survival and LC estimates in univariate analysis. A Cox regression model was used to identify potential prognostic factors for OS and LC in univariate and multivariate analyses. All analyses were performed using IBM SPSS ver. 20.0 (IBM Corp., Armonk, NY).

4. Ethical statement

This study was approved by the institutional review board of each participating institution. The requirement for informed consent was waived. We carried out this research according to the principles expressed in the declaration of Helsinki.

Results

1. Patient and treatment characteristics

The median age when performing IMRT-based reirradiation was 59 years (range, 20 to 90 years). Of the total patients, 95 patients (80.5%) had squamous cell carcinoma and 82 patients (69.5%) showed stage III/IV at initial presentation. The approach to the RSPHNC consisted of surgery for 40.7% (n=48; R0 resection in 29 patients and R1 resection in 19 patients) and chemotherapy for 72.9% (n=86) of the patients. Fractionation of IMRT-based reirradiation was once daily for all patients. The treatment volume included focal field in 84.7%, which was defined by the gross tumor or surgical bed plus a margin of 0.5-1.0 cm, and radical field in 15.3%, encompassing the gross tumor or surgical bed with an elective high-risk area plus a margin of 0.5-1.0 cm. The median interval period between RT courses was 29.4 months (range, 2.6 to 293.4 months). The median initial RT total dose, IMRT-based reirradiation total dose, and cumulative RT dose were 66 Gy (range, 40.0 to 78.6 Gy), 59.4 Gy (range, 36.0 to 75.0 Gy), and 124.9 Gy (range, 90.0 to 146.3 Gy), respectively. With regard

Table 1. Baseline characteristics

Variable	Total (n=118)
Initial presentation	
Age, median (range, yr)	56 (20-83)
Sex	
Male	92 (78.0)
Female	26 (22.0)
ECOG PS	
0-1	110 (93.2)
2-3	8 (6.8)
Primary subsite	
Nasopharynx	30 (25.4)
Oropharynx	15 (12.7)
Oral cavity	9 (7.6)
Paranasal sinus/Nasal cavity	23 (19.5)
Hypopharynx/Larynx	30 (25.4)
Other (SG, UP)	11 (9.3)
Histology	
SCC	95 (80.5)
Non-SCC	23 (19.5)
Stage	
I/II	31 (26.3)
III	16 (13.6)
IV	66 (55.9)
Unevaluable	5 (4.2)
Initial treatment	
Treatment modality	
Definitive RT/CRT	52 (44.1)
Surgery±PORT/CRT	48 (40.7)
Induction CTx+Definitive RT/CRT	13 (11.0)
Induction CTx+Surgery±PORT/CRT	3 (2.5)
Preoperative RT/CRT+Surgery	2 (1.6)
Initial RT total dose, median (range, Gy)	66.0 (40.0-78.6)
Initial RT fractional dose, median (range, Gy)	2.0 (1.2-2.5)
Second presentation	
Age, median (range, yr)	59 (20-90)
< 60	63 (53.4)
≥ 60	55 (46.6)
ECOG PS	
0-1	105.0 (89.0)
2-3	13.0 (11.0)
Presentation type	
Recurrent	109 (92.4)
SP	9 (7.6)
rStage	
rT0Nany	25 (21.2)
rT1Nany	13 (11.0)
rT2Nany	11 (9.3)
rT3Nany	19 (16.1)
rT4Nany	50 (42.4)
Failure type	
Local failure	74 (62.7)
Regional failure	24 (20.3)
Locoregional failure	20 (16.9)
Recurrent or SP tumor size (cm)	
Median, range	3.0 (0.5-11.0)
< 3	54 (45.8)
≥ 3	64 (54.2)
No. of recurrent or SP tumor	
1	72 (61.0)
≥ 2	46 (39.0)
Pre-existing organ dysfunction	
No	110 (93.2)
Yes[a]	8 (6.8)
RPA class[b]	
Class I	25 (21.2)
Class II	89 (75.4)
Class III	4 (3.4)
Second treatment	
Salvage surgery	
No	70 (59.3)
Yes[c]	48 (40.7)
Chemotherapy	
No	32 (27.1)
Yes	86 (72.9)
Reirradiation total dose (Gy)	
Median (range)	59.4 (36.0-75.0)
< 60	60 (50.8)
≥ 60	58 (49.2)
Reirradiation fractional dose, median (range, Gy)	2.1 (1.8-4.0)
Treatment volume of reirradiation[d]	
Focal field	100 (84.7)
Radical field	18 (15.3)
Cumulative RT dose, median (range, Gy)	124.9 (90.0-146.3)

(Continued to the next page)

(Continued)

Table 1. Continued

to RPA classes, class I, II, and III accounted for 21.2%, 75.4%, and 3.4%, respectively. The baseline characteristics of 118 patients from seven institutions are summarized in Table 1. Furthermore, the baseline characteristics according to each institution are shown in S1 Table.

2. Outcomes and prognostic factors

The median duration of follow-up after IMRT-based reirradiation was 18.5 months (range, 1.4 to 98.0 months). Twenty-nine patients (24.6%) remained alive at the time of the last observation. The median OS duration and 2-year OS rate were 20.1 months (range, 16.1 to 24.1 months) and 43.1%,

Table 1. Continued

Variable	Total (n=118)
Interval between RT courses (mo)	
Median (range)	29.4 (2.6-293.4)
< 24	52 (44.1)
≥ 24	66 (55.9)

ECOG PS, Eastern Cooperative Oncology Group performance status; SG, salivary gland; UP, unknown primary; SCC, squamous cell carcinoma; RT, radiotherapy; CRT, chemoradiotherapy; PORT, postoperative radiotherapy; CTx, chemotherapy; SP, second primary; rStage, recurrent tumor and nodal stage; RPA, recursive partitioning analysis. [a]Tracheostomy (n=6, 5.2%) or feeding tube dependence (n=2, 1.6%) prior to re-irradiation, [b]Prognostic groups associated with overall survival according to RPA defined by the Multi-Institution Reirradiation (MIRI) Collaborative, [c]Salvage surgery was performed in R0 resection for 29 patients and R1 resection for 19 patients, [d]Focal field included the gross tumor or surgical bed plus margin of 0.5-1.0 cm, whereas radical field encompassed the gross tumor or surgical bed with elective high risk area plus margin of 0.5-1.0 cm.

respectively (Fig. 1). The Kaplan-Meier curve of factors related to OS after reirradiation identified primary subsites ($p < 0.001$) (Fig. 2A), RSPHNC tumor size ($p < 0.001$) (Fig. 2B), number of RSPHNC ($p=0.041$), interval between RT courses ($p=0.007$) (Fig. 2C), and performance of salvage surgery for RSPHNC ($p=0.002$) (Fig. 2D) as significant factors. In a multivariate stepwise Cox regression model analysis, primary subsites (non-hypopharynx/larynx/oral cavity vs. hypopharynx/larynx/oral cavity; hazard ratio [HR], 0.457; $p=0.001$), tumor size of RSPHNC (≥ 3 cm vs. < 3 cm; HR, 2.119; $p=0.001$), interval between RT courses (≥ 24 months vs. < 24 months; HR, 0.460; $p < 0.001$), and salvage surgery (yes vs. no; HR, 0.586; $p=0.023$) were confirmed as independent prognostic factors affecting OS. All results from the univariate and multivariate Cox regression analyses related to OS are shown in Table 2.

Local progression within the reirradiation field was developed in 50 patients (42.4%). The median time to local failure and 2-year LC rate were 28.9 months (range, 8.23 to 49.57 months) and 53.5%, respectively (Fig. 1). Both univariate and multivariate Cox regression models revealed that the interval between RT courses ($p=0.078$ and $p=0.011$, respectively) and performance of salvage surgery for RSPHNC ($p=0.026$ and $p=0.042$, respectively) were significant prognostic factors associated with LC (Table 2). Fig. 3A and Fig. 3B show the Kaplan-Meier LC curve according to the interval between RT courses ($p=0.074$) and performance of salvage surgery ($p=0.023$), respectively.

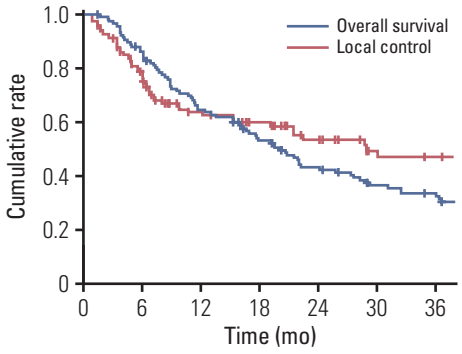

Fig. 1. Kaplan-Meier curve of overall survival and local control rates.

3. Survival validation according to MIRI RPA

We classified the patients into three prognostic classes according to the time interval between RT courses (< 2 years vs. ≥ 2 years), resectability (resected vs. unresected), and organ dysfunction (yes vs. no), as follows: those with interval > 2 years between RT courses with resected tumors (class I, n=25), those with interval > 2 years between RT courses with unresected tumors or with interval ≤ 2 years between RT courses without organ dysfunction (class II, n=89), and those with interval ≤ 2 years between RT courses with organ dysfunction (class III, n=4). The 2-year OS of each RPA class was 65.5% in class I, 38.0% in class II, and 25.0% in class III and was statistically significant ($p=0.001$) (Fig. 2D).

4. Toxicity

During IMRT-based reirradiation, no severe acute toxicity was recorded. At a median of 18.5 months after retreatment, grade ≥ 3 toxicity developed in 10 patients (8.5%), which consisted of grade 3 mucositis (n=2), interorgan fistula (n=4), dysphagia (n=2), and osteoradionecrosis (n=1) and grade 5 carotid blowout (n=1). With respect to organ dysfunction, 6 patients (5.1%) were tracheostomy-dependent, while 5 patients (4.2%) were feeding tube-dependent (Table 3).

Discussion

Our multi-center cohort study showed a 2-year OS of 43.1% and a 2-year LC of 53.5% after IMRT-based reirradiation for RSPHNC. The RSPHNC patients with small size tumors, a resectable status, and long interval between RT courses had a significantly better survival than their counterparts. We also validated the MIRI RPA classification by showing that RPA class I had a higher OS than class II or III. Regarding LC, we identified the independent impact of the interval between RT courses and performance of salvage surgery.

Previously published literature on IMRT for HNC reported that IMRT provides better oncologic outcomes and less toxicities than conventional RT [14,15]. Extending that view-

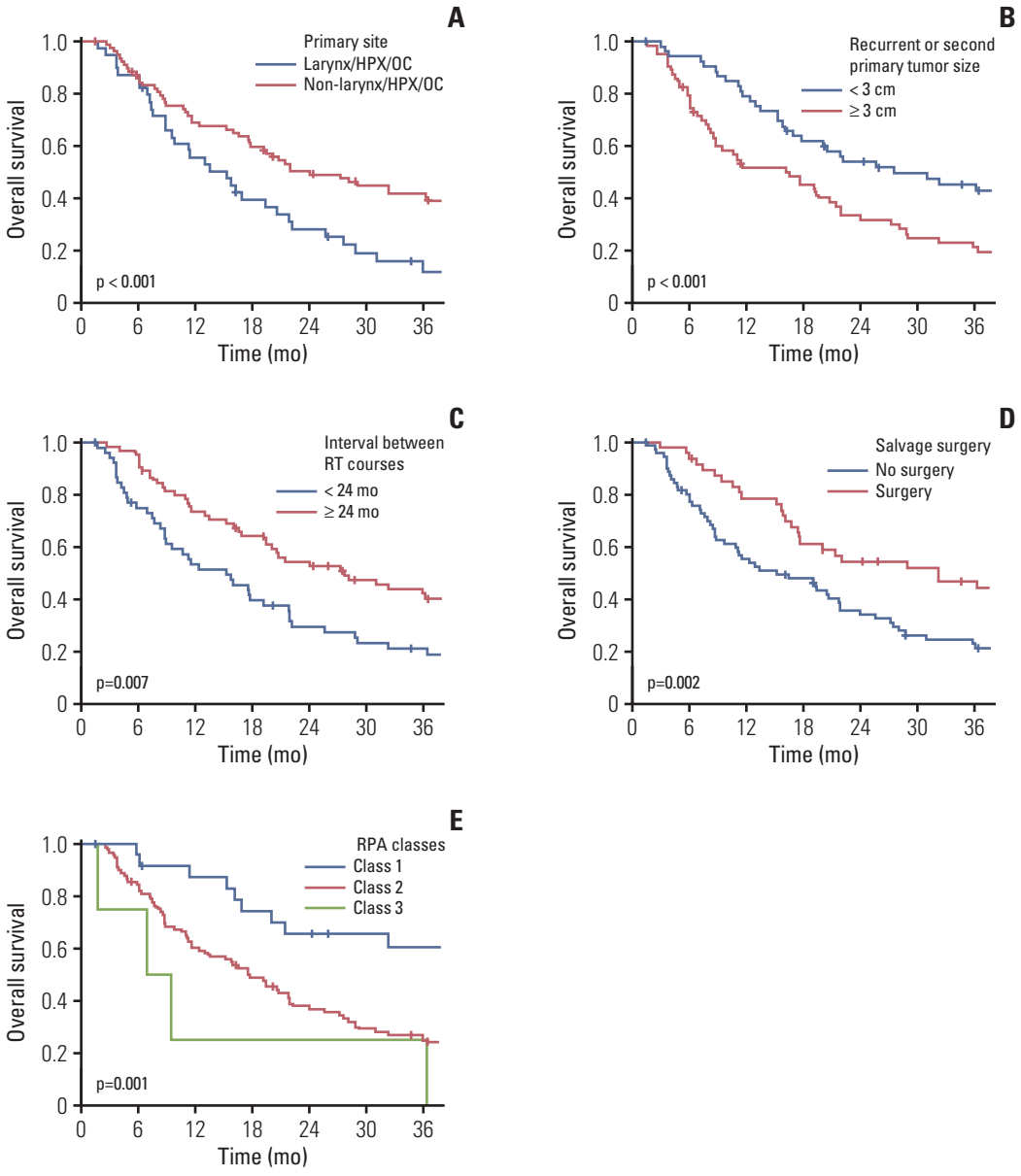

Fig. 2. Kaplan-Meier curve of overall survival rate according to primary subsite (A), tumor size of recurrent or second primary tumor (B), interval between radiotherapy (RT) courses (C), salvage surgery (D), and recursive partitioning analysis (RPA) classes defined by the Multi-Institution Reirradiation Collaborative (E).

point for RSPHNC patients, survival after IMRT-based reirradiation showed an improvement compared to conventional conformal reirradiation. The landmark prospective reirradiation trials in the pre-IMRT era including RTOG 9610 [16] and RTOG 9911 [17] reported that the 2-year OS ranged from 15% to 25% in patients who did not undergo salvage surgery. On the contrary, the MIRI group representatively showed an OS rate of 40% at 2 years following reirradiation of HNC in the IMRT era, which was 45% for postoperative patients and 36% for definitive patients [13]. Additionally, the Italy head and neck working group reported excellent outcomes of 44% OS at 5-year after reirradiation using advanced RT [18]. Of note, the current study showed that OS at 2 years was 43%, which was consistent with the abovementioned studies involving IMRT-based reirradiation. The favorable OS in our study could have resulted not only from this modern advanced RT technique but also from the high proportion of patients in RPA class I and II (96%), those who underwent salvage surgery (41%), those with a longer interval RT course application (56%), and those with no organ dysfunction at reirradiation (93%).

Specifically, our data supported that salvage surgery in

Table 2. Univariate and multivariate analysis affecting LC within reirradiation field and OS

Variable	OS				LC			
	UVA		MVA[a)]		UVA		MVA[a)]	
	HR (95% CI)	p-value	HR (95% CI)	p-value	HR (95% CI)	p-value	HR (95% CI)	p-value
Age at reirradiation (yr)								
< 60	Reference	0.089	-	-	Reference	0.494	-	-
≥ 60	1.438 (0.947-2.183)		-		1.214 (0.696-2.118)		-	
Sex								
Male	Reference	0.673	-	-	Reference	0.538	Reference	0.087
Female	0.897 (0.540-1.490)		-		1.227 (0.641-2.348)		1.845 (0.915-3.722)	
Histology								
SCC	Reference	0.137	-	-	Reference	0.851	-	-
Non-SCC	0.655 (0.375-1.144)		-		0.936 (0.467-1.873)		-	
Primary subsite								
Hypopharynx/Larynx/Oral cavity	Reference	0.001	Reference	0.001	Reference	0.403	-	-
Non-hypopharynx/Larynx/Oral cavity	0.463 (0.298-0.722)		0.457 (0.294-0.711)		0.762 (0.403-1.440)		-	
Presentation type								
Recurrent	Reference	0.068	-	-	Reference	0.550	-	-
Second primary	0.429 (0.173-1.063)		-		0.730 (0.260-2.048)		-	
Failure type								
Local failure	Reference	0.629	-	-	Reference	0.295	Reference	0.231
Regional failure	1.129 (0.663-1.924)	0.654	-	-	0.804 (0.369-1.750)	0.582	0.669 (0.285-1.570)	0.356
Locoregional failure	1.305 (0.747-2.280)	0.350	-	-	1.578 (0.792-3.144)	0.195	1.603 (0.670-3.834)	0.289
Recurrent or SP tumor size (cm)								
< 3	Reference	0.001	Reference	0.001	Reference	0.204	-	-
≥ 3	2.213 (1.377-3.275)		2.119 (1.345-3.339)		1.444 (0.819-2.545)		-	
No. of recurrent or SP tumors								
1	Reference	0.043	-	-	Reference	0.362	-	-
≥ 2	1.542 (1.013-2.346)		-		1.302 (0.738-2.297)		-	
Organ dysfunction								
No	Reference	0.110	-	-	Reference	0.649	-	-
Yes	1.887 (0.866-4.111)		-		0.719 (0.173-2.978)		-	
Interval between RT courses (mo)								
< 24	Reference	0.008	Reference	< 0.001	Reference	0.078	Reference	0.011
≥ 24	0.569 (0.375-0.865)		0.460 (0.300-0.705)		0.605 (0.346-1.057)		0.458 (0.250-0.837)	
Reirradiation dose (Gy)								
< 60	Reference	0.815	-	-	Reference	0.965	-	-
≥ 60	0.952 (0.628-1.443)		-		0.988 (0.567-1.720)		-	

(Continued to the next page)

Table 2. Continued

Variable	OS				LC			
	UVA		MVA[a]		UVA		MVA[a]	
	HR (95% CI)	p-value	HR (95% CI)	p-value	HR (95% CI)	p-value	HR (95% CI)	p-value
Treatment volume of reirradiation								
Focal field	Reference	0.616	-	-	Reference	0.146	Reference	0.063
Radical field	0.864 (0.488-1.530)		-		0.504 (0.200-1.270)		0.394 (0.148-1.050)	
Salvage surgery								
No	Reference	0.002	Reference	0.023	Reference	0.026	Reference	0.042
Yes	0.497 (0.319-0.776)		0.586 (0.369-0.930)		0.506 (0.278-0.922)		0.525 (0.282-0.977)	
Chemotherapy								
No	Reference	0.159	-	-	Reference	0.902	-	-
Yes	1.424 (0.871-2.327)		-		1.040 (0.561-1.929)		-	
MIRI RPA class[b]								
Class I	Reference	0.003	-	-	-	-	-	-
Class II	2.629 (1.419-4.869)	0.002	-	-	-	-	-	-
Class III	5.259 (1.677-16.488)	0.004	-	-	-	-	-	-

LC, local control; OS, overall survival; UVA, univariate analysis; MVA, multivariate analysis; HR, hazards ratio; CI, confidence interval; SCC, squamous cell carcinoma; SP, second primary; RT, radiotherapy; RPA, recursive partitioning analysis. [a]All variables (except RPA class) were analyzed using the binary Cox regression model with a backward stepwise method if $p \leq 0.10$, and they were removed when $p > 0.10$, [b]Prognostic groups defined according to RPA reported by the Multi-Institution Reirradiation (MIRI) Collaborative.

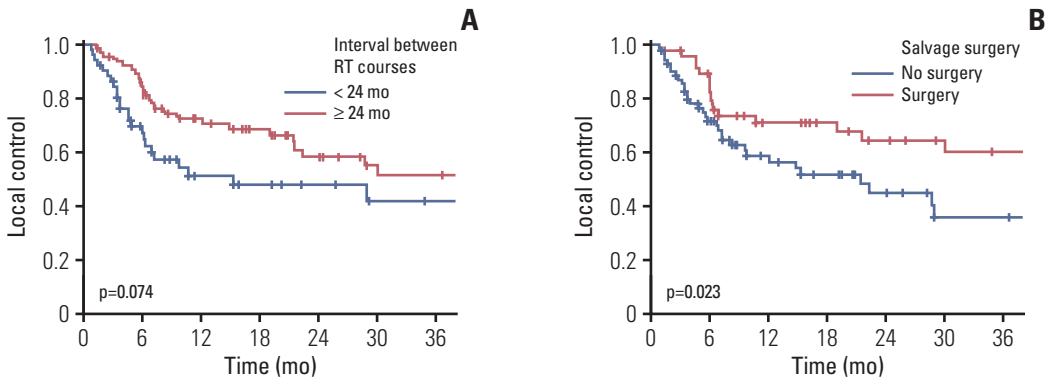

Fig. 3. Kaplan-Meier curve of local control rate according to interval between radiotherapy (RT) courses (A) and salvage surgery (B).

conjunction with IMRT reirradiation for RSPHNC improved OS and LC [13,19]. Surgical resection of RSPHNC could be an important factor considering that RSPHNC was generated from radioresistant clonogens after initial chemoradiation [20,21]. Finally, removing macroscopic tumors is a way to enhance retreatment effectiveness owing to the limited dose of IMRT-based reirradiation for gross tumors since the adjacent organ around the tumor was already irradiated with a high dose during previous RT. It was suggested that when patients with RSPHNC expected medically operable and convincing problem, salvage surgery should be encouraged cautiously. The higher LC and OS were the result of the longer interval between RT courses. The appropriate time interval between RT treatments for performing reirradiation is not established, although it depends on the relation between previous the irradiated dose to organs at risk and its tolerance dose associated with normal tissue damage repair [22,23]. Previous studies reported that a longer interval from the previous RT course contributed to improved outcomes [13,21,24,25]. This was explained by the fact that, the longer the interval between RT treatments, the greater the likelihood of LC and the lesser the aggressiveness of recurrent disease. It is noteworthy that in our patient population, organ dysfunction was not a part of prognostic factors affecting OS since we had only 6.8% of all patients with organ dysfunction. It shows that there was a bias in patient selection for reirradiation at each institution. It could be presumed that a patient without organ dysfunction was selected for retreatment with IMRT-based reirradiation.

We validated the MIRI RPA classification for the whole patients' population. The RPA classification differentiated the survival between class I and II/II. This difference was statistically significant. MIRI RPA class I cohort (66%) had a superior 2-year OS than class II and III (38% and 25%, respectively) cohorts. MIRI RPA class I might be the ideal subgroup who should undergo the active salvage treatment including IMRT reirradiation and/or surgical resection [13]. We found that the proposed RPA model might be applicable for our RSPHNC patient population and may help in patient selection for retreatment.

Table 3. Incidence of severe toxicity and organ dysfunction status following IMRT-based reirradiation

Variable	No. (%)
Grade ≥ 3 toxicity	10 (8.5)
Grade 3	
Mucositis	2 (1.7)
Interorgan fistula	4 (3.4)
Dysphagia	2 (1.7)
Osteoradionecrosis	1 (0.8)
Grade 5	
Carotid blowout	1 (0.8)
Organ dysfunction	11 (9.3)
Tracheostomy	6 (5.1)
Feeding tube dependence	5 (4.2)

IMRT, intensity-modulated radiotherapy.

Reirradiation for RSPHNC is a challenging issue owing to an increased risk of severe toxicities including fatality [23]. The rate of severe and fatal late toxicity in these cohorts was 8.5% and 0.8%, respectively, whereas previous prospective studies reported the severe toxicity ranging from 22% to 34% and fatality rates of 3.6% to 7.6%, respectively [16,17]. The amelioration of safety was likely attributed to not only the intensity-modulated technique, but also the conservative patient selection criteria of each institution prior to embarking the reirradiation course. The MIRI Collaborative group reported that in the modern reirradiation era, the risk of progression or death (64%) is four times the incidence of severe late toxicity following reirradiation (17%) [26]. Such risk of late toxicity was more dependent on patient or disease factors than treatment factors. This implied that future research related to patient selection benefiting from reirradiation is needed to elicit the effectiveness of reirradiation using modern technology including IMRT.

This current study has many limitations. The dominant weakness is in its retrospective nature and a heterogeneous population from multi-centers. Our cohort had various features in terms of patient selection and treatment characteristics according to the physician's discretion. Further, other limitations were the small number of patients from each center, which originated from the restriction of the cohort enrollment period, and the inherent limitations of IMRT. We did not identify the prognostic impact of human papillomavirus (HPV) in patients [27], especially those with oropharyngeal cancer undergoing reirradiation due to the availability of the HPV status of only 10 patients.

In conclusion, our multi-institutional study showed that IMRT-based reirradiation with a median dose of 60 Gy contributed to increased OS for patients with RSPHNC and had acceptable complications. Given the restricted salvage options, it could be considered an effective treatment for RSPHNC patients, especially those with small resectable tumors and a long interval between RT courses. Additionally, our cohort confirmed the prognostic validity of the survival rate of the MIRI RPA classification.

Electronic Supplementary Material

Supplementary materials are available at Cancer Research and Treatment website (https://www.e-crt.org).

Conflicts of Interest

Conflicts of interest relevant to this article was not reported.

Acknowledgments

This work was supported by Inha University Hospital Research Grant and the National Research Foundation of Korea (NRF) grant funded by the Korean government (MISP) under NRF-2014R1-A5A2009392.

References

1. Chao KS, Ozyigit G, Tran BN, Cengiz M, Dempsey JF, Low DA. Patterns of failure in patients receiving definitive and postoperative IMRT for head-and-neck cancer. Int J Radiat Oncol Biol Phys. 2003;55:312-21.
2. Ang KK, Zhang Q, Rosenthal DI, Nguyen-Tan PF, Sherman EJ, Weber RS, et al. Randomized phase III trial of concurrent accelerated radiation plus cisplatin with or without cetuximab for stage III to IV head and neck carcinoma: RTOG 0522. J Clin Oncol. 2014;32:2940-50.
3. Beitler JJ, Zhang Q, Fu KK, Trotti A, Spencer SA, Jones CU, et al. Final results of local-regional control and late toxicity of RTOG 9003: a randomized trial of altered fractionation radiation for locally advanced head and neck cancer. Int J Radiat Oncol Biol Phys. 2014;89:13-20.
4. Wong LY, Wei WI, Lam LK, Yuen AP. Salvage of recurrent head and neck squamous cell carcinoma after primary curative surgery. Head Neck. 2003;25:953-9.
5. Goodwin WJ Jr. Salvage surgery for patients with recurrent squamous cell carcinoma of the upper aerodigestive tract: when do the ends justify the means? Laryngoscope. 2000;110:1-18.
6. Cacicedo J, Navarro A, Alongi F, Gomez de Iturriaga A, Del Hoyo O, Boveda E, et al. The role of re-irradiation of secondary and recurrent head and neck carcinomas: is it a potentially curative treatment? A practical approach. Cancer Treat Rev. 2014;40:178-89.
7. Intensity Modulated Radiation Therapy Collaborative Working Group. Intensity-modulated radiotherapy: current status and issues of interest. Int J Radiat Oncol Biol Phys. 2001;51:880-914.
8. Puri DR, Chou W, Lee N. Intensity-modulated radiation therapy in head and neck cancers: dosimetric advantages and update of clinical results. Am J Clin Oncol. 2005;28:415-23.
9. Lee N, Puri DR, Blanco AI, Chao KS. Intensity-modulated radiation therapy in head and neck cancers: an update. Head Neck. 2007;29:387-400.
10. Ho JC, Phan J. Reirradiation of head and neck cancer using modern highly conformal techniques. Head Neck. 2018;40:2078-93.
11. Chen AM, Phillips TL, Lee NY. Practical considerations in the re-irradiation of recurrent and second primary head-and-neck cancer: who, why, how, and how much? Int J Radiat Oncol Biol Phys. 2011;81:1211-9.
12. Kim YS. Reirradiation of head and neck cancer in the era of intensity-modulated radiotherapy: patient selection, practical aspects, and current evidence. Radiat Oncol J. 2017;35:1-15.
13. Ward MC, Riaz N, Caudell JJ, Dunlap NE, Isrow D, Zakem SJ, et al. Refining patient selection for reirradiation of head and neck squamous carcinoma in the IMRT era: a multi-institution cohort study by the MIRI collaborative. Int J Radiat Oncol Biol Phys. 2018;100:586-94.
14. Toledano I, Graff P, Serre A, Boisselier P, Bensadoun RJ, Ortholan C, et al. Intensity-modulated radiotherapy in head and neck cancer: results of the prospective study GORTEC 2004-03. Radiother Oncol. 2012;103:57-62.
15. Zhang B, Mo Z, Du W, Wang Y, Liu L, Wei Y. Intensity-modulated radiation therapy versus 2D-RT or 3D-CRT for the treatment of nasopharyngeal carcinoma: a systematic review and meta-analysis. Oral Oncol. 2015;51:1041-6.
16. Spencer SA, Harris J, Wheeler RH, Machtay M, Schultz C, Spanos W, et al. Final report of RTOG 9610, a multi-institutional trial of reirradiation and chemotherapy for unresectable recurrent squamous cell carcinoma of the head and neck. Head Neck. 2008;30:281-8.
17. Langer CJ, Harris J, Horwitz EM, Nicolaou N, Kies M, Curran W, et al. Phase II study of low-dose paclitaxel and cisplatin in combination with split-course concomitant twice-daily reirradiation in recurrent squamous cell carcinoma of the head and

neck: results of Radiation Therapy Oncology Group Protocol 9911. J Clin Oncol. 2007;25:4800-5.
18. Orlandi E, Bonomo P, Ferella L, D'Angelo E, Maddalo M, Alterio D, et al. Long-term outcome of re-irradiation for recurrent or second primary head and neck cancer: a multi-institutional study of AIRO-Head and Neck working group. Head Neck. 2019;41:3684-92.
19. Riaz N, Hong JC, Sherman EJ, Morris L, Fury M, Ganly I, et al. A nomogram to predict loco-regional control after re-irradiation for head and neck cancer. Radiother Oncol. 2014;111:382-7.
20. Weichselbaum RR, Beckett MA, Schwartz JL, Dritschilo A. Radioresistant tumor cells are present in head and neck carcinomas that recur after radiotherapy. Int J Radiat Oncol Biol Phys. 1988;15:575-9.
21. Yard B, Chie EK, Adams DJ, Peacock C, Abazeed ME. Radiotherapy in the era of precision medicine. Semin Radiat Oncol. 2015;25:227-36.
22. Van der Schueren E, Van den Bogaert W, Vanuytsel L, Van Limbergen E. Radiotherapy by multiple fractions per day (MFD) in head and neck cancer: acute reactions of skin and mucosa. Int J Radiat Oncol Biol Phys. 1990;19:301-11.
23. Hoebers F, Heemsbergen W, Moor S, Lopez M, Klop M, Tesselaar M, et al. Reirradiation for head-and-neck cancer: delicate balance between effectiveness and toxicity. Int J Radiat Oncol Biol Phys. 2011;81:e111-8.
24. Velez MA, Veruttipong D, Wang PC, Chin R, Beron P, Abemayor E, et al. Re-irradiation for recurrent and second primary cancers of the head and neck. Oral Oncol. 2017;67:46-51.
25. Chopra S, Gupta T, Agarwal JP, Budrukkar A, Ghosh-Laskar S, Dinshaw K. Re-irradiation in the management of isolated neck recurrences: current status and recommendations. Radiother Oncol. 2006;81:1-8.
26. Ward MC, Lee NY, Caudell JJ, Zajichek A, Awan MJ, Koyfman SA, et al. A competing risk nomogram to predict severe late toxicity after modern re-irradiation for squamous carcinoma of the head and neck. Oral Oncol. 2019;90:80-6.
27. Velez MA, Wang PC, Hsu S, Chin R, Beron P, Abemayor E, et al. Prognostic significance of HPV status in the re-irradiation of recurrent and second primary cancers of the head and neck. Am J Otolaryngol. 2018;39:257-60.

pISSN 1598-2998, eISSN 2005-9256

Cancer Res Treat. 2020;52(4):1041-1049

https://doi.org/10.4143/crt.2020.057

Original Article

Open Access

Survival, Prognostic Factors, and Volumetric Analysis of Extent of Resection for Anaplastic Gliomas

Je Beom Hong, MD[1,2]
Tae Hoon Roh, MD, PhD[3]
Seok-Gu Kang, MD, PhD[2,4,5]
Se Hoon Kim, MD, PhD[4,6]
Ju Hyung Moon, MD[2,4]
Eui Hyun Kim, MD, PhD[2,4,5]
Sung Soo Ahn, MD, PhD[4,7]
Hye Jin Choi, MD, PhD[4,8]
Jaeho Cho, MD, PhD[4,9]
Chang-Ok Suh, MD, PhD[4,9]
Jong Hee Chang, MD, PhD[2,4,5]

[1]*Department of Neurosurgery, Kangbuk Samsung Hospital, Sungkyunkwan University School of Medicine, Seoul,* [2]*Department of Neurosurgery, Yonsei University College of Medicine, Seoul,* [3]*Department of Neurosurgery, Ajou University Hospital, Ajou University School of Medicine, Suwon,* [4]*Brain Tumor Center, Severance Hospital, Yonsei University Health System, Seoul,* [5]*Brain Research Institute, Yonsei University College of Medicine, Seoul, Departments of* [6]*Pathology,* [7]*Radiology,* [8]*Division of Oncology, Department of Internal Medicine, and* [9]*Department of Radiation Oncology, Yonsei University College of Medicine, Seoul, Korea*

Correspondence: Jong Hee Chang, MD, PhD
Department of Neurosurgery, Yonsei University College of Medicine, 50-1 Yonsei-ro, Seodaemun-gu, Seoul 03722, Korea
Tel: 82-2-2228-2162
Fax: 82-2-393-9979
E-mail: changjh@yuhs.ac

Received January 23, 2020
Accepted April 22, 2020
Published Online April 23, 2020

Purpose

The aim of this study is to evaluate the survival rate and prognostic factors of anaplastic gliomas according to the 2016 World Health Organization classification, including extent of resection (EOR) as measured by contrast-enhanced T1-weighted magnetic resonance imaging (MRI) and the T2-weighted MRI.

Materials and Methods

The records of 113 patients with anaplastic glioma who were newly diagnosed at our institute between 2000 and 2013 were retrospectively reviewed. There were 62 cases (54.9%) of anaplastic astrocytoma, isocitrate dehydrogenase (*IDH*) wild-type (AAw), 18 cases (16.0%) of anaplastic astrocytoma, *IDH*-mutant, and 33 cases (29.2%) of anaplastic oligodendroglioma, *IDH*-mutant and 1p/19q-codeleted.

Results

The median overall survival (OS) was 48.4 months in the whole anaplastic glioma group and 21.5 months in AAw group. In multivariate analysis, age, preoperative Karnofsky Performance Scale score, O^6-methylguanine-DNA methyltransferase (*MGMT*) methylation status, postoperative tumor volume, and EOR measured from the T2 MRI sequence were significant prognostic factors. The EOR cut-off point for OS measured in contrast-enhanced T1-weighted MRI and T2-weighted MRI were 99.96% and 85.64%, respectively.

Conclusion

We found that complete resection of the contrast-enhanced portion (99.96%) and more than 85.64% resection of the non-enhanced portion of the tumor have prognostic impacts on patient survival from anaplastic glioma.

Key words

Anaplastic glioma, Extent of resection, Survival, Prognosis

Introduction

Anaplastic gliomas, which account for 15%-20% of malignant gliomas [1], have poor prognosis despite modern multimodal treatments. To improve the accuracy of diagnosis and treatment, the 2016 World Health Organization (WHO) classification changed the three original categories from the 2007 classification, namely anaplastic astrocytoma, anaplastic

oligodendroglioma, and anaplastic oligoastrocytoma. These three categories were further subdivided as follows: anaplastic astrocytoma, isocitrate dehydrogenase (*IDH*)-mutant (AAm); anaplastic astrocytoma, *IDH*-wildtype (AAw); anaplastic astrocytoma, not otherwise specified (NOS); anaplastic oligodendroglioma, IDH-mutant and 1p/19q-codeleted (AOmc); anaplastic oligodendroglioma, NOS; and anaplastic oligoastrocytoma, NOS [2]. We obtained survival rates according to the new classification and examined the associated prognostic factors.

Extent of resection (EOR) has been known as an important prognosticator in anaplastic gliomas [3,4]. However, many studies have focused on only the contrast-enhanced parts of tumors observed in T1-weighted magnetic resonance imaging (MRI), despite many cases of anaplastic gliomas that are not enhanced or are only partially enhanced in contrast-enhanced T1-weighted images. In the present study, we investigated the tumor volume and EOR in both contrast-enhanced T1-weighted MRI and T2-weighted MRI sequences.

The aims of this study were (1) to identify the survival rate and prognostic factors in patients with anaplastic gliomas in the 2016 WHO classification; (2) to determine whether the volumetric measurement of EOR has prognostic value in contrast-enhanced T1-weighted MRI and T2-weighted MRI, and (3) to determine the prognostically meaningful cut-off value of resection volume in each MRI sequence.

Materials and Methods

1. Patient selection

We performed a retrospective analysis of the medical records and MRI features of 113 consecutive patients with anaplastic glioma who were newly diagnosed at our institute between 2000 and 2013, with neither prior radiotherapy nor chemotherapy. We excluded patients with gliomatosis cerebri (involving more than three lobes), midline location, and malignant transformation of a previously operated low-grade glioma. The medical records reviewed included sex, age at first diagnosis, preoperative Karnofsky Performance Scale (KPS) score, and postoperative treatment (radiotherapy, chemotherapy) (Table 1).

2. Histopathologic review

We investigated the molecular profiles of all patients including 1p/19q codeletion status, methylation of the O^6-methylguanine-DNA methyltransferase (MGMT) promoter and the state of *IDH* mutation. The *IDH* mutation status was initially assessed using immunostaining for the *IDH1*-R132H mutation. If immunohistochemistry did not show a mutation in *IDH1*-R132H, sequencing of *IDH1* codon 123 and *IDH2* codon 172 was performed. The 113 cases (grade III glioma based on the 2007 classification) were re-classified using the 2016 classification system: cases with wild-type IDH were classified as AAw, cases with non-codeleted 1p/19q and mutated *IDH* were classified as AAm, and cases with an *IDH* mutation and 1p/19q codeletion were classified as AOmc. This re-classification identified 62 cases of AAw, 18 cases of AAm, and 33 cases of AOmc. All pathological and molecular data were reviewed by a single pathologist (S.H.K.).

3. Imaging evaluation

MRI sequences, including T2-weighted, fluid-attenuated inversion recovery (FLAIR) and contrast-enhanced T1-weighted, were obtained preoperatively, postoperatively, and at regular follow-ups. Two experienced radiologists reviewed all patients' MRI data. Manual segmentation was performed to measure the tumor and resection volumes. We used OsiriX software (Pixmeo SARL, Bernex, Switzerland) to measure tumor volumes and EOR. Tumor volume was estimated based on the area of increased signal intensity on the contrast-enhanced T1-weighted images (enhancing lesions) or T2-weighted images (non-enhancing lesions). We tried to exclude any regions with cerebral edema on the T2-weighted images. The non-enhancing tumor was defined with regions of T2 hyperintensity (less than cerebrospinal fluid signal) that were associated with mass effect and architectural distortion, including blurring of the gray matter/white matter interface. Edema needed to be greater in signal than the non-enhancing tumor and lower than the cerebrospinal fluid on T2. The resection extent was calculated using early postoperative images (< 48 hours). EOR was calculated with the following equation: (preoperative tumor volume–postoperative tumor volume)/preoperative tumor volume. With respect to tumor location, deep lesions were defined as those that involved the brainstem, thalamus, basal ganglia, and the insula; superficial lesions involved only the cortex outside the insula.

4. Statistical analyses

We analyzed overall survival (OS) and progression-free survival (PFS) according to the specific pathology type using Kaplan-Meier curves and log-rank tests. To identify factors associated with PFS and OS, univariate and a multivariate Cox proportional regression analyses with stepwise methods (entry and exit criteria of $p < 0.05$) were performed, using the time from surgery to progression or death. Age, preoperative KPS score, tumor volume, and EOR were evaluated as continuous variables. OS was defined as the time from surgery to death from any cause or the last follow-up. PFS was defined as the time from surgery to the first instance of radiological signs of progression and/or deteriorated neurological status or death. We estimated optimal cut-off values for the dichotomization of the clinical outcome variable based on time-to-event data using the technique devised by Contal and O'Quigley [5]. The optimal cut-off point was selected by maximizing the hazard ratio. p-value < 0.05 was considered

Table 1. Baseline patient characteristics

	AAw	AAm	AOmc	Total
No. of patients	62 (54.9)	18 (16.0)	33 (29.2)	113 (100)
Age, median (range, yr)	48 (18-82)	36 (18-71)	45 (24-76)	40 (18-82)
Sex, female/male	27/35	8/10	14/19	49/64
Preoperative KPS, median (range)	80 (40-90)	80 (80-90)	80 (70-100)	80 (40-100)
Postoperative treatment				
CCRT	5 (4.4)	1 (0.9)	0	6 (5.3)
CCRT → CT	15 (13.3)	1 (0.9)	9 (8.0)	25 (22.1)
RT → CT	12 (10.6)	7 (6.2)	9 (8.0)	28 (24.8)
RT	20 (17.7)	8 (7.1)	15 (13.3)	43 (38.1)
None	4 (3.5)	0	0	4 (3.5)
Unknown	6 (5.3)	1 (0.9)	0	7 (6.2)
Chemotherapy regimen				
PCV	9 (8.0)	1 (0.9)	5 (4.4)	15 (13.3)
TMZ	21 (18.6)	8 (7.1)	12 (10.6)	41 (36.3)
Others[a)]	2 (1.8)	0	1 (0.9)	3 (2.7)
MGMT promoter status				
Methylated	20 (17.7)	15 (13.3)	29 (25.7)	64 (56.6)
Unmethylated	41 (36.3)	3 (2.7)	4 (3.5)	48 (42.5)
Missing	1 (0.9)	0	0	1 (0.9)
Tumor location				
Deep	24 (21.2)	4 (3.5)	5 (4.4)	33 (29.2)
Superficial	32 (28.3)	12 (10.6)	26 (23.0)	70 (61.9)
Volumetric analysis, mean (range)				
Preoperative (T1CE, cm^3)	14.6 (0.0-117.8)	3.2 (0.0-14.8)	18.0 (0-112.2)	13.8 (0.0-117.8)
Preoperative (T2, cm^3)	48.7 (0.8-197.2)	83.9 (13.5-232.9)	87.1 (6.2-212.3)	51.6 (0.8-232.9)
Postoperative (T1CE, cm^3)	2.62 (0-24.4)	0.0 (0-0)	0.1 (0-2.5)	1.0 (0-24.4)
Postoperative (T2, cm^3)	19.3 (0-166.5)	4.9 (0.7-27.3)	4.3 (0-26.9)	9.9 (0-166.5)
Extent of resection (T1CE, %)	81.5 (0-100)	100.0 (100-100)	95.9 (41.2-100)	90.6 (0-100)
Extent of resection (T2, %)	75.4 (0-100)	92.5 (52.7-100)	95.4 (76.5-100)	87.4 (0-100)

Values are presented as number (%) unless otherwise indicated. AAw, anaplastic astrocytoma, *IDH*-wildtype; AAm, anaplastic astrocytoma, *IDH*-mutant; AOmc, anaplastic oligodendroglioma, *IDH*-mutant, and 1p/19q-codeleted; KPS, Karnofsky Performance Scale; CCRT, concurrent chemo-radiation therapy; CT, chemotherapy; RT, radiation therapy; PCV, procarbazine, lomustine, and vincristine; TMZ, temozolomide; *MGMT*, O^6-methylguanine-DNA methyltransferase; T1CE, T1-weighted contrast-enhanced magnetic resonance imaging (MRI); T2, T2-weighted MRI. [a)]Others included fluorouracil +carboplatin, vincristine, and lomustine.

statistically significant. All statistical procedures were performed using SAS for Windows ver. 9.4 (SAS Institute Inc., Cary, NC).

5. Ethical statement

All methods were performed in accordance with the ethical guidelines of the 1975 Deceleration of Helsinki, as revised in 1983, and was approved by the institutional review board of Severance Hospital (Yonsei University Health System, Severance Hospital, 4-2019-0181). The written informed consent was waived by the institutional review board that approved this study's protocol because all the information was tabulated in anonymized and de-identified fashion.

Results

1. Patient characteristics

The clinical information of all 113 patients are listed in Table 1, stratified by the 2016 WHO classification. There were 62 patients (54.9%) in the AAw group, 18 (16.0%) in the AAm group, and 33 (29.2%) in the AOmc group. The median age at first diagnosis in the whole cohort was 40 years (range, 18 to 82 years). In total, 102 patients (90.3%) received postoperative radiotherapy and 59 (52.2%) received chemotherapy. Among the chemotherapy regimens, 15 cases (13.3%) were treated with PCV (procarbazine, lomustine, and vincristine) and 41 (36.3%) with temozolomide. The postoperative treatment modalities are also presented in Table 1. MGMT promoter methylation was detected in 64 cases (56.6%) of the

Table 2. Overall survival (OS) and progression-free survival (PFS)

Group	Median (mo)	Survival rate (%)				
		1-Year	2-Year	3-Year	4-Year	5-Year
OS						
GIII all	48.4	84.8	64.9	55.6	50.7	45.3
AAw	21.5	74.1	64.0	46.6	28.3	14.4
AAm	n.r.	69.3	55.4	55.4	55.4	55.4
AOmc	n.r.	96.3	85.9	85.9	85.9	85.9
PFS						
GIII all	31.8	76.7	58.7	49.2	43.1	41.8
AAw	16.4	80.6	64.5	45.7	25.8	9.0
AAm	n.r.	88.9	83.0	83.0	62.2	62.2
AOmc	130.0	96.4	92.4	82.6	82.6	82.6

GIII, grade III glioma; AAw, anaplastic astrocytoma, *IDH*-wildtype; AAm, anaplastic astrocytoma, *IDH*-mutant; n.r., not reached; AOmc, anaplastic oligodendroglioma, *IDH*-mutant and 1p/19q-codeleted.

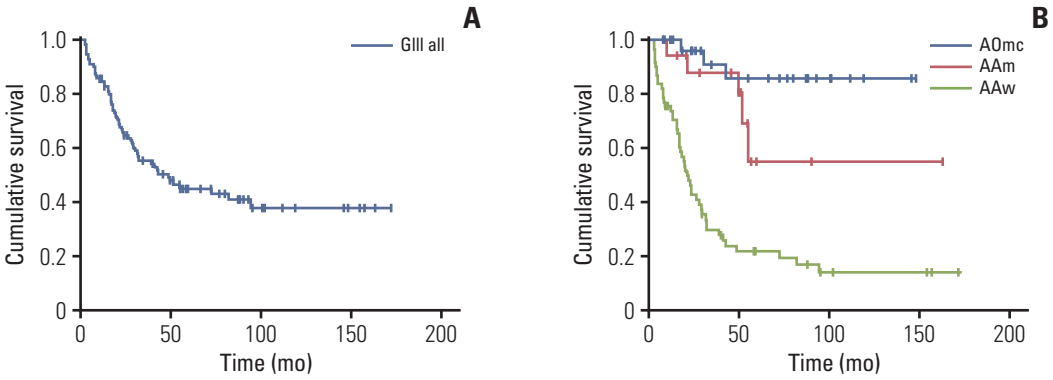

Fig. 1. Overall survival. (A) Kaplan-Meier representation of overall survival time for the entire group of 113 patients. (B) Kaplan-Meier representation of overall survival time for the AAw, AAm, AOmc each group. AAm, anaplastic astrocytoma, *IDH*-mutant; AAw, anaplastic astrocytoma, IDH-wildtype; AOmc, anaplastic oligodendroglioma, *IDH*-mutant and *1p/19q*-codeleted; GIII, grade III glioma.

whole cohort, 20 cases (17.7%) in the AAw subgroup, 15 cases (13.3%) in the AAm subgroup, and 29 cases (25.7%) in the AOmc subgroup.

2. Volumetric analysis

The mean tumor volumes in the contrast-enhanced T1-weighted and T2-weighted MRI sequences were respectively 13.8 cm^3 (range, 0.0 to 117.8 cm^3) and 51.6 cm^3 (range, 0.8 to 232.9 cm^3) preoperatively, and 1.0 cm^3 (range, 0.0 to 24.4 cm^3) and 9.9 cm^3 (range, 0.0 to 166.5 cm^3) postoperatively. The EOR measured in contrast-enhanced T1-weighted MRI (EOR-T1CE) was 90.6% (range, 0% to 100%), while it was 87.4% (0.0%-100%) in the T2-weighted MRI sequence. In our study biopsies were performed in 25 patients (22.1%).

3. Survival

After a median follow-up period of 66.1 months, the median OS was 48.4 months (95% confidence interval [CI], 15.1 to 81.7) for all patients and 21.5 months (95% CI, 17.2 to 25.8) in the AAw subgroup (Table 2, Fig. 1). The median OS was not reached in the other subgroups since more than half of the patients were still alive at the last follow-up. OS values for years 1-5 are presented in Table 2. PFS was 31.8 months (95% CI, 17.6 to 46.2) for all patients, 16.4 months (95% CI, 12.6 to 21.0) in the AAw subgroup, and 130.0 months (95% CI, 0.0 to 269.8) in the AOmc subgroup (Table 2, Fig. 2). PFS values for years 1-5 are presented in Table 2.

4. Prognostic factors

In univariate analysis, age, preoperative KPS score, tumor location, MGMT methylation status, postoperative residual tumor volume measured in contrast-enhanced T1-weighted MRI (RTV-T1CE), postoperative residual tumor volume measured in T2-weighted MRI (RTV-T2), EOR-T1CE, and EOR measured in T2-weighted MRI (EOR-T2) were statistically significant prognostic factors for OS and PFS (Table 3).

In the multivariate analysis, age, preoperative KPS, *MGMT* methylation status, RTV-T1CE, RTV-T2 and EOR-T2 were

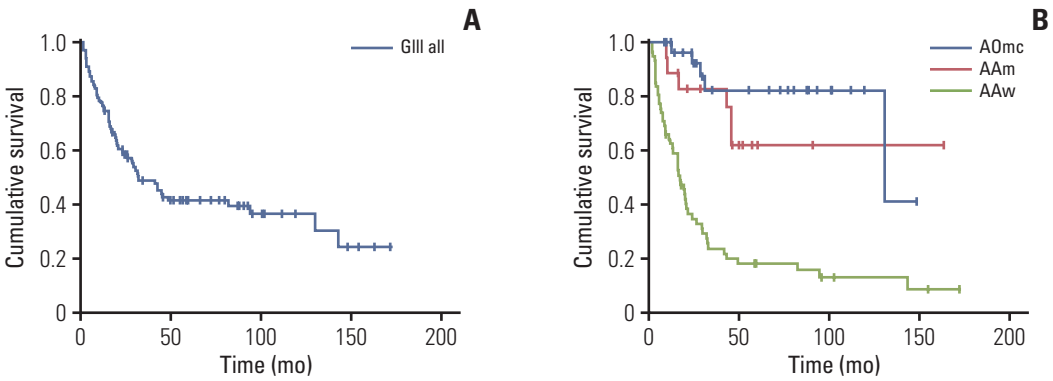

Fig. 2. Progression-free survival. (A) Kaplan-Meier representation of progression-free survival time for the entire group of 113 patients. (B) Kaplan-Meier representation of progression-free survival time for the AAw, AAm, AOmc each group. AAm, anaplastic astrocytoma, IDH-mutant; AAw, anaplastic astrocytoma, *IDH*-wildtype; AOmc, anaplastic oligodendroglioma, *IDH*-mutant and *1p/19q*-codeleted; GIII, grade III glioma.

Table 3. Univariate analysis of prognostic factors

	OS		PFS	
	HR (95% CI)	p-value	HR (95% CI)	p-value
Age	1.025 (1.008-1.042)	0.004	1.022 (1.006-1.038)	0.008
Sex	1.248 (0.729-2.135)	0.419	1.436 (0.856-2.408)	0.170
Preoperative KPS score	0.911 (0.866-0.958)	< 0.001	0.932 (0.893-0.972)	0.001
Deep location	0.333 (0.193-0.577)	< 0.001	0.316 (0.186-0.537)	< 0.001
MGMT methylation status	0.405 (0.236-0.694)	0.001	0.418 (0.251-0.696)	0.001
Chemotherapy	0.727 (0.427-1.237)	0.240	0.744 (0.450-1.231)	0.250
Preoperative T1CE tumor volume	1.006 (0.998-1.015)	0.160	1.005 (0.996-1.014)	0.296
Preoperative T2 tumor volume	0.995 (0.990-1.000)	0.073	0.995 (0.991-1.000)	0.057
Postoperative T1CE tumor volume	1.155 (1.085-1.229)	< 0.001	1.119 (1.058-1.184)	< 0.001
Postoperative T2 tumor volume	1.019 (1.009-1.030)	< 0.001	1.015 (1.006-1.025)	0.001
EOR (T1CE %)	0.985 (0.973-0.997)	0.013	0.986 (0.974-0.998)	0.018
EOR (T2 %)	0.976 (0.964-0.987)	< 0.001	0.977 (0.966-0.988)	< 0.001

OS, overall survival; PFS, progression-free survival; HR, hazard ratio; CI, confidence interval; KPS, Karnofsky performance status; MGMT, O^6-methylguanine-DNA methyltransferase; T1CE, T1-weighted contrast-enhanced magnetic resonance ima-ging (MRI); T2, T2-weighted MRI; EOR, extent of resection.

also statistically significant prognostic factor for OS, while age, *MGMT* methylation status, RTV-T1CE, RTV-T2, and EOR-T2 were statistically significant prognostic factors for PFS (Table 4).

5. Cut-off value of EOR

In cut-off value analysis using the Contal and O'Quigley method, age < 51 years, complete resection of the enhanced portion (99.96%), and more than 85.64% resection of the non-enhanced tumor portion showed prognostic impacts on OS in patients with anaplastic gliomas (Table 5, Fig. 3). As for PFS, age < 55 years, 72.73% resection of the contrast-enhanced portion, and 84.88% resection of the non-enhanced tumor portion demonstrated prognostic impacts (Table 5, Fig. 4).

Discussion

Despite multimodal treatment with surgery, radiotherapy, and chemotherapy, the prognosis for anaplastic glioma is poor. Several reports published in the past decade have shown survival times ranging from 19 months to 14.7 years for anaplastic gliomas [3,4,6-11]. Because of these varied prognoses, a new WHO 2016 classification, based on molecular markers, has been developed to promote more detailed and accurate diagnosis. Our study of 113 patients with anaplastic gliomas analyzed the survival, prognostic factors, and the cut-off value of extent of tumor resection, according to the 2016 WHO classification. Moreover, we found that the OS after surgery was 48.4 months for all anaplastic gliomas

Table 4. Multivariate analysis of prognostic factors

Variable	OS		PFS	
	HR (95% CI)	p-value	HR (95% CI)	p-value
Age	1.068 (1.023-1.115)	0.003	1.073 (1.029-1.118)	0.001
Preop KPS	0.889 (0.805-0.981)	0.019	0.921 (0.847-1.001)	0.052
Deep location	0.302 (0.083-1.101)	0.070	0.334 (0.104-1.077)	0.066
MGMT methylation status	0.150 (0.037-0.613)	0.008	0.092 (0.022-0.381)	0.001
Postoperative T1CE tumor volume	1.301 (1.056-1.602)	0.013	1.335 (1.071-1.663)	0.010
Postoperative T2 tumor volume	1.054 (1.009-1.100)	0.019	1.076 (1.027-1.129)	0.002
EOR (T1CE %)	0.999 (0.975-1.024)	0.925	0.993 (0.969-1.017)	0.578
EOR (T2 %)	0.951 (0.915-0.988)	0.010	0.942 (0.907-0.978)	0.002

OS, overall survival; PFS, progression-free survival; HR, hazard ratio; CI, confidence interval; KPS, Karnofsky performance status; MGMT, O^6-methylguanine-DNA methyltransferase; T1CE, T1-weighted contrast-enhanced magnetic resonance imaging (MRI); T2, T2-weighted MRI; EOR, extent of resection.

Table 5. Cut-off point (Contal and O'Quigley method)

Variable	OS			PFS		
	Cut point	HR (95% CI)	p-value	Cut point	HR (95% CI)	p-value
Age	≥ 51	2.911 (1.880-4.508)	< 0.001	≥ 55	2.971 (1.942-4.545)	< 0.001
EOR (T1CE %)	≥ 99.957	0.284 (0.154-0.524)	< 0.001	≥ 72.727	0.370 (0.227-0.602)	< 0.001
EOR (T2 %)	≥ 85.643	0.141 (0.075-0.267)	< 0.001	≥ 84.883	0.193 (0.112-0.331)	< 0.001

OS, overall survival; PFS, progression-free survival; HR, hazard ratio; CI, confidence interval; EOR, extent of resection; T1CE, T1-weighted contrast-enhanced magnetic resonance imaging (MRI); T2, T2-weighted MRI.

and 21.5 months in the AAw subgroup (Table 2).

Previously reported prognostic factors for anaplastic glioma include advanced patient age, preoperative neurological status, KPS, symptom duration, tumor location, EOR, adjuvant therapy (including radiation therapy and chemotherapy), preoperative MRI findings, as well as various molecular markers including *IDH* and *PTEN* mutations, 1p/19q codeletion, epidermal growth factor receptor (*EGFR*) amplification, and *MGMT* methylation [4,7-9,12-15]. The importance of these molecular markers for prognosis was reflected in the new WHO classification of 2016, which has had a great impact on the diagnostic criteria. Here, we have confirmed several prognostic factors including age, preoperative KPS, *MGMT* methylation status, postoperative tumor volume, and EOR.

Aggressive tumor resection can be dangerous for the patient's neurologic function, especially when the tumor is located deep inside the brain. Thus, when evaluating the association between survival and the EOR, it is important to take the tumor's location into account. In our series, tumor location was a statistically significant prognostic factor in univariate analysis, but its effect was lost in multivariate analysis. In addition, the association between preoperative tumor volume and survival rate was not statistically significant. These results suggest that the degree of surgical removal has a greater effect on the prognosis than the preoperative size and location.

In our univariate analysis, postoperative residual tumor volume and EOR were statistically significant prognostic factors for OS and PFS. This suggests that the extent of surgical resection and remaining tumor volume after surgery may have greater impacts on prognosis than preoperative volume (Table 3). However, in multivariate analysis, RTV-T1CE, RTV-T2, and EOR-T2 were statistically important prognostic factors (Table 4). The statistical insignificance of EOR-T1CE in multivariate analysis appears to be an effect of T2 lesions. Basically, T1 contrast-enhanced lesions are included in T2 lesions. Therefore, as shown in previous studies, we hypothesize that the EOR-T1CE still has significant prognostic value, and a study of the EOR cut-off value can be performed.

Malignant astrocytomas, including anaplastic glioma and glioblastoma multiforme, are difficult to resect curatively because of their invasive and infiltrative nature to the surrounding tissue [16]. This is especially difficult if the tumor is located in a functionally important region. However, microsurgical resection is a very important factor in the treatment of glioma, and maximal safe resection is known to be a good prognostic factor for all grades of gliomas [17-22].

In past, some studies had reported that there is no relationship between the EOR and survival in anaplastic gliomas

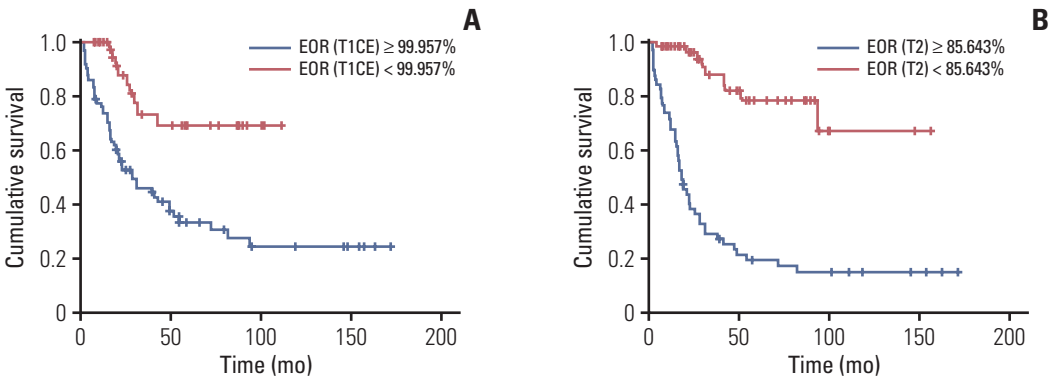

Fig. 3. Overall survival. (A) Kaplan-Meier representation of overall survival time according to EOR (T1CE). (B) Kaplan-Meier representation of overall survival time according to EOR (T2). EOR, extent of resection; T1CE, T1-weighted contrast-enhanced magnetic resonance imaging (MRI); T2, T2-weighted MRI.

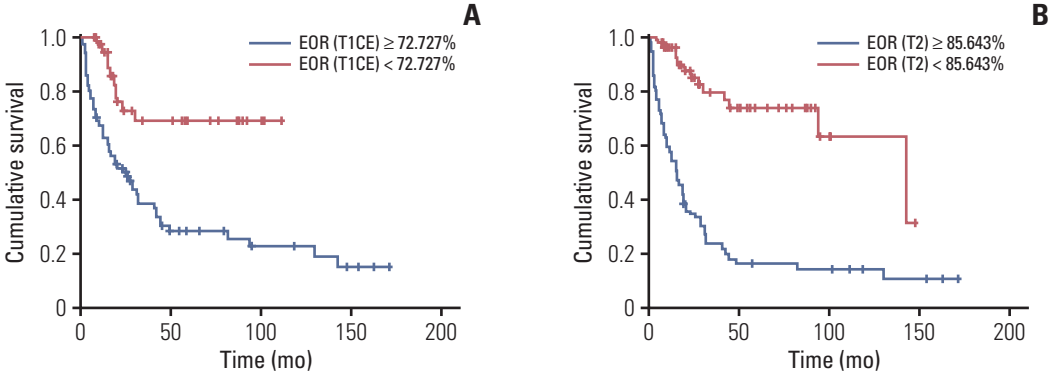

Fig. 4. Progression-free survival. (A) Kaplan-Meier representation of progression-free survival time according to EOR (T1CE). (B) Kaplan-Meier representation of progression-free survival time according to EOR (T2). EOR, extent of resection; T1CE, T1-weighted contrast-enhanced magnetic resonance imaging (MRI); T2, T2-weighted MRI.

[23,24]. However, recent studies have revealed that there is a relationship between the EOR and survival in anaplastic gliomas [3,25,26]. We performed volumetric analysis in the present study, confined to anaplastic gliomas, which have heterogenous features in MRI. A considerable proportion of anaplastic gliomas do not show contrast enhancement in T1-weighted MRI [15,17]. Therefore, to obtain a more accurate tumor volume, both abnormal T2/FLAIR hyperintense lesions as well as T1-weighted contrast-enhanced lesions should be considered. Previous studies analyzed EOR by combining tumor volume measured in T1-weighted contrast-enhanced images with that of T2/FLAIR image or T2 image alone [25,26]. To obtain more accurate information, we analyzed T2-weighted and T1 contrast-enhanced images separately and attempted to determine whether the EOR of each sequence affects survival rate.

Previous studies have found EOR thresholds of 76% in GIII glioma, 90% in GII glioma, 100% contrast enhancing resection with additional 53.21% of FLAIR hyperintense lesion in glioblastoma, and 53% in anaplastic astrocytoma and anaplastic oligoastrocytoma [18,22,25,26].

We investigated the cut-off value for the EOR on each MRI sequence (Table 5). The cut-off value of EOR affecting OS was 99.96% in contrast-enhanced T1-weighted MRI and 85.64% in T2-weighted MRI, so we propose that these EOR values are important for anaplastic gliomas. The use of multiple MRI sequences for suggesting the cut-off value of the volumetric EOR represents a strength of our study in the era of molecular glioma classification.

Age has already been identified as an important prognostic factor in several studies [3,7,24]. For example, a study has reported that an age of 65 years or older is a poor prognostic factor [27]. In the present study, we confirmed that age is an important factor affecting survival: 51 years old was the cut-off value that influenced the OS rate, while a cut-off of 55 years affected PFS.

Our study has some limitations. First, because of its retrospective nature from a single institution, there may be a selection bias of the patients. A few cases were excluded because of inadequate information of MRI available for

review. However, we tried to analyze a uniform patient population by examining consecutive patients. Second, there may be measuring bias. Because we measured T2-weighted hyperintense lesions separately, cerebral edema, ischemic change, and contusions may have been included to tumor volume in some degree. Third, patients have received various chemotherapeutic agents although the regimens of chemotherapy did not have a statistical significance in univariate analysis. And the postoperative radiation therapy was not controlled. In the future, more controlled multicenter validation studies are required.

In conclusion, the median OS was 48.4 months in the whole anaplastic glioma group and 21.5 months in the AAw group. We have also revealed that complete resection (more than 99.96%) of tumor volume measured in contrast-enhanced T1-weighted MRI, and more than 85.64% of tumor resection measured in T2-weighted MRI, have prognostic impacts on the survival of patients with anaplastic gliomas. Therefore, gross-total resection of at least the contrast-enhanced part of a lesion should be performed to prolong survival in anaplastic glioma patients.

Conflict of Interest

Conflict of interest relevant to this article was not reported.

Acknowledgments

This study was supported by the National Research Foundation of Korea (NRF) grant funded by the Korean government (NRF-2014R1A1A2058058) and a faculty research grant of Yonsei University College of Medicine (6-2018-0061).

References

1. Ostrom QT, Gittleman H, Fulop J, Liu M, Blanda R, Kromer C, et al. CBTRUS statistical report: primary brain and central nervous system tumors diagnosed in the United States in 2008-2012. Neuro Oncol. 2015;17 Suppl 4:iv1-62.
2. Louis DN, Perry A, Reifenberger G, von Deimling A, Figarella-Branger D, Cavenee WK, et al. The 2016 World Health Organization classification of tumors of the central nervous system: a summary. Acta Neuropathol. 2016;131:803-20.
3. Nuno M, Birch K, Mukherjee D, Sarmiento JM, Black KL, Patil CG. Survival and prognostic factors of anaplastic gliomas. Neurosurgery. 2013;73:458-65.
4. Rogne SG, Konglund A, Scheie D, Helseth E, Meling TR. Anaplastic astrocytomas: survival and prognostic factors in a surgical series. Acta Neurochir (Wien). 2014;156:1053-61.
5. Contal C, O'Quigley J. An application of changepoint methods in studying the effect of age on survival in breast cancer. Comput Stat Data Anal. 1999;30:253-70.
6. Cairncross G, Wang M, Shaw E, Jenkins R, Brachman D, Buckner J, et al. Phase III trial of chemoradiotherapy for anaplastic oligodendroglioma: long-term results of RTOG 9402. J Clin Oncol. 2013;31:337-43.
7. Chaichana KL, Kosztowski T, Niranjan A, Olivi A, Weingart JD, Laterra J, et al. Prognostic significance of contrast-enhancing anaplastic astrocytomas in adults. J Neurosurg. 2010;113:286-92.
8. van den Bent MJ, Brandes AA, Taphoorn MJ, Kros JM, Kouwenhoven MC, Delattre JY, et al. Adjuvant procarbazine, lomustine, and vincristine chemotherapy in newly diagnosed anaplastic oligodendroglioma: long-term follow-up of EORTC brain tumor group study 26951. J Clin Oncol. 2013;31:344-50.
9. Wick W, Hartmann C, Engel C, Stoffels M, Felsberg J, Stockhammer F, et al. NOA-04 randomized phase III trial of sequential radiochemotherapy of anaplastic glioma with procarbazine, lomustine, and vincristine or temozolomide. J Clin Oncol. 2009;27:5874-80.10.
10. Wick W, Roth P, Hartmann C, Hau P, Nakamura M, Stockhammer F, et al. Long-term analysis of the NOA-04 randomized phase III trial of sequential radiochemotherapy of anaplastic glioma with PCV or temozolomide. Neuro Oncol. 2016;18:1529-37.
11. Hildebrand J, Gorlia T, Kros JM, Afra D, Frenay M, Omuro A, et al. Adjuvant dibromodulcitol and BCNU chemotherapy in anaplastic astrocytoma: results of a randomised European Organisation for Research and Treatment of Cancer phase III study (EORTC study 26882). Eur J Cancer. 2008;44:1210-6.
12. Hartmann C, Hentschel B, Wick W, Capper D, Felsberg J, Simon M, et al. Patients with IDH1 wild type anaplastic astrocytomas exhibit worse prognosis than IDH1-mutated glioblastomas, and IDH1 mutation status accounts for the unfavorable prognostic effect of higher age: implications for classification of gliomas. Acta Neuropathol. 2010;120:707-18.
13. Paleologos NA, Merrell RT. Anaplastic glioma. Curr Treat Options Neurol. 2012;14:381-90.
14. Stupp R, Reni M, Gatta G, Mazza E, Vecht C. Anaplastic astrocytoma in adults. Crit Rev Oncol Hematol. 2007;63:72-80.
15. Wang Y, Wang K, Wang J, Li S, Ma J, Dai J, et al. Identifying the association between contrast enhancement pattern, surgical resection, and prognosis in anaplastic glioma patients. Neuroradiology. 2016;58:367-74.
16. Claes A, Idema AJ, Wesseling P. Diffuse glioma growth: a guerilla war. Acta Neuropathol. 2007;114:443-58.
17. Keles GE, Chang EF, Lamborn KR, Tihan T, Chang CJ, Chang SM, et al. Volumetric extent of resection and residual contrast enhancement on initial surgery as predictors of outcome in adult patients with hemispheric anaplastic astrocytoma. J Neurosurg. 2006;105:34-40.
18. Li YM, Suki D, Hess K, Sawaya R. The influence of maximum safe resection of glioblastoma on survival in 1229 patients: can we do better than gross-total resection? J Neurosurg. 2016;124:977-88.
19. McGirt MJ, Chaichana KL, Gathinji M, Attenello FJ, Than K, Olivi A, et al. Independent association of extent of resection

with survival in patients with malignant brain astrocytoma. J Neurosurg. 2009;110:156-62.
20. Nitta M, Muragaki Y, Maruyama T, Ikuta S, Komori T, Maebayashi K, et al. Proposed therapeutic strategy for adult low-grade glioma based on aggressive tumor resection. Neurosurg Focus. 2015;38:E7.
21. Sanai N, Polley MY, McDermott MW, Parsa AT, Berger MS. An extent of resection threshold for newly diagnosed glioblastomas. J Neurosurg. 2011;115:3-8.
22. Smith JS, Chang EF, Lamborn KR, Chang SM, Prados MD, Cha S, et al. Role of extent of resection in the long-term outcome of low-grade hemispheric gliomas. J Clin Oncol. 2008;26:1338-45.
23. Devaux BC, O'Fallon JR, Kelly PJ. Resection, biopsy, and survival in malignant glial neoplasms: a retrospective study of clinical parameters, therapy, and outcome. J Neurosurg. 1993; 78:767-75.
24. Tortosa A, Vinolas N, Villa S, Verger E, Gil JM, Brell M, et al. Prognostic implication of clinical, radiologic, and pathologic features in patients with anaplastic gliomas. Cancer. 2003;97: 1063-71.
25. Fujii Y, Muragaki Y, Maruyama T, Nitta M, Saito T, Ikuta S, et al. Threshold of the extent of resection for WHO grade III gliomas: retrospective volumetric analysis of 122 cases using intraoperative MRI. J Neurosurg. 2018;129:1-9.
26. Pessina F, Navarria P, Cozzi L, Ascolese AM, Simonelli M, Santoro A, et al. Value of surgical resection in patients with newly diagnosed grade III glioma treated in a multimodal approach: surgery, chemotherapy and radiotherapy. Ann Surg Oncol. 2016;23:3040-6.
27. Tanaka S, Meyer FB, Buckner JC, Uhm JH, Yan ES, Parney IF. Presentation, management, and outcome of elderly patients with newly-diagnosed anaplastic astrocytoma. J Neurooncol. 2012;110:227-35.

pISSN 1598-2998, eISSN 2005-9256

Cancer Res Treat. 2020;52(4):1050-1058 https://doi.org/10.4143/crt.2020.437

Original Article Open Access

Comparison between Craniospinal Irradiation and Limited-Field Radiation in Patients with Non-metastatic Bifocal Germinoma

Bo Li, MD, PhD[1,2]
Wenyi Lv, MM[1]
Chunde Li, MD[3]
Jiongxian Yang, MD[4]
Jiajia Chen, MD[5]
Jin Feng, MD[1]
Li Chen, MD[1]
Zhenyu Ma, MD[3]
Youqi Li, MM[1]
Jiayi Wang, MM[1]
Yanwei Liu, MD, PhD[1]
Yanong Li, MM[1]
Shuai Liu, MD, PhD[1]
Shiqi Luo, MD[3]
Xiaoguang Qiu, MD[1,2]

**A list of author's affiliations appears at the end of the paper.*

Correspondence: Shiqi Luo, MD
Department of Neurosurgery, Beijing Tiantan Hospital, Capital Medical University, No. 119, South 4th Ring West Road, Fengtai District, Beijing 100070, China
Tel: 86-10-67098006
Fax: 86-10-67098006
E-mail: bjthlsq@protonmail.com

Co-correspondence: Xiaoguang Qiu, MD
Department of Radiation Oncology, Beijing Tiantan Hospital, Capital Medical University, No. 119, South 4th Ring West Road, Fengtai District, Beijing 100070, China
Tel: 86-10-59975582
Fax: 86-10-67098587
E-mail: qiuxiaoguang@bjtth.org

Received May 9, 2020
Accepted July 8, 2020
Published Online July 9, 2020

*Bo Li and Wenyi Lv contributed equally to this work.

Purpose

Whether craniospinal irradiation (CSI) could be replaced by limited-field radiation in non-metastatic bifocal germinoma remains controversial. We addressed the issue based on the data from our series and the literature.

Materials and Methods

Data from 49 patients diagnosed with non-metastatic bifocal germinoma at our hospital during the last 10 years were collected. The Pediatric Quality of Life Inventory 4.0 was used to evaluate health-related quality of life (HRQOL). Additionally, 81 patients identified from the literature were also analyzed independently.

Results

In our cohort, 34 patients had tumors in the sellar/suprasellar (S/SS) plus pineal gland (PG) regions and 15 in the S/SS plus basal ganglia/thalamus (BG/T) regions. The median follow-up period was 52 months (range, 10 to 134 months). Our survival analysis showed that patients treated with CSI (n=12) or whole-brain radiotherapy (WBRT; n=34) had comparable disease-free survival (DFS; p=0.540), but better DFS than those treated with focal radiotherapy (FR; n=3, p=0.016). All 81 patients from the literature had tumors in the S/SS+PG regions. Relapses were documented in 4/45 patients treated with FR, 2/17 treated with whole-ventricle irradiation, 0/4 treated with WBRT, and 1/15 treated with CSI. Survival analysis did not reveal DFS differences between the types of radiation field (p=0.785). HRQOL analysis (n=44) in our cohort found that, compared with S/SS+PG germinoma, patients with BG/T involvement had significantly lower scores in social and school domains. However, HRQOL difference between patients treated with CSI and those not treated with CSI was not significant.

Conclusion

In patients with non-metastatic bifocal germinoma, it is rational that CSI could be replaced by limited-field radiation. HRQOL in patients with BG/T involvement was poorer.

Key words

Germinoma, Bifocal germinoma, Radiotherapy, Quality of life

Introduction

Intracranial germinoma is a rare malignancy mostly identified in children and adolescents. The incidence varies substantially across the continents, with North American and international data showing overall incidence of 0.6/million/yr in United States, 1.0/million/yr in Europe, 1.7/million/yr in Korea, and 2.7/million/yr in Japan [1,2]. The sellar/suprasellar (S/SS), pineal gland (PG), and basal ganglia/thalamus (BG/T) regions are the most common areas in which germinoma occurs, accounting for 23%-35%, 37%-66%, and 0%-8% of cases, respectively [2-5].

Craniospinal irradiation (CSI) used to be the standard of care for patients with germinoma. Although more than 90% of patients show long-term disease control, toxicities related to CSI are still concerning [6,7]. Thus, many researchers explored the possibility of limited-field irradiation such as focal radiotherapy (FR), whole ventricular irradiation (WVI), or whole-brain radiotherapy (WBRT) [8-11]. The emerging results showed that, combined with chemotherapy, reduction in the radiation dose and/or radiation field did not compromise the long-term survival of patients with localized disease. Interestingly, in clinical practice, some rare patients had synchronous lesions involving two intracranial locations; these cases are called bifocal germinoma. As dissemination within the central nervous system is characteristic of germinoma, treatment of cases with bifocal involvement is a dilemma at the time of decision-making, especially for radiation field selection.

Some pioneer researchers addressed the issue of bifocal germinoma treatment on the basis of their experience, and indicated that extended-field radiation could be avoided, if there is no evidence of metastasis or dissemination [12-14]. However, due to the scarcity of the disease, few studies have compared the difference between the above-mentioned radiation fields. Thus, evidence is still required to clarify the issue.

Classically, bifocal germinoma refers to patients with synchronous lesions involving S/SS and PG regions. However, we also identified a number of patients who have synchronous lesions involving S/SS and BG/T regions (Fig. 1, S1 Fig.). In the current study, we grouped them under the concept of bifocal germinoma and analyzed them together. Radiation strategies for patients with bifocal germinoma at our institute have evolved over the decades. Both CSI and FR were treatment options in the early years until WBRT became the standard of care. Here, we retrospectively analyzed clinical data from 49 patients to examine the survival of patients treated with different radiation fields. Moreover, we also independently analyzed 81 patients from the literature. In addition, since the long-term health-related quality of life (HRQOL) is another important factor that should be weighted at the time of radiation field selection, these data were also included in our study.

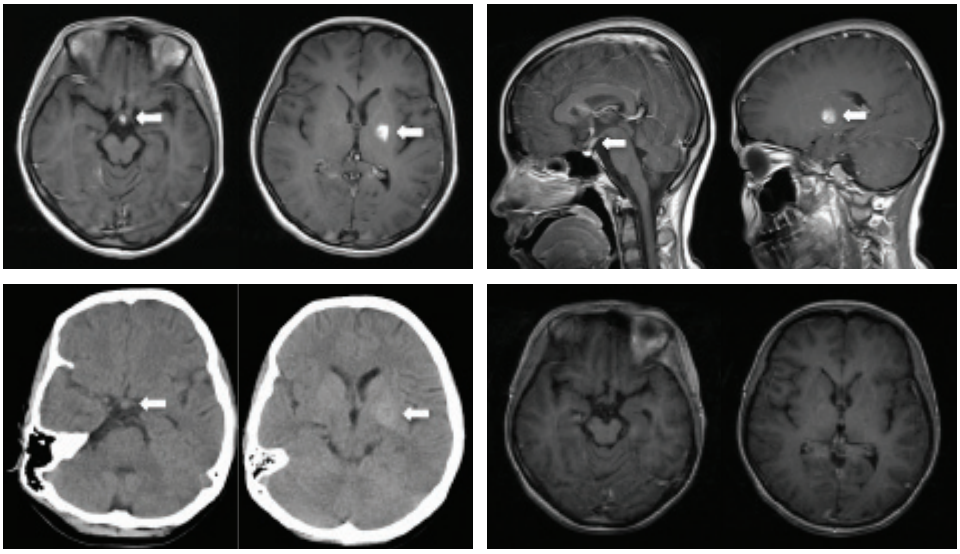

Fig. 1. Images of an 18-year-old girl who presented with right hemiparesis and adipsic diabetes insipitus. β-Human chorionic gonadotropin in the serum and cerebrospinal fluid was 39.4 IU/L and 77.2 IU/L, respectively. Radiological examinations revealed lesions located in the sellar and left thalamus area (tumors were indicated by the arrows). The first row shows axial and sagittal graphics on contrast-enhanced magnetic resonance image. Pituitary stalk enhancement and a left thalamus lesion with enhancement can be seen. The second row shows images on plain computed tomography scan. Lesions showed slightly higher intensity compared to the surrounding normal tissues. She was diagnosed as bifocal germinoma and chemoradiotherapy was applied. The third row shows the complete remission of the lesions after treatment.

Materials and Methods

1. Patients

Clinical data from 49 patients who were diagnosed with bifocal germinoma between January 2008 and January 2018 were analyzed. Diagnosis was established on the basis of histology and/or tumor makers (β-human chorionic gonadotropin [β-HCG] ≤ 100 IU/L and α-fetoprotein normal). Before treatment, all patients underwent baseline evaluation, including physical examination, blood tests, and radiographic examinations. Metastases were defined as any additional lesions documented on radiographic examinations and/or positive cerebrospinal fluid (CSF) cytology.

Considering the treatment strategy, two cycles of platinum-based chemotherapy (ifosfamide 1.5 g/m^2 days 1-3, etoposide 70 mg/m^2 days 1-3, and cisplatin 30 mg/m^2 days 1-3, repeated every 4 weeks) were initially performed after diagnosis. Subsequently, radiotherapy was applied and two additional cycles of chemotherapy were performed thereafter. The standard radiation dose in the current cohort was 40 Gy. In terms of radiation field at our institute, both FR and CSI (30 Gy) plus boosts had been considered for patients with bifocal disease, until WBRT (30 Gy) plus boost became the standard of care in 2008. Then, CSI plus boost was performed only in patients with evidence of metastases. Radiotherapy was applied at a daily dose of 1.6-1.8 Gy with five weekly fractions over 4.5-5 weeks. The gross target volume (GTV) was defined as the extent of the primary tumor(s) before treatment. The clinical target volume (CTV) was obtained by adding 0.5 cm to GTV. Additional 0.5-1 cm was added to CTV to create planning target volume (PTV). After treatment completion, routine follow-up was performed every 3-6 months for the first two years and every 6-12 months for the next 3 years.

2. Data from the literature

PubMed was used for literature searching. Patients who were eligible for the analysis must have information regarding diagnosis, tumor location, radiation field, radiation dose, chemotherapy, relapse status, and time to relapse. In addition, information about the age, sex, serum/CSF β-HCG level, CSF cytology results, and spinal magnetic resonance imaging (MRI) status were collected vigorously.

3. Health-related quality of life (HRQOL)

The Pediatric Quality of Life Inventory 4.0 (PedsQL 4.0) scale was used to evaluate HRQOL. The PedsQL 4.0 Generic Core Scale contains 23 items, which measure physical (eight items), emotional (five items), social (five items), and school functions (five items). HRQOL was provided as age-appropriate surveys for young children (5-7 years old), children (8-12 years old), teens (13-18 years old), young adults (18-25 years old), and adults (> 26 years old). The PedsQL 4.0 Generic Core Scale comprises parallel patient self-report and parent proxy-report formats. Items were reverse-scored and transformed to a 0-100 scale according to instructions, thus higher scores indicate better HRQOL. We attempted to contact all surviving patients via phone, and those who could be contacted received the electronic version of the PedsQL scale via e-mail and cell phone.

4. Statistical analysis

IBM SPSS Statistics for Windows, ver. 22.0 (IBM Corp., Armonk, NY), was used for data analysis. t test was employed for PedsQL scores analyses, which were considered as continuous variables. The Kaplan-Meier method was used to estimate survival. Disease-free survival (DFS) was calculated from the date of complete remission to the date of disease relapse. Disease relapse was defined as an elevation of tumor marker levels in the serum and/or CSF, the appearance of any new lesions on radiographic examinations, or both. Overall survival (OS) was determined from the date of diagnosis to the date of death or the last follow-up visit. Log-rank tests were used to compare survival curves. All statistical analyses used a significance level of 0.05, and all statistical tests were two-sided.

5. Ethical statement

This study was reviewed and approved by the Institutional Review Board of Beijing Tiantan Hospital (grant number: KY 2018-064-02). Informed written consent from patients was waived by the Institutional Review Board of Beijing Tiantan Hospital due to the retrospective study design.

Results

1. Patient characteristics

Among 49 patients included in our study, 34 were males (69.4%). The median age was 13 years (range, 5 to 47 years). Thirty-four patients had their lesions located in the S/SS and PG regions, while 15 patients had their lesions located in the S/SS and BG/T regions. Diagnosis was established based on histology in 13 patients and on levels of serum tumor markers in 36 patients. The non-metastatic status was determined based on both spinal MRI and CSF cytology in 46 patients. The remaining three patients showed negative findings on spinal MRI but had no CSF cytology data due to potential high intracranial pressure. In terms of radiotherapy, three patients underwent FR, 34 patients underwent WBRT plus boost, and 12 underwent CSI plus boost. The total radiation dose was 3,960 cGy in 43 patients, 4,500 cGy in two patients, and 5,040 in four patients. All but two patients in the CSI group received chemotherapy (Table 1).

The most common symptom was adipsic diabetes insipidus, which was documented in 44 patients (89.7%). Visual

Table 1. Patient characteristics

Characteristic	Our cohort (n=49)	Literature cohort (n=81)
Age, median (range, yr)	13 (5-47)	14 (4-28)
Not available	0	41
Primary tumor location		
S/SS+PG	34 (69.4)	81 (100)
S/SS+BG/T	15 (30.6)	0
Sex		
Male	34 (69.4)	27 (33.3)
Female	15 (30.6)	13 (16.0)
Not available	0	41 (50.7)
Method used to make the diagnosis		
Histology	13 (26.5)	64 (79.0)
TM	36 (73.5)	5 (6.2)
Serum β-HCG (IU/L)	14.56 (0.01-74)	-
CSF β-HCG (IU/L)	11.4 (0.01-87.7)	-
Clinical	0	11 (13.6)
Not available	0	1 (1.2)
Radiotherapy		
FR	3 (6.1)	45 (55.6)
WVI	0	17 (20.9)
WBRT+boost	34 (69.4)	4 (4.9)
CSI+boost	12 (24.5)	15 (18.6)
Dose of radiotherapy (Gy)		
≤ 40	43 (87.7)	56 (69.2)
> 40	6 (12.3)	21 (25.9)
Not available	0	4 (4.9)
Patients treated with chemotherapy	47 (95.9)	55 (67.9)

Values are presented as number (%) unless otherwise indicated. S/SS, sellar/suprasellar; PG, pineal gland; BG/T, basal ganglia/thalamus; TM, tumor marker; β-HCG, β-human chorionic gonadotropin; CSF, cerebrospinal fluid; FR, focal radiotherapy; WVI, whole ventricular irradiation; WBRT, whole-brain radiotherapy; CSI, craniospinal irradiation.

acuity decline was reported by 20 patients (40.8%). Sixteen patients (32.7%) had symptoms related to high intracranial pressure. Physical development abnormality was documented in 17 patients, seven of whom had precocious puberty (all male) and 10 had growth retardation (6 male and 4 female). Among 15 patients with S/SS+BG/T germinoma, five presented with hemiparesis.

2. Survival

The median follow-up period was 52 months (range, 10 to 134 months). The estimated 5-year DFS and OS were 96.7% and 97.3%, respectively. During the follow-up, all patients that underwent FR showed disease relapse. Among them, two patients with S/SS+PG germinoma had relapse in the spine and one patient with S/SS+BG/T germinoma had relapse in the left posterior limb of internal capsule. Only one patient with S/SS+PG germinoma in the WBRT group experienced disease relapse (in the spine); all patients in the CSI group were disease-free at the last follow-up. Survival analysis revealed that patients undergoing FR had the low-

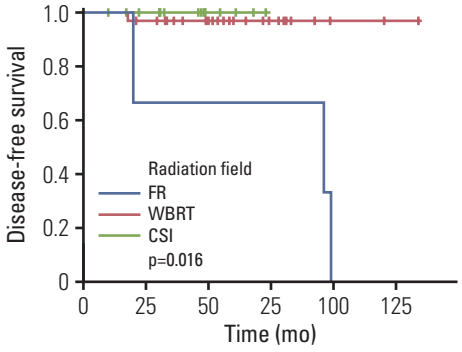

Fig. 2. Comparison of disease-free survival between patients undergoing focal radiotherapy (FR), whole-brain radiotherapy (WBRT), and craniospinal irradiation (CSI) (our cohort). Patients treated with CSI (n=12) or WBRT (n=34) had comparable disease-free survival (p=0.54), but better disease-free survival than those treated with FR (n=3, p=0.016).

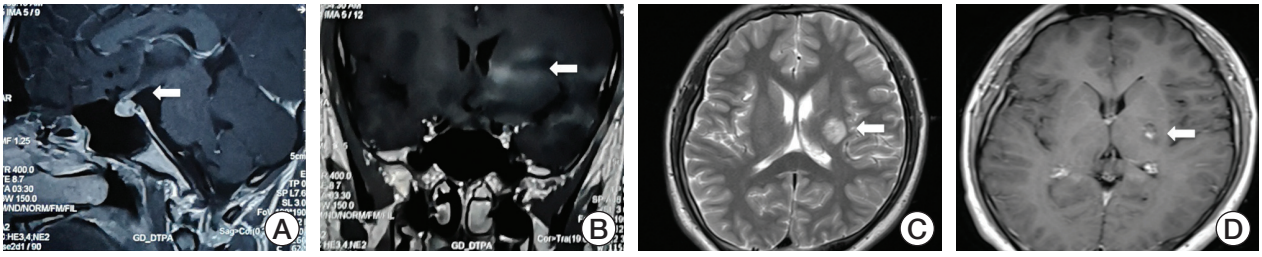

Fig. 3. Images of a 19-year-old boy who presented with adipsic diabetes insipitus only. β-Human chorionic gonadotropin (β-HCG) in the serum and cerebrospinal fluid was 22.4 IU/L and 41.9 IU/L, respectively. (A, B) Radiological examinations revealed pituitary stalk enhancement and left thalamus lesion with enhancement (tumors were indicated by the arrows). Then, four cycles of chemotherapy and focal radiotherapy were applied. (C, D) Twenty months later, enhanced lesion with cyst was identified in the left thalamus area (within the initial radiation field) (tumors were indicated by the arrows). β-HCG in the serum and cerebrospinal fluid was 716 IU/L and 442 IU/L, respectively. Then, salvage chemoradiotherapy was applied.

est DFS (66.6%) (FR vs. WBRT, p=0.008; FR vs. CSI, p=0.046; compared together, p=0.016), while those undergoing either WBRT (96.9%) or CSI (100%) had similar DFS (p=0.540) (Fig. 2).

At the time of relapse, three patients had negative serum/CSF β-HCG and serum β-HCG was 716 IU/L in the fourth patient (Fig. 3). Subsequently, four cycles of chemotherapy and CSI were applied. All patients have been successfully rescued and were disease-free at the last follow-up. The only death in the current cohort was documented in a male patient with histology-proven diagnosis, who underwent WBRT initially. Six years after treatment, left basal ganglia lesion was identified and biopsied. Histology indicated high-grade glioma. He died 2 months later. Consequently, the five-year OS was 100%, 90.9%, and 100% in FR, WBRT, and CSI groups, respectively (p=0.834).

3. Literature cohort

Totally, 81 non-metastatic bifocal germinoma patients were identified from the literature based on the authors' definition [9,12-22]. However, only 51 patients could be confirmed as both spinal MRI negative and CSF cytology negative. All patients had tumors in S/SS and PG regions. In terms of diagnosis, 64 patients were histology-proven, five showed elevated tumor markers, 11 were diagnosed clinically, and one had no available information. Relapses were documented in four of 45 receiving FR, two of 17 receiving whole-ventricle irradiation, 0 of 4 receiving WBRT, and 1 of 15 receiving CSI. DFS was not significantly different between radiation fields (p=0.785) (Fig. 4).

Out of seven relapsed patients, four had spinal lesions. All but one patient received subsequent salvage therapy, including chemoradiotherapy in five and chemotherapy alone in one patient. All were alive at the last follow-up (S2 Table).

4. HRQOL

Out of 48 surviving patients, 46 responded to our survey

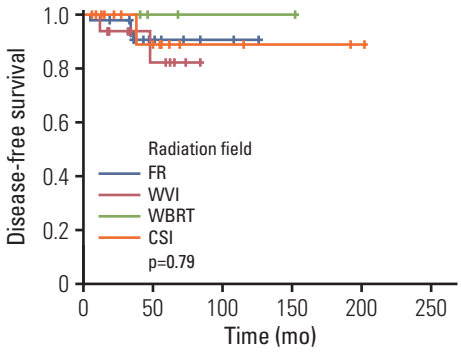

Fig. 4. Comparison of disease-free survival between patients undergoing focal radiotherapy (FR), whole-ventricle irradiation (WVI), whole-brain radiotherapy (WBRT), and craniospinal irradiation (CSI) (literature cohort). Survival analysis did not reveal disease-free survival differences between the types of radiation field (p=0.79).

with 44 having valid paired surveys. Subgroup analysis did not find HRQOL differences between sexes, radiation fields and dose. However, patients with S/SS+BG/T germinoma showed generally lower scores than those with S/SS+PG germinoma. Furthermore, their proxy-report total (p=0.001), emotional score (p=0.020), social score (p=0.018), school score (p=0.001) as well as self-report social score (p=0.024), and school score (p=0.012) were significantly reduced. Besides, better HRQOL were proved in patients surviving > 5 years compared with those surviving ≤ 5 years (Table 2).

Discussion

During the last decades, treatment strategies for patients with intracranial germinoma have greatly improved. Given the excellent prognosis, the primary goal should be to balance the cure rate against long-term toxicity. Thus, minimiz-

Table 2. PedsQL scores and subgroup analyses

	Total	p-value	Physical health	p-value	Emotional	p-value	Social	p-value	School	p-value
Proxy-report										
Sex										
Male (n=31)	71.5±17.7	0.592	69.2±26.2	0.911	78.3±18.88	0.331	75.0±22.5	0.902	65.0±23.6	0.242
Female (n=13)	66.9±19.7		70.7±31.4		70.0±17.7		73.7±19.5		51.2±26.8	
Origin										
S/SS+PG (n=30)	75.4±17.1	0.001	73.1±29.8	0.372	80.3±16.4	0.020	80.6±19.7	0.018	69.0±19.3	0.001
S/SS+BG/T (n=14)	52.6±7.1		60.0±18.6		59.0±15.5		56.0±11.9		31.0±18.8	
Radiation										
Non-CSI[a] (n=34)	79.2±15.2	0.264	81.2±16.3	0.374	81.2±22.5	0.464	82.5±17.0	0.401	70.0±21.2	0.091
CSI (n=10)	67.3±18.5		66.9±29.5		73.4±17.7		72.5±21.7		56.8±26.0	
Dose (Gy)										
≤ 40 (n=40)	66.5±13.1	0.251	68.7±22.8	0.280	74.6±16.1	0.801	70.0±18.5	0.383	51.3±23.1	0.101
> 40 (n=4)	73.1±18.9		77.1±21.7		73.1±17.8		76.3±22.3		63.6±20.4	
Follow-up (yr)										
≤ 5 (n=25)	59.4±13.4	0.007	63.9±19.1	0.403	64.0±15.3	0.002	63.1±16.3	0.013	44.3±16.7	0.001
> 5 (n=19)	76.8±17.2		72.3±31.8		84.1±14.7		82.5±20.1		70.8±20.9	
Self-report										
Sex										
Male (n=31)	65.0±17.1	0.982	65.9±24.5	0.833	68.5±20.4	0.571	68.5±22.8	0.962	56.5±25.8	0.430
Female (n=13)	64.7±24.9		62.5±36.1		62.0±20.7		69.0±24.5		67.0±18.2	
Origin										
S/SS+PG (n=30)	67.3±19.1	0.081	67.5±28.3	0.073	66.5±21.2	0.921	71.5±22.1	0.024	63.8±21.9	0.012
S/SS+BG/T (n=14)	48.9±12.2		46.8±17.6		65.0±14.1		50.0±21.2		35.0±21.2	
Radiation										
Non-CSI[a] (n=34)	79.3±19.5	0.153	84.3±14.3	0.102	80.0±26.4	0.190	81.6±23.6	0.282	68.3±23.6	0.513
CSI (n=10)	71.3±18.09		59.9±28.37		62.9±18.3		65.4±22.1		57.9±23.9	
Dose (Gy)										
≤ 40 (n=40)	65.2±16.9	0.481	67.3±24.5	0.572	67.7±20.1	0.762	67.2±20.4	0.381	57.2±24.6	0.701
> 40 (n=4)	69.4±14.3		72.0±19.1		70.0±18.1		74.0±18.9		60.3±16.7	
Follow-up (yr)										
≤ 5 (n=25)	58.7±14.3	0.141	60.4±18.2	0.474	60.0±16.0	0.143	64.5±19.3	0.364	49.1±17.2	0.042
> 5 (n=19)	69.8±19.5		68.1±31.0		72.0±20.5		73.0±23.2		67.5±22.2	

Values are presented as mean±standard deviation. S/SS, sellar/suprasellar; PG, pineal gland; BG/T, basal ganglia/thalamus; CSI, craniospinal irradiation. [a]Non-CSI group included two patients undergoing FR and 32 patients undergoing whole-brain radiotherapy.

ing the radiation field and dose is a priority, especially for localized disease. Physicians that treat patients with non-metastatic bifocal germinoma face a similar situation, which is challenging for their decision-making. In United States, bifocal germinoma used to be considered as a metastatic disease, and CSI was applied; however, in Europe, it was considered as a localized disease, and FR was applied [8,9,23]. Although emerging evidence shows that limited-field radiation is feasible in this setting, no data are available on the comparison of the efficacy between different radiation fields owing to the rarity of the disease [14,22].

Due to the development of various radiation strategies in our institute, we have an opportunity to compare the efficacy between different radiation fields. As it was shown in our cohort, CSI and WBRT showed comparable DFS, but better DFS than FR. Because WVI is another commonly used limited-field radiation that was not applied in our cohort, we intended to expand our findings based on the literature [9,12-22]. Among 81 patients identified from the literature, there were 7 relapses, including 4/45 receiving FR, 2/17 receiving WVI, 0/4 receiving WBRT, and 1/15 receiving CSI. Survival analysis in the literature cohort did not reveal any differences between CSI and other types of limited-field radiation. Taken together with the findings from our cohort, it could be advocated that limited-field radiotherapy, such as WVI or WBRT, may be considered as an option for patients with non-metastatic bifocal germinoma. We noticed that, among patients undergoing FR, higher relapse rate was observed in our cohort compared with that from the literature. We attributed it to inadequate margins. In some reports with available information, PTV was defined as 2 cm around primary lesions, where the most ventricular area could be covered due to bifocal origins. However, in our cohort, the minimum margins of the three patients that underwent FR were 1.2 cm, 1.3 cm, and 1.6 cm, which may have increased the possibility of tumor cell seeding. But for patient with higher β-HCG level at relapse, possible non-germinomatous germ cell tumors (NGGCTs) components existing could be responsible.

It is still uncertain whether bifocal lesions that presented synchronously at the time of diagnosis arise simultaneously or metastasize from one to the other. All lesions reported from literatures regarding bifocal cases were located in the S/SS and PG regions. Anatomically, both regions are in close contact with ventricles; therefore, CSF may mediate tumor transfer between these two regions. Furthermore, it is not uncommon that patients with localized S/SS or PG germinoma present with metastatic lesions at these sites at the time of treatment failure. Thus, the rationale of limited-field radiation application could be challenged. Interestingly, we identified a number of bifocal germinoma patients with lesions at S/SS and BG/T regions. Tumors originating from the BG/T region were generally surrounded by brain tissue, which showed no direct correlation with other origins. Thus, bifocal germinoma with S/SS and BG/T involvement probably provides another piece of evidence that bifocal germinoma may arise simultaneously in two regions. Consequently, application of limited-field radiation in patients with bifocal germinoma is justified, especially when no other evidence for metastasis is present.

To date, there are three commonly used limited-radiation fields in this setting, including FR, WVI, and WBRT. Many previous studies have shown that FR could lead to higher risk of relapse [9,11,24]. The relapse pattern showed that patients with S/SS and/or PG germinoma had higher risk of periventricular failure after FR [9,24]. Accordingly, WVI was proposed as potential optimal radiation field. Results from a prospective study showed that, among 23 patients with S/SS or PG germinoma, no one relapsed after WVI after 67 months follow-up [25]. However, in patients with BG/T area involvement, WVI may not be adequate since tumor invades deeply in the brain tissue. Probably due to these concerns, WBRT or CSI were the most commonly attempted radiation fields in published reports [26-28]. In our cohort, all 14 patients with non-metastatic S/SS+BG/T bifocal germinoma receiving WBRT were disease-free during the last visit. Based on our findings, WBRT could be considered as optimal radiation field in this population until new evidence emerges, while WVI should be optimal for patients with non-metastatic S/SS+PG bifocal germinoma.

As it was shown in our cohort, at the time of treatment failure, 3/4 relapses were located in the spinal area. Additionally, out of six patients who relapsed after limited-field radiation in the published data, four had spinal failure. Review of baseline evaluation revealed that CSF cytology and spinal MRI were not available for some patients. In our cohort, one patient with spinal failure did not receive CSF examination at diagnosis due to higher intracranial pressure. Therefore, full evaluation of spinal status seems more important in patients with bifocal germinoma, especially when limited-field radiation was considered. Furthermore, we also noticed that, some patients from the literature cohort were diagnosed clinically. A few physicians empirically treated patients with typical bifocal radiological presentations and negative tumor markers as germinoma patients. However, although rare, α-fetoprotein–negative NGGCTs do exist. Since the treatment strategy is totally different between germinoma and NGGCTs, empirical treatment would be problematic. Thus, histology is strongly recommended, especially in patients with negative tumor markers.

Since the onset of germinoma occurs near puberty, HRQOL is always a concern in long-term survivors. Data from our series showed that the HRQOL of patients surviving > 5 years was better. Another study conducted in brain tumor patients receiving proton therapy showed similar results, which HRQOL improving was documented during follow-

up [29]. Besides, we also found that patients with BG/T involvement had lower scores, especially in social and school domains. This finding was also indicated in other studies, which found that patients with BG/T germ cell tumors had worse HRQOL compared with patients with S/SS or PG germ cell tumors. In terms of treatment, some reports indicated that CSI led to lower PedsQL score and more severe neurocognitive impairments compared with limited-field radiations such as FR or WVI [29,30]. Unfortunately, this difference was not validated in our cohort, which may be attributed to WBRT application. However, given that the more extended treatment volume correlates with the higher probability of late-effects that patients encounter, the application of CSI should be confined where possible.

All in all, in the current study, we compared CSI and other limited-field radiation types in patients with non-metastatic bifocal germinoma. Based on the data both from our institute and published literature, CSI showed no advantage in terms of disease control and survival compared with WVI or WBRT. Thus, it is conceivable that CSI may be replaced by limited-field radiation. Furthermore, the HRQOL of this cohort is generally poor, especially for patients with BG/T involvement.

However, limitations do exist. Limited number of cases is still the main obstacle before the convincible conclusions. Although we recruited data from the literature, the inconsistence of screening, diagnosis, and treatments among authors should be concerned. Thus, multicenter study with unified regimen is warranted for the future investigation.

Electronic Supplementary Material

Supplementary materials are available at Cancer Research and Treatment website (https://www.e-crt.org).

Conflicts of Interest

Conflicts of interest relevant to this article was not reported.

Acknowledgments

This work received financial support from the Beijing Municipal Bureau of Health.

Author Details

[1]Department of Radiation Oncology, Beijing Tiantan Hospital, Capital Medical University, Beijing, [2]Beijing Neurosurgical Institute, Capital Medical University, Beijing, [3]Department of Neurosurgery, Beijing Tiantan Hospital, Capital Medical University, Beijing, [4]Department of Clinical Nutrition, Beijing Children's Hospital, Capital Medical University, Beijing, [5]Centre of Endocrinology Genetics and Metabolism, National Centre for Children's Health, Beijing Children's Hospital, Capital Medical University, Beijing, China

References

1. Lee SH, Jung KW, Ha J, Oh CM, Kim H, Park HJ, et al. Nationwide population-based incidence and survival rates of malignant central nervous system germ cell tumors in Korea, 2005-2012. Cancer Res Treat. 2017;49:494-501.
2. Murray MJ, Horan G, Lowis S, Nicholson JC. Highlights from the Third International Central Nervous System Germ Cell Tumour Symposium: laying the foundations for future consensus. Ecancermedicalscience. 2013;7:333.
3. Gao Y, Jiang J, Liu Q. Clinicopathological and immunohistochemical features of primary central nervous system germ cell tumors: a 24-years experience. Int J Clin Exp Pathol. 2014;7:6965-72.
4. Wong TT, Chen YW, Guo WY, Chang KP, Ho DM, Yen SH. Germinoma involving the basal ganglia in children. Childs Nerv Syst. 2008;24:71-8.
5. Rasalkar DD, Chu WC, Cheng FW, Paunipagar BK, Shing MK, Li CK. Atypical location of germinoma in basal ganglia in adolescents: radiological features and treatment outcomes. Br J Radiol. 2010;83:261-7.
6. Bamberg M, Kortmann RD, Calaminus G, Becker G, Meisner C, Harms D, et al. Radiation therapy for intracranial germinoma: results of the German cooperative prospective trials MAKEI 83/86/89. J Clin Oncol. 1999;17:2585-92.
7. Maity A, Shu HK, Janss A, Belasco JB, Rorke L, Phillips PC, et al. Craniospinal radiation in the treatment of biopsy-proven intracranial germinomas: twenty-five years' experience in a single center. Int J Radiat Oncol Biol Phys. 2004;58:1165-70.
8. Calaminus G, Frappaz D, Kortmann RD, Krefeld B, Saran F, Pietsch T, et al. Outcome of patients with intracranial non-germinomatous germ cell tumors-lessons from the SIOP-CNS-GCT-96 trial. Neuro Oncol. 2017;19:1661-72.
9. Calaminus G, Kortmann R, Worch J, Nicholson JC, Alapetite C, Garre ML, et al. SIOP CNS GCT 96: final report of outcome of a prospective, multinational nonrandomized trial for children and adults with intracranial germinoma, comparing craniospinal irradiation alone with chemotherapy followed by focal primary site irradiation for patients with localized disease. Neuro Oncol. 2013;15:788-96.
10. Goldman S, Bouffet E, Fisher PG, Allen JC, Robertson PL, Chuba PJ, et al. Phase II trial assessing the ability of neoadjuvant chemotherapy with or without second-look surgery to eliminate measurable disease for nongerminomatous germ cell tumors: a children's oncology group study. J Clin Oncol. 2015;33:2464-71.
11. Aoyama H, Shirato H, Ikeda J, Fujieda K, Miyasaka K, Sawamura Y. Induction chemotherapy followed by low-dose involved-field radiotherapy for intracranial germ cell tumors. J Clin Oncol. 2002;20:857-65.
12. Al-Mahfoudh R, Zakaria R, Irvine E, Pizer B, Mallucci CL. The management of bifocal intracranial germinoma in children. Childs Nerv Syst. 2014;30:625-30.
13. Lafay-Cousin L, Millar BA, Mabbott D, Spiegler B, Drake J,

Bartels U, et al. Limited-field radiation for bifocal germinoma. Int J Radiat Oncol Biol Phys. 2006;65:486-92.
14. Huang PI, Chen YW, Wong TT, Lee YY, Chang KP, Guo WY, et al. Extended focal radiotherapy of 30 Gy alone for intracranial synchronous bifocal germinoma: a single institute experience. Childs Nerv Syst. 2008;24:1315-21.
15. Weksberg DC, Shibamoto Y, Paulino AC. Bifocal intracranial germinoma: a retrospective analysis of treatment outcomes in 20 patients and review of the literature. Int J Radiat Oncol Biol Phys. 2012;82:1341-51.
16. van Battum P, Huijberts MS, Heijckmann AC, Wilmink JT, Nieuwenhuijzen Kruseman AC. Intracranial multiple midline germinomas: is histological verification crucial for therapy? Neth J Med. 2007;65:386-9.
17. Merchant TE, Sherwood SH, Mulhern RK, Rose SR, Thompson SJ, Sanford RA, et al. CNS germinoma: disease control and long-term functional outcome for 12 children treated with craniospinal irradiation. Int J Radiat Oncol Biol Phys. 2000;46:1171-6.
18. Ogawa K, Yoshii Y, Shikama N, Nakamura K, Uno T, Onishi H, et al. Spinal recurrence from intracranial germinoma: risk factors and treatment outcome for spinal recurrence. Int J Radiat Oncol Biol Phys. 2008;72:1347-54.
19. Baranzelli MC, Patte C, Bouffet E, Couanet D, Habrand JL, Portas M, et al. Nonmetastatic intracranial germinoma: the experience of the French Society of Pediatric Oncology. Cancer. 1997;80:1792-7.
20. Cuccia V, Alderete D. Suprasellar/pineal bifocal germ cell tumors. Childs Nerv Syst. 2010;26:1043-9.
21. Shikama N, Ogawa K, Tanaka S, Toita T, Nakamura K, Uno T, et al. Lack of benefit of spinal irradiation in the primary treatment of intracranial germinoma: a multiinstitutional, retrospective review of 180 patients. Cancer. 2005;104:126-34.
22. Sugiyama K, Uozumi T, Arita K, Kiya K, Kurisu K, Sumida M, et al. Clinical evaluation of 33 patients with histologically verified germinoma. Surg Neurol. 1994;42:200-10.
23. Rogers SJ, Mosleh-Shirazi MA, Saran FH. Radiotherapy of localised intracranial germinoma: time to sever historical ties? Lancet Oncol. 2005;6:509-19.
24. Alapetite C, Brisse H, Patte C, Raquin MA, Gaboriaud G, Carrie C, et al. Pattern of relapse and outcome of non-metastatic germinoma patients treated with chemotherapy and limited field radiation: the SFOP experience. Neuro Oncol. 2010;12:1318-25.
25. Lee DS, Lim DH, Kim IH, Kim JY, Han JW, Yoo KH, et al. Upfront chemotherapy followed by response adaptive radiotherapy for intracranial germinoma: prospective multicenter cohort study. Radiother Oncol. 2019;138:180-6.
26. Bowzyk Al-Naeeb A, Murray M, Horan G, Harris F, Kortmann RD, Nicholson J, et al. Current management of intracranial germ cell tumours. Clin Oncol (R Coll Radiol). 2018;30:204-14.
27. Sonoda Y, Kumabe T, Sugiyama S, Kanamori M, Yamashita Y, Saito R, et al. Germ cell tumors in the basal ganglia: problems of early diagnosis and treatment. J Neurosurg Pediatr. 2008;2:118-24.
28. Kamoshima Y, Sawamura Y. Update on current standard treatments in central nervous system germ cell tumors. Curr Opin Neurol. 2010;23:571-5.
29. Kuhlthau KA, Pulsifer MB, Yeap BY, Rivera Morales D, Delahaye J, Hill KS, et al. Prospective study of health-related quality of life for children with brain tumors treated with proton radiotherapy. J Clin Oncol. 2012;30:2079-86.
30. Liang SY, Yang TF, Chen YW, Liang ML, Chen HH, Chang KP, et al. Neuropsychological functions and quality of life in survived patients with intracranial germ cell tumors after treatment. Neuro Oncol. 2013;15:1543-51.

pISSN 1598-2998, eISSN 2005-9256

Cancer Res Treat. 2020;52(4):1059-1066

https://doi.org/10.4143/crt.2019.633

Original Article

Open Access

Real-World Data of Pyrotinib-Based Therapy in Metastatic HER2-Positive Breast Cancer: Promising Efficacy in Lapatinib-Treated Patients and in Brain Metastasis

Ying Lin, MD[1,2]
Mingxi Lin, MD[1,2]
Jian Zhang, MD, PhD[1,2]
Biyun Wang, MD, PhD[1,2]
Zhonghua Tao, MD, PhD[1,2]
Yiqun Du, MD, PhD[1,2]
Sheng Zhang, MD, PhD[1,2]
Jun Cao, MD, PhD[1,2]
Leiping Wang, MD, PhD[1,2]
Xichun Hu, MD, PhD[1,2]

[1]*Department of Medical Oncology, Fudan University Shanghai Cancer Center,* [2]*Department of Oncology, Shanghai Medical College, Fudan University, Shanghai, China*

Correspondence: Xichun Hu, MD, PhD
Department of Medical Oncology, Fudan University Shanghai Cancer Center and Department of Oncology, Shanghai Medical College, Fudan University, No. 270, Dong'an Road, Shanghai 200032, China
Tel: 86-21-64175590
Fax: 86-21-54561523
E-mail: xchu2009@hotmail.com

Co-correspondence: Jian Zhang, MD, PhD
Department of Medical Oncology, Fudan University Shanghai Cancer Center and Department of Oncology, Shanghai Medical College, Fudan University, No. 270, Dong'an Road, Shanghai 200032, China
Tel: 86-21-64175590
Fax: 86-21-54561523
E-mail: syner2000@163.com

Received October 21, 2019
Accepted April 24, 2020
Published Online April 24, 2020

*Ying Lin and Mingxi Lin contributed equally to this work.

Purpose

Pyrotinib is a newly-developed irreversible pan-ErbB receptor tyrosine kinase inhibitor. This study reported the first real-world data of pyrotinib-based therapy in metastatic human epidermal growth factor receptor 2 (HER2)-positive breast cancer (BC), focusing on efficacy in lapatinib-treated patients and in brain metastasis.

Materials and Methods

One hundred thirteen patients with metastatic HER2-positive BC treated with pyrotinib-based therapy in Fudan University Shanghai Cancer Center under non-clinical trial settings from September 1, 2018 to March 1, 2019 were included.

Results

Over half patients have received more than two lines of systematic therapy and exposed to two or more kinds of anti-HER2 agents. Most patients received a combined therapy, commonly of pyrotinib plus capecitabine, or vinorelbine or trastuzumab. Median progression-free survival (PFS) was 6.3 months (range, 5.54 to 7.06 months) and objective response rate (ORR) was 29.5%, with two patients (1.9%) achieving complete response. Lapatinib-naïve patients had significantly longer PFS than lapatinib-treated patients (9.0 months vs. 5.4 months, p=0.001). ORR for lapatinib-treated patients was 23.2%. Thirty-one of 113 patients have brain metastasis. Median PFS was 6.7 months and intracranial ORR was 28%. For patients without concurrent radiotherapy and/or brain surgery, the ORR was very low (6.3%). But for patients receiving concurrent radiotherapy and/or brain surgery, the ORR was 66.7%, and three patients achieved complete response. Most common adverse event was diarrhea.

Conclusion

Pyrotinib-based therapy demonstrated promising effects in metastatic HER2-positive BC and showed activity in lapatinib-treated patients. For patients with brain metastasis, pyrotinib-based regimen without radiotherapy showed limited efficacy, but when combined with radiotherapy it showed promising intracranial control.

Key words

Pyrotinib, HER2-positive breast cancer, Tyrosine kinase inhibitor, Lapatinib-treated, Brain metastasis

Introduction

Human epidermal growth factor receptor 2 (HER2)-positive breast cancer (BC) consists of 15%-20% of BC [1]. Before the era of HER2-targeted therapy, HER2-positive BC was aggressive, easily recurrent and had poor prognosis [1]. The development of anti-HER2 therapy has dramatically improved the survival of this BC subtype [1].

Recently pyrotinib, a novel oral pan-ErbB receptor tyrosine kinase inhibitor (TKI), has shown very promising results in

metastatic HER2-positive BC [2-5]. In a phase II study, pyrotinib plus capecitabine had significantly higher objective response rate (ORR) (78.5% vs. 57.1%, p=0.01) and longer progression-free survival (PFS; 18.1 months vs. 7.0 months, p < 0.001) compared to lapatinib plus capecitabine [5]. Recently, PHENIX study, a double-blinded, multicenter, randomized phase III study, showed that pyrotinib plus capecitabine significantly prolonged PFS (11.1 months vs. 4.1 months, p < 0.001) and increased ORR (68.6% vs. 16.0%, p < 0.001) than capetabine monotherapy [2]. Both studies included patients with metastatic HER2-positive BC previously treated with no more than two lines of systematic therapy. Pyrotinib was approved in China in August 2018 for metastatic HER2-positive BC because of the remarkable result of the above phase II study and is currently in phase I clinical trial in the United States.

Pyrotinib and neratinib are both irreversible ErbB receptor TKIs, which are different in nature from lapatinib, a reversible HER1 and HER2 receptor TKI. Both pyrotinib and neratinib were found to have superior efficacy than lapatinib [5,6]. The median PFS of 11.1 months in PHENIX study achieved by pyrotinib plus capecitabine is comparable to that of 8.8 months achieved by neratinib plus capetabine as third or later line therapy in NALA trial and that of 12.9 months achieved by neratinib plus paclitaxel as first-line treatment in the NEfERT-T trial [6,7], suggesting the potentially comparable efficacy of pyrotinib to neratinib. However, a common problem in both the phase II and phase III studies of pyrotinib is that patients were not optimally treated with anti-HER2 therapy before trials, and some patients were even naïve to trastuzumab [2,5]. Therefore, neither study could fully represent the major populations of global metastatic HER2-positive BC patients, who were usually optimally treated with multiple anti-HER2 agents, especially in western countries where more drugs were available [8]. Questions about whether the results pf pyrotinib clinical trials were applicable in the current setting for anti-HER2 therapy remains [8].

Another question is whether pyrotinib is effective in patients with exposure to lapatinib. As for neratinib, in lapatinib-treated cohort of TBCRC022 trial, neratinib plus capetabine arm had intracranial ORR of 33%, extracranial ORR of 43%, and median PFS of 3.1 months, demonstrating the activity of neratinib in lapatinib-treated patients [9]. However, no data so far is available regarding the activity of pyrotinib in lapatinib-treated patient.

HER2-positive BC has higher incidence of brain metastasis than other BC subtypes, with a risk as high as 35%-50% [10,11]. Brain metastasis in BC is associated with very poor clinical outcome, with 1-year overall survival (OS) less than 50% [11]. Blood brain barrier (BBB) hinders the efficacy of many drugs because of the limited penetration. Anti-HER2 TKIs have been widely exploited due to their small molecule property that enhances the ability to penetrate the BBB [11]. Radiotherapy also is a common option for local control of brain lesions. Despite these efforts, the treatments for brain metastasis are still limited. In the subgroup analysis of PHENIX study, 31 patients with brain metastasis were further analyzed, pyrotinib plus capetabine prolonged PFS by 2.7 months compared to capetabine (6.9 months vs. 4.2 months, p=0.011), showing promising efficacy in brain metastasis [2]. However, the sample size is small and more data is needed to verify the intracranial efficacy of pyrotinib.

This study aimed to evaluate the efficacy of pyrotinib-based therapy in metastatic HER2-positive BC in the real world, especially focusing on lapatinib-treated patients and on brain metastasis, and to explore the efficacy and safety when it is combined with agents other than capetabine. To our knowledge, this is the first real-world study of pyrotinib-based therapy, and first study evaluating the efficacy of pyrotinib in lapatinib-treated patients.

Materials and Methods

1. Patient population and data collection

Information of patients with metastatic HER2-positive BC treated with pyrotinib-based therapy in Fudan University Shanghai Cancer Center (FUSCC) under non-clinical trial settings from September 1, 2018 to March 1, 2019 was obtained. Eligible patients were women with histologically confirmed HER2-positive locally recurrent or metastatic BC. Patients who once received pyrotinib in clinical trial settings were excluded. For patients who underwent biopsies in the metastatic sites, hormone receptor and HER2 status were determined based on metastatic lesions. Last follow-up time was September 2019.

2. Treatment and dose modification

Patients were prescribed with pyrotinib in routine clinical practice. The standard dosage is 400 mg single dose orally per day. Starting dose, dose modification, dose interruption, treatment discontinuation, combination therapy with cytotoxic drugs and/or anti-HER2 agents and/or radiotherapy were determined by physicians' choice based on previous clinical trials results, general health status and willing of patients.

3. Efficacy and safety assessments

Tumor response assessments were based on Response Evaluation Criteria in Solid Tumor (RECIST) criteria (ver. 1.1) using radiologic scans, including computed tomography (CT) or magnetic resonance imaging (MRI). Adverse events (AEs) were assessed according to the National Cancer Institute Common Terminology Criteria for Adverse Events (CTCAE, 4.03). AEs were collected based on a patient self-reporting system and by reviewing biochemical test results.

The primary end point was PFS, which was defined as the time from initiating pyrotinib to date of disease progression confirmed by CT/MRI scan or death of any cause, regardless of whichever would occur first. Secondary endpoint included ORR, OS, and safety. The ORR was defined as the proportion of patients with complete response (CR) or partial response (PR). OS was defined as the time period from initiating pyrotinib treatment to the date of death of any cause. Disease-free interval was defined as the time from primary radical surgery to the date of relapse.

4. Statistical analysis

Median PFS and OS were calculated by the Kaplan-Meier method and the subgroup comparisons were evaluated using the log-rank test. Median follow-up period was calculated by reverse Kaplan-Meier method. Stepwise Cox regression model was used to analyze the correlations between factors and PFS. All statistical analyses were performed using SPSS ver. 19 (SPSS Inc., Chicago, IL). All statistical tests were two-tailed and $p < 0.05$ was considered statistically significant.

5. Ethical statement

This study was approved by the FUSCC Ethics Committee (approval No. 2003215-19) and performed in accordance with the 1964 Helsinki declaration and its later amendments or comparable ethical standards. Informed consents were obtained in accordance with study protocol.

Results

1. Baseline characteristics

A total of 122 patients were prescribed with pyrotinib under non-clinical settings in FUSCC from September 1, 2018, to March 1, 2019. Nine patients were excluded because they transferred to other hospital and no further information can be accessed. Therefore, 113 patients were included in our study. Median follow-up duration was 8.4 months (interquartile range, 7.0 to 9.9 months). Baseline characteristics were summarized in Table 1. Median age of patients was 53.4 years (range, 24 to 84 years). Thirty-one patients (27.4%) had brain metastasis. All patients except 1 (99.1%) were prior exposed to anti-HER2 therapy, with 99.1% patients exposed to trastuzumab and 50.4% exposed to lapatinib (Table 1). Ninety-one out of the 113 patients had received primary radical surgery when first diagnosed. Of the 91 patients with primary surgery, 43 (47.3%) have received standard 1-year adjuvant trastuzumab treatment, seven (7.7%) had inadequate adjuvant trastuzumab therapy due to all kinds of reasons, seven (7.7%) had primary resistance and relapsed during adjuvant trastuzumab therapy, and the remaining 34 (37.4%) did not receive any anti-HER2 adjuvant therapy. Sixty-one point nine percent of patients received more than two lines of systematic therapy before. Fifty-three (46.9%), 46 (40.7%), and 14 (12.4%) patients were exposed to 1, 2, and 3 kinds of anti-HER2 agents, respectively.

Table 1. Patient characteristics at baseline

Characteristic	No. (%) (n=113)
Age, median (range, yr)	53.4 (24-84)
HR status	
HR positive	45 (39.8)
HR negative	68 (60.2)
ECOG performance status	
0-1	107 (94.7)
≥ 2	5 (4.4)
Unknown	1 (0.9)
DFI	
Primary metastatic	22 (19.5)
DFI ≤ 1 yr	16 (14.2)
DFI > 1 yr	75 (66.4)
Metastatic sites	
Lymph nodes	74 (65.5)
Lung	63 (55.8)
Liver	57 (50.4)
Bone	48 (42.5)
Brain	31 (27.4)
Local recurrence	30 (26.5)
Pleura	21 (18.6)
Contralateral breast	6 (5.3)
No. of metastatic sites	
1	25 (22.1)
2	28 (24.8)
3	19 (16.8)
≥ 4	41 (36.3)
Visceral metastases	
Yes	100 (88.5)
No	13 (11.5)
Lines of systematic therapy of pyrotinib	
1	20 (17.7)
2	23 (20.4)
3	25 (22.1)
≥ 4	45 (39.8)
Prior HER2-targeted therapy	
Trastuzumab	112 (99.1)
Lapatinib	57 (50.4)
T-DM1	12 (10.6)
Pertuzumab	5 (4.4)

HR, hormone receptor; ECOG, Eastern Cooperative Oncology Group; DFI, disease-free interval; HER2, human epidermal growth factor receptor 2.

2. Treatment administration

Treatment administration was shown in Table 2. Most patients (96.5%) received a combined therapy. Besides the combination of pyrotinib plus capetabine previously studied in

Table 2. Treatment administration

Pyrotinib treatment	No. (%) (n=113)
Regimens	
Single agent	4 (3.5)
Combined therapy	
Pyrotinib+capetabine	67 (59.3)
Pyrotinib+trastuzumab+capetabine	14 (12.4)
Pyrotinib+vinorelbine	9 (8.0)
Pyrotinib+trastuzumab	8 (7.1)
Pyrotinib+paclitaxel	3 (2.7)
Other	8 (7.1)
Dosage	
Starting dosage (mg/day)	
160	1 (0.9)
240	1 (0.9)
320	3 (2.6)
400	108 (95.6)
Dose escalation (mg/day)	
160→400	1 (0.9)
240→400	1 (0.9)
320→400	1 (0.9)
Dose reduction (mg/day)	
400→320	24 (21.2)
400→320→240	2 (1.8)
Interruption of treatment	43 (38.1)
Treatment discontinuation due to AEs	7 (6.2)

AEs, adverse events.

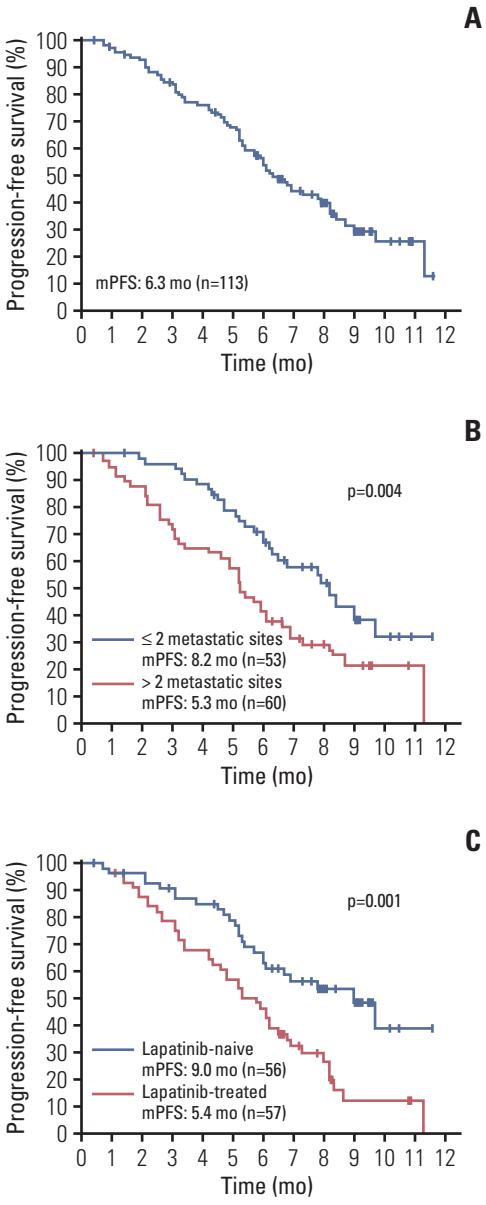

Fig. 1. Kaplan-Meier plot of progression-free survival and log-rank analysis of predictors of pyrotinib-based treatment. (A) Kaplan-Meier plot of progression-free survival of all patients treated with pyrotinib-based treatment. (B) Kaplan-Meier plot of progression-free survival for patients with ≤ 2 metastatic sites and > 2 metastatic sites. (C) Kaplan-Meier plot of progression-free survival for patients with and without prior lapatinib exposure. mPFS, median progression-free survival.

clinical trial, common combined agents also included vinorelbine and trastuzumab. Most patients started pyrotinib treatments at the standard dose of 400 mg/day, but 26 (23.0%) and 43 (38.1%) patients experienced dose reduction and treatment interruption respectively. The most common AEs causing dose reduction and treatment interruption were diarrhea, vomiting, nausea, and anorexia. Four patients were more than 70 years old, and they all started pyrotinib at standard dose of 400 mg. One out of four experienced dose reduction twice, and another one out of four experienced dose reduction once. Seven patients (6.2%) discontinued treatment permanently due to intolerant AEs, including three due to diarrhea, three due to vomiting and one due to simultaneous diarrhea and vomiting.

3. Efficacy in all patients

A total of 113 patients were included in PFS analysis. Median PFS was 6.3 months (range, 5.54 to 7.06 months) (Fig. 1A). Forty patients (35.4%) were still in treatment and median OS has not achieved by the time of this study.

A total of 105 patients were included in ORR analysis, with eight patients excluded because of lack of measurable lesions (Table 3). ORR was 29.5%, with 2 (1.9%) patients achieving CR. Of the two patients with CR response, one had a primary stage IV disease who has not been exposed to any anti-HER2 therapy and received pyrotinib plus trastuzumab plus docetaxel as first-line therapy. The other patient had a tumor with primary resistance to trastuzumab who experienced metastasis to brain during perioperative systematic therapy and received pyrotinib plus capetabine plus whole brain radiotherapy as first-line therapy.

Table 3. ORR rate in all patients and in patients with prior exposure to lapatinib

Response	No. (%)
All patients	105
Complete response	2 (1.9)
Partial response	29 (27.6)
Stable disease	44 (41.9)
Progressive disease	22 (21.0)
No data	8 (7.6)
ORR	31 (29.5)
Lapatinib-treated patients	56
Complete response	0
Partial response	13 (23.2)
Stable disease	26 (46.4)
Progressive disease	16 (28.6)
No data	1 (1.8)
ORR	13 (23.2)

ORR, objective response rate.

The number of metastatic sites (≤ 2 vs. > 2) and prior exposure to lapatinib were significantly correlated with PFS in log-rank analysis (p=0.004 and p=0.001, respectively) (Fig. 1B and C), and were independent predictors of PFS in Cox multivariate analysis (p=0.048 and p=0.002, respectively) (Table 4). Patients exposed to one kind of anti-HER2 agent had significantly longer PFS (9.0 months) than those exposed to 2 (5.9 months) or 3 (5.1 months) kinds of anti-HER2 agents (S1A Fig.).

4. Efficacy of pyrotinib-based therapy in lapatinib-treated patients

Fifty-seven patients were previously exposed to lapatinib and later received pyrotinib-based therapy. One patient lacked measurable lesions. Of the remaining 56 patients, 23.2% achieved PR response and no one achieved CR response (Table 3). Median PFS in patients with and without previous exposure to lapatinib were 5.4 months and 9.0 months, respectively (p=0.001) (Fig. 1C).

5. Efficacy of pyrotinib-based therapy in brain metastasis

Thirty-one patients had brain metastasis at baseline. There is no difference in PFS between patients with and without brain metastasis (p=0.696) (S1B Fig.). Fifty-four point eight percent of patients have received radiotherapy of brain lesions in the previous recurrence. Overall median PFS (intracranial and extracranial lesions considered) for patients with brain metastasis was 6.7 months (range, 4.69 to 8.71 months). By the time of the study, 10 patients were still undergoing treatment.

Table 4. Log-rank and Cox multivariate analysis of factors associated with progression-free survival

Characteristic	Log-rank analysis p-value	Cox multivariate analysis	
		p-value	Hazard ratio (95% CI)
DFI (> 1 yr vs. ≤ 1 yr vs. primary stage IV)	0.510	0.075	
> 1 yr vs. ≤ 1 yr			2.212 (1.079-4.535)
> 1 yr vs. primary stage IV			0.887 (0.477-1.650)
Types of metastasis (non-visceral vs. visceral)	0.428	0.890	1.064 (0.441-2.571)
No. of metastatic sites (≤ 2 vs. >2)	0.004	0.048	1.778 (1.005-3.145)
Prior exposure to lapatinib (no vs. yes)	0.001	0.002	2.313 (1.347-3.971)
HR status (HR+ vs. HR–)	0.145	0.552	1.174 (0.692-1.992)
Age group (> 60 yr vs. ≤ 60 yr)	0.556	0.948	1.018 (0.593-1.749)

CI, confidence interval; DFI, disease free interval; HR, hormone receptor.

Table 5. Objective response rate for brain lesions

Response	All patients (n=25)	Patients without concurrent radiotherapy or surgery (n=16)	Patients with concurrent radiotherapy and/or surgery (n=9)
Best response			
Complete response	3 (12.0)	0	3 (33.3)
Partial response	4 (16.0)	1 (6.3)	3 (33.3)
Stable disease	9 (36.0)	8 (50.0)	1 (11.1)
Progressive disease	5 (20.0)	5 (31.3)	0
No data	5 (20.0)	2 (12.5)	3 (33.3)
ORR	7 (28.0)	1 (6.3)	6 (66.7)

Values are presented as number (%). ORR, objective response rate.

Table 6. Grade 3 to 4 adverse events

Grade 3 to 4 adverse events	No. of patients (%)
Diarrhea	30 (26.5)
PPES	11 (9.7)
Neutropenia	5 (4.4)
Elevated aminotransferase	4 (3.5)
Anemia	4 (3.5)
Vomit	4 (3.5)
Leukopenia	3 (2.7)
Weight loss	2 (1.8)
Thrombocytopenia	2 (1.8)
Mucositis oral	1 (0.9)
Fatigue	1 (0.9)
Anorexia	1 (0.9)
Blood bilirubin increased	1 (0.9)

PPES, palmar-plantar erythrodysesthesia syndrome.

Twenty-five patients were included in the intracranial ORR analysis, with six patients excluded due to lack of measurable brain lesions (Table 5). Sixteen out of 25 patients did not receive concurrent radiotherapy or surgery of brain (Table 5). ORR was 28%, with 3/25 (12%) patients achieving CR and 4/25 (16%) patients achieving PR (Table 5). The three patients with CR response all received pyrotinib plus capetabine plus radiotherapy, and one of them has been exposed to three lines of systematic therapy before. In patients receiving pyrotinib-based systematic therapy and concurrent radiotherapy (8 patients) and/or surgery (1 patient) of the brain, the ORR was as high as 66.7% (6/9) (Table 5). After excluding those combined with radiotherapy, only 1/16 (6.3%) patients achieved PR and no patient achieved CR (Table 5).

6. Safety

As we used a patient self-reporting system to document AEs, and given the retrospective nature of the study, omission in reporting AEs was unavoidable. Here we report the grade 3 to 4 AEs (Table 6). The most common grade 3 to 4 AEs were diarrhea (26.5%), palmar-plantar erythrodysesthesia syndrome (PPES, 9.7%), neutropenia (4.4%). Excluding those with pyrotinib monotherapy and those combined with capetabine, toxicities remained tolerable. Most common grade 3 to 4 AEs were diarrhea (38.1%) and neutropenia (4.8%).

Discussion

The advent of HER2 targeted therapy has dramatically improved the prognosis of HER2-positive BC. Pyrotinib is a novel anti-HER2 TKI recently approved in China. Our study showed promising effects of pyrotinib-based therapy with a median PFS of 6.3 months and an ORR of 29.5% in metastatic HER2-positive BC. Comparing to the median PFS of 18.1 months and 11.1 months and the ORR of 78.5% and 68.6% achieved by pyrotinib plus capecitabine combination in previous phase II and III trials [2,5], our data were less fascinating. Several reasons should be taken into consideration. First of all, previous clinical trials included patients treated with two or less lines and some patients have not been exposed to any anti-HER2 therapy [2,5]. But in our cohort, over half patients were treated with more than two lines of systematic therapy, and over half received two or more kinds of anti-HER2 agents. Therefore, our cohort represented a treatment refractory population, and also the general population of patients with metastatic HER2-positive BC who were usually heavily treated with multiple anti-HER2 agents. Results of our study provided more experience outside the clinical trials for clinicians in treating general metastatic HER2-positive BC patients. Secondly, the follow-up time of our study is rather short and more than 30% of patients were still in treatment. However, we should also keep in mind that our study cohort included few patients previously exposed to pertuzumab and/or T-DM1. Pertuzumab and/or T-DM1 were common choices for front line treatments of HER2-positive BC patients globally. However, in China, pertuzumab was newly-approved and T-DM1 is waiting to be approved, which limited their usage in Chinese patients. Therefore, the role of pyrotinib in more heavily treated patients needs further global study. We hope the result from the phase I clinical trial of pyrotinib in the United States of America might shed some light on this question.

The efficacy of pyrotinib-based therapy was significantly better in lapatinib-naïve patients than in lapatinib-treated patients (Fig. 1C). In lapatinib-naïve group, pyrotinib-based therapy achieved a median PFS of 9.0 months, numerically comparable to that of neratinib plus capetabine arm (8.8 months) and better than that of lapatinib plus capetabine arm (6.6 months) in NALA study. In lapatinib-treated group, pyrotinib-based therapy had an ORR of 23.2%, which was a bit less than those from TBCRC022 trial (intracranial ORR 33% and extracranial ORR of 43%), but the median PFS of 5.4 months was numerically better than that from TBCRC022 trial (3.1 months). For the first time to our knowledge, this result provided evidence of the activity of pyrotinib-based therapy after failure of lapatinib-based treatment.

For HER2-positive BC, brain is always a sanctuary site [1]. For patients with brain metastasis, treatments remain limited and prognosis remains poor. Although anti-HER2 monoclonal antibodies and HER2-directed antibody drug conjugates were shown to improve survival in patients with brain metastasis in several studies [12-14], their intracranial effects remain controversial due to large-molecule property that hinders the infiltration through BBB. Anti-HER2 TKIs are important treatment options for brain metastasis. Petrelli et al. [15] conducted a pooled analysis including 12 studies

of the efficacy of lapatinib plus capecitabine in brain metastasis in HER2-positive BC. Results showed that lapatinib plus capecitabine achieved an ORR of nearly 30% and a median PFS of 4.1 months [15]. In the TBCRC022 trial, neratinib plus capecitabine has also shown promising efficacy in HER2-positive BC with brain metastasis with an ORR of 49% and 33% and median PFS of 5.5 and 3.1 months in lapatinib-naïve and lapatinib-treated patients respectively [9].

In our study, in patients with brain metastasis and only received pyrotinib-based therapy without local control of brain metastasis such as radiotherapy and surgery, the ORR was very low (6.3%), which was disappointing when compared to the efficacy of neratinib plus capetabine in brain metastasis in TBCRC022 trial. More data are needed to further evaluate the intracranial efficacy of pyrotinib. However, in patients combined pyrotinib-based systematic therapy with radiotherapy and/or surgery, the ORR was as high as 66.7%, and three out of nine patients achieved CR in brain lesions. This response rate was much higher than the previous study of lapatinib plus concurrent radiotherapy, which reported an ORR of 35%, in the treatment of brain metastasis [16], suggesting a possible treatment regimen of pyrotinib plus cytotoxic drugs plus radiotherapy for better intracranial control.

Pyrotinib-based therapy was generally well-tolerated. The most common grade 3 to 4 AEs was diarrhea, which was consistent with reports of the previous clinical trial. No severe AE was reported. Grade 3 to 4 PPES was less than that reported in clinical trials [2,5], mainly because about 40% of patients did not receive capecitabine as combined therapy. Combinations with agents other than capecitabine also demonstrated good safety profile, suggesting more combination options including anti-HER2 antibodies and cytotoxic drugs. However, given that a patient self-reporting system is used in reporting AEs and the retrospective nature of the study, oblivion in AE reporting was unavoidable.

Pyrotinib combination therapy demonstrated promising effects in metastatic HER2-positive BC with tolerable side effects, especially in lapatinib-naïve patients, and also some activity in lapatinib-treated patients. However, efficacy of pyrotinib-based therapy without concurrent radiotherapy in brain metastasis was not satisfying in our study and more investigations are needed in the future. But when combined with radiotherapy, pyrotinib-based therapy demonstrated remarkable intracranial disease control. More clinical trials are needed to further exploit the potential of this novel irreversible pan-ErbB receptor TKI.

Electronic Supplementary Material

Supplementary materials are available at Cancer Research and Treatment website (https://www.e-crt.org).

Conflicts of Interest

Conflicts of interest relevant to this article was not reported.

Acknowledgments

This study was supported by the Shanghai Municipal Science and Technology Commission Guidance Project, P.R. China (Contract No. 18411967800); Shanghai Municipal Commission of Health and Family Planning (Grant No. 201640069); Shanghai Natural Science Foundation (Grant No. 17ZR1405700); Research grant from Shanghai Hospital Development Center (Grant No. SHDC12018X03); and Shanghai Anticancer Association EYAS Project (Grant No. SACA-CY1B03). The authors would like to thank all the doctors, nurses, patients and their family members for their supports to our study.

References

1. Waks AG, Winer EP. Breast cancer treatment: a review. JAMA. 2019;321:288-300.
2. Jiang Z, Yan M, Hu X, Zhang Q, Ouyang Q, Feng J, et al. Pyrotinib combined with capecitabine in women with HER2+ metastatic breast cancer previously treated with trastuzumab and taxanes: a randomized phase III study. J Clin Oncol. 2019; 37(15 Suppl):1001.
3. Li X, Yang C, Wan H, Zhang G, Feng J, Zhang L, et al. Discovery and development of pyrotinib: a novel irreversible EGFR/HER2 dual tyrosine kinase inhibitor with favorable safety profiles for the treatment of breast cancer. Eur J Pharm Sci. 2017; 110:51-61.
4. Ma F, Li Q, Chen S, Zhu W, Fan Y, Wang J, et al. Phase I study and biomarker analysis of pyrotinib, a novel irreversible pan-ErbB receptor tyrosine kinase inhibitor, in patients with human epidermal growth factor receptor 2-positive metastatic breast cancer. J Clin Oncol. 2017;35:3105-12.
5. Ma F, Ouyang Q, Li W, Jiang Z, Tong Z, Liu Y, et al. Pyrotinib or lapatinib combined with capecitabine in HER2-positive metastatic breast cancer with prior taxanes, anthracyclines, and/or trastuzumab: a randomized, phase II study. J Clin Oncol. 2019;37:2610-9.
6. Saura C, Oliveira M, Feng YH, Dai MS, Hurvitz SA, Kim SB, et al. Neratinib + capecitabine versus lapatinib + capecitabine in patients with HER2+ metastatic breast cancer previously treated with ≥ 2 HER2-directed regimens: findings from the multinational, randomized, phase III NALA trial. J Clin Oncol. 2019;37(15 Suppl):1002.
7. Awada A, Colomer R, Inoue K, Bondarenko I, Badwe RA, Demetriou G, et al. Neratinib plus paclitaxel vs trastuzumab plus paclitaxel in previously untreated metastatic ERBB2-positive breast cancer: the NEfERT-T randomized clinical trial. JAMA Oncol. 2016;2:1557-64.
8. Gourd E. Pyrotinib versus lapatinib in HER2-positive breast cancer. Lancet Oncol. 2019;20:e562.
9. Freedman RA, Gelman RS, Anders CK, Melisko ME, Parsons

HA, Cropp AM, et al. TBCRC 022: a phase II trial of neratinib and capecitabine for patients with human epidermal growth factor receptor 2-positive breast cancer and brain metastases. J Clin Oncol. 2019;37:1081-9.
10. Martin AM, Cagney DN, Catalano PJ, Warren LE, Bellon JR, Punglia RS, et al. Brain metastases in newly diagnosed breast cancer: a population-based study. JAMA Oncol. 2017;3:1069-77.
11. Costa R, Carneiro BA, Wainwright DA, Santa-Maria CA, Kumthekar P, Chae YK, et al. Developmental therapeutics for patients with breast cancer and central nervous system metastasis: current landscape and future perspectives. Ann Oncol. 2017;28:44-56.
12. Brufsky AM, Mayer M, Rugo HS, Kaufman PA, Tan-Chiu E, Tripathy D, et al. Central nervous system metastases in patients with HER2-positive metastatic breast cancer: incidence, treatment, and survival in patients from registHER. Clin Cancer Res. 2011;17:4834-43.
13. Krop IE, Lin NU, Blackwell K, Guardino E, Huober J, Lu M, et al. Trastuzumab emtansine (T-DM1) versus lapatinib plus capecitabine in patients with HER2-positive metastatic breast cancer and central nervous system metastases: a retrospective, exploratory analysis in EMILIA. Ann Oncol. 2015;26:113-9.
14. Swain SM, Baselga J, Miles D, Im YH, Quah C, Lee LF, et al. Incidence of central nervous system metastases in patients with HER2-positive metastatic breast cancer treated with pertuzumab, trastuzumab, and docetaxel: results from the randomized phase III study CLEOPATRA. Ann Oncol. 2014;25:1116-21.
15. Petrelli F, Ghidini M, Lonati V, Tomasello G, Borgonovo K, Ghilardi M, et al. The efficacy of lapatinib and capecitabine in HER-2 positive breast cancer with brain metastases: A systematic review and pooled analysis. Eur J Cancer. 2017;84:141-8.
16. Kim JM, Miller JA, Kotecha R, Chao ST, Ahluwalia MS, Peereboom DM, et al. Stereotactic radiosurgery with concurrent HER2-directed therapy is associated with improved objective response for breast cancer brain metastasis. Neuro Oncol. 2019;21:659-68.

pISSN 1598-2998, eISSN 2005-9256

Cancer Res Treat. 2020;52(4):1067-1083

https://doi.org/10.4143/crt.2020.187

Original Article

Open Access

Elevated Expression of RIOK1 Is Correlated with Breast Cancer Hormone Receptor Status and Promotes Cancer Progression

Zhiqi Huang, MS[1]
Xingyu Li, MD[1]
Tian Xie, MS[2]
Changjiang Gu, MD[3]
Kan Ni, MS[3]
Qingqing Yin, MS[4]
Xiaolei Cao, PhD[1]
Chunhui Zhang, PhD[3]

[1]*Medical School of Nantong University, Nantong,* [2]*Department of Clinical Research Center, Nantong First People's Hospital, The Second Affiliated Hospital of Nantong University, Nantong,* [3]*Department of General Surgery, Affiliated Hospital of Nantong University, Nantong,* [4]*Research Center of Clinical Medicine, Affiliated Hospital of Nantong University, Nantong, China*

Correspondence: Chunhui Zhang, PhD
Department of General Surgery,
Affiliated Hospital of Nantong University,
No. 20, Xisi Road, Nantong 226001, China
Tel: 86-0513-81161201
Fax: 86-0513-81161201
E-mail: 783624840@qq.com

Co-correspondence: Xiaolei Cao, PhD
Medical School of Nantong University,
No. 19, Qixiu Road, Nantong 226001, China
Tel: 86-0513-85051729
Fax: 86-0513-85051729
E-mail: xiaolei@ntu.edu.cn

Received February 27, 2020
Accepted May 7, 2020
Published Online May 8, 2020

*Zhiqi Huang, Xingyu Li, and Tian Xie contributed equally to this work.

Purpose

RIOK1 has been proved to play an important role in cancer cell proliferation and migration in various types of cancers—such as colorectal and gastric cancers. However, the expression of RIOK1 in breast cancer (BC) and the relationship between RIOK1 expression and the development of BC are not well characterized. In this study, we assessed the expression of RIOK1 in BC and evaluated the mechanisms underlying its biological function in this disease context.

Materials and Methods

We used immunohistochemistry, western blot and quantitative real-time polymerase chain reaction to evaluate the expression of RIOK1 in BC patients. Then, knockdown or overexpression of RIOK1 were used to evaluate the effect on BC cells *in vitro* and *in vivo*. Finally, we predicted miR-204-5p could be a potential regulator of RIOK1.

Results

We found that the expression levels of RIOK1 were significantly higher in hormone receptor (HR)–negative BC patients and was associated with tumor grades (p=0.010) and p53 expression (p=0.008) and survival duration (p=0.011). Kaplan-Meier analysis suggested a tendency for the poor prognosis. *In vitro*, knockdown of RIOK1 could inhibit proliferation, invasion, and induced apoptosis in HR-negative BC cells and inhibited tumorigenesis *in vivo*, while overexpression of RIOK1 promoted HR-positive tumor progression. MiR-204-5p could regulate RIOK1 expression and be involved in BC progression.

Conclusion

These findings indicate that RIOK1 expression could be a biomarker of HR-negative BC, and it may serve as an effective prognostic indicator and promote BC progression.

Key words

Breast neoplasms, Hormone receptor, RIOK1, Prognosis, miR-204, PI3K

Introduction

Breast cancer (BC) remains the cancer type with the highest morbidity among women, with 1.67 million diagnoses and 521,900 deaths in 2012 alone [1]. In recent years the average 5-year survival of BC patients has risen significantly owing to advances in adjuvant and local therapeutic treatments, but in individuals with metastatic disease, such survival rates remain poor even following radical surgical treatment [2]. BC is a highly heterogeneous disease, with many recent efforts having been made to group BC patients according to a number of phenotypic parameters including

hormone receptor (HR) expression status and human epidermal growth factor receptor 2 (HER2) expression levels, leading to the definition of BC subtypes including luminal A, luminal B, HER2, and triple-negative BC [3]. Between 60% and 75% of BC cases are found to be HR-positive upon diagnosis [4]. The prognosis of BC patients is influenced by a range of different parameters, with HR-positive BC being known to have a significantly better average prognosis relative to HR-negative BC [5,6]. BC tumors that are positive for estrogen receptor (ER) are dependent upon active estrogen levels for growth, and as such patients can be treated with estrogen blockers such as tamoxifen or with inhibitors of estrogen production, leading to a better patient prognosis. Similarly, patients with HER2-positive BC often respond well to the monoclonal antibody trastuzumab, leading to significantly improved survival outcomes [7]. However, trastuzumab resistance also frequently manifests among these patients and is associated with significantly poorer survival outcomes. Triple-negative BC, in contrast, lacks any available targeted therapeutics and is thus associated with a poorer prognosis than other disease subtypes [8]. These findings emphasize the importance of identifying prognostic biomarkers and therapeutic targets which may allow for the better management and treatment of HR-negative BC patients.

Atypical protein kinases of the right open reading frame (RIO) family are present in almost all forms of life [9,10], with family members including RIOK1, RIOK2, and RIOK3. Both RIOK1 and RIOK2 are non-ribosomal proteins that are nonetheless essential for regulating ribosomal RNA biogenesis and cell cycle progression, with the depletion of either of these proteins in yeast having been shown to result in impaired 20S pre-ribosomal RNA processing. Similarly, RIOK2 is essential for 18S pre-rRNA production in human cells, whereas 21S pre-rRNA processing requires the activity of RIOK3 [11]. Proteins that regulate ribosomal biogenesis are known to have a profound impact of progression through the cell cycle, with RIOK1 depletion having been shown to result in S phase and mitotic arrest [12]. RIO kinases are also known to be important in the regulation of a wide range of disease types [13,14], with their overexpression having been previously detected in both non-small cell lung cancer (NSCLC) and colorectal cancer (CRC) [15]. In these contexts, RIOK1 has been shown to influence the proliferative, migratory, and invasive activity of tumor cells, although its exact mechanistic role in this context has not been fully [16]. Whether RIOK1 is similarly overexpressed and/or functionally important in BC remains uncertain, and further research is thus warranted to explore its relevance in this disease context.

Given that the biological function of RIOK1 in BC remains unclear, in the present study, we first evaluated the expression of RIOK1 in BC and then investigated the correlation between the RIOK1 expression and patient clinicopathological characteristics. We also evaluated the biological roles of RIOK1 by modulating its expression in BC cell lines. We found that knocking down RIOK1 was able to inhibit invasion, proliferation, G2/M cell cycle progression, and angiogenesis, while promoting cellular apoptosis via the phosphoinositide 3-kinase (PI3K)/AKT and mitogen-activated protein kinase (MAPK)/ERK pathway. Overexpression of RIOK1, in contrast, yielded the opposite phenotype. Bioinformatics analyses revealed that miR-204-5p was able to regulate the expression of RIOK1. Collectively, we found that RIOK1 plays an oncogenic role in BC and may represent a potential treatment target for BC patients.

Materials and Methods

1. Patient sample collection

Sixty BC patient tissue samples were collected from patients undergoing surgical resection for quantitative real-time polymerase chain reaction (qRT-PCR) and western blot in the general surgery department of the Affiliated Hospital of Nantong University between 2018 and 2019. Following collection, tissues were snap-frozen prior to use. In addition, 166 paraffin-embedded BC patient tissue blocks were collected in the department of pathology between 2010 and 2013 and were used for the retrospective study. All BC patient tumor samples had been independently evaluated by two pathologists, with differentiation, p53 expression levels, and HR/HER2 status being determined in light of the World Health Organization classification criteria. Patients that had undergone pre-surgical chemotherapy or radiotherapy were excluded from this analysis.

2. Immunohistochemistry and scoring

The expression of RIOK1 was assessed immunohistochemically in the 166 paraffin-embedded tumor tissue samples (5-μm-thick sections) discussed above using a tissue microarray approach, with each tissue sample having a core diameter of 2 mm. Sections were first treated with dimethyl benzene to achieve deparaffinization, after which an ethanol gradient was used to dehydrate samples. Antigen retrieval was conducted by heating samples at 100°C for 4 minutes and then at 95°C for 10 minutes in sodium citrate buffer (10 mM sodium-citrate mono-hydrate, pH 6.0), after which samples were allowed to cool to room temperature over 20 minutes prior to being washed with phosphate buffered saline (PBS). A 0.3% H_2O_2 solution was then applied to all samples for an additional 20 minutes in order to inhibit endogenous peroxidase activity, after which samples were probed overnight using anti-RIOK1 (1:100, Immunoway Group, Plano, TX) at 4°C. A two-step reagent kit (horseradish peroxidase [HRP] anti-mouse/rabbit IgG, Dako, Santa Clara, CA) was then used to detect this primary antibody, with diaminoben-

zidine (Dako) and hematoxylin counterstaining (Dako) being used to evaluate RIOK1 expression levels in these tissue samples. Two pathologists that had been blinded to patient outcomes next independently assessed RIOK1 staining in each tissue samples, scoring tissues according to staining intensity (with scores of 0, 1, 2, and 3 corresponding to no, weak, moderate, and strong staining, respectively) and the percentage of RIOK1-positive cells (with scores of 0, 1, 2, and 3 corresponding to 0%-30%, 31%-60%, 61%-80%, and 81%-100% RIOK1-positive, respectively). The product of these scores was then used to assess RIOK1 staining intensity, with an overall score of 0-3 being considered "low" and a score of 3 or higher being considered "high."

3. qRT-PCR

TRIzol (Thermo Fisher Scientific, Waltham, MA) was used to isolate total RNA from 60 BC patient tissue samples after which a spectrophotometer (NanoPhotometer, IMPLEN, Munich, Germany) was used to quantify the RNA contents in individual samples. Next, the RevertAid First Strand cDNA Synthesis Kit (Thermo Fisher Scientific) was used to prepare cDNA from 10 μL of each RNA sample using the following thermocycler settings: 42°C for 60 minutes and 70°C for 5 minutes. A Roche LightCycler 480 (Roche, Basel, Switzerland) was used to conduct qRT-PCR analyses of three replicate 2 μL cDNA samples, with individual reactions also containing 10 μL SYBR Green I Mix (Roche), 0.5 μL each of forward and reverse primers, and 7 μL nuclease-free H_2O. Thermocycler settings were as follows: 95°C for 5 minutes; 45 cycles of 95°C for 15 seconds, 60°C for 30 seconds, and 72°C for 30 seconds. Primers used in this study were as follows: RIOK1 (F, 5′-CCTTGGATTCTGATAACTGGAC-3′; R, 5′-AGGAAAATGGTGAAAACTTGG-3′), glyceraldehyde 3-phosphate dehydrogenase (GAPDH; F, 5′-CGCTGAGTACGTCGTGGAGTC-3′;R,5′-GCTGATGATCTTGAGGCTGTTGTC-3′). GAPDH expression was used for normalization purposes, with the $2^{-\Delta\Delta CT}$ approach used to assess relative RIOK1 expression levels in samples.

4. Western blot

RIPA lysis buffer containing protease inhibitors was used to lyse and BC tumor tissue samples, which were then spun for 20 minutes at 12,000 rpm at 4°C. Supernatants were then collected, with a BCA kit (Beyotime Institute of Biotechnology, Nantong, China) being used to quantify the protein contents within each sample. Samples were then boiled for 15 minutes in sodium dodecyl sulfate sample buffer, after which equal quantities of protein were separated via sodium dodecyl sulfate polyacrylamide gel electrophoresis and transferred to polyvinylidene difluoride membranes. Membranes were in turn blocked for 2 hours at room temperature with 5% skim milk in TBST. Blots were then probed with rabbit polyclonal anti-RIOK1 (1:1,000, Proteintech, Wuhan, China), anti–E-cadherin (1:1,000, Proteintech), anti-vimentin (1:1,000, CST, Danvers, MA); anti–N-cadherin (1:1,000, CST); PI3K (1:1,000, CST); p-AKT (1:2,000, CST); AKT (1:1,000, CST); cyclin B1 (1:500, Proteintech); p-ERK1/2 (1:1,000, Abcam, Cambridge, UK); ERK1/2 (1:2,000, Abcam). After washing in TBST, the membran washed thrice in TBST and incubated for 2 hours with appropriate HRP-conjugated secondary antibodies (1:1,000, Santa Cruz Biotechnology, Santa Cruz, CA). Enhanced che-miluminescence (Thermo Scientific) was then employed for protein detection, with analyses being repeated in triplicate.

5. Cell culture and transfection

BC cell lines MDA-MB-231 (HR-negative) and MCF-7 (HR-positive) were obtained from the Cell Bank of Type Culture Collection of the Chinese Academy of Sciences (Shanghai, China). MDA-MB-231 were maintained in Dulbecco's modified Eagle's medium (DMEM; Invitrogen, Carlsbad, CA) supplemented with 10% fetal bovine serum (GIBCO-BRL, Invitrogen), 100 μg/mL penicillin and 100 U/mL streptomycin (Shanghai Genebase Gen-Tech, Shanghai, China). MCF-7 cells were maintained in RPMI (Invitrogen) supplemented with 10% fetal bovine serum (GIBCO-BRL, Invitrogen), 100 ug/mL penicillin, and 100 U/mL streptomycin. All cells were within a humidified atmosphere containing 5% CO_2 at 37°C. MDA-MB-231 cells and MCF-7 cells were transfected with Lipofectamine 3000 Reagent (Invitrogen) following the manufacturer's protocol. Transfection efficiency was evaluated by western blot and quantitative polymerase chain reaction.

6. Flow cytometry

Flow cytometry analysis was performed detecting cell cycle distribution and cell apoptosis according to the manufacturer's protocol. Briefly, cells were trypsinized and fixed in centrifuge tubes containing 0.5 mL of 70% ethanol for at least 6 hours at 4°C, and then the suspension was centrifuged for 5 minutes at 1,000 rpm. Cell pellets were resuspended in 5 mL of PBS for approximately 30 seconds and centrifuged at 300 ×g for 5 minutes, then resuspended in 1 mL of propidium iodide staining solution and kept in the dark at 37°C for 10 minutes. Samples were analyzed by a flow cytometer (BD, Franklin Lakes, NJ). The percentage of the cells in G0-G1, S, and G2-M phase were collected and counted. When analyzing cell apoptosis, cells were washed by PBS and resuspended at a concentration of 1×10^6 cells/mL. Then an Annexin V-FITC Apoptosis Detection Kit (BD Biosciences, Oxford, UK) was used following the manufacturer's protocol. After incubation in the dark at room temperature for 20 minutes, the samples were immediately analyzed by a FACScan flow cytometer (Becton Dickinson, Franklin Lakes, NJ). Each assay was performed in triplicate.

7. Cell migration, invasion assay, and wound healing assay

For cell migration and invasion assays, the cells were performed using a transwell system that incorporated a polycarbonate filter membrane. The transfected cells (5×10^4 cells per well) were plated in the upper chamber containing 200 μL of serum-free media. The lower chambers contained 10% fetal bovine serum. After 24 hours of incubation, chambers were selected and fixed with paraformaldehyde, then stained with crystal violet for migration assays. For invasion assays, the filters were precoated with Matrigel (BD) and DMEM or RPMI media mixture in a ratio of 1:6. We selected chambers of MDA-MB-231 after 24 hours and those of MCF7 after 48 hours. The number of migrating or invading cells was counted on the captured images.

For wound healing assay, cells were plated and transfected on 6-well plates. After cells reached confluence, the cells were incubated in serum-free DMEM or RPMI media. Then an artificial scratch of the cells was wounded with a 10 μL pipette tip. Then the cells were washed by PBS twice and serum-free medium was added for a further 24 hours. Each experiment was repeated three times.

8. Cell proliferation assays

We used Cell Counting Kit-8 (CCK-8; Dojindo, Tokyo, Japan), colony formation, and EdU assays to estimate cell ability of proliferation. Three thousand transfected cells were seeded in the 96-well plates and added 10 μL solution per well; the absorbance was read on 450 nm for 24 hours, 48 hours, 72 hours, and 96 hours. For the colony formation assay, a total number of 800 transfected BC cells were plated in 6-well plates and cultured for about 2 weeks. Cell colonies were fixed with 4% methanol and stained with crystal violet. Colonies were counted and each experiment was repeated 3 times. EdU assay (5-ethynyl-20-deoxyuridine) was performed with a commercial kit (Ribobio, Guangzhou, China). The red staining represented proliferating cells and blue staining represented cell nucleus.

9. Tube formation assay

Two hundred microliters of Matrigel (BD) was plated in 24-well plates and incubated at 37°C for 30 minutes. When it became gel, 8×10^4 HUVECs were added in plates in two groups: supernatant from siNC transfection or siRIOK1 transfection of MDA-MB-231. After incubation at 37°C for 6 hours, tube formation was observed by microscope and saved.

10. Luciferase reporter assay

The wild type or mutation sequences within the predicted 3′ untranslated region binding sites of the RIOK1 were transfected into 293T cells along with miR-204 mimics or NC, carrying a luciferase reporter plasmid. After 48 hours, the luciferase activity was measured by Dual-Luciferase Reporter Assay Kit (Promega, Madison, WI).

11. Tumor xenografts

Four-week-old female nude mice were injected with MDA-MB-231 cells (1×10^7) with siRIOK1 or NC subcutaneously. After first injection, we transfected them *in vivo* each 5 days. The volume of xenograft tumors was measured every 5 days. After 30 days, the mice were executed and tumors were taken out for weighing.

12. Bioinformatics analysis

RIOK1 expression levels in a large BC patient cohort were assessed using the Oncomine database (https://www.oncomine.org) using the search terms "RIOK1," "Cancer VS. Normal/Cancer Analysis," and "Breast Cancer." Data were compared based upon log2 median-centered intensity in Oncomine microarray datasets. Kaplan-Meier Plotter (http://kmplot.com/analysis/) was further used to assess the relationship between RIOK1 expression levels and BC patient survival outcomes, yielding a survival curve for 3,951 BC patients and providing the corresponding p-value describing the relationship between RIOK1 expression and BC patient prognosis.

13. Statistical analysis

All statistical testing was conducted using SPSS ver. 20.0 (IBM Corp., Armonk, NY), and GraphPad Prism 6.0 (GraphPad Software Inc., San Diego, CA) was used to generate figures. Data are mean±standard deviation and were compared via Student's t tests, Kaplan-Meier survival analyses, chi-square tests, and Cox regression analyses as appropriate. For univariate and multivariate analyses of factors associated with BC patient prognosis, Cox proportional hazards regression models were used, with the results of these analyses reported as hazard ratios. $p < 0.05$ was the significance threshold.

14. Ethical statement

The xenograft mice were performed with the Afliated Hospital of Nantong University Animal Ethics Committee and according to the institutional guidelines.

The ethics committee of Nantong University Affiliated Hospital approved the present study, with all patients having provided written informed consent to participate.

Results

1. RIOK1 expression of BC patients in database

We began by analyzing the Oncomine database to assess RIOK1 expression levels in BC patients. This analysis revealed that patients with ER- or progesterone receptor (PR)–negative BC had higher average RIOK1 expression levels than did patients who were ER- or PR-positive ($p < 0.001$) (Fig.

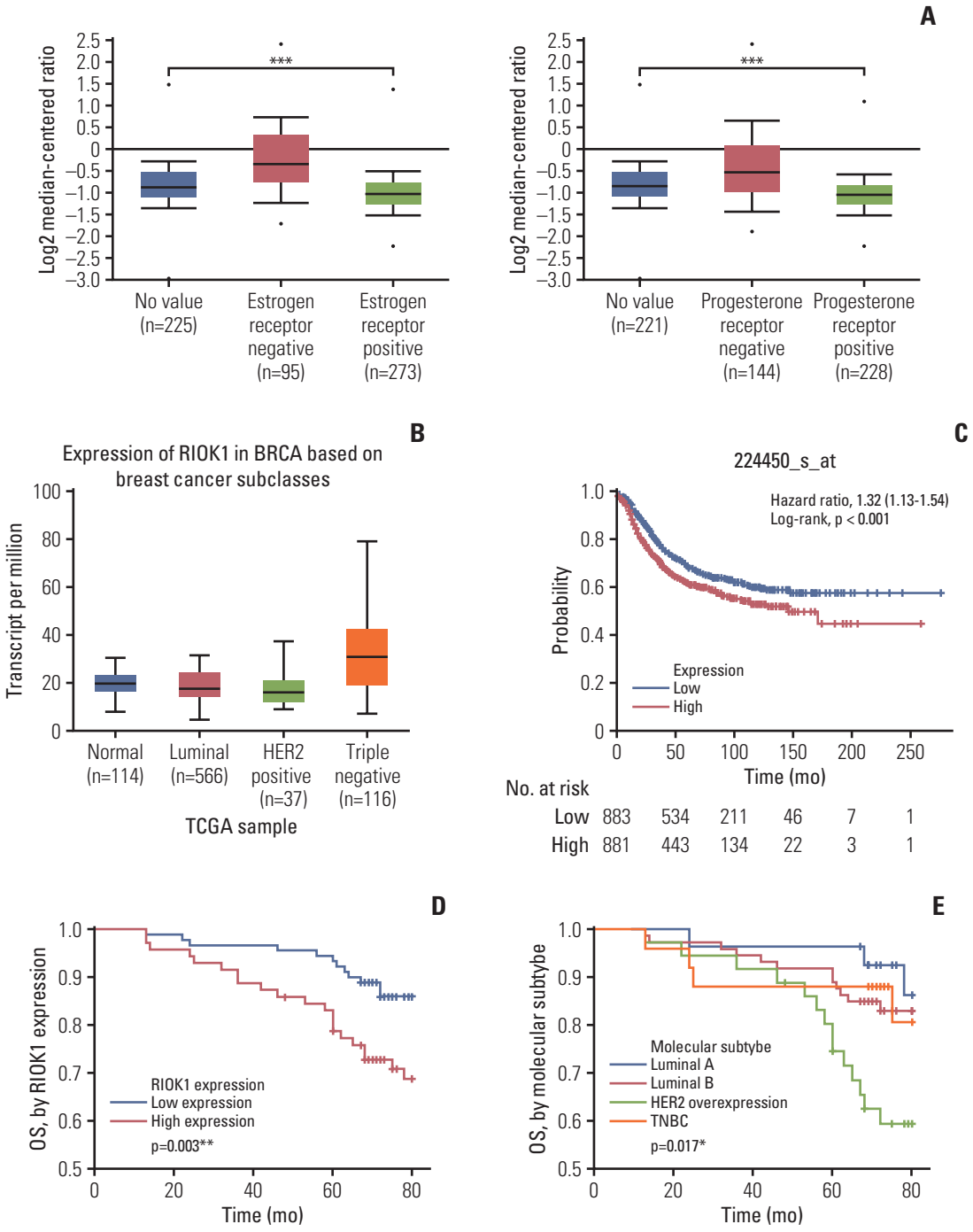

Fig. 1. The expression of RIOK1 was increased in breast cancer (BC) tissues and associated with poorer patient prognosis. (A, B) Expression of RIOK1 level in patients with hormone receptor (HR) status and different BC subclasses in The Cancer Genome Atlas (TCGA) database. (C) Kaplan-Meier survival curve of patients with BC from the TCGA database. (D) The overall survival (OS) of RIOK1-high patients (red) was significantly lower than that of RIOK1-low patients (blue). (E) The OS of HR-negative patients (green/orange) was significantly lower than that of HR-positive patients (red /blue). *$p < 0.05$, **$p < 0.01$, ***$p < 0.001$.

1A). The similar analysis showed the expression of RIOK1 was different depended on the subclass of BC (Fig. 1B). Furthermore, we found using Kaplan-Meier Plotter that BC patients with higher RIOK1 expression had a poorer prognosis than did patients with lower expression of this gene ($p < 0.001$) (Fig. 1C).

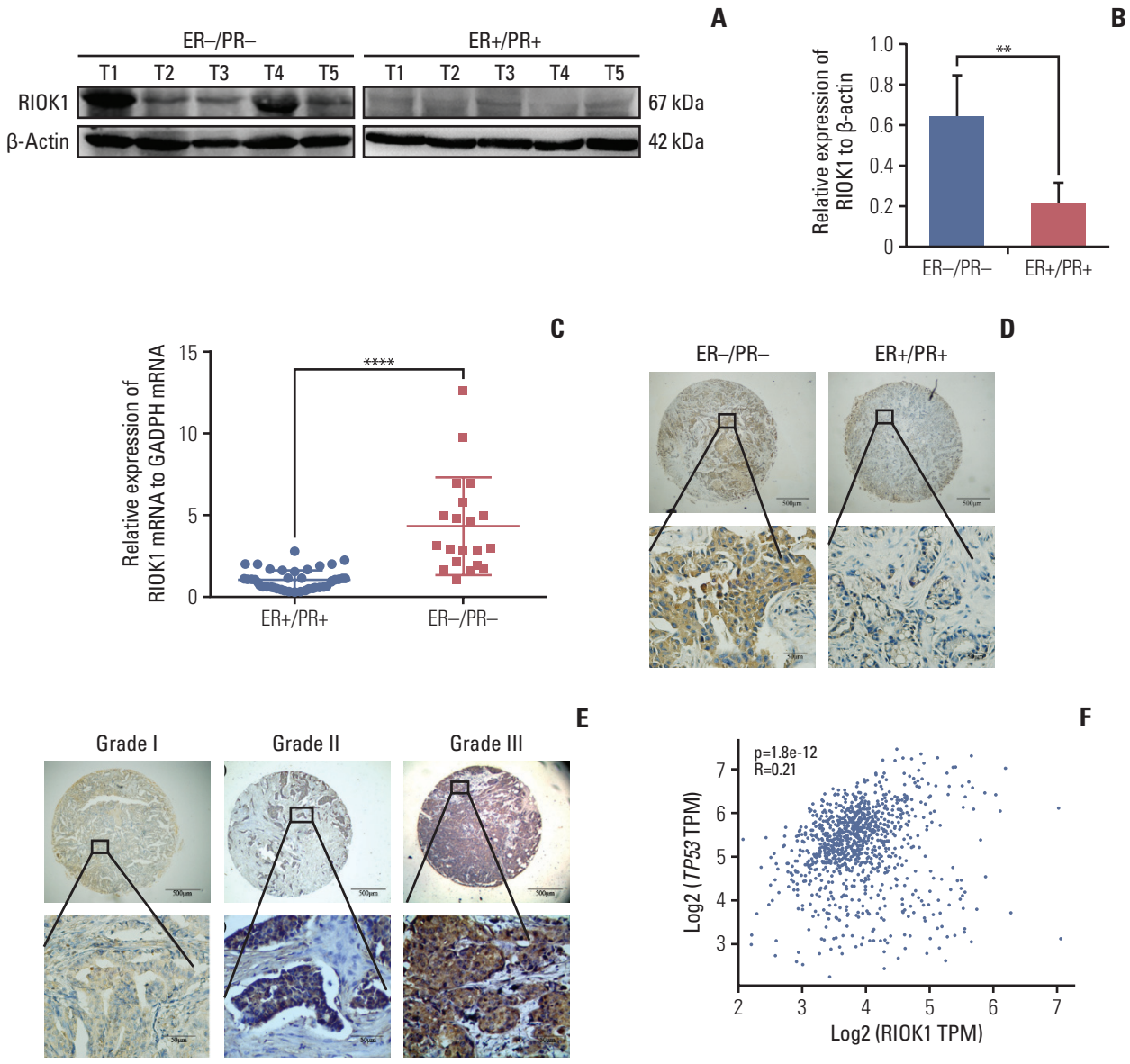

Fig. 2. RIOK1 was significantly upregulated in hormone receptor (HR)–negative tissues. (A, B) Assessment of RIOK1 expression in five HR-positive and five HR-negative breast cancer (BC) tissue samples as analyzed via Western blot. (C) The expression of RIOK1 at the mRNA level was assessed in 40 HR-positive and 20 HR-negative BC tissues via quantitative real-time polymerase chain reaction. (D) Staining in HR-negative BC tissue samples (left) and in HR-positive BC tissue samples (right) *in situ*. Original magnification: ×40 (upper), ×400 (lower). (E) RIOK1 staining was weak in grade I tumors (left), moderate in grade II tumors (middle), and strong in grade III tumors (right). Original magnification: ×40 (upper), ×400 (lower). (F) The database shows the relevance between RIOK1 and p53. ER, estrogen receptor; PR, progesterone receptor; GAPDH, glyceraldehyde 3-phosphate dehydrogenase; TPM, transcripts per million. $^{**}p < 0.01$, $^{****}p < 0.0001$ vs. HR-negative tissues.

2. RIOK1 is overexpressed in HR-negative BC tissues and correlates with clinicopathological parameters

We first quantified RIOK1 expression via western blot in five HR-positive and five HR-negative BC tumor samples and immunohistochemistry staining. This analysis showed that the expression of RIOK1 at the protein level was significantly higher in HR-negative BC tissue samples (Fig. 2A, B, and D). We further confirmed that RIOK1 expression was higher at the mRNA level in HR-negative BC tissue samples by comparing 40 HR-positive and 20 HR-negative samples via qRT-PCR ($p < 0.001$) (Fig. 2C). To explore the relationship between RIOK1 expression levels and BC disease progression using a tissue microarray of 166 BC patient samples. Of these 166 samples, 91 (54.8%) exhibited high RIOK1 immunohistochemical expression, while the remaining 75 (45.2%) are RIOK1-low (Table 1). Tumors that of a higher grade had

Table 1. The relationship between RIOK1 and p53 expression and clinicopathological parameters

Clinicopathological parameter	No.	RIOK1		p-value	p53		p-value
		Low or No	High		Low or No	High	
Total	166	91	75		108	58	
Age (yr)							
< 50	67	39	28	0.473	46	21	0.427
≥ 50	99	52	47		62	37	
Tumor diameter (mm)							
≤ 20	74	42	32	0.655	51	23	0.353
> 20	92	49	43		53	75	
Tumor stage (TNM)							
I	52	29	23	0.269	38	14	0.077
II	86	51	35		55	31	
III-IV	28	11	17		15	13	
Histological grade							
I	21	15	6	0.010*	17	4	0.263
II	99	59	40		62	37	
III	46	17	29		29	17	
Hormone receptor							
ER							
Negative	65	24	41	< 0.001***	35	30	0.015*
Positive	101	67	34		73	28	
PR							
Low	74	27	47	< 0.001***	39	35	0.003**
High	92	64	28		69	23	
HR status							
ER (+)/PR (+)	89	62	27	< 0.001***	66	23	0.003**
ER (–)/PR (+)	3	2	1		3	0	
ER (+)/PR (–)	12	5	7		7	5	
ER (–)/PR (–)	62	22	40		32	30	
Molecular type							
Luminal A	27	17	10	< 0.001***	23	4	0.012*
Luminal B	74	52	22		51	23	
HER2+	38	13	25		18	20	
TNBC	27	9	18		16	11	
Aggressive phenotype							
HER2							
Low	99	58	41	0.238	78	21	< 0.001***
High	67	33	34		30	37	
Triple-negative phenotype							
No	141	82	59	0.040*	93	48	0.568
Yes	25	9	16		15	10	
Lymph node metastasis							
Negative	92	54	38	0.263	54	38	0.263
Positive	74	37	37		37	37	
Ki67							
Low	70	43	27	0.129	49	21	0.237
High	96	47	49		58	37	
Survival time (mo)							
≥ 80	128	78	50	0.011*	88	40	0.228
< 80	33	12	21		19	14	

(Continued to the next page)

Table 1. Continued

Clinicopathological parameter	No.	RIOK1		p-value	p53		p-value
		Low or no	High		Low or no	High	
p53							
Low	115	65	40	0.008**	-	-	-
High	51	20	31		-	-	

Statistical analysis were carried out using Person χ^2 test. ER, estrogen receptor; PR, progesterone receptor; HR, hormone receptor; HER2, human epidermal growth factor receptor 2; TNBC, triple-negative breast cancer. *p < 0.05, **p < 0.01, ***p < 0.001.

Table 2. Assessment of prognostic factors associated with BC patient 80-month survival via univariate and multivariate approaches

Clinicopathological parameter	Univariate analysis		Multivariate analysis	
	Hazard ratio (95% CI)	p-value	Hazard ratio (95% CI)	p-value
RIOK1 (high vs. low)	2.473 (1.216-5.028)	0.012*	2.133 (1.041-4.372)	0.038*
Ki67 (high vs. low)	2.213 (1.028-4.763)	0.042*	-	-
Lymph node metastasis (yes or no)	3.364 (1.598-7.079)	0.001**	3.069 (1.449-6.498)	0.003**
p53 (high vs. low)	1.517 (0.749-3.071)	0.247	-	-
ER (yes or no)	0.551 (0.278-1.090)	0.086	-	-
PR (yes or no)	0.612 (0.308-1.215)	0.160	-	-
HER2 (yes or no)	2.132 (1.068-4.255)	0.031*	-	-
Age stage (≤ 50 yr vs. > 50 yr)	1.471 (0.713-3.033)	0.296	-	-
Tumor diameter (≤ 2 cm vs. > 2 cm)	1.852 (0.881-3.892)	0.104	-	-
Grade (well/moderately vs. poorly)	2.530 (0.605-10.577)	0.203	-	-

BC, breast cancer; CI, confidence interval; ER, estrogen receptor; PR, progesterone receptor; HER2, human epidermal growth factor receptor 2. *p < 0.05, **p < 0.01.

significantly increased RIOK1 protein expression levels (p=0.010) (Fig. 2E). In these samples, we found that RIOK1 expression was higher in HER2+ and triple-negative BC patient tumor samples relative to those from patients with luminal A or B disease based on HR status (p < 0.05). No relationship was observed between RIOK1 expression and patient age, tumor diameter, lymph node metastasis, or Ki67 expression. p53 staining results from the pathology department also revealed a significant association between RIOK1 and P53 levels in these BC patient tissue samples (p=0.008). Database also suggested a potential correlation between RIOK1 and p53 (Fig. 2F). Moreover, elevated RIOK1 expression was associated with an 80-month survival duration (p=0.011).

3. Correlation between RIOK1 expression and prognosis in BC patients

We next further assessed how RIOK1 expression in BC tumor tissues was associated with BC patient survival outcomes using Kaplan-Meier survival analyses. Through this approach, we observed significantly longer overall survival (OS) in BC patients with low RIOK1 expression levels relative to those with higher expression of this protein (p=0.003) (Fig. 1D). This analysis further confirmed that molecular subtype was another key determinant of BC patient survival outcomes (p=0.017) (Fig. 1E). When comparing RIOK1-positive and -negative samples, a crude HR of 2.473 was calculated. A univariate analysis revealed that elevated RIOK1 expression (p=0.012), Ki67 levels (p=0.042), lymph node metastasis (p=0.001), and HER-2 positive (p=0.032) were all associated with a poorer BC patient prognosis (Table 2). A subsequent multivariate analysis further confirmed that both lymph node metastasis and RIOK1 expression levels were independent predictors of BC patient (p=0.003 and p=0.038, respectively) (Table 2).

4. RIOK1 promotes migration, invasion, and angiogenesis in BC cells

As the expression of RIOK1 was higher in the MDA-MB-231 cell line relative to in MCF7 cells, we knocked down and overexpressed RIOK1 in these respective cell lines (Fig. 3A, S1 Fig.). Given that metastasis contributes to the low survival rate of BC patients, we evaluated the role of RIOK1 in BC migration and invasion. Transwell and wound healing analyses revealing that RIOK1 knockdown impaired cell motility, whereas RIOK1 overexpression had the opposite effect (Fig. 3B-D). Angiogenesis is an additional key driver of tumor metastasis. The tube formation assay revealed that when

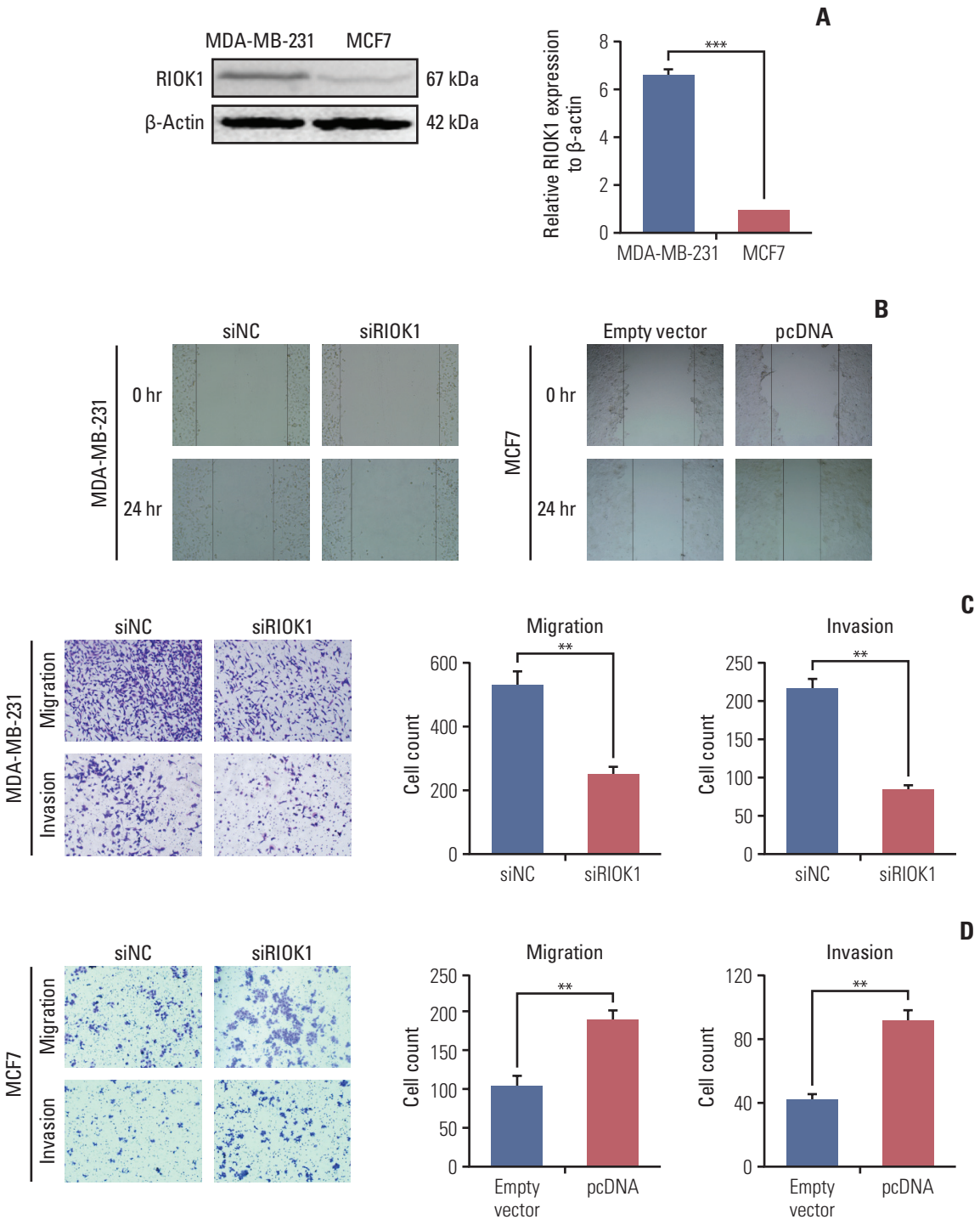

Fig. 3. Inhibiting RIOK1 expression decreased breast cancer (BC) cells migration, invasion, and angiogenesis. (A) Relative expression of RIOK1 in BC cell lines. (B) A wound healing assay was performed to determine the migration of MDA-MB-231 and MCF7 cells. (C, D) Transwell assay was used to measure the capacity of invasion and migration capacity on BC cells transfected with siRIOK1 or pcDNA compared with siNC or empty vector. *(Continued to the next page)*

RIOK1 was knocked down, tube formation was impaired in MDA-MB-231 cells (Fig. 3E). Consistent with these data, the expression of E-cadherin was increased and vimentin and N-cadherin were markedly downregulated when RIOK1 was knocked down (Fig. 3F).

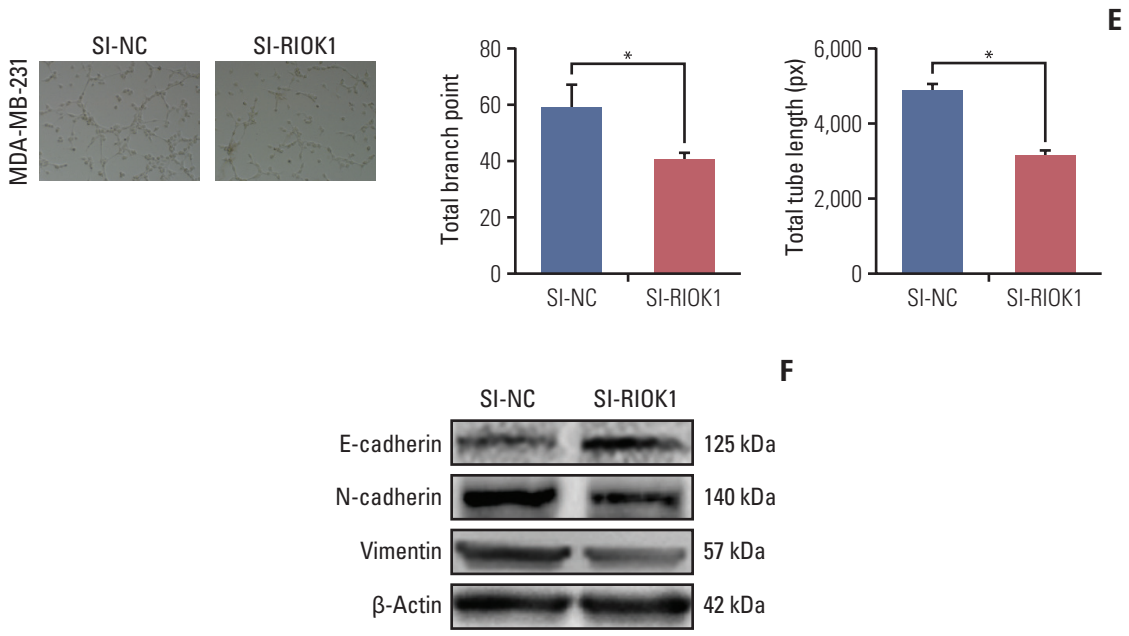

Fig. 3. *(Continued from the previous page)* (E) The effect of the RIOK1 expression of MDA-MB-231 cells on endothelial cell tube formation. (F) Western blot analysis was used to detect the RIOK1 level on epithelial-mesenchymal transition process markers. *$p < 0.05$, **$p < 0.01$, ***$p < 0.001$.

5. RIOK1 modulates BC cell proliferation, cell cycle progression, and apoptosis

CCK-8 and colony formation assays indicated that RIOK1 affected the proliferation of BC cells (Fig. 4A-D). We additionally used EdU incorporation assays to assess the percentage of proliferating BC cells when RIOK1 was knocked down (Fig. 4E). Flow cytometry revealed that BC cells exhibited G2/M phase arrest when RIOK1 was knocked down (Fig. 4F), with these cells additionally exhibiting increased rates of apoptosis, while apoptosis was inhibited in MCF7 cells overexpressing RIOK1 (Fig. 4G and H). We then used western blot to measure the expression of proteins related to the above analyses. In light of their importance in HR-negative BC, we analyzed the PI3K/AKT and MAPK/ERK signaling pathways in MDA-MB-231 cells, revealing that phospho-AKT and phospho-ERK1/2 levels were downregulated when RIOK1 was knocked down, indicating that RIOK1 may affect BC cells via these two pathways (Fig. 4I).

6. Knockdown of RIOK1 inhibits tumor growth *in vivo*

We next investigated whether RIOK1 was able to modulate BC tumorigenesis *in vivo*. MDA-MB-231 cells transfected with siRIOK1 or siNC were injected into nude mice and tumor growth was then monitored, revealing that tumors were smaller in mice in the siRIOK1 group relative to the siNC group (Fig. 5A-D). We additionally confirmed via qRT-PCR that RIOK1 expression was knocked down by siRIOK1 (Fig. 5E). These results thus suggested that knockdown of RIOK1 was able to inhibit tumor growth *in vivo*.

7. miR-204-5p modulates RIOK1 expression and impact HR-negative BC

To identify potential miRNAs that target RIOK1, we used TargetScan, miRDB, starBase, and Tarbase to identify miR-204-5p as the only predicted miRNA targeting this gene (Fig. 6A). We then detected the expression of RIOK1 in MDA-231 cells which was transfected with a miR-204-5p mimic or inhibitor (Fig. 6B). A luciferase reporter assay confirmed that miR-204-5p and RIOK1 were able to directly interact with one another in cells (Fig. 6C). Furthermore, we performed rescue assays to validate whether miR-204-5p was able to reverse the pro-tumorigenic role of RIOK1 in BC cells, and we determined that miR-204-5p/RIOK1 promoted BC cell proliferation and migration *in vitro* (Fig. 6D-F). Furthermore, through a database search, we found that lower miR-204 expression was predictive of a worse outcome in BC patients (S2 Fig.). Together, these data suggested that miR-204-5p was able to impact RIOK1 and to modulate its ability to influence tumor progression.

Discussion

RIOK1 is a key kinase in the RIO protein family. Kinases are essential regulators of all cellular processes, and make up roughly 2% of all eukaryotic genes [17], regulating transcription, translation, and protein function via phosphorylation of specific target proteins [18]. While best studied in yeast, RIO kinases are also thought to be key regulators of ribosomal

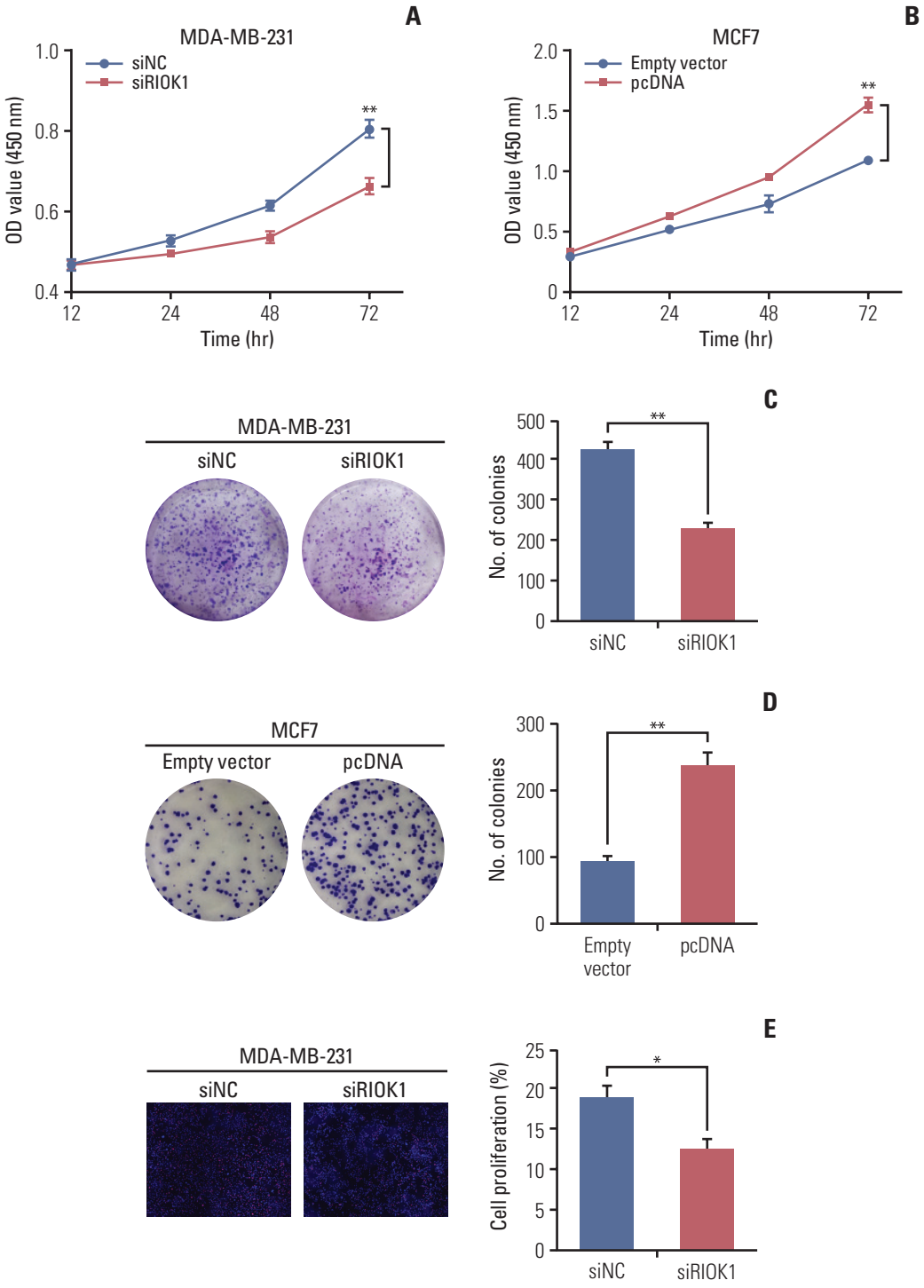

Fig. 4. RIOK1 promoted breast cancer (BC) cells proliferation, induced cell cycle arrest, and reduced cell apoptosis. (A, B) Cell Counting Kit-8 assay presented the proliferation capacity of MDA-MB-231 and MCF7 cells transfected with siRIOK1 or pcDNA compared with siNC or empty vector. (C, D) Colony formation assay was used to detect the proliferation of MDA-MB-231 and MCF7 cells transfected with siRIOK1 or pcDNA. (E) EdU assay was used to evaluate cell proliferation. Representative images for EdU-positive cells (red) and Hoechst-stained nuclei (blue) of MDA-MB-231 transfected with siRIOK1 or siNC were shown in the left. Quantification data was shown in the right. *(Continued to the next page)*

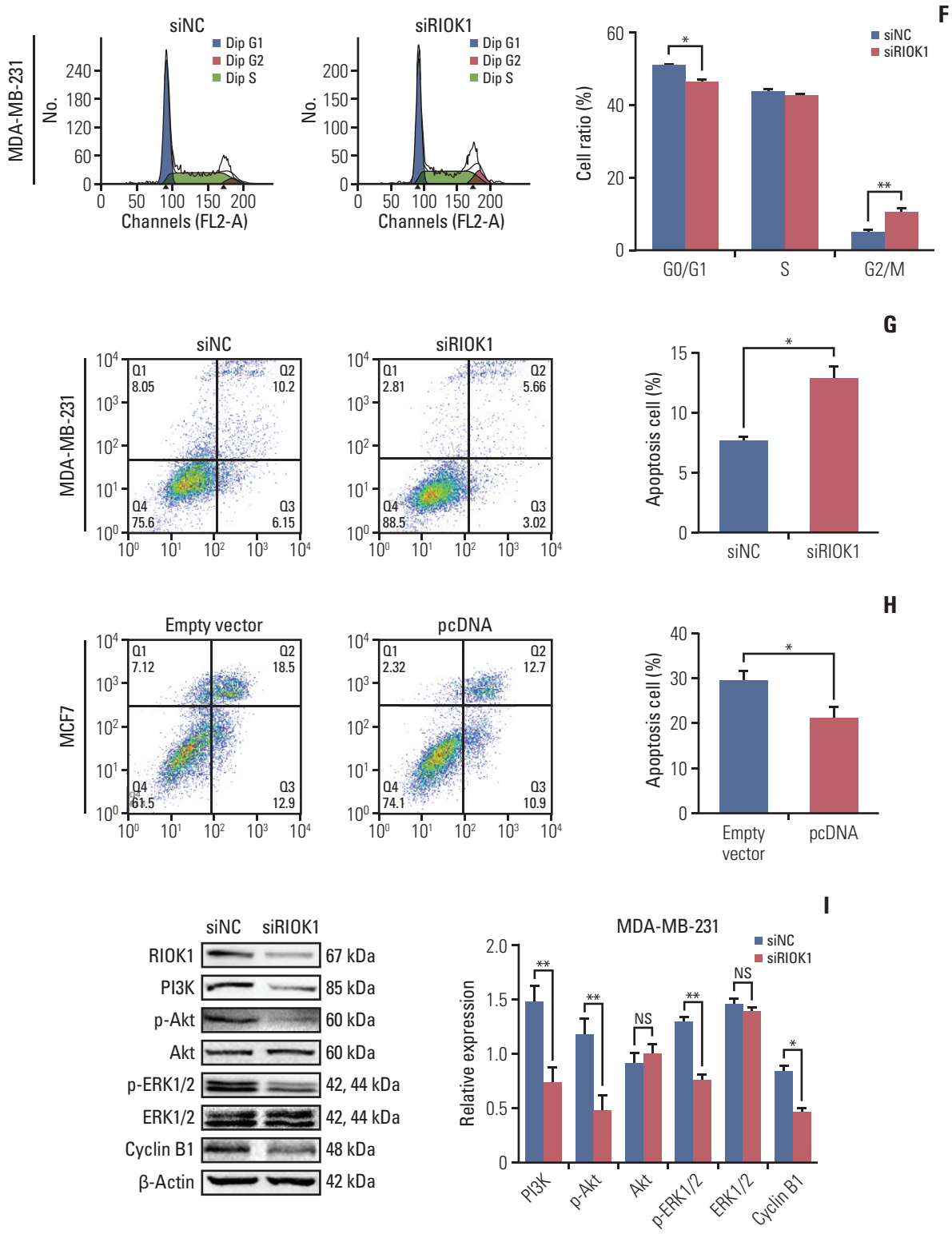

Fig. 4. *(Continued from the previous page)* (F) Flow cytometry of cell cycle was used to analyze the effect of siRIOK1 on MDA-MB-231 cells. (G, H) Induction of apoptosis of BC cells was analyzed by flow cytometry on MDA-MB-231 and MCF7 cells transfected with siRIOK1 or pcDNA compared with siNC or empty vertor. PI3K, phosphoinositide 3-kinase. (I) Western blot analysis of proliferation-related and apoptosis-related pathway proteins on MDA-MB-231 cells transfected with siRIOK1 or siNC. *$p < 0.05$, **$p < 0.01$.

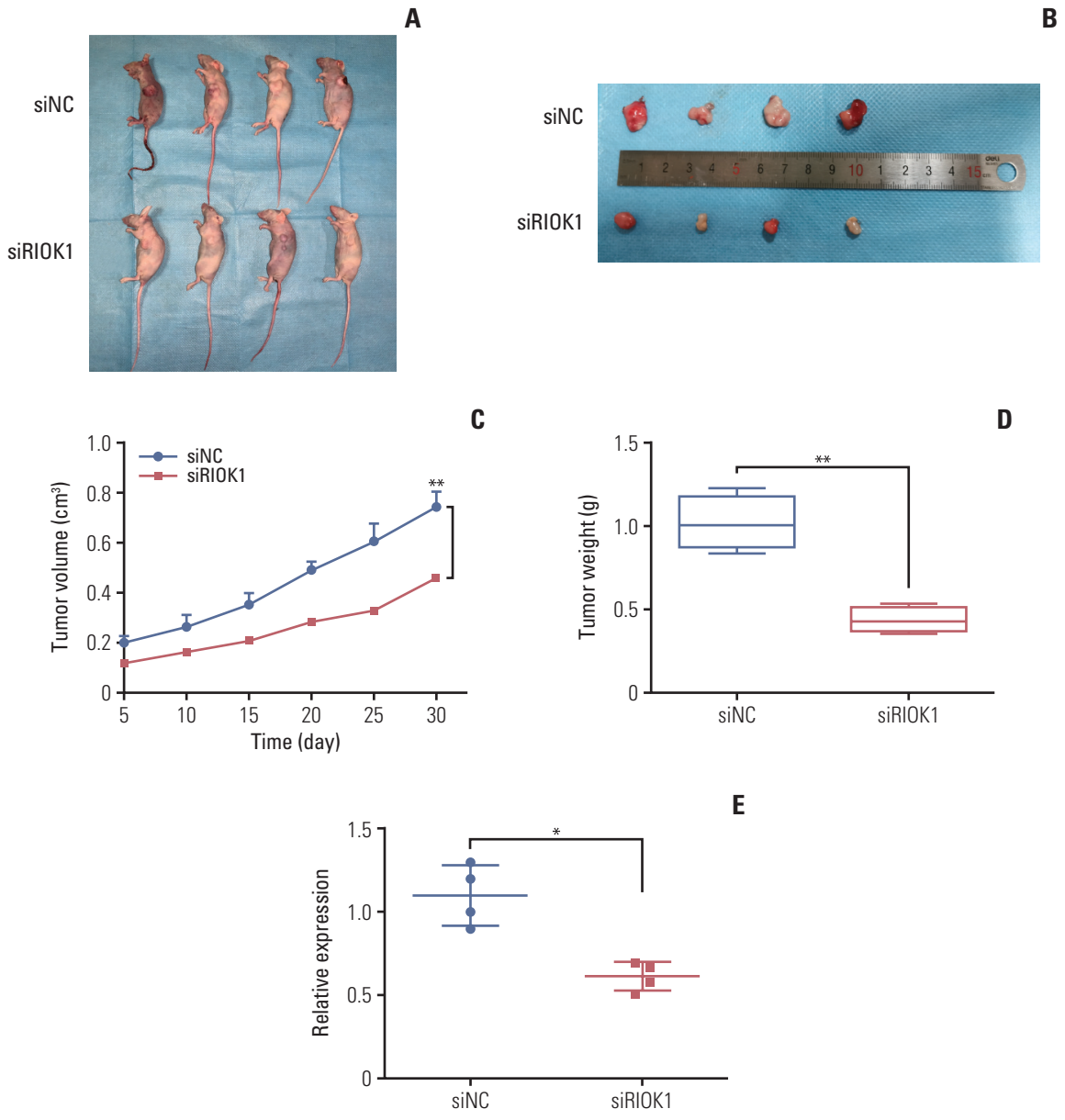

Fig. 5. Knockdown of RIOK1 inhibited tumor growth *in vivo*. (A, B) Knockdown of RIOK1 inhibited the growth of MDA-MB-231 cells in nude mice. (C) Growth curves of xenograft tumors with siRIOK1 or siNC. (D) The weight of tumors from two groups after removal. (E) RIOK1 expression in tumor tissues was detected by quantitative real-time polymerase chain reaction. *$p < 0.05$, **$p < 0.01$.

biogenesis in mammalian cells. Indeed, RIOK1 has been shown to be closely linked to mammalian cell proliferation, with its absence leading to cell cycle arrest at the G2/M checkpoint in affected cells [19]. The dependent of cell proliferation on RIOK1 activity was evident even in a study of RAS-driven tumor cells, suggesting that therapeutic targeting of RIOK1 may be a viable strategy for treating such RAS mutant cancers [20]. RIOK1 has also been shown to be overexpressed in CRC and NSCLC [15], but it has not been directly studied in the context of BC.

BC remains the most common invasive cancer type affecting women [21], with these tumors being classified using a number of different systems that offer insight into the associated disease prognosis and amenability to therapeutic treatment. In the present study, for the first time, we detected high RIOK1 expression in approximately half of BC patient tumors, with this protein primarily localizing to the cytoplasm in these cancer cells. These findings suggested that RIOK1 may not undergo nuclear translocation, or that higher expression may be associated with increased cytoplasmic localization. We similarly found that the expression of RIOK1 at both the mRNA and protein level was significantly corre-

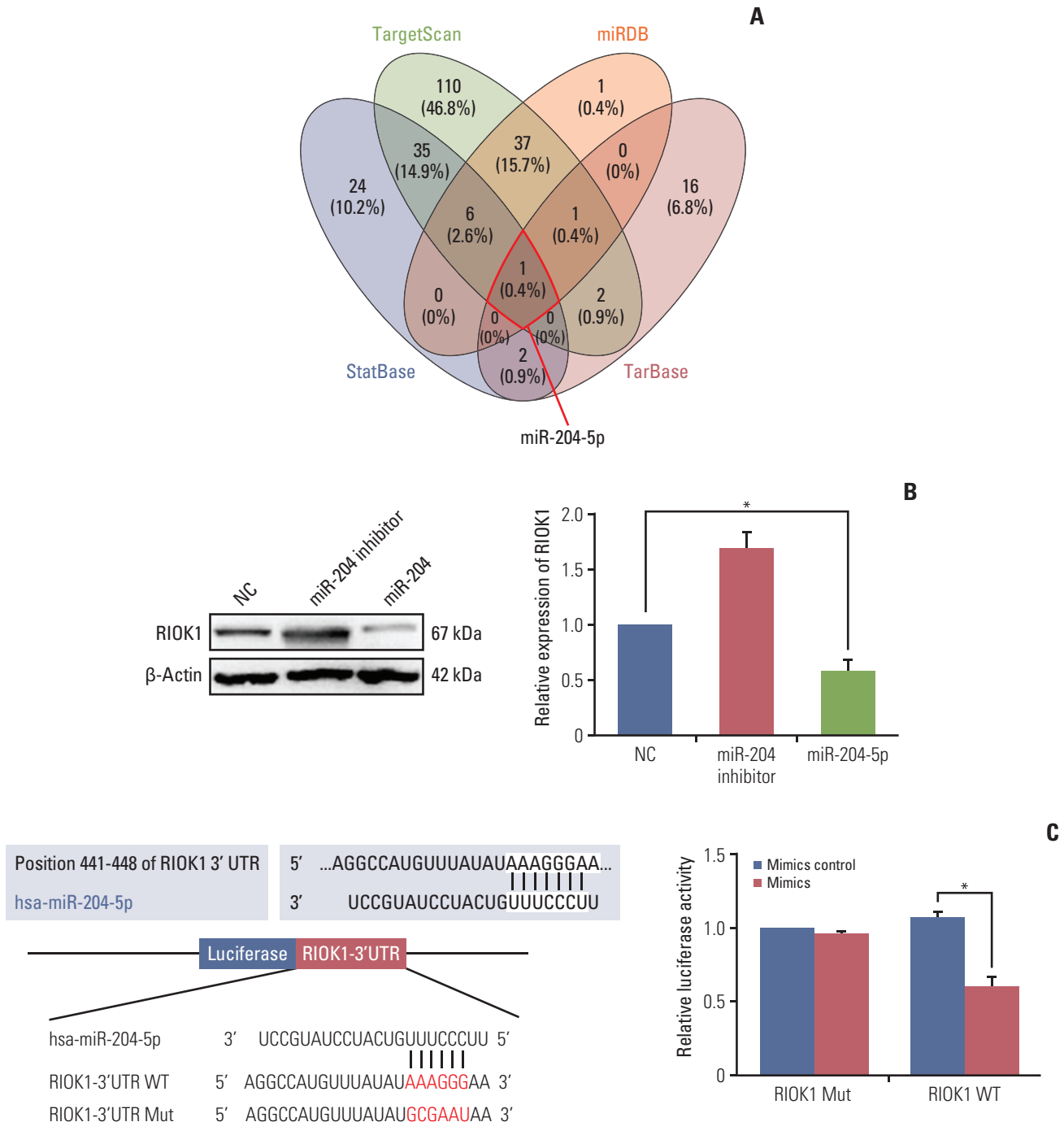

Fig. 6. miR-204-5p directly targeted on RIOK1 and regulated the effects of RIOK1 on hormone receptor (HR)–negative breast cancer (BC) cells. (A) Bioinformatics analysis of predicted miRNAs interacted with RIOK1. (B) Western blot analysis of RIOK1 expression in MDA-MB-231 after transfection with miR-204-5p or inhibitor. (C) The luciferase reporter assay showed a relationship between miR-204-5p and RIOK1. *(Continued to the next page)*

lated with tumor HR status, tumor grade, and with patient survival outcomes. Specifically, HR-negative tumors exhibited higher RIOK1 expression, and such elevated RIOK1 expression was in turn associated with reduced BC patient OS in both univariate and multivariate analyses. These results, therefore, indicated that RIOK1 expression level is an independent predictor of BC patient survival outcomes. HR status has been regarded as a determining factor of prognosis and lacked of specific molecular therapy. We found the clinical association between RIOK1 and HR, however, the

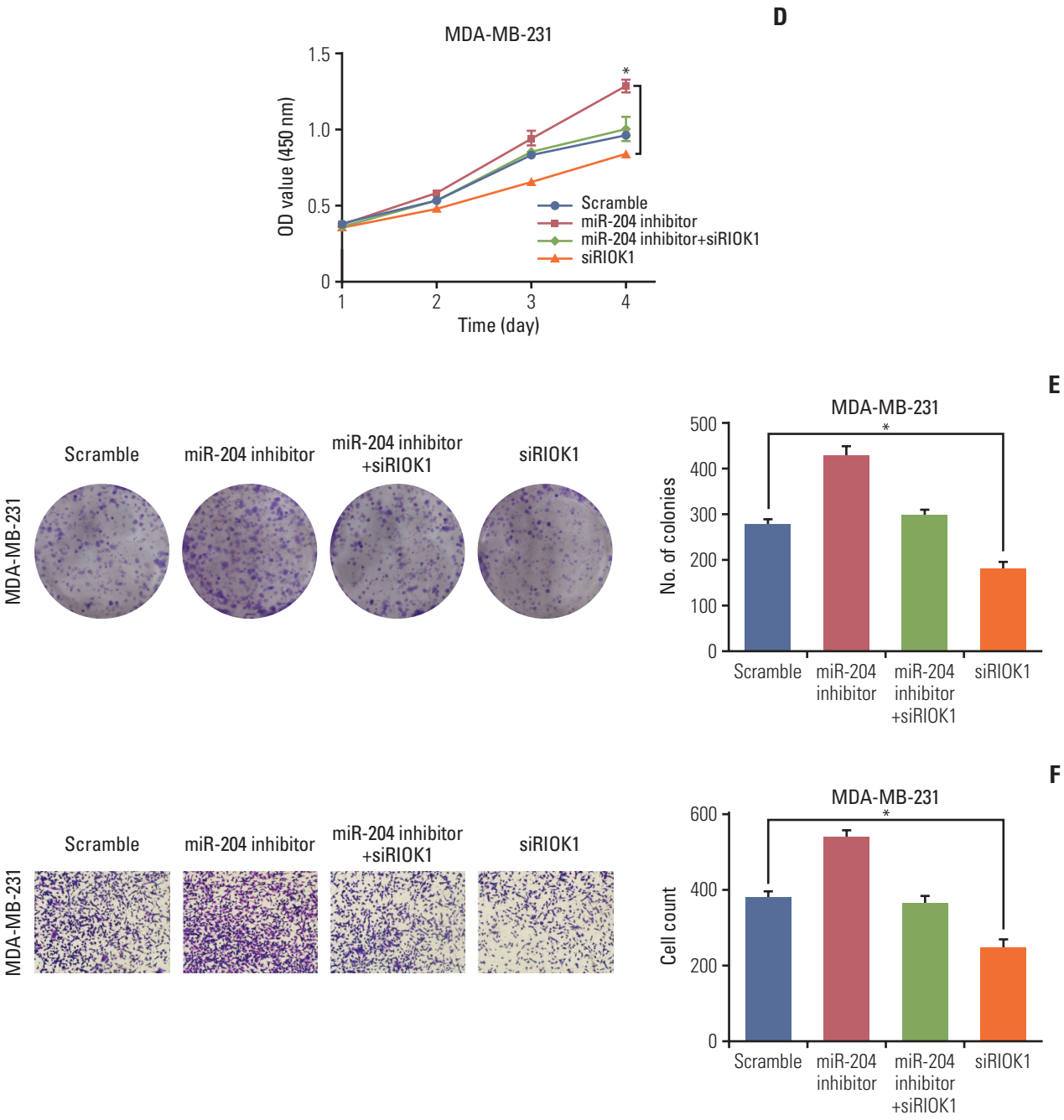

Fig. 6. *(Continued from the previous page)* (D, E) Effect of miR-204-5p and RIOK1 on BC cell proliferation capability. (F) Effect of miR-204-5p and RIOK1 on BC cell migration capability. *p < 0.05.

relationship between RIOK1 and HR was unclear, and further experiments are required to explore this association.

Interestingly, elevated RIOK1 expression was shown to be associated with elevated p53 levels in this analysis, and this has not been previously reported in other cancers. In addition, HR-negative BC patient samples exhibited elevated p53 levels in much the same way that they exhibited higher levels of RIOK1 expression. p53 is well known to function as a tumor suppressor gene, with the wildtype version of the p53 protein functioning to promote DNA repair and cell cycle arrest when it is [22,23]. Mutations that disrupt such wild type p53 functionality, however, are very common in tumors, affecting upwards of 80% of triple-negative BC and other serious tumor types [24]. As a result, such p53 mutations in immunohistochemistry are closely associated with reduced BC patient survival [25,26]. Previous work by Darb-Esfahani et al. [27] has further demonstrated that p53 levels are higher in triple-negative BC (74.8%) and HER2-pos-

itive BC (55.4%), suggesting that such tumors may express high levels of mutant p53 that are associated with a poorer patient prognosis. Previous studies have largely failed to address the relationship between RIO family proteins and p53, with just one study having demonstrated an interaction between these proteins and p53 activity [14]. In this study, only clarified the clinical link between RIOK1 and p53, but further follow-up experiments will be needed to understand the mechanistic basis for this association.

Finally, through cell phenotypes assays, we found RIOK1 could affected various tumor process such as proliferation, apoptosis, cell cycle, migration, and ivnvasion of BC cells. To investigate the mechanism on the subsequent studies, we detected several protein levels that regulate tumor process such as epithelial-mesenchymal transition, PI3K/AKT, and MAPK/ERK. To figure out what regulate RIOK1, we used four databases to find out the potential upstream miRNA. Only one miR-204-5p was in the list. MiR-204-5p was reported to be a tumor suppressor in BC patients and predicted poorer prognosis [28]. Shen et al. [29] revealed that the upregulation of miR-204-5p inhibits the proliferation, invasion, and migration of BC cells. In addition, in BC spheroids, miR-204 was downregulated in MDA-MB-231 cells than in MCF-7 cells, which means miR-204 could be associated with HR status, similarily [30]. We verified the relationship between miR-204 and RIOK1 by luciferase assay and co-transfected miR-204 and siRIOK1. According to our study, several assays indicated that miR-204-5p could regulate RIOK1 activity. Therefore, we speculated that miR-204-5p could be a potential regulator of RIOK1.

In summary, the results of this analysis for the first time indicate that HR-negative BC tumor tissues exhibit higher levels of RIOK1 expression, with RIOK1 expression also being associated with other clinicopathological characteristics in these patients. Importantly, elevated RIOK1 levels were associated with a poorer BC patient prognosis. RIOK1 expression levels were also associated with those of p53, which is already known to be a predictor of poor BC patient outcomes. RIOK1 could regulate BC cells proliferation, apoptosis, and metastasis by affecting the PI3K/AKT and MAPK/ERK signaling pathways in HR-negative BC cells. As such, we identified RIOK1 as a potential therapeutic target in patients with BC, although further in-depth multi-disciplinary studies will be needed to validate this possibility.

Electronic Supplementary Material

Supplementary materials are available at Cancer Research and Treatment website (https://www.e-crt.org).

Conflict of Interest

Conflict of interest relevant to this article was not reported.

Acknowledgments

We would like to thank Xingyu Li and Tian Xie for their support in data collection and analysis. This study was partially supported by a Nantong City-level Science and Technology Plan Project fund from Kan Ni (Number GJZ17086).

References

1. Ferlay J, Soerjomataram I, Dikshit R, Eser S, Mathers C, Rebelo M, et al. Cancer incidence and mortality worldwide: sources, methods and major patterns in GLOBOCAN 2012. Int J Cancer. 2015;136:E359-86.
2. Siegel R, Naishadham D, Jemal A. Cancer statistics, 2012. CA Cancer J Clin. 2012;62:10-29.
3. Coates AS, Winer EP, Goldhirsch A, Gelber RD, Gnant M, Piccart-Gebhart M, et al. Tailoring therapies: improving the management of early breast cancer: St Gallen International Expert Consensus on the Primary Therapy of Early Breast Cancer 2015. Ann Oncol. 2015;26:1533-46.
4. Beith J, Burslem K, Bell R, Woodward N, McCarthy N, De Boer R, et al. Hormone receptor positive, HER2 negative metastatic breast cancer: a systematic review of the current treatment landscape. Asia Pac J Clin Oncol. 2016;12 Suppl 1:3-18.
5. Gerratana L, Fanotto V, Bonotto M, Bolzonello S, Minisini AM, Fasola G, et al. Pattern of metastasis and outcome in patients with breast cancer. Clin Exp Metastasis. 2015;32:125-33.
6. Sihto H, Lundin J, Lundin M, Lehtimaki T, Ristimaki A, Holli K, et al. Breast cancer biological subtypes and protein expression predict for the preferential distant metastasis sites: a nationwide cohort study. Breast Cancer Res. 2011;13:R87.
7. Pienkowski T, Zielinski CC. Trastuzumab treatment in patients with breast cancer and metastatic CNS disease. Ann Oncol. 2010;21:917-24.
8. Vaz-Luis I, Lin NU, Keating NL, Barry WT, Winer EP, Freedman RA. Factors associated with early mortality among patients with de novo metastatic breast cancer: a population-based study. Oncologist. 2017;22:386-93.
9. LaRonde-LeBlanc N, Wlodawer A. A family portrait of the RIO kinases. J Biol Chem. 2005;280:37297-300.
10. LaRonde NA. The ancient microbial RIO kinases. J Biol Chem. 2014;289:9488-92.
11. Baumas K, Soudet J, Caizergues-Ferrer M, Faubladier M, Henry Y, Mougin A. Human RioK3 is a novel component of cytoplasmic pre-40S pre-ribosomal particles. RNA Biol. 2012;9:162-74.
12. Dez C, Tollervey D. Ribosome synthesis meets the cell cycle. Curr Opin Microbiol. 2004;7:631-7.
13. Kimmelman AC, Hezel AF, Aguirre AJ, Zheng H, Paik JH, Ying H, et al. Genomic alterations link Rho family of GTPases

to the highly invasive phenotype of pancreas cancer. Proc Natl Acad Sci U S A. 2008;105:19372-7.
14. Read RD, Fenton TR, Gomez GG, Wykosky J, Vandenberg SR, Babic I, et al. A kinome-wide RNAi screen in Drosophila Glia reveals that the RIO kinases mediate cell proliferation and survival through TORC2-Akt signaling in glioblastoma. PLoS Genet. 2013;9:e1003253.
15. Weinberg F, Reischmann N, Fauth L, Taromi S, Mastroianni J, Kohler M, et al. The atypical kinase RIOK1 promotes tumor growth and invasive behavior. EBioMedicine. 2017;20:79-97.
16. Hong X, Huang H, Qiu X, Ding Z, Feng X, Zhu Y, et al. Targeting posttranslational modifications of RIOK1 inhibits the progression of colorectal and gastric cancers. Elife. 2018;7:e29511.
17. Manning G, Plowman GD, Hunter T, Sudarsanam S. Evolution of protein kinase signaling from yeast to man. Trends Biochem Sci. 2002;27:514-20.
18. Manning G, Whyte DB, Martinez R, Hunter T, Sudarsanam S. The protein kinase complement of the human genome. Science. 2002;298:1912-34.
19. Angermayr M, Roidl A, Bandlow W. Yeast Rio1p is the founding member of a novel subfamily of protein serine kinases involved in the control of cell cycle progression. Mol Microbiol. 2002;44:309-24.
20. Cox AD, Fesik SW, Kimmelman AC, Luo J, Der CJ. Drugging the undruggable RAS: Mission possible? Nat Rev Drug Discov. 2014;13:828-51.
21. Alvarado R, Lari SA, Roses RE, Smith BD, Yang W, Mittendorf EA, et al. Biology, treatment, and outcome in very young and older women with DCIS. Ann Surg Oncol. 2012;19:3777-84.
22. Sionov RV, Haupt Y. The cellular response to p53: the decision between life and death. Oncogene. 1999;18:6145-57.
23. Vousden KH, Lu X. Live or let die: the cell's response to p53. Nat Rev Cancer. 2002;2:594-604.
24. Kandoth C, McLellan MD, Vandin F, Ye K, Niu B, Lu C, et al. Mutational landscape and significance across 12 major cancer types. Nature. 2013;502:333-9.
25. Langerod A, Zhao H, Borgan O, Nesland JM, Bukholm IR, Ikdahl T, et al. TP53 mutation status and gene expression profiles are powerful prognostic markers of breast cancer. Breast Cancer Res. 2007;9:R30.
26. Miller LD, Smeds J, George J, Vega VB, Vergara L, Ploner A, et al. An expression signature for p53 status in human breast cancer predicts mutation status, transcriptional effects, and patient survival. Proc Natl Acad Sci U S A. 2005;102:13550-5.
27. Darb-Esfahani S, Denkert C, Stenzinger A, Salat C, Sinn B, Schem C, et al. Role of TP53 mutations in triple negative and HER2-positive breast cancer treated with neoadjuvant anthracycline/taxane-based chemotherapy. Oncotarget. 2016;7:67686-98.
28. Li W, Jin X, Zhang Q, Zhang G, Deng X, Ma L. Decreased expression of miR-204 is associated with poor prognosis in patients with breast cancer. Int J Clin Exp Pathol. 2014;7:3287-92.
29. Shen SQ, Huang LS, Xiao XL, Zhu XF, Xiong DD, Cao XM, et al. miR-204 regulates the biological behavior of breast cancer MCF-7 cells by directly targeting FOXA1. Oncol Rep. 2017;38:368-76.
30. Boo L, Ho WY, Mohd Ali N, Yeap SK, Ky H, Chan KG, et al. Phenotypic and microRNA transcriptomic profiling of the MDA-MB-231 spheroid-enriched CSCs with comparison of MCF-7 microRNA profiling dataset. PeerJ. 2017;5:e3551.

pISSN 1598-2998, eISSN 2005-9256

Cancer Res Treat. 2020;52(4):1084-1102 https://doi.org/10.4143/crt.2020.093

Original Article Open Access

β1,4-Galactosyltransferase V Modulates Breast Cancer Stem Cells through Wnt/β-catenin Signaling Pathway

Wei Tang, BD[1]
Meng Li, MD[1]
Xin Qi, PhD[1]
Jing Li, PhD[1,2,3]

[1]*Key Laboratory of Marine Drugs, Chinese Ministry of Education, School of Medicine and Pharmacy, Ocean University of China, Qingdao,* [2]*Laboratory for Marine Drugs and Bioproducts of Qingdao National Laboratory for Marine Science and Technology, Qingdao,* [3]*Open Studio for Druggability Research of Marine Natural Products, Pilot National Laboratory for Marine Science and Technology (Qingdao), Qingdao, China*

Correspondence: Jing Li, PhD
Key Laboratory of Marine Drugs, Chinese Ministry of Education, School of Medicine and Pharmacy, Ocean University of China, Yushan Road No. 5, Qingdao 266003, China
Tel: 81-0532-82031980
Fax: 81-0532-82031980
E-mail: lijing_ouc@ouc.edu.cn

Received February 8, 2020
Accepted May 25, 2020
Published Online May 27, 2020

Purpose
Breast cancer stem cells (BCSCs) contribute to the initiation, development, and recurrence of breast carcinomas. β1,4-Galactosyltransferase V (B4GalT5), which catalyzes the addition of galactose to GlcNAcβ1-4Man of N-glycans, is involved in embryogenesis. However, its role in the modulation of BCSCs remains unknown.

Materials and Methods
The relationship between B4GalT5 and breast cancer stemness was investigated by online clinical databases and immunohistochemistry analysis. Mammosphere formation, fluorescence-activated cell sorting (FACS), and *in-vivo* assays were used to evaluate B4GalT5 expression in BCSCs and its effect on BCSCs. B4GalT5 regulation of Wnt/β-catenin signaling was examined by immunofluorescence and *Ricinus communis* agglutinin I pull-down assays. Cell surface biotinylation and FACS assays were performed to assess the association of cell surface B4GalT5 and BCSCs.

Results
B4GalT5, but not other B4GalTs, was highly correlated with BCSC markers and poor prognosis. B4GalT5 significantly increased the stem cell marker aldehyde dehydrogenase 1A1 (ALDH1A1) and promoted the production of $CD44^{+}CD24^{-/low}$ cells and the formation of mammospheres. Furthermore, B4GalT5 overexpression resulted in dramatic tumor growth *in vivo*. Mechanistically, B4GalT5 modified and protected Frizzled-1 from degradation via the lysosomal pathway, promoting Wnt/β-catenin signaling which was hyperactivated in BCSCs. B4GalT5, located on the surface of a small subset of breast carcinoma cells, was not responsible for the stemness of BCSCs.

Conclusion
B4GalT5 modulates the stemness of breast cancer through glycosylation modification to stabilize Frizzled-1 and activate Wnt/β-catenin signaling independent of its cell surface location. Our studies highlight a previously unknown role of B4GalT5 in regulating the stemness of breast cancer and provide a potential drug target for anticancer drug development.

Key words
β1,4-Galactosyltransferase V, Breast cancer stem cell, Cellular location, Frizzled-1, Glycosylation

Introduction

Breast cancer is one of the most common malignant cancers among women worldwide with more than 2 million new cases expected to be diagnosed and 600 thousand deaths in 2018 [1]. Although current treatments, to a certain extent, effectively reduce tumor bulk, many patients with breast cancer still experience recurrence, metastasis, and ultimately death.

Cancer stem cells (CSCs) are a small subset of poorly differentiated tumor cells within a tumor that show self-renewal and differentiation into heterogeneous lineages [2]. CSCs also account for chemo- and radioresistance, resulting in tumor recurrence and eventually metastasis due to the failure of current treatments [2]. Moreover, breast cancer stem cells (BCSCs) are regulated by several transcriptional factors

and signaling pathways, such as Nanog, Oct4, Notch pathway, and Wnt/β-catenin pathway [3]. Extensive evidence has shown that BCSCs are a crucial factor that contributes to the initiation, development, relapse, and chemoresistance of breast cancer.

A growing body of evidence supports aberrant glycosylation of cell surface receptors as a consequence of oncogenic transformation in different aspects of tumor progression, including proliferation, invasion, angiogenesis, and metastasis [4]. Within a tumor, altered glycosylation of proteins is frequently attributed to abnormal expression of glycosyltransferases [5]. Therefore, these enzymes are considered therapeutic targets, as aberrant glycans may be involved in promoting tumor progression and metastasis.

The β1,4-galactosyltransferase (B4GalT) family belongs to type II membrane-bound glycoproteins mainly located in the Golgi apparatus that exclusively transfer an active UDP-galactose in a β1,4 linkage to acceptor sugars [6]. There are currently seven members of the β4GalT gene family, B4Gal-T1-T7, which participate in the biosynthesis of different glycoconjugates and saccharide structures with slightly different substrate affinities and end products [6]. Specifically, B4GalT5 has been reported to catalyze the addition of galactose to GlcNAcβ1-4Man of glycans and functions as an important regulator in extraembryonic development [6]. Considerable research has revealed that extraembryonic development shares similarities with tumorigenesis in terms of biological behaviors (such as migration and invasion, gene expression and protein profiles, signaling pathways, and cell differentiation) [7], strongly suggesting that B4GalT5 may be involved in modulating the stemness of BCSCs. In this study, we demonstrated that B4GalT5 is upregulated in BCSCs to maintain the stemness of these cells by glycosylating the receptor Frizzled-1 and constantly activating Wnt/β-catenin signaling. Furthermore, we showed that B4GalT5 is located on the cell surface of a small subset of breast cancer cells, but cell surface localization did not play a decisive role in the stemness of BCSCs.

Materials and Methods

1. Reagents

Roswell Park Memorial Institute (RPMI) 1640 medium, minimum essential medium (MEM), Leibovitz's L-15 medium, Dulbecco's modified Eagle medium: nutrient mixture F-12 (DMEM/F-12), epidermal growth factor (EGF), basic fibroblast growth factor (bFGF), and B27 were purchased from Gibco (Grand Island, NY). Fetal bovine serum (FBS) and trypsin were purchased from Gibco-Invitrogen. Insulin and fluorescein isothiocyanate (FITC)-conjugated goat anti-rabbit antibody were purchased from Solarbio (Beijing, China). Antibodies to detect aldehyde dehydrogenase 1A1 (ALDH1A1), phosphorylated GSK3β (Ser 9), β-catenin, phosphorylated β-catenin (Ser 45), Erk, and His were products of Cell Signaling Technology (Boston, MA). SuperSignal West Femto Maximum Sensitivity Substrate, EZ-Link Sulfo-NHS-SS-Biotin, Pierce NeutrAvidin agarose, anti-B4GalT5, FITC-conjugated anti-CD44 and allophycocyanin (APC)-conjugated anti-CD24 antibodies were obtained from Thermo Scientific (Waltham, MA). Anti–Frizzled-1 and phycoerythrin (PE)-conjugated anti-His antibodies were purchased from R&D Systems (Minneapolis, MN). PE-conjugated anti–epithelial specific antigen antibody was purchased from Biolegend (San Diego, CA). The primary antibodies (β-actin and glyceraldehyde 3-phosphate dehydrogenase) and the secondary antibodies were purchased from HuaBio (Hangzhou, China). Horseradish peroxidase (HRP)-streptavidin, biotinylated *Ricinus communis* agglutinin I (RCA-I), and agarose-bound RCA-I were obtained from Vector Laboratories (Burlingame, CA). 3-(4,5-dimethyl-2-thiazolyl)-2,5-diphenyl-2-H-tetrazolium bromide (MTT) was purchased from Sigma-Aldrich (St. Louis, MO). The ALDEFLUOR Kit was purchased from Stem Cell Technologies (Vancouver, BC, Canada). The Mycoplasma PCR Detection Kit, DAPI, cell lysis buffer for western blot and immunoprecipitation (IP), phenylmethanesulfonylfluoride (PMSF), MG132, membrane and cytosol protein extraction kit and BCA Protein Assay Kit were purchased from Beyotime Institute of Biotechnology (Shanghai, China). B4GalT5 siRNA, NC siRNA, shB4GalT5 plasmid, and shNC plasmid were constructed by GenePharma (Shanghai, China). Triptolide with purity > 99% was obtained from Shanghai Institute of Materia Medica. Wnt 3β and leupeptin were obtained from the Laboratory of Molecular Medicine at Ocean University of China.

2. Tissue microarray

Tissue microarray (TMA; HBreD090CS01) was purchased from Shanghai Outdo Biotech Co., Ltd. (Shanghai, China). The TMA has 90 cores from 45 patients with invasive breast cancer, including 45 tumor tissues and 45 corresponding adjacent tissues. The immunohistochemical staining rate was classified as 0 (negative), 1 (1%-25% positive tumor cells), 2 (26%-50%), 3 (51%-75%), and 4 (76%-100%). Staining intensity was classified as 0 (absence of stained cells), 1 (weak staining), 2 (moderate staining), and 3 (strong staining). The immunohistochemistry (IHC) score was calculated by multiplying the staining rate and intensity. Correlations were determined by Spearman's coefficient of correlation.

3. Cell culture

MCF-7, adriamycin-resistant MCF-7 (MCF-7ADR), and MDA-MB-231 cell lines were purchased from the Cell Bank of the Chinese Academy of Sciences (Shanghai, China). Cell lines were validated using short tandem repeat analysis by Genesky Biotechnology Inc., Shanghai (Shanghai, China),

and tested for the absence of mycoplasma contamination by PCR using the Mycoplasma PCR Detection Kit. MCF-7 cells were maintained in MEM supplemented with 10% FBS, 0.01 mg/mL human recombinant insulin, and 1 μM nonessential amino acids. MCF-7ADR cells were cultured in RPMI-1640 medium supplemented with 10% FBS. MDA-MB-231 cells were cultured in L-15 medium supplemented with 15% FBS. Adriamycin was added on time to maintain the drug resistance phenotype of MCF-7ADR cells.

4. MTT assay

The MTT assay was used to measure the inhibitory effect of compounds on the viability of cancer cells. Adherent cells were seeded in 96-well plates at a density of 5,000 cells per well. After 24 hours, the cells were treated with different concentrations of triptolide for 72 hours. Twenty microliters of MTT solution was added to each well and incubated for 4 hours at 37°C. Then, dimethyl sulfoxide was added to the wells and incubated overnight at 37°C. The absorbance at 570 nm was measured using a microplate reader (BioTek, Winooski, VT).

5. Clinical dataset analysis

To analyze the expression of B4GalTs in invasive breast carcinomas compared with normal breast tissues, we used The Cancer Genome Atlas (TCGA) breast dataset from the Oncomine browser (https://www.oncomine.org).

Kaplan-Meier plotter (http://kmplot.com/analysis/index.php?p=background) was used to analyze the correlation between B4GalT5 expression and recurrence-free survival (RFS) in patients with breast cancer in 120 months [8].

The coexpression of B4GalT5 and CCR7, C-X-C chemokine receptor 4 (CXCR4), and ATP binding cassette subfamily B member 1 (ABCB1) was assessed in invasive breast invasive carcinoma samples from TCGA dataset by 'R2: Genomics Analysis and Visualization Platform' (http://r2.amc.nl). We also analyzed the coexpression of B4GalTs and ALDH1A1 and c-myc from GEPIA 2 from Zhang's lab [9]. Correlations were determined by Pearson's coefficient of correlation.

6. Flow cytometry analysis and sorting

For analysis of BCSC and non-BCSC cell fractions, cells were incubated with FITC-conjugated anti-CD44 antibody and PE or APC-conjugated anti-CD24 antibody in phosphate buffered saline (PBS) containing 2% FBS at 4°C for 30 minutes. BCSCs ($CD44^+CD24^{-/low}$) and non-BCSCs ($CD44^+CD24^+$) were analyzed and sorted by flow cytometry (MFLO XDP, Beckman Coulter, Pasadena, CA). The ALDEFLUOR Kit was used for the identification of BCSCs that express high levels of the enzyme aldehyde dehydrogenase (ALDH) according to the manufacturer's protocol.

For analysis of the proportions of the $CD24^{-/low}$ cell population in the His^+ cell population and His^- cell population, cells were incubated with PE-conjugated anti-His antibody and APC-conjugated anti-CD24 antibody in PBS containing 2% FBS at 4°C for 30 minutes. The samples were analyzed by flow cytometry (MFLO XDP, Beckman Coulter). The calculation method is as follows.

The proportion of $CD24^{-/low}$ cells in the His^+ cell population=$His^+CD24^{-/low}$ cells %/His^+ cells %.

The proportion of $CD24^{-/low}$ cells in the His^- cell population=$His^-CD24^{-/low}$ cells %/His^- cells %.

7. Plasmids

The DNA fragment for B4GalT5 was cloned from human cDNA using the corresponding primers and inserted into the pLVX-IRES-ZsGreen1 vector. The DNA fragment for B4GalT5-His was cloned from human cDNA using primers including His sequence and inserted into the pBABE-puro vector. These constructed vectors were transformed into DH5α cells and then amplified. The primers for B4GalT5 were 5′-CCGCTCGAGTGGCTGCAGCATGCGCG-3′ and 5′-CGCGGATCCTCAGTACTCGTTCACCTGAG-3′. The primers for B4GalT5-His were 5′-CGCGGATCCATGCGCGCCCGCCGGGGGCTGCT-3′ and 5′-CCGGAATTCTCAATGGTGATGGTGATGATGGT-3′.

8. siRNA and plasmid transfections

For siRNA transfection, cells were transfected at 80% confluency in 6-well plates with 50 nM control siRNA or B4GalT5-targeting siRNA (si-B4GalT5) (sense, 5′-CGGAGUGAGUGGCUUAACAdTdT-3′; antisense, 5′-UGUUAAGCCACUCACUCCGdTdT-3′) using Lipo2000 transfection reagents according to the manufacturer's instructions. The knockdown efficiency was examined by western blotting after 48 hours.

For plasmid transfection, cells were transfected with the plasmids using Lipo3000 transfection reagents according to the manufacturer's instructions. After 48 hours, the cells were treated with G418 or puromycin to screen for stably transfected MCF-7ADR cell lines. The stably transfected MCF-7ADR cell lines are as follows: B4GalT5-knockdown MCF-7ADR (MCF-7ADR/shB4GalT5), B4GalT5-overexpressing MCF-7ADR (MCF-7ADR/oe-B4GalT5), and MCF-7ADR expressing B4GalT5-His (MCF-7ADR/B4GalT5-His).

9. Mammosphere formation assay

For analysis of the effect of B4GalT5 on mammosphere formation, a single-cell suspension was quantified and seeded in ultralow attachment 6-well plates at a density of 2,000 cells per well at 37°C and 5% CO_2. Mammospheres were formed in serum-free DMEM/F-12 medium containing 20 ng/mL EGF, 10 ng/mL bFGF, 2% B27, and 5 μg/mL insulin. After 7 days, mammospheres with a diameter of > 50 μm were counted using a cell imaging multi-mode reader (BioTek).

For determination of the effect of triptolide on mammos-

pheres, single-cell suspensions were quantified and seeded in ultralow attachment 6-well plates at a density of 2,000 cells per well at 37°C and 5% CO_2. Mammospheres were formed in serum-free DMEM/F-12 medium containing 20 ng/mL EGF, 10 ng/mL bFGF, 2% B27, and 5 μg/mL insulin with treatment with PBS or different concentrations of triptolide. After 7 days, mammospheres with a diameter of > 50 μm were counted using a cell imaging multi-mode reader (Bio-Tek).

10. Colony formation assay

Five hundred microliters of pre-warmed 2×1,640 medium containing 20% FBS, 200 U/mL penicillin, 200 μg/mL streptomycin, and 500 μL of melted 1.2% agarose solution was mixed and transferred to a 6-well plate. When the bottom agar layer solidified, 1 mL of melted 0.7% agarose solution and 1 mL of single-cell suspension at a density of 500 cells per mL treated with increasing concentrations of triptolide were mixed and seeded on the bottom agar layer. The cells were incubated for 30 days at 37°C and 5% CO_2. The colonies were treated with 0.5 mL of MTT per well for 30 minutes at 37°C, and colonies containing up to 50 cells were counted.

11. Protein extraction, pull down, and immunoblotting

For the RCA-I pull-down assay, cells were lysed on ice for 30 minutes in cell lysis buffer for western and IP with 1 mM PMSF. Three hundred micrograms of total cell lysates were centrifuged at 12,000 ×g and 4°C for 10 minutes and then incubated with RCA-I agarose beads at 4°C overnight. After the samples were washed three times using cell lysis buffer, pulled-down proteins were subjected to western blotting. Total Frizzled-1 expression level was used as loading control.

For western blotting, membrane and cytosol proteins of MCF-7ADR cells were extracted by the membrane and cytosol extraction kit according to the manufacturer's instructions. Total cell lysates were prepared using loading buffer on ice for 45 minutes and denatured at 95°C for 15 minutes followed by sodium dodecyl sulfate polyacrylamide gel electrophoresis (SDS-PAGE). Then, the samples were transferred to Immobilon-P polyvinylidene difluoride membranes, blocked with 5% non-fat milk, and incubated with the indicated antibodies. SuperSignal West Femto Maximum Sensitivity Substrate was used to detect HRP-conjugated secondary antibodies.

12. Cell surface biotinylation assay

After the samples were washed twice with cold PBS, MCF-7ADR cells were incubated with EZ-Link Sulfo-NHS-SS-Biotin at a final concentration of 0.5 mg/mL for 60 minutes at 4°C, followed by a 50 mM glycine/PBS wash and two washes with PBS. Biotinylated cells were lysed with cell lysis buffer for western and IP and then centrifuged for 15 minutes at 12,000 ×g and 4°C. The supernatant was incubated with PNeutrAvidin agarose beads and mixed at 4°C overnight. Biotinylated proteins were eluted from the beads by heating to 100°C for 5 minutes in SDS-PAGE sample buffer before loading into the SDS-PAGE gel for western blotting.

13. Immunofluorescence assay

For detection of the p-GSK3β (Ser 9) and B4GalT5 expression levels, cells were cultured on a 96-well black-wall glass bottom plate for 24 hours. They were fixed with 4% paraformaldehyde for 30 minutes, permeabilized with 0.3% Triton X-100 for 20 minutes and blocked with 1% bovine serum albumin (BSA) in PBS for 1 hour. The cells were incubated with primary antibody (1:50) in blocking buffer. After sufficient washing, the cells were incubated with FITC-conjugated goat anti-rabbit antibody to detect the primary antibody. The cells were incubated with DAPI for 10 minutes. The resulting images were taken using a laser scanning confocal microscope (Carl Zeiss, Jena, Germany).

For detection of B4GalT5-His and CD24 on the cell surface, the cells were digested and resuspended in 1% BSA in PBS. The cells were incubated with anti-His antibody (1:50) in 1% BSA. After sufficient washing, the cells were incubated with FITC-conjugated goat anti-rabbit antibody and APC-conjugated anti-CD24 antibody for 1 hour. The resulting images were taken using a laser scanning confocal microscope (Carl Zeiss).

14. Animal studies

MCF-7ADR/NC and B4GalT5-overexpressing MCF-7ADR (MCF-7ADR/oe-B4GalT5) cells were subcutaneously transplanted into 14-15 g, 6-week-old female BALB/c nude mice (Beijing Vital River Laboratory Animal Technology Co., Ltd., Beijing, China) at a concentration of 2×10^6 cells per site. Five mice were used in each group for analysis of B4GalT5-induced tumor initiation. The tumor volumes of these mice were measured every week to assess tumor initiation and growth. These tumors were dissected 9 weeks after transplantation and weighed. Then, these tumors were excised, ground, and lysed in loading buffer on ice for 45 minutes. Protein lysates were boiled for 10 minutes and then subjected to western blotting.

15. Statistical analysis

Statistical comparisons between two groups were performed by two-tailed Student's t tests. The means were calculated using at least three biological replicates. Error bars represent the standard error of the mean for three independent experiments. p-values of < 0.05 were considered statistically significant.

16. Ethical statement

This study was approved by School of Medicine and Pharmacy, Ocean University of China, and performed in accord-

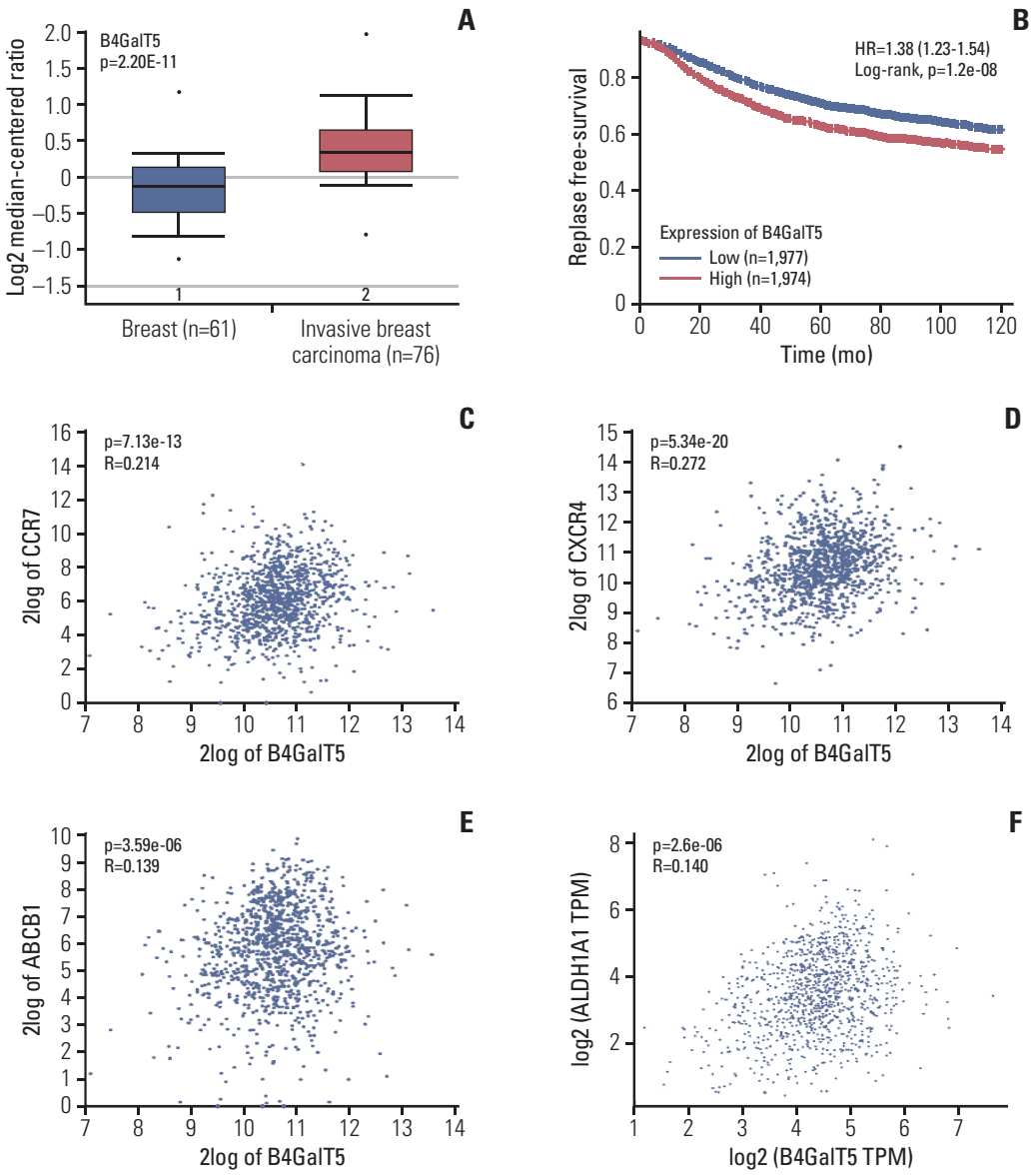

Fig. 1. β1,4-Galactosyltransferase V (B4GalT5) is associated with the stemness of breast cancer. (A) The Cancer Genome Atlas (TCGA) breast dataset analysis of B4GalT5 mRNA levels in invasive breast carcinomas (n=76) and normal breast tissues (n=61) using the Oncomine browser. (B) Kaplan-Meier survival curves for patients with breast cancer (n=3,955) in 120 months. The correlation between B4GalT5 expression and relapse-free survival of patients with breast cancer were analyzed using Kaplan-Meier plotter. (C-E) Correlation between B4GalT5 and CC-chemokine receptor 7 (CCR7) (C), C-X-C chemokine receptor 4 (CXCR4) (D), or ATP binding cassette subfamily B member 1 (ABCB1) (E) mRNA levels in invasive breast carcinoma samples from TCGA dataset (n=1,097) using 'R2: Genomics Analysis and Visualization Platform.' (F) The correlation between B4GalT5 and aldehyde dehydrogenase 1A1 (ALDH1A1) mRNA levels in breast carcinoma patients from TCGA dataset using GEPIA 2. *(Continued to the next page)*

ance with the National Institutes of Health Guide for the Care and Use of Laboratory Animals (NIH publication, 8th edition, 2011).

Results

1. B4GalT5 is associated with the stemness of breast carcinoma

To investigate the relationship between B4GalT5 and BCSCs, we first used online database analysis to compare the B4GalT5 expression level in invasive breast carcinomas with that in normal breast tissues, as CSCs are thought to be close-

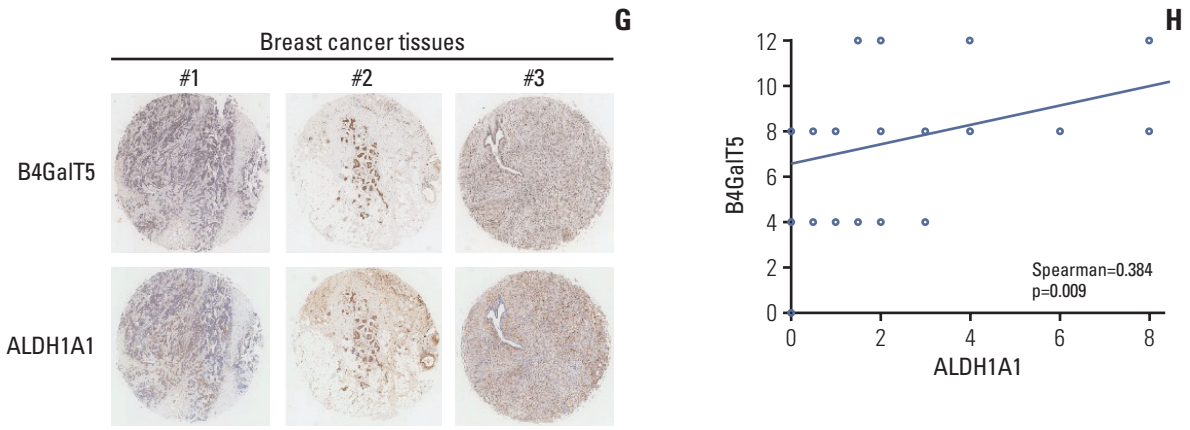

Fig. 1. *(Continued from the previous page)* (G) Representative images of B4GalT5 and ALDH1A1 expression in the breast tumor microarray by immunohistochemistry (IHC) analysis. (H) The correlation between B4GalT5 and ALDH1A1 IHC scores of 45 cores of the breast tumor microarray.

Table 1. B4GalTs mRNA levels in invasive breast carcinomas (n=76) and normal breast tissues (n=61)

Gene	Fold change (vs. normal)	p-value[a)]
B4GalT1	1.579	9.65e-7
B4GalT2	1.589	1.91e-9
B4GalT3	2.059	7.05e-27
B4GalT4	1.393	2.50e-9
B4GalT5	1.507	2.20E-11
B4GalT6	–1.615	1.000
B4GalT7	1.459	1.48e-6

B4GalT, β1,4-galactosyltransferase V. [a)]$p < 0.01$, statistically significant.

Table 2. Correlation between B4GalTs and ALDH1A1 in breast carcinoma samples from TCGA breast dataset

Gene	r (Pearson)[a)]	p-value[b)]
B4GalT1	–0.026	0.39
B4GalT2	–0.091	0.0026
B4GalT3	–0.038	0.21
B4GalT4	0.034	0.27
B4GalT5	0.14	2.6e-06
B4GalT6	0.2	2.4e-11
B4GalT7	–0.042	0.16

B4GalT, β1,4-galactosyltransferase V; ALDH1A1, aldehyde dehydrogenase 1A1; TCGA, The Cancer Genome Atlas. [a)]$r > 0$, positive correlation; $r < 0$, negative correlation, [b)]$p < 0.01$, statistically significant.

ly correlated with the migration and invasiveness of cancer cells [2]. The TCGA breast dataset showed that B4GalT5 was highly expressed in invasive breast carcinomas (Fig. 1A). Kaplan-Meier survival curves for patients with breast cancer (n=3,955) also showed that patients with high expression of B4GalT5 had lower RFS than those with low expression (Fig. 1B, S1 Table). Because BCSCs can establish metastasis and evade traditional anti-tumor therapies [2], we further examined the correlation between B4GalT5 and these malignant phenotypes. Online database analysis showed a positive correlation between B4GalT5 and CC-chemokine receptor 7 (CCR7; R=0.214, p=7.13e-13) (Fig. 1C), CXCR4 (R=0.272, p=5.34e-20) (Fig. 1D), and multidrug resistance protein 1 (ABCB1) (R=0.139, p=3.59e-06) (Fig. 1E), which are involved in tumor metastasis and chemoresistance [10,11]. These results indicate that B4GalT5 is correlated with cancer progression and may be related to BCSCs. ALDH1A1 is related to cancer stem-like features and its high expression and activity has also been proposed as a reliable CSC marker [12]; therefore, we further detected the correlation between B4GalT5 and ALDH1A1. We found that B4GalT5 was positively associated with ALDH1A1 (R=0.14, p=2.6e-06) (Fig. 1F). Since the B4GalT family has seven members, we further investigated the relationship of other B4GalTs and the malignancy of breast carcinoma by online database analysis and found that most B4GalTs (except B4GalT6) were highly expressed in invasive breast carcinomas compared with normal breast tissues (Table 1). Of note, B4GalT5 was the only member positively correlated with the BCSC marker ALDH1A1 (Table 2). For further verification, the expression of B4GalT5 and ALDH1A1 was detected in a tumor microarray containing 45 cancer tissues from patients with invasive breast cancer. Pathologic information regarding these patients is presented in S2 Table. There was a positive correlation between B4GalT5 and ALDH1A1 expression (Spearman=0.384, p=0.009) in 45 patients (Fig. 1G and H). Collectively, these results suggest a critical role of B4GalT5 in regulating the stemness of BCSCs.

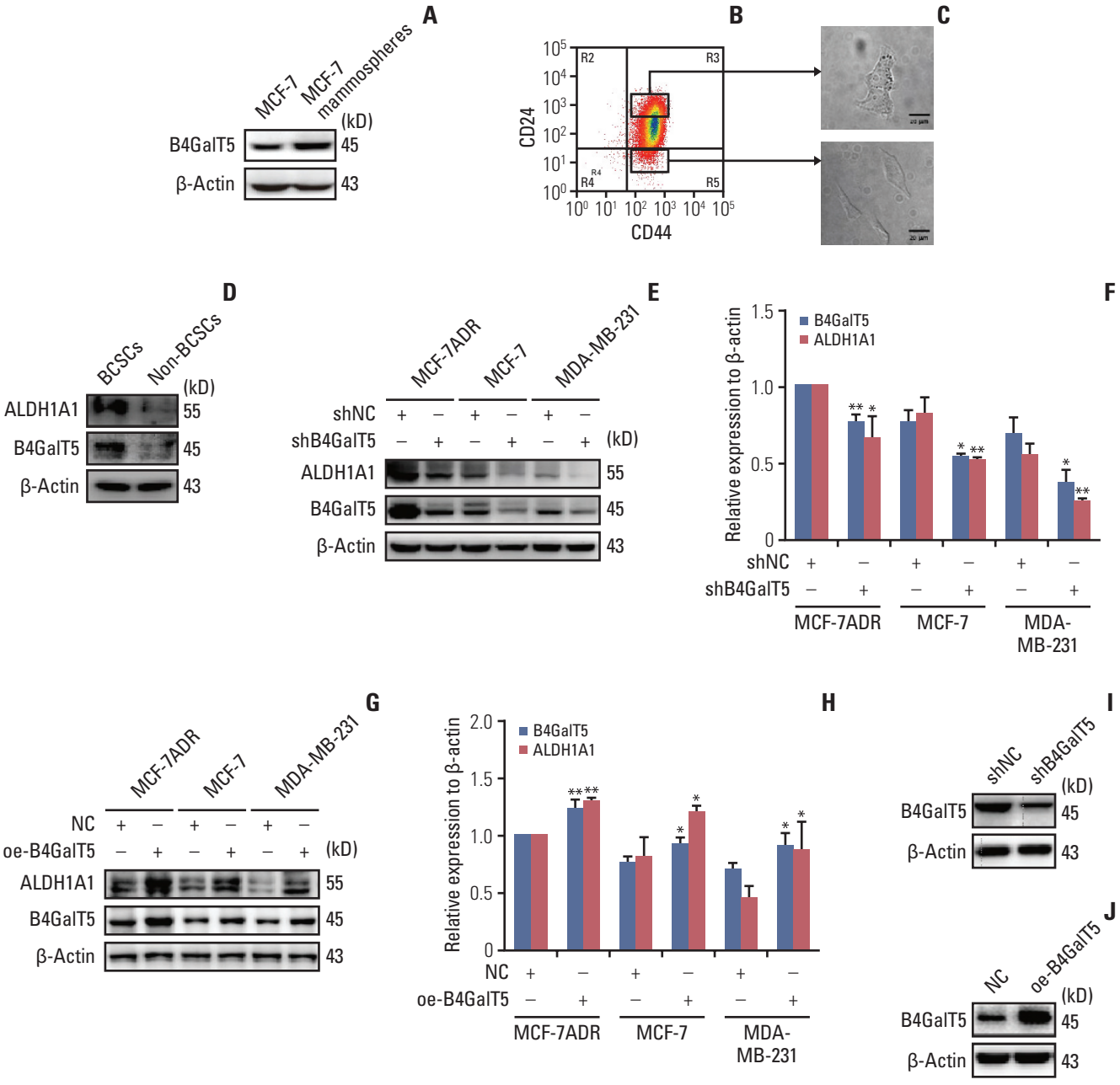

Fig. 2. β1,4-Galactosyltransferase V (B4GalT5) is required for maintaining the stemness of breast cancer. (A) Western blotting analysis of B4GalT5 expression levels in intact MCF-7 cells and MCF-7 mammospheres. (B) Flow cytometry (FCM) analysis and sorting of $CD44^{+}CD24^{-/low}$ cells (breast cancer stem cells [BCSCs]) and $CD44^{+}CD24^{+}$ cells (non-BCSCs) in MCF-7ADR cells. (C) Patterns of BCSCs and non-BCSCs sorted from MCF-7ADR cells. Scale bars=20 μm. (D) Western blotting analysis of B4GalT5 and aldehyde dehydrogenase 1A1 (ALDH1A1) expression levels in BCSCs and non-BCSCs sorted from MCF-7ADR cells. (E-H) Effects of B4GalT5 on ALDH1A1 expression in breast cancer cells by western blotting. MCF-7, MCF-7ADR, and MDA-MB-231 cells were transfected using shB4GalT5 (E, F) or B4GalT5 (G, H) plasmids for 48 hours and subjected to western blotting compared to the negative control. Protein band densities were quantified by normalizing to β-actin. (I, J) Expression levels of B4GalT5 in MCF-7ADR/shB4GalT5 (I) and MCF-7ADR/oe-B4GalT5 (J) compared to the negative control. *(Continued to the next page)*

2. B4GalT5 is required for maintaining the stemness of breast cancer

To further investigate the relationship between B4GalT5 and BCSCs, we performed *in vitro* studies using MCF-7 and MCF-7ADR breast cancer cell lines. CSCs can form mammospheres in serum-free culture medium supplemented

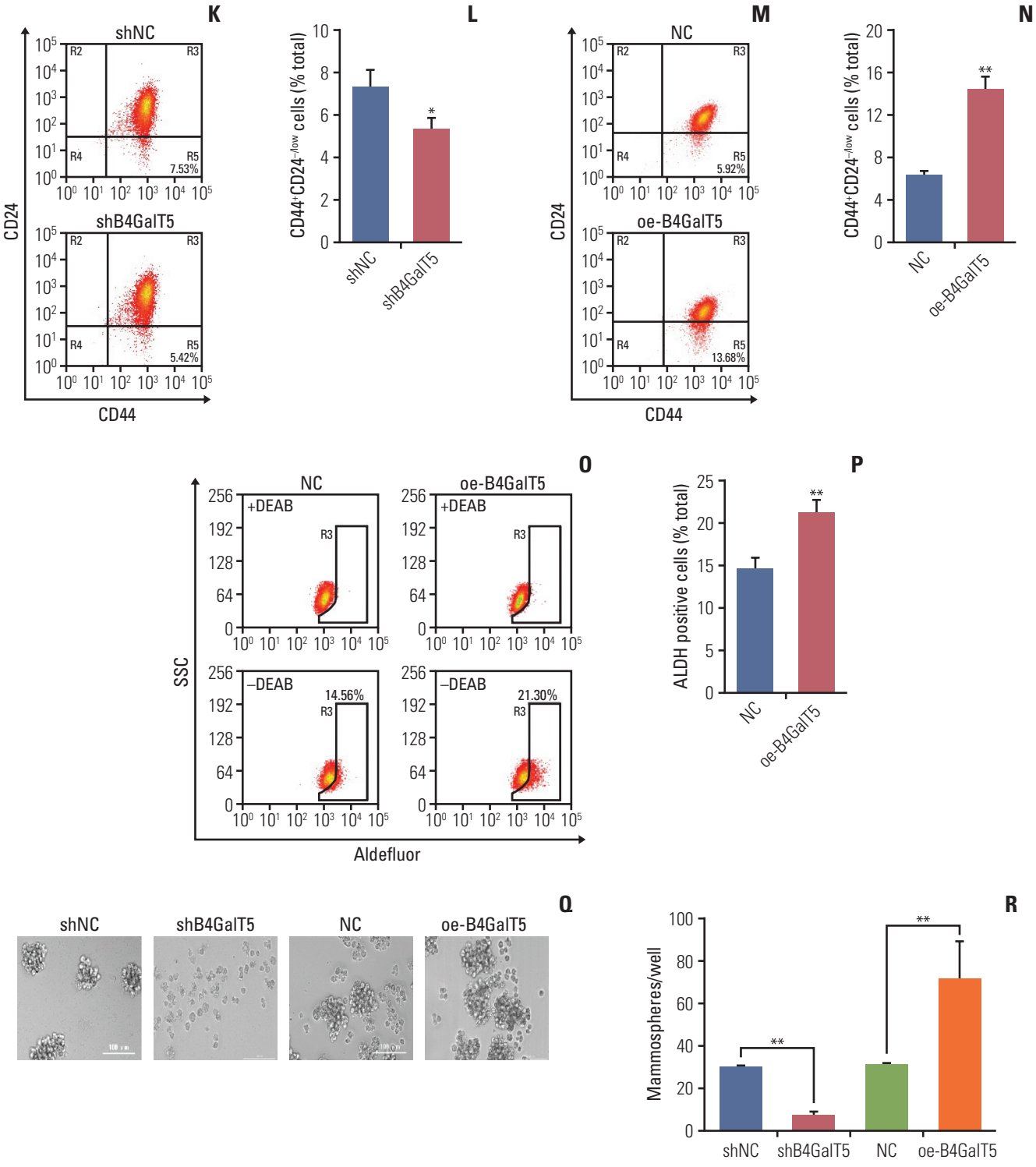

Fig. 2. *(Continued from the previous page)* (K-N) Influences of B4GalT5 on the proportion of $CD44^{+}CD24^{-/low}$ cells in MCF-7ADR/shB4GalT5 (K, L) or MCF-7ADR/oe-B4GalT5 (M, N) cells compared to the negative control. Cells were stained with anti-CD44 and anti-CD24 antibodies and analyzed by FCM. (O, P) FCM analysis of ALDH+ cells in MCF-7ADR/oe-B4GalT5 cells compared to MCF-7ADR/NC cells. The cells were stained and analyzed as described. (Q, R) The sizes and numbers of mammospheres formed by MCF-7ADR/shB4GalT5 and MCF-7ADR/oe-B4GalT5 compared to the negative control groups. Two thousand cells per well were cultured in serum-free medium for seven days. Formed mammospheres were quantified, and images of formed spheres with a diameter of > 50 μm were taken with a light microscope. Scale bars=100 μm. *(Continued to the next page)*

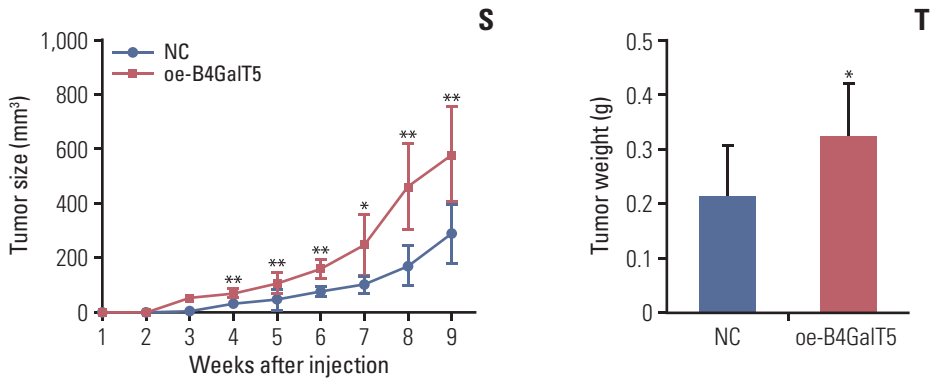

U

Days after injection	1	28	35	42	49	56	63
NC	0/5	0/5	0/5	0/5	2/5	3/5	5/5
oe-B4GalT5	0/5	3/5	4/5	5/5	5/5	5/5	5/5

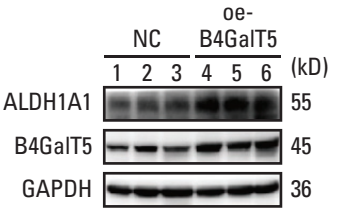

Fig. 2. *(Continued from the previous page)* (S, T) Volumes (S) and weights (T) of tumor formed by MCF-7ADR/NC and MCF-7ADR/oe-B4GalT5 cells in BALB/c nude mice. MCF-7ADR/NC and MCF-7ADR/oe-B4GalT5 cells were subcutaneously transplanted into female BALB/c nude mice at the concentration of 2×10^6 cells per site. After 9 weeks, the mice were sacrificed for measurement of tumor weights (n=5, per group). (U) Statistics of tumors with a volume of 100 mm^3 after subcutaneous injection of MCF-7ADR cells. (V) Western blotting analysis of B4GalT5 and ALDH1A1 expression in tumor tissues. All experiments were performed in three replicates. All data are representative and shown as means±standard error of the mean. *$p < 0.05$, **$p < 0.01$, vs. negative control (NC).

with appropriate growth factors due to their capacity for self-renewal and multipotent differentiation; the mammosphere formation assay is also widely used in the isolation and enrichment of CSCs. First, we compared the B4GalT5 expression in MCF-7 mammospheres versus intact MCF-7 cells. As shown in Fig. 2A, western blotting analysis showed that B4GalT5 was highly expressed in the MCF-7 mammospheres.

Because $CD44^+CD24^{-/low}$ is identified as the molecular marker of BCSCs [2], we next verified whether the expression of B4GalT5 was associated with $CD44^+CD24^{-/low}$ cells. Multiple forms of drug resistance induced by continuous exposure of cells to chemotherapeutics usually generate a high proportion of BCSCs [13]. We therefore chose the adriamycin-resistant breast cancer cell line MCF-7ADR for further research. $CD44^+CD24^{-/low}$ cells (BCSCs) and $CD44^+CD24^+$ cells (non-BCSCs) were sorted from MCF-7ADR cells aseptically by flow cytometry (Fig. 2B), cultured and subjected to western blotting. Strikingly, the $CD44^+CD24^{-/low}$ cells displayed a more malignant phenotype than the $CD44^+CD24^+$cells and had a spindle shape and limited cell-cell contacts; in contrast, the $CD44^+CD24^+$ cells displayed a cobblestone epithelial morphology (Fig. 2C), which is consistent with a previous report showing that $CD44^+CD24^{-/low}$ cells were representative of BCSCs. Furthermore, western blotting analysis showed that B4GalT5 was significantly overexpressed in the $CD44^+CD24^{-/low}$ cells versus the $CD44^+CD24^+$ cells; in addition, the BCSC marker ALDH1A1 was increased along with overexpression of B4GalT5 (Fig. 2D). Together, these results indicate that B4GalT5 is highly expressed in BCSCs.

To explore the role of B4GalT5 in regulating the stemness of BCSCs, we first detected the effect of B4GalT5 on stem cell marker ALDH1A1 expression in breast cancer cells and found an obvious reduction in ALDH1A1 expression in MCF-7ADR, MCF-7, and MDA-MB-231 cell lines (Fig. 2E and F). In contrast, B4GalT5 overexpression (oe-B4GalT5) significantly augmented ALDH1A1 expression in breast cancer cells (Fig. 2G and H). Moreover, we constructed MCF-7ADR cells with stable knockdown of B4GalT5 (referred to as shB4GalT5, Fig. 2I) and stable overexpression of B4GalT5 (referred to as oe-B4GalT5) (Fig. 2J), followed by *in vitro* and *in vivo* studies. We observed a significant decline in the $CD44^+CD24^{-/low}$ cells (Fig. 2K and L) in shB4GalT5 cells, as previously observed in siB4GalT5 transfected MCF-7ADR cells. In contrast, B4GalT5 overexpression significantly increased the percentage of $CD44^+CD24^{-/low}$ cells (Fig. 2M and N), accompanied by increased ALDH activity (Fig. 2O and P), indicating that B4GalT5 induces the formation of BCSC stemness. Moreover, we performed a mammosphere formation assay to assess the self-renewal ability of BCSCs and the expression

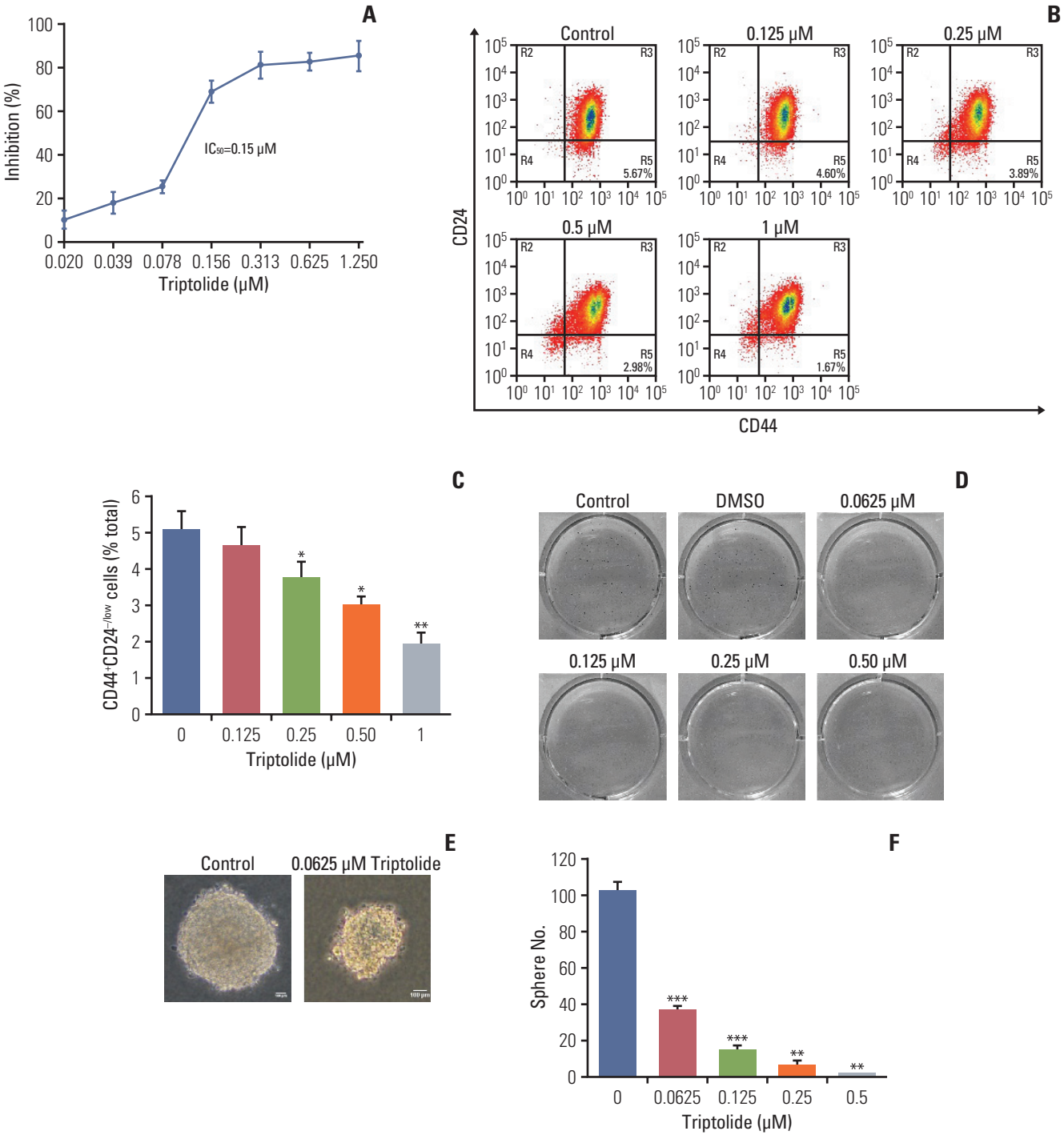

Fig. 3. β1,4-Galactosyltransferase V (B4GalT5) is involved in the inhibition of breast cancer stem cells by triptolide. (A) IC_{50} of triptolide against MCF-7ADR cells using MTT assay. Cells were treated with increasing concentrations of triptolide for 72 hours and MTT assay was performed. NC, normal control. (B, C) Inhibitory effect of triptolide on the proportion of $CD44^{+}CD24^{-/low}$ cells in MCF-7ADR cells. Cells were treated with increasing concentrations of triptolide for 48 hours, then stained with anti-CD44 and anti-CD24 antibodies and analyzed by flow cytometry. (D) Images of colonies in the soft agar. Five hundred MCF-7ADR cells per well were plated in the upper agar for 30 days with the treatment with triptolide before MTT dye was added. Images of formed colonies containing up to 50 cells with a light microscope are shown. (E) Images of colonies magnified treated with dimethyl sulfoxide (DMSO) or 0.0625 μM triptolide using a light microscope. Scale bars=100 μm. (F) Quantification of the number of colonies. *(Continued to the next page)*

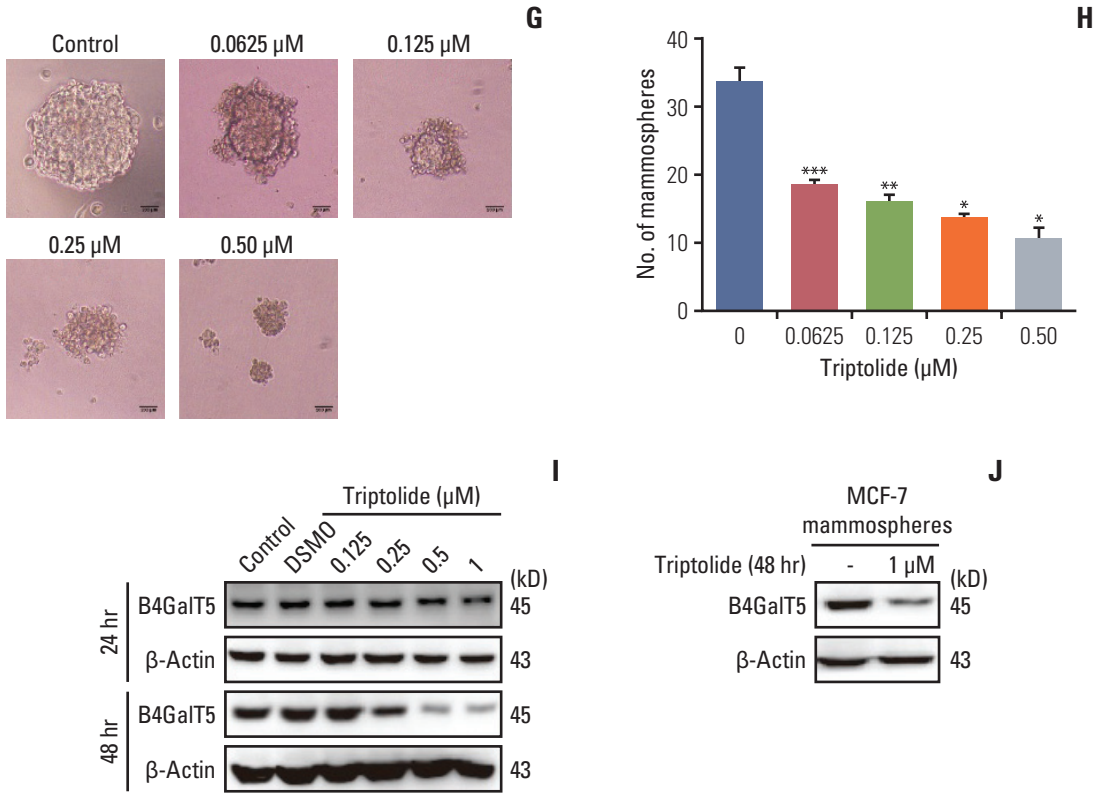

Fig. 3. *(Continued from the previous page)* (G) Images of mammospheres in serum-free medium. 2000 MCF-7 cells per well were cultured in serum-free medium with treatment with phosphate buffered saline (PBS) or different concentrations of triptolide. After 7 days, pictures were taken using light microscopy with a camera. Scale bars=200 μm. (H) Quantification of the number of colonies. (I) Inhibitory effect of triptolide on B4GalT5 expression in MCF-7ADR cells in dose- and time-dependent manners. MCF-7ADR cells were treated with different concentrations of triptolide for 24 hours and 48 hours. Then cells were subjected to western blotting. (J) Inhibitory effect of triptolide on B4GalT5 expression in MCF-7 mammospheres by western blotting. All experiments were performed in three replicates. All data are representative and shown as means±standard error of the mean. *$p < 0.05$, **$p < 0.01$, ***$p < 0.001$, vs. the former group.

level of B4GalT5. We found that the size and number of the mammospheres were markedly restrained in the shB4GalT5 cells, whereas B4GalT5 overexpression promoted the formation of mammospheres (Fig. 2Q and R). It has been reported that CSCs drive tumor initiation, progression, and recurrence [2]. We then subcutaneously injected constructed MCF-7ADR cells into female BALB/c nude mice and found that the group with B4GalT5 overexpression exhibited a dramatic increase in tumor growth and weight compared with the control group (Fig. 2S and T). Specifically, the oe-B4GalT5 cells formed tumors with a volume of 100 mm^3 volume earlier than the cells without B4GalT5 overexpression, as plotted in Fig. 2U, further highlighting the strong tumorigenicity conferred by B4GalT5. Furthermore, we found that tumor tissue with B4GalT5 overexpression had higher expression levels of ALDH1A1, as assessed by western blot, than the tissues of the control group (Fig. 2V). Consequently, these results confirm that B4GalT5 plays an important role in maintaining the stemness of BCSCs.

3. B4GalT5 is involved in the inhibition of BCSCs by triptolide

Triptolide, a diterpene triepoxide of extracts derived from the medicinal plant *Tripterygium Wilfordii Hook F*, has been reported to inhibit the stemness of various cancers, including triple-negative breast cancer and pancreatic cancer [14]. Therefore, we wondered whether B4GalT5 was involved in the inhibition of BCSCs by triptolide. We found that MCF-7ADR cell viability was inhibited by treatment with triptolide, with an IC_{50} of 0.15 μM (Fig. 3A). In addition, triptolide dramatically reduced the percentage of $CD44^+CD24^{-/low}$ cells, suggesting that triptolide significantly eliminated BCSCs (Fig. 3B and C). Furthermore, we found that triptolide apparently suppressed colony growth in soft agar (Fig. 3D-F) and the formation of mammospheres in serum-free medium supplemented with certain cytokines (Fig. 3G and H). All these results confirmed that triptolide was indeed a pharmacological inhibitor of BCSCs. We further investigated whether inhibition of BCSCs by triptolide was accompanied by a decrease in B4GalT5. In the presence of triptolide, the

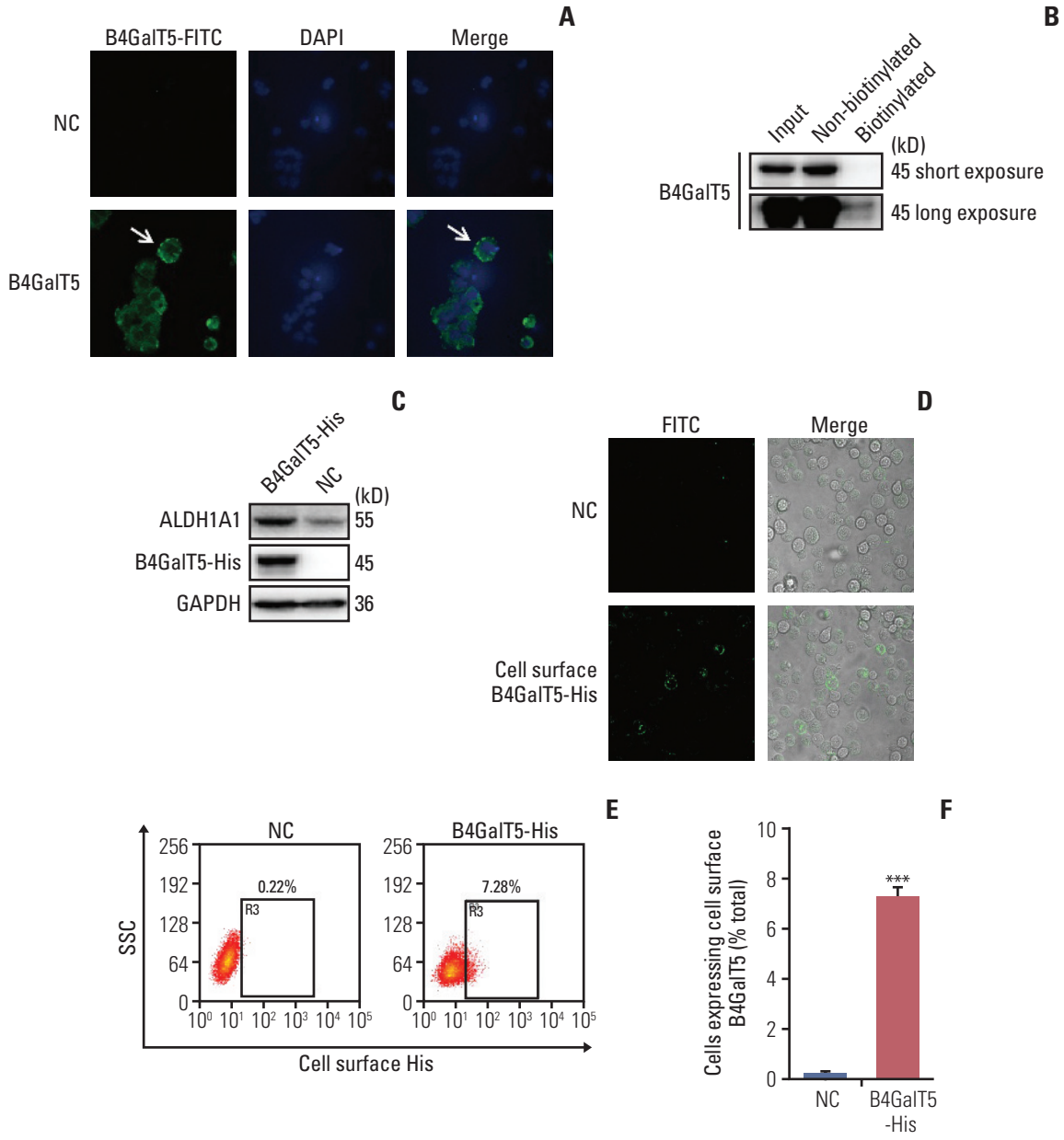

Fig. 4. Cell surface β1,4-galactosyltransferase V (B4GalT5) is not responsible for the stemness of breast cancer. (A) Immunofluorescence analysis of B4GalT5 expression in MCF-7ADR cells. Cells were stained with IgG or anti-B4GalT5 antibody followed by fluorescein isothiocyanate (FITC)–conjugated anti-Rabbit antibodies as described and analyzed by a laser scanning confocal microscope. (B) Cell surface biotinylation assay to compare B4GalT5 localization in plasma membrane and cytoplasmic fractions of MCF-7ADR cells. (C) Construction of MCF-7ADR cells that stably expresses B4GalT5 with a C-terminal 6×His tag. MCF-7ADR cells were transfected with pBABE-B4GalT5-His-IRES-puro plasmid for 48 hours and then selected with 150 μg/mL puromycin. Expression of corresponding proteins was examined by western blotting. (D) Representative images of B4GalT5-His expression on the cell surface of MCF-7ADR/B4GalT5-His and MCF-7ADR/NC cells. After digested and resuspended, the cells were stained with anti-His antibody at room temperature for 1 hour followed by FITC-conjugated anti-rabbit antibody at room temperature for 1 hour. Pictures were taken by a laser scanning confocal microscope. (E, F) Flow cytometry (FCM) analysis of B4GalT5-His expression on the cell surface of MCF-7ADR/B4GalT5-His and MCF-7ADR/NC cells. Cells were stained with phycoerythrin (PE)-conjugated anti-His antibody at room temperature for 1 hour and analyzed by Moflo XDP. Error bars represent standard error of the mean (n=3, ***$p < 0.001$, t test). *(Continued to the next page)*

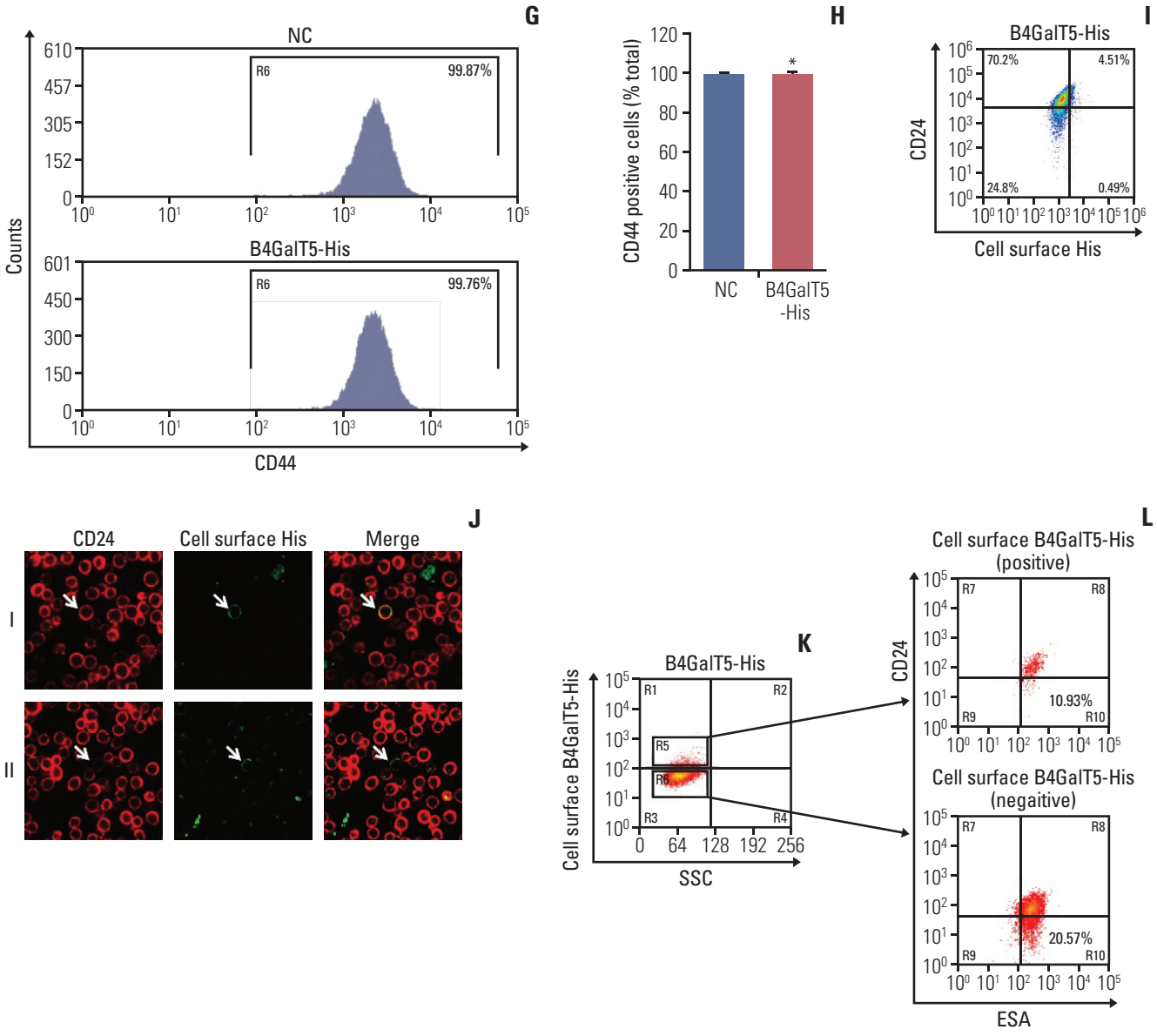

Fig. 4. *(Continued from the previous page)* (G, H) FCM analysis of CD44 expression in MCF-7ADR/B4GalT5-His and MCF-7ADR/NC cells. The cells were stained with FITC-conjugated CD44 antibody at 4°C for 30 minutes and analyzed using Moflo XDP. Error bars represent SEM (n=3; *p > 0.05, t test). (I) FCM analysis of $CD24^{-/low}$ cells in B4GalT5-His positive on the cell surface of MCF-7ADR/B4GalT5-His cells. MCF-7ADR/B4GalT5-His and MCF-7ADR/NC cells were stained with APC-conjugated anti-CD24 and PE-conjugated anti-His antibodies and analyzed by Moflo XDP. (J) Representative images of CD24 and B4GalT5-His expression on the cell surface of MCF-7ADR/B4GalT5-His and MCF-7ADR/NC cells. After digested and resuspended, the cells were stained with anti-CD24 and anti-His antibodies. Pictures were taken by a laser scanning confocal microscope. (K, L) FCM analysis of $ESA^{+}CD24^{-/low}$ cells in B4GalT5-His positive (K, R5) and negative (K, R6) on the cell surface of MCF-7ADR/B4GalT5-His cells; NC, negative control; GAPDH, glyceraldehyde 3-phosphate dehydrogenase; SSC, Side Scatter; ESA, epithelial specific antigen. All experiments were performed in three replicates.

expression level of B4GalT5 was significantly decreased in a dose- and time-dependent manner (Fig. 3I). In particular, B4GalT5 expression in MCF-7 mammospheres was inhibited by treatment with 1 μM triptolide (Fig. 3J). Together, these results further indicate that B4GalT5 is closely correlated with the stemness of breast cancer.

4. Cell surface B4GalT5 is not responsible for the stemness of breast cancer

It has been reported that B4GalT show cell surface expression for cell spreading and migration in migratory 3T3 cells [15], indicating that cell surface B4GalTs correlates with cancer malignancy. Thus, we tested whether cell sur-

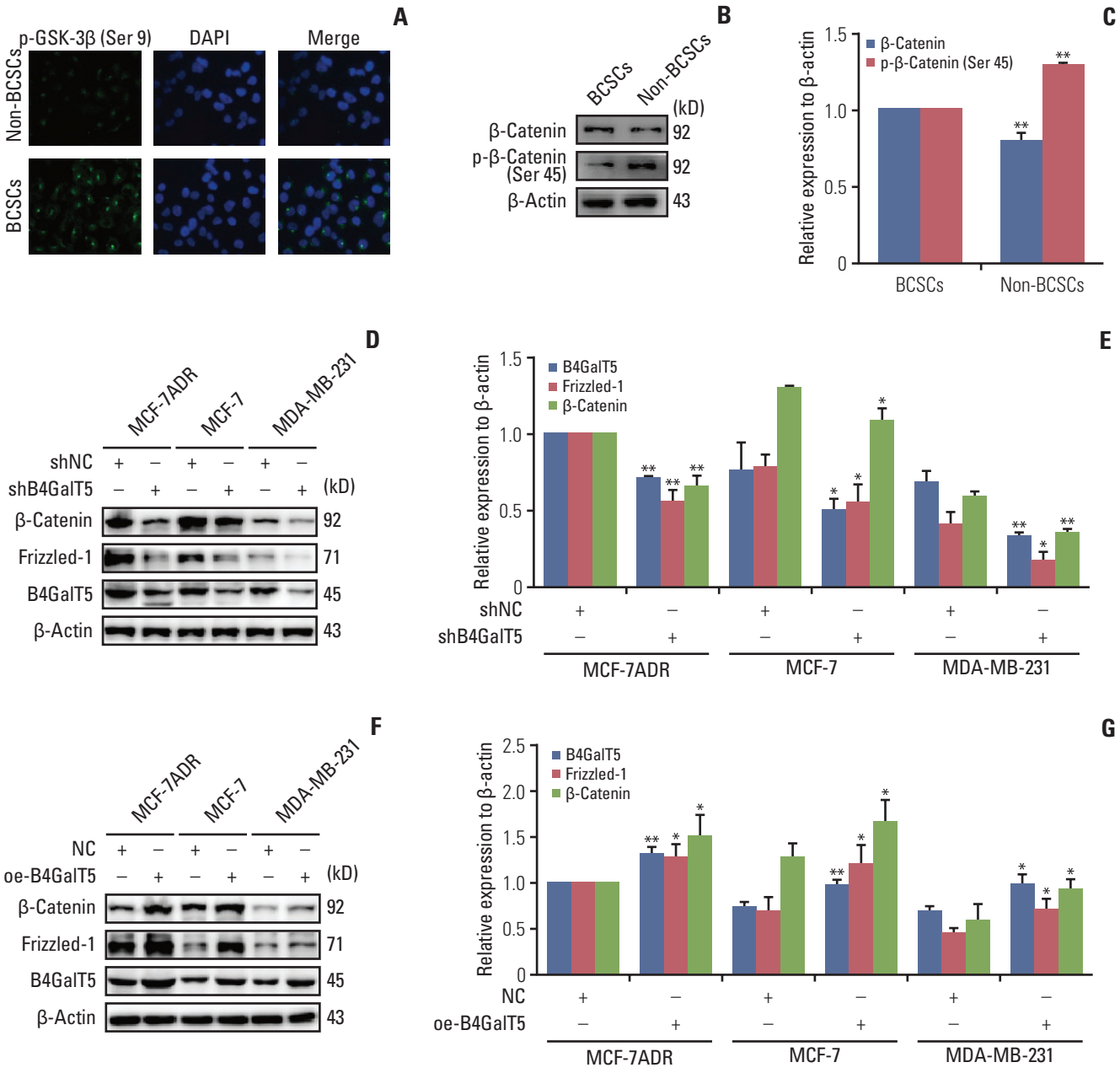

Fig. 5. β1,4-Galactosyltransferase V (B4GalT5) promotes Wnt/β-catenin signaling that is hyperactivated in breast cancer stem cells (BCSCs). (A) Immunofluorescence analysis of phosphorylated-GSK3β (Ser 9) expression in BCSCs and non-BCSCs. MCF-7ADR cells were sorted into BCSCs and non-BCSCs, then stained with antibodies and DAPI as described and analyzed by a laser scanning confocal microscope. (B, C) Western blotting analysis of β-catenin and phosphorylated-β-catenin (Ser 45) expression levels in BCSCs and non-BCSCs. Protein band densities were quantified by normalizing to β-actin. (D, E) The effect of B4GalT5 knockdown on Frizzled-1, β-catenin, and B4GalT5 expression levels in MCF-7ADR, MCF-7, and MDA-MB-231 cell lines by western blotting analysis. Protein band densities were quantified by normalizing to β-actin. (F, G) The effect of B4GalT5 overexpression on Frizzled-1, β-catenin, and B4GalT5 expression levels in MCF-7ADR, MCF-7, and MDA-MB-231 cell lines by western blotting analysis. Protein band densities were quantified by normalizing to β-Actin. *(Continued to the next page)*

face B4GalT5 was correlated with the stemness of BCSCs. As shown in Fig. 4A, cell surface B4GalT5 was found in a small portion of MCF-7ADR cells by confocal microscopy. Further, we carried out a cell surface biotinylation assay and proved that the expression level of cell surface B4GalT5 was much lower than that of cytoplasmic B4GalT5 in MCF-7ADR cells (Fig. 4B), indicating that a small proportion of the cells expresses cell surface B4GalT5. These results were consist-

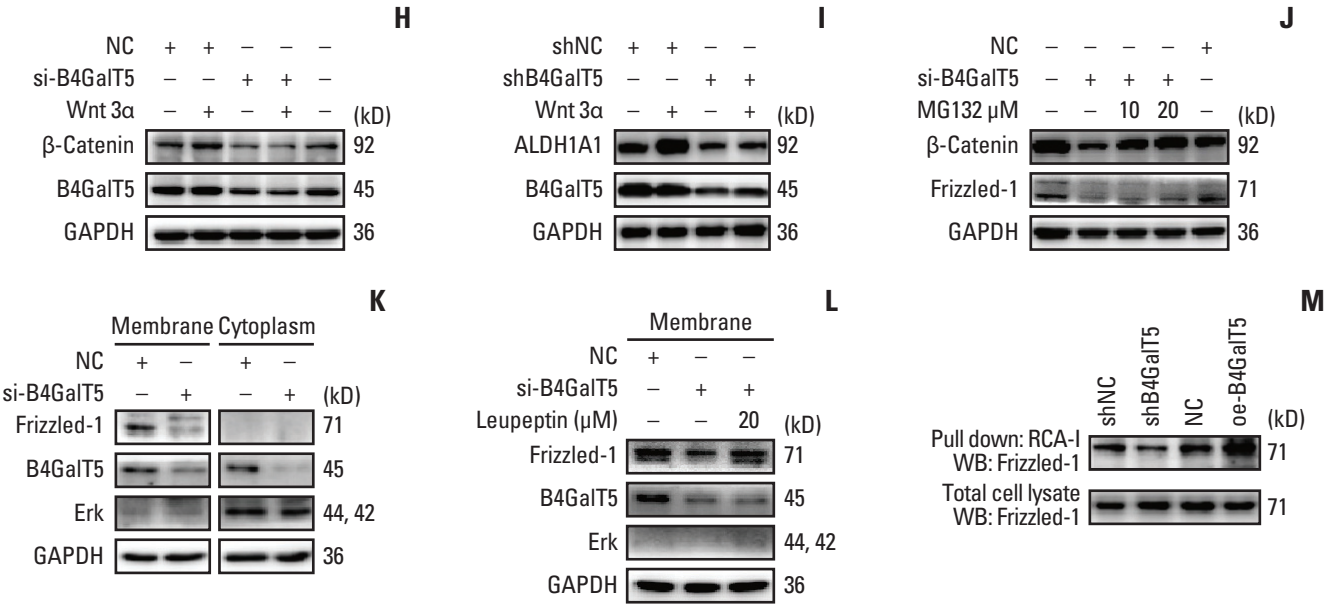

Fig. 5. *(Continued from the previous page)* (H) The effect of B4GalT5 on wnt 3α induced Wnt/β-catenin signaling by western blotting (WB). After transfected using B4GalT5 siRNA for 12 hours, MCF-7ADR cells were starved for 36 hours followed by adding wnt 3α, and subjected to western blotting. (I) The effect of B4GalT5 on Wnt 3α induced ALDH1A1 expression by western blotting. MCF-7ADR/shNC and MCF-7ADR/shB4GalT5 cells were starved for 36 hours followed by adding Wnt 3α, and subjected to western blotting. (J) The degradation pathway of β-catenin due to B4GalT5 knockdown. After transfected using B4GalT5 siRNA for 41 hours, MCF-7ADR cells were treated with MG132 (protease inhibitor) for 7 hours. Protein levels were examined by western blotting. (K) Western blotting analysis of membrane and cytosol proteins in MCF-7ADR cells. MCF-7ADR cells were transfected using B4GalT5 siRNA for 48 hours, extracted into membrane and cytosol proteins and then subjected to western blotting. Erk was used for examining purity of membrane proteins. (L) The degradation pathway of Frizzled-1 on the cell surface of MCF-7ADR cells due to B4GalT5 knockdown. After transfected using B4GalT5 siRNA for 40 hours, MCF-7ADR cells were treated with 20 μM leupeptin (lysosome inhibitor) for 8 hours. The membrane proteins were extracted as described and then subjected to western blotting. Erk was used for examining purity of membrane proteins. (M) The effect of B4GalT5 on biosynthesis of galactosyl-oligosaccharides in glycans of Frizzled-1 by RCA-I lectin pull-down assay. MCF-7ADR/shNC, MCF-7ADR/shB4GalT5, MCF-7ADR/NC, and MCF-7ADR/oe-B4GalT5 cells were lysed and incubated with agarose-bound RCA-I overnight. Total Frizzled-1 was used as loading control. All experiments were performed in three replicates. Data are presented as means±standard error of the mean. *$p < 0.05$, **$p < 0.01$ versus the control group.

ent with a feature of CSCs, namely a small subset of poorly differentiated tumor cells within a tumor. To further validate the relationship of B4GalT5 expression on the cell surface and BCSCs, we first constructed MCF-7ADR cells that stably overexpressed B4GalT5 with a C-terminal 6×His tag for immunofluorescence staining due to lack of the antibody recognizing its extracellular fragment (Fig. 4C). Western blotting analysis showed that ALDH1A1 was highly expressed in the B4GalT5-His–transfected cells, which suggested the successful construction of cells with active expression of B4GalT5-His (Fig. 4C). We then performed live cell staining using anti-His antibody. B4GalT5-His was detected in a small subset of cells by confocal microscopy without cell membrane permeabilization (Fig. 4D). Furthermore, fluorescence-activated cell sorting (FACS) analysis showed that cell surface B4GalT5-His was expressed in approximately 7.62% of MCF-7ADR cells (Fig. 4E and F). From these results, B4GalT5 was shown to partially localize to the cell membrane with its C-terminus extracellular region, and cell surface B4GalT5 still belonged to type II membrane-bound proteins, consistent with the normal localization of B4GalT5 on the Golgi apparatus [6].

Next, we explored the association between cell surface B4GalT5 and BCSCs by a series of *in vitro* assays. For convenient detection, we first detected the effect of B4GalT5 on CD44 expression by FACS analysis and observed that CD44 expression in MCF-7ADR cells was almost completely positive and not influenced by B4GalT5 overexpression (Fig. 4G and H). We then investigated the expression of CD24 and B4GalT5 on the cell surface of B4GalT5-His–expressing cells and found that the population with low and negative expression of CD24 ($CD44^{+}CD24^{-/low}$, BCSCs) accounted for 9.80% of the B4GalT5-His^{+} cells, whereas this population accounted for 26.10% of the B4GalT5-His^{-} cells (Fig. 4I). We also found that B4GalT5-His^{+} cells overlapped with not only $CD24^{+}$ cells but also $CD24^{-/low}$ cells, as observed by confocal microscopy analysis (Fig. 4J). These results suggested

that cell surface B4GalT5 may not be a marker of BCSCs. $ESA^+CD44^+CD24^{-/low}$ cells have also been reported to possess BCSC properties based on their high spheroid formation and *in vivo* tumor formation ability; hence, the molecular marker group is a more precise way to recognize BCSCs [2]. For further confirmation of the correlation of cell surface B4GalT5 and the stemness of BCSCs, the population rates of $ESA^+CD44^+CD24^{-/low}$ cells were detected in $CD44^+$ cells positive or negative for B4GalT5-His. As shown in Fig. 4K and L, FACS analysis demonstrated that the population with $ESA^+CD44^+CD24^{-/low}$ accounted for 10.93% of the B4GalT5-His^+ cells, while this population accounted for 20.57% of the B4GalT5-His^- cells, which was consistent with the results in Fig. 4H. Together, these results strongly suggest that there is no internal connection between cell surface B4GalT5 and BCSCs, and cell surface B4GalT5 is not responsible for the stemness of breast cancer.

5. B4GalT5 promotes Wnt/β-catenin signaling that is hyperactivated in BCSCs

Aberrant Wnt/β-catenin signaling is involved in multiple cancers and closely correlates with cell proliferation, invasion, metastasis, and CSC survival [16]. We tested whether Wnt/β-catenin signaling mediated the regulation of B4GalT5 on the stemness of BCSCs. To validate the relationship between Wnt/β-catenin signaling and BCSCs, we isolated $CD44^+CD24^{-/low}$ cells (BCSCs) and $CD44^+CD24^{-/low}$ cells (non-BCSCs) from MCF-7ADR cells using FACS, followed by immunofluorescence and western blotting analysis. GSK3β is reported to be phosphorylated at Ser 9 and thereby inactivated by AKT, resulting in a decrease in β-catenin degradation and activation of Wnt/β-catenin signaling [17]. We found that inactive phosphorylated-Gsk3β (Ser 9) is highly expressed in BCSCs (Fig. 5A). As the substrate of GSK3β, β-catenin showed low phosphorylation at Ser 45 and its expression was upregulated in BCSCs versus non-BCSCs, indicating that the stability of β-catenin was maintained in BCSCs (Fig. 5B and C). All these results suggest that Wnt/β-catenin signaling is hyperactivated in BCSCs compared with non-BCSCs.

To investigate the role of B4GalT5 in regulating Wnt/β-catenin signaling, we first depleted B4GalT5 using B4GalT5 siRNA in multiple breast cancer cell lines, including MCF-7ADR, MCF-7 and MDA-MB-231, and found that the expression levels of the Wnt/β-catenin signaling-related molecules Frizzled-1 and β-catenin were decreased significantly (Fig. 5D and E). In contrast, B4GalT5 overexpression significantly augmented the amounts of Frizzled-1 and β-catenin (Fig. 5F and G). As a canonical Wnt protein, wnt 3α is widely expressed and a representative ligand that interacts with the receptor Frizzled-1 and thereby activates the β-catenin–dependent pathway in Wnt signaling [18]. As shown in Fig. 5H and I, wnt 3α did not successfully induce activation of Wnt/β-catenin signaling and failed to reverse the decrease in stem cell marker ALDH1A1 expression in the B4GalT5-knockdown MCF-7ADR cells, further indicating that B4GalT5 regulates the stemness of breast cancer via activation of Wnt/β-catenin signaling.

We next elucidated the mechanisms underlying the decrease in β-catenin and Frizzled-1 induced by B4GalT5. While Wnt/β-catenin signaling is inactivated, the β-catenin destruction complex is formed and induces β-catenin phosphorylation and degradation by the proteasome system [18]. We observed that the proteasome inhibitor MG132 reversed the decrease in β-catenin in the B4GalT5-knockdown MCF-7ADR cells, whereas the amount of Frizzled-1 was not affected (Fig. 5J). In addition to the proteasomal pathway, the lysosomal system is the other major pathway for protein degradation, especially for cell surface receptors [19]. As the receptor of Wnt signaling, Frizzled-1 was found to be almost completely located on the cell membrane (Fig. 5K), and treatment with the lysosome inhibitor leupeptin clearly blocked B4GalT5 knockdown-induced downregulation of Frizzled-1 in MCF-7ADR cells (Fig. 5L). Together, these results indicate that B4GalT5 knockdown induces degradation of Frizzled-1 via the lysosomal pathway and thereby contributes to β-catenin degradation by the proteasomal pathway, which leads to inactivation of Wnt/β-catenin signaling.

Frizzled-1 is a receptor glycoprotein with N-glycosylation modification, as reported on the Uniprot website (http://www.uniprot.org). Glycans, which are bulky hydrophilic polymers, often contribute to increased stability against proteolysis. Moreover, the covalent binding of glycans to the protein surface may inherently enhance the thermal and kinetic stability of proteins [20]. B4GalT5 participates in the biosynthesis of N-linked oligosaccharides containing galactose residues [6]. Therefore, we assessed whether B4GalT5 participated in the N-glycosylation modification of Frizzled-1 and consequently affected Wnt/β-catenin signaling. RCA-I binds to galactose or N-acetylgalactosamine residues of membrane glycoconjugates, and RCA-I pull-down assays indicated that B4GalT5 knockdown significantly blocked the biosynthesis of galactosyl-oligosaccharides in the glycans of Frizzled-1, while B4GalT5 overexpression increased its biosynthesis (Fig. 5M), indicating a positive correlation between B4GalT5 and Frizzled-1 N-glycosylation. Above all, these findings strongly indicate that B4GalT5 promotes N-glycosylation of Frizzled-1 and its downstream signaling, thereby regulating the stemness of BCSCs.

Discussion

Increasing evidence suggests that BCSCs are involved in tumor progression, recurrence and resistance to chemo- and radiotherapies [3]; thus, identifying specific factors that can regulate BCSC properties is important for reducing recur-

rence and thereby improving the therapeutic effect on breast cancer. In this paper, we demonstrated that B4GalT5-mediated regulation of BCSCs positively correlated with malignant phenotypes and poor prognosis of breast cancer by a series of online database analyses and IHC analyses followed by *in vitro* and *vivo* studies.

A characteristic feature of the malignant transformation of tumor cells is the alteration of highly branched N-linked oligosaccharides on glycoproteins [4]. Abnormal expression of B4Gal-T1-T7 has been reported to be involved in changes in highly branched N-linked oligosaccharides, which are implicated in a number of diseases, including various cancers, inflammation, and viral infection [6]. For example, B4GalT2 is a critical effector involved in neuronal development, congenital muscular dystrophies and astrocytoma [21]. B4GalT4 overexpression is closely associated with colorectal cancer metastasis and poor prognosis in patients [22]. B4GalT5 and B4GalT6 are responsible for the production of lactosylceramide (LacCer) synthase, which functions in the initial step of ganglioside biosynthesis [23]. Moreover, B4GalT5 participates in the synthesis of both N-linked oligosaccharides and various glycolipids, contributing to highly galactosylated cell surface proteins that are associated with extraembryonic development and the tumorigenesis of astrocytoma, melanoma and glioma [6]. Finally, B4GalT7 regulates the synthesis of glycosaminoglycans that play a central role in many pathophysiological events [24]. In this paper, we found that the expression levels of B4GalTs (except B4GalT6) were upregulated in invasive breast carcinomas compared with mammary tissues, yet only B4GalT5 was found to be positively associated with the BCSC marker ALDH1A1, indicating that B4GalT5 displays CSC-related specificity and might play important roles in breast cancer.

Several studies have reported that Wnt/β-catenin signaling is aberrantly activated in various human malignancies, including breast, colorectal, gastric, lung, ovary, pancreatic, prostate and uterine cancers, leukemia and melanoma, and is involved in CSC survival, bulk tumor expansion and metastasis [25]. In this pathway, the Wnt ligand interacts with the receptor Frizzled-1, inhibiting the degradation of β-catenin and subsequently translocating into the cell nucleus, which can regulate the transcription of a number of target genes related to cancer development [25]. Our studies also confirmed that Wnt/β-catenin signaling was more active in BCSCs than in non-BCSCs. As the receptor of Wnt/β-catenin signaling, Frizzled-1 shows N-glycosylation that has been demonstrated to play an important role in regulating biological activity, intracellular targeting, protein folding, and maintenance of protein stability [26]. We propose for the first time that B4GalT5 mediates the biosynthesis of galactosyl-oligosaccharides in the N-glycosylation modification of Frizzled-1, which contributes to the activation of Wnt/β-catenin signaling and thereby regulates the stemness of breast cancer. Furthermore, we found that B4GalT4 knockdown promoted Frizzled-1 degradation by the lysosomal pathway and then contributed to the degradation of β-catenin through the proteasomal pathway. Previous studies have reported that incomplete N-glycosylation affects the stability of cell surface proteins, such as N-cadherin and programmed death-ligand 1, and leads to their ubiquitylation and subsequent proteasomal degradation [27,28], which is inconsistent with our findings. Since proteins on the cell membrane recycle from endosomes to the plasma membrane or are transported to lysosomes for degradation [29], we believe that incomplete N-glycosylation resulting from the depletion of B4GalT5 affects the stability of Frizzled-1 located in the cell membrane and eventually results in its degradation through the lysosomal pathway.

In addition to the location of B4GalTs in the Golgi complex, glycosyltransferases are present on the cell surface, where they function as adhesion molecules that are involved in cell-to-cell and cell-to-extracellular matrix interactions as well as cell spreading and migration, and associated with signal transduction cascades [15,30]. Consistent with these previous studies, our data also showed that B4GalT5 was located on the cell surface of MCF-7ADR cells and first confirmed that it is a type II membrane-bound protein. As B4GalT5, located partly on the cell surface, was related to cell spreading and migration [15], cell surface B4GalT5 may be a molecular marker for the stemness of BCSCs. However, flow cytometry and immunofluorescence assays revealed that cell surface B4GalT5 was not responsible for the stemness of BCSC. These results in turn demonstrated that B4GalT5 canonically located in the Golgi complex, which affected the level of Frizzled-1 by glycosylation modification on the cell surface, was responsible for the stemness of breast cancer through Wnt/β-catenin signaling. The biological function of cell surface B4GalT5 may only mediate spreading and migration of a small number of cells. The finding of a correlation between glycosyltransferase distribution and its function in BCSCs provides more foundations for drug design to target BCBCs.

In conclusion, we showed that B4GalT5 is overexpressed in invasive breast carcinomas, positively associated with poor survival, and closely related to the stemness of BCSCs. We have demonstrated for the first time that B4GalT5 regulates BCSC properties by affecting the N-glycosylation modification of Frizzled-1, thereby affecting its stability on the cell membrane and inhibiting downstream signaling in BCSCs, which is independent of the B4GalT5 location in cells. Our findings provide novel insights into the important role of B4GalT5 in BCSCs. This study also suggests that targeting B4GalT5 may be a promising strategy to suppress or eliminate CSCs in breast cancer.

Electronic Supplementary Material

Supplementary materials are available at Cancer Research and Treatment website (https://www.e-crt.org).

Conflicts of Interest

Conflicts of interest relevant to this article was not reported.

Acknowledgments

This work was supported by the National Natural Science Foundation of China [No. 81673450] and the NSFC Shandong Joint Fund [U1606403]; the Scientific and Technological Innovation Project was financially supported by Qingdao National Laboratory for Marine Science and Technology [No. 2015ASKJ02], the Fundamental Research Funds for the Central Universities [No. 201762002] and the National Science and Technology Major Project for Significant New Drugs Development (2018ZX09735-004).

References

1. Bray F, Ferlay J, Soerjomataram I, Siegel RL, Torre LA, Jemal A. Global cancer statistics 2018: GLOBOCAN estimates of incidence and mortality worldwide for 36 cancers in 185 countries. CA Cancer J Clin. 2018;68:394-424.
2. Visvader JE, Lindeman GJ. Cancer stem cells: current status and evolving complexities. Cell Stem Cell. 2012;10:717-28.
3. Ghasemi F, Sarabi PZ, Athari SS, Esmaeilzadeh A. Therapeutics strategies against cancer stem cell in breast cancer. Int J Biochem Cell Biol. 2019;109:76-81.
4. Fuster MM, Esko JD. The sweet and sour of cancer: glycans as novel therapeutic targets. Nat Rev Cancer. 2005;5:526-42.
5. Pinho SS, Reis CA. Glycosylation in cancer: mechanisms and clinical implications. Nat Rev Cancer. 2015;15:540-55.
6. Wassler M. β1,4-galactosyltransferases, potential modifiers of stem cell pluripotency and differentiation. In: Bhartiya D, Lenka, N, editors. Pluripotent stem cells. Rijeka: InTech; 2013. p. 345-72.
7. Ma Y, Zhang P, Wang F, Yang J, Yang Z, Qin H. The relationship between early embryo development and tumourigenesis. J Cell Mol Med. 2010;14:2697-701.
8. Gyorffy B, Lanczky A, Eklund AC, Denkert C, Budczies J, Li Q, et al. An online survival analysis tool to rapidly assess the effect of 22,277 genes on breast cancer prognosis using microarray data of 1,809 patients. Breast Cancer Res Treat. 2010;123:725-31.
9. Tang Z, Li C, Kang B, Gao G, Li C, Zhang Z. GEPIA: a web server for cancer and normal gene expression profiling and interactive analyses. Nucleic Acids Res. 2017;45:W98-W102.
10. Muller A, Homey B, Soto H, Ge N, Catron D, Buchanan ME, et al. Involvement of chemokine receptors in breast cancer metastasis. Nature. 2001;410:50-6.
11. Robey RW, Pluchino KM, Hall MD, Fojo AT, Bates SE, Gottesman MM. Revisiting the role of ABC transporters in multidrug-resistant cancer. Nat Rev Cancer. 2018;18:452-64.
12. Ciccone V, Terzuoli E, Donnini S, Giachetti A, Morbidelli L, Ziche M. Stemness marker ALDH1A1 promotes tumor angiogenesis via retinoic acid/HIF-1alpha/VEGF signalling in MCF-7 breast cancer cells. J Exp Clin Cancer Res. 2018;37:311.
13. Li Y, Xian M, Yang B, Ying M, He Q. Inhibition of KLF4 by statins reverses adriamycin-induced metastasis and cancer stemness in osteosarcoma cells. Stem Cell Reports. 2017;8:1617-29.
14. Yang A, Qin S, Schulte BA, Ethier SP, Tew KD, Wang GY. MYC inhibition depletes cancer stem-like cells in triple-negative breast cancer. Cancer Res. 2017;77:6641-50.
15. Youakim A, Dubois DH, Shur BD. Localization of the long form of beta-1,4-galactosyltransferase to the plasma membrane and Golgi complex of 3T3 and F9 cells by immunofluorescence confocal microscopy. Proc Natl Acad Sci U S A. 1994;91:10913-7.
16. Lim SK, Lu SY, Kang SA, Tan HJ, Li Z, Adrian Wee ZN, et al. Wnt signaling promotes breast cancer by blocking ITCH-mediated degradation of YAP/TAZ transcriptional coactivator WBP2. Cancer Res. 2016;76:6278-89.
17. Chung J, Karkhanis V, Baiocchi RA, Sif S. Protein arginine methyltransferase 5 (PRMT5) promotes survival of lymphoma cells via activation of WNT/beta-catenin and AKT/GSK3beta proliferative signaling. J Biol Chem. 2019;294:7692-710.
18. Rada P, Rojo AI, Offergeld A, Feng GJ, Velasco-Martin JP, Gonzalez-Sancho JM, et al. WNT-3A regulates an Axin1/NRF2 complex that regulates antioxidant metabolism in hepatocytes. Antioxid Redox Signal. 2015;22:555-71.
19. Cooper GM. The cell: a molecular approach. 2nd ed. Sunderland, MA: Sinauer Associates Inc.; 2000.
20. Sola RJ, Griebenow K. Effects of glycosylation on the stability of protein pharmaceuticals. J Pharm Sci. 2009;98:1223-45.
21. Sasaki N, Manya H, Okubo R, Kobayashi K, Ishida H, Toda T, et al. beta4GalT-II is a key regulator of glycosylation of the proteins involved in neuronal development. Biochem Biophys Res Commun. 2005;333:131-7.
22. Chen WS, Chang HY, Li CP, Liu JM, Huang TS. Tumor beta-1,4-galactosyltransferase IV overexpression is closely associated with colorectal cancer metastasis and poor prognosis. Clin Cancer Res. 2005;11(24 Pt 1):8615-22.
23. Yoshihara T, Satake H, Nishie T, Okino N, Hatta T, Otani H, et al. Lactosylceramide synthases encoded by B4galt5 and 6 genes are pivotal for neuronal generation and myelin formation in mice. PLoS Genet. 2018;14:e1007545.
24. Talhaoui I, Bui C, Oriol R, Mulliert G, Gulberti S, Netter P, et al. Identification of key functional residues in the active site of human {beta}1,4-galactosyltransferase 7: a major enzyme in the glycosaminoglycan synthesis pathway. J Biol Chem. 2010;285:37342-58.
25. Katoh M. Canonical and non-canonical WNT signaling in cancer stem cells and their niches: cellular heterogeneity, omics reprogramming, targeted therapy and tumor plasticity

(Review). Int J Oncol. 2017;51:1357-69.
26. Wang H, Zhou T, Peng J, Xu P, Dong N, Chen S, et al. Distinct roles of N-glycosylation at different sites of corin in cell membrane targeting and ectodomain shedding. J Biol Chem. 2015;290:1654-63.
27. Li CW, Lim SO, Xia W, Lee HH, Chan LC, Kuo CW, et al. Glycosylation and stabilization of programmed death ligand-1 suppresses T-cell activity. Nat Commun. 2016;7:12632.
28. Xu Y, Chang R, Xu F, Gao Y, Yang F, Wang C, et al. N-glycosylation at Asn 402 stabilizes N-cadherin and promotes cell-cell adhesion of glioma cells. J Cell Biochem. 2017;118:1423-31.
29. Yonamine I, Bamba T, Nirala NK, Jesmin N, Kosakowska-Cholody T, Nagashima K, et al. Sphingosine kinases and their metabolites modulate endolysosomal trafficking in photoreceptors. J Cell Biol. 2011;192:557-67.
30. Rodeheffer C, Shur BD. Targeted mutations in beta1,4-galactosyltransferase I reveal its multiple cellular functions. Biochim Biophys Acta. 2002;1573:258-70.

pISSN 1598-2998, eISSN 2005-9256

Cancer Res Treat. 2020;52(4):1103-1111

https://doi.org/10.4143/crt.2020.337

Original Article

Open Access

Challenge for Diagnostic Assessment of Deep Learning Algorithm for Metastases Classification in Sentinel Lymph Nodes on Frozen Tissue Section Digital Slides in Women with Breast Cancer

Young-Gon Kim, PhD[1]
In Hye Song, MD, PhD[2]
Hyunna Lee, PhD[3]
Sungchul Kim, BS[1]
Dong Hyun Yang, MD, PhD[4]
Namkug Kim, PhD[5]
Dongho Shin, BS[6]
Yeonsoo Yoo, BS[6]
Kyowoon Lee, BS[7]
Dahye Kim, BBA[8]
Hwejin Jung, PhD[9]
Hyunbin Cho, BS[9]
Hyungyu Lee, PhD[9]
Taeu Kim, BA[10]
Jong Hyun Choi, BA[11]
Changwon Seo, MS[9]
Seong Il Han, BS[12]
Young Je Lee, BE[13]
Young Seo Lee, BA[14]
Hyung-Ryun Yoo, BS[15]
Yongju Lee, PhD[16]
Jeong Hwan Park, MD, PhD[17]
Sohee Oh, PhD[18]
Gyungyub Gong, MD, PhD[19]

**A list of author's affiliations appears at the end of the paper.*

Correspondence: Gyungyub Gong, MD, PhD
Department of Pathology, Asan Medical Center, University of Ulsan College of Medicine, 88 Olympic-ro 43-gil, Songpa-gu, Seoul 05505, Korea
Tel: 82-2-3010-4554
Fax: 82-2-472-7898
E-mail: gygong@amc.seoul.kr

Received April 20, 2020
Accepted June 29, 2020
Published Online June 30, 2020

*Young-Gon Kim and In Hye Song contributed equally to this work.

Purpose

Assessing the status of metastasis in sentinel lymph nodes (SLNs) by pathologists is an essential task for the accurate staging of breast cancer. However, histopathological evaluation of SLNs by a pathologist is not easy and is a tedious and time-consuming task. The purpose of this study is to review a challenge competition (HeLP 2018) to develop automated solutions for the classification of metastases in hematoxylin and eosin–stained frozen tissue sections of SLNs in breast cancer patients.

Materials and Methods

A total of 297 digital slides were obtained from frozen SLN sections, which include post–neoadjuvant cases (n=144, 48.5%) in Asan Medical Center, South Korea. The slides were divided into training, development, and validation sets. All of the imaging datasets have been manually segmented by expert pathologists. A total of 10 participants were allowed to use the Kakao challenge platform for 6 weeks with two P40 GPUs. The algorithms were assessed in terms of the area under receiver operating characteristic curve (AUC).

Results

The top three teams showed 0.986, 0.985, and 0.945 AUCs for the development set and 0.805, 0.776, and 0.765 AUCs for the validation set. Micrometastatic tumors, neoadjuvant systemic therapy, invasive lobular carcinoma, and histologic grade 3 were associated with lower diagnostic accuracy.

Conclusion

In a challenge competition, accurate deep learning algorithms have been developed, which can be helpful in making frozen diagnosis of intraoperative SLN biopsy. Whether this approach has clinical utility will require evaluation in a clinical setting.

Key words

Breast neoplasms, Deep learning, Frozen sections, Neoplasm metastasis, Sentinel lymph node

Introduction

Recently, implementation of digital pathology has been rising because of workforce crisis and increased need of consultation and collaboration. Digital pathology has many advantages in terms of time saving, slide storage, remote working, and second-opinion practice, and is becoming a part of routine procedure in diverse areas such as primary diagnosis, multidisciplinary clinic, and frozen section diagnosis [1]. Owing to rapid progress of technology, machine learning techniques using digital histopathological images have been investigated and showed satisfactory results in the detection of tumor areas and lymph node metastases in prostate, lung, and breast cancers [2-4].

Breast cancer is the most common cancer in women, accounting for approximately one-third of all cancers in women globally. For patients with localized breast cancer, the treatment of choice is surgical removal of the primary tumor [5]. In order to reduce disease recurrence or metastasis, lymph node sampling or dissection should be performed during surgery. Because axillary lymph node dissection may cause morbidity, such as arm-lymphedema and nerve injury, sentinel lymph node (SLN) sampling is recommended in order to determine the nodal metastases status and if extensive lymph node dissection is required [6-9]. Although some recent studies suggested that the role of SLN biopsy has been diminished in early breast cancer patients [10-13], SLN sampling is still considered important due to its cost- and time-effectiveness and usually performed intraoperatively using the frozen section technique and which allows surgeons to make immediate decisions during surgery [14]. However, pathologists frequently experience problems while making diagnoses of frozen sections.

First, frozen section diagnosis should be made as quickly as possible in order to minimize the waiting time for surgeons which can cause surgical and anesthetic complications. The turnaround time of the frozen section diagnosis is usually kept less than 20 to 30 minutes, including the gross examination, tissue cutting, and staining, and the microscopic examination [15]. Second, microscopic examination of a frozen section is more difficult than that of a conventional section because of inferior quality of the sections due to the frozen artifact. There are also components, such as capillaries, histiocytes, and germinal centers, in lymph nodes and which can be mistaken for metastatic carcinoma. Furthermore, frozen section diagnosis is extremely difficult in some patients who have underwent neoadjuvant systemic therapy before surgery. In order to overcome such difficulties, the deep learning algorithm might be helpful. For example, the 'CAncer MEtastases in LYmph nOdes challeNge' (CAMELYON16 and CAMELYON17) competitions disclosed that some deep learning algorithms achieved better diagnostic performance than a panel of 11 pathologists participating in a simulation exercise designed to mimic routine pathology workflow [4,16]. However, digital slides which were used in most of those previous studies had not been created from frozen tissue sections, but from formalin-fixed paraffin-embedded (FFPE) tissue sections. To our best knowledge, there has not been any reported

Table 1. Clinicopathologic characteristics of the patients (resolution [width×height] of digital slide: 93,970×234,042)

	Training set (n=157)	Development set (n=40)	Validation set (n=100)	p-value[a]
Age (yr)	50 (28-80)	49 (30-68)	47 (34-75)	
Sex				
Female	157 (100)	40 (100)	100 (100)	> 0.99
Metastatic carcinoma				
Present, size > 2 mm	68 (43.3)	14 (35.0)	40 (40.0)	0.158
Present, size ≤ 2 mm	35 (22.3)	5 (12.5)	15 (15.0)	
Absent	54 (34.4)	21 (52.5)	45 (45.0)	
Neoadjuvant systemic therapy				
Not received	80 (51.0)	28 (70.0)	45 (45.0)	0.027
Received	77 (49.0)	12 (30.0)	55 (55.0)	
Histologic type				
IDC	149 (94.9)	32 (80.0)	86 (86.0)	0.005[b]
ILC	8 (5.1)	5 (12.5)	11 (11.0)	
MC	0	0	3 (3.0)	
Metaplastic carcinoma	0	3 (7.5)	0	
Histologic grade				
1 or 2	118 (75.2)	34 (85.0)	86 (86.0)	0.074
3	39 (24.8)	6 (15.0)	14 (14.0)	

Values are presented as median (range) or number (%). IDC, invasive ductal carcinoma; ILC, invasive lobular carcinoma; MC, mucinous carcinoma. [a]p-values, calculated using the chi-square test, [b]For the histologic type, a chi-square test was conducted between IDC and non-IDC.

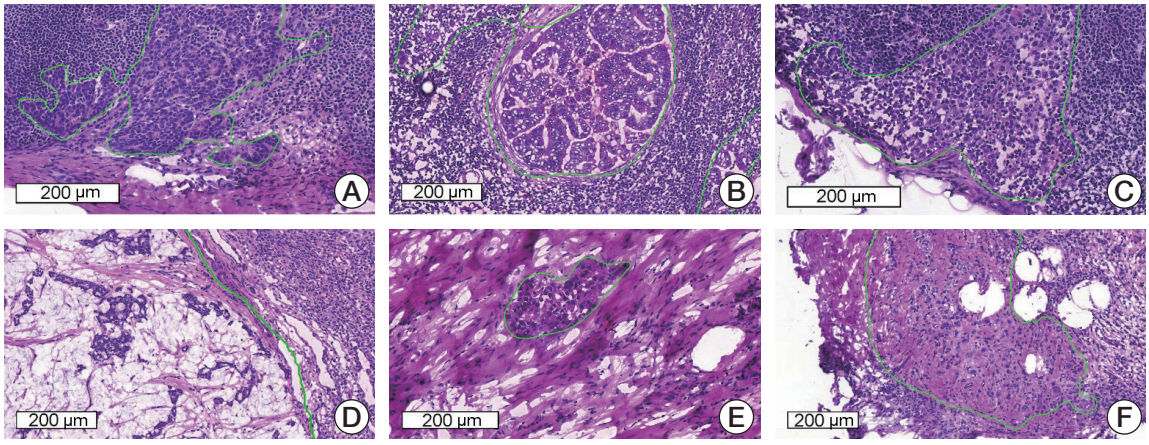

Fig. 1. Representative microscopic images of various metastatic carcinomas with annotation (H&E staining). (A) Invasive ductal carcinoma, histologic grade 2, consists of medium-sized tumor cells with moderate glandular formation. (B) Invasive ductal carcinoma, histologic grade 3, shows large-sized tumor cells with poor glandular formation. (C) Tumor cells are small- to medium-sized and poorly cohesive in invasive lobular carcinoma. (D) Mucinous carcinoma contains abundant extracellular mucin. (E, F) Invasive ductal carcinoma after neoadjuvant systemic therapy shows fragmented clusters of tumor cells (E) or singly scattered, atypical tumor cells (F) in the fibrotic background.

study using frozen tissue section of SLNs until the present time. In addition, the previous studies did not include post–neoadjuvant cases, which has been increasing but difficult to histologically examine [17].

In the challenge competition originating from the HeLP (HEalthcare ai Learning Platform), several models have been developed. In this challenge setting, we aimed to evaluate the models' performances for classification of metastases per slide in hematoxylin and eosin–stained frozen tissue sections of SLNs of breast cancer patients.

Materials and Methods

1. Data description

During routine surgical procedure for breast cancer in our institution, the excised SLNs were immediately submitted for frozen section. All of the SLNs were cut into 2-mm slices, entirely embedded in optimum cutting temperature compound, and frozen in –20°C to –30°C. For each lymph node, 5-μm-thick frozen sections were cut and one or two sections were picked up on glass slides and stained with hematoxylin and eosin. In this study, a total of 297 digital slides of SLNs from 132 patients were retrospectively collected. Among those, 144 slides were made from SLNs of patients who had received neoadjuvant therapy (48.5%). The slides were divided into a training set, a development set, and a validation set (157, 40, and 100 digital slides, respectively) without consideration of distribution of histologic type. Slides before a specific point in time were used as the training and development sets, and the other digital slides after that were used as the validation set. Patient demographics are summarized in Table 1. The slides were scanned using a digital microscopy scanner (Pannoramic 250 FLASH, 3DHISTECH Ltd., Budapest, Hungary) in MIRAX format (.mrxs) and with a resolution of 0.221 μm per pixel.

2. Reference standard

All the imaging datasets were segmented manually by one rater, and their annotations were confirmed by two clinically expert pathologists with 6 and 20 years' experience in breast pathology. Regions of metastatic carcinoma larger than 200 μm in the greatest dimension were annotated as cancer with the in-house labeling tool, as shown in Fig. 1.

3. Challenge competition environment

The challenge competition platform developed by Kakao was used to allocate two GPUs to each team. All of the competitors were allowed to access only paths of digital slides and corresponding mask images with Kakao platform. Docker image files that enables any of deep learning platform to run were used to train models and inference development and validation sets. Each team was given two P40 GPUs (NVIDIA, Santa Clara, CA) resources for training models. Kakao platform used CUDA 9,0 and cuDNN 7.

During the first stage for four weeks, competitors were given 197 digital slides as the training and development set for four weeks. The training set (157 digital slides) with annotated masks was given for training the model, while the development set (40 digital slides) without masks was given for tuning the model. Model performance calculated by the evaluation matrix was listed on the leader board after inferencing the development set which was used for tuning the model. During the second stage for additional 2 weeks, the

Table 2. Algorithm descriptions and hyper parameters

Team	Architecture	Input size (slide layer level)	Optimization (learning rate)	Augmentation real-time	Pre-processing	Post-processing; inference for confidence
Fiffeb	Inception v3, RFC	256×256×3 (6) Patch	SGD (0.9)	Color augmentation, horizontal flip, random rotation	Otsu thresholding, tumor (> 90%) and non-tumor (0% and > 20%)	Generation of heat map with image level 7 and feeding morphological information into FRC; RFC output
DoAI	U-Net	512×512×3 (0) Patch	SGD (1e-1, decay 0.1 each 2 epochs)	Rotation, horizontal and vertical flip	None	De-noising for false-positive reduction; CNN output
GoldenPass	U-Net, Inception v3	256×256×3 (4) Patch	Adam (1e-3, 5e-4)	Rotation, horizontal and vertical flip, brightness (0.5-1)	Otsu thresholding, tumor (> 100%)	None; Max value for heat-map
SOG	Simple CNN	300×300×3 (4) Slide	Adadelta (1e-3)	None	None	None; CNN output

SGD, stochastic gradient descent; RFC, random forest classifier; CNN, convolutional neural network.

Table 3. Performance and average time comparison for classification of tumor slide

Team	Development set AUC	Validation set AUC	Validation set					Time (min)
			ACC	TPR	TNR	PPV	NPV	
Fiffeb	0.986	0.805	0.770	0.727	0.822	0.833	0.712	10.8
DoAI	0.985	0.776	0.750	0.800	0.689	0.759	0.738	0.6
GoldenPass	0.945	0.760	0.730	0.782	0.667	0.741	0.714	3.9
SOG	0.595	0.540	0.510	0.145	0.956	0.800	0.478	-

AUC, area under the curve; ACC, accuracy; TPR, true positive rate; TNR, true negative rate; PPV, positive predictive value; NPV, negative predictive value.

competitors were given 100 additional digital slides for final evaluation of their models with the optimal model derived from the development set.

4. Evaluation metric

The algorithms were assessed for classifying between "metastasis" or "normal." Area under receiver operating characteristic curve (AUC) was evaluated by receiver operating characteristic (ROC) analysis.

5. Competitors

Forty-five competitors who were interested in digital pathology or machine learning registered for this challenge within 4 weeks from the beginning of November 2018. Ten competitors were selected according to their inner commitments in accordance with the limited platform environment. Ten competitors were composed of students, researchers, and doctors experienced in medical image analysis using machine learning or deep learning. Only four competitors submitted their results on the leaderboard. The methodological description is summarized in Table 2. All of the competitors selected only deep learning as the main architecture such as Inception v3 [18] for classification of the tumor patch or U-Net [19] for segmentation of the tumor region. Instead of modifying their models, they focused on pre- and post-processing steps to achieve optimal results. In one team which ranked high, random forest regression [20] was used to inference confidence by extracting high level features including the number of tumor regions, percentage of the tumor region over the entire tissue region, the area of the largest tumor regions, etc., from the heat map generated using the deep learning method. Real time-based augmentation methods were adjusted while training models. Detailed descriptions of each algorithm are listed in Table 2.

6. Ethical statement

The institutional review board for human investigations at Asan Medical Center (AMC) approved the study protocol with removal of all patient identifiers from the images and they waived the requirement for informed consent, in accordance with the retrospective design of this study.

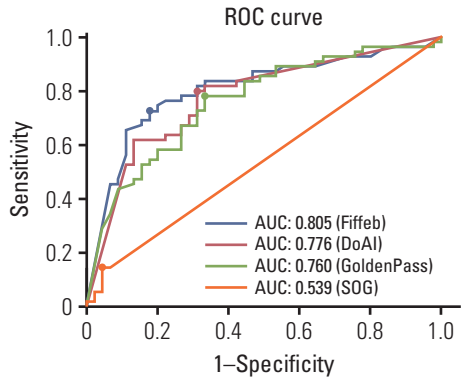

Fig. 2. Receiver operating characteristics (ROC) comparisons of models trained by four algorithms for the validation set and cut-off threshold value of each algorithm. The cutoff threshold value is dotted on each ROC curve. AUC, area under ROC.

Results

Model performances were sorted in descending order for the validation set as shown in Table 3 and Fig. 2. Four teams submitted their results on the leader board in development and validation sets. For the development set, the Four algorithms showed 0.986, 0.985, 945, and 0.595 AUCs. For the validation set which consisted of 100 digital slides, the Fiffeb team showed the highest AUC 0.805 in the validation set compared with other teams such as the DoAI, GoldenPass, and SOG teams at AUC 0.776, 0.760, and 0.540 respectively. Average times of the first three teams (Fiffeb, DoAI, and GoldenPass) in validation set were 10.8, 0.6, and 3.9 minutes, respectively.

For more detailed analysis, each algorithm was evaluated

Table 4. Performance comparison for determining the clinicopathologic characteristics of tumors

	Team			
	Fiffeb	DoAI	GoldenPass	SOG
Metastatic tumor size				
≤ 2 mm (n=33)				
TPR	0.600	0.667	0.667	0.067
FNR	0.400	0.333	0.333	0.933
> 2 mm (n=22)				
TPR	0.775	0.850	0.825	0.175
FNR	0.225	0.150	0.175	0.825
Neo-adjuvant therapy				
Not received (n=45)				
TPR	0.731	0.808	0.808	0.154
TNR	0.842	0.737	0.632	0.895
Received (n=55)				
TPR	0.724	0.793	0.759	0.138
TNR	0.808	0.654	0.692	1.000
Histologic type				
IDC (n=86)				
TPR	0.723	0.766	0.766	0.149
TNR	0.795	0.667	0.641	0.949
ILC (n=11)				
TPR	0.833	1.000	1.000	0.000
TNR	1.000	0.800	0.800	1.000
MC (n=3)				
TPR	0.500	1.000	0.500	0.500
TNR	1.000	1.000	1.000	1.000
Histologic grade				
1 or 2 (n=86)				
TPR	0.735	0.816	0.796	0.163
TNR	0.838	0.676	0.649	0.946
3 (n=14)				
TPR	0.667	0.667	0.667	0.000
TNR	0.750	0.750	0.750	1.000

TPR, true positive rate; FNR, false negative rate; TNR, true negative rate; IDC, invasive ductal carcinoma; ILC, invasive lobular carcinoma; MC, mucinous carcinoma.

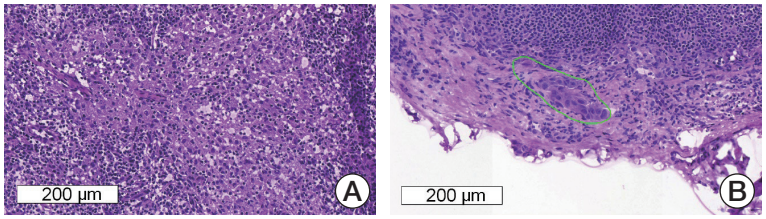

Fig. 3. Representative microscopic images of false-positive (A) and false-negative (B) cases. (A) Reactive histiocytes show abundant, eosinophilic cytoplasm and can be misinterpreted as metastatic carcinoma. (B) A very small focus of metastatic carcinoma (approximately 200 μm in the greatest dimension) is seen and which was missed by all four of the teams.

with the cutoff threshold determined by the Youden index [21] from the ROC curve in the validation set in terms of the accuracy (ACC), true positive rate (TPR), true negative rate (TNR), positive predictive value (PPV), and negative predictive value (NPV). The first-placed team Fiffeb showed the highest AUC (0.805), ACC (0.770), TNR (0.822), and PPV (0.833), while the second-placed team DoAI showed the highest TPR (0.800) and NPV (0.738).

In addition, model performance comparisons with clinical information for more detail, such as the metastatic tumor size (smaller or larger than 2 mm in the greatest dimension), whether patients had received neoadjuvant systemic therapy, histologic type of tumor, and the histologic grade of the tumor was measured, as shown in Table 4. Four teams showed higher TPR and lower false-negative rate in lymph nodes with larger metastatic tumors. In lymph nodes obtained from patients who had received neoadjuvant systemic therapy, four teams showed lower TPR and two teams showed lower TNR. In terms of the histologic type, three teams showed higher TPR and four teams higher TNR in the invasive lobular carcinoma group than in the invasive ductal carcinoma group. When comparing performance between the histologic grades, four teams showed higher TPR, but only one team showed higher TNR in grade 1 or 2 than in grade 3.

Among the 100 slides in the validation set, 57 slides were correctly categorized by all top three teams (35 slides, true-positive; 22 slides, true-negative), four slides were incorrectly categorized as positive (false-positive) by the top three teams, and six slides were incorrectly categorized as negative (false-negative) by the top three teams, as shown in Fig. 3. All of the four false-positive slides were obtained from patients with invasive ductal carcinoma, histologic grade 2, and two slides were from neoadjuvant systemic therapy patients. Similarly, all of the six false-negative slides were obtained from patients with invasive ductal carcinoma, i.e., five from histologic grade 2 patients and one from a histologic grade 3 patient, and three were from neoadjuvant systemic therapy patients. Four of the six false-negative slides had micrometastases. The size range of metastatic carcinoma in the false-negative slides was 0.13 to 4.45 mm.

Discussion

In this current study, all of the competitors adopted convolutional neural network (CNN)–based deep learning methods as the main idea such as the classification or segmentation network, and which showed high performance at 0.805, 0.776, and 0.760 in terms of AUC for the top three teams.

Interestingly, in all four teams, AUC was lower in the validation set compared to that in the development set. This might be due to the difference in patient demographics, particularly with regard to neoadjuvant systemic therapy. Distribution of histologic type is different between training, development, and validation sets as shown in Table 1. Especially in the validation set, the number of slides obtained from patients after neoadjuvant systemic therapy was significantly higher than that in the development set. Neoadjuvant systemic therapy often causes fibrosis and macrophage infiltration in the tumor area and fragmentation and/or scattering of tumor clusters [17], and which can lead to difficulty in histologic examination. It might be suggested that this neoadjuvant systemic therapeutic effect caused a decrease of AUC in the validation set.

Inference time is also key point with this challenge so that methods can be adopted in routine clinical practice. Turnaround time between receiving samples and reporting in conventional frozen section diagnosis has been variably reported around 20-30 minutes, including gross examination, freezing, cutting, staining, and microscopic examination [22]. Time consumed for scanning can be varied upon the size of sections, type of scanning machine, magnification, and focus layering, but recent studies have reported that 3-9 minutes of median handling time for scanning [22,23]. Two different types of patch-based CNN methods, classification and segmentation network, have shown pros and cons. The number of outputs of the classification network in this challenge is same with the number of classes that the model classifies input patch into (i.e., 1 or 2) by encoding all input dimensions to compressed features for a precise decision. In case of segmentation network, the number of outputs is same with the number of input dimensions (i.e., 448×448=200,704), which is approximately 100K or 200K times more than that

of classification network. It is a factor reducing computational time. In our results, the first-placed team using only classification network showed 0.3 higher AUC than that of the second-placed team using only segmentation network, but too slow to deploy this into the real clinical routine while the computational time of the second-placed team took 18.8 times faster than that of the first-placed team. Ensemble of those different types of CNN networks should be considered to enhance model performance in routine clinical practice.

Next, we compared model performances according to the clinicopathologic factors of the patients. It is generally known that in manual examination of intraoperative SLN biopsy, false-negative results are more likely in micrometastases and favorable and/or lobular histology [24]. In the validation set, the top three teams showed better performances in lymph nodes with macrometastatic tumor, and which is consistent with manual examination and the CAMELYON16 study [4]. Lymph nodes which were obtained from non-neoadjuvant systemic therapy patients also revealed better performances, as discussed above. Lymph nodes from invasive lobular carcinoma patients revealed better TPR in the first three teams and better TNR in four teams than those from invasive ductal carcinoma patients, although the number of slides from invasive lobular carcinoma patients is limited. This is in accordance with the general results in manual examination and the CAMELYON16 study. In the CAMELYON16 study, 29 among 32 teams showed higher AUC in the invasive ductal carcinoma set than in the non-invasive ductal carcinoma set. In addition, tumors of histologic grade 1 or 2 showed higher TPR in the top three teams, but lower TNR in two of the three teams than tumors of histologic grade 3, and which requires further studies.

We found that some cases were wrongly categorized by the first three teams. All of six false-negative cases showed small-sized metastatic carcinoma, and which could result in false negativity. In contrast, four false-positive cases did not reveal any common clinicopathologic feature. However, we assume that reactive histiocytic infiltration or prominent germinal centers in lymph nodes might cause false positivity. Manual confirmation is probably necessary, and so a screening tool that would expedite this process might have broad appeal. Interestingly, TPR of mucinous carcinoma cases (0.5-1.0) was not lower than those of invasive ductal carcinoma (0.149-0.766) or invasive lobular carcinoma (0.000-1.000), although mucinous carcinoma was not included in training and validation sets. This might be due to some histologic similarities between mucinous carcinoma and other carcinomas, such as cluster formation, bigger cell size than lymphocytes, and nuclear size enlargement.

Our study has some strong significance compared to previously reported studies about possible usefulness of deep learning algorithm in diagnosis of SLN metastasis [4,16]. First, we used digital slides from frozen sections which were made intraoperatively, while previous studies used FFPE sections. Since frozen sections have lower quality due to tissue artifact compared with FFPE sections, it is more difficult to examine frozen sections than FFPE sections. However, what is used to determine the surgical extent intraoperatively in the real world is frozen sections, not FFPE sections. Therefore, we suggest that studies of the deep learning algorithm with SLNs would be more practical if frozen sections are used. Second, our dataset includes a high proportion (48.5%) of post-neoadjuvant patients. The role of neoadjuvant therapy in breast cancer treatment has been increasing these days, but it is much more difficult to histologically diagnose SLN metastasis after neoadjuvant therapy [17]. During case selection, we included more post-neoadjuvant cases than clinical setting with an intention of making our dataset unique and more useful. To reduce false-positive or false-negative issues technically, the deep learning models should be re-trained with those regions and different hyper-parameters such as class weights or loss weights. Those regions with different hyper-parameters have deep learning models intensively trained as strong positive regions with this strategy. Applications using these methods can be adopted in routine clinical practice by showing attention map with augmented reality and training itself robustly with false-positive cases selected by pathologists with on-line learning.

Our contest has several limitations. First, only paths to access the training, development, and validation sets were given to competitors, which means that they had no way to check the heat map generated by their models as all dataset contests provided were not available in public. Competitors were not allowed to check processing in the middle of training for the same reason. Only less than 1 MB log data could be saved and given to competitors for the purpose of debugging after training processing to check if and how the training is going well. It was also not available how much time was spent for training and analyses. This might be one of key reasons of the models with relatively low accuracies. Second, only two GPUs were given to each competitor, and it could be limited resource, although this constraint makes competitors fair. Third, we did not perform immunohistochemistry to confirm metastatic carcinoma on frozen section slides. On the contrary to FFPE sections, multiple frozen sections which were made from the same tissue fragment showed quite different shapes due to the tissue artifact. Therefore, immunohistochemistry is not as helpful in frozen sections as in FFPE sections to annotate tumor cells. In addition, it is impossible to retrospectively perform immunohistochemistry on frozen sections. Instead, when we annotate tumor cells in frozen sections, we review matched FFPE sections with cytokeratin immunohistochemistry in order to minimize annotation error. Finally, the high proportion of post–neoadjuvant cases or cases with micrometastases could have negatively affected the diagnostic accuracy of algorithms in this study. It

would have been nicer if we could divide the dataset into multiple groups and develop different algorithms based on patients' information, such as neoadjuvant status, histologic type, or histologic grade of tumor. However, it was impossible due to the limited number of digital slides. We hope to expand our dataset and include such analysis in our further study. Finally, the model performance can be influenced by various parameters including quality of tissue sections, staining quality and color differences, type of scanning machine, scanning environment, and accuracy of segmentation. Therefore, further studies for optimization of pre-processing of digital images might improve models' diagnostic performances.

Possibly because of the characteristics of our dataset and the above limitations, even the top three algorithms in this study showed relatively lower performance than the other first prized in CAMELYON16, and lower diagnostic accuracy than average of pathologists [25]. However, we believe that it is worth holding a digital pathology challenge competition using frozen tissue sections in open innovation manner. For adjusting algorithms into routine clinical practice, HeLP is preparing another challenge competition to handle other problems such as localization of micro-metastasis and processing time.

Recognition abilities of deep learning and human could be complement each other. In addition, algorithms with deep learning can be used as computer aided system to help doctors diagnose. For example, virtual reality technology can help making quack accurate decision or alert a doctor who misses critical parts.

We held a challenge competition during six weeks to resolve the problem for classification of digital pathology slides with metastases in hematoxylin and eosin–stained frozen tissue sections of SLNs of breast cancer patients. The top three competitor teams achieved very high AUCs in the development set while they performed slightly lower AUC in the validation set. In this open innovation manner, the deep learning algorithms could be developed and evaluated, which might be helpful in the frozen diagnosis of intraoperative, SLN biopsy. Further studies are required in order to increase the accuracy and decrease the time consuming required to apply the deep learning algorithm in the clinical setting.

Conflicts of Interest

Conflicts of interest relevant to this article was not reported.

Acknowledgments

This work was supported by Kakao and Kakao Brain corporations and a grant of the Korea Health Technology R&D Project through the Korea Health Industry Development Institute (KHIDI), funded by the Ministry of Health & Welfare, Republic of Korea (HI18C0022).

Author Details

[1]Department of Biomedical Engineering, Asan Institute of Life Science, Asan Medical Center, University of Ulsan College of Medicine, Seoul, [2]Department of Hospital Pathology, Seoul St. Mary's Hospital, College of Medicine, The Catholic University of Korea, Seoul, [3]Health Innovation Big Data Center, Asan Institute for Life Science, Asan Medical Center, Seoul, Departments of [4]Radiology and [5]Convergence Medicine, Asan Medical Center, University of Ulsan College of Medicine, Seoul, [6]KakaoBrain-BrainCloud Team, Seongnam, [7]Department of Computer Science and Engineering, Ulsan National Institute of Science and Technology, Ulsan, [8]Image Laboratory, School of Computer Science and Engineering, Chung-Ang University, Seoul, [9]DoAI Inc., Seoul, [10]Department of Business Management and Convergence Software, Sogang University, Seoul, [11]Data Science & Business Analytics Lab, School of Industrial Management Engineering, College of Engineering, Korea University, Seoul, [12]Software Graduate Program, School of Computing, College of Engineering, Korea Advanced Institute of Science and Technology, Seoul, [13]Department of Biomedical Engineering, Yonsei University, Seoul, [14]Department of Social Studies Education, College of Education, Ewha Womans University, Seoul, [15]Department of Math, University of Kwangwoon, Seoul, [16]Department of Electrical and Computer Engineering, Seoul National University, Seoul, Departments of [17]Pathology and [18]Biostatistics, Seoul National University College of Medicine and SMG-SNU Boramae Medical Center, Seoul, [19]Department of Pathology, Asan Medical Center, University of Ulsan College of Medicine, Seoul, Korea

References

1. Williams BJ, Bottoms D, Treanor D. Future-proofing pathology: the case for clinical adoption of digital pathology. J Clin Pathol. 2017;70:1010-8.
2. Wang S, Chen A, Yang L, Cai L, Xie Y, Fujimoto J, et al. Comprehensive analysis of lung cancer pathology images to discover tumor shape and boundary features that predict survival outcome. Sci Rep. 2018;8:10393.
3. Litjens G, Sanchez CI, Timofeeva N, Hermsen M, Nagtegaal I, Kovacs I, et al. Deep learning as a tool for increased accuracy and efficiency of histopathological diagnosis. Sci Rep. 2016;6:26286.
4. Ehteshami Bejnordi B, Veta M, Johannes van Diest P, van Ginneken B, Karssemeijer N, Litjens G, et al. Diagnostic assessment of deep learning algorithms for detection of lymph node metastases in women with breast cancer. JAMA. 2017;318:2199-210.
5. Kasper DL, Fauci AS, Hauser SL, Longo DL, Jameson JL, Loscalzo J. Harrison's principles of internal medicine. 19th ed.

New York: McGraw-Hill; 2015.
6. Hayes SC, Janda M, Cornish B, Battistutta D, Newman B. Lymphedema after breast cancer: incidence, risk factors, and effect on upper body function. J Clin Oncol. 2008;26:3536-42.
7. Fleissig A, Fallowfield LJ, Langridge CI, Johnson L, Newcombe RG, Dixon JM, et al. Post-operative arm morbidity and quality of life: results of the ALMANAC randomised trial comparing sentinel node biopsy with standard axillary treatment in the management of patients with early breast cancer. Breast Cancer Res Treat. 2006;95:279-93.
8. Lyman GH, Temin S, Edge SB, Newman LA, Turner RR, Weaver DL, et al. Sentinel lymph node biopsy for patients with early-stage breast cancer: American Society of Clinical Oncology clinical practice guideline update. J Clin Oncol. 2014;32:1365-83.
9. Manca G, Rubello D, Tardelli E, Giammarile F, Mazzarri S, Boni G, et al. Sentinel lymph node biopsy in breast cancer: indications, contraindications, and controversies. Clin Nucl Med. 2016;41:126-33.
10. Galimberti V, Cole BF, Viale G, Veronesi P, Vicini E, Intra M, et al. Axillary dissection versus no axillary dissection in patients with breast cancer and sentinel-node micrometastases (IBCSG 23-01): 10-year follow-up of a randomised, controlled phase 3 trial. Lancet Oncol. 2018;19:1385-93.
11. Giuliano AE, Ballman KV, McCall L, Beitsch PD, Brennan MB, Kelemen PR, et al. Effect of axillary dissection vs no axillary dissection on 10-year overall survival among women with invasive breast cancer and sentinel node metastasis: the ACOSOG Z0011 (Alliance) randomized clinical trial. JAMA. 2017;318:918-26.
12. Wang J, Tang H, Li X, Song C, Xiong Z, Wang X, et al. Is surgical axillary staging necessary in women with T1 breast cancer who are treated with breast-conserving therapy? Cancer Commun (Lond). 2019;39:25.
13. Donker M, van Tienhoven G, Straver ME, Meijnen P, van de Velde CJ, Mansel RE, et al. Radiotherapy or surgery of the axilla after a positive sentinel node in breast cancer (EORTC 10981-22023 AMAROS): a randomised, multicentre, open-label, phase 3 non-inferiority trial. Lancet Oncol. 2014;15:1303-10.
14. Celebioglu F, Sylvan M, Perbeck L, Bergkvist L, Frisell J. Intraoperative sentinel lymph node examination by frozen section, immunohistochemistry and imprint cytology during breast surgery: a prospective study. Eur J Cancer. 2006;42:617-20.
15. Chen Y, Anderson KR, Xu J, Goldsmith JD, Heher YK. Frozen-section checklist implementation improves quality and patient safety. Am J Clin Pathol. 2019;151:607-12.
16. Bandi P, Geessink O, Manson Q, Van Dijk M, Balkenhol M, Hermsen M, et al. From detection of individual metastases to classification of lymph node status at the patient level: the CAMELYON17 challenge. IEEE Trans Med Imaging. 2019;38:550-60.
17. Honkoop AH, Pinedo HM, De Jong JS, Verheul HM, Linn SC, Hoekman K, et al. Effects of chemotherapy on pathologic and biologic characteristics of locally advanced breast cancer. Am J Clin Pathol. 1997;107:211-8.
18. Szegedy C, Vanhoucke V, Ioffe S, Shlens J, Wojna Z. Rethinking the inception architecture for computer vision. In: 2016 Proceedings of the IEEE Conference on Computer Vision and Pattern Recognition; 2016 Jun 27-30; Las Vegas, NV, USA.
19. Ronneberger O, Fischer P, Brox T. U-net: convolutional networks for biomedical image segmentation. In: International Conference on Medical Image Computing and Computer-Assisted Intervention (MICCAI); 2015 Oct 5-9; Munich, Germany. Cham: Springer; 2015. p. 234-41.
20. Liaw A, Wiener M. Classification and regression by random forest. R News. 2002;2:18-22.
21. Youden WJ. Index for rating diagnostic tests. Cancer. 1950;3:32-5.
22. Laurent-Bellue A, Poullier E, Pomerol JF, Adnet E, Redon MJ, Posseme K, et al. Four-year experience of digital slide telepathology for intraoperative frozen section consultations in a two-site French academic department of pathology. Am J Clin Pathol. 2020;154:414-23.
23. Menter T, Nicolet S, Baumhoer D, Tolnay M, Tzankov A. Intraoperative frozen section consultation by remote whole-slide imaging analysis: validation and comparison to robotic remote microscopy. J Clin Pathol. 2020;73:350-2.
24. Akay CL, Albarracin C, Torstenson T, Bassett R, Mittendorf EA, Yi M, et al. Factors impacting the accuracy of intra-operative evaluation of sentinel lymph nodes in breast cancer. Breast J. 2018;24:28-34.
25. Houpu Y, Fei X, Yang Y, Fuzhong T, Peng L, Bo Z, et al. Use of Memorial Sloan Kettering Cancer Center nomogram to guide intraoperative sentinel lymph node frozen sections in patients with early breast cancer. J Surg Oncol. 2019;120:587-92.

pISSN 1598-2998, eISSN 2005-9256

Cancer Res Treat. 2020;52(4):1112-1119 https://doi.org/10.4143/crt.2020.245

Original Article Open Access

Real-World Experience of Nivolumab in Non-small Cell Lung Cancer in Korea

Sun Min Lim, MD, PhD[1]
Sang-We Kim, MD, PhD[2]
Byoung Chul Cho, MD, PhD[1]
Jin Hyung Kang, MD, PhD[3]
Myung-Ju Ahn, MD, PhD[4]
Dong-Wan Kim, MD, PhD[5]
Young-Chul Kim, MD, PhD[6]
Jin Soo Lee, MD, PhD[7]
Jong-Seok Lee, MD, PhD[8]
Sung Yong Lee, MD, PhD[9]
Keon Uk Park, MD, PhD[10]
Ho Jung An, MD, PhD[11]
Eun Kyung Cho, MD, PhD[12]
Tae Won Jang, MD, PhD[13]
Bong-Seog Kim, MD, PhD[14]
Joo-Hang Kim, MD, PhD[15]
Sung Sook Lee, MD, PhD[16]
Im-Il Na, MD, PhD[17]
Seung Soo Yoo, MD, PhD[18]
Ki Hyeong Lee, MD, PhD[19]

**A list of author's affiliations appears at the end of the paper.*

Correspondence: Ki Hyeong Lee, MD, PhD
Division of Hematology-Oncology, Department of Internal Medicine, Chungbuk National University Hospital, Chungbuk National University College of Medicine, 776 ilsunhwan-ro, Heungdeok-gu, Cheongju 28644, Korea
Tel: 82-43-269-6015
Fax: 82-43-269-6899
E-mail: kihlee@chungbuk.ac.kr

Received March 24, 2020
Accepted May 9, 2020
Published Online May 15, 2020

Purpose
The introduction of immune checkpoint inhibitors represents a major advance in the treatment of lung cancer, allowing sustained recovery in a significant proportion of patients. Nivolumab is a monoclonal anti–programmed death cell protein 1 antibody licensed for the treatment of locally advanced or metastatic non-small cell lung cancer (NSCLC) after prior chemotherapy. In this study, we describe the demographic and clinical outcomes of patients with advanced NSCLC treated with nivolumab in the Korean expanded access program.

Materials and Methods
Previously treated patients with advanced nonsquamous and squamous NSCLC patients received nivolumab at 3 mg/kg every 2 weeks up to 36 months. Efficacy data including investigator-assessed tumor response, progression data, survival, and safety data were collected.

Results
Two hundred ninety-nine patients were treated across 36 Korean centers. The objective response rate and disease control rate were 18% and 49%, respectively; the median progression-free survival was 2.1 months (95% confidence interval [CI], 1.87 to 3.45), and the overall survival (OS) was 13.2 months (95% CI, 10.6 to 18.9). Patients with smoking history and patients who experienced immune-related adverse events showed a prolonged OS. Cox regression analysis identified smoking history, presence of immune-related adverse events as positive factors associated with OS, while liver metastasis was a negative factor associated with OS. The safety profile was generally comparable to previously reported data.

Conclusion
This real-world analysis supports the use of nivolumab for pretreated NSCLC patients, including those with an older age.

Key words
Non-small cell lung cancer, Anti–PD-1, Real-world data

Introduction

The introduction of immune checkpoint inhibitors (ICIs) has led to tremendous changes in the treatment of advanced stage non-small cell lung cancer (NSCLC), and ICIs have emerged as one of the most effective anticancer agents. ICIs can block inhibitory pathways that control the immune response, restoring and sustaining the immune system against cancer cells. Programmed death cell protein 1 (PD-1) is a promising target of immunotherapy, and tumor expression of

programmed death-ligand 1 (PD-L1) has been widely investigated as a predictive marker of response, although its sensitivity and specificity is modest [1]. Recent pivotal studies have assessed the role of immunotherapy in metastatic NSCLCs in both squamous and nonsquamous histology, and three agents (nivolumab, pembrolizumab, atezolizumab) have been investigated for the treatment of previously treated metastatic NSCLC.

Nivolumab is a human IgG4 monoclonal antibody that blocks PD-1, and is now approved in second-line therapy of metastatic NSCLC patients. Nivolumab was tested in the open label, randomized phase 3 trials of CheckMate 017 and 057 [2,3] for previously treated squamous and nonsquamous NSCLC, respectively, and showed significantly improved OS compared to docetaxel in both trials. Recently, 5-year pooled OS rates for CheckMate017 and CheckMate057 were reported to be 13.4% for nivolumab, whereas it was 2.6% for docetaxel [4]. However, these clinical trials have excluded patients with poor performance status, brain metastases, and epidermal growth factor receptor (*EGFR*)/anaplastic lymphoma kinase (*ALK*) genomic alterations. About one-third of lung cancer patients present with poor performance status (Eastern Cooperative Oncology Group performance status [ECOG PS] ≥ 2) in the real world, although they have been excluded from most clinical trials [5]. While there is a higher frequency of *EGFR* and *ALK*-altered patients in Asia, this subgroup of patients cannot be overlooked in the era of immunotherapy. Moreover, elderly patients are frequently under-represented in clinical trials, despite the growing population worldwide [6].

Nivolumab was provided by Ono Pharmaceuticals through an expanded access program (EAP) from February 2016 to March 2019 for both squamous and nonsquamous NSCLC patients in Korea. The EAP program enrolled 300 advanced NSCLC patients from 36 sites in Korea, and represents the largest nation-wide representation of real-world practice. Here, we present the characteristics of response and toxicity of nivolumab treatment in multiple centers in Korea.

Materials and Methods

1. Patients and data collection

Advanced NSCLC patients were screened and recruited from 36 academic hospitals across the Republic of Korea. Eligibility criteria included locally advanced or metastatic NSCLC that had progressed despite standard therapy, an ECOG PS of 0 to 2, and adequate organ function and laboratory results. Key exclusion criteria included active brain metastases, autoimmune diseases, and patients with a life expectancy of < 6 weeks. Nivolumab was given 3 mg/kg intravenously every 2 weeks for a maximum of 36 months or until disease progression, unacceptable toxicity, or withdrawal of consent. Dose escalation or reduction was not allowed.

2. Efficacy assessment

Baseline tumor assessment was performed before the start of treatment, and response evaluation was performed by computed tomography imaging at least every 3 months, according to the local standard of practice. Tumor size measurement was performed according to RECIST 1.1 criteria [7]. An overall response was defined as a complete response (CR) or partial response (PR). Other efficacy parameters included disease control rate, duration of response, progression-free survival (PFS), and overall survival (OS). PFS was defined as the time from the start of nivolumab treatment to disease progression or death from any cause. OS was defined as the time from the start of nivolumab treatment to death from any cause.

3. Safety assessment

Safety was assessed at each patient visit by routine physical examination and laboratory assessment as needed by the physician. Blood tests included hematology, routine chemistry (including liver, kidney function, and pancreatic enzymes) and hormonal measurements (thyroid, adrenal function). Toxicity was classified according to Common Terminology Criteria for Adverse Events ver. 4 (CTCAE v4.0), and data regarding immune-related adverse events (irAEs) were reported retrospectively by patient chart review and laboratory reports.

4. Statistical analysis

All patients who received at least one dose of nivolumab were included in the intention-to-treat analyses for efficacy and safety. Data were summarized using descriptive statistics or contingency tables for demographic and baseline characteristics, response measurements, and safety measurements. All survival analyses were estimated using Kaplan-Meier curves and compared using the log-rank test. Hazard ratios and corresponding confidence intervals were estimated with the Cox proportional hazards model. All statistical analyses were performed with SPSS ver. 25.0 (IBM Corp., Armonk, NY).

5. Ethical statement

This program was performed in accordance with the principles of the Good Clinical Practice and was approved by the institutional review board of each hospital. All patients provided written informed consent before participation in the EAP.

Results

1. Baseline characteristics

From February 2016 to September 2016, a total of 334 patients were screened and 300 patients were enrolled in the

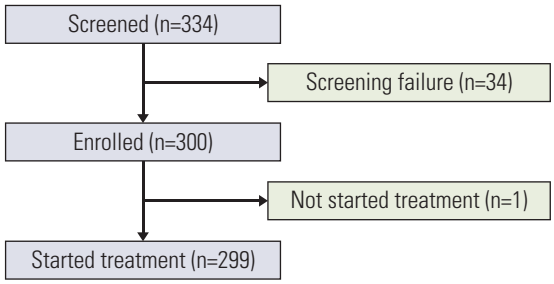

Fig. 1. Flow diagram of the study patients. Three hundred thirty-four patients were nominated for treatment in the nivolumab EAP. Thirty-four patients did not meet the study criteria and failed the screening. A total of 300 patients were enrolled, but one patient did not start the treatment. Overall, 299 patients were included in the analysis.

EAP. One patient did not start the treatment, so a total of 299 patients were evaluated for intention-to-treat analysis (Fig. 1). Median follow up time was 30.1 months (95% confidence interval [CI], 0 to 36.3), and a median of 6 doses of nivolumab were administered (range, 1 to 79). The median age of all patients was 61 (range, 31 to 85 years), and 206 (68.9%) were male patients. Most patients (87.3%) had ECOG PS 0-1, but 38 patients (12.7%) had ECOG PS 2. By histology, 198 (66.2%) patients had adenocarcinoma, 85 (28.4%) had squamous cell carcinoma, 6 (2%) had large cell carcinoma. Distant metastasis was identified in 275 (91.9%) patients, and the most common site of metastasis was bone (27.1%), followed by lung (24.4%) and brain (20.1%). Regarding smoking history, 108 (36.1%) patients were never-smokers, and former or current smokers (63.9%) were more prevalent. Most patients (86.9%) had stage IV disease and were former or current smokers (63.9%). As previous therapy, 61.5% of patients had surgery, 51.8% had radiotherapy, and 27.1% had received one line of chemotherapy before nivolumab. The majority of patients (72.9%) had received two or more lines of chemotherapy, ranging from 2 to 7 (Table 1).

As PD-L1 testing was optional in this program, PD-L1 immunohistochemistry results were available in only 17 patients (5.7%), *EGFR* mutations were identified in 48 patients (16.1%), and *ALK* translocations were identified in five patients (1.7%), but *EGFR* and *ALK* gene status was not available in 155 (51.8%) and 176 (58.9%) patients, respectively.

Table 1. Baseline characteristics of all patients

Characteristic	No. (%) (n=299)
Sex	
Male	206 (68.9)
Female	93 (31.1)
Age (yr)	
Median (range)	61 (31-85)
ECOG PS	
0-1	261 (87.3)
2	38 (12.7)
Histology	
Adenocarcinoma	198 (66.2)
Squamous cell carcinoma	85 (28.4)
Large cell carcinoma	6 (2.0)
Other	10 (3.3)
Metastasis site	
Adrenal glands	31 (10.4)
Bone	81 (27.1)
Brain	60 (20.1)
Liver	32 (10.7)
Lung ipsilateral	55 (18.4)
Lung contralateral	73 (24.4)
Other	109 (36.5)
Clinical stage	
IIIA	2 (0.7)
IIIB	37 (12.4)
IV	260 (87.0)
Smoking history	
Never	108 (36.1)
Former	171 (57.2)
Current	20 (6.7)
Previous therapy	
Surgery	
Yes	115 (38.5)
No	184 (61.5)
Radiotherapy	
Yes	144 (48.2)
No	155 (51.8)
Chemotherapy	
1	81 (27.1)
≥ 2	218 (72.9)

ECOG PS, Eastern Cooperative Oncology Group performance status.

2. Efficacy

Response evaluation was available in 256 patients, and 43 patients (14%) had missing evaluation scans due to progressive disease or death before first evaluation (Table 2). Best objective overall response (ORR) in the evaluable population was: CR in four patients (2%), PR in 49 patients (16%), stable disease in 92 patients (31%), and progressive disease in 111 (37%) patients. The ORR was 18%, and disease control rate (DCR) was 49%. The median time to response was 1.8 months (range, 1.3 to 18.2 months), and the median duration of response in those who achieved objective response was 21.0 months (range, 0.8+ to 33.2+ months). We compared ORR according to histology (squamous cell carcinoma vs. adenocarcinoma) and smoking status (never vs. former/current). The ORR (24.7% vs. 13.6%, p=0.023) and DCR (56.5% vs. 42.9%, p=0.036) in squamous cell carcinoma patients were both significantly higher than adenocarcinoma patients, while the ORR and DCR did not differ between never-

Table 2. Overall objective response

	Total (n=299)	Histology		Smoking	
		Squamous (n=85)	Adenocarcinoma (n=198)	Never (n=108)	Former or current (n=191)
Objective response rate[a]	53 (18)	21 (25)	27 (14)	13 (12)	40 (21)
Disease control rate[b]	145 (49)	48 (56)	85 (43)	45 (42)	100 (52)
Best overall response					
CR	4 (2)	2 (2)	2 (1)	1 (1)	3 (2)
PR	49 (16)	19 (22)	25 (13)	12 (11)	37 (19)
SD	92 (31)	27 (32)	58 (29)	32 (30)	60 (31)
PD	111 (37)	28 (33)	79 (40)	43 (40)	68 (36)
NE	43 (14)	1 (1)	0	0	1 (1)
Duration of response[c] **(mo)**	21.03 (0.79+ to 33.15+)	16.9 (1.94 to 33.08+)	26.8 (0.79+ to 32.85+)	20.4 (2.43 to 32.39+)	26.8 (0.79+to 33.15+)

Values are presented as number (%) or median (range). CR, complete response; PR, partial response; SD, stable disease; PD, progressive disease; NE, not evaluable. [a]Best overall response is CR or PR, [b]Best overall response is CR or PR or SD, [c]The duration of response was defined as the time from the date of first response (CR/PR) to the date of first documented disease progression/death (event), or last tumor assessment (censored).

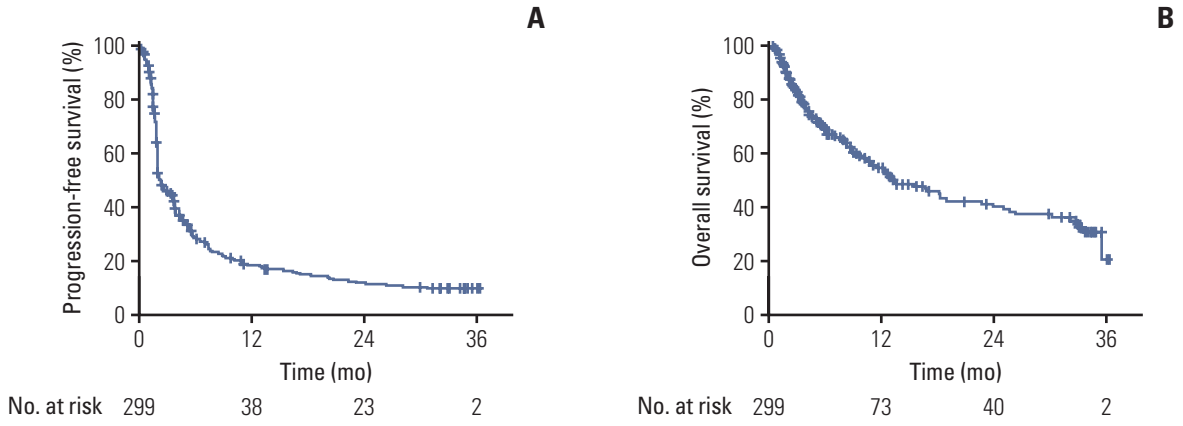

Fig. 2. Kaplan-Meier curves of progression-free survival and overall survival in non-small cell lung cancer patients treated with nivolumab. (A) Progression-free survival of all patients. (B) Overall survival of all patients.

smokers and former/current smokers. The Kaplan-Meier estimates for PFS and OS are reported in Fig. 2A and B. The median PFS was 2.1 months (95% CI, 1.87 to 3.45), and the median OS was 13.2 months (95% CI, 10.6 to 18.9). The 1-year and 2-year PFS rate was 18.2% and 11.7% and, 1-year and 2-year OS rate was 54.5%, 40.1%, respectively. Next, PFS and OS were compared between specific patient subgroups. Former or current smokers showed significantly longer OS, but not PFS, compared to never-smokers (Fig. 3A and B). PFS and OS were not significantly different according to tumor histology (Fig. 3C and D).

3. Efficacy in specific patients' subgroups

We compared ORR according to different clinical parameters including metastatic site, ECOG PS, prior treatment line, presence of immune-related AE (irAE), and *EGFR* mutation status (S1 Table). We noted a significantly higher ORR in patients who presented with irAE than those who did not (32% vs. 11%, $p < 0.001$). In addition, patients who received one prior therapy showed higher ORR than those who received two or more prior therapies (27% vs. 14%, p=0.009). However, there were no significant differences in ORR according site of metastasis, ECOG PS or *EGFR* mutation status.

When PFS and OS were compared between specific patient subgroups, we noted that patients who were aged 75 or older showed a significantly prolonged PFS (p=0.046) compared to patients under 75 years (S2A Fig.), while OS was not different (S2B Fig.). There were no differences in PFS or OS according to ECOG PS (S2C and S2D Fig.). Patients who experienced irAEs showed a significantly prolonged PFS and OS compared to those who did not ($p < 0.001$) (S2E and S2F Fig.).

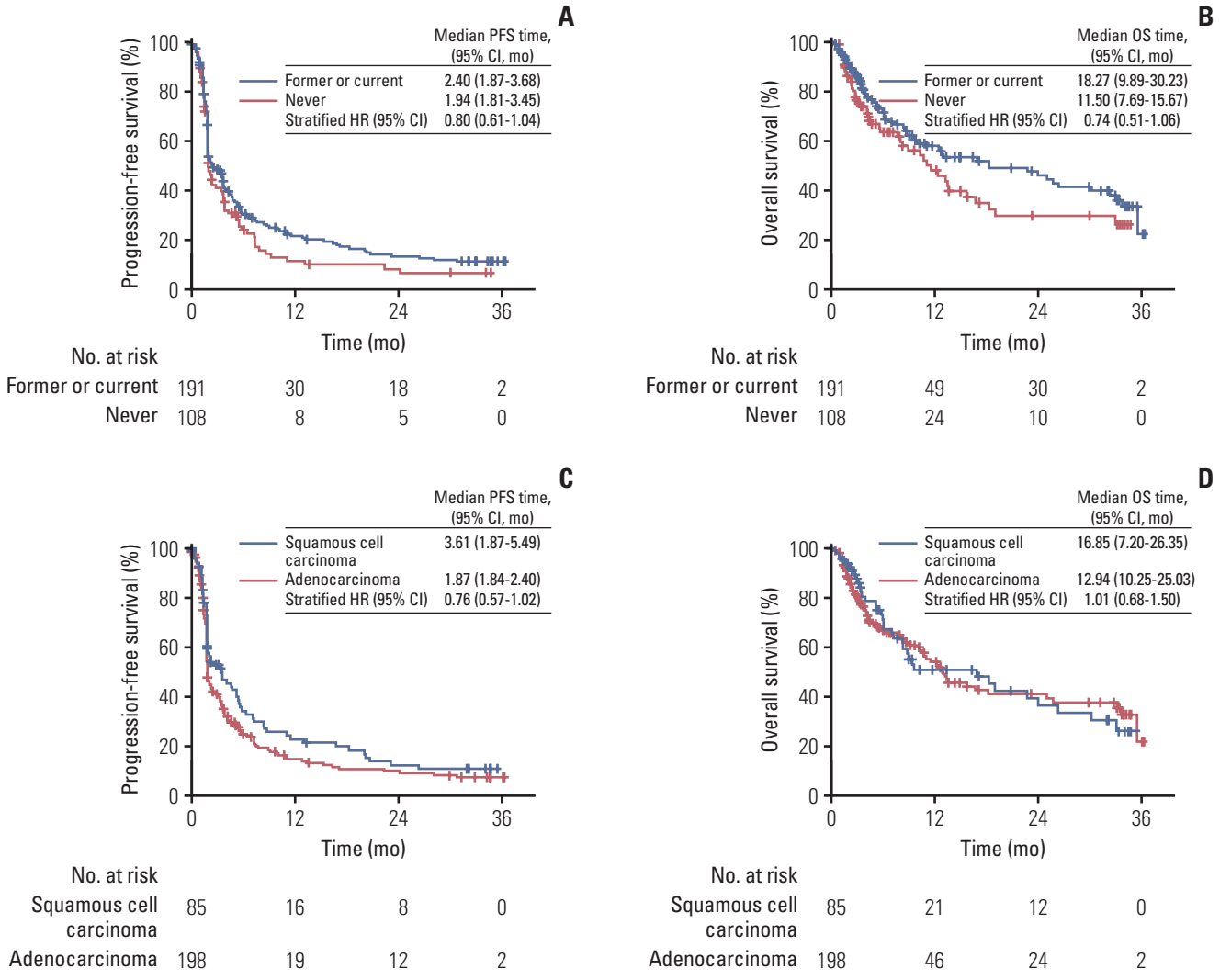

Fig. 3. Kaplan-Meier curves. (A) Comparison of progression-free survival between former or current smokers versus never-smokers. (B) Comparison of overall survival between former or current smokers versus never-smokers. (C) Comparison of progression-free survival between squamous cell carcinoma and adenocarcinoma. (D) Comparison of overall survival between squamous cell carcinoma and adenocarcinoma. HR, hazard ratio; CI, confidence interval.

On the other hand, patients who presented with concomitant brain and liver metastases showed the shortest PFS and OS compared to those with brain, liver, or other metastases (data not shown).

Ninety-three patients were treated beyond progression, and of these patients, two (2%) achieved objective response beyond progression, and disease control was achieved in 18 (19%) patients. The median OS of patients who received nivolumab beyond PD was 13.2 months (95% CI, 9.59 to 23.95), which was significantly longer from those who withdrew after PD (8.28 months; 95% CI, 6.05 to 12.35; p=0.048).

When we compared clinical or tumor characteristics between early progressors (< 4 cycles) and long-term responders (≥ 48 cycles), no baseline clinical or tumor characteristics clearly distinguished long-term survivors (data not shown). There was a trend toward long-term efficacy in patients with squamous histology and patients with smoking history.

4. Univariate and multivariate analyses

We next performed univariate and multivariate analyses to assess the role of each clinical parameter on OS and PFS. Cox regression analysis identified smoking history, presence of irAE as positive factors associated with OS, and liver metastasis was negative factor associated with OS. At multivariate analysis, all three factors maintained their independent prognostic role (Table 3). In addition, the presence of irAEs was also a positive factor associated with PFS (S3 Table).

Table 3. Cox proportional hazard model for overall survival

Variable	Reference	Univariate analysis			Multivariate analysis		
		Hazard ratio	95% CI	p-value	Hazard ratio	95% CI	p-value
Age							
≥ 75 yr	< 75 yr	0.62	0.31-1.23	0.172	-	-	-
Smoking history							
Former or current	Never	0.66	0.46-0.96	0.028	0.65	0.44-0.94	0.024
Histology							
Squamous cell carcinoma	Adenocarcinoma	0.92	0.62-1.38	0.697	-	-	-
Brain metastasis							
Yes	No	1.40	0.93-2.11	0.110	-	-	-
Liver metastasis							
Yes	No	2.38	1.52-3.75	< 0.001	2.18	1.37-3.47	0.001
ECOG PS							
2	0-1	1.60	0.97-2.65	0.067	-	-	-
Previous treatment line							
≥ 2	1	1.42	0.94-2.15	0.094	-	-	-
Immune-related AE							
Yes	No	0.44	0.29-0.67	< 0.001	0.50	0.33-0.76	0.001
AE							
Yes	No	0.77	0.44-1.35	0.360	-	-	-
EGFR							
Positive	Negative	0.94	0.52-1.72	0.854	-	-	-

CI, confidence interval; ECOG PS, Eastern Cooperative Oncology Group performance status; AE, adverse effect; *EGFR*, epidermal growth factor receptor.

5. Safety

Treatment-related AE of any grade, and treatment-related AE of grade 3-4 events were reported in 63% and 18% of patients, respectively. The discontinuation rate due to treatment-related AEs was 8%. No treatment-related deaths were reported. IrAEs were reported in 32% of patients (S4 Table). The most common treatment-related AEs were decreased appetite (9.7%), pruritus (8.0%), pneumonia (7.0%), fatigue (7.0%) and diarrhea (7.0%). The most common treatment-related grade 3-4 AEs were dyspnea (1.7%), hepatotoxicity (1.3%), and pleural effusion (1%) (S5 Table). The most common irAEs was skin toxicity, occurring in 11% of patients, followed by endocrine (8%) and gastrointestinal (7%) (S6 Table). The following treatment-related grade 3/4 irAEs were notable: skin toxicity presenting as erythematous skin rash (n=1) and rash acneiform (n=1), pulmonary toxicity presenting as pneumonitis (n=2), hepatotoxicity presenting as aspartate aminotransferase/alanine transaminase increased (n=2), musculoskeletal toxicity presenting as myalgia (n=1), and endocrine toxicity presenting as thyroid-stimulating hormone increase (n=1).

Discussion

In this real-world analysis, efficacy and safety of nivolumab were comparable to previous phase 3 results. ORR, PFS, and OS in our population were similar to the observations in the CheckMate017 and CheckMate057 studies [2,3]. In addition, 3-year OS was 20.4% in our study, while it was 17.1% in the pooled phase 3 analyses [4]. There were no new safety signals identified in our study. Unlike clinical trials, we included patients with ECOG PS 2 and those who were previously heavily treated, thus this EAP represents a sizeable real-world experience with nivolumab.

Subgroup analyses showed that patients who experienced irAEs showed significantly higher ORR, PFS, and OS. The correlation between irAEs and efficacy has been previously reported [8-12]. In a recent study conducted in Spain, the probability of having a clinical response was 23 times higher in those patients who showed an irAE [8]. In a series of cases from clinical trials at MD Anderson, patients who were treated with ICIs showed better ORR and PFS if they experienced severe irAEs [10]. In a Japanese lung cancer cohort treated with nivolumab, patients with early irAEs showed improved ORR and PFS compared with those without [12]. However, these reports were retrospective in nature, similar to ours, and whether or not the presence of irAEs could be a novel predictor of response should be further validated in

prospective trials. One possibility is that the longer exposure to nivolumab increases the risk of developing irAEs. Still, the association between irAEs and the efficacy of ICIs highlights the need for better management of irAEs so that patients can continue treatment as long as possible.

We noted that elderly patients demonstrated similar benefits compared to those in the overall population. Efficacy was similar among patients aged < 65, 65 to < 75, ≥ 75 years, and safety profiles were also similar. When age group was divided into < 75, and ≥ 75 years, patients who were aged ≥ 75 showed a significantly longer PFS, although this was no longer significant in Cox proportional hazard models. While elderly patients are often under-represented in clinical trials [13], recent real-world data suggests that the efficacy of ICIs does not deteriorate in elderly patients [14,15]. In a large French study, advanced NSCLC patients aged 80 years or over showed similar median OS compared to patients under 80 years, suggesting that no specific tolerability issue arose in this age group [15]. In an Italian EAP study, tumor response was similar across patients aged < 65, 65 to < 75, and ≥ 75 years [14]. Therefore, we cautiously suggest that old age alone should not be a barrier to anti–PD-1/PD-L1 treatment, but further study of larger elderly populations is warranted.

In our study, squamous histology seemed associated with higher ORR, although it did not lead to improved survival outcomes. This could be explained by the higher prevalence of oncogenic driver mutations in adenocarcinomas, which are reported to be less responsive to anti–PD-1/PD-L1 therapy [16,17]. Similarly, former or current smokers had a prolonged OS compared to never-smokers, and smoking status maintained significant after multivariate analysis. This is in line with a recent meta-analysis that PD-1 and PD-L1 inhibitors significantly prolonged the OS in smoking patients [18].

Liver metastasis was associated with poor survival outcome in our study. The presence of liver metastasis significantly increased the likelihood of death (hazard ratio, 2.18; p=0.001) in multivariate analysis. A recent study which explored the association of liver metastasis and response in patients with melanoma and lung cancer also suggested that liver metastasis was associated with reduced response and shorter PFS [19]. In this study, reduced $CD8^+$ T cell density at the invasive tumor margin was observed in liver biopsies, providing a possible background for poor survival. Multiple mechanisms have been suggested to explain liver-induced immune tolerance, such as poor CD4+ T cell activation [20], and Kupffer cells activating regulatory T cells [21]. Further mechanistic studies may aid to explain factors influencing response to ICIs.

The presence of *EGFR* mutation in tumor is known to be poorly responsive to ICIs. In a meta-analysis by Lee et al. [22], ICIs were not superior to docetaxel in *EGFR*-mutant subset, and in another meta-analysis, the PFS was in fact worse in patients with *EGFR*-mutant subset treated with PD-1/PD-L1 inhibitors versus docetaxel [23]. In our study, ORR, PFS, and OS were not different according to *EGFR* mutation status, but this may be due to small number of *EGFR*-mutant patients and *EGFR* mutation status was largely unavailable in most patients.

Thirty-eight patients (12.7%) with ECOG PS 2 were enrolled in our study, and efficacy results showed that ORR, PFS, and OS were not significantly inferior in ECOG PS 2 patients. This indicates that, unlike clinical trials, ECOG PS 2 patients can also benefit from ICIs in the real-world setting.

Our study has some limitations. The EAP did not require the PD-L1 status of tumor tissue for enrollment, so our data lacks analysis on the PD-L1 status and efficacy. Furthermore, there were no data on brain response evaluation to evaluate intracranial efficacy.

In conclusion, the efficacy of nivolumab in real-world patients seems to be comparable to that of clinical trials, and nivolumab is a viable option in the previously treated NSCLC patients.

Electronic Supplementary Material

Supplementary materials are available at Cancer Research and Treatment website (https://www.e-crt.org).

Conflict of Interest

Conflict of interest relevant to this article was not reported.

Author Details

[1]Division of Medical Oncology, Yonsei Cancer Center, Yonsei University College of Medicine, Seoul, [2]Division of Oncology, Department of Internal Medicine, Asan Medical Center, University of Ulsan College of Medicine, Seoul, [3]Division of Medical Oncology, Department of Internal Medicine, Seoul St. Mary's Hospital, College of Medicine, The Catholic University of Korea, Seoul, [4]Division of Hematology-Oncology, Samsung Medical Center, Sungkyunkwan University School of Medicine, Seoul, [5]Department of Internal Medicine, Seoul National University Hospital, Seoul, [6]Department of Internal Medicine, Chonnam National University Hwasun Hospital, Hwasun, [7]Center for Lung Cancer, National Cancer Center, Goyang, [8]Division of Hematology and Medical Oncology, Department of Internal Medicine, Seoul National University Bundang Hospital, Seongnam, [9]Department of Internal Medicine, Korea University Guro Hospital, Seoul, [10]Department of Hematology/Oncology, Keimyung University Dongsan Hospital, Daegu, [11]Division of Medical Oncology, Department of Internal Medicine, St. Vincent's Hospital, College of Medicine, The Catholic University of Korea, Suwon, [12]Division of Oncology, Department of Internal Medicine, Gachon University Gil Medical Center, Incheon, [13]Department of Internal Medicine, Kosin University Gospel Hospital, Busan, [14]Department of Internal Medicine, Veterans Health Service Medical Center, Seoul, [15]Department of Internal Medicine, CHA Bundang Medical Center, CHA University, Seongnam, [16]Department of Hematology-Oncology, Inje University Haeundae Paik Hospital,

Busan, [17]Division of Hematology/Oncology, Department of Internal Medicine, Korea Cancer Center Hospital, Korea Institute of Radiological and Medical Sciences, Seoul, [18]Department of Internal Medicine, Kyungpook National University Hospital, School of Medicine, Kyungpook National University, Daegu, [19]Division of Hematology-Oncology, Department of Internal Medicine, Chungbuk National University Hospital, Chungbuk National University College of Medicine, Cheongju, Korea

References

1. Taube JM, Klein A, Brahmer JR, Xu H, Pan X, Kim JH, et al. Association of PD-1, PD-1 ligands, and other features of the tumor immune microenvironment with response to anti-PD-1 therapy. Clin Cancer Res. 2014;20:5064-74.
2. Borghaei H, Paz-Ares L, Horn L, Spigel DR, Steins M, Ready NE, et al. Nivolumab versus docetaxel in advanced nonsquamous non-small-cell lung cancer. N Engl J Med. 2015;373:1627-39.
3. Brahmer J, Reckamp KL, Baas P, Crino L, Eberhardt WE, Poddubskaya E, et al. Nivolumab versus docetaxel in advanced squamous-cell non-small-cell lung cancer. N Engl J Med. 2015;373:123-35.
4. Gettinger S, Borghaei H, Brahmer J, Chow L, Burgio M, De Castro Carpeno J, et al. Five-year outcomes from the randomized, phase 3 trials CheckMate 017/057: nivolumab vs docetaxel in previously treated NSCLC. In: 2019 World Conference on Lung Cancer; 2019 Sep 7-10; Barcelona, Spain, Abstract No. OA14.04.
5. Lilenbaum RC, Cashy J, Hensing TA, Young S, Cella D. Prevalence of poor performance status in lung cancer patients: implications for research. J Thorac Oncol. 2008;3:125-9.
6. Sacco PC, Casaluce F, Sgambato A, Rossi A, Maione P, Palazzolo G, et al. Current challenges of lung cancer care in an aging population. Expert Rev Anticancer Ther. 2015;15:1419-29.
7. Eisenhauer EA, Therasse P, Bogaerts J, Schwartz LH, Sargent D, Ford R, et al. New response evaluation criteria in solid tumors: Revised RECIST guideline (version 1.1). Eur J Cancer. 2009;45:228-47.
8. Rogado J, Sanchez-Torres JM, Romero-Laorden N, Ballesteros AI, Pacheco-Barcia V, Ramos-Levi A, et al. Immune-related adverse events predict the therapeutic efficacy of anti-PD-1 antibodies in cancer patients. Eur J Cancer. 2019;109:21-7.
9. Sato K, Akamatsu H, Murakami E, Sasaki S, Kanai K, Hayata A, et al. Correlation between immune-related adverse events and efficacy in non-small cell lung cancer treated with nivolumab. Lung Cancer. 2018;115:71-4.
10. Fujii T, Colen RR, Bilen MA, Hess KR, Hajjar J, Suarez-Almazor ME, et al. Incidence of immune-related adverse events and its association with treatment outcomes: the MD Anderson Cancer Center experience. Invest New Drugs. 2018;36:638-46.
11. Teraoka S, Fujimoto D, Morimoto T, Kawachi H, Ito M, Sato Y, et al. Early immune-related adverse events and association with outcome in advanced non-small cell lung cancer patients treated with nivolumab: a prospective cohort study. J Thorac Oncol. 2017;12:1798-805.
12. Haratani K, Hayashi H, Chiba Y, Kudo K, Yonesaka K, Kato R, et al. Association of immune-related adverse events with nivolumab efficacy in non-small-cell lung cancer. JAMA Oncol. 2018;4:374-8.
13. Shenoy P, Harugeri A. Elderly patients' participation in clinical trials. Perspect Clin Res. 2015;6:184-9.
14. Grossi F, Crino L, Logroscino A, Canova S, Delmonte A, Melotti B, et al. Use of nivolumab in elderly patients with advanced squamous non-small-cell lung cancer: results from the Italian cohort of an expanded access programme. Eur J Cancer. 2018;100:126-34.
15. Assie JB, Cotte F, Levra MG, Calvet C, Jolivel R, Jouaneton B, et al. Nivolumab outcomes in octogenarian patients with advanced non-small cell lung cancer in a French real-world setting. J Thorac Oncol. 2019;14(10 Suppl):S708.
16. Soo RA, Lim SM, Syn NL, Teng R, Soong R, Mok TS, et al. Immune checkpoint inhibitors in epidermal growth factor receptor mutant non-small cell lung cancer: current controversies and future directions. Lung Cancer. 2018;115:12-20.
17. Sakamoto H, Tanaka H, Shiratori T, Baba K, Ishioka Y, Itoga M, et al. The efficacy of immune checkpoint inhibitors in advanced non-small cell lung cancer harboring driver mutations. Mol Clin Oncol. 2019;10:610-4.
18. Li B, Huang X, Fu L. Impact of smoking on efficacy of PD-1/PD-L1 inhibitors in non-small cell lung cancer patients: a meta-analysis. Onco Targets Ther. 2018;11:3691-6.
19. Tumeh PC, Hellmann MD, Hamid O, Tsai KK, Loo KL, Gubens MA, et al. Liver metastasis and treatment outcome with anti-PD-1 monoclonal antibody in patients with melanoma and NSCLC. Cancer Immunol Res. 2017;5:417-24.
20. Wang JC, Livingstone AM. Cutting edge: CD4+ T cell help can be essential for primary CD8+ T cell responses in vivo. J Immunol. 2003;171:6339-43.
21. Jenne CN, Kubes P. Immune surveillance by the liver. Nat Immunol. 2013;14:996-1006.
22. Lee CK, Man J, Lord S, Links M, Gebski V, Mok T, et al. Checkpoint inhibitors in metastatic EGFR-mutated non-small cell lung cancer: a meta-analysis. J Thorac Oncol. 2017;12:403-7.
23. Dong ZY, Zhang JT, Liu SY, Su J, Zhang C, Xie Z, et al. EGFR mutation correlates with uninflamed phenotype and weak immunogenicity, causing impaired response to PD-1 blockade in non-small cell lung cancer. Oncoimmunology. 2017;6:e1356145.

pISSN 1598-2998, eISSN 2005-9256

Cancer Res Treat. 2020;52(4):1120-1134

https://doi.org/10.4143/crt.2020.307

Original Article

Open Access

Genetic Alterations in Preinvasive Lung Synchronous Lesions

Soyeon Ahn, PhD[1]
Jisun Lim, PhD[1]
Soo Young Park, PhD[2]
Hyojin Kim, MD, PhD[2]
Hyun Jung Kwon, MD[2]
Yeon Bi Han, MD[2]
Choon-Taek Lee, MD, PhD[3]
Sukki Cho, MD, PhD[4]
Jin-Haeng Chung, MD, PhD[2]

[1]Division of Statistics, Medical Research Collaborating Center, Departments of [2]Pathology and Translational Medicine, [3]Internal Medicine, and [4]Thoracic and Cardiovascular Surgery, Seoul National University Bundang Hospital, Seongnam, Korea

Correspondence: Jin-Haeng Chung, MD, PhD
Department of Pathology, Seoul National University Bundang Hospital, 82 Gumi-ro 173beon-gil, Bundang-gu, Seongnam 13620, Korea
Tel: 82-31-787-7713
Fax: 82-31-787-4012
E-mail: chungjh@snu.ac.kr

Co-correspondence: Soyeon Ahn, PhD
Division of Statistics, Medical Research Collaborating Center, Seoul National University Bundang Hospital, 82 Gumi-ro 173beon-gil, Bundang-gu, Seongnam 13620, Korea
Tel: 82-31-787-8121
Fax: 82-31-787-4825
E-mail: ahnsoyeon@snubh.org

Received April 14, 2020
Accepted June 4, 2020
Published Online June 5, 2020

Purpose

Despite advances in treatment, lung cancer remains the leading cause of cancer mortality. This study aimed to characterise genome-wide tumorigenesis events and to understand the hypothesis of the multistep carcinogenesis of lung adenocarcinoma (LUAD).

Materials and Methods

We conducted multiregion whole-exome sequencing of LUAD with synchronous atypical adenomatous hyperplasia (AAH), adenocarcinoma *in situ*, or minimally invasive adenocarcinoma of 19 samples from three patients to characterize genome-wide tumorigenesis events and validate the hypothesis of the multistep carcinogenesis of LUAD. We identified potential pathogenic mutations preserved in preinvasive lesions and supplemented the finding by allelic variant level from RNA sequencing.

Results

Overall, independent mutational profiles were observed per patient and between patients. Some shared mutations including epidermal growth factor receptor (*EGFR* , p.L858R) were present across synchronous lesions.

Conclusion

Here, we show that there are driver gene mutations in AAH, and they may exacerbate as a sequence in a histological continuum, supporting the Darwinian evolution model of cancer genome. The intertumoral and intratumoral heterogeneity of synchronous LUAD implies that multi-biomarker strategies might be necessary for appropriate treatment.

Key words

Adenocarcinoma of lung, Atypical adenomatous hyperplasia, Mutation, Clonal evolution, Whole exome sequencing

Introduction

Although molecular targeted therapies and immune checkpoint inhibitors have markedly improved treatment outcomes in lung cancer, it remains the leading cause of cancer deaths [1]. Lung adenocarcinoma (LUAD) is the most common subtype of lung cancer, accounting for approximately 28%-50% of all cases [2,3], and its incidence is continuously increasing. LUAD is often diagnosed at an advanced stage, leading to a poor prognosis. Multiregional sequencing in lung cancer showed high degree of intratumoral heterogeneity [4], highlighting that understanding the processes of LUAD genome evolution by accumulating somatic mutations over time is important for the early diagnosis and prevention of LUAD.

LUAD with ground-glass/lepidic feature is hypothesised

to follow a multistep tumorigenesis starting from atypical adenomatous hyperplasia (AAH), to adenocarcinoma *in situ* (AIS), to minimally invasive adenocarcinoma (MIA), and finally to invasive or lepidic-predominant adenocarcinoma (ADC) as a histologic stepwise continuum [5,6]. AAH is the only reported precursor lesion to LUAD and is occasionally discovered in the surgically resected lung tissue harboring lung cancer [6]. However, studies on AAH are limited due to its rarity and small lesion size.

The first targeted sequencing study on AAH and paired ADC lesions reported increasing mutational abundance of synchronous epidermal growth factor receptor (*EGFR*), *KRAS*, and *TP53* mutations in the tumor [7]. Another targeted sequencing study combined with transcriptome analysis suggested that exclusive pathways in the driver gene *BRAF* or *KRAS* mutate and initiate the progression of precursor lesions to malignancy [8]. Recently, we reported targeted deep sequencing in sequential lesions [9]. The increased proportions of overall mutated lesions in advanced lesions and shared mutations of *EGFR* between synchronous lesions implied a linear stepwise progression of LUAD [10]. However, the interlesional and intralesional heterogeneity reported in previous AAH studies and the analysis being limited to the focused gene list make it difficult to understand the overall genetic alteration events.

This study aimed to characterize genome-wide tumorigenesis events and to elucidate the hypothesis of the multistep carcinogenesis of LUAD. Towards this goal, we conducted multiregion whole-exome sequencing (WES) of LUAD and preinvasive lesions and paired normal tissue samples.

Materials and Methods

1. Sample selection

We used patients' specimens collected in the previous targeted sequencing study [9]. Histologic slides from patients who underwent wedge resection or lobectomy were stained with haematoxylin and eosin for routine pathologic diagnosis. From each formalin-fixed, paraffin-embedded (FFPE) tissue, 10 μm-thick sections were cut for DNA extraction after minimum trimming, and pathologists reviewed cases and microdissected the area containing > 60% neoplastic cells. Three patients (P1, P5, and P8) with complete AAH-AIS-MIA-ADC sequences of synchronous lesions were chosen. For WES, the remaining extracted DNA from the FFPE tissues were prepared. The characteristics of the entire paired samples for WES, targeted sequencing, and RNA sequencing are summarized in S1 Table.

Information regarding patient characteristics and sample collections was detailed in the previously reported paired targeted sequencing study [9].

2. DNA and total RNA preparation

For RNA sequencing (RNA-seq), total RNAs were extracted from additional FFPE tissue sections from the same patients, and cDNA were synthesized according to the manufacturer's protocol. Non-tumorous samples were used as controls for RNA-seq. Genomic DNA was extracted using the Maxwell (R) 16 FFPE Plus LEV DNA Purification Kit (Promega, Mannheim, Germany) and quantified with PicoGreen dsDNA quantitation assay (Molecular Probes, Eugene, OR). All samples passed the in-house quality control criteria of next-generation sequencing library. The library preparation was performed through Agilent SureSect V5 (Agilent Technologies, Santa Clara, CA) and TruSeqProtocol with TruSeq Exome Enrichment (Illumina, San Diego, CA). DNA sequencing and RNA-seq was performed using an Illumina HiSeq 2500 with 100 bp×2 paired-end reads.

3. Somatic DNA variant calling

WES variants were called with three different caller strategies: Genomon2 pipeline, Mutect (ver. 1.1.4), and MuTect2 (S2 Fig.). Genomon2 pipeline with default parameters identified any potential somatic mutation if Fisher exact test resulted in a p-value < 0.05. For Mutect and MuTect2, raw reads were aligned using BWA (ver. 0.7.12) and then preprocessed using GATK (ver. 32.6) per the best practices recommended by the Broad Institute. To maximize sensitivity, MuTect2 was run with a low cut-off (--max_alt_alleles_in_normal_count 10000000 --max_alt_allele_in_normal_fraction 0.10). Single-nucleotide variants (SNVs) were filtered with a minimum read depth of 20 in the lesions and the matched control, and variant allele frequency (VAF) of being greater than 4% in any lesions and less than 1% in the matched control was set as cut-off values. The 4% cut-off was decided based on the paired comparison between the WES samples and the targeted sequencing samples (S2 Fig.). Variants were annotated via ANNOVAR (ver. 2016-02-01) or Cancer Genome Interpreter [11], and only exonic variants were further filtered. Read depth was obtained via bam-readcount (ver. 0.8.0). Insertions and deletions (indels) were identified with the same read-depth and VAF filter criteria and manually reviewed using the Integrative Genomics Viewer.

4. Copy number analysis

Copy number analysis was performed using Sequenza (ver. 2.1.2) and Excavator2. Segmental somatic copy number alterations (CNAs) were defined according to the intersection between Sequenza (filtered by Bayes factor > 0.3) and Excavator2 (filtered by call probability > 0.9).

5. Inferred clonal tree construction

An individual inferred clonal tree was constructed based on the VAF matrix with SNV as rows and samples as columns. Clonal sequences rather than multiregion trees were

used to avoid biased inference of the underlying subcolonal structures [12]. For each patient, two VAF and read-depth matrices (size of [no. of SNVs]×number of lesions) were decomposed into a genotype matrix (size of [no. of SNVs]× no. of clones) and a clone frequency matrix (size of [no. of clone]×no. of lesions) using an Expectation-Maximization algorithm. The algorithm required a fixed clone number, which we set as four. As a result, the genotype matrix determined the clonal membership of each variant, and each clone was linked to lesions according to the estimated clone frequencies. An unrooted phylogenetic tree was drawn from the inferred clones based on the minimum evolution algorithm. The Clomial and ape R packages were used. LUAD driver genes taken from Bailey et al. [13] were depicted in the trees.

6. Pathway analysis/functional annotation

The mutated genes were investigated further via pathway enrichment analysis using REACTOME (ver. 66, https://reactome.org). The pathogenic status of mutations of driver genes were reviewed via the NCBI ClinVar (https://www.ncbi.nlm.nih.gov/clinvar/, accessed on November 18, 2018).

7. Mutational signature analysis

Somatic mutational signatures were generated and compared to the 30 known mutational signatures in the Catalogue of Somatic Mutations in Cancer database (http://cancer.sanger.ac.uk/cosmic/signatures) using deconstructSigs R package. It quantified the linear combination of well-annotated Catalogue of Somatic Mutations in Cancer (COSMIC) signatures from a single sample input. SNVs were annotated with one of 96 trinucleotide-context substitutions, and the prevalent mutation signatures were illustrated as lego plots.

8. Somatic allelic imbalance

Mutational abundance between the genome and the transcriptome was generally consistent, showing that the mutated allele was expressed according to its mutational frequency in the genome. By contrast, somatic allelic imbalance is a deviation of a consistent expression of somatic alleles, and several studies reported that preferentially allelic selections may be associated with the functionality of cancer genomes [14]. We first included genes with a minimum RNA read depth of 20 and fitted a regression model between RNA VAF versus WES VAF. We then defined somatic allelic imbalance using a data-driven binomial model. For each SNV found in WES, unlikely observation of the read number of RNA was calculated given the WES VAF as the expected probability of binomial distribution. Either SOM-L or SOM-E was defined if the adjusted p-value of Hochberg method is < 0.05. The protein-protein interaction graph was drawn using Cytoscape (ver. 3.7.0) with a STRING database (ver. 10.5) plugin.

9. Ethical statement

This study was approved by the Institutional Review Board of Seoul National University Bundang Hospital and all the patients provided written informed consent (IRB No. B-1607/355-301), and all methods were performed in accordance with the relevant guidelines and regulations.

Results

1. Mutational landscape of synchronous LUAD

Initially, 26 samples from three patients were prepared for WES. Of these, four AAH samples that did not pass the quality control and three non-tumorous normal samples were excluded in the analysis. In total, 19 samples (5 AAH, 3 AIS, 4 MIA, 4 ADC, and 3 matched lymph node controls) were included. WES was conducted with an on-target average depth of 217× (range, 185 to 268) per sample. We found an average of 205 exonic mutations (range, 45 to 682) per sample, and 63% (range, 51% to 70%) of these were nonsynonymous somatic mutations (S2 and S3 Figs.). On average, we identified 251 mutations in smokers (P1 and P8) and 66 mutations in a nonsmoker (P5), consistent with previous studies showing that smoking contributed to higher mutational burden [15]. There was no increasing pattern in tumor mutational burden across sequential lesions (75, 341, 196, and 275 variants in AAH, AIS, MIA, and ADC, respectively), but the VAF tended to increase from preinvasive to invasive lesions (6.1%, 9.7%, 9.2%, and 15.2%) (S4 Fig.). A total of 2,198 genes were affected in all patients, and 172 genes were mutated in more than one patient. Mutations were largely private (82%), that is, mutations were observed in a single sample. Among the driver genes in LUAD, *EGFR* had mutated across two patients (P1 and P5). Moreover, other frequently mutated genes in LUAD had recurrently mutated within one patient (*TP53* for P1 and *KRAS* and *BRAF* for P8) (Table 1). Our data also showed that mutations in *KRAS* and *EGFR* genes are mutually exclusive [16], while *TP53* and *EGFR* genes are commutated [17]. However, we observed concomitant *KRAS* and *BRAF* mutations, which were in contrast to previous studies [8,18]. On average, 62%, 61%, and 65% of the mutations were annotated as passenger mutations in P1, P5, and P8, respectively. Similarly, the proportion of passenger mutations or not protein-affecting mutations were 92%, 89%, and 94%, respectively, which implies that most of mutations in smokers were non-driver mutations.

2. Interlesional heterogeneity

To characterize interlesional heterogeneity, multiregional VAF distributions were mapped (Fig. 1). We found some shared mutations that existed in multiple samples, including *EGFR* mutation (encoding p.L858R) in P5 with increasing mutational abundance throughout the sequential histologi-

Table 1. Variant allele frequencies of driver gene mutations

Gene	Amino acid change	Clinical significance (CliniVar ID)	P1								P5				P8			
			AAH1	AAH2	AAH3	AIS	MIA1	MIA2	ADC1	ADC2	AAH	AIS	MIA	ADC	AAH	AIS	MIA	AD
EGFR	p.G719D		-	-	-	-	-	-	-	9	-	-	-	-	-	-	-	-
	p.G719C	Pathogenic (45225)	-	-	-	-	-	-	-	-	-	17	-	-	-	-	-	-
	p.L858R	Drug response (16609)	-	-	-	-	-	-	-	-	20	0.5[a]	15	30	-	-	-	-
TP53	c.240_240delinsT		-	-	-	-	13	-	-	-	-	-	-	-	-	-	-	-
	p.Q60X (stopgain)		-	-	-	-	-	-	42	43	-	-	-	-	-	-	-	-
KRAS	p.Q61H	Pathogenic/likely pathogenic (177881)	-	-	-	-	-	-	-	-	-	-	-	-	7	-	-	-
	p.G13C	Pathogenic (45123)	-	-	-	-	-	-	-	-	-	-	-	-	-	-	-	8
	p.G12V	Pathogenic (12583)	-	-	-	-	-	-	-	-	-	-	-	-	-	-	15	-
BRAF	p.G466V	Pathogenic/likely pathogenic (13967)	-	-	-	-	-	-	-	-	-	-	-	-	-	-	-	15
	p.G464R	Pathogenic (279992)	-	-	-	-	-	-	-	-	-	-	-	-	-	-	16	-
SETD2	p.P2124Q		-	-	-	-	-	-	-	-	-	-	-	-	-	4	-	-
	p.R441Q		-	5	-	-	-	-	-	-	-	-	-	-	-	-	-	-
CTNNB1	p.D115V		-	-	-	-	12	11	-	-	-	-	-	-	-	-	-	-
NF1	p.N1388K		-	-	-	-	-	-	-	-	5	-	-	-	-	-	-	-
RBM10	p.Y505X		-	-	-	-	-	-	-	-	-	-	8	-	-	-	-	-
	c.2337_2337delins-G		-	-	-	-	27	13	-	-	-	-	-	-	-	-	-	-
	p.G780V		-	-	-	-	28	14	-	-	-	-	-	-	-	-	-	-
RBM23	p.A355A		-	-	-	-	-	-	-	-	20	19	22	-	-	17	15	19
SMARCA4	p.E1133E		-	-	-	12	-	-	-	-	-	-	-	-	-	-	-	-
U2AF1	p.S34F	Likely pathogenic (376025)	-	-	-	-	-	-	-	-	-	-	-	-	-	-	-	46
MUC4	p.P1952S		10	7	11	8	8	7	17	-	-	-	-	-	-	-	-	-
	p.N2437D		-	-	-	-	-	-	-	-	-	-	-	-	17	-	16	32
	p.P540P		-	-	-	-	-	-	-	-	-	5	-	-	-	-	-	-
	p.G154R		-	-	-	-	-	-	-	-	-	-	-	-	-	4	-	-
HLA-DQB2	p.G250S		-	-	-	-	-	-	-	-	6	20	11	16	-	-	-	-
	p.R247H		-	-	-	-	-	-	-	-	-	-	-	-	5	20	8	14
ALK	p.H755A		-	-	-	11	-	-	-	-	-	-	-	-	-	-	-	-

Values are presented as percentage. AAH, atypical adenomatous hyperplasia; AIS, adenocarcinoma *in situ*; MIA, minimally invasive adenocarcinoma; ADC, adenocarcinoma. [a]Epidermal growth factor receptor (*EGFR*) mutation (p.L858R) in P5 AIS was not called because it failed to pass the cut-off of 4%.

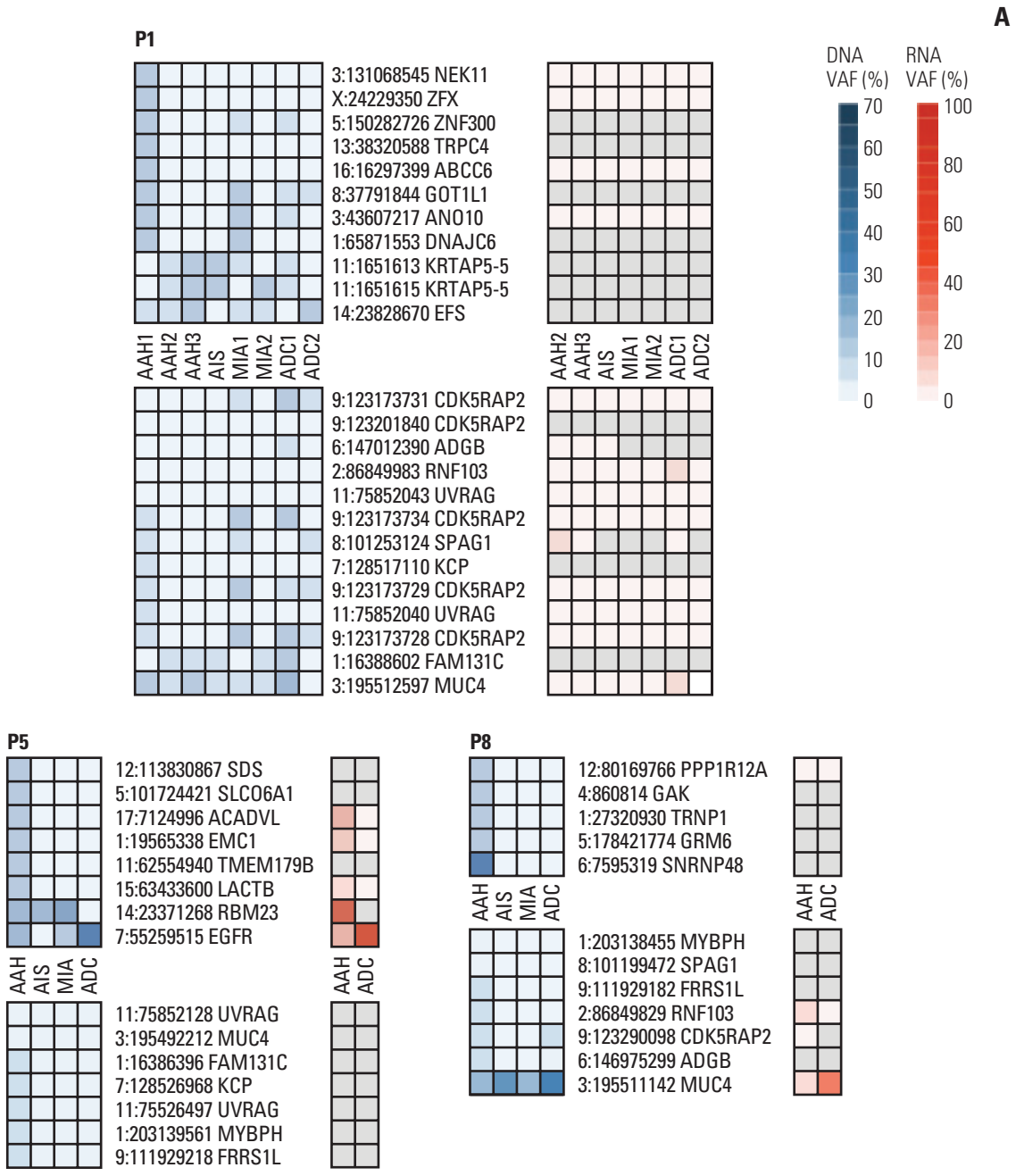

Fig. 1. Multiregional variant allele frequency. Blue and red colours denote the heatmap of variant allele frequency (VAF) of the genome and the transcriptome, respectively. The upper panel shows the private mutations, while the lower panel shows gene mutations found in at least two patients. (A) Atypical adenomatous hyperplasia (AAH). *(Continued to the next page)*

cal continuum. *MUC4* in P1 (p.P1952S) and P8 (p.N2437D), and *HLA-DQB2* in P8 (p.G250S and p.R247H) also showed increase VAF in advanced lesions (Table 1). However, the multiregional heatmaps in the overall population indicated few overlapping mutations (S5 Fig.). Indels of *DNAH7*, *NDUFA10*, and *WDR88* recurrently occurred in more than one patient, and 129 detected indels were mutated within one patient.

3. Intrapatient heterogeneity

To explore intrapatient heterogeneity, a clone relationship was inferred by estimating the hidden clonal status using observed VAFs (Fig. 2). Associated driver genes were portrayed on the inferred clonal trees. In P1, one clone containing *TP53* mutation (c.240_240delinsT-) was detected in AIS, and an *EGFR* mutation (p.G719D) was detected in ADC. Another clone in P1 lacked *TP53* (p.Q60X) in ADC. In P5,

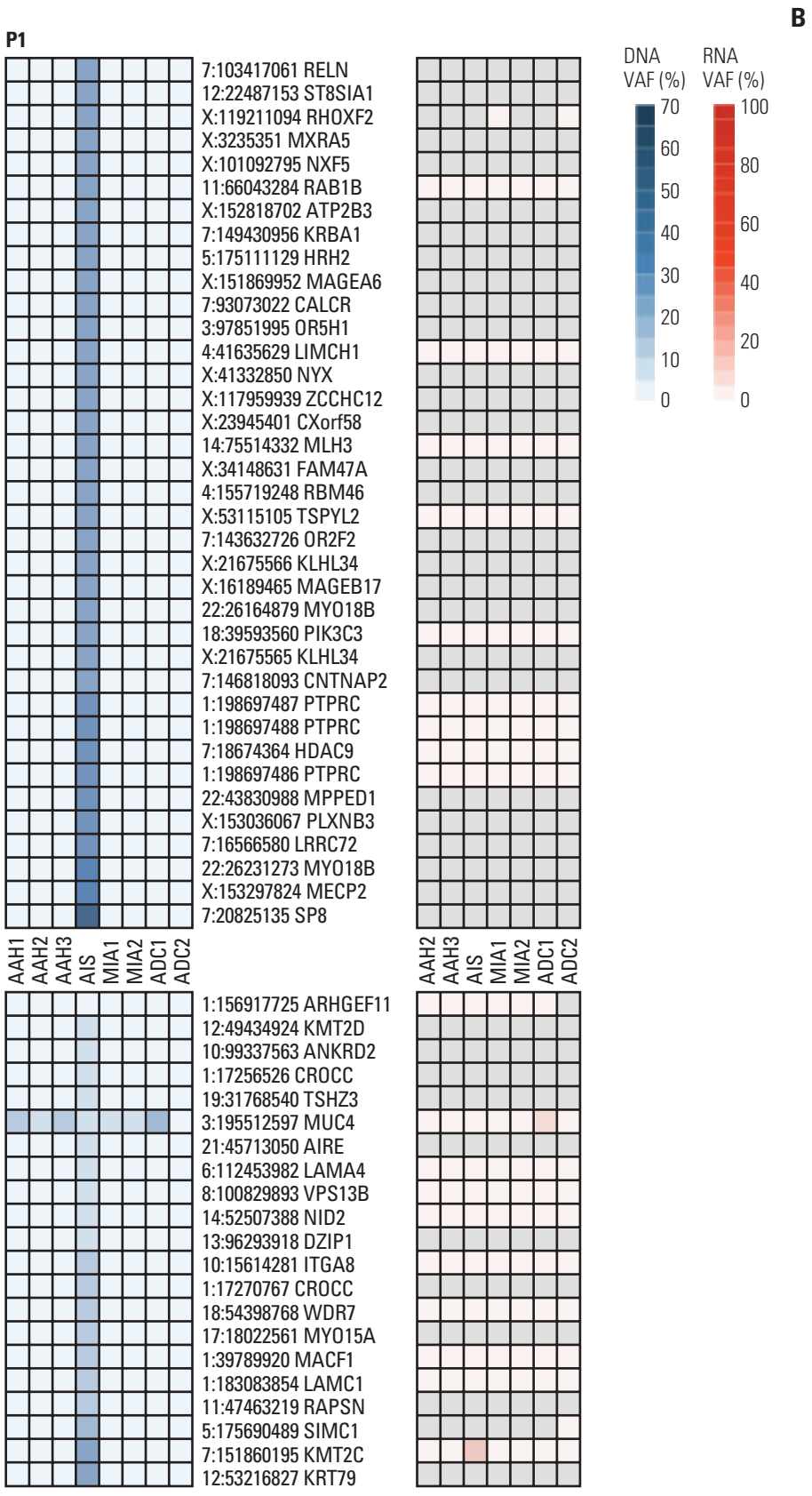

Fig. 1. *(Continued from the previous page)* (B) Adenocarcinoma *in situ* (AIS). *(Continued to the next page)*

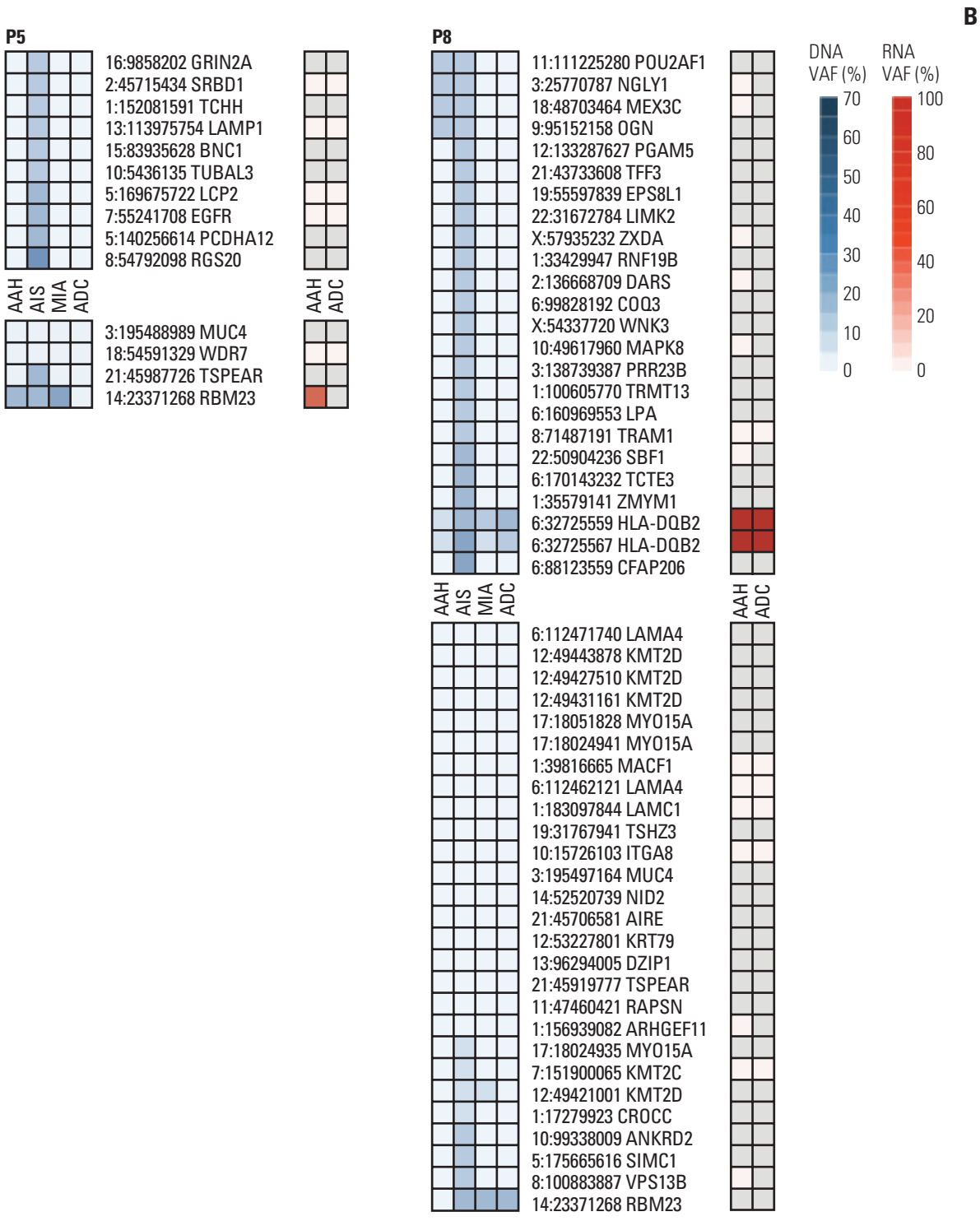

Fig. 1. *(Continued from the previous page) (Continued to the next page)*

EGFR mutation (p.L858R) appeared pre-dominant at the root, and other clones were divergent from each other. Only one clone included *NF1* mutation (p.N1388K) in AAH. In P8, however, multiple clones simultaneously had pathogenic or likely pathogenic mutations. One clone had *KRAS* mutation (p.G12V) coupled with *BRAF* mutation (p.G464R) in MIA, and another clone had *KRAS* (p.G13C) and *BRAF* (p.G466V) in ADC.

CNAs were recurrently observed in 1p13.3, 3q13.33, 4q13.2, 5q35.1, 5q35.3, 8q23.1, 10q21.3, 11p15.5, 14q11.2, 14q13.2, 16p-

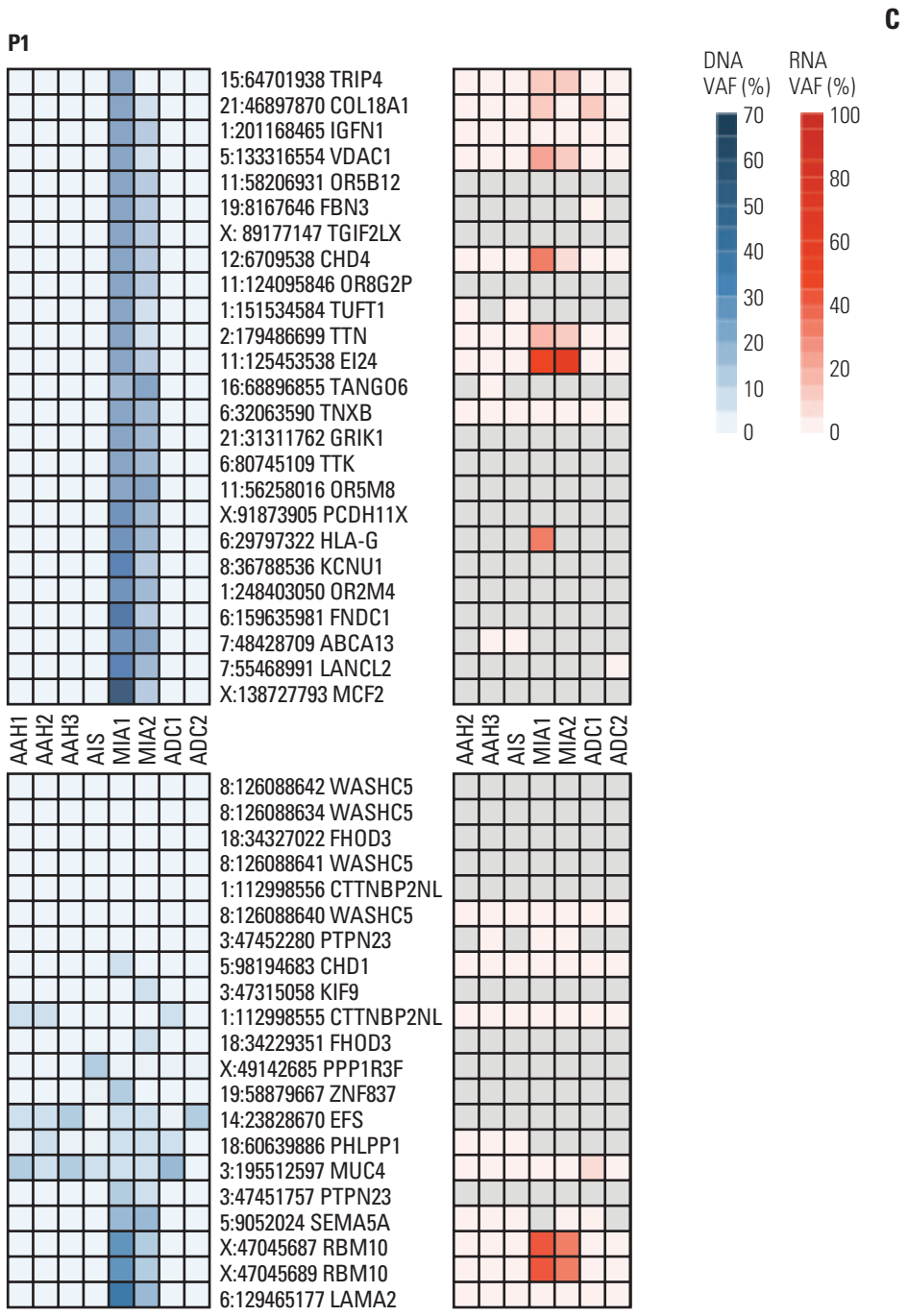

Fig. 1. *(Continued from the previous page)* (C) Minimally invasive adenocarcinoma (MIA). *(Continued to the next page)*

13.3, 19q13.42, 20p13, and 22q11.23 (S6 Fig.).

4. Mutation signature analysis

We observed that C:G>A:T transitions were more dominant types in smokers (41% in P1, 51% in P8) than in nonsmokers (30% in P5). Meanwhile, C:G>T:A transitions were more frequent in nonsmokers (38% in P5, 32% in P1, and 27% in P8) [15]. We then further performed the mutation base-substitution signatures (Fig. 3, S7 Fig.) [19]. Overall, signatures associated with smoking (signature 4 [smoking] and 29 [tobacco] chewing]) and aging (signature 1) were highly enriched. Signature 1, composed of C:G>T:A single-base substitutions at CpG sites, was frequently observed in all cancer types. Signatures 4 and 29 were characterized mainly by C:G>A:T mutations with transcriptional strand bias. P1 was a 20 pack-year male current smoker who showed smoking-

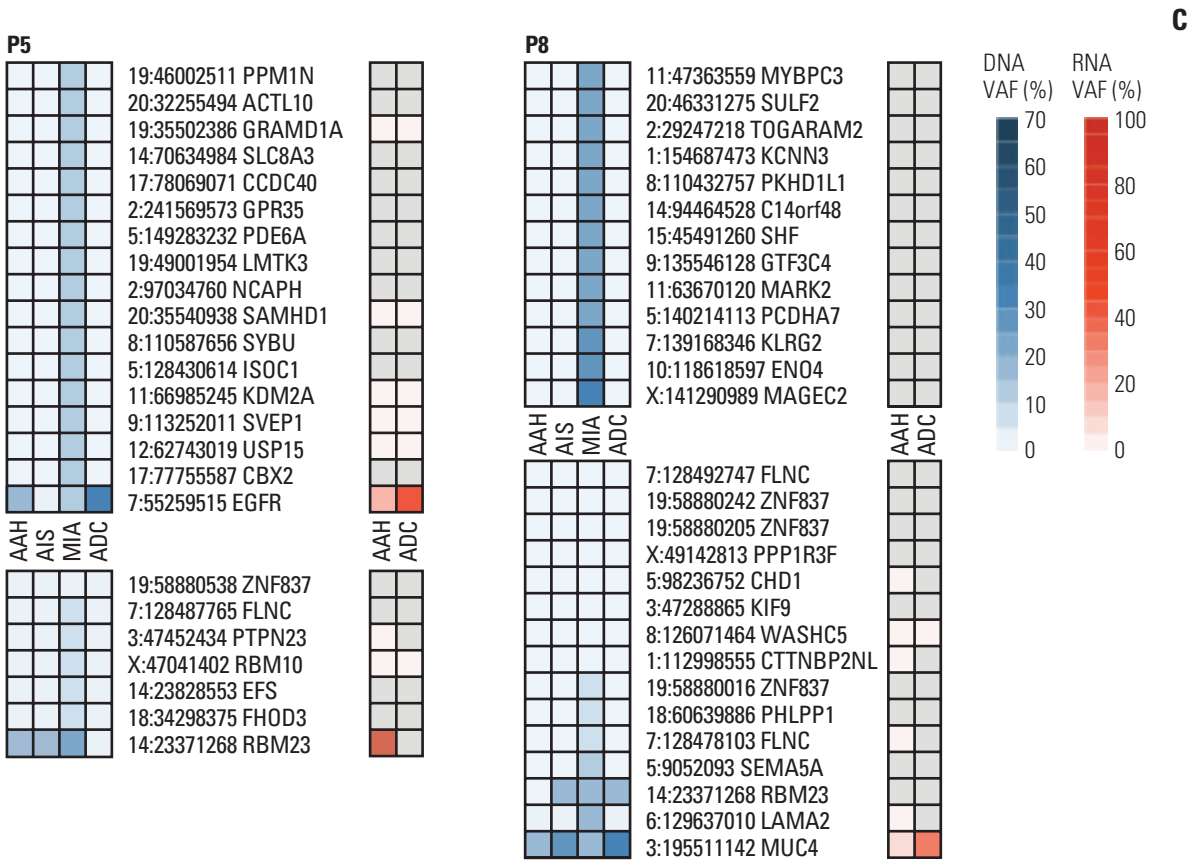

Fig. 1. *(Continued from the previous page) (Continued to the next page)*

related signatures, whereas P5 was a never-smoker female and showed abnormalities in DNA maintenance across all lesions (signatures 6 and 15 [DNA mismatch repair (MMR)] and 3 and 20 [defective DNA repair]). P8, a previous smoker male patient with a 30 pack-year history, showed a combination of smoking-related and DNA MMR-related signatures. Exposure to ultraviolet light, which is a mutagenic agent, was common in the AAHs of P1 and P5. The TRACERx study reported a significant relationship between pack-years and smoking-related signature in late clonal mutations, consistent with the enrichment of signature 4 or 29 in our data [20]. Interestingly, differential signature patterns were observed in P1, where signature 4 was dominant in AAH1 and signature 1 was common in AAH2 and AAH3. This suggested that clonal compositions even in preneoplasia lesions could be different, which was also implied in the clonal status analysis (Fig. 2).

5. RNA-seq for allele-specific expression

A total of 14 RNA samples were used in this study. We determined allele-specific expression to compare RNA VAF and WES VAF. A linear regression model showed that RNA VAF was concordant with WES VAF (RNA VAF-1.1×WES VAF; Pearson correlation coefficient, 0.46) (S8 Fig.). Although we did not find similar findings that missense or silent variants in the genome implicated overexpression of certain alleles (S9 Fig.), somatic variant lost in the transcriptome (SOM-L) and somatic variant overexpressed in the transcriptome (SOM-E) variants were discovered in P1, and protein interaction graphs within each lesion type in P1 were derived (S10 Fig.). In AIS, oncogene Yes-associated protein 1 and enzyme ubiquitin-specific peptidase 9, X-linked were found, indicating that preinvasive lesion is related to loss of function in suppressed tumor growth related to the Hippo signaling pathway [21]. In MIA, genes related to mitochondrial outer member, including voltage-dependent anion channel 1 and inner mitochondrial membrane 22, were overexpressed. In ADC, loss alleles of integrin alpha 1 (*ITGA1*) and Versican core protein precursor (*VCAN*) interacted with overexpressed allele of *EGFR* [22]. *ITGA1* and *EGFR* are well-documented prognostic markers, whereas *VCAN* enhances tumor recurrence [23].

In genes in which mutant allelic expression levels were maintained at least 4%, REACTOME analysis revealed that the biological processes of P1, P5, and P8 were regulation of *TP53* expression (*TP53*), fibroblast growth factor receptor 2

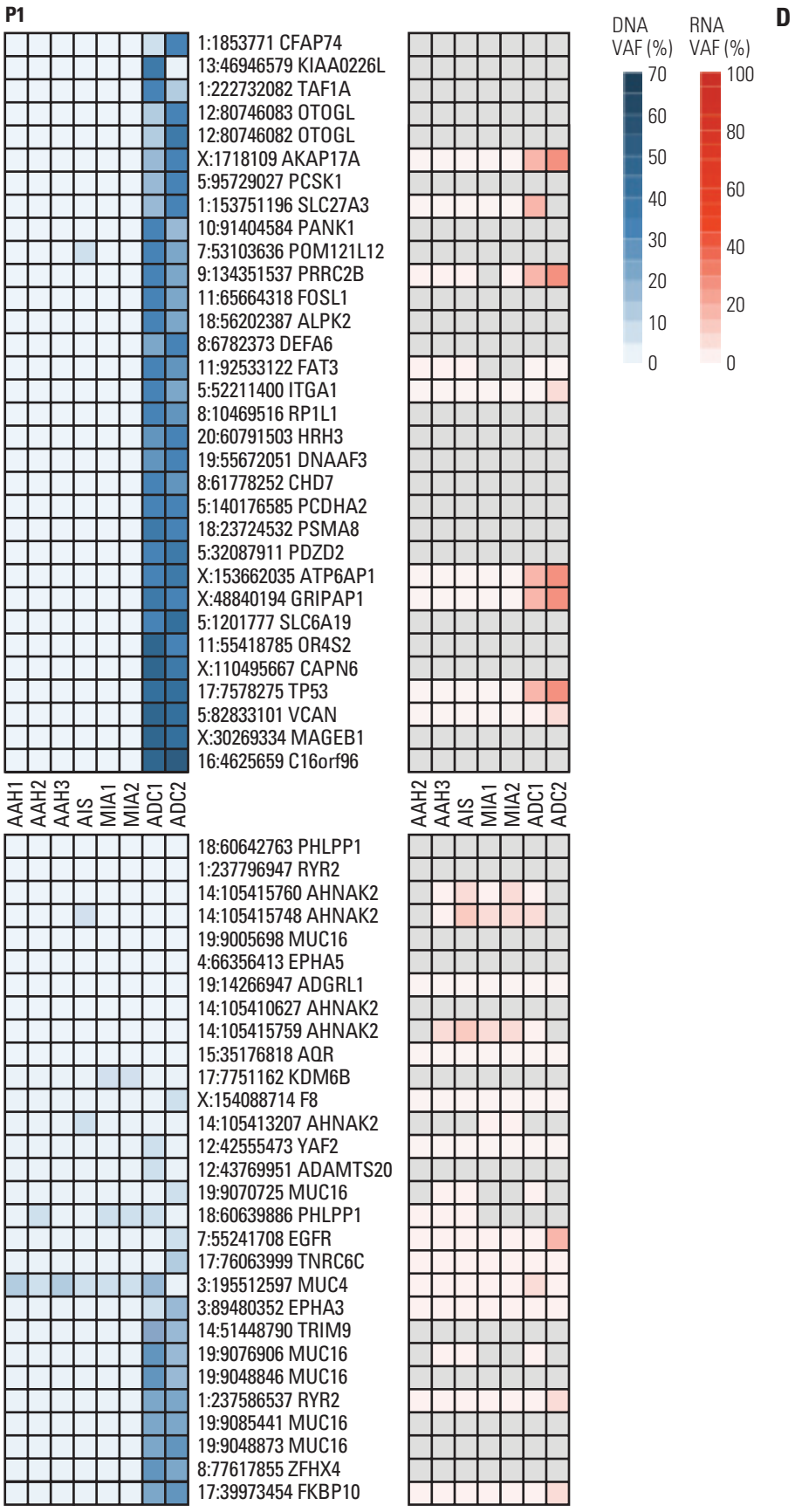

Fig. 1. *(Continued from the previous page)* (D) Adenocarcinoma (ADC). *(Continued to the next page)*

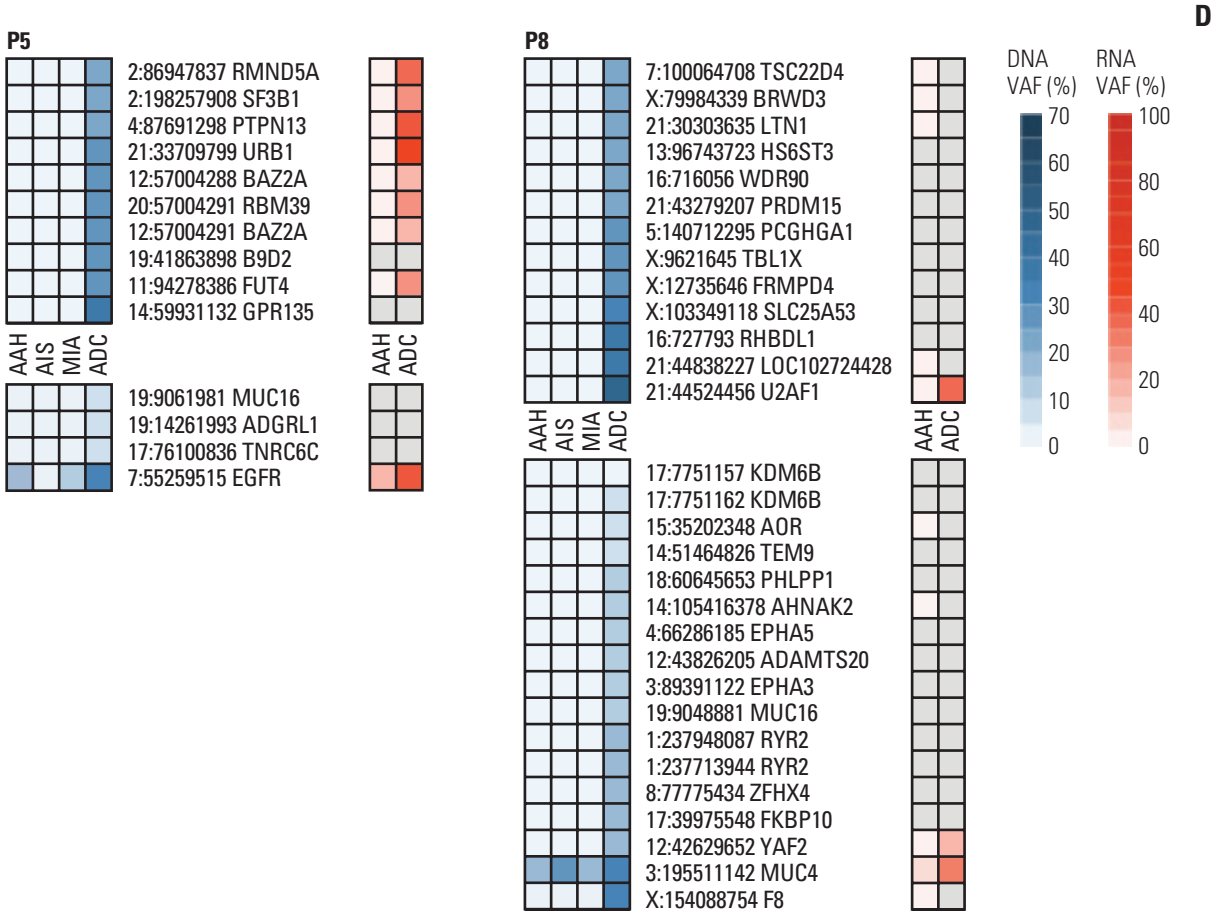

Fig. 1. *(Continued from the previous page)* ADC-N, non-invasive portion of ADC.

(*FGFR2*) mutant receptor activation, *PI3K* cascade (*FGFR2*), and *RAS* signaling downstream of NF1 loss-of-function variants and RAF activation (*KRAS* and *BRAF*), respectively (S11 Table).

Discussion

In this study, we identified the genomic alterations in the precursor lesions of LUAD and inferred clonal evolution in LUAD development through WES supplemented with transcriptome analysis. Shared *EGFR* pathogenic mutation was observed across synchronous lesions, indicating that identical mutations occurred in the early tumorigenesis. Overall increase in VAF but not in tumor burden (mutation number) in invasive lesions indicated that accumulated mutation of certain driver genes is functionally important in cancer development [24]. Furthermore, heterogeneous mutation profiles strongly implied that each lesion underwent largely independent genetic alteration events. Although mutation signature analyses beyond single-gene mutations helped in understanding the combinatory base change mechanism associated with smoking and aging, the individual pathway was evitable.

The receptor tyrosine kinase/RAS/RAF pathway was frequently mutated and crucial in the development of LUAD [6]. Our results are consistent with those of previous studies on AAH showing the exclusive nature of *EGFR* mutation and *KRAS* mutations, and they were frequently observed in nonsmokers and smokers, respectively. EGFR is a receptor tyrosine kinase belonging to the ERBB family, and its mutations are more widespread in the Asian population and more common in women and nonsmokers. P5, a nonsmoker female Asian patient, harbored the most common pathogenic mutations in *EGFR* (p.L858R) across all lesions, which exemplified the role of *EGFR*-L858R mutation in tumor invasiveness during the early stage of lung cancer. Meanwhile, *KRAS* oncogenes encoding guanosine-5′-triphosphate-binding proteins contribute to invasive lesions when supplementary genomic alternations occur. P8, a male current smoker patient with a 30 pack-year history, had *KRAS* mutation in preinvasive and invasive lesions and *UTAF1* and *BRAF* mutations in invasive lesions. We can further postulate the interaction between *KRAS* and human leukocyte antigen (*HLA*) genes in

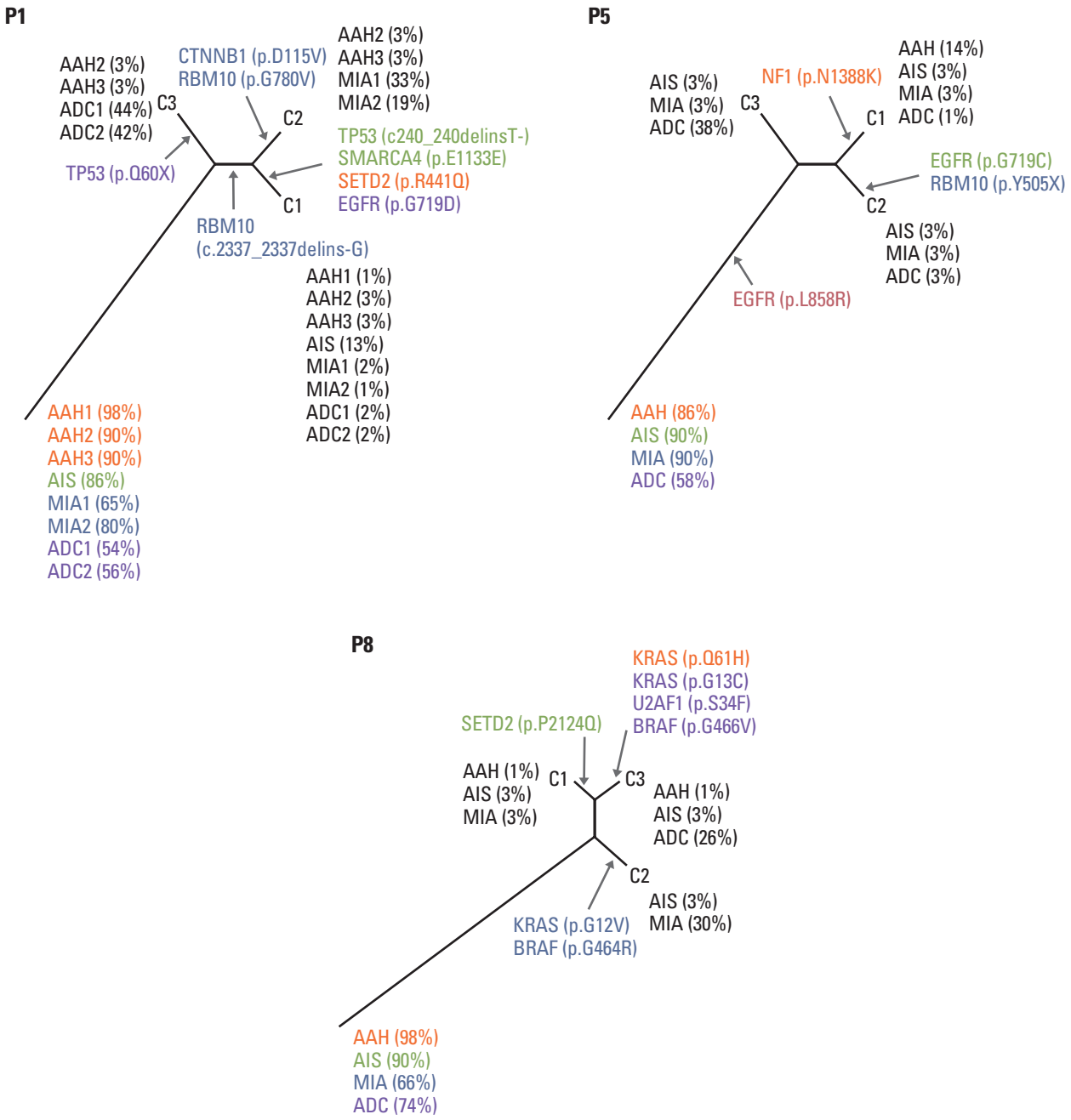

Fig. 2. Inferred clone status. For each patient, two variant allele frequency (VAF) and read-depth matrices [(no. of mutations)×(no. lesions)] were decomposed into a genotype matrix [(no. of mutations)×(no. of clones)] and a clone frequency matrix [(no. of clone)×(no. lesions)]. C1-C3 represents inferred clones. Clone frequencies (i.e., the proportion of a clone in each lesion) are shown in parenthesis. Colours matched to the legions where the mutation occurred (orange, atypical adenomatous hyperplasia [AAH]; green, adenocarcinoma *in situ* [AIS]; blue, minimally invasive adenocarcinoma [MIA]; purple, adenocarcinoma [ADC]; red, all lesions). For example, C3 clone in P1 occupied 3% of AAH2 and AAH3, 44% of ADC1, and 42% of ADC2.

this patient because *HLA-DQB2* mutations were prevalent. The specific role of *HLA-DQB2* in cancer genomics was not reported, but immunological function may be affected by mutant neoantigen peptides of hotspot mutations [25].

P1, a 20 pack-year previous smoking male patient, showed combination pathways related to chromatin remodeling (*SETD2* and *RBM10*) and clinical prognosis (co-mutation of *TP53* and *EGFR*) [26]. We found that recurrent mutations of tubulin tyrosine ligase-like protein 5 (*TTLL5*) appeared in preinvasive lesions among known co-mutated genes with SET

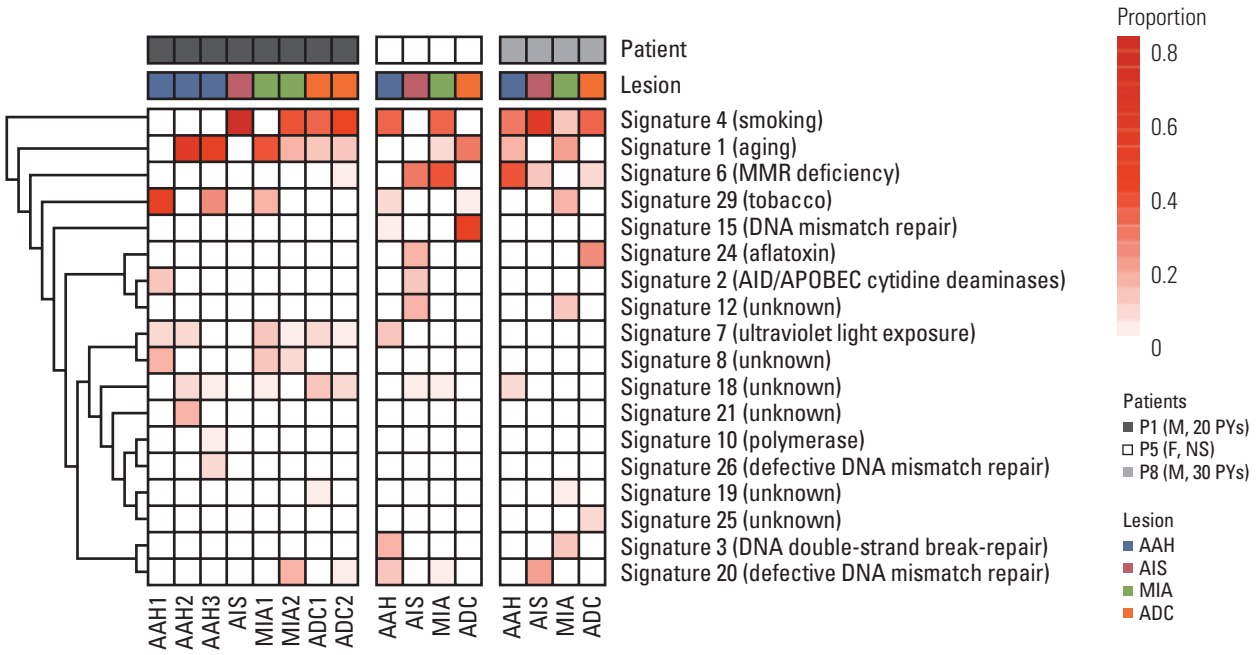

Fig. 3. Mutation signature analysis. Somatic mutational signatures were generated and compared to the 30 known mutational signatures in the Catalogue of Somatic Mutations in Cancer (COSMIC) database. AAH, atypical adenomatous hyperplasia; AIS, adenocarcinoma *in situ*; MIA, minimally invasive adenocarcinoma; ADC, adenocarcinoma.

domain containing 2 (*SETD2*), a histone methyltransferase (S12 Table). *SETD2* has been reported to be co-mutated with polybromo 1 (*PBRM1*), particularly in renal cell cancer [27] and in lung cancer [28]. Although WES did not show *PBRM1* mutation in this patient, a previous study using paired targeted sequencing indicated that the patient harbored *PBRM1* mutation (p.K135X) in ADC1 with low frequency (S12 Table, S13 Fig.). We also noted enriched mutations in chromatic-modifying genes (*SMARCA4* [p.E1133E]) and RNA-splicing genes (*RBM10* [c.2337_2337delins-G, and p.G780V]). These findings indicate that accumulated *SETD2* tumor suppressor mutations along with *TTLL5* enzyme mutations in preinvasive lesions exacerbated methylation and chromatic remodeling dysfunction through *SMARCA4*, *RBM10*, and *PBRM1* mutations [29] (S14 Table). The copy number analysis indicated that P1 had aberrant copy number status in invasive lesions (S15 Fig., S16 Table). In a large cohort of 100 early stage lung cancer patients, DNA instability was found to possibly play a key role in cancer malignancy as it can have invasive capacity induced by environmental diversity and can thus be a predictor of clinical outcome [20].

The cancer evolution models are primarily divided into the neutral evolution ('a big bang model') [30] and the Darwinian evolution, depending on the differential clonal selection modes and rates [31]. Darwinian evolution selecting the fittest subclone was further divided into branched, linear, convergent, and parallel evolution. In our study, a linear evolutionary pattern can explain the EGFR-driven selective sweeps. Our data showed that genes related to epithelial cell proliferation and differentiation (*MUC4*) may be a part of the selective subclonal mechanism. We also conjectured that not only drive specific genomic changes, but also environmental factors contribute to clonal compositions.

The study has limitations. First, because our samples were cross-sectionally obtained at a single time point, the lesions may not be in chronological orders. Second, the patient number was small. Third, our adjusted cut-off value of VAF was extremely lower compared to that in conventional next-generation sequencing studies, although variants with low VAF values are frequently observed in clinical cancer samples [32]. Meanwhile, the major strengths of this study include the series of multiple continuum lesions within a patient and the reproducibility of results through multiple sequencing platforms (WES, targeted, and RNA-seq). We also observed that the mutation signature patterns were consistent to those reported in large-scale studies of early lung cancer patients. Collectively, the variants repeatedly confirmed in our studies may have potential utility for studying neoplastic progression (S17 Table, S18 Fig.).

In summary, we performed a comprehensive analysis of somatic alterations across synchronous lesion mutations and identified the multiple evolutionary trajectories of LUAD rooted in preinvasive lesions toward advanced lesions. We observed few shared somatic mutations and cellular heterogeneity in lung cancer, which implied the independent tumorigenic event within certain genes. The intertumoral

and intratumoral heterogeneity of synchronous LUAD implies that multi-biomarker strategies might be necessary for appropriate treatment decisions. The distinct genetic origin implicates that individualized screening strategies are needed. Our finding implied that genomic variant in *EGFR*, *TP53*, *KRAS*, and *BRAF* could occur early in the process of tumor evolution, and different pathways may involve between a smoker and a non-smoker. The multi-modality tests such as imaging with diagnostic test like cell free DNA testing may lead to identifying certain clonal expansions.

Electronic Supplementary Material

Supplementary materials are available at Cancer Research and Treatment website (https://www.e-crt.org).

Conflicts of Interest

Conflicts of interest relevant to this article was not reported.

Acknowledgments

This research was supported by the Basic Science Research Program through the National Research Foundation of Korea (NRF) funded by the Ministry of Education (NRF-2015R1D1A1A02061597 to SA and 2019R1A2C1006890 to JHC) and by Seoul National University Bundang Hospital (grant number 13-2016-013 to JHC).

References

1. Siegel RL, Miller KD, Jemal A. Cancer statistics, 2018. CA Cancer J Clin. 2018;68:7-30.
2. Pakkala S, Ramalingam SS. Personalized therapy for lung cancer: striking a moving target. JCI Insight. 2018;3:e120858.
3. Choi CM, Kim HC, Jung CY, Cho DG, Jeon JH, Lee JE, et al. Report of the Korean Association of Lung Cancer Registry (KALC-R), 2014. Cancer Res Treat. 2019;51:1400-10.
4. Zhang J, Fujimoto J, Zhang J, Wedge DC, Song X, Zhang J, et al. Intratumor heterogeneity in localized lung adenocarcinomas delineated by multiregion sequencing. Science. 2014;346:256-9.
5. Travis WD, Nicholson AG. WHO classification of tumours of the lung, pleura, thymus and heart. Lyon: International Agency for Research on Cancer; 2015.
6. Inamura K. Clinicopathological characteristics and mutations driving development of early lung adenocarcinoma: tumor initiation and progression. Int J Mol Sci. 2018;19:1259.
7. Izumchenko E, Chang X, Brait M, Fertig E, Kagohara LT, Bedi A, et al. Targeted sequencing reveals clonal genetic changes in the progression of early lung neoplasms and paired circulating DNA. Nat Commun. 2015;6:8258.
8. Sivakumar S, Lucas FA, McDowell TL, Lang W, Xu L, Fujimoto J, et al. Genomic landscape of atypical adenomatous hyperplasia reveals divergent modes to lung adenocarcinoma. Cancer Res. 2017;77:6119-30.
9. Park E, Ahn S, Kim H, Park SY, Lim J, Kwon HJ, et al. Targeted sequencing analysis of pulmonary adenocarcinoma with multiple synchronous ground-glass/lepidic nodules. J Thorac Oncol. 2018;13:1776-83.
10. Noguchi M. Stepwise progression of pulmonary adenocarcinoma: clinical and molecular implications. Cancer Metastasis Rev. 2010;29:15-21.
11. Tamborero D, Rubio-Perez C, Deu-Pons J, Schroeder MP, Vivancos A, Rovira A, et al. Cancer Genome Interpreter annotates the biological and clinical relevance of tumor alterations. Genome Med. 2018;10:25.
12. Alves JM, Prieto T, Posada D. Multiregional tumor trees are not phylogenies. Trends Cancer. 2017;3:546-50.
13. Bailey MH, Tokheim C, Porta-Pardo E, Sengupta S, Bertrand D, Weerasinghe A, et al. Comprehensive characterization of cancer driver genes and mutations. Cell. 2018;173:371-85.
14. Rhee JK, Lee S, Park WY, Kim YH, Kim TM. Allelic imbalance of somatic mutations in cancer genomes and transcriptomes. Sci Rep. 2017;7:1653.
15. Govindan R, Ding L, Griffith M, Subramanian J, Dees ND, Kanchi KL, et al. Genomic landscape of non-small cell lung cancer in smokers and never-smokers. Cell. 2012;150:1121-34.
16. Cancer Genome Atlas Research Network. Comprehensive molecular profiling of lung adenocarcinoma. Nature. 2014;511:543-50.
17. Labbe C, Cabanero M, Korpanty GJ, Tomasini P, Doherty MK, Mascaux C, et al. Prognostic and predictive effects of TP53 co-mutation in patients with EGFR-mutated non-small cell lung cancer (NSCLC). Lung Cancer. 2017;111:23-9.
18. Schmid K, Oehl N, Wrba F, Pirker R, Pirker C, Filipits M. EGFR/KRAS/BRAF mutations in primary lung adenocarcinomas and corresponding locoregional lymph node metastases. Clin Cancer Res. 2009;15:4554-60.
19. Alexandrov LB, Nik-Zainal S, Wedge DC, Aparicio SA, Behjati S, Biankin AV, et al. Signatures of mutational processes in human cancer. Nature. 2013;500:415-21.
20. Jamal-Hanjani M, Wilson GA, McGranahan N, Birkbak NJ, Watkins TB, Veeriah S, et al. Tracking the evolution of non-small-cell lung cancer. N Engl J Med. 2017;376:2109-21.
21. Valero V 3rd, Pawlik TM, Anders RA. Emerging role of Hpo signaling and YAP in hepatocellular carcinoma. J Hepatocell Carcinoma. 2015;2:69-78.
22. Zheng W, Jiang C, Li R. Integrin and gene network analysis reveals that ITGA5 and ITGB1 are prognostic in non-small-cell lung cancer. Onco Targets Ther. 2016;9:2317-27.
23. Pirinen R, Leinonen T, Bohm J, Johansson R, Ropponen K, Kumpulainen E, et al. Versican in nonsmall cell lung cancer: relation to hyaluronan, clinicopathologic factors, and prognosis. Hum Pathol. 2005;36:44-50.
24. Ma P, Fu Y, Cai MC, Yan Y, Jing Y, Zhang S, et al. Simultaneous evolutionary expansion and constraint of genomic heteroge-

neity in multifocal lung cancer. Nat Commun. 2017;8:823.
25. He XP, Song FJ, Liu XY, Wang Z, Li XX, Liu FY, et al. The relationship between KRAS gene mutations and HLA class I antigen downregulation in the metastasis of non-small cell lung cancer. J Int Med Res. 2013;41:1473-83.
26. Blakely CM, Watkins TB, Wu W, Gini B, Chabon JJ, McCoach CE, et al. Evolution and clinical impact of co-occurring genetic alterations in advanced-stage EGFR-mutant lung cancers. Nat Genet. 2017;49:1693-704.
27. Hakimi AA, Pham CG, Hsieh JJ. A clear picture of renal cell carcinoma. Nat Genet. 2013;45:849-50.
28. Ahn JW, Kim HS, Yoon JK, Jang H, Han SM, Eun S, et al. Identification of somatic mutations in EGFR/KRAS/ALK-negative lung adenocarcinoma in never-smokers. Genome Med. 2014;6:18.
29. Park IY, Powell RT, Tripathi DN, Dere R, Ho TH, Blasius TL, et al. Dual chromatin and cytoskeletal remodeling by SETD2. Cell. 2016;166:950-62.
30. Sottoriva A, Kang H, Ma Z, Graham TA, Salomon MP, Zhao J, et al. A Big Bang model of human colorectal tumor growth. Nat Genet. 2015;47:209-16.
31. Venkatesan S, Birkbak NJ, Swanton C. Constraints in cancer evolution. Biochem Soc Trans. 2017;45:1-13.
32. Shin HT, Choi YL, Yun JW, Kim NK, Kim SY, Jeon HJ, et al. Prevalence and detection of low-allele-fraction variants in clinical cancer samples. Nat Commun. 2017;8:1377.

pISSN 1598-2998, eISSN 2005-9256

Cancer Res Treat. 2020;52(4):1135-1144

https://doi.org/10.4143/crt.2020.218

Original Article

Open Access

A Phase II Study of Avelumab Monotherapy in Patients with Mismatch Repair–Deficient/Microsatellite Instability–High or *POLE*-Mutated Metastatic or Unresectable Colorectal Cancer

Jwa Hoon Kim, MD[1]
Sun Young Kim, MD, PhD[1]
Ji Yeon Baek, MD, PhD[2]
Yong Jun Cha, MD, PhD[2]
Joong Bae Ahn, MD, PhD[3]
Han Sang Kim, MD, PhD[3]
Keun-Wook Lee, MD, PhD[4]
Ji-Won Kim, MD, PhD[4]
Tae-You Kim, MD, PhD[5]
Won Jin Chang, MD, PhD[6]
Joon Oh Park, MD, PhD[7]
Jihun Kim, MD, PhD[8]
Jeong Eun Kim, MD, PhD[1]
Yong Sang Hong, MD, PhD[1]
Yeul Hong Kim, MD, PhD[6]
Tae Won Kim, MD, PhD[1]

**A list of author's affiliations appears at the end of the paper.*

Correspondence: Tae Won Kim, MD, PhD
Department of Oncology, Asan Medical Center, University of Ulsan College of Medicine, 88 Olympic-ro 43-gil, Songpa-gu, Seoul 05505, Korea
Tel: 82-2-3010-3910
Fax: 82-2-3010-6961
E-mail: twkimmd@amc.seoul.kr

Received March 13, 2020
Accepted April 23, 2020
Published Online April 24, 2020

Purpose

We evaluated the efficacy and safety of avelumab, an anti–PD-L1 antibody, in patients with metastatic or unresectable colorectal cancer (mCRC) with mismatch repair deficiency (dMMR)/microsatellite instability-high (MSI-H) or *POLE* mutations.

Materials and Methods

In this prospective, open-label, multicenter phase II study, 33 patients with mCRC harboring dMMR/MSI-H or POLE mutations after failure of ≥ 1st-line chemotherapy received avelumab 10 mg/kg every 2 weeks. dMMR/MSI-H was confirmed with immunohistochemical staining (IHC) by loss of expression of MMR proteins or polymerase chain reaction (PCR) for micro-satellite sequences. *POLE* mutation was confirmed by next-generation sequencing (NGS). The primary endpoint was the objective response rate (ORR) by Response Evaluation Criteria in Solid Tumors ver. 1.1.

Results

The median age was 60 years, and 78.8% were male. Thirty patients were dMMR/MSI-H and three had *POLE* mutations. The ORR was 24.2%, and all of the responders were dMMR/MSI-H. For 21 patients with MSI-H by PCR or NGS, the ORR was 28.6%. At a median follow-up duration of 16.3 months, median progression-free survival and overall survival were 3.9 and 13.2 months in all patients, and 8.1 months and not reached, respectively, in patients with MSI-H by PCR or NGS. Dose interruption and discontinuation due to treatment-related adverse events occurred in four and two patients, respectively, with no treatment-related deaths.

Conclusion

Avelumab displayed antitumor activity with manageable toxicity in patients with previously treated mCRC harboring dMMR/MSI-H. Diagnosis of dMMR/MSI-H with PCR or NGS could be complementary to IHC to select patients who would benefit from immunotherapy.

Key words

Colorectal neoplasms, Mismatch repair deficiency, Microsatellite instability, *POLE* mutation, Avelumab

Introduction

Colorectal cancer (CRC) is one of the leading causes of cancer-related death worldwide and the third most common cancer in Korea [1]. Standard palliative treatment for metastatic or unresectable CRC (mCRC) is fluorouracil-based combination chemotherapy (with oxaliplatin or irinotecan), with or without agents targeting angiogenesis (bevacizumab) or epidermal growth factor receptor (cetuximab). The available therapeutic options for later-line chemotherapy are limited; regorafenib and TAS-102 showed only a modest clinical benefit in these patients. The objective response rate (ORR) with regorafenib and TAS-102 was approximately 1%, and median progression-free survival (PFS) was around 2 months for both treatments [2,3]. The long-term outcomes of mCRC are still poor [1], and novel therapeutic approaches are needed.

Growing evidence suggests that patients with mCRC harboring deficient mismatch repair protein (dMMR)/microsatellite instability–high (MSI-H) can obtain clinical benefit from immune checkpoint inhibitors (ICIs) [4-7]. Pembroli-

zumab and nivolumab, which are anti–programmed death 1 (anti–PD-1) inhibitors, improved ORR and PFS in selected patients with dMMR/MSI-H mCRC [4-7]. Failure to repair DNA replication-associated errors in dMMR/MSI-H mCRC is associated with high mutation loads, tumor neoantigen loads, and dense immune cell infiltration [8]. In fact, the whole-exome sequences revealed higher somatic mutation loads (1,782 mutations per tumor) in patients with dMMR/MSI-H than in patients with proficient MMR (73 mutations per tumor) (p=0.007), and a greater density of CD8-positive lymphocytes and a higher expression of PD-ligand 1 (PD-L1) were observed in patients with dMMR/MSI-H than in patients with proficient MMR [4]. However, the clinical benefit of ICIs is confined to a small proportion of patients, because dMMR/MSI-H is identified in only about 5% in patients with mCRC [9]. This raises the need to expand the number of potential candidates for immunotherapy.

The *POLE* gene is located in 12q24.33 and encodes the proofreading (exonuclease) subunit of polymerase epsilon (POLE) with 2,286 amino acids [10]. This *POLE* mutation has been reported in approximately 3% of proficient MMR CRC and represents high somatic mutation loads [10]. According to the Cancer Genome Atlas, up to one-quarter of hypermutated CRC carry somatic mutations in POLE [10]. Because high mutation loads are considered a mechanism of the response of dMMR/MSI-H to ICIs, *POLE*-mutated cancer may also be susceptible to ICIs. However, to date, clinical data regarding the response to ICIs in *POLE*-mutated cancer are lacking.

Treatment with avelumab, an anti–PD-L1 inhibitor, achieved an ORR of 33% in patients with previously treated metastatic Merkel cell carcinoma and was approved for the treatment of metastatic Merkel cell carcinoma in early 2017 [11]. Subsequently, avelumab has shown promising antitumor activity in various solid tumors, such as genitourinary tract [12,13], gynecologic [14], and lung [15], but its activity in mCRC harboring dMMR/MSI-H has not been investigated. This study aimed to evaluate the efficacy and safety of avelumab in patients with previously treated CRC with deficient MMR/MSI-H as well as those with *POLE* mutations.

Materials and Methods

1. Study design and patients

This study is a prospective, open-label, multicenter phase II study conducted as a substudy of the K-MASTER project, a nationwide, government-funded precision medicine initiative [16]. Eligible patients were aged ≥ 20 years and had histologically or cytologically confirmed metastatic or unresectable adenocarcinoma of the colon or rectum after failure of first-line or later chemotherapy, including fluoropyrimidine, oxaliplatin, or irinotecan, with or without targeted agents (bevacizumab or cetuximab). Patients were enrolled if dMMR/ MSI-H was confirmed by either immunohistochemistry (IHC) or polymerase chain reaction (PCR) by local test at each site, or if *POLE* mutation was confirmed by next-generation sequencing (NGS) certified by the Ministry of Food and Drug Safety, Korea. MMR protein was determined to be deficient by loss of expression of one or more of the following on IHC: MLH1, MSH2, MSH6, and PMS2. MSI-H was diagnosed by PCR if two or more microsatellite markers (BAT-25, BAT-26, D2S123, D5S346, and D17S250) were detected. *POLE* mutations included hotspots such as P286R and other sites. Eligible patients had at least one measurable disease, an Eastern Cooperative Oncology Group (ECOG) performance status of 0 or 1, and adequate organ function. Any prior treatment with anti–PD-1 or PD-L1 inhibitors was not permitted, and prior immunosuppressive treatment or the last dose of chemotherapy should not be administered within 28 days before the first dose of study drug. Prior radiotherapy was permitted if it was not administered to the target lesions selected for this study.

2. Treatment and evaluation

Avelumab was administered at 10 mg/kg intravenously every 2 weeks until disease progression, unacceptable toxicity, or patient refusal occurred. Dose modification was not allowed, but dose delay was permitted at the investigator's discretion in case of clinically significant events. Study treatment was discontinued if there were more than 4 weeks of delay. Response assessment was performed by computed tomography (CT) scan according to Response Evaluation Criteria in Solid Tumors (RECIST) ver. 1.1 every 6 weeks. After the end of treatment, patients were followed up for disease status and survival information every 3 months. The medical histories of all patients were obtained before treatment, including physical examination, complete blood count with differential count, serum chemistry, electrolytes, coagulation, carcinoembryonic antigen, thyroid function test (thyroid-stimulating hormone and free thyroxine), urinalysis, electrocardiogram, chest X-ray, CT scan, and other scans if clinically indicated. Adverse events were assessed every cycle according to the National Cancer Institute Common Terminology Criteria for Adverse Events (NCI-CTCAE), version 4.0.

3. Statistical analysis

The sample size was calculated using the Simon two-stage optimal design. The target response rate was set to 30%, and a rate of 10% or below was considered failure, allowing early termination of any ineffective treatment early in the study. With a one-sided type I error of 5% and a power of 0.8, the planned study was to proceed in two steps. If a tumor response occurred in at least two patients after the first 10 patients were listed, the study proceeded to the second stage with 19 additional patients. A total of 29 patients were requi-red, and enrollment of 33 patients was planned,

Table 1. Baseline characteristics of the study patients

Characteristic	No. (%)
Age, median (range, yr)	60 (25-88)
Sex	
Male	26 (78.8)
Female	7 (21.2)
ECOG performance status	
0	10 (30.3)
1	23 (69.7)
Primary tumor	
Right-sided colon	22 (66.7)
Left-sided colon	5 (15.2)
Rectum	6 (18.2)
Histology	
Well differentiated	6 (18.2)
Moderately differentiated	19 (57.6)
Poorly differentiated	5 (15.2)
Not assessable	3 (9.1)
***RAS* status**	
Wild	11 (33.3)
Mutant	20 (60.6)
Not done	2 (6.1)
***BRAF* status**	
Wild	22 (66.7)
Mutant	4 (12.1)
Not done	7 (21.2)
Sites of metastasis	
Liver	15 (45.5)
Lung	11 (33.3)
Lymph node, abdomen	20 (60.6)
Peritoneum/Omentum	9 (27.3)
Bone	2 (6.1)
Family history of cancer in any first-degree relative	7 (21.2)
Previous chemotherapy regimen	
FOLFOX	24 (72.7)
FOLFIRI	15 (45.5)
XELOX	4 (12.1)
Capecitabine	10 (30.3)
Others	2 (6.1)
Previous targeted treatment	
Bevacizuamb	25 (75.8)
Cetuximab	2 (6.1)
Prior radiotherapy	7 (21.2)
Prior surgery	
Primary site resection	31 (93.9)
Metastasectomy	9 (27.3)
Prior lines of therapy	
1	16 (48.5)
2	11 (33.3)
≥ 3	6 (18.2)

ECOG, Eastern Cooperative Oncology Group; FOLFOX, 5-fluorouracil, leucovorin, and oxaliplatin; FOLFIRI, 5-fluorouracil, leucovorin, and irinotecan; XELOX, capecitabine and oxaliplatin.

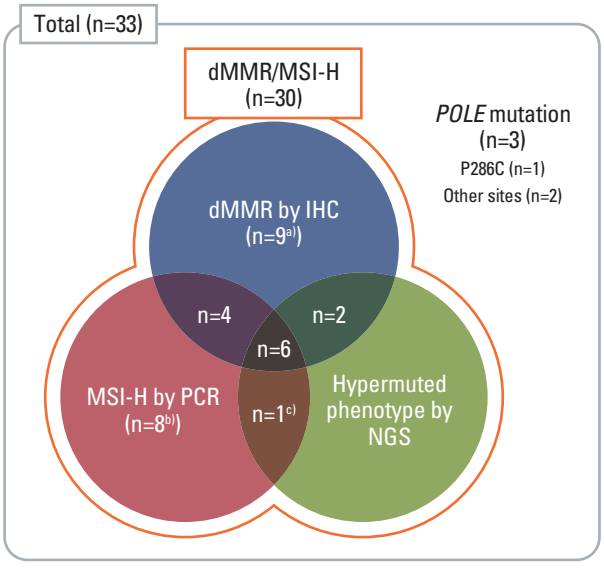

Fig. 1. Status of mismatch repair by immunohistochemistry (IHC) or microsatellite instability (MSI) by polymerase chain reaction (PCR) and *POLE* mutation. dMMR, mismatch repair deficiency; MSI-H, MSI-high; MSS, microsatellite stable; NGS, next-generation sequencing; p-MMR, proficient-microsatellite instability. [a]Six of nine were MSS by PCR or NGS, [b]One of eight was p-MMR by IHC, [c]p-MMR by IHC.

given a dropout rate of 10%.

The primary endpoint was the ORR by RECIST ver. 1.1; the secondary endpoints included the disease control rate (DCR), PFS, overall survival (OS), and adverse events. DCR was defined as the proportion of patients with complete response (CR), partial response (PR), or stable disease (SD) sustained for ≥ 6 weeks. PFS was calculated from the first date of avelumab administration to the date of disease progression or death from any cause. OS was calculated from the first date of avelumab administration to the date of death from any cause. Survival rates were estimated using the Kaplan-Meier method. A two-sided p-value < 0.05 was considered to indicate statistical significance, and all statistical analyses were performed using IBM SPSS Statistics for Windows ver. 21.0 (IBM Corp., Armonk, NY).

4. Ethical statement

All procedures followed were in accordance with the ethi-

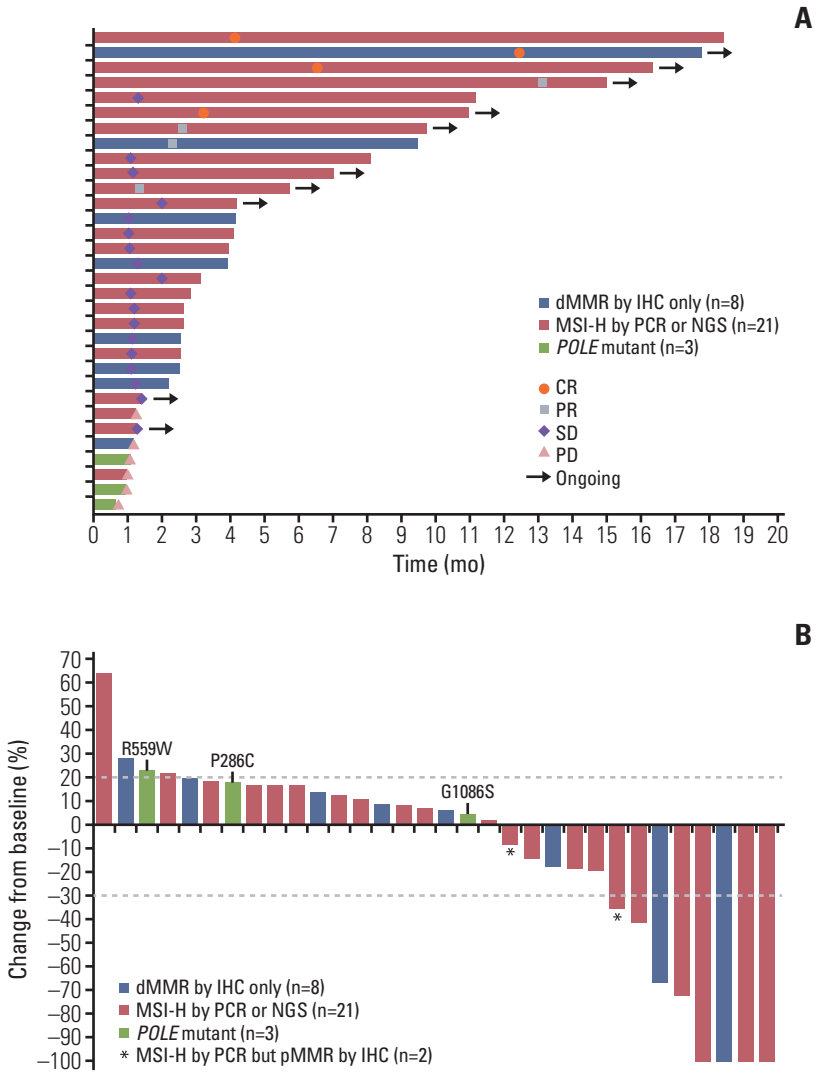

Fig. 2. Antitumor activity of avelumab in patients with metastatic or unresectable colorectal cancer harboring deficient mismatch repair (dMMR)/microsatellite instability-high (MSI-H) or *POLE* mutations. (A) Treatment duration of avelumab for all patients. (B) Best change from baseline in target lesion size after avelumab. CR, complete response; IHC, immunohistochemistry; NGS, next-generation sequencing; PCR, polymerase chain reaction; PD, progressive disease; p-MMR, proficient-microsatellite instability; PR, partial response; SD, stable disease.

cal standards of the responsible committee on human experimentation (institutional and national) and the Helsinki Declaration of 1964 and later versions. The study protocol was approved by the institutional review board of each participating center and the Korean Cancer Study Group (KCSG; protocol No. KCSG-CO-17-07). This trial was registered on http://www.clinicaltrials. gov with the identifier NCT0315-0706. Informed consent or a substitute was obtained from all patients before inclusion in the study.

Results

1. Patient characteristics

Between May 2017 and April 2019, a total of 34 patients were initially enrolled at seven clinical sites in South Korea; one patient failed the screening tests, and thus, 33 patients with histologically or cytologically confirmed, previously treated, metastatic or unresectable CRC were enrolled in the final analysis. Table 1 summarizes the baseline characteristics of the 33 study patients. The median age was 60 years (range, 25 to 88), and 78.8% were male. Two-thirds of the patients (n=22, 66.7%) had right-sided colon cancer, and 20 patients (60.6%) had RAS mutation. Seven patients had a family his-

Table 2. Clinical response to avelumab monotherapy

Response	All patients (n=33)		MSI high by PCR or NGS (n=21)	
	No. (%)	95% CI (%)	No. (%)	95% CI (%)
Complete response	4 (12.1)	0.97-23.2	3 (14.3)	0-29.3
Partial response	4 (12.1)	0.97-23.2	3 (14.3)	0-29.3
Stable disease	18 (54.5)	37.5-71.5	13 (61.9)	41.1-82.7
Progressive disease	6 (18.2)	5.0-31.4	2 (9.5)	0-22.0
Not assessable[a)]	1 (3.0)	0-8.8	0	-
Objective response rate	8 (24.2)	9.4-38.6	6 (28.6)	9.3-47.9
Disease control rate	26 (78.8)	64.9-92.7	19 (90.5)	77.9-103

MSI, microsatellite instability; PCR, polymerase chain reaction; NGS, next-generation sequencing. [a)]Lost to follow-up (n=1).

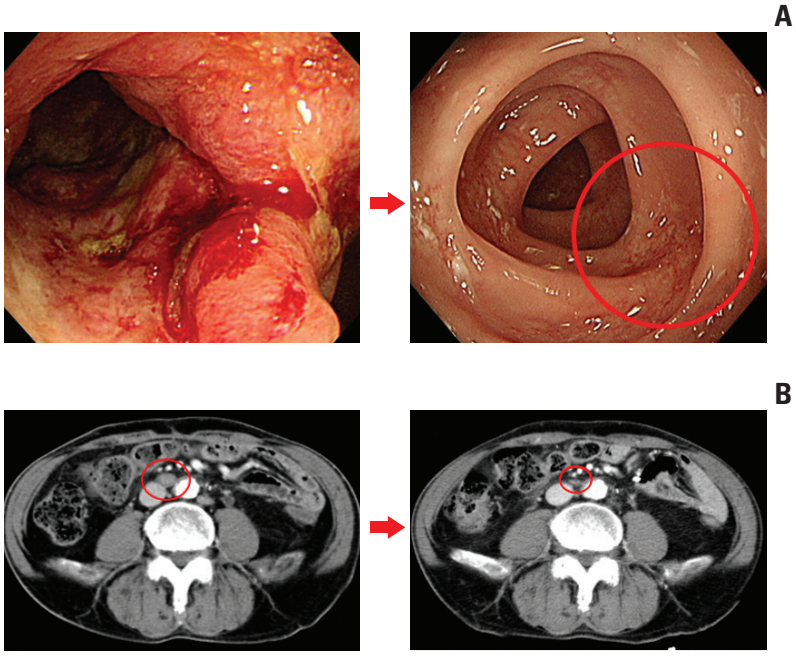

Fig. 3. Representative images of two patients who achieved partial response during avelumab monotherapy. (A) Endoscopic images of a 44-year-old man with initially metastatic T-colon cancer harboring microsatellite instability-high (MSI-H) by both immunohistochemistry (IHC) and next-generation sequencing. (B) Computed tomography scans of 75-year-old man with recurrent rectal cancer harboring MSI-H by IHC.

tory of cancer in a first-degree relative.

2. Deficient MMR or MSI high and *POLE* mutation

Among the 33 patients, 30 patients had dMMR/MSI-H CRC, and three patients had *POLE*-mutated CRC. *POLE* mutation was identified at the P286C, R559W, and G1086S sites. NGS revealed hypermutated phenotype CRC in only one patient with a P286C mutation, but the other sites (R559W and G1086S) were not associated with high tumor mutation burden (TMB) in each different NGS panel (S1 Table).

Among 30 patients with dMMR/MSI-H, IHC, and PCR were performed both in 23 patients, respectively. Both tests at the same time were performed in 16 patients, among whom 10 (62.5%) showed concordance between IHC and PCR. NGS, which was not mandatory for detecting dMMR/ MSI-H, was performed in 12 patients with dMMR/MSI-H.

The distribution of patients according to different detection methods is shown in Fig. 1. Twenty-one patients were diagnosed with dMMR by IHC, and 19 were diagnosed with MSI-H by PCR. Discordance between the IHC and PCR results was found as follows: six of nine patients with dMMR by IHC only showed microsatellite stable (MSS) CRC by PCR or NGS, and one of eight patients with MSI-H by PCR only showed proficient MMR by IHC. One patient who was diagnosed as MSI-H by PCR and NGS was diagnosed as proficient MMR by IHC.

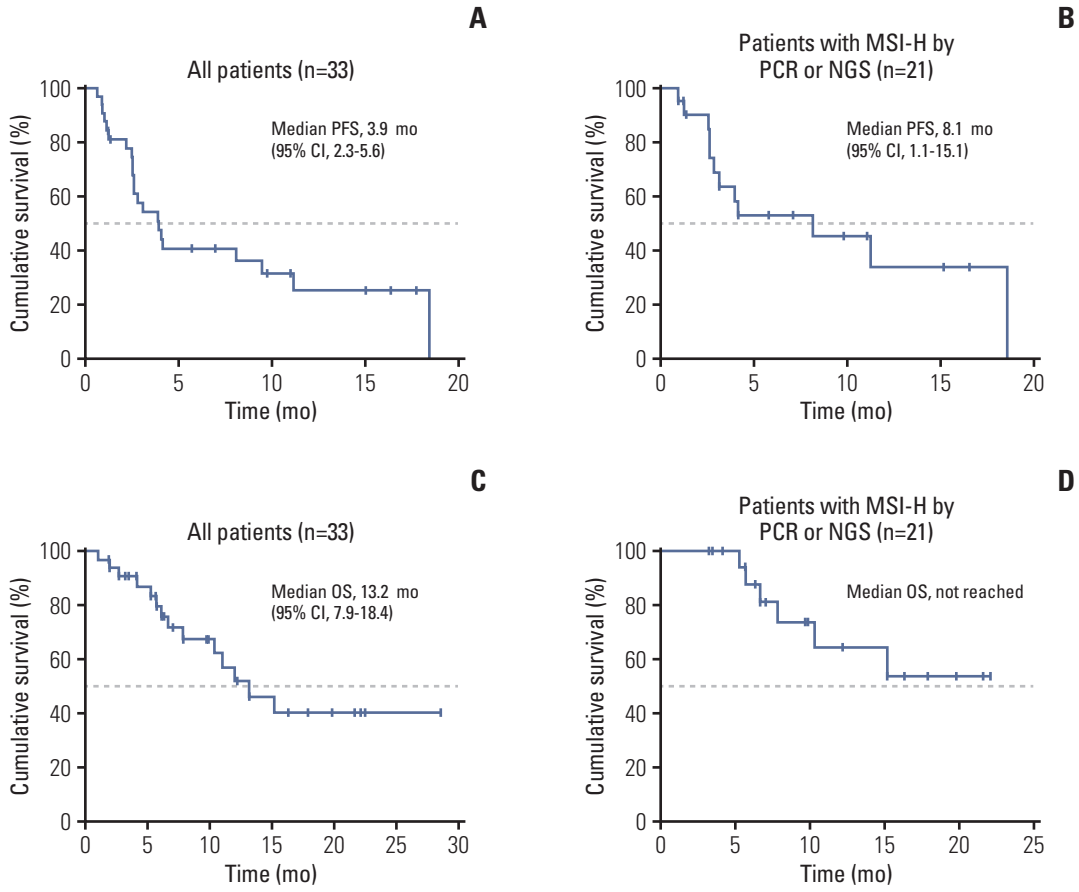

Fig. 4. Median progression-free survival (PFS) (A, B) and overall survival (OS) (C, D) in all patients (A, C) and patients with microsatellite instability high (MSI-H) (B, D) by polymerase chain reaction (PCR) or next-generation sequencing (NGS). CI, confidence interval.

3. Clinical response to avelumab

Avelumab was discontinued mainly due to disease progression (n=22, 66.7%), followed by loss to follow-up (n=1, 0.03%); the remaining 10 patients were treated with ongoing avelumab (Fig. 2A). The median time to response was 4.2 months, and the median duration of response was 13.9 months (Fig. 2A). Among the 33 patients, four (12.1%) had CR, four (12.1%) had PR, 18 (54.5%) had SD, 6 (18.2%) had progressive disease (PD), and one (3.0%) was not assessable (Table 2). The ORR and DCR were 24.2% and 78.8%, respectively. Of 21 patients with MSI-H by PCR or NGS, three (14.3%) had CR, three (14.3%) had PR, 13 (61.9%) had SD, and two (9.5%) had PD (Table 2). The ORR and DCR were 28.6% and 90.5%, respectively. All responders had dMMR/MSI-H CRC, and no patients with a *POLE* mutation achieved response.

The best percentage changes from baseline in target lesion size are shown in Fig. 2B. Six of eight patients with CR or PR showed MSI-H by PCR or NGS. Among six patients with PD, two patients with *POLE* mutations (G1086S and P286C) had PD based on unequivocal progression of nontarget lesions, and all three patients with *POLE* mutations had PD without any tumor shrinkage. One patient with proficient MMR by IHC only but MSI-H by PCR achieved PR. Representative images of two responders are shown in Fig. 3.

Given the discrepancies between IHC and PCR results and the need to investigate their association with the response to avelumab, IHC results were separately reviewed in available eight of nine patients with dMMR by IHC only at each clinical site. dMMR was revised to proficient MMR by IHC in five patients, who also showed MSS by PCR or NGS. Four of them did not achieved response; however, the other patient achieved CR despite proficient MMR revised after review of the IHC result and MSS by PCR.

4. PFS and OS

With a median follow-up duration of 16.3 months (95% confidence interval [CI], 5.6 to 27.1 months), median PFS was 3.9 months (95% CI, 2.3 to 5.6 months) in all patients and 8.1 months (95% CI, 1.1 to 15.1 months) in patients with MSI-H by PCR or NGS (Fig. 4A and B). Median OS was 13.2 months (95% CI, 7.9 to 18.4 months) in all patients and not reached in patients with MSI-H by PCR or NGS (Fig. 4C and D). Overall, the 12-month PFS and OS rates were 36.4% and 66.7%,

Table 3. Treatment-related adverse events

Event	All patients (n=33, 100%)	
	Any grade	Grade ≥ 3
Any TRAE	24 (72.7)	6 (18.2)
Myalgia	6 (18.2)	0
Chills	5 (15.2)	0
Infusion-related reaction	5 (15.2)	0
Pruritus	5 (15.2)	0
Thyroid dysfunction	4 (12.1)	0
Skin rash	4 (12.1)	0
Diarrhea	3 (9.1)	2 (6.1)
Fever	3 (9.1)	0
Increased AST or ALT	3 (9.1)	0
Hypomagnesemia	3 (9.1)	0
Fatigue	2 (6.1)	0
Anorexia	2 (6.1)	0
Hyperglycemia	2 (6.1)	1 (3.0)
Increased amylase or lipase	1 (3.0)	2 (6.1)
Nausea	1 (3.0)	0
Sweating	1 (3.0)	0
Dry skin	1 (3.0)	0
Anemia	1 (3.0)	0
Hyperbilirubinemia	0 (0.0)	1 (3.0)

Values are presented as number (%). TRAE, treatment-related adverse event; AST, aspartate aminotransferase; ALT, alanine aminotransferase.

respectively, and 47.6% and 76.2%, respectively, in patients with MSI-H by PCR or NGS.

5. Treatment-related adverse events

Treatment-related adverse events (TRAEs) with avelumab are shown in Table 3. TRAEs of any grade were observed in 24 patients (72.7%). Common TRAEs of any grade included myalgia (n=6, 18.2%), chills (n=5, 15.2%), infusion-related reaction (n=5, 15.2%), pruritus (n=5, 15.2%), thyroid dysfunction (n=4, 12.1%), and skin rash (n=4, 12.1%). Grade 3 or 4 TRAEs occurred in six patients (18.2%). Dose interruption due to TRAEs occurred in four patients (12.1%): grade 3 hyperglycemia (n=1), grade 3 lipase increase (n=1), grade 2 aspartate aminotransferase increase (n=1), and grade 2 fever (n=1). There were two discontinuations of treatment due to treatment-related grade 3 hyperbilirubinemia (n=1) and probable treatment-related grade 4 tumor bleeding (n=1) after response to avelumab as a serious adverse event. There were no deaths due to TRAE.

Discussion

In this open-label, multicenter, phase II study, avelumab showed promising antitumor activity and manageable toxicity in patients with mCRC harboring dMMR/MSI-H or *POLE* mutation. The ORR and median PFS were 24.2% and 3.9 months, respectively, and six of eight responders were continuing avelumab treatment with durable response at the end of the analysis. Of note, the ORR and median PFS were 28.6% and 8.1 months, respectively, in patients with MSI-H by PCR or NGS, which were thought to be more reliable methods of determining the MSI status than IHC. Although no patients with *POLE* mutations had response to avelumab, the limitations of small sample size and variation in mutation sites need to be taken into account. TRAEs of any grade and TRAEs of grade 3 or 4 were observed in 72.7% and 18.2% of patients, respectively, which was consistent with previous studies [17]. There were two discontinuations of treatment, one because of a TRAE and the other because of a serious adverse event, probably related to treatment. There were no treatment-related deaths.

The efficacy of avelumab (an anti–PD-L1 inhibitor) for mCRC with dMMR/MSI-H, specifically in patients with MSI-H by PCR or NGS, is comparable to that of pembrolizumab and nivolumab (anti–PD-1 inhibitors) in this setting. In the KEYNOTE-016 trial, only patients with MSI-H CRC had the objective response to pembrolizumab (ORR 40%), whereas none of those with MSS CRC had the objective response [4]. A subsequent multicenter trial of pembrolizumab for dMMR/MSI-H CRC, the KEYNOTE-164 phase II study, resulted in an ORR of 33% and a median PFS of 4.1 months; the 12-month PFS and OS rates were 34% to 41% and 72% to 76%, respectively, according to prior line of treatment [6,7]. Nivolumab also showed promising antitumor activity in terms of ORR (31.1%) in dMMR/MSI-H CRC, and the 12-month PFS and OS rates were 50% and 73%, respectively [5]. All these favorable results in dMMR/MSI-H CRC contrast sharply with those of later-line conventional chemotherapy for overall mCRC with treatments such as regorafenib or TAS-102, which resulted in ORR of only 1% and median PFS of around 2 months [2,3].

Several phase I results from the JAVELIN Solid Tumor Trials have shown promising ORRs and disease stabilization with avelumab in various types of advanced tumors. Specifically, among 53 patients with metastatic or locally advanced previously treated solid tumors, four (8%) achieved responses and 30 (57%) had SD [18]. The ORR with avelumab ranged from 6.7% to 18.2%, depending on tumor type such as metastatic or unresectable previously treated renal cell carcinoma [12], urothelial carcinoma [13], non-small cell lung cancer [15], and ovarian cancer [14]. In a phase II study of 88 patients with chemotherapy-refractory metastatic Merkel cell carcinoma [11], the ORR with avelumab was 33%, including a CR rate of 11.4%. To date, avelumab has been approved for treatment of previously treated metastatic Merkel cell carcinoma, urothelial carcinoma, and renal cell carcinoma in combination with axitinib. Several explorations to expand

its use in various clinical settings are ongoing. The present study adds to the evidence of clinical activity of avelumab by showing durable objective responses in mCRC with dMMR/MSI-H.

dMMR/MSI-H is an established biomarker for the efficacy of ICIs in mCRC, and its predictive value has also been confirmed in other various tumors. MSI-H metastatic gastric cancer (mGC) had a higher ORR with pembrolizumab than did MSS mGC (57% vs. 9%) in the KEYNOTE-059 study [19]. Recently, the clinical benefit of pembrolizumab was demonstrated among patients with dMMR/MSI-H non-CRC, including endometrial cancer, gastric cancer, cholangiocarcinoma, and pancreatic cancer in terms of ORR (34.3%) and median PFS (4.1 months) [20]. Although the exact mechanism is unknown, there are several proposed explanations for T-cell checkpoint blockade [21]. Since dMMR/MSI-H results in diverse neoantigens, T-cell epitopes that are newly formed as a consequence of tumor-specific mutations, which can increase neoantigen-driven T-cell response. Another possible explanation is that dMMR/MSI-H is associated with the activation of signaling pathways through altered cytokines or chemokines, resulting in the tumor microenvironment becoming more inflamed. Cellular stress induced by dMMR/MSI-H promotes innate immune cells, such as T cells and natural killer cells, or tumor recognition.

However, not all patients with mCRC harboring dMMR/MSI-H respond to ICIs, and the TMB varies even within dMMR/MSI-H mCRC. The updated analysis from the initial single-center study showed an ORR of 50% [4], but subsequent multicenter phase II trials revealed ORR of around 30% [5-7]. In the present study, the ORR was 28.6% in patients with MSI-H by PCR or NGS. Approximately 37 to 41 mutations per megabase may be a cutoff value, and low TMB was significantly associated with poor response to ICIs and worse PFS within the dMMR/MSI-H population, which may be an explanation for the heterogeneity in response in recent clinical trials of dMMR/MSI-H CRC [22]. Moreover, substantial genomic variation is observed within dMMR/MSI-H tumors. In particular, the genome-wide intensity of MSI and the accumulation of insertion–deletion mutational loads are responsible for a wide diversity of clinical benefits with ICIs [23], and the activated WNT/β-catenin signaling pathway is associated with immune escape, despite a high TMB and high numbers of tumor-infiltrating lymphocytes [24].

In fact, a considerable portion of the primary resistance of mCRC treated with ICIs may be due to misdiagnosis of dMMR/MSI-H. One study showed that three of five patients (60%) who had PD at the first evaluation were reassessed as MSS by central review with PCR, contrary to the diagnosis of dMMR/MSI-H by local assessment [25]. In the CheckMate-142 study, there were discrepancies between local and central assessments in 14 of 74 patients (19%) [5]. Most of the patients with assessments (10/14) were initially determined as dMMR by IHC at the local laboratory, but central review with PCR reclassified them as MSS [5]. In this study, there were some discrepancies between IHC and PCR results, and six of nine patients with dMMR by IHC only showed MSS by PCR or NGS, leading to different ORRs depending on how dMMR/MSI-H CRC was defined. After review of the available IHC results in eight of these patients, five patients were revised to proficient MMR, while their PCR or NGS showed all MSS. The reliability and reproducibility of IHC results have always been a concern, because IHC results are largely affected by intra- and interobserver variation and tissue preservation status [26], and local assessment without central review contributed to these results. Likewise, in the recent phase II study with a similar design, differences in ORRs with avelumab in patients with previously treated endometrial cancer were observed between dMMR determined by IHC only and MSI-H determined by NGS (26.7% vs. 30%) [27]. dMMR/MSI-H could be misdiagnosed if IHC results are not supported by PCR or NGS, so the IHC test alone should be carefully interpreted by experienced pathologists. Further, IHC tests on tumor samples achieved after chemoradiotherapy, old samples, or poorly preserved samples are associated with a high risk of unreliable results.

POLE-mutated CRC has been characterized by young age, male predominance, right-sided CRC, earlier stage of disease, and excellent prognosis [10]. *POLE* has a crucial role in chromosomal DNA replication by its proofreading capacity and is known to be mutually exclusive with dMMR/MSI-H [10]. Because of high immunogenicity and enrichment of mutation-associated neoantigens, *POLE*-mutated cancer has been considered a candidate for treatment with ICIs. However, there are limited data, and there is only one case report [28] of a patient with mCRC harboring a *POLE* mutation (V411L) and MSS. This patient had a response after three cycles of pembrolizumab, and CD8 infiltrating lymphocytes with PD-1 expression were observed in the primary colon tumor. All responders in previous reports had mutations at the P286R or V411L sites, which are considered hotspots of *POLE* mutation [10]. Unfortunately, three patients with *POLE* mutations did not respond to ICIs in the present study. One patient with a P286C mutation was associated with a hypermutation phenotype by NGS, but the other two (with R559W and G1086S mutations) did not show high TMB, although they were tested with different panels (S1 Table), and the identified sites of *POLE* mutation might not have been hotspots, which could have led to negative results. Further clinical studies with larger sample sizes are necessary to evaluate the activity of ICIs and its association with sites in *POLE*-mutated CRC.

One of the responders initially showed dMMR by IHC and MSS by PCR at the time of enrollment. However, the IHC result was revised to proficient MMR in the post hoc review. Although NGS could not be performed due to an inadequate

amount of tumor tissue, leaving the *POLE* mutation status of this patient unknown, he achieved CR and has continued avelumab treatment for approximately 18 months (Fig. 3). In this regard, there may be unknown factors to explain the mechanism of response to ICIs other than MMR/MSI status or *POLE* mutation, such as PD-L1 or PD-L2 amplification [29,30], although we could not explore the cause of responsiveness in this patient due to the lack of adequate tumor tissue.

This study has several limitations. The consistency of eligibility and response evaluation could not be fully ensured, because central adjudication of the dMMR/MSI status of tumor tissue and central review of the radiologic response were not performed. Tumor samples were not collected prospectively for research purposes, and therefore translational studies, such as investigation of TMB, tumor-infiltrating lymphocytes, PD-L1 expression, or transcriptome, have not yet been performed. Further *post hoc* studies are planned with available tissue samples to elucidate their association with the response to ICIs.

In conclusion, avelumab is a promising anti–PD-L1 inhibitor in patients with metastatic or unresectable CRC harboring dMMR/MSI-H or POLE mutations. For the determination of dMMR/MSI-H, the conventional IHC method alone appears to be insufficient to select patients who would benefit from immunotherapy. Further studies to identify accurate strategies to select optimal candidates for immu-notherapy are needed.

Electronic Supplementary Material

Supplementary materials are available at Cancer Research and Treatment website (https://www.e-crt.org).

Conflicts of Interest

Avelumab was kindly provided by Merck Korea, Seoul, Korea; an affiliate of Merck KGaA, Darmstadt, Germany, as part of an alliance between Merck KGaA and Pfizer. Merck KGaA, Darmstadt, Germany and Pfizer reviewed the manuscript for medical accuracy only before journal submission.

Acknowledgments

This research was supported by a grant of the Korea Health Technology R&D Project through the Korea Health Industry Development Institute (KHIDI), funded by the Ministry of Health & Welfare, Republic of Korea (grant number: HI17C2206).

We thank Dr. Joon Seo Lim from the Scientific Publications Team at Asan Medical Center for his assistance with scientific editing of this manuscript.

Author Details

[1]Department of Oncology, Asan Medical Center, University of Ulsan College of Medicine, Seoul, [2]Center for Colorectal Cancer, Research Institute and Hospital, National Cancer Center, Goyang, [3]Division of Medical Oncology, Department of Internal Medicine, Severance Hospital, Yonsei University College of Medicine, Seoul, [4]Division of Hematology and Medical Oncology, Department of Internal Medicine, Seoul National University Bundang Hospital, Seoul National University College of Medicine, Seongnam, [5]Department of Internal Medicine, Seoul National University Hospital, Seoul National University College of Medicine, Seoul, [6]Division of Oncology/Hematology, Department of Internal Medicine, Korea University Anam Hospital, Korea University College of Medicine, Seoul, [7]Division of Hematology-Oncology, Department of Medicine, Samsung Medical Center, Sungkyunkwan University School of Medicine, Seoul, [8]Department of Pathology, Asan Medical Center, University of Ulsan College of Medicine, Seoul, Korea

References

1. Jung KW, Won YJ, Kong HJ, Lee ES; Community of Population-Based Regional Cancer Registries. Cancer statistics in Korea: incidence, mortality, survival, and prevalence in 2015. Cancer Res Treat. 2018;50:303-16.
2. Grothey A, Van Cutsem E, Sobrero A, Siena S, Falcone A, Ychou M, et al. Regorafenib monotherapy for previously treated metastatic colorectal cancer (CORRECT): an international, multicentre, randomised, placebo-controlled, phase 3 trial. Lancet. 2013;381:303-12.
3. Mayer RJ, Van Cutsem E, Falcone A, Yoshino T, Garcia-Carbonero R, Mizunuma N, et al. Randomized trial of TAS-102 for refractory metastatic colorectal cancer. N Engl J Med. 2015;372:1909-19.
4. Le DT, Uram JN, Wang H, Bartlett BR, Kemberling H, Eyring AD, et al. PD-1 blockade in tumors with mismatch-repair deficiency. N Engl J Med. 2015;372:2509-20.
5. Overman MJ, McDermott R, Leach JL, Lonardi S, Lenz HJ, Morse MA, et al. Nivolumab in patients with metastatic DNA mismatch repair-deficient or microsatellite instability-high colorectal cancer (CheckMate 142): an open-label, multicentre, phase 2 study. Lancet Oncol. 2017;18:1182-91.
6. Le DT, Kavan P, Kim TW, Burge ME, Van Cutsem E, Hara H, et al. KEYNOTE-164: Pembrolizumab for patients with advanced microsatellite instability high (MSI-H) colorectal cancer. J Clin Oncol. 2018;36(15 Suppl):3514.
7. Le DT, Kim TW, Van Cutsem E, Geva R, Jager D, Hara H, et al. Phase II open-label study of pembrolizumab in treatment-refractory, microsatellite instability-high/mismatch repair-deficient metastatic colorectal cancer: KEYNOTE-164. J Clin Oncol. 2020;38:11-9.
8. Llosa NJ, Cruise M, Tam A, Wicks EC, Hechenbleikner EM, Taube JM, et al. The vigorous immune microenvironment of microsatellite instable colon cancer is balanced by multiple counter-inhibitory checkpoints. Cancer Discov. 2015;5:43-51.

9. Koopman M, Kortman GA, Mekenkamp L, Ligtenberg MJ, Hoogerbrugge N, Antonini NF, et al. Deficient mismatch repair system in patients with sporadic advanced colorectal cancer. Br J Cancer. 2009;100:266-73.
10. Palles C, Cazier JB, Howarth KM, Domingo E, Jones AM, Broderick P, et al. Germline mutations affecting the proofreading domains of POLE and POLD1 predispose to colorectal adenomas and carcinomas. Nat Genet. 2013;45:136-44.
11. Kaufman HL, Russell J, Hamid O, Bhatia S, Terheyden P, D'Angelo SP, et al. Avelumab in patients with chemotherapy-refractory metastatic Merkel cell carcinoma: a multicentre, single-group, open-label, phase 2 trial. Lancet Oncol. 2016;17:1374-85.
12. Vaishampayan U, Schoffski P, Ravaud A, Borel C, Peguero J, Chaves J, et al. Avelumab monotherapy as first-line or second-line treatment in patients with metastatic renal cell carcinoma: phase Ib results from the JAVELIN Solid Tumor trial. J Immu-nother Cancer. 2019;7:275.
13. Patel MR, Ellerton J, Infante JR, Agrawal M, Gordon M, Aljumaily R, et al. Avelumab in metastatic urothelial carcinoma after platinum failure (JAVELIN Solid Tumor): pooled results from two expansion cohorts of an open-label, phase 1 trial. Lancet Oncol. 2018;19:51-64.
14. Disis ML, Taylor MH, Kelly K, Beck JT, Gordon M, Moore KM, et al. Efficacy and safety of avelumab for patients with recurrent or refractory ovarian cancer: phase 1b results from the JAVELIN solid tumor trial. JAMA Oncol. 2019;5:393-401.
15. Gulley JL, Rajan A, Spigel DR, Iannotti N, Chandler J, Wong DJ, et al. Avelumab for patients with previously treated metastatic or recurrent non-small-cell lung cancer (JAVELIN Solid Tumor): dose-expansion cohort of a multicentre, open-label, phase 1b trial. Lancet Oncol. 2017;18:599-610.
16. Choi YJ, Kim YH. The cancer precision medicine diagnosis and treatment (K-MASTER) enterprise. Korean J Med. 2019;94:246-51.
17. Kelly K, Infante JR, Taylor MH, Patel MR, Wong DJ, Iannotti N, et al. Safety profile of avelumab in patients with advanced solid tumors: a pooled analysis of data from the phase 1 JAVELIN solid tumor and phase 2 JAVELIN Merkel 200 clinical trials. Cancer. 2018;124:2010-7.
18. Heery CR, O'Sullivan-Coyne G, Madan RA, Cordes L, Rajan A, Rauckhorst M, et al. Avelumab for metastatic or locally advanced previously treated solid tumours (JAVELIN Solid Tumor): a phase 1a, multicohort, dose-escalation trial. Lancet Oncol. 2017;18:587-98.
19. Fuchs CS, Doi T, Jang RW, Muro K, Satoh T, Machado M, et al. Safety and efficacy of pembrolizumab monotherapy in patients with previously treated advanced gastric and gastroesophageal junction cancer: phase 2 clinical KEYNOTE-059 trial. JAMA Oncol. 2018;4:e180013.
20. Marabelle A, Le DT, Ascierto PA, Di Giacomo AM, De Jesus-Acosta A, Delord JP, et al. Efficacy of pembrolizumab in patients with noncolorectal high microsatellite instability/mismatch repair-deficient cancer: results from the phase II KEYNOTE-158 study. J Clin Oncol. 2020;38:1-10.
21. Kelderman S, Schumacher TN, Kvistborg P. Mismatch repair-deficient cancers are targets for anti-PD-1 therapy. Cancer Cell. 2015;28:11-3.
22. Schrock AB, Ouyang C, Sandhu J, Sokol E, Jin D, Ross JS, et al. Tumor mutational burden is predictive of response to immune checkpoint inhibitors in MSI-high metastatic colorectal cancer. Ann Oncol. 2019;30:1096-103.
23. Mandal R, Samstein RM, Lee KW, Havel JJ, Wang H, Krishna C, et al. Genetic diversity of tumors with mismatch repair deficiency influences anti-PD-1 immunotherapy response. Science. 2019;364:485-91.
24. Grasso CS, Giannakis M, Wells DK, Hamada T, Mu XJ, Quist M, et al. Genetic mechanisms of immune evasion in colorectal cancer. Cancer Discov. 2018;8:730-49.
25. Cohen R, Hain E, Buhard O, Guilloux A, Bardier A, Kaci R, et al. Association of primary resistance to immune checkpoint inhibitors in metastatic colorectal cancer with misdiagnosis of microsatellite instability or mismatch repair deficiency status. JAMA Oncol. 2019;5:551-5.
26. Klarskov L, Ladelund S, Holck S, Roenlund K, Lindebjerg J, Elebro J, et al. Interobserver variability in the evaluation of mismatch repair protein immunostaining. Hum Pathol. 2010;41:1387-96.
27. Konstantinopoulos PA, Luo W, Liu JF, Gulhan DC, Krasner C, Ishizuka JJ, et al. Phase II study of avelumab in patients with mismatch repair deficient and mismatch repair proficient recurrent/persistent endometrial cancer. J Clin Oncol. 2019;37:2786-94.
28. Gong J, Wang C, Lee PP, Chu P, Fakih M. Response to PD-1 blockade in microsatellite stable metastatic colorectal cancer harboring a POLE mutation. J Natl Compr Canc Netw. 2017;15:142-7.
29. Sorscher S, Resnick J, Goodman M. First case report of a dramatic radiographic response to a checkpoint inhibitor in a patient with proficient mismatch repair gene expressing metastatic colorectal cancer. JCO Precis Oncol. 2017 Feb 23 [Epub]. https://doi.org/10.1200/PO.16.00005.
30. Goodman AM, Piccioni D, Kato S, Boichard A, Wang HY, Frampton G, et al. Prevalence of PDL1 amplification and preliminary response to immune checkpoint blockade in solid tumors. JAMA Oncol. 2018;4:1237-44.

pISSN 1598-2998, eISSN 2005-9256

Cancer Res Treat. 2020;52(4):1145-1152

https://doi.org/10.4143/crt.2020.208

Original Article

Open Access

Evaluation of the American Joint Committee on Cancer (AJCC) 8th Edition Staging System for Hepatocellular Carcinoma in 1,008 Patients with Curative Resection

Sujin Park, MD[1]
Sangjoon Choi, MD[1]
Yoon Ah Cho, MD, PhD[1]
Dong Hyun Sinn, MD, PhD[2]
Jong Man Kim, MD, PhD[3]
Cheol-Keun Park, MD, PhD[1,4]
Sang Yun Ha, MD, PhD[1]

Departments of [1]Pathology and Translational Genomics, [2]Internal Medicine, and [3]Surgery, Samsung Medical Center, Sungkyunkwan University School of Medicine, Seoul, [4]Anatomic Pathology Reference Lab, Seegene Medical Foundation, Seoul, Korea

Correspondence: Sang Yun Ha, MD, PhD
Department of Pathology and Translational Genomics, Samsung Medical Center, Sungkyunkwan University School of Medicine, 81 Irwon-ro, Gangnam-gu, Seoul 06351, Korea
Tel: 82-2-3410-1586
Fax: 82-2-3410-0025
E-mail: sangyun.ha@skku.edu

Received March 10, 2020
Accepted April 28, 2020
Published Online April 28, 2020

Purpose

Recently, the 8th edition staging system of the American Joint Committee on Cancer (AJCC) for hepatocellular carcinoma (HCC) was released, including a change in T category. We aimed to validate the new AJCC system.

Materials and Methods

The predictive value of the new AJCC was validated in comparison to the previous edition, in a total 1,008 patients who underwent curative resection for HCC as initial treatment.

Results

The 2-year area under the curve values for recurrence-free survival (RFS) and overall survival (OS) were comparable in the 7th and 8th editions. Stage migration was observed in 63 patients (6.3%); from T2 to T1a for 44 patients and from T3 to T4 for 19 patients. The RFS and OS were not different between T1a and T1b in the 8th edition. For solitary tumors ≤ 2 cm, those with microvascular invasion had lower RFS and OS values than those without although they were all classified as T1a in the 8th edition. Tumors involving a major branch of the portal or hepatic vein (T4 by the 8th edition and T3b by the 7th edition) had shorter RFS and OS than multifocal tumors, at least one of which was > 5 cm (T3 by the 8th edition and T3a by the 7th edition).

Conclusion

The AJCC 8th edition staging system for HCC showed comparable predictive performance to the 7th edition. It is desirable in a future revision to consider sub-stratification of solitary tumors ≤ 2 cm (T1a) depending on the presence of vascular invasion, which is not included in the 8th edition.

Key words

Hepatocellular carcinoma, Stage, Prognosis, Microvascular invasion

Introduction

Hepatocellular carcinoma (HCC) comprises 75%-85% of primary liver cancer, which is the sixth most commonly diagnosed cancer and the fourth leading cause of cancer death worldwide [1].

Although hepatic resection is the treatment of choice in HCC, it is not curative because of the high recurrence rate of up to 70% [2]. Therefore, prediction of recurrence and appropriate treatment are important for improved patient outcomes [3].

Among multiple staging systems proposed for stratifying patients with HCC, the American Joint Committee on Cancer (AJCC) staging system for HCC is one of the most commonly used, and the 7th edition of the AJCC system has been validated by various external studies in terms of usefulness and clinical relevance [4-6].

As of January 1, 2018, AJCC 8th edition staging has been used for cancer staging, and there were some notable changes in the T category of HCC compared to the previous version [7,8]. First, solitary tumors with size up to 2 cm are now staged as T1a regardless of the presence of microvascular invasion, unlike in the previous 7th edition, where the presence of microvascular invasion determined whether the tumor is T1 or T2 based on size 2 cm or less. Second, categories named T3b and T4 in the 7th edition are merged into a single T4 category in the new edition and T3a of the 7th edition is renamed as T3 in the 8th edition.

In this study, we validated the predictive value of the new AJCC 8th staging system in comparison to the previous 7th

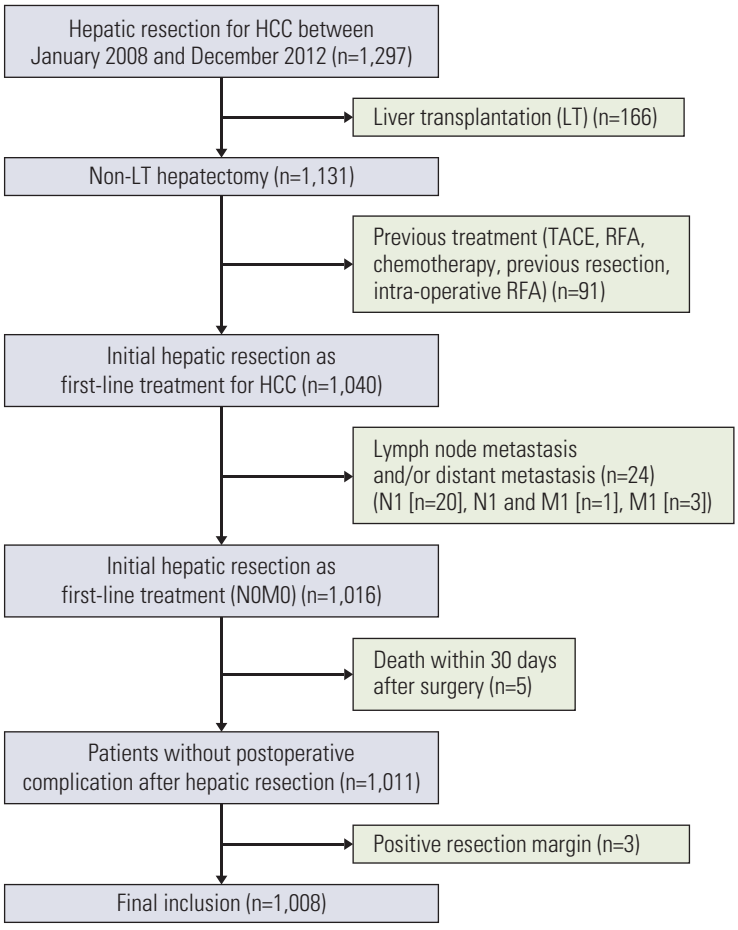

Fig. 1. Summary of patient selection. HCC, hepatocellular carcinoma; TACE, transarterial chemoembolization; RFA, radiofrequency ablation.

edition in a single-institution study population of 1,008 cases. We also attempted to determine how the change in T category predicts prognosis in this population.

Materials and Methods

1. Study patients

Between January 2008 and December 2012, a total of 1,297 patients underwent hepatic resection for HCC at Samsung Medical Center. Initially, 166 liver transplantation (LT) cases were excluded from the study; among the 1,131 non-LT cases, 89 were excluded because they were treated with other modalities before surgery. Other treatment modalities included transarterial chemoembolization, radiofrequency ablation (RFA) and chemotherapy. Two patients were additionally excluded due to previous operative history and intraoperative RFA, respectively. Among the remaining 1,040 patients who underwent hepatic resection as the initial curative treatment for HCC, an additional 32 patients were excluded as follows: five patients died within 30 days after hepatic resection, three patients showed positive resection margins on pathologic examination, and 24 patients had lymph node metastasis or distant metastasis. Finally, 1,008 cases that were appropriate for tumor staging for HCC were considered in retrospective analysis. The process of case selection is summarized in Fig. 1.

2. Clinicopathologic data acquisition and tumor staging

The medical records of patients meeting all inclusion criteria were reviewed for demographic information of sex, age, and clinically underlying etiology of chronic liver disease, if present. The histopathologic features of HCC are collected by reviewing the pathology reports as follow: tumor number, maximal tumor size, differentiation, microvascular invasion, and major branch of portal vein invasion, and the T category was determined using the 7th and 8th editions of the AJCC staging system [7,8]. Presence of chronic hepatitis and fibrosis stage in the background liver parenchyma was also evaluated. The histological differentiation of HCC was graded by the Edmondson and Steiner system, which classifies HCC into four grades from I to IV [9].

Table 1. Summary of clinicopathologhic characteristics of the patients

Characteristic	No. (%)
Sex	
Male	816 (81.0)
Female	192 (19.0)
Age, median (range, yr)	56 (20-83)
Tumor numbers	
Solitary	876 (86.9)
Multifocal	132 (13.1)
Tumor size (cm)	
≤ 2	224 (22.2)
> 2 and ≤ 5	554 (55.0)
> 5	230 (22.8)
Edmondson grade	
I	63 (6.3)
II	872 (86.5)
III	68 (6.7)
IV	5 (0.5)
Microvascular invasion	
(–)	520 (51.6)
(+)	488 (48.4)
Major branch of portal vein invasion	
(–)	989 (98.1)
(+)	19 (1.9)
7th AJCC T category	
T1	472 (46.8)
T2	477 (47.3)
T3a	35 (3.5)
T3b	19 (1.9)
T4	5 (0.5)
8th AJCC T category	
T1a	201 (19.9)
T1b	315 (31.3)
T2	433 (43.0)
T3	35 (3.5)
T4	24 (2.4)
Etiology	
HBV	812 (80.6)
HCV	45 (4.5)
HBV and HCV	4 (0.3)
Alcohol	34 (3.4)
Others	113 (11.2)
Fibrosis stage	
No cirrhosis	564 (56.0)
Cirrhosis	443 (44.0)
Non-diagnostic[a]	1 (0.0)
Recurrence	
(–)	584 (57.9)
(+)	424 (42.1)
Death	
(–)	792 (78.6)
(+)	216 (21.4)

AJCC, American Joint Committee on Cancer; HBV, hepatitis B virus; HCV, hepatitis C virus. [a]Evaluation of fibrosis was limited due to insufficient background not-tumor tissue in one case.

3. Surveillance for tumor recurrence and survival

After surgical resection for HCC, the patients were regularly monitored by dynamic contrast-enhanced computer tomography (CT) and/or magnetic resonance imaging (MRI) and a serum tumor marker such as α-fetoprotein every 3 to 6 months. Diagnosis of recurrence was dependent on radiologic evaluation of CT and/or MRI results. Survival data such as overall survival (OS) and recurrence-free survival (RFS) were also recorded. The durations of RFS and OS were calculated from the date of surgical resection to the date of each event or the last day of follow-up, respectively.

4. Statistical analysis

RFS and OS were estimated using the Kaplan-Meier method and compared by log-rank test. SPSS Statistics ver. 25.0 (IBM Inc., Armonk, NY) was utilized in this analysis. Analysis of the time-dependent receiver operating characteristic (ROC) curves for censored survival data was used to compare the capability of the two models to predict tumor recurrence. This analysis was executed using SAS ver. 9.4 (SAS Institute Inc., Cary, NC) and R 3.6.1 (Vienna, Austria; http://www.R-project.org/). All p-values lower than 0.05 were considered statistically significant.

5. Ethical statement

The Institutional Review Board of Samsung Medical Center approved this study and waived informed consent (IRB No. 2019-08-018).

Results

1. Patients and characteristics

The median age of 1,008 patients was 56 years (range, 20 to 83 years), 816 patients (81.0%) were male and 192 patients (19.0%) were female. The median follow-up period was 64.8 months (standard deviation, 29.7 months; range, 0.7 to 112.5 months). The characteristics of the 1,008 enrolled cases are summarized in Table 1.

2. Stage distribution and migration

When staged by the AJCC 7th edition, the distribution of T category was as follows: T1 (n=472, 46.8%), T2 (n=477,

Table 2. Distribution and migration of T category according to American Joint Committee on Cancer (AJCC) 7th and 8th edition staging system

	Pathologic T category by AJCC 8th edition					Total
	T1a	T1b	T2	T3	T4	
Pathologic T category by AJCC 7th edition						
T1	157	315	0	0	0	472
T2	44	0	433	0	0	477
T3a	0	0	0	35	0	35
T3b	0	0	0	0	19	19
T4	0	0	0	0	5	5
Total	201	315	433	35	24	1,008

47.3%), T3a (n=35, 3.5%), T3b (n=19, 1.9%), and T4 (n=5, 0.5%). When the 8th edition was applied to our study population, the distribution was as follows: T1a (n=201, 19.9%), T1b (n=315, 31.3%), T2 (n=433, 43.0%), T3 (n=35, 3.5%), and T4 (n=24, 2.4%) (Table 2).

Among 472 patients who were staged as T1 by the 7th edition, 157 were reclassified as T1a by the 8th edition, and 315 were reclassified as T1b. Stage migration was also observed. Among the 477 patients that were staged as T2 by the 7th edition, 44 patients migrated to T1a when staged by the 8th edition. Additionally, among 54 patients that were previously staged as T3, 19 migrated to T4 when staged by the 8th edition. In total, the T categories of 63 patients (6.3% of 1,008 patients) were scored differently by the 7th and 8th editions.

3. Prognostic effect of T category in the 7th and 8th editions

The 1-, 3-, and 5-year RFS rates were 74.7%, 55.6%, and 37.9%, respectively, while those of OS were 93.3%, 79.4%, and 58.1%. The survival curves according to the 7th and 8th editions are shown in Figs. 2 and 3. Overall, RFS and OS were different according to T category of both the 7th and 8th editions. However, they were not different between T3b and T4 with the 7th edition or between T1a and T1b in the 8th edition.

According to the survival curves by the 7th edition, both RFS and OS were different between T3a and T3b (p=0.015 for RFS and p=0.035 for OS), but they were not significantly different between T3a and T4 (p=0.306 for RFS and p=0.055 for OS) or T3b and T4 (p=0.886 for RFS and p=0.559 for OS). According to the survival curves for the 8th edition, however, both RFS and OS were not different between T1a and T1b (p=0.380 for RFS and p=0.777 for OS).

The area under the ROC curve (AUC) graphs for recurrence and death were obtained for both the 7th and 8th editions (Fig. 4). The 2-year AUC value for RFS was 0.693 by the 7th edition and 0.690 by the 8th edition (p=0.737). Similarly, the 2-year AUC value for OS was 0.770 by the 7th edition and 0.765 by the 8th edition (p=0.715). These results indicate comparable predictive abilities of T staging by the AJCC 7th and 8th editions in HCC.

4. Prognostic effect of microvascular invasion in HCC ≤ 2 cm

The tumor sizes of 224 cases (22.2% of the 1,008 cases) were 2 cm or less; among these, 201 cases (19.9%) were solitary tumors that were staged as T1a by the AJCC 8th edition. Although they were staged the same, when these 201 cases were classified into two groups according to presence of microvascular invasion, both RFS and OS were statistically significantly lower in the group with microvascular invasion (n=157) than in those without microvascular invasion (n=44) (p=0.037 for RFS and p < 0.001 for OS) (Fig. 5).

5. Involvement of a major branch of the portal or hepatic vein

Of all tumors, 19 (1.9%) involved a major branch of portal vein or hepatic vein and showed T-category migration from T3b by 7th to T4 by the 8th edition. The patients with these tumors had significantly lower RFS and OS values than the 35 cases (34.7%) with multifocal tumors, at least one of which was larger than 5 cm and were classified as T3a by the 7th edition and T3 by the 8th edition (p=0.015 for RFS and p=0.035 for OS) (Fig. 6). These results support the change of 8th edition.

Discussion

The prognostic effect of microvascular invasion has been reported in several previous studies as a negative effector in patient survival [10-12]. A recent meta-analysis study incorporating 14 studies involving 3,033 patients confirmed this issue [13]. However, it is debatable that the prognostic effect of microvascular invasion in small-size HCC ≤ 2 cm is significant. In one study published in 2013 by Shindoh et al. [14], however, the long-term survival of 155 patients (14.0%) with solitary HCC ≤ 2 cm was not affected by microvascular invasion. Based on these data, a part of the pathologic T cat-

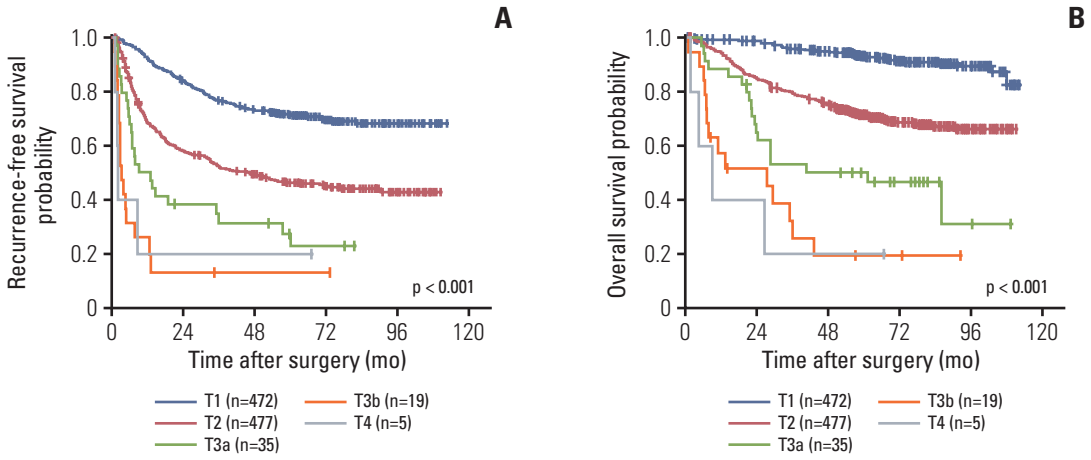

Fig. 2. Kaplan-Meir survival curves according to the American Joint Committee on Cancer T category of the 7th edition: recurrence-free survival (A) and overall survival (B).

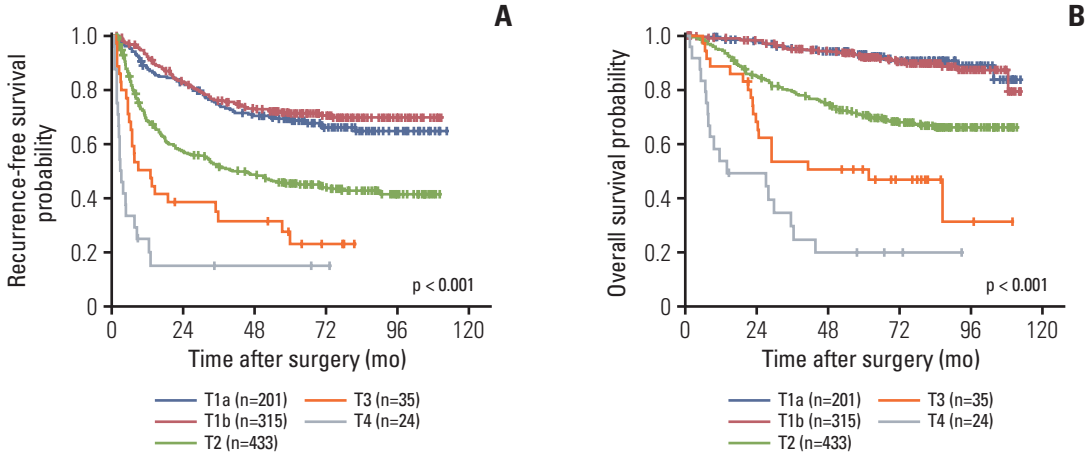

Fig. 3. Kaplan-Meir survival curves according to the American Joint Committee on Cancer T category of the 8th edition: recurrence-free survival (A) and overall survival (B).

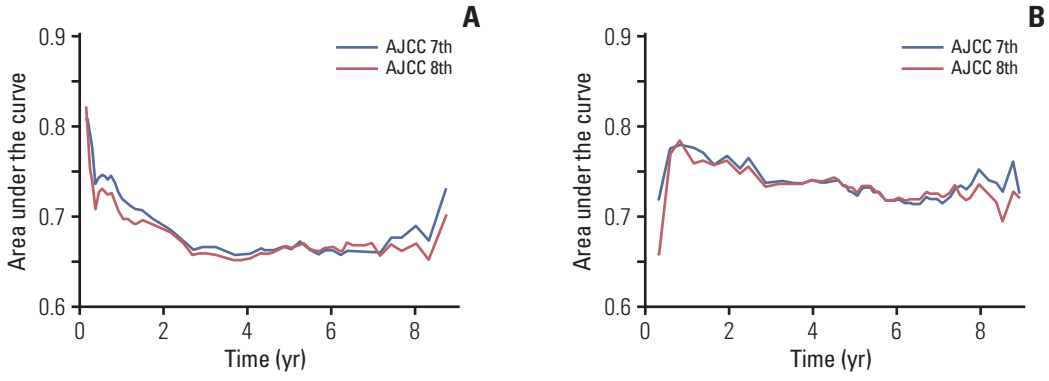

Fig. 4. The area under the curve graphs for recurrence (A) and death (B) by the 7th and 8th editions of the American Joint Committee on Cancer (AJCC) T category.

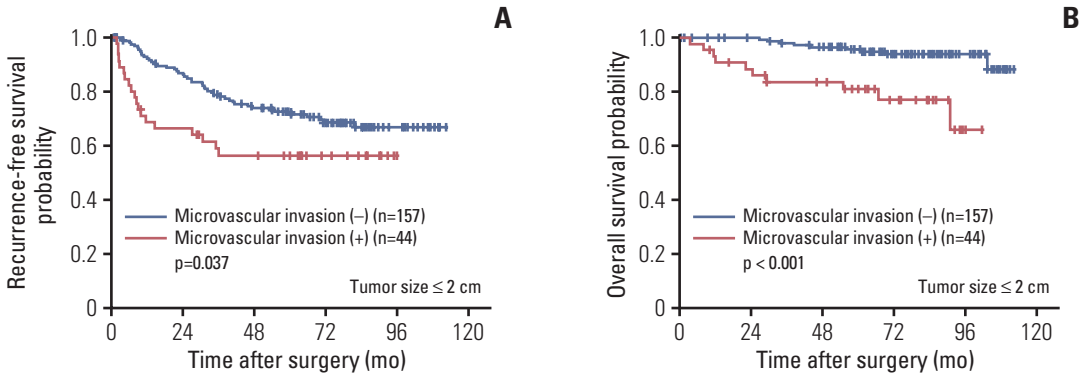

Fig. 5. Kaplan-Meir survival curves of single hepatocellular carcinoma ≤ 2 cm according to presence of microvascular invasion: recurrence-free survival (A) and overall survival (B).

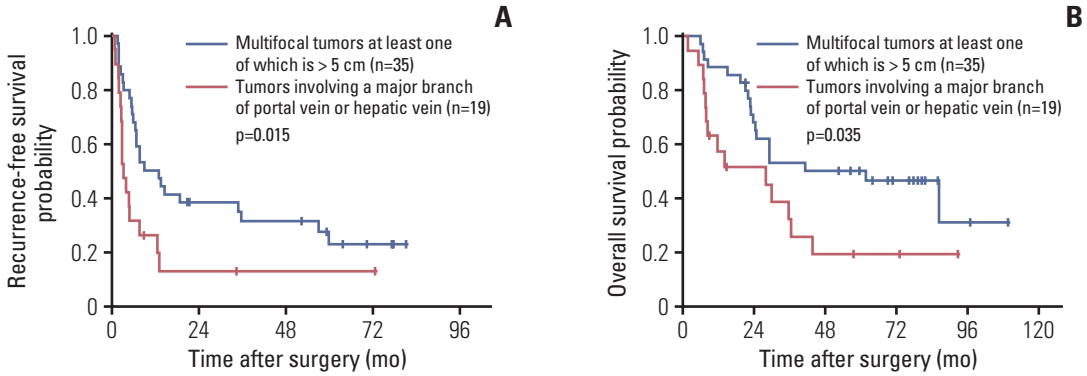

Fig. 6. Kaplan-Meir survival curves of the American Joint Committee on Cancer T category 3a versus 3b of the 7th edition: recurrence-free survival (A) and overall survival (B).

egory was modified from the AJCC 7th edition to the 8th edition. According to the 7th edition, a T1 tumor refers only to a solitary tumor without vascular invasion. If there is vascular invasion, it is staged as T2 even if the tumor is solitary. But, in the 8th edition, the size of the tumor is the determining factor, and all solitary tumors with size 2 cm or less are staged as T1a regardless of the presence of vascular invasion. Tumors are staged as at least T1b when their size is larger than 2 cm, and the presence of vascular invasion determines whether the tumor is T1b or T2. In short, in smaller tumors that are 2 cm or less, the presence of vascular invasion is not considered as a prognostic factor in the updated AJCC 8th edition.

One of the main findings of our study was that solitary tumors ≤ 2 cm with microvascular invasion showed lower RFS and OS values than those without microvascular invasion. The discrepancy between the studies by Shindoh et al. [14] and our group may have been caused by the characteristics of the study population, since people in South Korea receive medical services from tertiary medical institutions due to the national health insurance system. Thus, early-stage cancers can be detected more frequently. The proportion of solitary tumors ≤ 2 cm was higher in our study than in the study by Shindoh et al. [14] (19.9% vs. 14.0%, p < 0.001). Another possible explanation is that there is no standardized guideline for pathologic evaluation of microvascular invasion, but this effect might be limited because the frequency of microvascular invasion in solitary HCC ≤ 2 cm was comparable in these two studies (26.5% vs. 22.3%, p=0.48).

There are some reports supporting our results. Recently, Wang et al. [15] demonstrated that microvascular invasion predicts poor prognosis of solitary HCC ≤ 2 cm based on propensity score matching analysis of 496 patients. Meta-analyses by Chen et al. [13] also showed a prognostic effect of microvascular invasion in solitary HCC ≤ 2 cm.

Another major change in T staging is that T3a in the 7th edition is now re-categorized as T3 in the 8th edition, and tumors involving a major branch of the portal or hepatic vein, which were categorized as T3b in the 7th edition, are reclassified as T4 in the 8th edition. This change was based on a long-term survival study of 754 patients [16], which showed no survival difference between patients with T3a and those with T3b tumors (p=0.073) or between patients with T3b and those with T4 tumors (p=0.227). In our study,

tumors involving a major branch of the portal or hepatic vein (T4 by the 8th edition and T3b by the 7th edition, n=19) showed lower RFS and OS than multifocal tumors, at least one of which was > 5 cm (T3 by the 8th edition and T3a by the 7th edition, n=35) (p=0.015 for RFS and p=0.035 for OS), supporting the change in the 8th edition.

In the RFS and OS curves generated according to AJCC 7th edition T staging (Fig. 2), the curves of the T4 tumors did not follow the estimated survival. Since the inclusion criteria of this study were designed to strictly involve only resectable cases, there are only five cases staged as T4 after resection. The key information related to these T4 tumors is summarized in S1 Table. As described above, neither RFS nor OS was different between T3a and T4 (p=0.055 for RFS and p=0.306 for OS) or T3b and T4 (p=0.886 for RFS and p=0.559 for OS) by the 7th edition. Therefore, although it was a small group, our results related to T4 tumors suggest that tumors involving a major branch of the portal vein or hepatic vein (T3b) may not show better prognosis in the long term than those involving adjacent organs (other than gallbladder) to a resectable extent. This idea is consistent with the change of AJCC staging, since T3b and T4 categories in the 7th edition are merged into the same T4 category in the 8th edition.

The major limitation of this study is that only curatively resected HCCs were enrolled for analysis. Surgical resection is the only modality with which we can definitely determine the presence of microvascular invasion by pathologic evaluation. Since HCCs can be treated by various treatment modalities based on the status of the patients, study population should be extended to overcome this limitation. In further studies, population-based or multicenter analysis that also include HCC cases treated with other modalities other than surgical resection is required to validate the findings of this study and eventually to modify future AJCC staging systems of HCC with the results.

The T category of AJCC 8th edition had comparable predictive performance to the 7th edition, and T4 in the 8th edition, which was established by combining T3b and T4 of the 7th edition, better predicted the prognosis of tumors with higher T category. However, presence of microvascular invasion still has prognostic value in smaller solitary tumors (size ≤ 2 cm), which are all staged as T1a by the AJCC 8th edition. Further studies such as population-based or multicenter analysis incorporating of HCCs with various treatment modalities other than surgical resection are required to validate these findings and to apply the results to future AJCC staging systems for HCC.

Electronic Supplementary Material

Supplementary materials are available at Cancer Research and Treatment website (https://www.e-crt.org).

Conflict of Interest

Conflicts of interest relevant to this article was not reported.

Acknowledgments

This study was funded by the Samsung Medical Center intramural Grant (#SMO1161731) and the Basic Science Research Program through the National Research Foundation of Korea (NRF), funded by the Ministry of Education (NRF-2017R1C1B5017890).

References

1. Bray F, Ferlay J, Soerjomataram I, Siegel RL, Torre LA, Jemal A. Global cancer statistics 2018: GLOBOCAN estimates of incidence and mortality worldwide for 36 cancers in 185 countries. CA Cancer J Clin. 2018;68:394-424.
2. Sherman M. Recurrence of hepatocellular carcinoma. N Engl J Med. 2008;359:2045-7.
3. Portolani N, Coniglio A, Ghidoni S, Giovanelli M, Benetti A, Tiberio GA, et al. Early and late recurrence after liver resection for hepatocellular carcinoma: prognostic and therapeutic imp-lications. Ann Surg. 2006;243:229-35.
4. Cheng CH, Lee CF, Wu TH, Chan KM, Chou HS, Wu TJ, et al. Evaluation of the new AJCC staging system for resectable hepatocellular carcinoma. World J Surg Oncol. 2011;9:114.
5. Kee KM, Wang JH, Lee CM, Chen CL, Changchien CS, Hu TH, et al. Validation of clinical AJCC/UICC TNM staging system for hepatocellular carcinoma: analysis of 5,613 cases from a medical center in southern Taiwan. Int J Cancer. 2007;120: 2650-5.
6. Varotti G, Ramacciato G, Ercolani G, Grazi GL, Vetrone G, Cescon M, et al. Comparison between the fifth and sixth editions of the AJCC/UICC TNM staging systems for hepatocellular carcinoma: multicentric study on 393 cirrhotic resected patients. Eur J Surg Oncol. 2005;31:760-7.
7. Amin MB, Edge S, Greene F, Byrd DR, Brookland RK, Washington MK, et al. AJCC cancer staging manual. 8th ed. New York: Springer; 2017.
8. Edge SB, Byrd DR, Compton CC, Fritz AG, Greene FL, Trotti A. AJCC cancer staging manual. 7th ed. New York: Springer; 2010.
9. Edmondson HA, Steiner PE. Primary carcinoma of the liver: a study of 100 cases among 48,900 necropsies. Cancer. 1954;7: 462-503.
10. Jonas S, Bechstein WO, Steinmuller T, Herrmann M, Radke C, Berg T, et al. Vascular invasion and histopathologic grading determine outcome after liver transplantation for hepatocellular carcinoma in cirrhosis. Hepatology. 2001;33:1080-6.
11. Barreto SG, Brooke-Smith M, Dolan P, Wilson TG, Padbury RT, Chen JW. Cirrhosis and microvascular invasion predict outcomes in hepatocellular carcinoma. ANZ J Surg. 2013;83: 331-5.

12. Rodriguez-Peralvarez M, Luong TV, Andreana L, Meyer T, Dhillon AP, Burroughs AK. A systematic review of microvascular invasion in hepatocellular carcinoma: diagnostic and prognostic variability. Ann Surg Oncol. 2013;20:325-39.
13. Chen ZH, Zhang XP, Wang H, Chai ZT, Sun JX, Guo WX, et al. Effect of microvascular invasion on the postoperative long-term prognosis of solitary small HCC: a systematic review and meta-analysis. HPB (Oxford). 2019;21:935-44.
14. Shindoh J, Andreou A, Aloia TA, Zimmitti G, Lauwers GY, Laurent A, et al. Microvascular invasion does not predict long-term survival in hepatocellular carcinoma up to 2 cm: reappraisal of the staging system for solitary tumors. Ann Surg Oncol. 2013;20:1223-9.
15. Wang H, Wu MC, Cong WM. Microvascular invasion predicts a poor prognosis of solitary hepatocellular carcinoma up to 2 cm based on propensity score matching analysis. Hepatol Res. 2019;49:344-54.
16. Chan AC, Fan ST, Poon RT, Cheung TT, Chok KS, Chan SC, et al. Evaluation of the seventh edition of the American Joint Committee on Cancer tumour-node-metastasis (TNM) staging system for patients undergoing curative resection of hepatocellular carcinoma: implications for the development of a refined staging system. HPB (Oxford). 2013;15:439-48.

pISSN 1598-2998, eISSN 2005-9256

Cancer Res Treat. 2020;52(4):1153-1161

https://doi.org/10.4143/crt.2020.173

Original Article

Open Access

A Multi-cohort Study of the Prognostic Significance of Microsatellite Instability or Mismatch Repair Status after Recurrence of Resectable Gastric Cancer

Ji Yeong An, PhD[1]
Yoon Young Choi, PhD[2,3]
Jeeyun Lee, PhD[4]
Woo Jin Hyung, PhD[2]
Kyoung-Mee Kim, PhD[5]
Sung Hoon Noh, PhD[2]
Min-Gew Choi, PhD[1]
Jae-Ho Cheong, PhD[2,3,6,7]

[1]Department of Surgery, Samsung Medical Center, Sungkyunkwan University School of Medicine, Seoul, [2]Department of Surgery, Yonsei University Health System, Seoul, [3]Yonsei Biomedical Research Institute, Yonsei University Health System, Seoul, [4]Division of Hematology-Oncology, Department of Medicine, [5]Department of Pathology and Translational Genomics, Samsung Medical Center, Sungkyunkwan University School of Medicine, Seoul, [6]YUHS-KRIBB Medical Convergence Research Institute, Seoul, [7]Brain Korea 21 PLUS Project for Medical Science, Yonsei University College of Medicine, Seoul, Korea

Correspondence: Jae-Ho Cheong, MD, PhD
Department of Surgery, Yonsei University College of Medicine, 50 Yonsei-ro, Seodaemun-gu, Seoul 03722, Korea
Tel: 82-2-2228-2094
Fax: 82-2-313-8289
E-mail: JHCHEONG @yuhs.ac

Received March 2, 2020
Accepted May 1, 2020
Published Online May 4, 2020

*Ji Yeong An and Yoon Young Choi contributed equally to this work.

Purpose

High microsatellite instability (MSI) is related to good prognosis in gastric cancer. We aimed to identify the prognostic factors of patients with recurrent gastric cancer and investigate the role of MSI as a prognostic and predictive biomarker of survival after tumor recurrence.

Materials and Methods

This retrospective cohort study enrolled patients treated for stage II/III gastric cancer who developed tumor recurrence and in whom the MSI status or mismatch repair (MMR) status of the tumor was known. MSI status and the expression of MMR proteins were evaluated using polymerase chain reaction and immunohistochemical analysis, respectively.

Results

Of the 790 patients included, 64 (8.1%) had high MSI status or MMR deficiency. The tumor-node-metastasis stage, type of recurrence, Lauren classification, chemotherapy after recurrence, and interval to recurrence were independently associated with survival after tumor recurrence. The MSI/MMR status and receiving adjuvant chemotherapy were not associated with survival after recurrence. In a subgroup analysis of patients with high MSI or MMR-deficient gastric cancer, those who did not receive adjuvant chemotherapy had better treatment response to chemotherapy after recurrence than those who received adjuvant chemotherapy.

Conclusion

Patients with high MSI/MMR-deficient gastric cancer should be spared from adjuvant chemotherapy after surgery, but aggressive chemotherapy after recurrence should be considered. Higher tumor-node-metastasis stage, Lauren classification, interval to recurrence, and type of recurrence are associated with survival after tumor recurrence and should thus be considered when establishing a treatment plan and designing clinical trials targeting recurrent gastric cancer.

Key words

Stomach neoplasms, Recurrence, Microsatellite instability, Prognosis, Biomarker

Introduction

Gastric cancer is among the leading causes of cancer-related death worldwide [1,2]. Surgery and additional chemotherapy with and without radiation therapy are the standard treatment modalities for curative intent of locally advanced gastric cancer [3]. However, over 40% of patients treated with surgery and additional chemotherapy develop tumor recurrence that results in mortality [3,4]. Consequently, the prognostic factors of survival after recurrence (SAR) are clinically important in the treatment of gastric cancer. Nonetheless, only few studies have addressed this issue in

gastric cancer [4,5].

Recent studies on the biology of gastric cancer [6-8] have identified predictive biomarkers of prognosis and chemotherapy response [8-10]. Microsatellite instability (MSI) is one such biomarker. MSI-high (MSI-H) is known to be related to good prognosis and no benefit or even harmful effect from additional chemotherapy after surgery for stage II/III gastric cancer [4,11,12]. These clinical characteristics imply that surgery alone would be an effective strategy for patients with MSI-H gastric cancer. However, some patients with MSI-H still experience tumor recurrence, and thus, clinicians hesitate while forgoing additional chemotherapy because of the fear that no chemotherapy may increase the risk of tumor recurrence [13]. It is unclear whether chemotherapy after recurrence yields a similar benefit between gastric cancer patients who did and did not receive postoperative chemotherapy before recurrence [5,14], particularly according to the MSI status. Thus, this study aimed to identify prognostic factors of patients with recurrent gastric cancer and investigate the role of the MSI status as a prognostic and predictive biomarker of SAR.

Materials and Methods

1. Population

Two large cohorts, namely the Y-cohort and S-cohort, were included in this study. The Y-cohort was based on the population of a previous study that reported the clinical implication of the MSI status for stage II/III gastric cancer [15], while the S-cohort was based on the population of previous studies on various biomarkers and molecular markers [7]. All patients underwent gastrectomy for curative intent and were pathologically confirmed to have stage II or III gastric cancer according to the 8th edition of the American Joint Committee on Cancer [16]. The additional chemotherapy and follow-up strategy were employed according to the guidelines [17,18]. We included patients with tumor recurrence and in whom the MSI or mismatch repair (MMR) status was known. Patients who received chemotherapy or radiation therapy before surgery and whose primary cancer was in the remnant stomach were excluded. Patients in whom the cancer was in the remnant stomach after initial gastrectomy but were treated via surgery with curative intent were also excluded.

2. Clinicopathologic variables

We retrospectively reviewed the clinicodemographic characteristics, including sex and age during initial gastric cancer diagnosis, presence of serosa invasion and lymph node metastasis, TNM stage, Lauren classification, location of tumor, MSI/MMR status, whether or not the patient received adjuvant chemotherapy, type of recurrence, interval between initial gastrectomy to tumor recurrence (< 1 year, ≥ 1 year and < 2 years, ≥ 2 years), and whether or not the patient received chemotherapy after recurrence. The type of recurrence was classified as locoregional, hematogenous, peritoneum, any combination, and ovarian metastasis only. Recurrence and survival were determined based on records from the hospital and the Korean National Statistical Office and through telephone surveys.

3. Definition of MSI and MMR

The MSI status was evaluated in the Y-cohort using polymerase chain reaction (PCR). DNA was extracted from paired normal tissue and tumor tissue that were formalin-fixed, paraffin embedded, and amplified using PCR for two mononucleotide repeat markers (BAT25 and BAT26) and three dinucleotide markers (D5S346, D2S123, and D17S250) [19]. MSI-H was defined as an instability at two or more markers; otherwise, it was defined as microsatellite stable (MSS).

The expression of MMR proteins was evaluated in the S-cohort via immunohistochemical (IHC) analysis. Samples from tissue microarray blocks were used to prepare 3- to 4-μm-thick sections for analysis, and monoclonal antibodies, including mouse anti-MLH1 (#PA0610, Leica Biosystem, Buffalo Grove, IL), mouse anti-MSH2 (#286M-16, Cell Marque, Rocklin, CA), mouse anti-MSH6 (#610919, BD Transduction, San Jose, CA), and rabbit anti-PMS2 (#288M-16, Cell Marque), were used for staining. Deficient MMR (dMMR) was defined as loss of any MMR protein expression in ≥ 80% of tumor cells while internal control nuclei (lymphocytes and stromal cells) are stained [20]. Two pathologists independently performed the evaluations.

4. Statistical analysis

Statistical analysis was performed using SPSS ver. 20.0 for Windows (IBM Corp., Armonk, NY) and R software ver. 3.4.3. Categorical variables are described as numbers and proportions and were compared using a chi-square test. Continuous variables are described as mean with standard deviation and were compared using an independent t test. Patient prognosis was evaluated according to SAR, which was defined as the time from recurrence to death due to any cause. The SAR of each group was generated using Kaplan-Meier curves and compared using log-rank test. A Cox proportional hazard model was used with the hazard ratio (HR) and its 95% confidence interval (CI). Institution was used as the adjustment variable for the overall analysis. Subgroup analysis was conducted with respect to each institution. The final multivariable model comprised variables that were statistically significant in the univariable analysis and were selected using likelihood forward methods. A two-sided p-value of < 0.05 was considered statistically significant.

Table 1. Clinicopathologic characteristics of the patients, initial gastric cancer stage, and treatments

Characteristic	No. (%) (n=790)
Age, mean±SD (yr)	57.18±12.53
Sex	
Male	521 (65.9)
Female	269 (34.1)
Serosa invasion	
Negative	355 (44.9)
Positive	435 (55.1)
LN metastasis	
Negative	64 (8.1)
Positive	726 (91.9)
TNM stage	
II	188 (23.8)
III	602 (76.2)
Lauren classification	
Intestinal	293 (37.1)
Diffuse/Mixed	497 (62.9)
Tumor location	
UB/Whole	133 (16.8)
MB/LB	657 (83.2)
MSI/MMR	
MSS/pMMR	726 (91.9)
MSI-H/dMMR	64 (8.1)
Adjuvant CTx[a]	
No	214 (27.3)
Yes	570 (72.7)
Interval to recurrence (yr)	
< 1	322 (40.8)
≥ 1, < 2	237 (30.0)
≥ 2	231 (29.2)
Type of recurrence	
Locoregional	132 (16.7)
Hematogenous	154 (19.5)
Peritoneum	336 (42.5)
Any combination	142 (18.0)
Krukenberg only	26 (3.3)
CTx after recurrence[a]	
No	265 (35.1)
Yes	489 (64.9)

LN, lymph node; UB, upper body; MB, mid-body; LB, lower body; MSI, microsatellite instability; MMR, mismatch repair; MSS, microsatellite stable; pMMR, proficient mismatch repair; MSI-H, microsatellite instability high; dMMR, deficient mismatch repair; CTx, chemotherapy. [a]Information was incomplete in some patients because of transfer to other hospital, loss of follow-up, and unclear medical records.

5. Ethical statement

This study was approved by the Institutional Review Board (approval number 4-2019-0244), and the need for informed consent was waived.

Results

1. Baseline characteristics of the patients, initial gastric cancer stage, and treatment

The overall cohort comprised 790 patients (439 and 351 patients from the Y-cohort and the S-cohort, respectively); of these, 65.9% were men. In total, 602 patients (76.2%) were treated for stage III gastric cancer. With respect to Lauren histology, 293 (37.1%) and 497 (62.9%) patients had an intestinal and diffuse/mixed type, respectively. There were 64 patients with MSI-H/dMMR gastric cancer (8.1%), and 570 patients (72.7%) received adjuvant chemotherapy after gastrectomy. Over 70% of patients developed tumor recurrence within 2 years after initial surgery; the most common type was peritoneal recurrence (42.5%). Furthermore, 64.9% of patients were administered chemotherapy after tumor recurrence (Table 1). The proportion of serosa-positive cases, MSI-H/dMMR cases, and cases treated with both adjuvant and post-recurrence chemotherapy; TNM stage; interval to recurrence; and type of recurrence were significantly different between the Y-cohort and S-cohort (S1 Table).

Consequently, institution was used as an adjustment variable in the following analysis. The type of recurrence was similar between MSI-H/dMMR and MSS/proficient MMR (pMMR) tumors (S2 Table).

2. Factors related to prognosis after recurrence

In the overall population, age (adjusted HR, 1.007; 95% CI, 1.011 to 1.013; p=0.025), serosa invasion (adjusted HR, 1.324; 95% CI, 1.128 to 1.555; p=0.001), TNM stage (adjusted HR, 1.288; 95% CI, 1.086 to 1.527; p=0.004), Lauren classification (adjusted HR, 1.470; 95% CI, 1.264 to 1.708; p < 0.001), chemotherapy after recurrence (adjusted HR, 0.363; 95% CI, 0.306 to 0.431; p < 0.001), interval from surgery to recurrence (p < 0.001), and type of recurrence (p < 0.001) were significantly associated with SAR (Table 2); in contrast, sex, presence of lymph node metastasis, location of tumor, and receiving adjuvant chemotherapy were not. The associations between clinicopathologic variables, except MSI/MMR status, and SAR were similar in both cohorts (S3 Table).

In the overall cohort, MSI-H/dMMR was not associated with SAR (adjusted HR, 1.155; 95% CI, 0.885 to 1.506; p=0.290) (Table 2, S4A Fig.). However, in the subgroup analysis by institutions, MSI-H was related to poor SAR in the Y-cohort (HR, 1.544; 95% CI, 1.038 to 2.298; p=0.032) (S3 Table, S4B Fig.), while there were no significant differences in SAR according to the MMR status in the S-cohort (HR, 0.950; 95% CI, 0.667 to 1.354; p=0.777) (S3 Table, S4C Fig.). In the institution-adjusted multivariable analysis, TNM stage, Lauren classification, interval to recurrence, type of recurrence, and chemotherapy after recurrence were independent factors related to SAR (Table 3).

Table 2. Univariable Cox proportional hazard model for survival after recurrence

	Overall cohort	
	Adjusted HR[a] (95% CI)	p-value
Age	1.007 (1.001-1.013)	0.025
Sex		0.362
Male	1	
Female	1.072 (0.923-1.246)	
Serosa invasion		0.001
Negative	1	
Positive	1.324 (1.128-1.555)	
LN metastasis		0.325
Negative	1	
Positive	1.141 (0.878-1.482)	
TNM stage		0.004
II	1	
III	1.288 (1.086-1.527)	
Lauren classification		< 0.001
Intestinal	1	
Diffuse/Mixed	1.470 (1.264-1.708)	
Tumor location		0.202
UB/Whole	1	
MB/LB	1.135 (0.934-1.378)	
MSI/MMR		0.290
MSS/pMMR	1	
MSI-H/dMMR	1.155 (0.885-1.506)	
Adjuvant CTx		0.176
No	1	
Yes	0.894 (0.760-1.052)	
Interval to recurrence (yr)		< 0.001
< 1	1	
≥ 1, < 2	0.768 (0.647-0.912)	0.003
≥ 2	0.650 (0.545-0.776)	< 0.001
Type of recurrence		< 0.001
Locoregional	1	
Hematogenous	1.010 (0.793-1.288)	0.935
Peritoneum	1.434 (1.163-1.768)	0.001
Any combination	1.603 (1.256-2.045)	< 0.001
Krukenberg only	0.614 (0.393-0.961)	0.033
CTx after recurrence		< 0.001
No	1	
Yes	0.363 (0.306-0.431)	

HR, hazard ratio; CI, confidence interval; LN, lymph node; UB, upper body; MB, mid-body; LB, lower body; MSI, microsatellite instability; MMR, mismatch repair; MSS, microsatellite stable; pMMR, proficient mismatch repair; MSI-H, microsatellite instability high; dMMR, deficient mismatch repair; CTx, chemotherapy. [a]Adjusted by institution.

3. Effect of chemotherapy according to MSI/MMR status

Additional analyses were conducted to evaluate the effects of adjuvant chemotherapy and chemotherapy after recurrence in the overall cohort and according to the MSI/MMR status. In the overall cohort, patients who received chemotherapy after recurrence had longer SAR regardless of whether or not they received adjuvant chemotherapy (log-rank $p < 0.001$) (Table 4, Fig. 1A), and a similar finding was noted in both cohorts (log-rank $p < 0.001$ and $p < 0.001$ in the Y-cohort and S-cohort, respectively) (S5A and S5B Fig.). A similar finding was observed in MSS/pMMR tumors of overall cohort and in both cohorts (Fig. 1B, S6A and S6B Fig.).

Among patients with MSI-H/dMMR tumors, those who

Table 3. Multivariable Cox proportional hazard model for survival after recurrence in the overall cohort

	Adjusted HR[a] (95% CI)	p-value
TNM		0.049
II	1	
III	1.199 (1.001-1.435)	
Lauren classification		< 0.001
Intestinal	1	
Diffuse/Mixed	1.515 (1.294-1.775)	
Interval to recurrence (yr)		< 0.001
< 1	1	
≥ 1, < 2	0.754 (0.631-0.902)	0.002
≥ 2	0.648 (0.539-0.778)	< 0.001
Type of recurrenc[b]		< 0.001
Locoregional/Hematogenous	1	
Peritoneum/Combination	1.326 (1.085-1.620)	0.006
Krukenberg only	0.665 (0.416-1.061)	0.087
Chemotherapy after recurrence		< 0.001
No	1	
Yes	0.367 (0.309-0.435)	

HR, hazard ratio; CI, confidence interval. [a]Adjusted by institution, [b]Variables were categorized into three according to having similar HRs.

received chemotherapy only after recurrence had the longest SAR (Table 4), and the prognosis of patients who received adjuvant chemotherapy was similar regardless of whether they did or did not receive chemotherapy after recurrence (log-rank p=0.020) (Fig. 1C). Similar findings were observed in the Y-cohort (log-rank p=0.080) and S-cohort (log-rank p=0.053) (S7A and S7B Fig.).

Discussion

This study investigated the prognostic factors of patients with recurrent gastric cancer and the role of the MSI status as a prognostic and predictive biomarker of SAR. We found that among patients with MSI-H/dMMR recurrent gastric cancer, treatment response to chemotherapy after recurrence differed according to whether or not the patient received adjuvant chemotherapy. To the best of our knowledge, this is the first study to report such a result. This finding is clinically valuable because chemotherapy in the adjuvant setting would be detrimental to patients with stage II/III MSI-H/dMMR gastric cancer when they develop tumor recurrence. Given that patients with MSI-H/dMMR stage II/III gastric cancer generally have favorable prognosis and that adjuvant/perioperative chemotherapy yields no benefit in reducing the risk of tumor recurrence [4,11,12], these patients should be spared from adjuvant chemotherapy, with surgery alone being the most effective treatment strategy. This finding may be due to the acquired resistance from adjuvant chemotherapy and the negative effects of chemotherapy on patient immunity. The mechanism for this has been hypothesized as follows: (1) DNA-targeted cytotoxic chemotherapy increases treatment resistance in tumors lacking MMR activity, causing the selection of resistant MMR-deficient tumors, and this condition could increase genetic instability, heterogeneity, and selection of more invasive tumor cells [21]. Consequently, adjuvant chemotherapy for patients with MSI-H/dMMR gastric cancer could cause chemotherapy resistance without reducing the risk of tumor recurrence, and recurrence leads to poor prognosis. (2) MSI-H/dMMR tumors are related to enriched immune cells that may be responsible for the suppression of residual micrometastases after surgery [22,23], and chemotherapy may induce immune suppression [24]. In addition, chemotherapy may have a negative effect on immune surveillance, and the innate benefit from a hypermutated phenotype could be attenuated [12]. These negative effects of chemotherapy on the patient's immunity could lead to poor prognosis after tumor recurrence.

Our findings could lead to a clinical dilemma because not all patients with MSI-H/dMMR can be cured via surgery alone, and a tangible clinical benefit could be expected from adjuvant treatment in some patients with high-risk MSI-H/dMMR gastric cancer [13,25]. Because patients with MSI-H/dMMR tumors are possible candidates for immune-checkpoint inhibitor treatment [26,27], adjuvant immunotherapy would be a better strategy than conventional chemotherapy for this population. However, the superiority of adjuvant immunotherapy still needs to be verified. In addition, given that the prognosis of MSI-H/dMMR tumors could vary according to certain biomarkers [28,29], secondary biomarkers that can be used to guide adjuvant treatment for this spe-

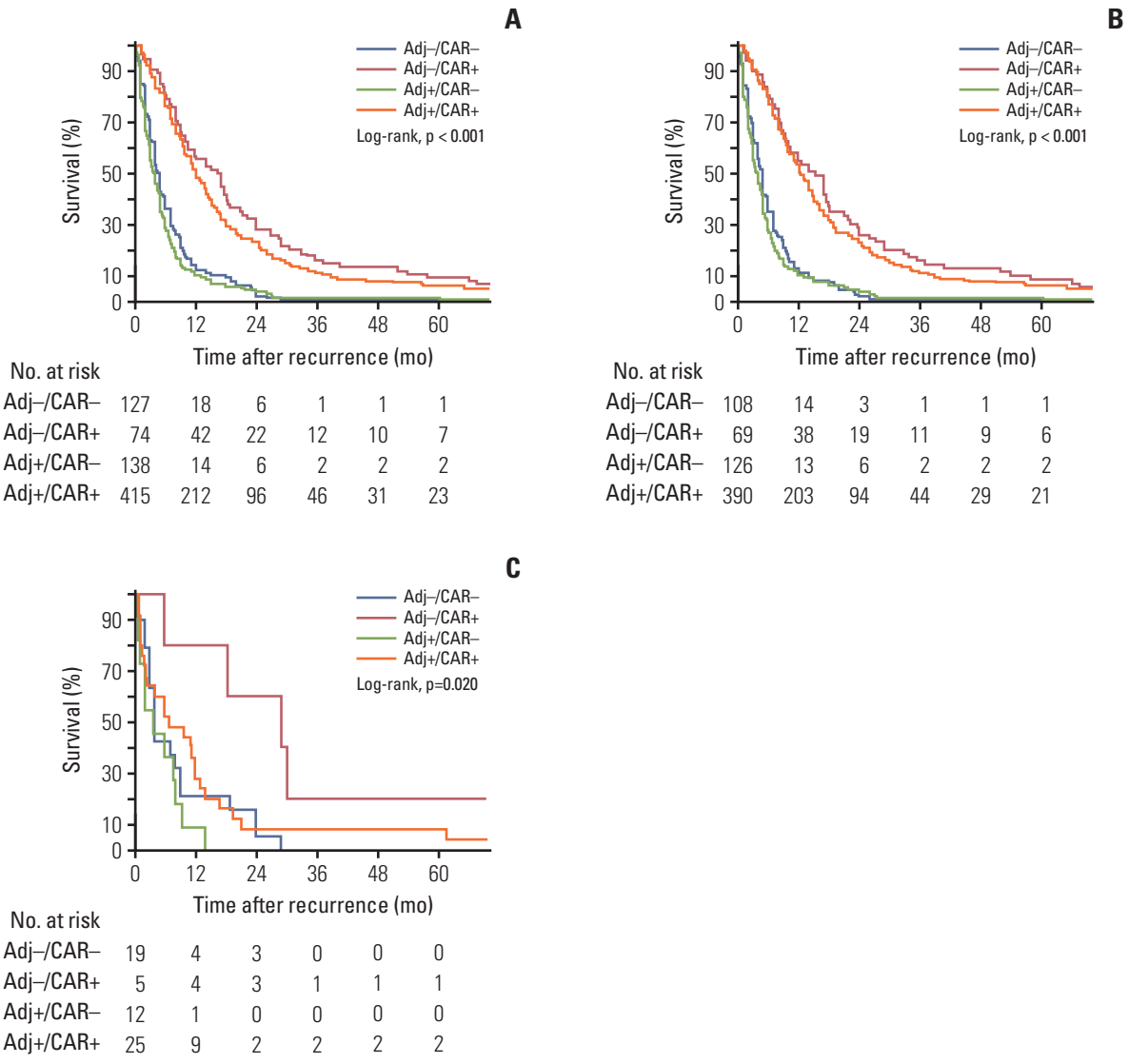

Fig. 1. Kaplan-Meier curves for survival after recurrence according to receiving adjuvant chemotherapy and chemotherapy after recurrence. (A) Regardless of the MSI/MMR status. (B) MSS/pMMR tumor. (C) MSI-H/dMMR tumors in the overall cohort. MSI, microsatellite instability; MRR, mismatch repair; MSS, microsatellite stable; pMMR, proficient MMR; MSI-H, MSI-high; dMMR, deficient MMR; n, number of patients; Adj, adjuvant chemotherapy; CAR, chemotherapy after recurrence.

cific type of gastric cancer should be investigated [13].

In this study, SAR was not statistically different according to the MSI/MMR status, but it differed according to the cohort. MSI-H was related to shorter SAR in the Y-cohort, while there was no difference in SAR between dMMR and pMMR patients in the S-cohort. This finding may be due to the following reasons: (1) the effect of chemotherapy might differ according to the MSI/MMR status, and the proportion of patients receiving adjuvant chemotherapy and chemotherapy after recurrence differed significantly between the cohorts in this study. (2) The Y-cohort was derived from a consecutive cohort enrolled between 2000 and 2010, while the S-cohort was derived from molecular or biomarker studies conducted between 1995 and 2008. (3) The MSI/MMR status was assessed using different methods in the cohorts, i.e., PCR in the Y-cohort and IHC analysis in the S-cohort. In colorectal cancer, the association between the MSI/MMR status and prognosis after recurrence has been conflicting. A study on the molecular subtypes of colorectal cancer reported worse survival after relapse in those with MSI-H type [30], while a study of two randomized clinical trials reported longer SAR among patients with dMMR colon cancers [28] and attributed this to the difference in recurrence pattern according to the MMR status (regional vs. distant type). A similar recurrence pattern of MSI-H/dMMR and MSS/pMMR tumors in this study resulted in a similar SAR, and

Table 4. Association between treatment and survival after recurrence in the overall cohort and by MSI/MMR status

	Adjusted HR[a] (95% CI)	p-value
Overall		< 0.001
Adj–/CAR+	1	
Adj+/CAR+	1.229 (0.947-1.596)	0.121
Adj–/CAR–	2.820 (2.062-3.856)	< 0.001
Adj+/CAR–	3.583 (2.658-4.831)	< 0.001
MSS/pMMR		< 0.001
Adj–/CAR+	1	
Adj+/CAR+	1.133 (0.867-1.481)	0.359
Adj–/CAR–	2.798 (2.012-3.890)	< 0.001
Adj+/CAR–	3.356 (2.464-4.570)	< 0.001
MSI-H/dMMR		< 0.001
Adj–/CAR+	1	
Adj+/CAR+	5.360 (1.472-19.517)	0.011
Adj–/CAR–	4.491 (1.412-14.290)	0.011
Adj+/CAR–	12.052 (3.065-47.391)	< 0.001

MSI, microsatellite instability; MMR, mismatch repair; HR, hazard ratio; CI, confidence interval; Adj, adjuvant chemotherapy; CAR, chemotherapy after recurrence; MSS, microsatellite stable; pMMR, proficient mismatch repair; MSI-H, microsatellite instability high; dMMR, deficient mismatch repair. [a]Adjusted by age, sex, and institution.

the effect of chemotherapy when administered before and after recurrence needs to be considered when evaluating the prognosis after recurrence according to the MSI/MMR status. Additional evidence is needed to determine whether the MSI/MMR status could be a useful biomarker even after tumor recurrence.

Given that initial tumor stage, Lauren classification, interval to recurrence, and type of recurrence were significantly related to SAR, these factors should be considered for patient stratification in clinical trials for recurrent gastric cancer. More advanced initial tumor stage may be related to more subclinical metastases and aggressive biologic behaviors that result in more progressive recurrence [14]. The diffuse histology of gastric cancer is related to cancer stemness and being refractory to chemotherapy [6,8], and this could lead to shorter SAR. Tumors that recur at a longer interval from initial treatment may tend to behave in a more indolent manner after recurrence. Peritoneal and combination recurrence would be less responsive to oral or intravenous chemotherapy and may yield a higher tumor burden that could cause shorter SAR.

This study enrolled patients from the two largest gastric cancer-specialized centers in Korea. Considering the low prevalence of MSI-H/dMMR gastric cancer with its favorable prognosis, this cohort may be the largest to date. In addition, this study is the first to evaluate the effects of both chemotherapy before and after recurrence according to SAR biomarkers of gastric cancer. However, there are also possible limitations of this study that need to be addressed. The effects of chemotherapy after recurrence were likely overestimated as some patients died before chemotherapy could be implemented after tumor recurrence. Moreover, the retrospective design of this study and the different chemotherapy regimens used for adjuvant chemotherapy and chemotherapy after recurrence made it difficult to conduct more subgroup analysis for the effect of chemotherapies before and after recurrence by MSI/MMR status, and it might be another limitation. Despite these limitations, our results provide clinical insight into the behavior of MSI-H/dMMR gastric cancer in the setting of standard of care and provide instrumental information for deciding on the appropriate treatment strategy for recurrent gastric cancer.

In conclusion, chemotherapy only after recurrence yields high SAR in gastric cancer patients with MSI-H/dMMR. This shows that in MSI gastric cancer, only post-recurrence chemotherapy and not adjuvant chemotherapy is beneficial. Furthermore, TNM stage, Lauren classification, interval to recurrence, and type of recurrence are associated with SAR and should thus be considered when creating the treatment plan and designing clinical trials targeting recurrent gastric cancer.

Electronic Supplementary Material

Supplementary materials are available at Cancer Research and Treatment website (https://www.e-crt.org).

Conflict of Interest

Conflict of interest relevant to this article was not reported.

References

1. Bray F, Ferlay J, Soerjomataram I, Siegel RL, Torre LA, Jemal A. Global cancer statistics 2018: GLOBOCAN estimates of incidence and mortality worldwide for 36 cancers in 185 countries. CA Cancer J Clin. 2018;68:394-424.
2. Jung KW, Won YJ, Kong HJ, Lee ES. Cancer statistics in Korea: incidence, mortality, survival, and prevalence in 2016. Cancer Res Treat. 2019;51:417-30.
3. Noh SH, Park SR, Yang HK, Chung HC, Chung IJ, Kim SW, et al. Adjuvant capecitabine plus oxaliplatin for gastric cancer after D2 gastrectomy (CLASSIC): 5-year follow-up of an open-label, randomised phase 3 trial. Lancet Oncol. 2014;15:1389-96.
4. Pietrantonio F, Miceli R, Raimondi A, Kim YW, Kang WK, Langley RE, et al. Individual patient data meta-analysis of the value of microsatellite instability as a biomarker in gastric cancer. J Clin Oncol. 2019;37:3392-400.
5. Ito S, Ohashi Y, Sasako M. Survival after recurrence in patients with gastric cancer who receive S-1 adjuvant chemotherapy: exploratory analysis of the ACTS-GC trial. BMC Cancer. 2018;18:449.
6. Cancer Genome Atlas Research Network. Comprehensive molecular characterization of gastric adenocarcinoma. Nature. 2014;513:202-9.
7. Cristescu R, Lee J, Nebozhyn M, Kim KM, Ting JC, Wong SS, et al. Molecular analysis of gastric cancer identifies subtypes associated with distinct clinical outcomes. Nat Med. 2015;21:449-56.
8. Cheong JH, Yang HK, Kim H, Kim WH, Kim YW, Kook MC, et al. Predictive test for chemotherapy response in resectable gastric cancer: a multi-cohort, retrospective analysis. Lancet Oncol. 2018;19:629-38.
9. Yong WP, Rha SY, Tan IB, Choo SP, Syn NL, Koh V, et al. Real-time tumor gene expression profiling to direct gastric cancer chemotherapy: proof-of-concept "3G" trial. Clin Cancer Res. 2018;24:5272-81.
10. Roh CK, Choi YY, Choi S, Seo WJ, Cho M, Jang E, et al. Single patient classifier assay, microsatellite instability, and Epstein-Barr virus status predict clinical outcomes in stage II/III gastric cancer: results from CLASSIC trial. Yonsei Med J. 2019;60:132-9.
11. Choi YY, Kim H, Shin SJ, Kim HY, Lee J, Yang HK, et al. Microsatellite instability and programmed cell death-ligand 1 expression in stage II/III gastric cancer: post hoc analysis of the CLASSIC randomized controlled study. Ann Surg. 2019;270:309-16.
12. Smyth EC, Wotherspoon A, Peckitt C, Gonzalez D, Hulkki-Wilson S, Eltahir Z, et al. Mismatch repair deficiency, microsatellite instability, and survival: an exploratory analysis of the Medical Research Council Adjuvant Gastric Infusional Chemotherapy (MAGIC) trial. JAMA Oncol. 2017;3:1197-203.
13. Choi YY, Cheong JH. Comment on "To treat, or not to treat, that is the question: biomarker-guided adjuvant chemotherapy for stage II and III gastric cancer". Ann Surg. 2019;270:e40-1.
14. O'Connell MJ, Campbell ME, Goldberg RM, Grothey A, Seitz JF, Benedetti JK, et al. Survival following recurrence in stage II and III colon cancer: findings from the ACCENT data set. J Clin Oncol. 2008;26:2336-41.
15. Kim SY, Choi YY, An JY, Shin HB, Jo A, Choi H, et al. The benefit of microsatellite instability is attenuated by chemotherapy in stage II and stage III gastric cancer: results from a large cohort with subgroup analyses. Int J Cancer. 2015;137:819-25.
16. Amin MB, Edge SB, Greene FL, Byrd DR, Brookland RK, Washington MK, et al. AJCC cancer staging manual. 8th ed. New York: Springer; 2017.
17. Guideline Committee of the Korean Gastric Cancer Association (KGCA), Development Working Group and Review Panel. Korean practice guideline for gastric cancer 2018: an evidence-based, multi-disciplinary approach. J Gastric Cancer. 2019;19:1-48.
18. Japanese Gastric Cancer Association. Japanese gastric cancer treatment guidelines 2014 (ver. 4). Gastric Cancer. 2017;20:1-19.
19. Boland CR, Thibodeau SN, Hamilton SR, Sidransky D, Eshleman JR, Burt RW, et al. A National Cancer Institute Workshop on Microsatellite Instability for cancer detection and familial predisposition: development of international criteria for the determination of microsatellite instability in colorectal cancer. Cancer Res. 1998;58:5248-57.
20. Cho J, Kang SY, Kim KM. MMR protein immunohistochemistry and microsatellite instability in gastric cancers. Pathology. 2019;51:110-3.
21. Meyers M, Wagner MW, Hwang HS, Kinsella TJ, Boothman DA. Role of the hMLH1 DNA mismatch repair protein in fluoropyrimidine-mediated cell death and cell cycle responses. Cancer Res. 2001;61:5193-201.
22. Grogg KL, Lohse CM, Pankratz VS, Halling KC, Smyrk TC. Lymphocyte-rich gastric cancer: associations with Epstein-Barr virus, microsatellite instability, histology, and survival. Mod Pathol. 2003;16:641-51.
23. Chiaravalli AM, Feltri M, Bertolini V, Bagnoli E, Furlan D, Cerutti R, et al. Intratumour T cells, their activation status and survival in gastric carcinomas characterised for microsatellite instability and Epstein-Barr virus infection. Virchows Arch. 2006;448:344-53.
24. Onyema OO, Decoster L, Njemini R, Forti LN, Bautmans I, De Waele M, et al. Chemotherapy-induced changes and immunosenescence of CD8+ T-cells in patients with breast cancer. Anticancer Res. 2015;35:1481-9.
25. Mondaca S, Yoon SS, Strong VE, Ku GY, Ilson DH, Greally M, et al. Comment on "Microsatellite instability as a predictive biomarker for adjuvant chemotherapy in gastric cancer": are we there yet? Ann Surg. 2019;270:e39-40.
26. First tissue-agnostic drug approval issued. Cancer Discov. 2017;7:656.
27. Le DT, Uram JN, Wang H, Bartlett BR, Kemberling H, Eyring AD, et al. PD-1 blockade in tumors with mismatch-repair deficiency. N Engl J Med. 2015;372:2509-20.
28. Sinicrope FA, Shi Q, Allegra CJ, Smyrk TC, Thibodeau SN, Goldberg RM, et al. Association of DNA mismatch repair and mutations in BRAF and KRAS with survival after recurrence in stage III colon cancers: a secondary analysis of 2 rand-

omized clinical trials. JAMA Oncol. 2017;3:472-80.
29. Cho J, Lee J, Bang H, Kim ST, Park SH, An JY, et al. Programmed cell death-ligand 1 expression predicts survival in patients with gastric carcinoma with microsatellite instability. Oncotarget. 2017;8:13320-8.
30. Guinney J, Dienstmann R, Wang X, de Reynies A, Schlicker A, Soneson C, et al. The consensus molecular subtypes of colorectal cancer. Nat Med. 2015;21:1350-6.

pISSN 1598-2998, eISSN 2005-9256

Cancer Res Treat. 2020;52(4):1162-1177 https://doi.org/10.4143/crt.2020.138

Original Article Open Access

FGFR4 Gly388Arg Polymorphism Affects the Progression of Gastric Cancer by Activating STAT3 Pathway to Induce Epithelial to Mesenchymal Transition

Yanwei Ye, PhD[1]
Jie Li, MD[2]
Dongbao Jiang, MD[3]
Jingjing Li, PhD[4]
Chuangfeng Xiao, MD[1]
Yingze Li, MD[1]
Chao Han, PhD[5]
Chunlin Zhao, PhD[1]

[1]*Department of Gastrointestinal Surgery and Institute of Clinical Medicine, The First Affiliated Hospital of Zhengzhou University, Zhengzhou,* [2]*Department of General Surgery, Tongchuan People's Hospital, Shanxi,* [3]*Department of Thyroid, and Breast Surgery, Xinxiang Central Hospital, Xinxiang, Departments of* [4]*Infectious Disease and* [5]*Pharmacy, The First Affiliated Hospital of Zhengzhou University, Zhengzhou, China*

Correspondence: Yanwei Ye, PhD
Department of Gastrointestinal Surgery and Institute of Clinical Medicine, The First Affiliated Hospital of Zhengzhou University, 1 Eastern Jian-She Road, Zhengzhou, Henan 450052, China
Tel: 86-13838389763
Fax: 86-037167967236
E-mail: yeyanwei66@163.com

Received February 24, 2020
Accepted May 24, 2020
Published Online May 25, 2020

*Yanwei Ye and Jie Li contributed equally to this work.

Purpose
Fibroblast growth factor receptor 4 (FGFR4) plays a critical role in cancer progression involving in tumor proliferation, invasion, and metastasis. This study clarified the role of FGFR4-Arg388 variant in gastric cancer (GC), and more importantly highlighted the possibility of this single nucleotide polymorphism (SNP) as potential therapeutic targets.

Materials and Methods
FGFR4 polymorphism was characterized in advanced GC patients to perform statistical analysis. FGFR4-dependent signal pathways involving cell proliferation, invasion, migration, and resistance to oxaliplatin (OXA) in accordance with the SNP were also assessed in transfected GC cell lines.

Results
Among 102 GC patients, the FGFR4-Arg388 patients showed significantly higher tumor stage (p=0.047) and worse overall survival (p=0.033) than the Gly388 patients. Immunohistochemical results showed that FGFR4-Arg388 patients were more likely to have higher vimentin (p=0.025) and p-STAT3 (p=0.009) expression compared with FGFR4-Gly388 patients. In transfected GC cells, the overexpression of FGFR4-Arg388 variant increased proliferation and invasion of GC cells, increasing resistance of GC cells to OXA compared with cells overexpressing the Gly388 allele.

Conclusion
The exploration mechanism may be through FGFR4-Arg388/STAT3/epithelial to mesenchymal transition axis regulating pivotal oncogenic properties of GC cells. The FGFR4-Arg388 variant may be a biomarker and a candidate target for adjuvant treatment of GC.

Key words
Fibroblast growth factor receptor 4, Gly388Arg polymorphism, Gastric neoplasms, STAT3, Epithelial to mesenchymal transition

Introduction

The U.S. Food and Drug Administration (FDA) approved herceptin and ramucirumab for the treatment of advanced gastric cancer (GC), while the overall effect was not satisfactory. Therefore, whether there are new molecular markers to be pivotal in the occurrence and development of GC, as well as further targeted drugs worthy of research and development, will become a further breakthrough in the field of GC research.

In recent years, a mass of molecular changes having an important role in the pathogenesis and prognosis of tumor patients have been confirmed. The fibroblast growth factor receptor 4 (FGFR4) has been proven therapeutic potential in a variety of cancer types [1], which has been connected with process and prognosis in several kinds of cancer, involving GC [2-4]. FGFR-Arg388 variant (rs351855 at the genotype level), contains an amino acid rep-lacement of an arginine for a glycine at codon 388. FGFR4-Arg388 variant plays a role in susceptibility to oral squamous cell carcinoma,

pituitary tumors, and neuroblastoma [5-7]. FGFR4-Arg388 variant was a new independent prognostic factor and correlated with tumor poorer prognosis in various tumors [8-10]. FGFR4-Arg388 variant also affects the tumor biological behavior. For example, FGFR4-Gly388 tumors express incremental prolactin and less growth hormone, whereas tumors holding the polymorphic variant of FGFR4-Arg388 express enhancive growth hormone with respect to prolactin [11].

The FGFR4-Arg388 variant has been declared to be associated with multiple signaling pathways. Ulaganathan and Ullrich [12] believe FGFR4-Arg388 variant might expose a proximal STAT3 binding site and have confirmed that FGFR4-Arg388 variant could induce enhanced STAT3 signal. The FGFR4-Arg388 allele produces a receptor variant that preferentially promotes STAT3/5 signaling, transcriptionally inducing Grb-14 in pancreatic endocrine cells to promote insulin secretion [13]. Moreover, FGFR4-Arg388 variant has been related to epithelial to mesenchymal transition (EMT), inducing expression of EMT-associated proteins [14,15]. The FGFR4 variant induces STAT3 activation and the expression of EMT-related genes, thereby causing pro-oncogenic effects in lung cancer *in vitro* and *in vivo* [16]. In the current research, we aimed to explore the potential effect of the FGFR4-Arg388 variant on GC biological behavior, its resistance to oxaliplatin (OXA), its impact on patients' pathological features and prognosis in this setting, whether it was caused by EMT and STAT3 pathways, with exploration of the relationship creatively.

Materials and Methods

1. Patients

Collection of 102 consecutive primary GC tissue samples was in the First Affiliated Hospital of Zhengzhou University (Zhengzhou, China). All patients were diagnosed and treated at this hospital. All GC patients without any chemotherapy, radiotherapy, and other therapies prior to radical gastrectomy. All cases were pathologically recorded and approved by the hospital ethics committee to record personal files for clinical data. Staging must be based on the American Joint Committee on Cancer (AJCC) tumor, lymph node metastasis system (TNM) staging for GC staging (7th edition, 2010) [17]. Follow-up data were acquired by telephone, letter acquisition, and outpatient clinical database. The survival time was calculated based on the date from the completion of the surgery to the date of death or the date of the last follow-up. Follow-up time was from January 2010 to December 2017.

2. Immunohistochemical staining

The expression of FGFR4, E-cadherin (E-cad), vimentin (Vim), STAT3, and p-STAT3 in paraffin-embedded tumor specimens of all selected patients was detected by immunohistochemistry. The concentrations of antibodies and positive sites were as follows: anti-FGFR4, dilution 1:500, positive site was cytoplasm; anti–E-cad, dilution 1:200, positive site was cell membrane; anti-Vim, dilution 1:500, positive site was cytoplasm; anti-STAT3, dilution of 1:100, the positive sites were the nucleus and cytoplasm; anti–p-STAT3, dilution of 1:200, the positive sites were the nucleus and cytoplasm; the negative control (NC) was achieved by incubating the parallel slides to omit the accordingly primary antibody.

3. Immunohistochemical staining scoring

Slides were semi-quantitatively evaluated by two independent pathologists who were blinded to the patient's clinical data when scoring the immunohistochemical results of the archival tissue samples. Cytoplasmic FGFR4 immunostaining was scored (quaternary system): negative (–), low (+), intermediate (++), and high expression (+++) [18]. Finally, the percentage of positive staining cells was scored according to the intensity score of each part: Vim of positive tumor cells dispersed throughout the section, constituting at least 10% [19]; When > 10% of tumor membranes were stained, E-cad expression was positive [20]. Overexpression of STAT3 and p-STAT3 were defined as nuclear staining of more than 30% of tumor cells in GC [21].

4. Genotyping

Genomic DNA was removed from the 102 tumor tissue stored in 4% paraformaldehyde. A 120-bp fragment possessing the Gly388Arg polymorphism was polymerase chain reaction (PCR) amplified using polymerized forward primer, 5′-CAGTACCTGTCGGGCCAGAG-3′; reverse, 5′-CTTGGCTGTGCTCCTGCTG-3′. One microliter of PCR products were labeled with the BigDye sequencing kit (Applied Biosystems, Foster City, CA) and the recommended operating conditions were on the basis of the manufacturer's instructions. The sequence data were interpreted with the DNSstar software (Fig. 1A).

5. Cell lines and cell culture

Human GC cell lines AGS, NCI-N87, MGC803, and MKN-45 were obtained from the American Type Culture Collection. The BGC803 and SGC7901 cell lines were purchased from the Chinese Academy of Sciences, Science Bank of the typical Culture Collection (CBTCCCAS, Shanghai, China). Cell lines were cultured in RPMI-1640 medium (Gibco, Grand Island, NY) supplemented with 10% fetal bovine serum (FBS; Gibco), 100 U/mL penicillin and 100 μg/mL streptomycin (Caisson Labs, North Logan, UT) with a humidified atmosphere containing 5% CO_2 at 37°C.

6. Antibodies and reagents

Rabbit monoclonal anti–E-cad (#3195), anti-Vim (#5741),

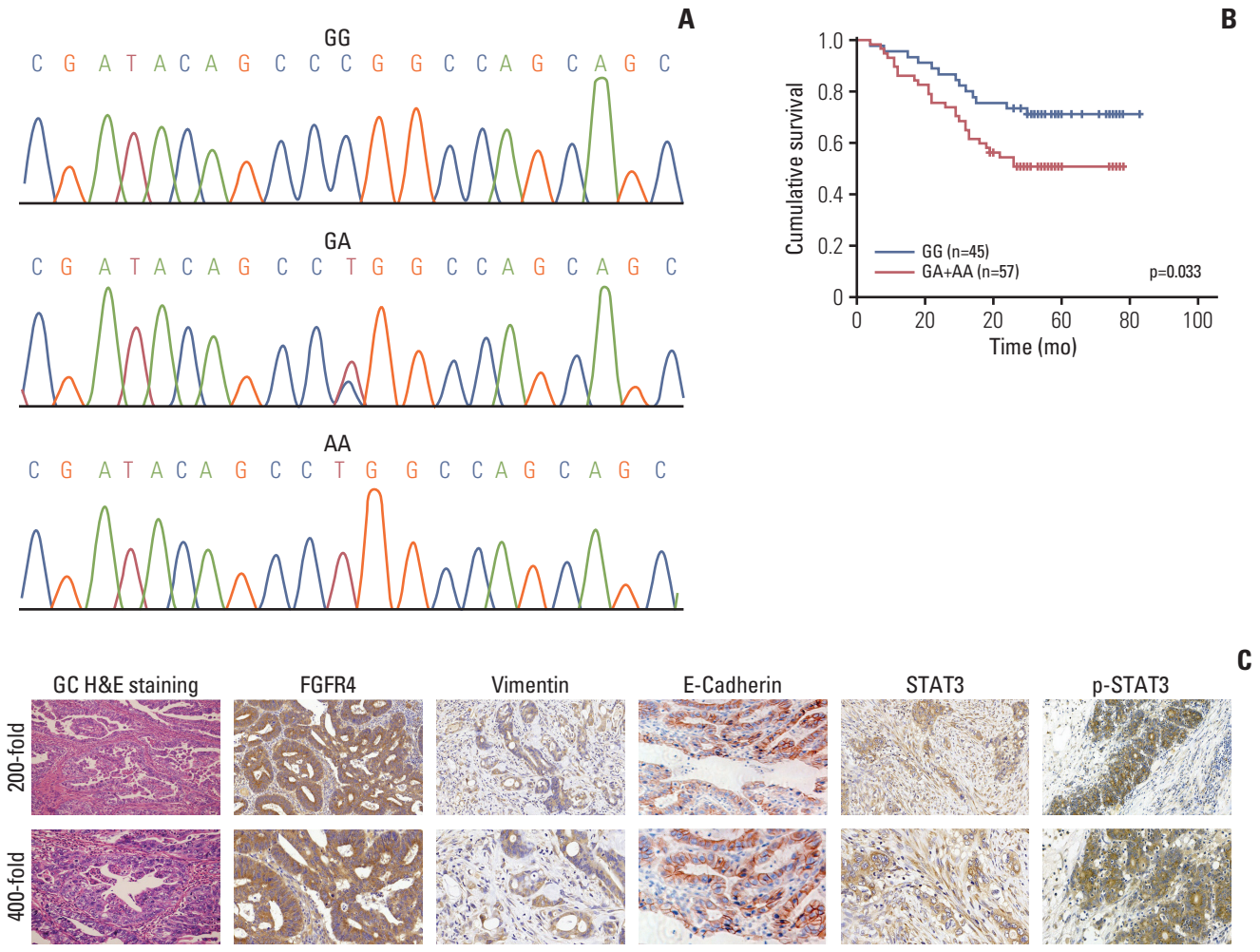

Fig. 1. (A) Gene sequencing including three specific fibroblast growth factor receptor 4 (*FGFR4*) Gly388Arg polymorphic genotype (including Gly/Gly, Gly/Arg, and Arg/Arg). (B) Significant difference was observed between patients with FGFR4-Gly388 allele and FGFR4-Arg388 variant among 102 gastric cancer (GC) patients after stratified Kaplan-Meier survival analysis. (C) Strong positive expressions of immunohistochemical markers in GC tissue were demonstrated. All H&E staining and immunohistochemical pictures were amplified 200-fold (upper) and 400-fold (lower).

anti–p-STAT3 (#9145), anti–caspase-3 (#14220), and anti–cleaved caspase-3 (#9664) as well as mouse monoclonal anti–β-actin (#3700) and anti-STAT3 (#9139) were all bought in Cell Signaling Technology (Beverly, MA). The anti-FGFR4 antibody was purchased by Proteintech (#11098-1-AP) (Wuhan, China). Secondary horseradish peroxidase-conjugated antibodies were goat anti-mouse and goat anti-rabbit from Sigma-Aldrich Corp. (St. Louis, MO). AG490 was bought from Sigma-Aldrich Corporation (Shanghai, China). In addition, OXA came from our clinical trial group at the research center.

7. Lentiviral overexpression vector construction and transfection

Lentiviral overexpression vector construction and transfection (pHBLV-CMV-MCS-3flag-EF1-puro, including FGFR4-Gly388, FGFR4-Arg388, and NC) were completed by Hanbio (Shanghai, China). The primer sequences of FGFR4-Gly388 were as follows: 5′-ggatctattccggtGaattcGCCACCATGCGGCTGCTGCTGGCCCTGTT-3′ and 5′-CTTAAGCTTGGTACCGAggatccTGTCTGCACCCCAGACCCGAA-3′. The primer sequences of FGFR4-Arg388 were as follows: 5′-ggatctatttccggtGaattcGCCACCATGCGGCTGCTGCTGGCCCTGTT-3′ and 5′-CTTAAGCTTGGTACCGAggatccTGTCTGCACCCCAGACCCGAA-3′. GC cells were seeded in a 24-well plate at a density of 5×10^5 cells per well for 24 hours, then infected by adding the prepared virus according to the manufacturer's instructions. After the virus control group completely died under the action of puromycin, the cells of the experimental group were considered to be completely screened.

8. Reverse transcription PCR and quantitative real-time PCR

Total RNA was collected from GC cell lines using TRIzol reagent. DNA synthesis kit (MBI, Fermentas, Canada) was reversely transcribed into cDNA of each RNA sample. Primers were: FGFR4, 5′-agatactcaaagacaacgcct-3′ and 5′-cgcactccacgatcacgta-3′; β-actin, 5′-cacgatggaggggccggactcatc-3′ and 5′-taaagacctctatgccaacacacagt-3′. Two Taq PCR MasterMix (Takara, Tokyo, Japan) was used for PCR amplification. *FGFR4* annealing temperature for 57°C. PCR products were electrophoresis with 2% agarose gel and stained with ethyl bromide. According to the instructions of Takara, the mRNA expression of FGFR4 in six GC cell lines was detected by quantitative real-time PCR (q-PCR). Repeat the experiment three times. Relative differences were calculated according to the comparative Ct method.

9. Protein extraction and western blot

Whole cell lysates were prepared using protein extraction reagents (Merck, Darmstadt, Germany). Protein samples boiled for 10 minutes (30 μg per protein) were added to a 10% sodium dodecyl sulfate polyacrylamide gel for electrophoretic separation and transferred to a polyvinylidene difluoride (PVDF) membrane. The PVDF membrane was blocked in phosphate buffered saline (PBS) containing 0.05% Tween-20 and 5% skim milk powder for 1 hour at room temperature, and incubated with primary antibody overnight at 4°C. Then wash the PVDF membrane three times with PBS containing 0.05% Tween-20 and 1% skim milk powder. The PVDF membrane was then incubated with the secondary antibody for 1 hour at room temperature. The protein imprint was detected by an ECL detection system (Image-Quant LAS 3000, General Electric Co., Fairfield, CT). At least all samples were performed on three independent western blot analyses.

10. Apoptosis assay

GC cells, including mock, NC, and FGFR4-Gly388 and FGFR4-Arg388 overexpression groups were dealt with OXA at proper concentration (average value of IC_{50} of mock group and NC group) for 24 hours. Annexin V and propidium iodide (PI) were used for cell apoptosis detection by flow cytometry and fluorescence microscope (Nikon, Tokyo, Japan). Then cells were combined in 500 μL annexin V binding buffer and incubated with 5 μL Annexin V–PI in the dark and at room temperature for 15 minutes. After that, all samples were analyzed by FACS Calibur flow cytometry with CellQuest software (Thermo Fisher Scientific, Waltham, MA) and photographed under a fluorescence microscope.

11. Cell proliferation assays

Cell viability was assessed using Cell Counting Kit-8 (CCK-8) reagent (Dojindo Laboratories, Kumamoto, Japan) and EdU reagent (Ribobio, Guangzhou, China).

1) CCK-8 proliferation assay

One hundred microliters of cell medium containing 2,000 cells was seeded into each well of 96-well plates. After 1, 2, 3, 4, and 5 days of culture respectively, the supernatant was removed. The absorbance at 450 nm was measured using a microplate reader.

2) Gradient concentration CCK-8 assays

After culturing for 24 hours, cells were dealt with OXA at different concentrations ladder (0, 1, 2, 4, 8, 16, 32, 64, 128, and 256 μg). After 72 hours of culture, the supernatant was removed. The absorbance was measured at 450 nm with a microplate reader. Cell viability and IC_{50} were calculated for subsequent experiments.

3) EdU proliferation assay

Cells were seeded in 24-well plates at 4×10^5 cells/well in 1 mL of culture medium. Each hole was incubated at room temperature for 30 minutes with 300-400 μL cell stationary fluids (PBS containing 4% paraformaldehyde). Two hundred microliters of 1× Apollo staining reaction solution was added to each well to mark EdU. Each well was incubated with 200 μL 1× Hoechst 33342 reaction solutions at room temperature and decolorize shaker for 30 minutes for DNA staining. Under ultraviolet light, the cell nuclei were all stained blue, and the proliferating nuclei were stained red under a green light.

12. Matrigel invasion and invasion assay

The polycarbonate filter (8-μm pore size) was covered with Matrigel gel (BD Biosciences, Franklin Lakes, NJ) at a concentration of 1 μg/mL and placed in a 24-well cell culture plate. Each well was inoculated 1×10^5 cells of 100 μL of FBS-free medium in the upper part of the chamber, while the lower part of the chamber was filled with medium containing 20% FBS as a control. After incubation at 37°C for 72 hours, cells invaded with Matrigel membrane were fixed with 4% formaldehyde and stained with hematoxylin and eosin (H&E) reagent. Wipe off the non-migrating cells on the upper side of the filter. Calculate at least 10 locations per filter. For cell scratch assays, SGC7901 and BGC803 cells (mock, NC, FGFR4-Gly388, and FGFR4-Arg388) in 6-well plates were scored with well-defined scratches and cultured for 24 hours. Obtain images under the fluorescence microscope at the same interval for 8 hours. The migration distance is quantified by Image-Pro Plus software (Media Cybemetics, Rockville, MD).

13. Statistical analysis

The connection between FGFR4 expression and clinicopathological factors as well as other immunohistochemical markers was assessed by chi-square test. Survival curves

Table 1. Association analysis of the *FGFR4* Gly388Arg polymorphism and clinicopathological parameters in gastric cancer patients

Variable	Total (n=102)	GG (n=45)	GA+AA (n=57)	Pearson's χ^2 value	p-value
Age (yr)					
< 60	52	23	29	0.001	> 0.99
≥ 60	50	22	28		
Sex					
Male	74	35	39	1.105	0.373
Female	28	10	18		
Tumor size (cm)					
< 4	67	30	37	0.004	> 0.99
≥ 4	34	15	19		
Differentiation					
G1+G2	44	16	28	1.887	0.227
G3+G4	58	29	29		
T category					
T1+T2	43	24	19	4.125	0.047
T3+T4	59	21	38		
N category					
N0	47	29	28	0.607	0.436
N1+N2+N3	54	26	28		
M category					
M0	95	41	51	2.713	0.130
M1	7	1	6		
Borrmann type					
Local type (early GC+I+II)	50	15	35	3.494	0.071
Infiltrating type (III+IV)	52	25	27		
Lauren type					
Intestinal type	45	17	28	0.070	0.840
Diffuse infiltration type	57	23	34		
WHO type					
Tubular adenocarcinoma	42	17	25	3.264	0.515
Papillary adenocarcinoma	3	0	3		
Mucous adenocarcinoma	3	2	1		
Signet ring cell carcinoma	18	8	10		
Poorly differentiated adenocarcinoma	36	13	23		
FGFR4 status					
Low expression	33	17	16	1.083	0.394
High expression	69	28	41		
STAT3 status					
Negative	37	14	23	0.929	0.408
Positive	65	31	34		
p-STAT3 status					
Negative	46	27	19	7.222	0.009
Positive	56	18	38		
Vimentin status					
Negative	41	24	17	5.781	0.025
Positive	61	21	40		
E-cadherin status					
Negative	35	12	23	2.089	0.208
Positive	67	33	34		

FGFR4, fibroblast growth factor receptor 4; GC, gastric cancer; WHO, World Health Organization.

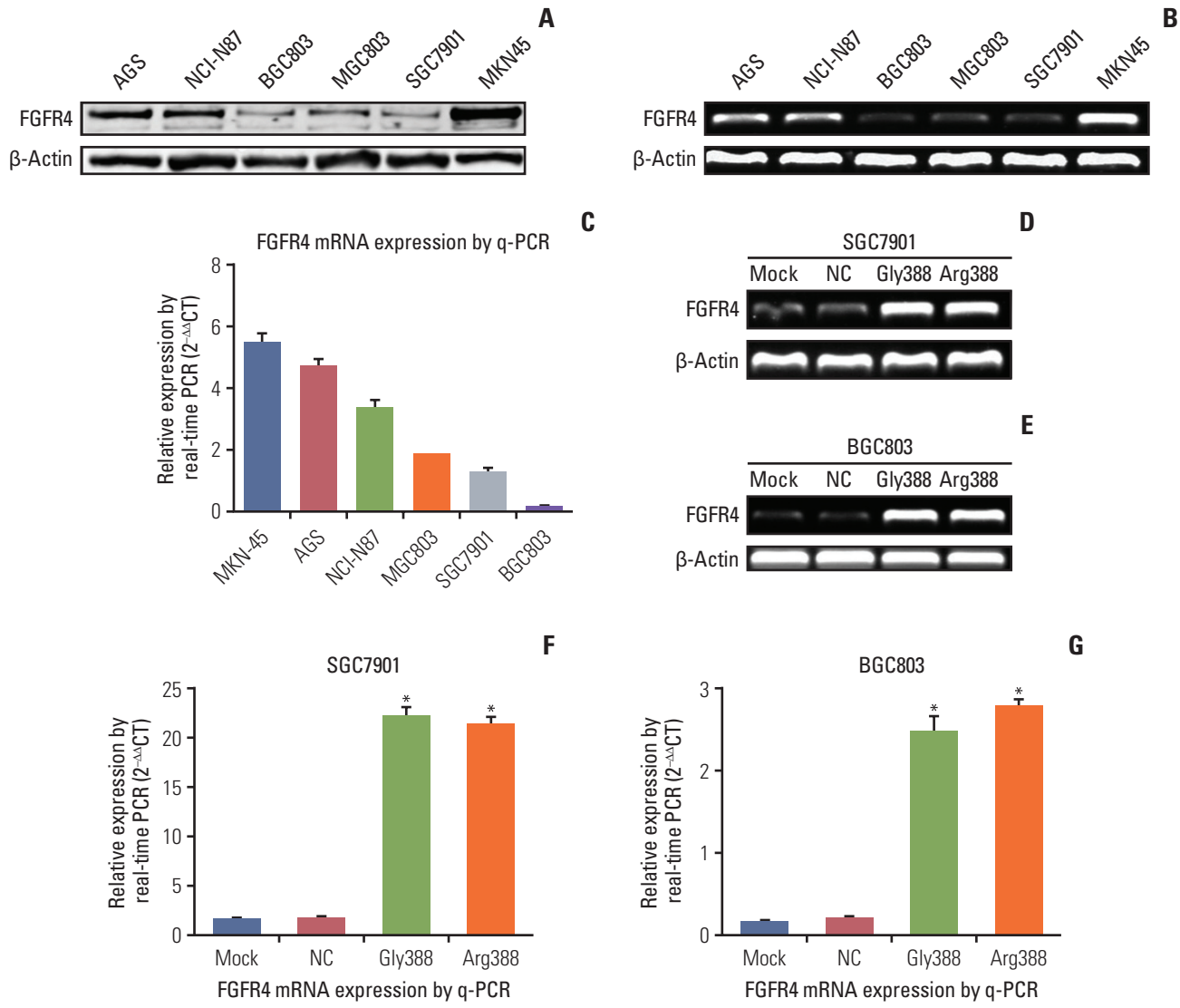

Fig. 2. The expressions of fibroblast growth factor receptor 4 (FGFR4) mRNA and protein were illustrated in various gastric cancer (GC) cell lines and transfected cells. (A) Expressions of FGFR4 protein in different GC cell lines by western blot. (B) Expressions of FGFR4 mRNA in different GC cells by reverse transcription polymerase chain reaction (RT-PCR). (C) Expressions of FGFR4 mRNA in different GC cells by quantitative real-time polymerase chain reaction (q-PCR). Expressions of FGFR4 mRNA in SGC7901 (D) and BGC803 (E) cells (mock, negative control [NC], Gly388-transfected, and Arg388-transfected) by RT-PCR. Expressions of FGFR4 mRNA in SGC7901 (F) and BGC803 (G) cells (mock, NC, Gly388-transfected, and Arg388-transfected) by q-PCR. β-Actin was served as loading control. At least three independent detecting were performed. *$p < 0.05$.

were calculated by Kaplan-Meier method, and differences between survival curves were examined with the log-rank test. All the statistical tests were bilateral, with a significance at the 0.05 level. SPSS ver. 17.0 statistical software (SPSS Inc., Chicago, IL) was used for statistical analysis and graph drawing, which was used to collect and classify patients' clinical pathology and follow-up data, covering sex, age, tumor size, differentiation, tumor stage, lymph node status, distant metastases, Borrmann type (divided into local type including early GC, uplift type [I], ulcer type [II] and infiltrating type including infiltrating ulcer type [III] and diffuse infiltrating type [IV]), Lauren type, World Health Organization type (WHO), and expression of relevant tumor markers.

14. Ethical statement

The study was approved by the Institutional Review Board of The First Affiliated Hospital of Zhengzhou University (IRB No. YB M-05-02) and performed in accordance with the principles of the Declaration of Helsinki. Written informed consents were obtained.

Results

1. Correlation of *FGFR4* Gly388Arg single nucleotide polymorphism with clinicopathological characteristics and prognosis of GC patients

The relationship between pathological parameters and related protein expression in 102 GC patients and *FGFG4* polymorphism was summarized in Table 1. We then stratified FGFR4-Gly388 and FGFR4-Arg388 patients according to *FGFR4* single nucleotide polymorphism (SNP). FGFR4-Arg388 variant was observed in GC patients with higher tumor stage (T3+T4) (p=0.047), while no correlation with sex (p=0.373), age (p > 0.99), tumor size (p > 0.99), differentiation (p=0.227), lymph node status (p=0.436), distant metastases (p=0.130), Borrmann type (p=0.071), Lauren type (p=0.840), and WHO type (p=0.515). It was worth mentioning that Borrmann type (p=0.071) may be statistically significant if the sample size was increased. A significant correlation was observed between FGFR4-Arg388 variant and the expression of Vim (p=0.025) as well as p-STAT3 (p=0.009) expression in GC, while no correlation with the expression of FGFR4 (p=0.394), STAT3 (p=0.408), and E-cad (p=0.208). Moreover, Kaplan-Meier survival analysis showed that FGFR4-Arg388 variant in GC patients were significantly correlated with a poorer prognosis in terms of cumulative survival compared with FGFR4-Gly388 allele (p=0.033) (Fig. 1B). Typical immunohistochemical positive expression of the five related molecules and H&E staining for morphological features of GC can be seen in Fig. 1C.

2. FGFR4 expression differed in various GC cell lines

FGFR4 was expressed in GC lines at mRNA and protein levels using q-PCR, reverse transcription PCR (RT-PCR), and western blot analysis. As Fig. 2A displayed, the protein expression of FGFR4 was more obvious in MKN45 and AGS, while weaker in MGC803, SGC7901, and BGC803. RT-PCR results showed that mRNA expression of FGFR4 was distinctly stronger in MKN45 and AGS than in the other four GC cell lines (Fig. 2B). As showed in Fig. 2C, the quantitative analysis results by q-PCR verified that the mRNA expression of FGFR4 in SGC7901 and BGC803 was weaker than the other GC cell lines. Hence, the SGC7901 and BGC803 cell lines which were utilized to construct different *FGFR4* genetic phenotype were chosen to conduct subsequent assays.

3. FGFR4-Gly388 allele and FGFR4-Arg388 allele were verified to be over-expressed

The stable overexpression of FGFR4-Gly388 and FGFR4-Arg388 in GC cells were conducted by transfection of lentiviral overexpression vector (pHBLV-CMV-MCS-3flag-EF1-puro) for the following functional assays. The efficiency of transfection of vector was checked by RT-PCR and q-PCR. As Fig. 2D and E shown, the expression of FGFR4-Gly388 and FGFR4-Arg388 mRNA was remarkably increased in SGC7901 and BGC803 (vector transfection groups) compare with mock and NC groups. As shown in Fig. 2F and G, the quantitative analysis results by q-PCR also verified that FGFR4 mRNA expression in SGC7901 and BGC803 vector transfection groups was significantly higher. Actually, all tests had proved effective in increasing FGFR4 mRNA expression, as measured by RT-PCR and q-PCR.

4. FGFR4-Arg388 allele enhanced proliferation, invasion, and migration

Compared with mock and NC cells, the proliferation of Gly388-transfected and Arg388-transfected cells was considerably enhanced. Results of CCK-8 proliferation assay showed that the absorbency was higher in FGFR4-Arg388 groups than that in FGFR4-Gly388 groups, particularly after 3, 4, and 5 days of culture (Student's t test, $p < 0.05$) (Fig. 3A). Similarly, proliferation of BGC803 Arg388-tranfected cells obviously increased in comparison to the other three groups ($p < 0.05$) (Fig. 3B). The same results were achieved for EdU proliferation assay. The proportion of Arg388-transfected cells proliferation were higher compared to the other three groups in SGC7901 (Students t test, $p < 0.05$) (Fig. 3C and E) and BGC803 (Student's t test, $p < 0.05$) (Fig. 3D and F). When compared with mock and NC groups, Gly388-transfected and Arg388-transfected cells showed significantly more cell invasion. As shown in Fig. 3G, the number of SGC7901 cells invading the Matrigel-coated membrane in the FGFR4-Arg388 group was much higher than that in the FGFR4-Gly388 group ($p < 0.05$) (Fig. 3I). Similarly, the number of BGC803 cells in the FGFR4-Arg388 group was significantly higher than that in the FGFR4-Gly388 group (Fig. 3H), and the difference was statistically significant ($p < 0.05$) (Fig. 3J). Similar results were also observed using a cell scratch assay in SGC-7901 (Fig. 3K and M) and BGC803 ($p < 0.05$) (Fig. 3L and N). Together, these results indicated that both the Arg388-transfected and Gly388-transfected cells evidently increased the proliferation, migration, and invasion in GC cells, whereas that overexpression of the FGFR4-Arg388 variant was stronger than Gly388 allele.

5. FGFR4-Arg388 variant can increase the resistance of OXA

To assess the effect of OXA on the growth of SGC7901 and BGC803 cells at different concentrations, we used CCK-8 proliferation assay to observe cell viability. Fig. 4A and B show the cell viability of SGC7901 and BGC803 cells at different concentrations of OXA, and the IC_{50} in Arg388-transfected, Gly388-transfected, mock and NC were 12.83, 10.46, 5.77, and 5.12 μg, respectively (Fig. 4A and B). When OXA was treated BGC803 cells, the cell viability also decreased with increasing concentration. The IC_{50} in Arg388-transfected, Gly-388-transfected, mock, and NC were 11.67, 6.86, 1.96, and

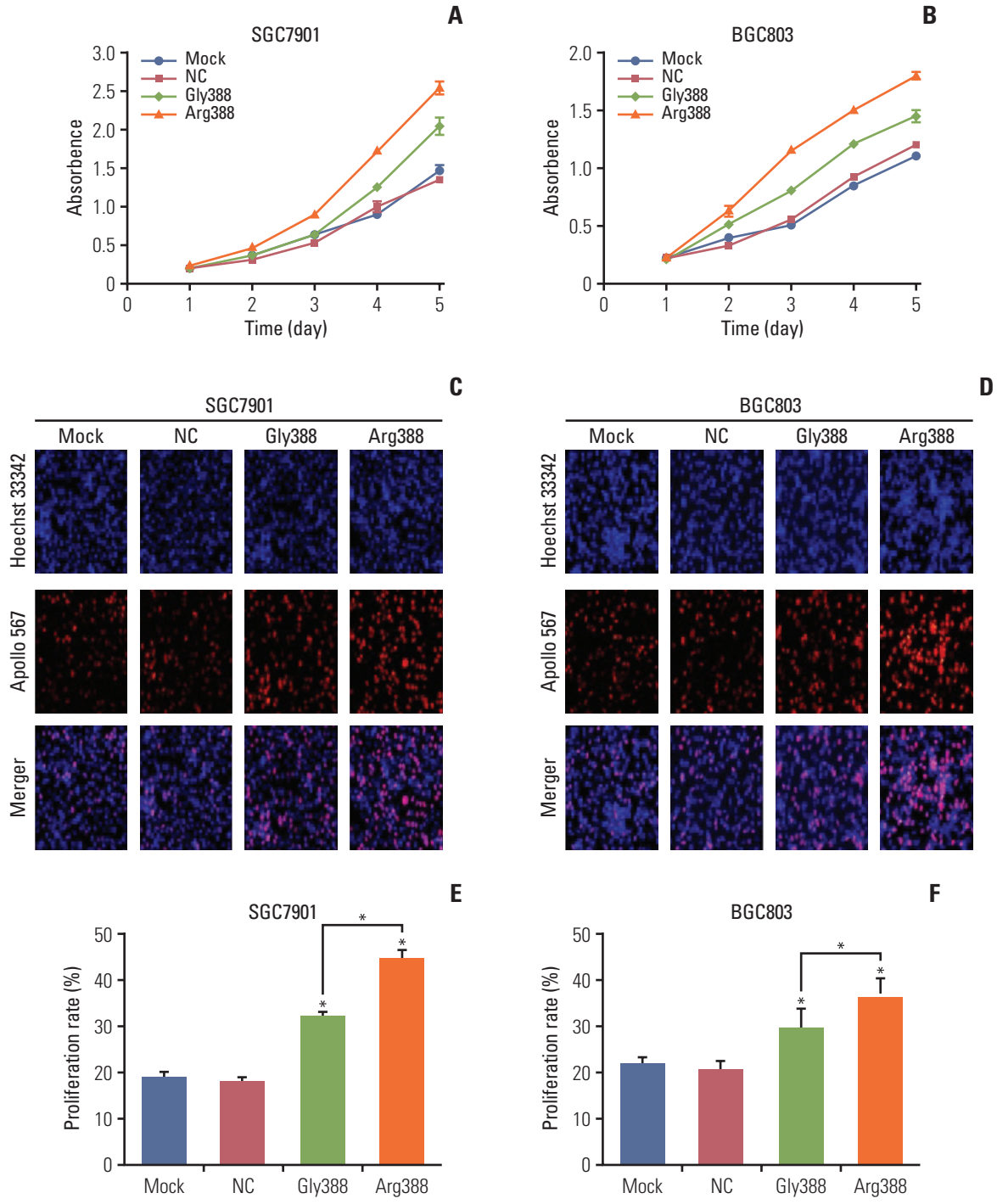

Fig. 3. Effect of fibroblast growth factor receptor 4 (*FGFR4*) genotype on proliferation, invasion, and migration. (A, B) Compared with mock and negative control (NC) cells, the proliferation of Gly388- and Arg388-transfected cells was significantly enhanced. In addition, Arg388-transfected cells have a faster proliferation than Gly388-transfected cells. In addition, Arg388-transfected cells have a faster proliferation than Gly388-transfected cells. Similar results were also observed in the EdU fluorescence staining test (C-F), Transwell chambers invasion assay (G-J), and cell scratch assay (K-N). *p < 0.05. *(Continued to the next page)*

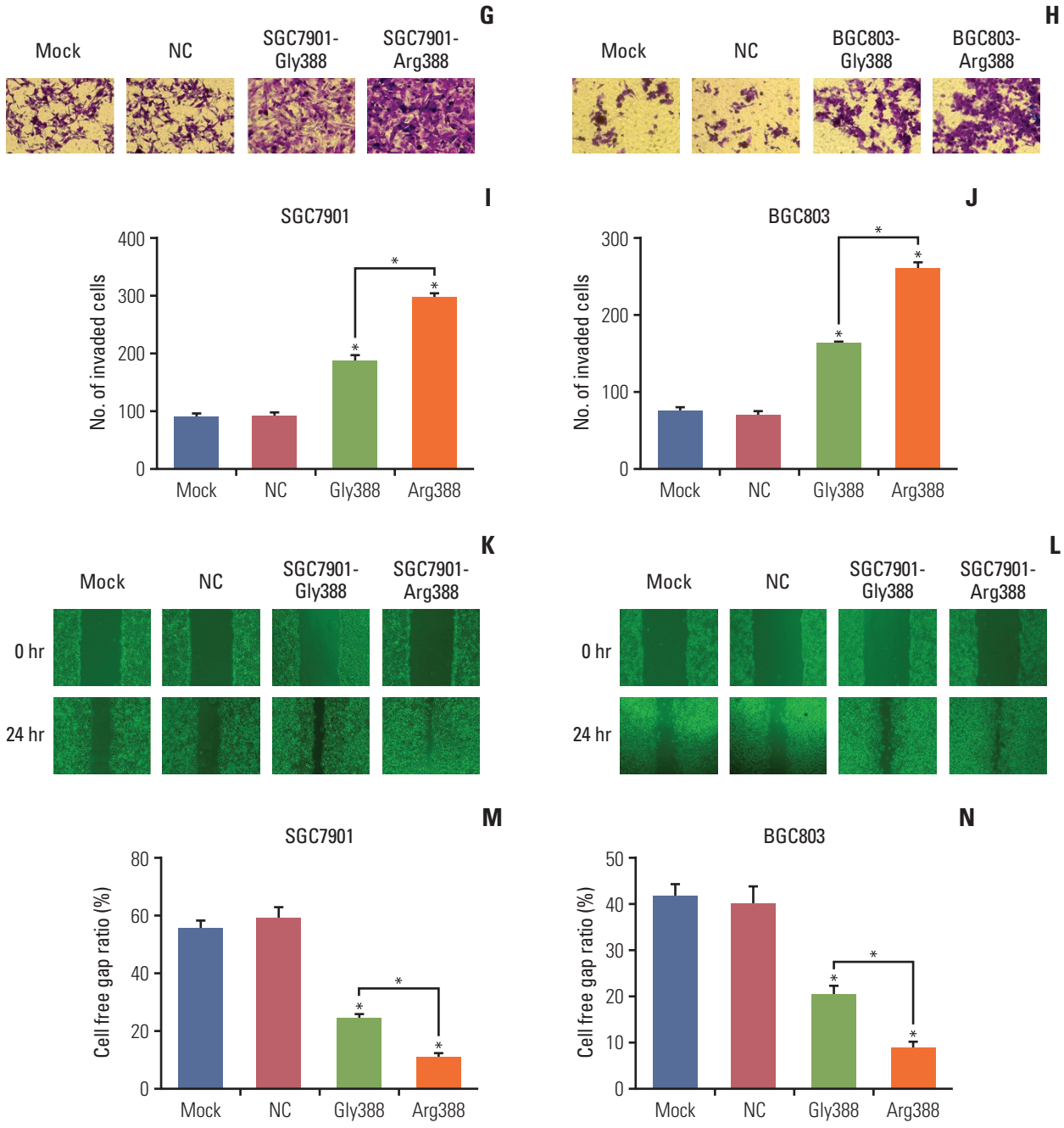

Fig. 3. *(Continued from the previous page)* Similar results were also observed in the EdU fluorescence staining test (C-F), Transwell chambers invasion assay (G-J), and cell scratch assay (K-N). *$p < 0.05$.

2.27 μg, respectively (Fig. 4C and D). Based on the above results, the appropriate concentration of OXA for later apoptosis experiments was 5 μg in SGC7901 cells and 2 μg in BGC803 cells, respectively (average value of IC_{50} for mock and NC group).

In cell apoptosis flow cytometry assay, when compared to mock and NC group, the Gly388- and Arg388-transfected group distinctly reduced the apoptosis rate of SGC7901 cells (Student's t test, $p < 0.05$) (Fig. 4E and G) and BGC803 cells (Student's t test, $p < 0.05$) (Fig. 4F and H). Moreover, the apoptosis rate of Arg388-transfected group was less than that of Gly388-transfected group in both of these GC cells. Furthermore, similar results could be shown in fluorescent staining for apoptosis (Fig. 4I-L), which suggested that FGFR4 overexpression can weaken the chemotherapy effect of OXA, and it was important to note that the FGFR4-Arg388 variant was superior to the FGFR4-Gly388 allele to increase the resistance of OXA.

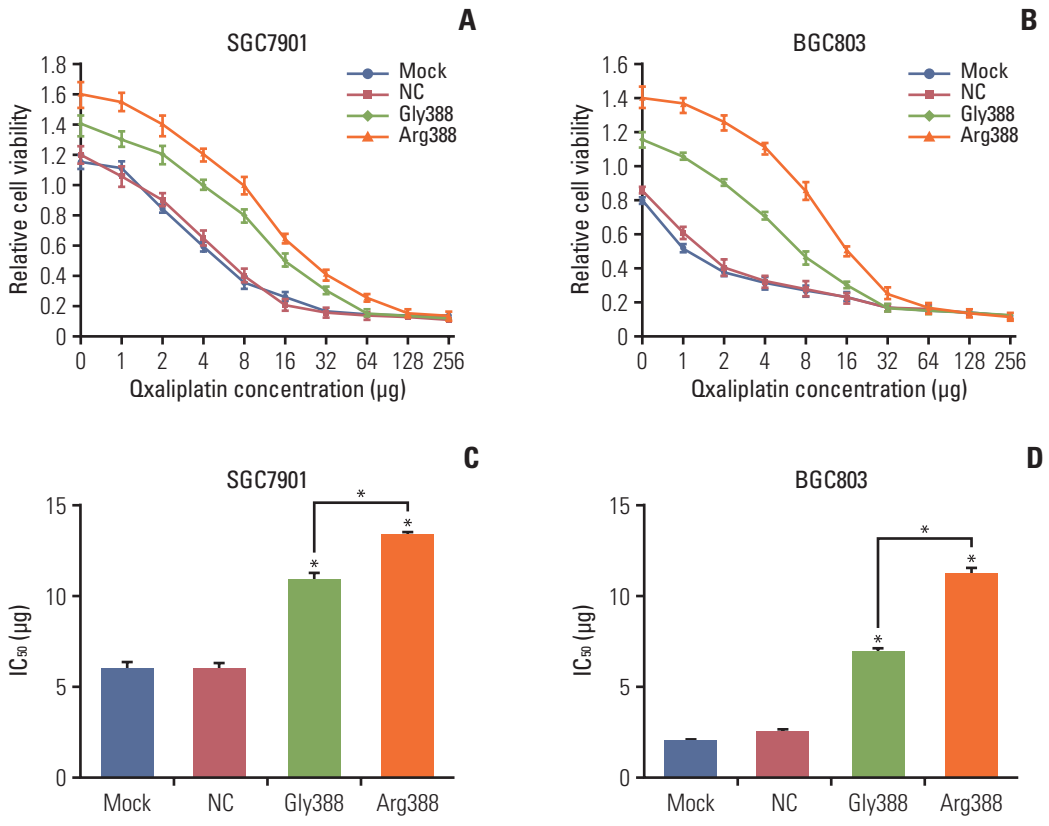

Fig. 4. The relationship between fibroblast growth factor receptor 4 (FGFR4) genotype and oxaliplatin (OXA) resistance. (A-D) Effects of different OXA concentrations on the activity of SGC7901 and BGC803 cells. NC, normal control. *(Continued to the next page)*

After 24 hours of OXA culture, expressions of caspase-3 and cleaved caspase-3 increased substantially in SGC7901 cells. Compared with mock, NC, and Gly388-transfected groups, the Arg388-transfected group decreased the expressions of caspase-3 and cleaved caspase-3, whether adding OXA or not, which confirmed that the apoptosis rate of FGFR4-Arg388 variant group was lower than the other three groups (Fig. 4M). Moreover, similar results could be observed in BGC803 cells (Fig. 4N).

6. FGFR4-Arg388 variant affects the EMT process and STAT3 signaling pathway, and inhibition of the STAT3 pathway reduces Arg388 variant induced EMT

To investigate the mechanism of how FGFR4-Arg388 variant affected the proliferation, invasion, and apoptosis of GC cells, we observed the expression change of associated molecules through western blot. Compared with mock and NC groups, the expression of FGFR4 in the Gly388- and Arg388-transfected SGC7901 cells were equally increased, which were actually shown to be effective in increasing FGFR4 protein expression in transfected GC cells. When the relationship between FGFR4 genotype and STAT3 signaling pathway was studied, the expression of STAT3 was obviously increased in Gly388- and Arg388-transfected SGC7901 cells. The expression of p-STAT3 was substantially increased in Arg388-transfected SGC7901 cells when compared with other three groups. This indicates that the FGFR4-Arg388 variant affects STAT3 signaling pathway. To study the role of the FGFR4 genotype in the EMT, we assessed the roles of the FGFR4-Arg388 variant compared with the FGFR4-Gly388 allele during induction of EMT changes in stably transfected GC cells. Western blot analyses showed there was an increased expression of Vim in Arg388-transfected SGC7901 cells compared with Gly388-transfected and control cells. While E-cad was significantly reduced in Arg388-transfected SGC-7901 cells when compared with other three groups. These results implied that the FGFR4-Arg388 variant promotes the EMT process (Fig. 5A). Similar results were also found in BGC803 cells (Fig. 5B).

To explore if FGFR4-Arg388 induced EMT could be decreased by inhibition of STAT3 activation, we cultivated the GC cells with the Jak2 inhibitor AG490 to block STAT3 activation and reduced expression of STAT3 protein. STAT3 and p-STAT3 have the same molecular weight, the expression of two proteins cannot be displayed in one PVDF membrane, that is why we used two internal reference proteins as a control for loading. STAT3 pathway inhibition was followed by growth of E-cad and reduction of Vim both

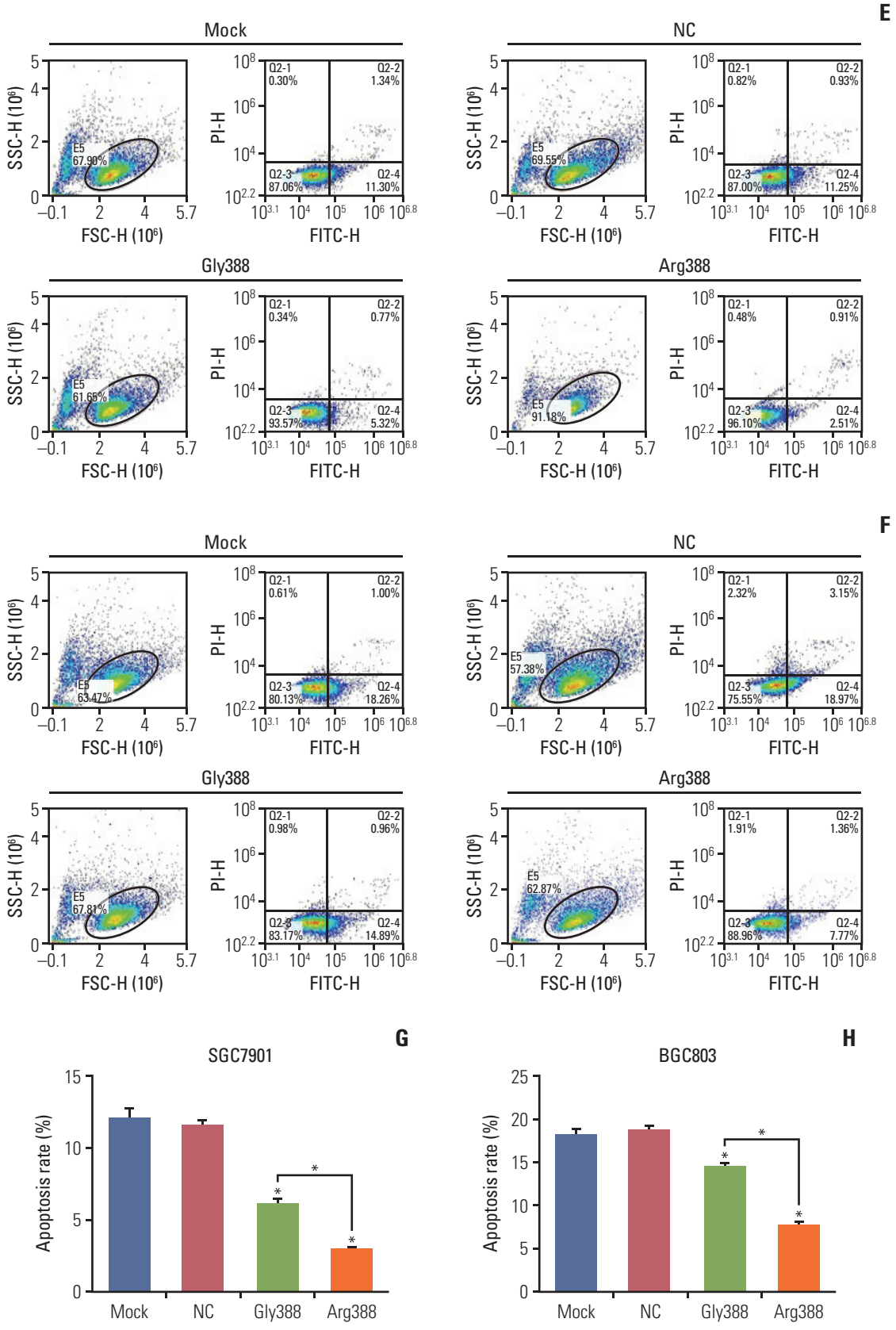

Fig. 4. *(Continued from the previous page)* (E-H) Flow cytometry: apoptosis rate of gastric cancer (GC) cells with different *FGFR4* genotypes after OXA addition for 24 hours. *(Continued to the next page)*

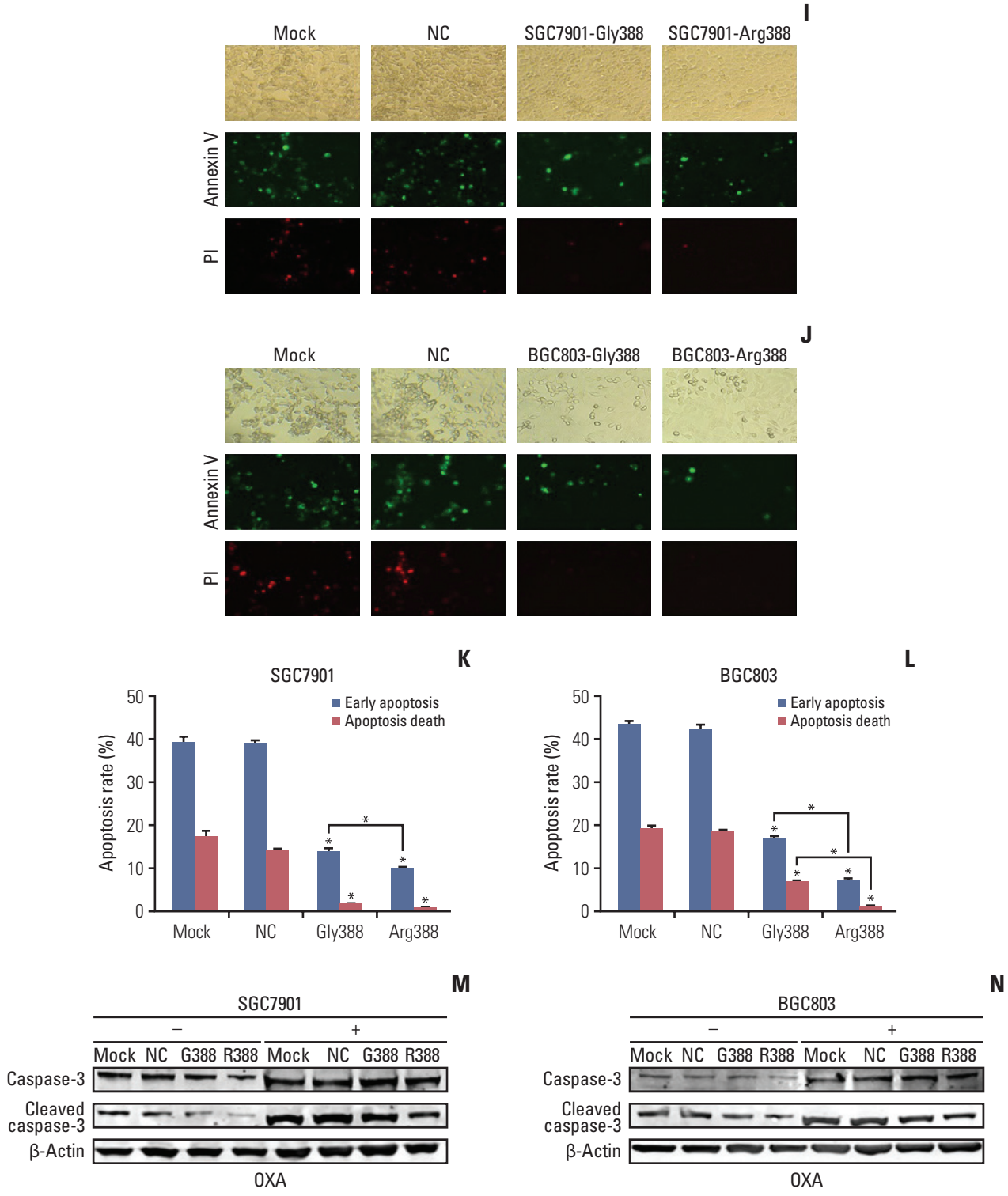

Fig. 4. *(Continued from the previous page)* (I-L) Fluorescent staining for apoptosis of GC cells with different *FGFR4* genotypes (green represents early apoptosis and red represents apoptosis death). PI, propidium iodide. (M, N) Western bolt was used to detect the changes of apoptosis molecules in GC cells with different *FGFR4* genotypes before and after OXA addition. *$p < 0.05$.

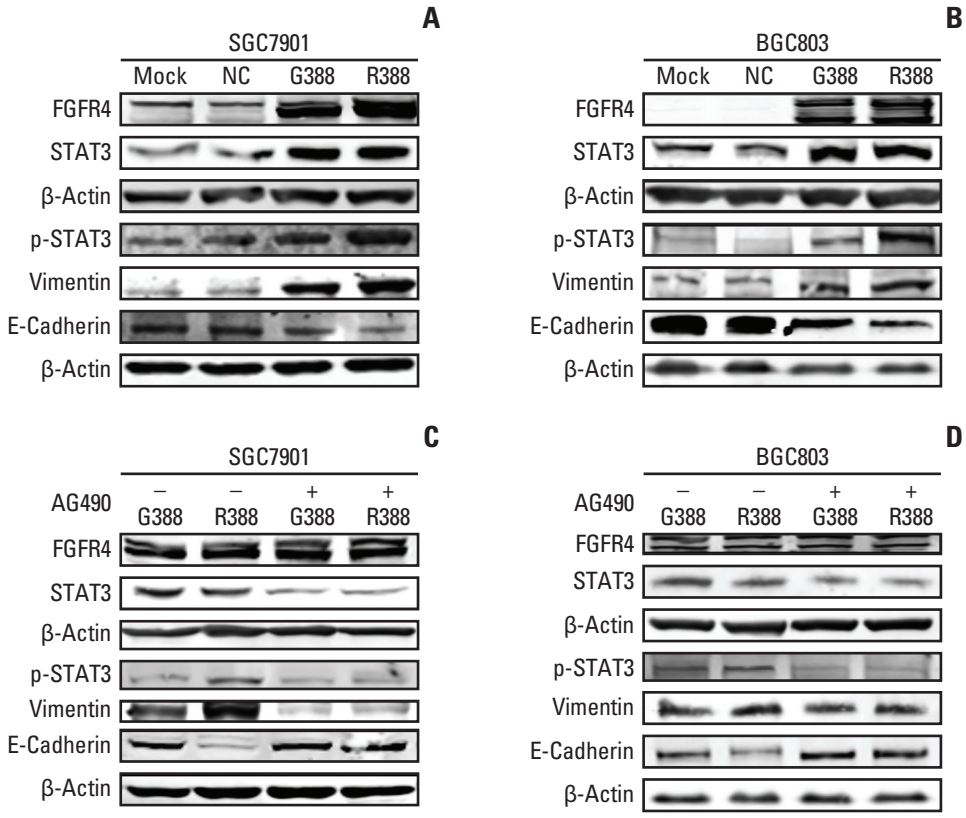

Fig. 5. The mechanism of fibroblast growth factor receptor 4 (FGFR4)-Arg388 influencing the oncogenic properties of gastric cancer cells. (A, B) Western blot detection of the expression of related molecules including FGFR4, signal pathway (STAT3), and epithelial to mesenchymal transition (E-cadherin and vimentin) in SGC7901 and BGC803 cells with different FGFR4 genotypes (mock, normal control [NC], Gly388, and Arg388). (C, D) The changes of related molecules between overexpression Gly388- and Arg388-transfected cells were detected, when cells were incubated with the Jak2 inhibitor AG490 to block STAT3 activation.

in Gly388- and Arg388-transfected cells, while the effect of inhibiting EMT on Arg388 variant was significantly stronger than that of Gly388 allele (Fig. 5C). Notably, similar results were shown in BGC803 cells (Fig. 4D). These results confirmed that FGFR4-Arg388 induced EMT could be reduced by STAT3 pathway obstruction.

Discussion

The presence of the FGFR4-Arg388 variant correlated with higher tumor stage (T3+T4) in clinical GC samples (p=0.047). The results indicated that the FGFR4-Arg388 variant might accelerate the progression of GC. Serra et al. [22] discovered that FGFR4-Arg388 variant promoted tumor progression by increasing peritoneal spread and the growth of metastatic lesions in the liver in the pancreatic endocrine tumor mouse model transfected with FGFR4-Gly388 or Arg388. This may be one of the reasons that the FGFR4-Arg388 variant influenced the progression of GC. Our research found that the overall survival (OS) of GC patients with FGFR4-Arg388 variant was worse than that of FGFR4-Gly388 patients (p=0.033). Quintanal-Villalonga et al. [16,23]. indicated that the presence of the FGFR4-Arg388 variant is associated with poorer prognosis in clinical non-small cell lung cancer samples and lung squamous cell carcinoma samples. Multivariate analysis supported the independent prognostic role of the FGFR4-Arg388 variant in OS [16,23]. Similar results were found FGFR4-Arg388 variant had a predictive role in the response of esophageal cancer patients to chemoradiotherapy with a worse trend for OS than Gly388 in the early stages [24]. Immunohistochemistry results demonstrated that the expression of Vim, STAT3, and p-STAT3 in FGFR4-Arg388 group was significantly higher than that in Gly388 allele, suggesting that the biological behavior was more aggressively in GC patients with high expression of FGFR4-Arg388, who might be suitable to undergo the chemotherapy after surgery. This may be an explanation that tumor stage was higher and OS was lower in GC patients with FGFR4-Arg388 comparing to that in Gly388 group.

Our previous studies have found that overexpression of FGFR4 continued to increase the infiltration and prolifera-

tion capacity of GC cells [2]. More importantly, in the present study we focus on comparing the differences in tumor carcinogenic behavior between the two types of overexpression FGFR4 genotypes. Our function assays *in vitro* revealed that the proliferation, invasion and migration abilities of SGC7901 and BGC803 cells with FGFR4-Arg388 were much stronger than those in FGFR4-Gly388 cells, indicating that the FGFR4 might increase the malignancy of GC cells, which confirmed once again the previous findings. *FGFR4* gene could accelerate progression of GC [2]. Similar results were discovered in colorectal cancer by Cho et al. [15].

The proliferation ability of SGC7901 and BGC803 cells with FGFR4-Gly388, Arg388, mock, and NC was significantly weakened when dealt with by different concentration of OXA. Transfection groups had significantly higher IC_{50} than the mock and NC groups, and the Arg388-transfected group had a higher IC_{50} than Gly388-transfected group, which suggested that overexpression of FGFR4 was resistant to OXA, whereas FGFR4-Arg388 variant was more effective. This conclusion was confirmed by the apoptosis assay that the apoptosis rates of Arg388-transfected group were markedly decreased in SGC7901 and BGC803 cells treated with the single concentration of OXA compared with others. In molecular level, the expression of caspase-3 and cleaved caspase-3 obviously weakened in Arg388 group treated with OXA, which supported the results of apoptosis assay. Our former studies have found that FGFR4 overexpression can weaken the effects of 5-fluorouracil, BGJ398 (an inhibitor of FGFR4), and PD173074 (an inhibitor of FGFR4) [2,3]. This study reconfirms the role of FGFR4 to weaken the effects of OXA, a novel clinical chemotherapy drug. Gao et al. [25] showed that inhibition of FGFR4 signaling significantly overcomes sorafenib resistance in hepatocellular carcinoma. Serra et al. [22] showed that unlike FGFR4-Gly388, FGFR4-Arg388 tumors exhibited diminished responsiveness to everolimus (an inhibitor of mammalian target of rapamycin signal). Few studies have been conducted on resistance of *FGFR4* Gly388Arg polymorphisms to chemotherapeutic drugs, while we found that FGFR4-Arg388 variant was indeed resistant to OXA compared with Gly388 allele.

Studies have revealed that the FGFR4-Arg388 variant can induce EMT [15,16], activating the STAT3 signaling pathway by promoting phosphorylation of STAT3 [13]. Therefore, we explored the correlation between *FGFR4* Gly388Arg polymorphism and EMT as well as STAT3 signaling pathways in GC. The results of western blot showed the expression of STAT3 was obviously increased in Gly388- and Arg388-transfected cells. The expression of p-STAT3 was substantially increased in Arg388-transfected cells when compared with other three groups, while there was no difference in expression of STAT3 between Gly388- and Arg388-transfected groups. Immunohistochemical results showed that the expressions of p-STAT3 were relatively higher in Arg388 GC patients, which were in accordance with western bolt results. This suggests that the FGFR4-Arg388 variant affects the STAT3 signaling pathway, possibly increasing the phosphorylation of STAT3. Ezzat et al. [6] showed that FGFR4-Arg388 pituitary cells have higher mitochondrial STAT3 serine phosphorylation driving basal and maximal oxygen consumption rate than ones expressing the more common FGFR4-Gly388 allele. This phenomenon may be ascribed to that FGFR4-Arg388 can expose a proximal STAT3 binding site [12]. A large number of studies have found STAT3 activation was involved in regulating expression of apoptosis genes, yet continuous activation of STAT3 signaling would grant resistance to apoptosis in breast cancer cells [26,27]. FGFR4-Arg388 variant could activate STAT3 signal, which may be the reason why Arg388 had the least apoptosis of GC cells treated with OXA.

Western bolt showed there was a higher expression of Vim and lower expression of E-cad in FGFR4-Arg388 group, which suggested that Arg388 variant may induce EMT. Elevated Vim protein levels and reduced E-cad protein levels are usually associated with cancer cell metastasis and the EMT process. Cho et al. [15] had similar findings in colorectal cancer that FGFR4-Arg388 could induce EMT. Quintanal-Villalonga et al. [16] found that the poorer prognostic role of this FGFR4-Arg388 variant in lung cancer may be mediated by the induction of N-cadherin expression (an EMT molecular). The relationship between FGFR4-Arg388 and E-cad showed differences in immunohistochemistry and western blot results, possibly due to the small number of clinical cases leading to false positive or negative results in immunohistochemistry.

Plenty of studies have found that constitutive STAT3 expression promoted and sustained the EMT phenotype [28-30]. Meanwhile, we found that FGFR4-Arg388 was substantially correlated with the molecules of EMT and STAT3 signal. Thus, we proposed a hypothesis that FGFR4-Arg388, STAT3, and EMT make up a functional signal axis that regulates carcinogenesis of GC and inhibition of FGFR4-Arg388/STAT3/EMT signal axis was possible to reverse the EMT. After final verification, the activation of STAT3 inhibited by AG490 increased the expression of E-cad and decreased the expression of Vim, indicating that the inhibition of STAT3 attenuated the process of EMT. Finally, it can be understood that blocking this signal axis can reverse the EMT process. We also found AG490 inhibits overexpression of FGFR4-Arg388 variant induced EMT more significantly than Gly388 allele, which could be due to FGFR4-Arg388 promotes STAT3 phosphorylation more effectively [6,12]. It is worth further explore the exact mechanisms involved FGFR4-Arg388/STAT3/EMT regulating the biological function of tumor cells.

Collectively, this study elucidated the role of FGFR4-Arg388 variant in GC, and emphasized the probability of this SNP as potential therapeutic targets. FGFR4-Arg388 variant

was linked to poor prognosis of GC patients. FGFR4-Arg388 variant increased proliferation and invasion GC cells, weakening the effects of OXA. The exploration mechanism may be through FGFR4-Arg388/STAT3/EMT axis regulating pivotal oncogenic properties of GC cells.

Conflict of Interest

Conflicts of interest relevant to this article was not reported.

Acknowledgments

This study was supported by Department of Gastrointestinal Surgery and Institute of Clinical Medicine, The First Affiliated Hospital, Zhengzhou University and National Natural Science Foundation of China, Grant No. 81201955. Furthermore, this work was supported by the Foundation of Henan Educational Committee (Grant No.19A320080).

References

1. Katoh M. Genetic alterations of FGF receptors: an emerging field in clinical cancer diagnostics and therapeutics. Expert Rev Anticancer Ther. 2010;10:1375-9.
2. Li J, Ye Y, Wang M, Lu L, Han C, Zhou Y, et al. The overexpression of FGFR4 could influence the features of gastric cancer cells and inhibit the efficacy of PD173074 and 5-fluorouracil towards gastric cancer. Tumour Biol. 2016;37:6881-91.
3. Ye Y, Jiang D, Li J, Wang M, Han C, Zhang X, et al. Silencing of FGFR4 could influence the biological features of gastric cancer cells and its therapeutic value in gastric cancer. Tumour Biol. 2016;37:3185-95.
4. Ye Y, Shi Y, Zhou Y, Du C, Wang C, Zhan H, et al. The fibroblast growth factor receptor-4 Arg388 allele is associated with gastric cancer progression. Ann Surg Oncol. 2010;17:3354-61.
5. Chou CH, Hsieh MJ, Chuang CY, Lin JT, Yeh CM, Tseng PY, et al. Functional FGFR4 Gly388Arg polymorphism contributes to oral squamous cell carcinoma susceptibility. Oncotarget. 2017;8:96225-38.
6. Ezzat S, Wang R, Pintilie M, Asa SL. FGFR4 polymorphic alleles modulate mitochondrial respiration: a novel target for somatostatin analog action in pituitary tumors. Oncotarget. 2017;8:3481-94.
7. Whittle SB, Reyes S, Du M, Gireud M, Zhang L, Woodfield SE, et al. A polymorphism in the FGFR4 gene is associated with risk of neuroblastoma and altered receptor degradation. J Pediatr Hematol Oncol. 2016;38:131-8.
8. Morimoto Y, Ozaki T, Ouchida M, Umehara N, Ohata N, Yoshida A, et al. Single nucleotide polymorphism in fibroblast growth factor receptor 4 at codon 388 is associated with prognosis in high-grade soft tissue sarcoma. Cancer. 2003;98:2245-50.
9. Streit S, Mestel DS, Schmidt M, Ullrich A, Berking C. FGFR4 Arg388 allele correlates with tumour thickness and FGFR4 protein expression with survival of melanoma patients. Br J Cancer. 2006;94:1879-86.
10. Yu W, Feng S, Dakhova O, Creighton CJ, Cai Y, Wang J, et al. FGFR-4 Arg(3)(8)(8) enhances prostate cancer progression via extracellular signal-related kinase and serum response factor signaling. Clin Cancer Res. 2011;17:4355-66.
11. Jalali S, Monsalves E, Tateno T, Zadeh G. Role of mTOR inhibitors in growth hormone-producing pituitary adenomas harboring different FGFR4 genotypes. Endocrinology. 2016;157:3577-87.
12. Ulaganathan VK, Ullrich A. Membrane-proximal binding of STAT3 revealed by cancer-associated receptor variants. Mol Cell Oncol. 2016;3:e1145176.
13. Ezzat S, Zheng L, Florez JC, Stefan N, Mayr T, Hliang MM, et al. The cancer-associated FGFR4-G388R polymorphism enhances pancreatic insulin secretion and modifies the risk of diabetes. Cell Metab. 2013;17:929-40.
14. Sugiyama N, Varjosalo M, Meller P, Lohi J, Chan KM, Zhou Z, et al. FGF receptor-4 (FGFR4) polymorphism acts as an activity switch of a membrane type 1 matrix metalloproteinase-FGFR4 complex. Proc Natl Acad Sci U S A. 2010;107:15786-91.
15. Cho SH, Hong CS, Kim HN, Shin MH, Kim KR, Shim HJ, et al. FGFR4 Arg388 is correlated with poor survival in resected colon cancer promoting epithelial to mesenchymal transition. Cancer Res Treat. 2017;49:766-77.
16. Quintanal-Villalonga A, Ojeda-Marquez L, Marrugal A, Yague P, Ponce-Aix S, Salinas A, et al. The FGFR4-388arg variant promotes lung cancer progression by N-cadherin induction. Sci Rep. 2018;8:2394.
17. Edge SB, Compton CC. The American Joint Committee on Cancer: the 7th edition of the AJCC cancer staging manual and the future of TNM. Ann Surg Oncol. 2010;17:1471-4.
18. Thussbas C, Nahrig J, Streit S, Bange J, Kriner M, Kates R, et al. FGFR4 Arg388 allele is associated with resistance to adjuvant therapy in primary breast cancer. J Clin Oncol. 2006;24:3747-55.
19. Myoteri D, Dellaportas D, Lykoudis PM, Apostolopoulos A, Marinis A, Zizi-Sermpetzoglou A. Prognostic evaluation of vimentin expression in correlation with Ki67 and CD44 in surgically resected pancreatic ductal adenocarcinoma. Gastroenterol Res Pract. 2017;2017:9207616.
20. Gao H, Lan X, Li S, Xue Y. Relationships of MMP-9, E-cadherin, and VEGF expression with clinicopathological features and response to chemosensitivity in gastric cancer. Tumour Biol. 2017;39:1010428317698368.
21. Zhang S, Huang S, Deng C, Cao Y, Yang J, Chen G, et al. Co-ordinated overexpression of SIRT1 and STAT3 is associated with poor survival outcome in gastric cancer patients. Oncotarget. 2017;8:18848-60.
22. Serra S, Zheng L, Hassan M, Phan AT, Woodhouse LJ, Yao JC, et al. The FGFR4-G388R single-nucleotide polymorphism alters pancreatic neuroendocrine tumor progression and response to mTOR inhibition therapy. Cancer Res. 2012;72:5683-91.
23. Quintanal-Villalonga A, Carranza-Carranza A, Melendez R,

Ferrer I, Molina-Pinelo S, Paz-Ares L. Prognostic role of the FGFR4-388Arg variant in lung squamous-cell carcinoma patients with lymph node involvement. Clin Lung Cancer. 2017;18:667-74.
24. Shim HJ, Shin MH, Kim HN, Kim JH, Hwang JE, Bae WK, et al. The prognostic significance of FGFR4 Gly388 polymorphism in esophageal squamous cell carcinoma after concurrent chemoradiotherapy. Cancer Res Treat. 2016;48:71-9.
25. Gao L, Wang X, Tang Y, Huang S, Hu CA, Teng Y. FGF19/FGFR4 signaling contributes to the resistance of hepatocellular carcinoma to sorafenib. J Exp Clin Cancer Res. 2017;36:8.
26. Calo V, Migliavacca M, Bazan V, Macaluso M, Buscemi M, Gebbia N, et al. STAT proteins: from normal control of cellular events to tumorigenesis. J Cell Physiol. 2003;197:157-68.
27. Okabe M, Miyabe S, Nagatsuka H, Terada A, Hanai N, Yokoi M, et al. MECT1-MAML2 fusion transcript defines a favorable subset of mucoepidermoid carcinoma. Clin Cancer Res. 2006;12:3902-7.
28. Sullivan NJ, Sasser AK, Axel AE, Vesuna F, Raman V, Ramirez N, et al. Interleukin-6 induces an epithelial-mesenchymal transition phenotype in human breast cancer cells. Oncogene. 2009;28:2940-7.
29. Cheng GZ, Zhang WZ, Sun M, Wang Q, Coppola D, Mansour M, et al. Twist is transcriptionally induced by activation of STAT3 and mediates STAT3 oncogenic function. J Biol Chem. 2008;283:14665-73.
30. Zang C, Liu X, Li B, He Y, Jing S, He Y, et al. IL-6/STAT3/TWIST inhibition reverses ionizing radiation-induced EMT and radioresistance in esophageal squamous carcinoma. Oncotarget. 2017;8:11228-38.

pISSN 1598-2998, eISSN 2005-9256

Cancer Res Treat. 2020;52(4):1178-1187

https://doi.org/10.4143/crt.2020.313

Original Article

Open Access

Adjuvant Chemotherapy in Microsatellite Instability–High Gastric Cancer

Jin Won Kim, MD, PhD[1]
Sung-Yup Cho, MD, PhD[2,3]
Jeesoo Chae, PhD[2]
Ji-Won Kim, MD, MS[1]
Tae-Yong Kim, MD, PhD[3,4]
Keun-Wook Lee, MD, PhD[1]
Do-Youn Oh, MD, PhD[3,4]
Yung-Jue Bang, MD, PhD[3,4]
Seock-Ah Im, MD, PhD[3,4]

[1]*Division of Hematology and Medical Oncology, Department of Internal Medicine, Seoul National University Bundang Hospital, Seoul National University College of Medicine, Seongnam,* [2]*Department of Biomedical Sciences, Seoul National University College of Medicine, Seoul,* [3]*Cancer Research Institute, Seoul National University College of Medicine, Seoul,* [4]*Division of Hematology and Medical Oncology, Department of Internal Medicine, Seoul National University Hospital, Seoul National University College of Medicine, Seoul, Korea*

Correspondence: Seock-Ah Im, MD, PhD
Department of Internal Medicine,
Seoul National University College of Medicine,
101 Daehak-ro, Jongno-gu, Seoul 03080, Korea
Tel: 82-2-2072-0850
Fax: 82-2-765-7081
E-mail: moisa@snu.ac.kr

Received April 14, 2020
Accepted June 10, 2020
Published Online June 11, 2020

Purpose

Microsatellite instability (MSI) status may affect the efficacy of adjuvant chemotherapy in gastric cancer. In this study, the clinical characteristics of MSI-high (MSI-H) gastric cancer and the predictive value of MSI-H for adjuvant chemotherapy in large cohorts of gastric cancer patients were evaluated.

Materials and Methods

This study consisted of two cohorts. Cohort 1 included gastric cancer patients who received curative resection with pathologic stage IB-IIIC. Cohort 2 included patients with MSI-H gastric cancer who received curative resection with pathologic stage II/III. MSI was examined using two mononucleotide markers and three dinucleotide markers.

Results

Of 359 patients (cohort 1), 41 patients (11.4%) had MSI-H. MSI-H tumors were more frequently identified in older patients ($p < 0.001$), other histology than poorly cohesive, signet ring cell type (p=0.005), intestinal type (p=0.028), lower third tumor location (p=0.005), and absent perineural invasion (p=0.027). MSI-H status has a tendency of better disease-free survival (DFS) and overall survival (OS) in multivariable analyses (hazard ratio [HR], 0.4; p=0.059 and HR, 0.4; p=0.063, respectively). In the analysis of 162 MSI-H patients (cohort 2), adjuvant chemotherapy showed a significant benefit with respect to longer DFS and OS (p=0.047 and p=0.043, respectively). In multivariable analysis, adjuvant chemotherapy improved DFS (HR, 0.4; p=0.040).

Conclusion

MSI-H gastric cancer had distinct clinicopathologic findings. Even in MSI-H gastric cancer of retrospective cohort, adjuvant chemotherapy could show a survival benefit, which was in contrast to previous prospective studies and should be investigated in a further prospective trial.

Key words

Microsatellite instability, Adjuvant chemotherapy, Stomach neoplasms

Introduction

Microsatellite instability (MSI) is characterized as the increased rate of uncorrected replication errors at the simple repeat sequence caused by a DNA mismatch repair gene (MMR) defect [1,2]. MSI-high (MSI-H) results in accelerated mutations in oncogenes and tumor suppressor genes and a phenotype of hypermutational status [3,4]. Tumor-specific neopeptides may be generated during MSI-H carcinogenesis. A protective role of lymphocytes against MSI-H colorectal cancer that prevents tumor metastasis was reported [5]. Because of the immunologic aspect of MSI status, it was recently highlighted as a predictive marker in immunotherapy. MSI-H tumors have been shown to benefit from immunotherapy, and anti–programmed death-1 antibody (pembrolizumab) has finally been approved by the U.S. Food and Drug Administration for the treatment of MSI-H tumors regardless of the tumor type [6,7].

In an adjuvant setting, MSI-H could be a prognostic and predictive marker. In colorectal cancer, MSI-H tumor showed better prognosis than microsatellite stable (MSS)/MSI-low (MSI-L) tumors [8,9]. Patients with MSI-H colorectal cancer did not benefit from adjuvant chemotherapy. Particularly, adjuvant chemotherapy with 5-fluorouracil alone in patients with stage II colorectal cancer may be even worse than no adjuvant chemotherapy [8]. Therefore, adjuvant chemotherapy with 5-fluorouracil alone in stage II colorectal cancer patients is not recommended by several guidelines [10,11].

In gastric cancer, adjuvant chemotherapy with capecitabine plus oxaliplatin or S1 has been proven to prolong survival after D2 resection of stage II/III gastric cancer in CLASSIC and ACTS-GC study [12,13]. MSI-H status is relatively common in gastric cancer and occurs in approximately 9% of surgically resected gastric cancer [4,14-16]. In the CLASSIC trial, compared with the overall positive results, patients with MSI-H gastric cancer did not experience any survival benefit from adjuvant chemotherapy [13,15]. Similarly, in the MAGIC trial, which evaluated the role of perioperative chemotherapy for resectable gastric cancer, MSI-H status had an improved prognosis in the surgery-alone treatment arm, but a worse survival outcome in the chemotherapy-plus-surgery arm compared with an MSS/MSI-L [17,18]. A recently published paper of pooled individual patient data from four large randomized clinical trials conducted in patients with resectable gastric cancer (MAGIC [18], CLASSIC [13], ARTIST [19] which evaluated the concurrent irradiation with adjuvant chemotherapy [capecitabine plus cisplatin], and ITACA-S [20] which evaluated an intensified combination chemotherapy schedule [fluorouracil plus leucovorin plus irinotecan followed by cisplatin plus docetaxel] compared with single-agent chemotherapy [fluorouracil plus leucovorin]) showed that patients with MSI-L/MSS gastric cancer benefited from chemotherapy plus surgery, but those with MSI-H gastric cancer did not [16]. However, in the CLASSIC and MAGIC trial, only 40 and 20 patients had MSI-H tumors. In a pooled analysis of four clinical trials, 121 patients had MSI-H tumors, and just 33 patients with MSI-H tumor who received surgery alone were included in the control group. Therefore, despite these results from randomized clinical trials and pooled analysis, there is limited statistical power for the use of MSI/MMR deficiency testing as a predictive marker for adjuvant chemotherapy in patients with curatively resected gastric cancer.

Therefore, we evaluated the predictive value of MSI-H tumor for the benefit of adjuvant chemotherapy in large cohorts of gastric cancer patients. The clinical characteristics of MSI-H gastric cancer were also evaluated.

Materials and Methods

1. Patients

This study consisted of two cohorts. In cohort 1, the clinical features of MSI-H compared with MSS/MSI-L were analyzed. Cohort 1 included gastric cancer patients who received curative resection with pathologic stage IB-IIIC from February 2005 to January 2006 at Seoul National University Hospital (SNUH). Cohort 2 was used for the analysis of the efficacy of adjuvant chemotherapy in MSI-H gastric cancer. Cohort 2 included patients with MSI-H gastric cancer who received curative resection with pathologic stage II/III from January 2007 to February 2012 at Seoul National University Bundang Hospital (SNUBH) and from December 2004 to June 2012 at SNUH. MSI-H patients in cohort 1 were included in cohort 2. Clinical data were retrieved from the medical records of patients. The American Joint Committee on Cancer (AJCC) 7th edition was used.

2. Test for MSI

Genomic DNA of the formalin-fixed gastric cancer tissues was extracted using standard proteinase-K digestion and a phenol/chloroform procedure. MSI was examined using two mononucleotide markers: BAT 25 (located 4q12-13 *KIT* gene, intron 16, T25 repeat) and BAT 26 (located 2p22-21, *hMSH2* gene, exon5, A26 repeat) and three dinucleotide markers: DS123 (located 2p 16.3, CA repeat), D5S346 (located 5q22.2, CA repeat), and D17S250 (located 17q12, CA repeat). Polymerase chain reaction (PCR) reactions were conducted in 10 μL reaction volumes with fluorescent dye 50-end labeled primers. PCR products were denatured in formamide for 2 minutes at 95°C and electrophoresed on denaturing 8% polyacrylamide sequencing gels. MSI status was analyzed using GeneScan software in an ABI 3100 sequencer (Foster City, CA). Tissue samples that exhibited abnormal band patterns were considered to indicate MSI. According to the number of markers displaying instability of each tumor, the tumors were divided into MSI-H, MSI-L, and MSS. MSI-H indicated instability in two or more of five markers. MSI-L indicated instability in one of five markers. MSS indicated there was no instability in the five markers [1].

3. Statistical analysis

The differences in clinicopathologic findings according to MSI status were evaluated using chi-square analysis. Disease-free survival (DFS) was defined as the duration between the surgical operation and disease relapse, any cause of death before disease relapse, or the last follow-up. The event for DFS was defined as relapse and any cause of death. Overall survival (OS) was measured from the surgical operation to the last follow-up or any cause of death. The event for OS was defined as any cause of death. The Kaplan-Meier method was used for survival analysis with the log-rank test. The Cox

Table 1. Characteristics of gastric cancer patients with MSS/MSI-L and MSI-H (cohort 1)

Characteristic	MSS/MSI-L (n=318, 88.6%)	MSI-H (n=41, 11.4%)	p-value
Age (yr)			
Median (range)	60 (28-87)		
< 70	269 (92.4)	22 (7.6)	< 0.001
≥ 70	49 (72.1)	19 (27.9)	
Sex			
Male	214 (90.7)	22 (9.3)	0.083
Female	104 (84.6)	19 (15.4)	
Operation			
Total gastrectomy	109 (93.2)	8 (6.8)	0.066
Subtotal gastrectomy	191 (85.3)	33 (14.7)	
Partial gastrectomy	17 (100)	0	
Whipple	1 (100)	0	
Histology			
Tubular, well to poorly differentiated	253 (86.9)	38 (13.1)	0.045
Poorly cohesive, signet ring cell type	42 (100)	0	
Other histological variants	23 (88.5)	3 (11.5)	
Lauren[a]			
Diffuse	126 (92.0)	11 (8.0)	0.028
Intestinal	147 (84.0)	28 (16.0)	
Mixed	42 (95.5)	2 (4.5)	
Location			
Upper third	21 (100)	0	0.005
Mid third	169 (92.3)	14 (7.7)	
Lower third	128 (82.6)	27 (17.4)	
Stage			
Ib	65 (85.5)	11 (14.5)	0.285
IIA	71 (85.5)	12 (14.5)	
IIB	56 (90.3)	6 (9.7)	
IIIA	36 (83.7)	7 (16.3)	
IIIB	58 (95.1)	3 (4.9)	
IIIC	32 (94.1)	2 (5.9)	
Lymphatic			
Absent	127 (92.7)	10 (7.3)	0.054
Present	191 (86.0)	31 (14.0)	
Venous			
Absent	271 (88.0)	37 (12.0)	0.386
Present	47 (92.2)	4 (7.8)	
Perineural			
Absent	136 (84.5)	25 (15.5)	0.027
Present	182 (91.9)	16 (8.1)	
Adjuvant chemotherapy			
Not applied	143 (78.1)	40 (21.9)	0.113
Applied	149 (84.7)	27 (15.3)	

Values are presented as number (%) unless otherwise indicated. [a]Unknown patients (n=3).

proportional hazards regression model was used to calculate hazard ratio (HR) in univariable and multivariable analysis. All statistical analyses were performed using SPSS Statistics ver. 25 (IBM Corp., Armonk, NY).

4. Ethical statement

This study was conducted in accordance with the ethical standards of the Declaration of Helsinki and the national and international guidelines. This study was approved by the institutional review board at SNUBH (B-1207-164-107) and

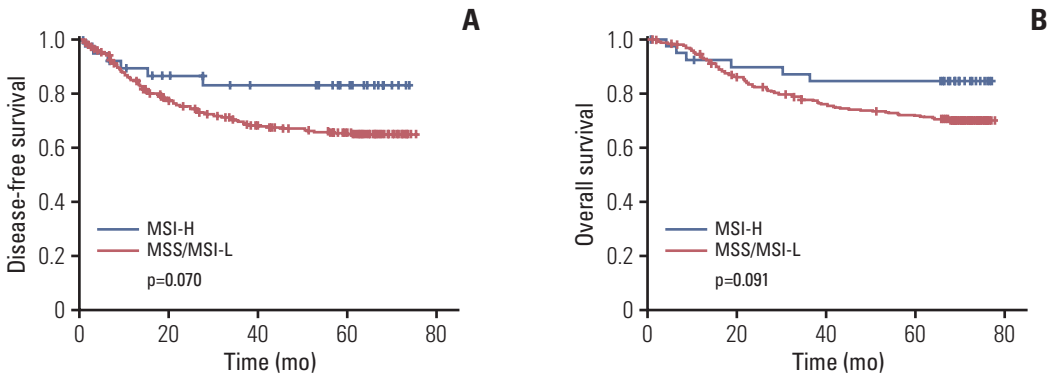

Fig. 1. Disease-free survival (A) and overall survival (B) according to microsatellite instability (MSI) status. p-value calculated by a Kaplan-Meier method. MSI-H, MSI-high; MSI-L, MSI-low; MSS, microsatellite stable.

SNUH (H-1208-100-422) and acquired a waiver of informed consent.

Results

1. Characteristics of patients with MSI-H gastric cancer compared with MSS/MSI-L gastric cancer (cohort 1)

Cohort 1 was analyzed to evaluate the characteristics of MSI-H gastric cancer patients who received curative gastrectomy. A total of 731 patients with gastric cancer received the curative operation with D2 dissection. Among these patients, 366 patients with stage IA were excluded. MSI data were available in 359 of 365 patients with stages IB-IIIC. Cohort 1 consisted of these 359 patients (Table 1). MSI-H status was seen in 41 patients (11.4%) and was associated with older age (27.9% vs. 7.6%, $p < 0.001$), other histology than poorly cohesive, signet ring cell type (p=0.045), Lauren's intestinal type (16% vs. 8.0% of disuse type, p=0.028), and lower third tumor location (17.4% vs. 7.7% of mid-third location, p=0.005). In contrast, there were no patients who had MSI-H tumors with poorly cohesive, signet ring cell type (0/42, 0.0%). There was no significant correlation according to stage (p=0.285), lymphatic invasion (p=0.054), or venous invasion (p=0.386), but MSI-H was identified more frequently in absent perineural invasion (p=0.027).

2. Survival of patients with MSI-H gastric cancer compared with MSS/MSI-L gastric cancer (cohort 1)

In cohort 1, the median follow-up duration was 71.1 months after surgery. Univariable analysis between clinicopathologic factors and survival was done (S1 Table). Patients with MSI-H gastric cancer had better 5-year DFS rate (83.2% vs. 65.5%, respectively; p=0.070) (Fig. 1A), and 5-year OS rate (84.4% vs. 71.7%, respectively; p=0.091) (Fig. 1B) than those with MSS/MSI-L, although there was not significant. In the multivariable analysis with MSI status, sex, age, World Health Organization histology, Lauren classification, tumor location, lymphatic invasion, venous invasion, perineural invasion, and the use of adjuvant chemotherapy, MSI-H status showed an better survival although there was not statistical significance (for DFS: HR, 0.4; 95% confidence interval [CI], 0.2 to 1.0; p=0.059; for OS: HR, 0.4; 95% CI, 0.2 to 1.0; p=0.063) (Table 2).

In terms of the role of adjuvant chemotherapy in MSS/MSI-L tumors, patients with adjuvant chemotherapy had the prolonged survival (for DFS: p=0.176 and $p < 0.001$; for OS: p=0.225 and $p < 0.001$ in stage II and stage III, respectively). However, in MSI-H tumors, patients with adjuvant chemotherapy did not show the prolonged survival because of small sample size (for DFS: p=0.439 and p=0.836; for OS: p=0.439 and p=0.933 in 18 patients with stage II and 12 stage III, respectively).

3. Characteristics of MSI-H gastric cancer patients (cohort 2)

We next evaluated the efficacy of adjuvant chemotherapy in more MSI-H gastric cancer patients who received a curative gastrectomy (cohort 2). In total, 5,983 patients were screened who received a gastrectomy and an MSI test. Of these 5,983 patients, 578 patients (9.7%) were confirmed as MSI-H. Finally, 162 patients who underwent R0 resection, were diagnosed with pathologic stage II/III, and were a candidate for adjuvant chemotherapy were included in cohort 2 (S2 Fig.). The baseline characteristics of these patients are shown in Table 3. In this cohort, 38.9% of patients were over 70 years old, and 58% were male. Tumor location of the lower third was observed in 62.3%. Intestinal type was found in 52.5%. All patients had MSI-H gastric cancer, and 69.8% of patients showed instability in all five MSI markers. Pathologic stage II and stage III were identified in 77 (47.5%) and 85 (52.5%), respectively. Lymph invasion, vascular invasion, and perivascular invasion were identified in 77.8%, 15.4%, and 37.7%, respectively. In addition, 75 patients (46.3%) were not treated with adjuvant chemotherapy. Fluoropyrimidine treatment alone, such as S1 or uracil and tegafur/leucovorin,

Table 2. Multivariable analysis for disease-free survival and overall survival (cohort 1)

Characteristic	No.	Disease-free survival			Overall survival		
		Hazard ratio	95% Confidence interval	p-value[a]	Hazard ratio	95% Confidence interval	p-value[a]
MSI							
MSS or MSI-L	318	1			1		
MSI-H	41	0.4	0.2-1.0	0.059	0.4	0.2-1.0	0.063
Sex							
Male	291	1			1		
Female	68	0.5	0.3-0.9	0.010	0.6	0.4-1.0	0.051
Age (yr)							
< 70	236	1			1		
≥ 70	123	1.6	0.9-2.6	0.091	1.9	1.1-3.3	0.017
Histology							
Poorly cohesive, signet ring cell type	42	1			1		
Other	317	1.1	0.7-1.7	0.779	0.9	0.5-1.4	0.535
Lauren							
Diffuse	137	1			1		
Intestinal	175	0.7	0.4-1.1	0.114	0.7	0.4-1.1	0.129
Mixed	44	1.0	0.5-1.8	0.943	1.0	0.5-1.8	0.939
Location							
Upper third	21	1			1		
Mid third	183	1.0	0.4-2.5	0.943	3.0	0.7-12.4	0.135
Lower third	155	1.1	0.4-2.8	0.844	3.7	0.9-15.6	0.073
Stage							
Ib	76	1			1		
II	145	2.8	1.0-7.5	0.044	4.1	1.2-14.2	0.025
III	138	14.0	5.2-38.2	< 0.001	20.0	5.8-69.6	< 0.001
Lymphatic							
Absent	137	1			1		
Present	222	2.1	1.2-3.6	0.010	1.8	1.0-3.2	0.048
Venous							
Absent	308	1			1		
Present	51	2.5	1.6-3.9	< 0.001	2.5	1.6-4.0	< 0.001
Perineural							
Absent	161	1			1		
Present	198	1.1	0.7-1.7	0.722	1.1	0.7-1.8	0.734
Adjuvant chemotherapy							
Not applied	183	1			1		
Applied	176	0.4	0.3-0.7	< 0.001	0.5	0.3-0.8	0.005

MSI, microsatellite instability; MSS, microsatellite stable; MSI-L, MSI-low; MSI-H, MSI-high. [a]The Cox proportional hazards regression model was used.

was used in 42 patients (25.9%), whereas 40 patients (24.7%) were treated with fluoropyrimidine plus platinum, including 5-fluorouracil plus cisplatin or capecitabine plus oxaliplatin. There was no difference in the use of adjuvant chemotherapy by stage, but the application of adjuvant chemotherapy decreased significantly with age (p=0.521 and p < 0.001). Of the patients who were ≥ 80 years old, 81.8% did not receive chemotherapy. In contrast, 82.4% of the patients under 60 years old were treated with adjuvant chemotherapy, and 51.0% received combination therapy with fluoropyrimidine and platinum (p < 0.001) (S3 Table).

4. Survival according to adjuvant chemotherapy in MSI-H gastric cancer patients (cohort 2)

In cohort 2, the median follow-up duration was 87.9 months after surgery. Median DFS and OS of all patients

Table 3. Characteristics of gastric cancer patients with MSI-H (cohort 2)

Characteristic	No. (%) (n=162)
Age (yr)	
Median (range)	66.5 (37-95)
≤ 59	55 (34.0)
60-69	44 (27.2)
70-79	52 (32.1)
≥ 80	11 (6.8)
Sex	
Male	94 (58.0)
Female	68 (42.0)
Tumor location	
Upper third	16 (9.9)
Mid third	41 (25.3)
Lower third	101 (62.3)
Whole	4 (2.5)
WHO classification	
Tubular, well differentiated	1 (0.6)
Tubular, moderately differentiated	77 (47.5)
Tubular, poorly differentiated	71 (43.8)
Other histological variants	13 (8.0)
Lauren classification	
Diffuse	50 (30.9)
Intestinal	85 (52.5)
Mixed	27 (16.7)
Instable microsatellite marker	
2	18 (11.1)
3	2 (1.2)
4	29 (17.9)
5	113 (69.8)
Pathologic stage	
IIA	19 (11.7)
IIB	58 (35.8)
IIIA	43 (26.5)
IIIB	27 (16.7)
IIIC	15 (9.3)
Lymphatic invasion	
Absent	36 (22.2)
Present	126 (77.8)
Venous invasion	
Absent	137 (84.6)
Present	25 (15.4)
Perineural invasion	
Absent	101 (62.3)
Present	61 (37.7)
Adjuvant chemotherapy	
No adjuvant therapy	75 (46.3)
Fluoropyrimidine alone (S1, UFTE/LV)	42 (25.9)
Fluoropyrimidine plus platinum (FP, XELOX)	40 (24.7)
Unknown	5 (3.1)

MSI-H, microsatellite instability-high; WHO, World Health Organization; UFTE, uracil and tegafur; LV, leucovorin.

were not reached. The result of univariable analysis between clinicopathologic factors and survival was shown in S4 Table. MSI-H patients treated with adjuvant chemotherapy showed longer DFS and OS than patients without chemotherapy (p=0.047 and p=0.043, respectively) (Fig. 2A and B). In MSI-H patients with stage II, this benefit of adjuvant chemotherapy was observed (p=0.001 in DFS, p=0.001 in OS) but not in MSI-H patients with stage III (p=0.867 in DFS, p=0.840 in OS). In patients who received fluoropyrimidine alone, the 5-year DFS and OS rates were 87.0% and 94.8%, respectively, which were higher than in the no adjuvant chemotherapy group (5-year DFS rate, 72.9%; p=0.044 [Bonferroni-corrected]; 5-year OS rate, 78.3%; p=0.022 [Bonferroni-corrected]) (Fig. 2C and D). In the fluoropyrimidine plus platinum group, the 5-year DFS and OS rates were 72.4% and 89.5%, respectively, which were not significantly different from the no adjuvant chemotherapy (p=0.880 [Bonferroni-corrected] and p=0.956 [Bonferroni-corrected], respectively). In addition, multivariable analysis with clinically significant factors, such as sex, age, stage, lymphatic invasion, venous invasion, perineural invasion, Lauren classification, and adjuvant chemotherapy, indicated that adjuvant chemotherapy in MSI-H gastric cancer patients was a significant independent prognostic factor for DFS (HR, 0.4; 95% CI, 0.2 to 1.0; p=0.040) (Table 4).

Discussion

In this study, the clinical features and predictive role of MSI-H for adjuvant chemotherapy were evaluated in curatively resected gastric cancer. MSI-H gastric cancer had a tendency of better prognosis than MSS/MSI-L after curative resection. In terms of the efficacy of adjuvant chemotherapy in MSI-H tumors, patients who received adjuvant chemotherapy could experience longer survival than those without adjuvant chemotherapy. Particularly, even adjuvant chemotherapy with fluoropyrimidine alone showed better survival than without adjuvant chemotherapy.

The clinical characteristics of MSI-H in curatively resected gastric cancer were distinctive from MSS/MSI-L. MSI-H tumor was diagnosed more frequently in older patients. In addition, MSI-H tumor was more common in patients with the intestinal type, other histology than poorly cohesive, signet ring cell type, and lower third tumor location. These findings were in accordance with previous studies [14,16]. In this study, MSI-H tumor was associated with present lymphatic invasion and absent perineural invasion. MSI was not correlated with early-stage cancers. This could be attributed to the exclusion of IA stage patients. In a previous study that included stage IA patients, MSI was observed more frequently in stage I (64.1%; T1, 44.1%; N0, 63.5%). Among stage II/III that were candidates for adjuvant chemotherapy, MSI-H was not observed frequently in earlier stage tumors [16].

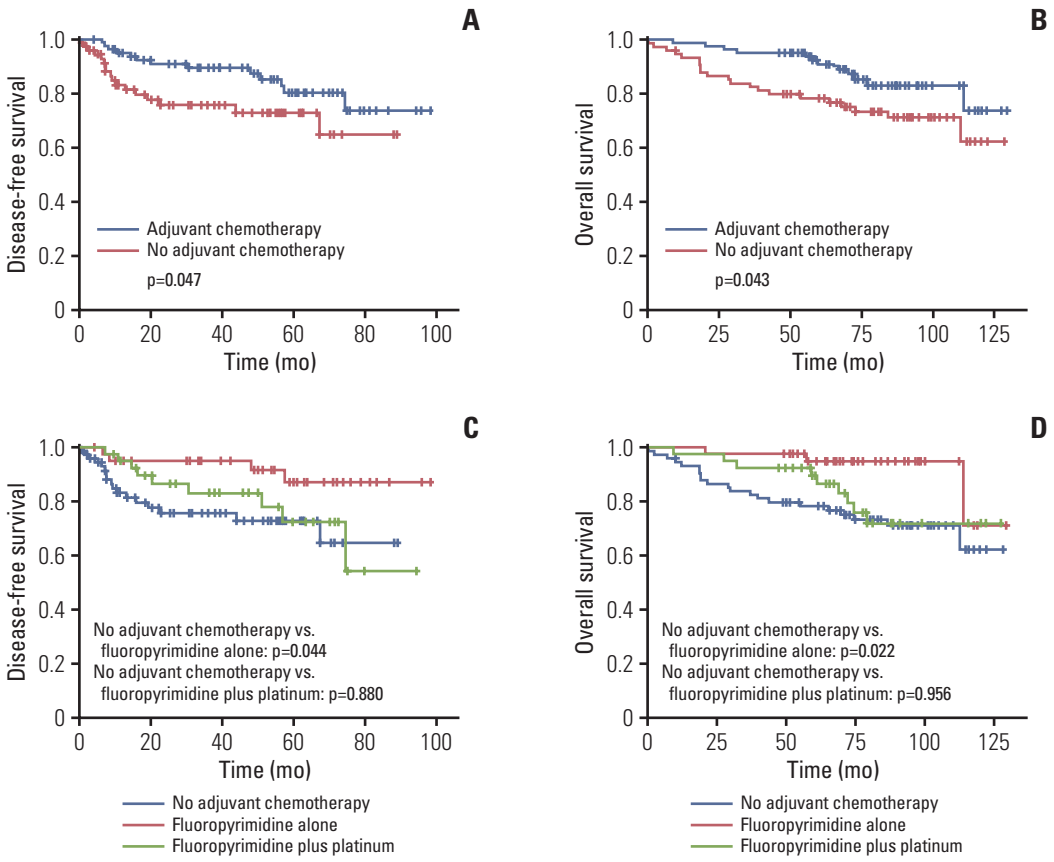

Fig. 2. Survival according to adjuvant chemotherapy in microsatellite instability–high gastric cancer. Bonferroni-corrected p-values, calculated by a Kaplan-Meier method. (A) Disease-free survival according to adjuvant chemotherapy. (B) Overall survival according to adjuvant chemotherapy. (C) Disease-free survival according to chemotherapy regimen. (D) Overall survival according to chemotherapy regimen.

MSI-H may be identified in just 7%-9% of resectable gastric cancers [14,16]. In the early stage that is not a candidate for adjuvant chemotherapy, MSI-H might be more frequently identified. Therefore, evaluation of the efficacy of adjuvant chemotherapy in MSI-H should be limited due to the small sample size. In previous studies related to the effects of adjuvant chemotherapy in MSI-H gastric cancer, only 40 and 20 MSI-H patients from the CLASSIC and the MAGIC study were included [15,17]. Just 33 MSI-H patients who received surgery alone and 88 patients with MSI-H tumor who received preoperative or adjuvant chemotherapy were included in the pooled analysis of four randomized trials [16]. In a retrospective study of a large cohort of 1,990 patients, just 54 patients with stage II/III were included for analysis of 5-fluorouracil adjuvant chemotherapy [14]. These studies demonstrated that MSI-H tumors did not benefit from adjuvant chemotherapy compared with MSS/MSI-L. However, due to small sample sizes, the use of these results to guide the application of adjuvant chemotherapy according to MSI status is limited. Although our study had a limitation due to its retrospective design, the population that was analyzed included 162 pathologic stage II/II patients with MSI-H tumor who were a candidate for adjuvant chemotherapy. This sample size was much larger than in previous studies. In contrast to previous studies, adjuvant chemotherapy could prolong the survival of patients, even in MSI-H gastric cancer. The efficacy of adjuvant chemotherapy in MSI-H patients could be an important clinical issue considering that MSI-H is more prevalent in older patients and those with an early stage of the disease. Therefore, this controversial result should be investigated in a further prospective study. Additionally, adjuvant chemotherapy with fluoropyrimidine alone showed a benefit in terms of survival, but fluoropyrimidine and platinum combination did not show better survival as an adjuvant therapy significantly. There was not significant effect of adjuvant chemotherapy in stage III in which more fluoropyrimidine and platinum combination was applied. Based on these findings of our study, platinum could be assumed to have a detrimental effect in MSI-H gastric cancer. In most previous studies related with adjuvant therapy in MSI-H gastric cancer, fluoropyrimidine and platinum combination was used. Fluoropyrimidine alone as an adjuvant chemotherapy in MIS-H gastric cancer was not evaluated. Therefore, adjuvant effect of fluoropyrimidine alone in MSI-

Table 4. Multivariable analysis for disease-free survival and overall survival (cohort 2)

Characteristic	No.	Disease-free survival			Overall survival		
		Hazard ratio	95% Confidence interval	p-value[a]	Hazard ratio	95% Confidence interval	p-value[a]
Sex							
Male	94	1			1		
Female	68	0.9	0.4-2.1	0.939	0.9	0.4-1.8	0.685
Age (yr)							
< 70	99	1			1		
≥ 70	63	1.1	0.5-2.5	0.771	2.4	1.1-5.3	0.028
Lauren							
Diffuse	50	1			1		
Intestinal	85	0.7	0.3-1.5	0.319	0.7	0.3-1.6	0.443
Mixed	27	0.4	0.1-1.5	0.166	0.3	0.1-1.2	0.076
Lymphatic invasion							
Absent	36	1			1		
Present	126	2.1	0.7-6.6	0.184	0.9	0.4-2.3	0.898
Venous invasion							
Absent	137	1			1		
Present	25	5.6	2.4-12.8	< 0.001	2.0	0.8-4.9	0.141
Perineural invasion							
Absent	101	1			1		
Present	61	1.0	0.5-2.1	0.948	1.0	0.5-2.1	0.960
Stage							
II	77	1			1		
III	85	2.1	0.9-4.9	0.077	1.3	0.6-2.7	0.553
Adjuvant chemotherapy							
No adjuvant therapy	75	1			1		
Adjuvant chemotherapy	82	0.4	0.2-1.0	0.040	0.7	0.3-1.5	0.327

[a]The Cox proportional hazards regression model was used.

H gastric cancer should be also evaluated in a further study.

In cases of MSI-H colorectal cancers, adjuvant chemotherapy with 5-fluorouracil alone may even have a detrimental effect on survival [8]. Therefore, recent guidelines do not recommend adjuvant chemotherapy with 5-fluorouracil alone in patients with MSI-H colorectal cancer [10,11]. However, it was reported that adding oxaliplatin could overcome this detrimental effect of 5-fluorouracil on patient survival in MSI-H colorectal cancers and that MSI-H alone did not affect survival in the case of adding oxaliplatin to treat stage III patients [21-24]. Inversely, in our study, adjuvant chemotherapy with fluoropyrimidine alone showed a benefit in terms of survival, which was different from the results obtained in colorectal cancer patients. It was reported that MSI status did not influence the survival of patients treated with 5-fluorouracil and the *in vitro* antitumor activity of 5-fluorouracil in gastric cancer cells [25]. This difference between gastric cancer and colorectal cancer could be attributed to the biologic differences of MSI-H according to tumor type [26]. In our analysis for mutational profiles of MSI-H gastric and colorectal cancers from The Cancer Genome Atlas database, the mutational profile was different between gastric cancer and colon cancer (S5 Fig.). MSI-H colon cancer showed an increased rate of *BRAF* mutations compared with MSI-H gastric cancer (55% vs. 22%), but MSI-H gastric cancer exhibited more *ARID1A*, *KMT2D*, and *RNF43* mutations than MSI-H colon cancer (S5 Fig.).

In conclusion, MSI-H tumor in patients with curatively resected gastric cancer had distinct characteristics with older age, intestinal type, other histology than poorly cohesive, signet ring cell type, lower third location, and absent perineural invasion. MSI-H could be a better prognostic marker in curatively resected gastric cancer. In MSI-H gastric cancer, adjuvant chemotherapy could show a survival benefit, which was in contrast to previous prospective studies and should be investigated in a further prospective trial.

Electronic Supplementary Material

Supplementary materials are available at Cancer Research and Treatment website (https://www.e-crt.org).

Conflicts of Interest

Conflicts of interest relevant to this article was not reported.

Acknowledgments

This study was supported by grant no. 11-2012-010 from the SNUBH research fund.

References

1. Boland CR, Thibodeau SN, Hamilton SR, Sidransky D, Eshleman JR, Burt RW, et al. A National Cancer Institute Workshop on Microsatellite Instability for cancer detection and familial predisposition: development of international criteria for the determination of microsatellite instability in colorectal cancer. Cancer Res. 1998;58:5248-57.
2. Boland CR, Goel A. Microsatellite instability in colorectal cancer. Gastroenterology. 2010;138:2073-87.
3. Yuza K, Nagahashi M, Watanabe S, Takabe K, Wakai T. Hypermutation and microsatellite instability in gastrointestinal cancers. Oncotarget. 2017;8:112103-15.
4. Hause RJ, Pritchard CC, Shendure J, Salipante SJ. Classification and characterization of microsatellite instability across 18 cancer types. Nat Med. 2016;22:1342-50.
5. Buckowitz A, Knaebel HP, Benner A, Blaker H, Gebert J, Kienle P, et al. Microsatellite instability in colorectal cancer is associated with local lymphocyte infiltration and low frequency of distant metastases. Br J Cancer. 2005;92:1746-53.
6. Marcus L, Lemery SJ, Keegan P, Pazdur R. FDA approval summary: pembrolizumab for the treatment of microsatellite instability-high solid tumors. Clin Cancer Res. 2019;25:3753-8.
7. Le DT, Uram JN, Wang H, Bartlett BR, Kemberling H, Eyring AD, et al. PD-1 blockade in tumors with mismatch-repair deficiency. N Engl J Med. 2015;372:2509-20.
8. Sargent DJ, Marsoni S, Monges G, Thibodeau SN, Labianca R, Hamilton SR, et al. Defective mismatch repair as a predictive marker for lack of efficacy of fluorouracil-based adjuvant therapy in colon cancer. J Clin Oncol. 2010;28:3219-26.
9. Gryfe R, Kim H, Hsieh ET, Aronson MD, Holowaty EJ, Bull SB, et al. Tumor microsatellite instability and clinical outcome in young patients with colorectal cancer. N Engl J Med. 2000;342:69-77.
10. Costas-Chavarri A, Nandakumar G, Temin S, Lopes G, Cervantes A, Cruz Correa M, et al. Treatment of patients with early-stage colorectal cancer: ASCO resource-stratified guideline. J Glob Oncol. 2019;5:1-19.
11. Labianca R, Nordlinger B, Beretta GD, Mosconi S, Mandala M, Cervantes A, et al. Early colon cancer: ESMO clinical practice guidelines for diagnosis, treatment and follow-up. Ann Oncol. 2013;24 Suppl 6:vi64-72.
12. Sasako M, Sakuramoto S, Katai H, Kinoshita T, Furukawa H, Yamaguchi T, et al. Five-year outcomes of a randomized phase III trial comparing adjuvant chemotherapy with S-1 versus surgery alone in stage II or III gastric cancer. J Clin Oncol. 2011;29:4387-93.
13. Noh SH, Park SR, Yang HK, Chung HC, Chung IJ, Kim SW, et al. Adjuvant capecitabine plus oxaliplatin for gastric cancer after D2 gastrectomy (CLASSIC): 5-year follow-up of an open-label, randomised phase 3 trial. Lancet Oncol. 2014;15:1389-96.
14. An JY, Kim H, Cheong JH, Hyung WJ, Kim H, Noh SH. Microsatellite instability in sporadic gastric cancer: its prognostic role and guidance for 5-FU based chemotherapy after R0 resection. Int J Cancer. 2012;131:505-11.
15. Choi YY, Kim H, Shin SJ, Kim HY, Lee J, Yang HK, et al. Microsatellite instability and programmed cell death-ligand 1 expression in stage II/III gastric cancer: post hoc analysis of the CLASSIC randomized controlled study. Ann Surg. 2019;270:309-16.
16. Pietrantonio F, Miceli R, Raimondi A, Kim YW, Kang WK, Langley RE, et al. Individual patient data meta-analysis of the value of microsatellite instability as a biomarker in gastric cancer. J Clin Oncol. 2019;37:3392-400.
17. Smyth EC, Wotherspoon A, Peckitt C, Gonzalez D, Hulkki-Wilson S, Eltahir Z, et al. Mismatch repair deficiency, microsatellite instability, and survival: an exploratory analysis of the Medical Research Council Adjuvant Gastric Infusional Chemotherapy (MAGIC) trial. JAMA Oncol. 2017;3:1197-203.
18. Cunningham D, Allum WH, Stenning SP, Thompson JN, Van de Velde CJ, Nicolson M, et al. Perioperative chemotherapy versus surgery alone for resectable gastroesophageal cancer. N Engl J Med. 2006;355:11-20.
19. Lee J, Lim DH, Kim S, Park SH, Park JO, Park YS, et al. Phase III trial comparing capecitabine plus cisplatin versus capecitabine plus cisplatin with concurrent capecitabine radiotherapy in completely resected gastric cancer with D2 lymph node dissection: the ARTIST trial. J Clin Oncol. 2012;30:268-73.
20. Bajetta E, Floriani I, Di Bartolomeo M, Labianca R, Falcone A, Di Costanzo F, et al. Randomized trial on adjuvant treatment with FOLFIRI followed by docetaxel and cisplatin versus 5-fluorouracil and folinic acid for radically resected gastric cancer. Ann Oncol. 2014;25:1373-8.
21. Gavin PG, Colangelo LH, Fumagalli D, Tanaka N, Remillard MY, Yothers G, et al. Mutation profiling and microsatellite instability in stage II and III colon cancer: an assessment of their prognostic and oxaliplatin predictive value. Clin Cancer Res. 2012;18:6531-41.
22. Kim ST, Lee J, Park SH, Park JO, Lim HY, Kang WK, et al. Clinical impact of microsatellite instability in colon cancer following adjuvant FOLFOX therapy. Cancer Chemother Pharmacol. 2010;66:659-67.
23. Oh SY, Kim DY, Kim YB, Suh KW. Oncologic outcomes after adjuvant chemotherapy using FOLFOX in MSI-H sporadic stage III colon cancer. World J Surg. 2013;37:2497-503.
24. Kim JE, Hong YS, Kim HJ, Kim KP, Kim SY, Lim SB, et al. Microsatellite instability was not associated with survival in stage III colon cancer treated with adjuvant chemotherapy of oxaliplatin and infusional 5-fluorouracil and leucovorin (FOLFOX). Ann Surg Oncol. 2017;24:1289-94.

25. Oki E, Kakeji Y, Zhao Y, Yoshida R, Ando K, Masuda T, et al. Chemosensitivity and survival in gastric cancer patients with microsatellite instability. Ann Surg Oncol. 2009;16:2510-5.

26. Imai K, Yamamoto H. Carcinogenesis and microsatellite instability: the interrelationship between genetics and epigenetics. Carcinogenesis. 2008;29:673-80.

pISSN 1598-2998, eISSN 2005-9256

Cancer Res Treat. 2020;52(4):1188-1198

https://doi.org/10.4143/crt.2020.402

Original Article

Open Access

Tumor Control and Overall Survival after Stereotactic Body Radiotherapy for Pulmonary Oligometastases from Colorectal Cancer: A Meta-Analysis

Hoon Sik Choi, MD, MS[1]
Bae Kwon Jeong, MD, PhD[2]
Ki Mun Kang, MD, PhD[1]
Hojin Jeong, PhD[2]
Jin Ho Song, MD, PhD[3]
In Bong Ha, MD, MS[2]
Oh-Young Kwon, MD, PhD[4]

[1]Department of Radiation Oncology and Institute of Health Science, Gyeongsang National University Changwon Hospital, Gyeongsang National University College of Medicine, Changwon, [2]Department of Radiation Oncology and Institute of Health Science, Gyeongsang National University Hospital, Gyeongsang National University College of Medicine, Jinju, [3]Department of Radiation Oncology, Seoul St. Mary's Hospital, College of Medicine, The Catholic University of Korea, Seoul, [4]Department of Neurology and Institute of Health Science, Gyeongsang National University Hospital, Gyeongsang National University College of Medicine, Jinju, Korea

Correspondence: Oh-Young Kwon, MD, PhD
Department of Neurology and Institute of Health Science, Gyeongsang National University Hospital, Gyeongsang National University College of Medicine, 79 Gangnam-ro, Jinju 52727, Korea
Tel: 82-55-750-8288
Fax: 82-55-750-1709
E-mail: oykwon@gnu.ac.kr

Received April 29, 2020
Accepted July 19, 2020
Published Online July 21, 2020

*Hoon Sik Choi and Bae Kwon Jeong contributed equally to this work.

Purpose

In pulmonary oligometastases from colorectal cancer (POM-CRC), the primarily recommended local therapy is metastasectomy. Stereotactic body radiotherapy (SBRT) is another local therapy modality that is considered as an alternative option in patients who cannot undergo surgery. The purpose of this meta-analysis is to demonstrate the effects of SBRT on POM-CRC by integrating the relevant studies.

Materials and Methods

The authors explored MEDLINE, EMBASE, Cochrane Library, Web of Science, and SCOPUS, and selected studies including patients treated with SBRT for POM-CRC and availability of local control (LC) or overall survival (OS) rate. In this meta-analysis, the effect of SBRT was presented in the form of the LC and OS rates for 1, 2, 3, and 5 years after SBRT as pooled estimates, and the frequency of pulmonary toxicity of grade 3 or higher after SBRT (PTG3-SBRT).

Results

Fourteen full texts among the searched 4,984 studies were the objects of this meta-analysis. The overall number of POM-CRC patients was 495 as per the integration of 14 studies. The pooled estimate LC rate at 1, 2, 3, and 5 years after SBRT was 81.0%, 71.5%, 56.0%, and 61.8%, and the OS rate was 86.9%, 70.1%, 57.9%, and 43.0%, respectively. The LC and OS rates gradually declined until 3 years after SBRT in a similar pattern. Among the 14 studies, only two studies reported PTG3-SBRT as 2.2% and 10.8%, respectively.

Conclusion

For POM-CRC, SBRT is an ablative therapy with a benefit on LC and OS rates and less adverse effects on the lung.

Key words

Colorectal neoplasms, Lung metastasis, Radiosurgery, Meta-analysis

Introduction

The limited number of metastatic tumors occurring at restricted sites are termed as oligometastases (OM). OM is an intermediate state of tumors, between widespread and localized, and implies the applicability of local therapy [1]. Unfortunately, colorectal cancer (CRC) recurs in more than half of patients even after definitive radical surgery [2,3]. In such patients, CRC recurs frequently in the form of OM in the liver and lung [4,5]. In patients with pulmonary OM from CRC (POM-CRC), metastasectomy along with systemic therapy leads to improvement in survival outcomes [6-10]. National

Comprehensive Cancer Network (NCCN) and European Society for Medical Oncology (ESMO) groups also recommend metastasectomy as an ablative therapy for POM-CRC [11-13].

Patients with metastatic cancer often refuse surgery or are medically or surgically inoperable. Stereotactic body radiotherapy (SBRT) can be an alternative ablative option for metastasectomy because it allows precise irradiation to lesions and minimal radiation exposure to surrounding normal tissues. The NCCN and ESMO groups also recommend SBRT as an alternative treatment modality for OM patients who are incapable of undergoing surgery. To present the effects of SBRT for POM-CRC, several studies with various publication types including original study, systematic review, and meta-analysis have been published [14,15]. Although previous studies have shown excellent tumor control ability of SBRT, physicians still do not have a clear reason to choose SBRT over surgery for POM-CRC patients. To directly or indirectly compare the treatment effect of surgery and SBRT, it is important to investigate the overall survival (OS) after SBRT in detail based on every year and to grasp the association between local control (LC) and OS rate.

This meta-analysis aimed to investigate the LC and OS rates of POM-CRC patients after SBRT serially at yearly time points and to investigate the relationship between them. The other goal was to investigate the frequency of pulmonary toxicity of grade 3 or higher after SBRT (PTG3-SBRT).

Materials and Methods

1. Search strategy

A meta-analysis was performed in compliance with 'the Preferred Reporting Items for Systematic Review and Meta-Analysis (PRISMA)' guidelines [16]. The protocol of this meta-analysis has been submitted to The International prospective register of systematic reviews (PROSPERO) (CRD-42020164111) [17].

To establish a strategy to find all studies that could be the subject of this meta-analysis as a study that applied SBRT as a local therapy to patients with POM-CRC and observed its outcome, appropriate search terms were selected. The words and phrases chosen were lung, pulmonary, metastasis, recurrence, colorectal, colon, sigmoid, rectal, cancer, carcinoma, tumor, neoplasm, radiosurgery, stereotactic body radiotherapy, stereotactic radiotherapy, stereotactic ablative radiotherapy, stereotactic radiosurgery, SBRT, stereotactic radiotherapy, and stereotactic ablative radiotherapy. While performing for relevant studies, the publication date chosen was from database inception to September 3, 2019. MEDLINE, EMBASE, Cochrane Library, Web of Science, and SCOPUS were the online databases used. Other bibliographies, such as reference lists and gray literature were also examined. There was no limitation with regard to publication date or language. EndNote X9.2 was the software used to handle the searched studies [18].

2. Study selection

For this meta-analysis, the following inclusion criteria were set: original researches, studies having information about CRC as primary cancer and pulmonary metastasis as OM, and studies providing information on at least one of LC and OS rates. The studies that included patients with concurrent uncontrolled extrathoracic metastasis when performing SBRT were excluded because it can significantly affect survival. If there were multiple reports from an institution and it seemed that the patient samplings included the same patients, only one study was left by applying the following priority principle: single topic, more sampling of patients, and more up-to-date study.

The searched data was sent to EndNote X9.2. Immediately after the sending, the automatic check function of EndNote removed duplicated studies. After removing the duplicated studies, the initial screening process of the searched data was embarked. In the initial screening process, the studies with irrelevant subjects were removed using titles and abstracts. The studies filtered in the initial screening process entered into the second selection process. In this course, the researchers reviewed the full texts of the screened studies carefully and selected studies that suited the purpose of this meta-analysis. In this process, four reviewers (H.S. Choi, B.K. Jeong, I.B. Ha, and K.M. Kang) worked independently. For the disagreements that occurred between the four reviewers, the authors reappraised the studies through discussion or consultation with other authors (H. Jeong and J.H. Song).

3. Data synthesis and analysis

Information extracted from the selected studies was general data (authors, publication years, study design, and OM definition), patient details (sample number, age, sex, tumor size, and follow-up duration), treatment profiles (SBRT dose, fractionation, and presence of concurrent chemotherapy) and outcome (LC rate, OS rate, and PTG3-SBRT).

For this meta-analysis, we used R ver. 3.5.3 (The R Foundation for Statistical Computing, Vienna, Austria) [19]. LC and OS rates were extracted as effect sizes to calculate pooled estimates at the time points of 1 year, 2 years, 3 years, and 5 years after SBRT for patients with POM-CRC. The selected studies were conducted on similar patients treated with standardized modalities and provided LC rate, OS rate, or both. Thus, we used a fixed-effects model for the meta-analysis as a predetermined way on the viewpoint that heterogeneity did not seem clinically significant among the studies. The studies included in this meta-analysis adopted one of the Common Terminology Criteria for Adverse Events (CTCAE) and Radiation Therapy Oncology Group (RTOG) scale to evaluate pulmo-

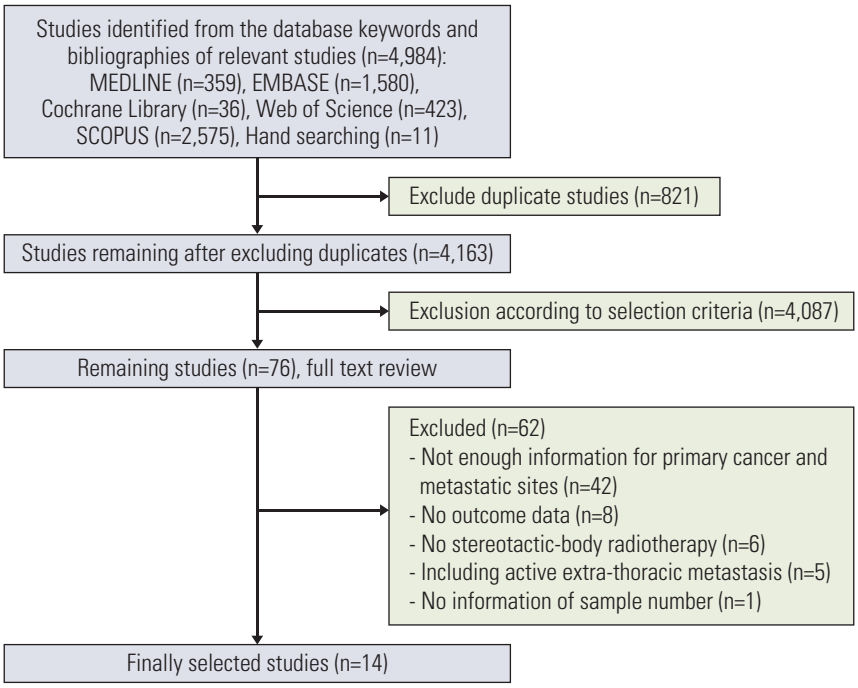

Fig. 1. Flow map for identification of relevant studies.

nary toxicity. The frequency of PTG3-SBRT was reviewed.

A forest plot for each meta-analysis was generated to display the findings. For visual evaluation of heterogeneity, the forest plots were used. Cochrane's Q and I^2 were calculated for each analysis as statistical methods for measuring the heterogeneity. When the p-value of Cochran's Q was less than 0.1 or the I^2 was more than 50%, heterogeneity was considered significant among the studies.

Eventually, 14 studies were selected in this meta-analysis. The authors, however, should perform different meta-analyses with recombination of the studies. The recombination was according to the types of outcomes and the time points of observation. As the number of studies incorporated in each meta-analysis was less than 10, evaluation of the publication bias was inappropriate in this review.

4. Quality assessment of literature

The Newcastle-Ottawa-Scale (NOS) is a checklist for assessing the quality of literature in meta-analyses for non-randomized studies [20]. In this meta-analysis, the cohort version NOS was used for quality assessment of the literature. When evaluating each of the finally selected studies as the NOS, two authors (H.S. Choi, O.Y. Kwon) independently evaluated and formed a consensus. The NOS for cohort studies consists of nine items grouped into three dimensions: selection, comparability, and outcome. It uses a star system that assesses each item and gives one star if the study has the highest quality for that. The only item of comparability can have two stars as an exception. Therefore, the number of stars that each study can have in the evaluation by the NOS ranges between 0-9. The NOS scores 7-9 refer to high-quality and 4-6 refer to medium quality.

Results

1. Identification of relevant studies

Using the initially set search strategy, we collected 4,984 studies that could be the probable subject of research: 359 from MEDLINE, 1,580 from EMBASE, 36 from Cochrane Library, 423 from Web of Science, 2,575 from SCOPUS, and 11 from hand searching. Immediately after the collection, we excluded 821 duplicate studies. Through the initial screening process with the remaining 4,163 studies, 4,087 studies were eliminated from the data. Through the secondary selection process with the full texts of the remaining 76 studies, 62 studies were excluded for the following reasons: not enough information for being aware of primary cancer and metastatic sites (n=42), no outcome data (n=8), no SBRT (n=6), including active extrathoracic metastasis (n=5), and no information about the sample number (n=1). Finally, 14 studies encompassing 495 patients with POM-CRC who underwent SBRT entered in this meta-analysis [21-34]. The process for study inclusion is presented in Fig. 1.

2. Features of the included studies

As shown in Table 1, 14 studies were selected for this meta-analysis. The publication year of the studies was between

Table 1. Characteristics of the 14 studies selected for the meta-analysis

Study	Design of study	Definition of OMS[a)]	Tumor size, median (cm)	BED10 (median, Gy)	Concurrent CTx	No. of samples	Age, median (yr)	Female (%)	FU, median (mo)
Dell'Acqua (2019) [27]	R	5	NA	NA	Yes	54	NA	NA	NA
Jingu (2017) [29]	R	NA	1.5	105.6	NA	93	69	35.5	28.0
Kinj (2017) [31]	R	4	1.6	180.0	NA	53	69	66.0	33.0
Agolli (2016) [21]	R	4	NA	NA	NA	44	68	27.0	36.0
Aoki (2016) [22]	R	3	NA	NA	No	13	NA	NA	NA
Binkley (2015) [24]	R	NA	NA	NA	NA	26	NA	NA	NA
Carvajal (2015) [25]	P	1	1.0	149.6	NA	13	69	30.5	9.2
Filippi (2015) [28]	R	5	NA	93.6	No	40	70	50.0	20.0
Jung (2015) [30]	R	3	NA	105.6	NA	50	65	NA	42.8
Comito (2014) [26]	P	3	NA	105.6	No	40	NA	NA	NA
Navarria (2014) [32]	P	5	NA	NA	NA	29	NA	NA	NA
Bae (2012) [23]	R	4	NA	NA	NA	12	NA	NA	NA
Takeda (2011) [33]	R	NA	1.8	100.0	No	15	61	13.3	29.0
Kim (2009) [34]	R	3	2.1	112.5	No	13	54	53.8	28.0

OMS, oligometastases; BED10, biologically effective dose with an alpha/beta ratio of 10; CTx, chemotherapy; FU, follow-up; R, retrospective; P, prospective; NA, not available. [a)]Maximum allowable number of metastatic pulmonary lesions.

Table 2. Clinical outcomes and data on pulmonary toxicity after stereotactic body radiotherapy

Study	Local control (%)				Overall survival (%)				Toxicity	
	1-Year	2-Year	3-Year	5-Year	1-Year	2-Year	3-Year	5-Year	≥ Grade 3	Criteria
Dell'Acqua (2019) [27]	78.0	75.0	45.0	NA	NA	NA	NA	NA	0.0	CTCAE 4.0
Jingu (2017) [29]	NA	NA	65.2	56.2	88.7	61.3	55.9	42.7	2.2	CTCAE 4.0
Kinj (2017) [31]	79.8	78.2	75.0	70.0	83.8	69.3	62.0	58.3	0.0	NA
Agolli (2016) [21]	NA	NA	NA	NA	82.8	67.7	50.8	NA	0.0	CTCAE 4.0
Aoki (2016) [22]	NA	70.0	67.6	NA	NA	NA	60.6	NA	0.0	CTCAE 4.0
Binkley (2015) [24]	74.5	57.8	NA	NA	NA	NA	NA	NA	NA	CTCAE 4.0
Carvajal (2015) [25]	92.3	92.3	NA	NA	92.3	92.3	66.7	NA	0.0	CTCAE 3.0
Filippi (2015) [28]	NA	NA	NA	NA	88.0	73.0	50.0	39.0	10.8	RTOG
Jung (2015) [30]	88.7	74.0	70.6	NA	95.0	75.0	64.0	35.0	0.0	CTCAE 4.0
Comito (2014) [26]	85.0	75.0	70.0	NA	87.0	68.0	58.0	NA	0.0	CTCAE 3.0
Navarria (2014) [32]	89.7	NA	NA	NA	NA	78.0	NA	NA	0.0	CTCAE 3.0
Bae (2012) [23]	NA	NA	66.0	66.0	NA	NA	57.0	34.0	NA	CTCAE 3.0
Takeda (2011) [33]	80.0	73.0	40.0	NA	NA	NA	NA	NA	NA	CTCAE 3.0
Kim (2009) [34]	76.9	52.7	52.7	NA	100	75.5	64.7	NA	0.0	CTCAE 2.0

NA, not available; CTCAE, Common Terminology Criteria for Adverse Events; RTOG, Radiation Therapy Oncology Group.

Table 3. Local control and overall survival as pooled estimates after SBRT

Elapsed years after SBRT	Local control rate				Overall survival rate			
	Pooled estimate (%)	95% CI	No. of studies	Study	Pooled estimate (%)	95% CI	No. of studies	Study
1 Year	81.0	77.8-83.8	9	Dell'Acqua (2019) [27], Kinj (2017) [31], Binkley (2015) [24], Carvajal (2015) [25], Jung (2015) [30], Comito (2014) [26], Navarria (2014) [32], Takeda (2011) [33], Kim (2009) [34]	86.9	83.0-90.0	8	Jingu (2017) [29], Kinj (2017) [31], Agolli (2016) [21], Carvajal (2015) [25], Filippi (2015) [28], Jung (2015) [30], Comito (2014) [26], Kim (2009) [34]
2 Years	71.5	67.9-74.8	9	Dell'Acqua (2019) [27], Kinj (2017) [31], Aoki (2016) [22], Binkley (2015) [24], Carvajal (2015) [25], Jung (2015) [30], Comito (2014) [26], Takeda (2011) [33], Kim (2009) [34]	70.1	65.7-74.16	9	Jingu (2017) [29], Kinj (2017) [31], Agolli (2016) [21], Carvajal (2015) [25], Filippi (2015) [28], Jung (2015) [30], Comito (2014) [26], Navarria (2014) [32], Kim (2009) [34]
3 Years	56.0	52.2-59.8	9	Dell'Acqua (2019) [27], Jingu (2017) [29], Kinj (2017) [31], Aoki (2016) [22], Jung (2015) [30], Comito (2014) [26], Bae (2012) [23], Takeda (2011) [33], Kim (2009) [34]	57.9	53.5-62.2	10	Jingu (2017) [29], Kinj (2017) [31], Agolli (2016) [21], Aoki (2016) [22], Carvajal (2015) [25], Filippi (2015) [28], Jung (2015) [30], Comito (2014) [26], Bae (2012) [23], Kim (2009) [34]
5 years	61.8	54.6-68.6	3	Jingu (2017) [29], Kinj (2017) [31], Bae (2012) [23]	43.0	37.2-49.0	5	Jingu (2017) [29], Kinj (2017) [31], Filippi (2015) [28], Jung (2015) [30], Bae (2012) [23]

SBRT, sterotactic-body radiotherapy; CI, confidence interval.

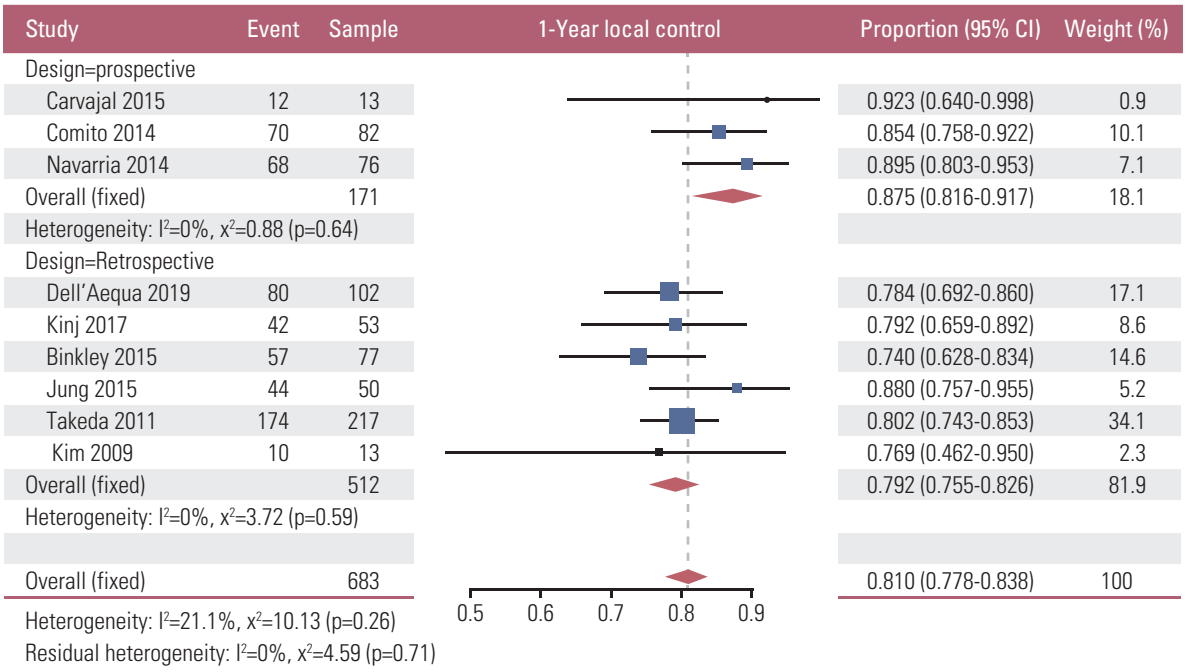

Fig. 2. Pooled estimates of local control rate at 1 year after stereotactic body radiotherapy [24-27,30-34]. CI, confidence interval.

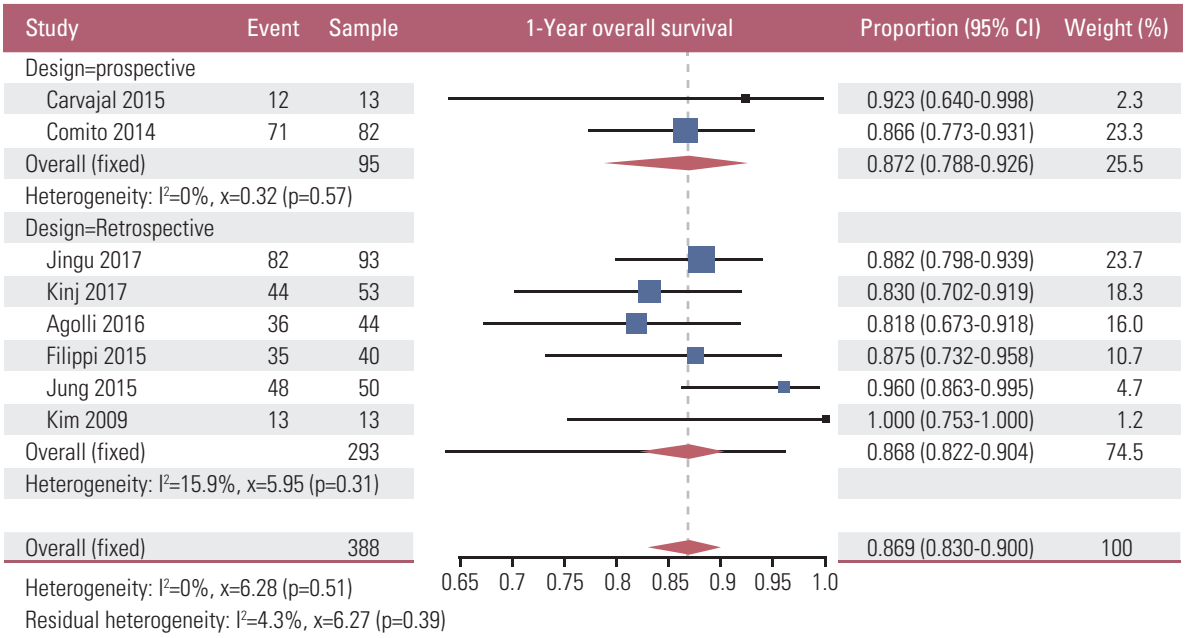

Fig. 3. Pooled estimates of overall survival rate at 1 year after stereotactic body radiotherapy [21,25,26,28-31,34]. CI, confidence interval.

2009 and 2019. The design was retrospective in 11 studies and prospective in the other three studies. Six of 14 studies reported whether chemotherapy was concurrently given, during the SBRT period: a study [27] allowed concurrent chemotherapy in the study design; and the other five studies [22,26,28,33,34] excluded these patients from the analysis. OM was defined based on the number of lesions in 11 of 14 studies. The maximum allowable number of pulmonary lesions as OM in each study ranged from 1 to 5; the median was four. The median value of metastatic tumor size from five studies ranged from 1.0 to 2.1 cm; the median was 1.6 cm. The median prescription doses of SBRT collected from eight studies were converted based on a biologically effective dose with an alpha/beta ratio of 10 (BED10). The median of

BED10 was 105.6 Gy and ranged from 93.6 to 180 Gy. For the finally selected 14 studies, the sample number varied from 12 to 93 and the median was 34.5. The median age of patients from eight studies ranged from 54 to 70 years, and the median of the medians was 68.5 years. The median percentage of females was 35.5% (13.3%-66.0%) among the seven studies, which provided sex distribution. The median follow-up duration in eight studies ranged from 9.2 to 42.8 months, and the median was 28.5 months.

The effect sizes of LC and OS rate at 1, 2, 3, and 5 years after SBRT were extracted from each primary study and shown in Table 2. The median rate of LC, at 1, 2, 3, and 5 years was 80.0% (74.5%-92.3%, n=9), 74.0% (52.7%-92.3%, n=9), 66.0% (40.0%-75.0%, n=9), and 66.0% (56.2%-70.0%, n=3), respectively. The median rate of OS at 1, 2, 3, and 5 years was 88.4% (82.8%-100.0%, n=8), 73.0% (61.3%-92.3%, n=9), 59.3% (50.0%-66.7%, n=10), and 39.0% (34.0%-58.3%, n=5), respectively. All the finally selected studies provided information on the frequency of PTG3-SBRT. As criteria for evaluating the toxicity of SBRT, the CTCAE was applied in 12 studies (ver. 2.0 for one, ver. 3.0 for five, and ver. 4.0 for six) and the RTOG in one study. The remaining study did not provide information about the criteria. There were two of 14 studies that provided information about PTG3-SBRT. In a study using the CTCAE as an evaluation tool, PTG3-SBRT occurred in 2.2% of patients [29]. Another study, which evaluated the toxicity based on RTOG, reported PTG3-SBRT as a dense radiographic appearance in 10.8% of patients, but all the patients were asymptomatic [28].

3. Pooled estimates

The pooled estimates of the LC and the OS rate at 1, 2, 3, and 5 years after SBRT are shown in Table 3. Nine studies reported the LC rate at 1 year after SBRT, with a pooled estimate of 81.0% (95% confidence interval [CI], 77.8 to 83.8); for this, I^2 was 21.1%, and Q-value was 10.13 (p=0.26). The estimate was 87.5% (95% CI, 81.6 to 91.7) in three prospective studies and 79.2% (95% CI, 75.5 to 82.6) in six retrospective studies in the subgroup analysis performed according to the study designs. The Q-value was 5.54 between the subgroups (p=0.019) and 4.59 within the subgroups (p=0.71) (Fig. 2). Combination of nine studies revealed the pooled estimate of the LC rate at 2 years after SBRT as 71.5% (95% CI, 67.9 to 74.8), I^2 was 37.9%, and Q-value was 12.88 (p=0.12). The pooled estimate was 77.0% (95% CI, 67.3 to 84.5) for two prospective studies and 70.7% (95% CI, 66.8 to 74.3) for seven retrospective studies in the subgroup analysis. Q was 1.53 (p=0.22) between the groups and 11.35 (p=0.12) within the groups. The pooled estimate at 3 years after SBRT was 56.0% (95% CI, 52.2 to 59.8) when collecting LC rates at 3 years after SBRT from 9 studies. I^2 was 84.8% and Q-value was 52.72 ($p < 0.01$) for this analysis. One of the nine studies was a prospective study and eight were retrospective. While collecting three retrospective studies reporting LC at 5 years after SBRT, the pooled estimate, I^2, and Q-value were 61.8% (95% CI, 54.6 to 68.6), 34.8%, and 3.07 (p=0.22), respectively.

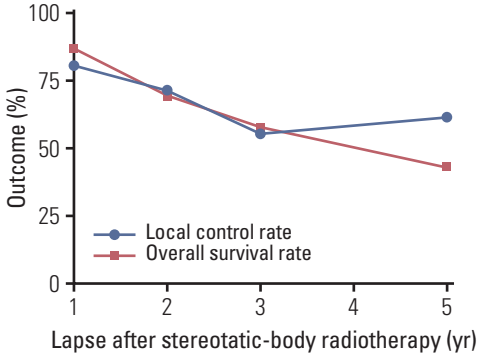

Fig. 4. Local control and overall survival at 1, 2, 3, and 5 years after stereotactic body radiotherapy with trend lines.

Eight out of 14 studies reported OS rate at 1 year after SBRT, and the pooled estimate, I^2, and Q-value were 86.9% (95% CI, 83.0 to 90.0), 0.0%, and 6.28 (p=0.51), respectively (Fig. 3). In the subgroup analysis for the study design, the pooled estimate was 87.2% (95% CI, 78.8 to 92.6) for two prospective studies out of the eight studies and 86.8% (95% CI, 82.2 to 90.4) for the other six retrospective ones. Q was 0.01 (p=0.92), between the subgroups and 6.27 (p=0.39) within the subgroups (Fig. 3). Nine studies reported OS rate at 2 years after SBRT. The pooled estimate was 70.1% (95% CI, 65.7 to 74.2), I^2 was 14.1%, and Q-value was 9.32 (p=0.32). The pooled estimate was 73.4% (95% CI, 66.1 to 79.6) for the three prospective studies out of the nine studies and 68.3% (95% CI, 62.7 to 73.4) for the other six retrospective ones. Q-value was 1.27 (p=0.26) between the subgroups and 8.04 (p=0.33) within the subgroups. Ten studies provided afforded OS rate at 3 years after SBRT. The pooled estimate was 57.9% (95% CI, 53.5 to 62.2), I^2 was 0.0%, and Q-value was 4.46 (p=0.88). For the subgroup analysis, the pooled estimate was 59.9% (95% CI, 49.8 to 69.3) for the two prospective studies out of the 10 studies and 57.4% (95% CI, 52.5 to 62.2) for the other eight retrospective studies. Q-value was 0.19 (p=0.66) between the subgroups and was 4.27 (p=0.81) within the subgroups. The pooled OS rate was 43.0% (95% CI, 37.2 to 49.0) at 5 years after SBRT, and I^2 was 46.4, and Q-value was 7.46 (p=0.11) as per the five retrospective studies.

A line graph showing the serial rates of LC and OS was created to observe the relation between them (Fig. 4). The trend line of LC showed a gradual decrease pattern until three years after the SBRT and no further decrease at five years after SBRT. Meanwhile, that of OS showed a continuous decrease until five years after SBRT. Both the trend lines showed very similar changes up to 3 years after SBRT.

4. Study quality assessment

A star for the item 'selection of the non-exposed cohort' and 'comparability' for all studies while assessing the quality of primary studies could not be provided in this meta-analysis through NOS due to the absence of controls in all the studies. In six studies, the follow-up period was less than 2 years and it was judged that the periods were not sufficient for observing the outcome and toxicity. A star could not be given for six studies for the item 'length of outcome' in NOS. As a result, six out of 14 studies subjected to this meta-analysis received five stars in the NOS evaluation, and the remaining eight studies received six stars. Therefore, all subjects of this meta-analysis had medium quality. The results of the assessment are provided in S1 Table.

Discussion

A meta-analysis was conducted by collecting 14 studies that reported the effect of SBRT for POM-CRC. Overall, 495 patients were included in the study. The average number of metastatic lung lesions was 1.4 per patient, and the median prescription dose of SBRT for the POM-CRC was 105.6 Gy of BED10. The primary goal of this meta-analysis was to combine LC and OS rates over time after SBRT for POM-CRC. The investigated time points were 1 year, 2 years, 3 years, and 5 years after SBRT. For each time points, the LC rate was 81.0%, 71.5%, 56.0%, and 61.8%, respectively, and the OS rate was 86.9%, 70.1%, 57.9%, and 43.0%, respectively. A gradual decrease in the LC and OS rates was observed with a similar pattern from 1 year to 3 years after SBRT. However, after 3 years, only the OS rate decreased and no change was observed in the LC rate. Only two studies reported PTG3-SBRT with a frequency of 2.2% and 10.8%, respectively.

NCCN and ESMO groups prefer metastasectomy as an ablative therapy for POM-CRC and consider SBRT as another option when surgery is not possible. Several retrospective studies have reported the effect of pulmonary metastasectomy in POM-CRC patients with a 5-year OS rate of 32.4%-43% [7-10]. A meta-analysis involving 25 retrospective studies reported the effects of lung metastasectomy in POM-CRC patients with OS rate as a range value and the 5-year OS rate as 27%-68% [6]. A randomized clinical trial demonstrated the effect of metastasectomy for POM-CRC, the researchers compared the outcome of patients between a group with metastasectomy plus chemotherapy, and chemotherapy only as controls. At five years after treatment, the estimated survival rate was 38% and 29% for the metastasectomy group and controls, respectively [35]. As the study was terminated prematurely with only 65 participants due to recruiting difficulty, the data has weak evidence. Nonetheless, the information helps to assess the meaning of the present meta-analysis. The present meta-analysis revealed that the 5-year survival rate was 43% among the POM-CRC patients treated with SBRT. Although most of the primary studies included in this meta-analysis included the patients whose conditions were too poor to endure the operation in their cohort, the effects of SBRT for POM-CRC seemed comparable to metastasectomy effects demonstrated by previous studies. The information provided by the present meta-analysis suggests a new perspective that the SBRT can be a valuable option as a primary treatment of POM-CRC.

Despite comparable treatment outcomes, there are several obstacles for selecting SBRT as the first choice of ablative therapy for POM-CRC. Compared to other primary cancers, the presence of numerous hypoxic cells may make POM-CRC more radioresistant [36]. Clinical studies on SBRT in POM-CRC or POM from other primary cancers reported that the former had a lower LC rate after SBRT than the latter [33,37]. Nevertheless, it has become increasingly evident that higher radiation doses can surpass CRC radioresistance. A few studies have shown a significant benefit of the SBRT dose more than 100 Gy or 120 Gy (BED10) for the LC rate of POM-CRC [24,25,29]. Another study also found a dose-dependent effect of SBRT with BED10 more than 120 Gy for the OM that occurred in the liver, lymph nodes, and lung [23].

It is not clear if the LC derived by SBRT improves the survival rate in the POM-CRC patients [38]. Theoretically, SBRT, a local therapy method similar to surgery, can improve survival. The information provided by this meta-analysis provides a cue to get a solution to this issue. From yearly outcome information to the third year after SBRT, the sequential changes in the LC and OS rates are similar. Accordingly, up to 3 years after SBRT, the LC derived from SBRT in POM-CRC patients is hypothesized to have an association with the OS. Conversely, after 3 years, survival may be inhibited by other factors such as extrapulmonary metastases or the patient's general condition than the POM control, so additional survival improvement could be obtained through appropriate systemic therapy with supportive care.

Lung lesions move concordantly with the breath of the patients. Therefore, when physicians use radiotherapy as a treatment modality of POM-CRC, there is a concern that it is difficult to irradiate the correct location on the lesion. However, advances in the SBRT technique have put forward more effective and less toxic treatment by delivering high radiation dose to the targets and stiff dose gradient between normal tissues. Our meta-analysis also showed that SBRT is a less toxic and safe treatment option.

A previously reported systematic review gathered studies that investigated the effect of SBRT on POM-CRC without providing pooled estimates through meta-analysis [14]. Two previously reported meta-analyses investigated the effects of SBRT on POM-CRC. One of them presented pooled estimates as the odds ratio of local failure [39]. The other meta-analysis reported the LC, OS, and progression-free survival

rates after SBRT for POM-CRC [15]. Compared to information provided by the previous studies, our meta-analysis has an additional strength. For consistent and comprehensive integration, the studies whose cohort included the patients having active metastatic lesions outside the lung were excluded. The pooled estimates of the LC and OS rates obtained through the integration of the present meta-analysis may make the outcome information of POM-CRC treated with SBRT clearer.

The compositions were identical among the 14 studies chosen for the present meta-analysis. The primary studies enrolled in the present meta-analysis seemed not to vary in their characteristics. First, from the time we selected the studies, the inclusion criteria were set to recruit studies with possible homogeneity. All the primary studies had data for the POM-CRC patients without metastatic lesions when treated with SBRT. In particular, the authors selected only the studies that used the standardized SBRT with breath correction without concurrent chemotherapy and only the studies that reported LC and OS as outcomes. After collecting the studies, it was also possible to discover that there was homogeneity somewhat, among the studies. The average age of the patients included in each study was similar. Eight studies were available to obtain information on average age, with a distribution of age 54-70. In six of these studies, the mean age of the patient group was 65 or older. The design of the study also showed a low degree of heterogeneity among the included studies. Of the 14 subjects, 11 had a retrospective design, and only three had a prospective design. The quality assessment of the literature evaluated by the NOS also revealed low heterogeneity. The NOS scores of all the 14 research studies were 5-6 points, which was the medium quality. So, the authors presumed that the clinical heterogeneity was low and chose the fixed-effects model as a preset mode for the statistical method. The choice seemed appropriate, as the heterogeneity was also weak in terms of statistical figures and forest plots. Just at three years after SBRT, the LC rate showed substantial heterogeneity with an I^2 value of 88%. Nevertheless, it seemed to be a statistical coincidence because the heterogeneities of other meta-analyses, including the same studies, were low.

The present review has a limitation that most of the studies included in the meta-analysis were retrospective. Another limitation is that all the included studies lacked proper controls. Since studies comparing the SBRT treatment group with the surgical treatment group or chemotherapy only group were not in the finally selected studies, it was difficult to demonstrate whether SBRT improved outcomes statistically. Such limitations may have originated in a clinical environment that is difficult for researchers to overcome. It would be challenging to envision randomized controlled studies, given the cancer patient's right to choose the treatment. Despite such difficulties, more reliable information could be obtained if additional prospective studies emerge added later, and scholars gather and meta-analyze them.

In conclusion, we demonstrated that SBRT has been useful for the treatment of POM-CRC throughout this meta-analysis. This review demonstrates the relationship between LC and OS rates and the probable presence of a similar trend of gradual decrement up to 3 years after SBRT. Besides, this review shows that SBRT-related pulmonary toxicity might be acceptable for the treatment of POM-CRC. It is suggested that SBRT in POM-CRC could be an effective and safe ablative therapy and option for metastasectomy.

Electronic Supplementary Material

Supplementary materials are available at Cancer Research and Treatment website (https://www.e-crt.org).

Conflicts of Interest

Conflict of interest relevant to this article was not reported.

References

1. Hellman S, Weichselbaum RR. Oligometastases. J Clin Oncol. 1995;13:8-10.
2. Elias D, Benizri E, Vernerey D, Eldweny H, Dipietrantonio D, Pocard M. Preoperative criteria of incomplete resectability of peritoneal carcinomatosis from non-appendiceal colorectal carcinoma. Gastroenterol Clin Biol. 2005;29:1010-3.
3. Galandiuk S, Wieand HS, Moertel CG, Cha SS, Fitzgibbons RJ Jr, Pemberton JH, et al. Patterns of recurrence after curative resection of carcinoma of the colon and rectum. Surg Gynecol Obstet. 1992;174:27-32.
4. Lee WS, Yun SH, Chun HK, Lee WY, Yun HR, Kim J, et al. Pulmonary resection for metastases from colorectal cancer: prognostic factors and survival. Int J Colorectal Dis. 2007;22:699-704.
5. Van Cutsem E, Nordlinger B, Adam R, Kohne CH, Pozzo C, Poston G, et al. Towards a pan-European consensus on the treatment of patients with colorectal liver metastases. Eur J Cancer. 2006;42:2212-21.
6. Gonzalez M, Poncet A, Combescure C, Robert J, Ris HB, Gervaz P. Risk factors for survival after lung metastasectomy in colorectal cancer patients: a systematic review and meta-analysis. Ann Surg Oncol. 2013;20:572-9.
7. Pfannschmidt J, Muley T, Hoffmann H, Dienemann H. Prognostic factors and survival after complete resection of pulmonary metastases from colorectal carcinoma: experiences in 167 patients. J Thorac Cardiovasc Surg. 2003;126:732-9.
8. Saito Y, Omiya H, Kohno K, Kobayashi T, Itoi K, Teramachi M, et al. Pulmonary metastasectomy for 165 patients with colo-

rectal carcinoma: a prognostic assessment. J Thorac Cardiovasc Surg. 2002;124:1007-13.
9. Yedibela S, Klein P, Feuchter K, Hoffmann M, Meyer T, Papadopoulos T, et al. Surgical management of pulmonary metastases from colorectal cancer in 153 patients. Ann Surg Oncol. 2006;13:1538-44.
10. Zampino MG, Maisonneuve P, Ravenda PS, Magni E, Casiraghi M, Solli P, et al. Lung metastases from colorectal cancer: analysis of prognostic factors in a single institution study. Ann Thorac Surg. 2014;98:1238-45.
11. National Comprehensive Cancer Network. Rectal cancer (version 1. 2020) [Internet]. Plymouth Meeting, PA: National Comprehensive Cancer Network; 2020 [cited 2020 Jul 19]. Available from: https://www.nccn.org/professionals/physician_gls/pdf/rectal.pdf.
12. National Comprehensive Cancer Network. Colon cancer (version 1. 2020) [Internet]. Plymouth Meeting, PA: National Comprehensive Cancer Network; 2020 [cited 2020 Jul 19]. Available from: https://www.nccn.org/professionals/physician_gls/pdf/colon.pdf.
13. Van Cutsem E, Cervantes A, Adam R, Sobrero A, Van Krieken JH, Aderka D, et al. ESMO consensus guidelines for the management of patients with metastatic colorectal cancer. Ann Oncol. 2016;27:1386-422.
14. Kobiela J, Spychalski P, Marvaso G, Ciardo D, Dell'Acqua V, Kraja F, et al. Ablative stereotactic radiotherapy for oligometastatic colorectal cancer: systematic review. Crit Rev Oncol Hematol. 2018;129:91-101.
15. Cao C, Wang D, Tian DH, Wilson-Smith A, Huang J, Rimner A. A systematic review and meta-analysis of stereotactic body radiation therapy for colorectal pulmonary metastases. J Thorac Dis. 2019;11:5187-98.
16. Moher D, Liberati A, Tetzlaff J, Altman DG; PRISMA Group. Preferred reporting items for systematic reviews and meta-analyses: the PRISMA statement. Ann Intern Med. 2009;151:264-9.
17. Booth A, Clarke M, Dooley G, Ghersi D, Moher D, Petticrew M, et al. The nuts and bolts of PROSPERO: an international prospective register of systematic reviews. Syst Rev. 2012;1:2.
18. Clarivate Analytics. Endnote X9.2. Philadelphia, PA: Clarivate Analytics; 2019.
19. R Core Team. R: A language and environment for statistical computing [Internet]. Vienna: R Foundation for Statistical Computing; 2019 [cited 2020 Jul 19]. Available from: https://www.R-project.org/.
20. Wells G, Shea B, O'Connell D, Peterson J, Welch V, Losos M, et al. The Newcastle-Ottawa Scale (NOS) for assessing the quality of norandomized wtudies in meta-analysis [Internet]. Ottawa: Ottawa Hospital Research Institue; 2000 [cited 2020 Jul 19]. Available from: http://www.ohri.ca/programs/clinical_epidemiology/oxford.asp.
21. Agolli L, Bracci S, Nicosia L, Valeriani M, De Sanctis V, Osti MF. Lung metastases treated with stereotactic ablative radiation therapy in oligometastatic colorectal cancer patients: outcomes and prognostic factors after long-term follow-up. Clin Colorectal Cancer. 2017;16:58-64.
22. Aoki M, Hatayama Y, Kawaguchi H, Hirose K, Sato M, Akimoto H, et al. Stereotactic body radiotherapy for lung metastases as oligo-recurrence: a single institutional study. J Radiat Res. 2016;57:55-61.
23. Bae SH, Kim MS, Cho CK, Kang JK, Kang HJ, Kim YH, et al. High dose stereotactic body radiotherapy using three fractions for colorectal oligometastases. J Surg Oncol. 2012;106:138-43.
24. Binkley MS, Trakul N, Jacobs LR, von Eyben R, Le QT, Maxim PG, et al. Colorectal histology is associated with an increased risk of local failure in lung metastases treated with stereotactic ablative radiation therapy. Int J Radiat Oncol Biol Phys. 2015;92:1044-52.
25. Carvajal C, Navarro-Martin A, Cacicedo J, Ramos R, Guedea F. Stereotactic body radiotherapy for colorectal lung oligometastases: preliminary single-institution results. J BUON. 2015;20:158-65.
26. Comito T, Cozzi L, Clerici E, Campisi MC, Liardo RL, Navarria P, et al. Stereotactic ablative radiotherapy (SABR) in inoperable oligometastatic disease from colorectal cancer: a safe and effective approach. BMC Cancer. 2014;14:619.
27. Dell'Acqua V, Surgo A, Kraja F, Kobiela J, Zerella MA, Spychalski P, et al. Stereotactic radiation therapy in oligometastatic colorectal cancer: outcome of 102 patients and 150 lesions. Clin Exp Metastasis. 2019;36:331-42.
28. Filippi AR, Badellino S, Ceccarelli M, Guarneri A, Franco P, Monagheddu C, et al. Stereotactic ablative radiation therapy as first local therapy for lung oligometastases from colorectal cancer: a single-institution cohort study. Int J Radiat Oncol Biol Phys. 2015;91:524-9.
29. Jingu K, Matsuo Y, Onishi H, Yamamoto T, Aoki M, Murakami Y, et al. Dose escalation improves outcome in stereotactic body radiotherapy for pulmonary oligometastases from colorectal cancer. Anticancer Res. 2017;37:2709-13.
30. Jung J, Song SY, Kim JH, Yu CS, Kim JC, Kim TW, et al. Clinical efficacy of stereotactic ablative radiotherapy for lung metastases arising from colorectal cancer. Radiat Oncol. 2015;10:238.
31. Kinj R, Bondiau PY, Francois E, Gerard JP, Naghavi AO, Leysalle A, et al. Radiosensitivity of colon and rectal lung oligometastasis treated with stereotactic ablative radiotherapy. Clin Colorectal Cancer. 2017;16:e211-20.
32. Navarria P, Ascolese AM, Tomatis S, Cozzi L, De Rose F, Mancosu P, et al. Stereotactic body radiotherapy (sbrt) in lung oligometastatic patients: role of local treatments. Radiat Oncol. 2014;9:91.
33. Takeda A, Kunieda E, Ohashi T, Aoki Y, Koike N, Takeda T. Stereotactic body radiotherapy (SBRT) for oligometastatic lung tumors from colorectal cancer and other primary cancers in comparison with primary lung cancer. Radiother Oncol. 2011;101:255-9.
34. Kim MS, Yoo SY, Cho CK, Yoo HJ, Choi CW, Seo YS, et al. Stereotactic body radiation therapy using three fractions for isolated lung recurrence from colorectal cancer. Oncology. 2009;76:212-9.
35. Treasure T, Farewell V, Macbeth F, Monson K, Williams NR, Brew-Graves C, et al. Pulmonary Metastasectomy versus Continued Active Monitoring in Colorectal Cancer (PulMiCC): a multicentre randomised clinical trial. Trials. 2019;20:718.
36. van Laarhoven HW, Kaanders JH, Lok J, Peeters WJ, Rijken PF, Wiering B, et al. Hypoxia in relation to vasculature and

proliferation in liver metastases in patients with colorectal cancer. Int J Radiat Oncol Biol Phys. 2006;64:473-82.
37. Franceschini D, Cozzi L, De Rose F, Navarria P, Franzese C, Comito T, et al. Role of stereotactic body radiation therapy for lung metastases from radio-resistant primary tumours. J Cancer Res Clin Oncol. 2017;143:1293-9.
38. Siva S, MacManus M, Ball D. Stereotactic radiotherapy for pulmonary oligometastases: a systematic review. J Thorac Oncol. 2010;5:1091-9.
39. Jingu K, Matsushita H, Yamamoto T, Umezawa R, Ishikawa Y, Takahashi N, et al. Stereotactic radiotherapy for pulmonary oligometastases from colorectal cancer: a systematic review and meta-analysis. Technol Cancer Res Treat. 2018;17:1533033818794936.

pISSN 1598-2998, eISSN 2005-9256

Cancer Res Treat. 2020;52(4):1199-1210

https://doi.org/10.4143/crt.2020.303

Original Article

Open Access

High Systemic Inflammation Response Index (SIRI) Indicates Poor Outcome in Gallbladder Cancer Patients with Surgical Resection: A Single Institution Experience in China

Lejia Sun, MD[1]
Wenmo Hu, MD[1]
Meixi Liu, MD[2]
Yang Chen, MD[2]
Bao Jin, MD[1]
Haifeng Xu, MD[1]
Shunda Du, MD[1]
Yiyao Xu, MD[1]
Haitao Zhao, MD[1]
Xin Lu, MD[1]
Xinting Sang, MD[1]
Shouxian Zhong, MD[1]
Huayu Yang, PhD[1]
Yilei Mao, MD, PhD[1]

[1]*Department of Liver Surgery, Peking Union Medical College (PUMC) Hospital, PUMC and Chinese Academy of Medical Sciences, Beijing,* [2]*Peking Union Medical College (PUMC), PUMC and Chinese Academy of Medical Sciences, Beijing, China*

Correspondence: Yilei Mao, MD, PhD
Department of Liver Surgery, Peking Union Medical College (PUMC) Hospital, PUMC and Chinese Academy of Medical Sciences, Beijing 100730, China
Tel: 86-10-69156042
Fax: 86-10-69156042
E-mail: pumch-liver@hotmail.com

Co-correspondence: Huayu Yang, PhD
Department of Liver Surgery, Peking Union Medical College (PUMC) Hospital, PUMC and Chinese Academy of Medical Sciences, Beijing 100730, China
Tel: 86-10-69152831
Fax: 86-10-69152831
E-mail: dolphinyahy@hotmail.com

Received April 13, 2020
Accepted July 20, 2020
Published Online July 21, 2020

*Lejia Sun, Wenmo Hu, and Meixi Liu contributed equally to this work.

Purpose

The systemic inflammation response index (SIRI) has been reported to have prognostic ability in various solid tumors but has not been studied in gallbladder cancer (GBC). We aimed to determine its prognostic value in GBC.

Materials and Methods

From 2003 to 2017, patients with confirmed GBC were recruited. To determine the SIRI's optimal cutoff value, a time-dependent receiver operating characteristic curve was applied. Univariate and multivariate Cox analyses were performed for the recognition of significant factors. Then the cohort was randomly divided into the training and the validation set. A nomogram was constructed using the SIRI and other selected indicators in the training set, and compared with the TNM staging system. C-index, calibration plots, and decision curve analysis were performed to assess the nomogram's clinical utility.

Results

One hundred twenty-four patients were included. The SIRI's optimal cutoff value divided patients into high (≥ 0.89) and low SIRI (< 0.89) groups. Kaplan-Meier curves according to SIRI levels were significantly different ($p < 0.001$). The high SIRI group tended to stay longer in hospital and lost more blood during surgery. SIRI, body mass index, weight loss, carbohydrate antigen 19-9, radical surgery, and TNM stage were combined to generate a nomogram (C-index, 0.821 in the training cohort, 0.828 in the validation cohort) that was significantly superior to the TNM staging system both in the training (C-index, 0.655) and validation cohort (C-index, 0.649).

Conclusion

The SIRI is an independent predictor of prognosis in GBC. A nomogram based on the SIRI may help physicians to precisely stratify patients and implement individualized treatment.

Key words

Gallbladder neoplasms, Systemic inflammation response index (SIRI), Overall survival, Prognosis, Nomogram

Introduction

Gallbladder cancer (GBC) is a relatively rare tumor type with a poor prognosis [1]. With surgical resection currently the only curative therapy, median survival is approximately 25 months after curative resection according to a multicenter study in the United States conducted in 2016 [2]. It is also a significant source of mortality among countries in Asia and Latin America [3]. As Dr. Fortner and Pack stated in 1958, "the 5-year survival of a patient with GBC constitutes a medical curiosity" [4]. For many decades, physicians have been devoted to making more precise predictions of outcome for patients with GBC. To date, the TNM staging system, which was proposed by the American Joint Committee on Cancer (AJCC), remains the gold standard in cancer management [5]. However, other factors such as patients' demographic features, symptoms, and laboratory test data may also have important effects on the prognosis of GBC patients, which will lead to great divergence in clinical outcome even in patients at the same TNM stage. Therefore, more accurate and reliable prognostic models for GBC are urgently required in clinical practice.

In cancer development and progression, the inflammatory response is widely recognized as an important factor [6]. Some inflammation-based biomarkers, such as the platelet-to-lymphocyte ratio (PLR), monocyte-to-lymphocyte ratio (MLR), and neutrophil-to-lymphocyte ratio (NLR) have been proposed, and their potential to predict prognosis of GBC has been reported [7]. Recently, a novel inflammation-based biomarker combining peripheral monocytes, neutrophils, and lymphocytes count, named the systemic inflammation response index (SIRI), was proposed by Qi et al. [8], and shows good prognostic ability in some solid tumors including pancreatic, gastric, esophageal, and nasopharyngeal cancer [9-11]. However, there is still no evidence demonstrating whether the SIRI can act as a prognostic indicator to precisely predict GBC patient outcome. Additionally, to the best of our knowledge, there is no prediction model that includes inflammation-based biomarkers for GBC.

Hence, the aims of our study were to investigate the SIRI's prognostic value using our cohort of patients with GBC, and to construct a prognostic prediction model incorporating the SIRI and test its predictive accuracy.

Materials and Methods

1. Patients

From 1 December 2003 to 30 June 2017, a total of 124 patients diagnosed as GBC with pathological confirmation after surgical resection at Peking Union Medical College Hospital (PUMCH) in Beijing, China, were retrospectively recruited to this study.

The inclusion criteria were described as follows: (1) GBC confirmed by histopathological examination as the primary diagnosis; (2) surgical resection for GBC performed; (3) routine blood test, serum tumor biomarker test, and infection test results measured within 7 days before surgery; and (4) complete clinicopathological information and postoperative follow-up data available.

The exclusion criteria included: (1) lack of clear histopathological diagnosis; (2) missing clinicopathological information; (3) incomplete follow-up data; (4) other malignant tumors present; and (5) distant metastasis.

2. Data collection

Demographic and clinical information were manually reviewed from the medical records. We collected demographic data, symptoms such jaundice, fever, and weight loss, medical history including hypertension and diabetes, serum laboratory test results, physical examination findings, surgical records, and histopathological reports retrospectively. The SIRI was defined as: SIRI=N×M/L, in which N, L, and M refer to peripheral counts of neutrophils, lymphocytes, and monocytes. Since preoperative inflammatory status could affect the results of the complete blood count and thus had effect on the value of the SIRI, we also collected patients' preoperative inflammation status and antibiotics usage. We defined the combined inflammatory status as one of the following situations: (1) having acute inflammatory disease including acute pancreatitis, acute cholecystitis, or acute cholangitis at admission; (2) body temperature ≥ 37.3°C at admission with white blood cell (WBC) > 10×10^9/L. GBC stage and postoperative pathological TNM information were determined with the use of the AJCC 8th edition classification system [12]. The maximal tumor size, tumor differentiation grade, and incisional margins were judged based on observations made during surgery and the final histopathological reports. R0 resection was defined as microscopically negative incisional margins. And radical surgery was defined when the radical surgical protocols were carried out and R0 resection was achieved as well. The specific radical surgical protocols were determined by the preoperative staging, operative findings and the results of cryosection biopsy. In details, for patients at the stage Tis or T1a, simple cholecystectomy was performed; for patients at the stage T1b or T2a or T2b, cholecystectomy with > 2 cm hepatic wedge resection were performed; for patients at the stage T3, most of them were received cholecystectomy with en bloc hepatic resection (segments IVB and V), and the other also received extra hemihepatectomy and/or bile duct excision; and for patients at the stage T4, extended radical resection including cholecystectomy, major hepatic resection, peripheral organ resection (omentum, stomach, duodenum, etc.) were performed according to standard radical surgical procedures. For patients at the stage T1b or higher, regional lymphad-

Table 1. Baseline characteristics of all patients

Characteristic	Total	High SIRI (≥ 0.89)	Low SIRI (< 0.89)	p-value
Sex				
Male	69 (55.6)	34 (50.0)	35 (62.5)	0.204
Female	55 (44.4)	34 (50.0)	21 (37.5)	
Age (yr)				
≤ 65	72 (58.1)	37 (54.4)	35 (62.5)	0.465
> 65	52 (41.9)	31 (45.6)	21 (37.5)	
Jaundice				
No	104 (83.9)	56 (82.4)	48 (85.7)	0.635
Yes	20 (16.1)	12 (17.6)	8 (14.3)	
Fever				
No	112 (90.3)	58 (85.3)	54 (96.4)	0.064
Yes	12 (9.7)	10 (14.7)	2 (3.6)	
Fatigue				
No	115 (92.7)	61 (89.7)	54 (96.4)	0.182
Yes	9 (7.3)	7 (10.3)	2 (3.6)	
Weight loss				
No	78 (62.9)	41 (60.3)	37 (66.1)	0.577
Yes	46 (37.1)	27 (39.7)	19 (33.9)	
Gallstone				
No	69 (55.6)	43 (63.2)	26 (46.4)	0.071
Yes	55 (44.4)	25 (36.8)	30 (53.6)	
Hypertension				
No	86 (69.4)	52 (76.5)	34 (60.7)	0.078
Yes	38 (30.6)	16 (23.5)	22 (39.3)	
Diabetes				
No	97 (78.2)	54 (79.4)	43 (76.8)	0.828
Yes	27 (21.8)	14 (20.6)	13 (23.2)	
Combined inflammatory status				
No	120 (96.8)	65 (95.6)	55 (98.2)	0.626
Yes	4 (3.2)	3 (4.4)	1 (1.8)	
Preoperative antibiotics usage				
No	116 (93.5)	62 (91.2)	54 (96.4)	0.292
Yes	8 (6.5)	6 (8.8)	2 (3.6)	
BMI (kg/m²)				
≥ 24	56 (45.2)	29 (42.6)	27 (48.2)	0.589
< 24	68 (54.8)	39 (57.4)	29 (51.8)	
CA19-9 (U/mL)				
> 40	62 (50.0)	41 (60.3)	21 (37.5)	0.019
≥ 40	62 (50.0)	27 (39.7)	35 (62.5)	
Maximum tumor size (cm)	3.00 (1.77-4.85)	3.00 (1.87-5.00)	2.60 (1.60-4.50)	0.341
Histologic type				
Adenocarcinoma	119 (96.0)	64 (94.1)	55 (98.2)	0.377
Other	5 (4.0)	4 (5.9)	1 (1.8)	
Resection (R0)				
No	43 (34.7)	33 (48.5)	10 (17.9)	0.001
Yes	81 (65.3)	35 (51.5)	46 (82.1)	
Radical surgery				
No	54 (43.5)	39 (57.4)	15 (26.8)	0.001
Yes	70 (56.5)	29 (42.6)	41 (73.2)	

(Continued to the next page)

Table 1. Continued

Characteristic	Total	High SIRI (≥ 0.89)	Low SIRI (< 0.89)	p-value
Tumor differentiation				
G1	28 (22.6)	12 (17.6)	16 (28.6)	0.371
G2	44 (35.5)	24 (35.3)	20 (35.7)	
G3	37 (29.8)	24 (35.3)	13 (23.2)	
Gx	15 (12.1)	8 (11.8)	7 (12.5)	
TNM stage				
0	4 (3.2)	2 (2.9)	2 (3.6)	0.024
I	11 (8.9)	2 (2.9)	9 (16.1)	
IIA	12 (9.7)	5 (7.4)	7 (12.5)	
IIB	2 (1.6)	1 (1.5)	1 (1.8)	
IIIA	39 (31.5)	20 (29.4)	19 (33.9)	
IIIB	41 (33.1)	26 (38.2)	15 (26.8)	
IVA	4 (3.2)	2 (2.9)	2 (3.6)	
IVB	11 (8.9)	10 (14.7)	1 (1.8)	
Follow-up (mo)	20.00 (7.75-34.00)	12.50 (6.00-29.50)	27.00 (16.25-48.25)	0.009
Death				
No	45 (36.3)	17 (25.0)	28 (50.0)	0.005
Yes	79 (63.7)	51 (75.0)	28 (50.0)	

Values are presented as number (%) or median (range). SIRI, systemic inflammation response index; BMI, body mass index; CA19-9, carbohydrate antigen 19-9; TNM, tumor-node-metastasis.

enectomy was performed. Patients who received palliative surgery were based on one of the following reasons: (1) unresectable disease by operative findings; (2) comorbidity and aging, which could not bear the radical surgery; (3) false cryosection biopsy reports during operation; and (4) declined by the patient's relatives. The purpose of the palliative surgery was to clarify of diagnosis and relieve of the symptoms such as jaundice and abdominal pain. After discharge, all patients were regularly followed up. The last follow-up time and survival status were recorded. Overall survival (OS) was defined as the interval between the date of surgery and death or the last follow-up time. The last follow-up time was February 2020. After screening, the inclusion criteria were met by 124 patients that were included afterwards.

3. Statistical analysis

Categorical variables are presented as numbers and percentages, whereas continuous variables including the SIRI are presented by the median and first and third quartiles. Continuous variables such as body mass index (BMI) and carbohydrate antigen 19-9 (CA19-9) were transformed into categorical variables on the basis of routine cutoff values in the clinical application. The SIRI's optimal cutoff value for OS was calculated by applying a time-dependent receiver operating characteristic (ROC) analysis. Survival curves were plotted through the Kaplan-Meier method. Log-rank test was used to compare the differences between subgroups. Based on the SIRI cutoff value, patients were divided into high SIRI and low SIRI group. The correlations between different SIRI groups and clinicopathological variables were analyzed by Mann-Whitney U tests or two-sample t tests for continuous variables based on its normality, and by Fisher exact tests or Pearson chi-square tests for categorical variables.

Cox regression methodology was applied for univariate analysis. Variables with a p-value no more than 0.1 in univariate analysis and other potential confounding variables (e.g., the combined inflammatory status and preoperative antibiotics usage) were then subjected to the multivariate Cox proportional hazard regression model. The independent prognostic variables were selected according to the results of Cox proportional analyses. Then, we randomly divided the whole cohort into the nomogram development set and validation set in a proportion of 1:1. A prognostic nomogram was established for predicting OS in the training cohort and Harrell's concordance index (C-index) was used to measure the predictive accuracy both in the training and the validation cohort. Validation was based on 1,000 bootstrap re-samplings. Nomogram performance was evaluated using calibration plots. The prognostic nomogram was then compared with the traditional TNM staging system using the C-index and decision curve analysis both in the training and the validation cohort [13]. All statistical analyses were performed using SPSS ver. 25.0 (IBM Corp., Armonk, NY) and R 3.6.2 software (Institute of Statistics and Mathematics, Vienna, Austria). A two-sided p-values < 0.05 were considered statistically significant.

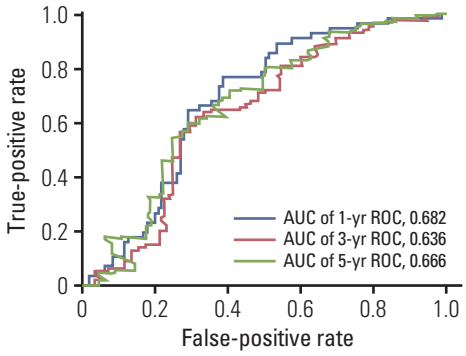

Fig. 1. Time-dependent receiver operating characteristic (ROC) analysis of systemic inflammation response index (SIRI) for 1-, 3-, and 5-year survival. AUC, area under the curve.

4. Ethical statement

The study was approved by the Ethics Committee of PUMCH and CAMS & PUMC (approval decision number: S-K1110) and was conducted according to the ethical standards of the World Medical Association Declaration of Helsinki [14]. In accordance with the committee's regulations, written informed consent was obtained from all patients who were alive.

Results

1. Patient baseline characteristics

A total of 124 patients with GBC were investigated in this study. Study patients' baseline characteristics are shown in Table 1. Sixty-nine patients (55.6%) were male and 55 (44.4%) were female. The median follow-up time was 20 months (range, 0.5 to 153 months). Twenty (16.1%), 12 (9.7%), nine (7.3%), and 46 (37.1%) patients developed jaundice, fever, fatigue, and weight loss, respectively, when diagnosed with GBC. Elevated preoperative serum CA19-9 was observed in 62 (50%) patients. Before operation for GBC, three patients had acute pancreatitis but no one had acute cholecystitis or cholangitis. Another one patient had elevated body temperature (≥ 37.3°C) with WBC > 10×10^9/L. In total, four patients were defined to have the combined inflammatory status as previously described. Eight patients had preoperative antibiotics usage. Eighty-five patients (68.5%) were intended to perform radical surgery and 70 of them (82.4%) achieved negative margins (R0 resection). The other 39 patients (31.5%)

Table 2. The relationship between the SIRI and surgical outcome

Characteristic	Total	High SIRI	Low SIRI	p-value
Length of stay in hospital (day)	15.00 (10.25-20.00)	16.00 (10.75-20.00)	12.00 (9.00-16.50)	0.007
Hemorrhage during operation (mL)	200 (50-400)	200 (100-400)	200 (50-300)	0.001
Barthel score (before operation-after operation)	35 (15-45)	35 (10-45)	40 (15-4)	0.768
Complications				
Bleeding				
No	120 (96.8)	64 (94.1)	56 (100)	0.127
Yes	4 (3.2)	4 (5.9)	0	
Infection				
No	107 (86.3)	58 (85.3)	49 (87.5)	0.799
Yes	17 (13.7)	10 (14.7)	7 (12.5)	
Liver failure				
No	124 (100)	68 (100)	56 (100)	-
Yes	0	0	0	
Biliary fistula				
No	120 (96.8)	65 (95.6)	55 (98.2)	0.627
Yes	4 (3.2)	3 (4.4)	1 (1.8)	
Ascites				
No	121 (97.6)	66 (97.1)	55 (98.2)	> 0.99
Yes	3 (2.4)	2 (2.9)	1 (1.8)	
Others				
No	113 (91.1)	60 (88.2)	53 (94.6)	0.342
Yes	11 (8.9)	8 (11.8)	3 (5.4)	
Complications				
No	95 (76.6)	49 (72.1)	46 (82.1)	0.286
Yes	29 (23.4)	19 (27.9)	10 (17.9)	

Values are presented as median (range) or number (%). SIRI, systemic inflammation response index.

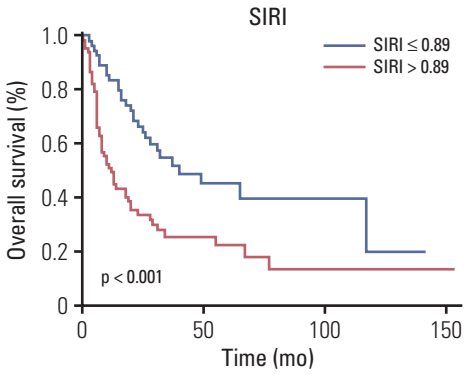

Fig. 2. Kaplan-Meier survival curves of different systemic inflammation response index (SIRI) groups.

received palliative surgery. According to the AJCC 8th edition, 39 patients were diagnosed as stage IIIA and 41 patients were stage IIIB. Postoperative histopathological reports revealed that the majority of our patients (119 patients, 96%) had adenocarcinoma, four patients had adenosquamous carcinoma, and one patient had intracholecystic papillary neoplasm. Finally, 79 patients (63.7%) were followed until death.

2. Clinicopathological features according to the SIRI

To calculate the SIRI's optimal cutoff value, we first generated 1-, 3-, and 5-year time-dependent ROC curves according to the SIRI's OS, as shown in Fig. 1, with areas under the curve (AUC) of 0.682, 0.636, and 0.666 respectively. Then we determined the SIRI's optimal cutoff value to be 0.89 using the 1-year time-dependent ROC curve. Based on this cutoff value, we divided the patients into high SIRI and low SIRI groups; the patients' characteristics of each group are also summarized in Table 1. Compared with the low SIRI group, there were more patients with high CA19-9 (> 40 U/mL) in the high SIRI group (60.3% vs. 37.5%, p=0.019). The surgical margin as R0 tended to be harder to achieve in the high SIRI group (51.5% vs. 82.1%, p=0.001). The patients in the high SIRI group tended to have higher TNM staging distribution (p=0.024). Furthermore, the median follow-up time was sig-

Table 3. Univariate and multivariate Cox proportional hazards analysis for OS in 124 patients with GBC

Characteristic	Univariate analysis			Multivariate analysis		
	HR	95% CI	p-value	HR	95% CI	p-value
Demographics						
Sex (female/male)	1.126	0.759-1.671	0.573	-	-	-
Age (> 65 yr/≤ 65 yr)	1.385	0.941-2.038	0.106	-	-	-
BMI (< 24 kg/m^2/≥ 24 kg/m^2)	1.988	1.268-3.118	0.002	2.008	1.162-3.471	0.013
Symptoms						
Jaundice (yes/no)	1.490	0.949-2.340	0.083	1.107	0.583-2.101	0.755
Weightloss (yes/no)	1.781	1.206-2.629	0.004	1.729	1.004-2.976	0.048
Fatigue (yes/no)	1.426	0.691-2.944	0.338	-	-	-
Fever (yes/no)	1.128	0.600-2.120	0.708	-	-	-
Past medical history						
Gallstone (yes/no)	1.115	0.760-1.635	0.600	-	-	-
Hypertension (no/yes)	1.442	0.928-2.243	0.127	-	-	-
Diabetes (no/yes)	1.184	0.739-1.897	0.500	-	-	-
Preoperative inflammation status						
Combined inflammatory status (yes/no)	1.230	0.447-3.383	0.688	1.624	0.197-13.386	0.652
Preoperative antibiotics usage (yes/no)	1.221	0.516-2.888	0.649	1.781	0.533-5.944	0.348
Inflammation-based biomarkers						
SIRI (high/low)	2.208	1.484-3.286	< 0.001	1.753	1.027-2.991	0.040
Blood test						
CA19-9 (> 40 IU/mL/≤ 40 IU/mL)	3.659	2.347-5.705	< 0.001	2.162	1.194-3.916	0.011
Post-operation						
Tumor size (> 5 cm/≤ 5 cm)	1.125	0.637-1.986	0.686	-	-	-
Adenocarcinoma (no/yes)	2.104	0.767-5.774	0.148	-	-	-
TNM stage (III-IV/0-II)	7.516	3.249-17.380	< 0.001	7.523	1.558-36.329	0.012
Radical surgery (no/yes)	3.945	2.629-5.920	< 0.001	2.940	1.676-5.159	< 0.001
Grade (G3/G1 or G2)	1.549	1.005-2.387	0.044	1.175	0.686-2.013	0.556

OS, overall survival; GBC, gallbladder cancer; HR, hazard ratio; CI, confidence interval; BMI, body mass index; SIRI, systemic inflammation response index; CA19-9, carbohydrate antigen 19-9; TNM, tumor-node-metastasis.

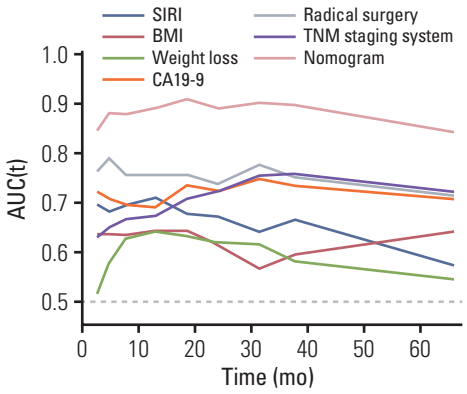

Fig. 3. Time-dependent receiver operating characteristic analysis of each of the selected factors and the prognostic model. SIRI, systemic inflammation response index; BMI, body mass index; CA19-9, carbohydrate antigen 19-9; AUC, area under the curve.

nificantly shorter in the high SIRI group (12.5 months vs. 27 months, p=0.009), with more patients reaching the state of death (75.0% vs. 50.0%, p=0.005).

3. The relationship between the SIRI and surgical outcome

To determine whether the SIRI can predict patients' surgical outcome, we compared the high SIRI group with the low SIRI group in terms of length of stay in hospital, hemorrhage during surgery, the change in Barthel score after surgery, and different kinds of complications including bleeding, infection, liver failure, biliary fistula, ascites, and others (Table 2). The patients in the high SIRI group tended to stay longer in hospital as compared with the low SIRI group (16 days vs. 12 days, p=0.007). Furthermore, during surgery, patients in the high SIRI group lost more blood than those in the low SIRI group, though the median blood losses were equal (200 mL vs. 200 mL, p=0.001). However, no significant differences were observed in the change in Barthel score and the incidence rates of all types of postoperative complications. Combining the occurrence of all the complications, there was still no significant difference between the high and low SIRI groups (p=0.286).

4. Factors predicting OS

The Kaplan-Meier curves of OS according to the SIRI showed significant difference, as confirmed by the log-rank test ($p < 0.001$) (Fig. 2). Moreover, upon univariate analysis, BMI ≥ 24, jaundice, weight loss, CA19-9 > 40 U/mL, radical surgery, TNM stage, tumor differentiation grade, and SIRI showed statistically significant associations with OS. Multivariate analysis revealed that BMI < 24 (hazard ratio [HR], 2.008; 95% confidence interval [CI], 1.162 to 3.471; p=0.013), weight loss (HR, 1.729; 95% CI, 1.004 to 2.976; p=0.048), high SIRI (HR, 1.753; 95% CI, 1.027 to 2.991; p=0.040), CA19-9

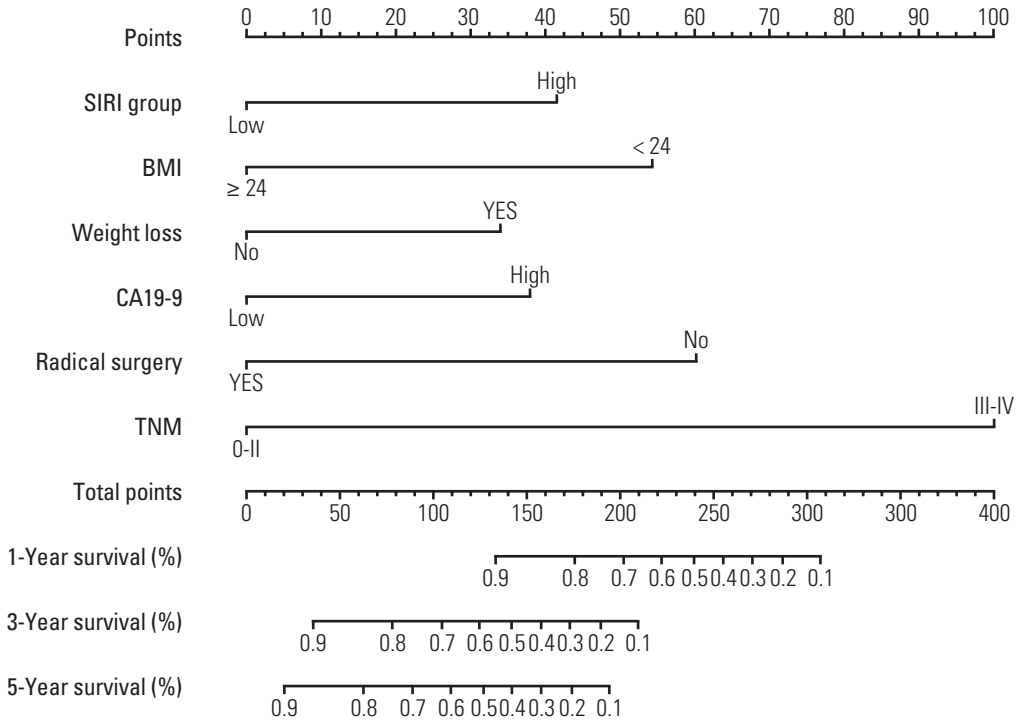

Fig. 4. Prognostic nomogram for predicting 1-, 3-, and 5-year overall survival probability based on the systemic inflammation response index (SIRI) group, body mass index (BMI), weight loss, carbohydrate antigen 19-9 (CA19-9), radical surgery, and TNM stage in patients with gallbladder cancer.

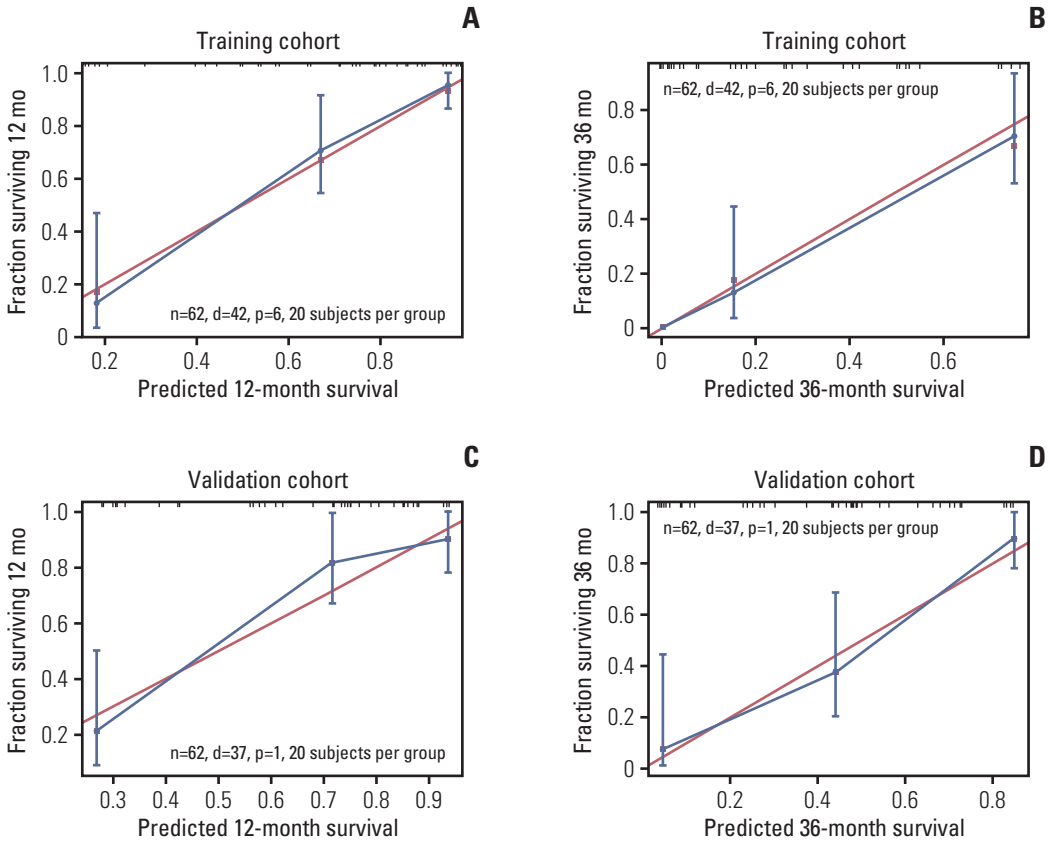

Fig. 5. Nomogram calibration plot for predicting overall survival probabilities at 1 year (A, C) and 3 years (B, D).

> 40 U/mL (HR, 2.162; 95% CI, 1.194 to 3.916; p=0.011), no radical surgery (HR, 2.940; 95% CI, 1.676 to 5.159; p < 0.001), and TNM stage (III-IV) (HR, 7.523; 95% CI, 1.558 to 36.329; p=0.012) were independent factors for OS (Table 3).

5. Prognostic model for prediction of OS

We first randomly equally divided the patients into the training cohort and the validation cohort. In order to build the prognostic model for OS prediction in the training cohort, the resulting variables from the multivariate Cox analysis were included. The prognostic factors included six risk factors, including BMI, weight loss, SIRI, CA19-9, radical surgery, and TNM stage. The time-dependent ROC curves of each included factor and the prognostic model are shown in Fig. 3, which showed that the SIRI's AUCs were higher than BMI and weight loss, but lower than CA19-9, radical surgery, TNM stage. Furthermore, the prognostic model combining all six factors had better predictive accuracy than any of the single factors, with AUCs of 1, 3, and 5 years as 0.897, 0.912, and 0.913, respectively. To visualize the prognostic model and make it more practical, a nomogram containing these six factors was constructed (Fig. 4). Each factor in the nomogram was assigned with a point based on its status. Summing the total points from all variables and drawing a vertical line at the location of the total points scale allowed us to predict the probabilities of the outcomes in terms of 1-, 3-, and 5-year OS probability.

6. Comparison of predictive accuracy for OS between the nomogram and the TNM staging system

The model's predictive ability was assessed by calculating the C-index, which was 0.821 (95% CI, 0.759 to 0.883) in the training cohort and 0.828 (95% CI, 0.762 to 0.894), demonstrating the nomogram's good predictive accuracy. Additionally, the nomogram's performance was graphically evaluated by making 1- and 3-year calibration plots (Fig. 5). The predicted line was very close to the reference line both in the training and the validation cohort, which indicates the model's good performance. Finally, to test the clinical usefulness of our model, decision curve analysis was performed (Fig. 6). Compared with the TNM staging system, our model offered much better clinical utility.

We developed histograms of the nomogram-predicted probability of 12-month survival according to different AJCC TNM staging groupings. As shown in Fig. 7, in patients with TNM stage IIIA and IIIB, there was a wide variety in the distribution of nomogram-predicted probabilities, ranging from 0.05 to 0.95. Additionally, the C-index of the AJCC TNM sys-

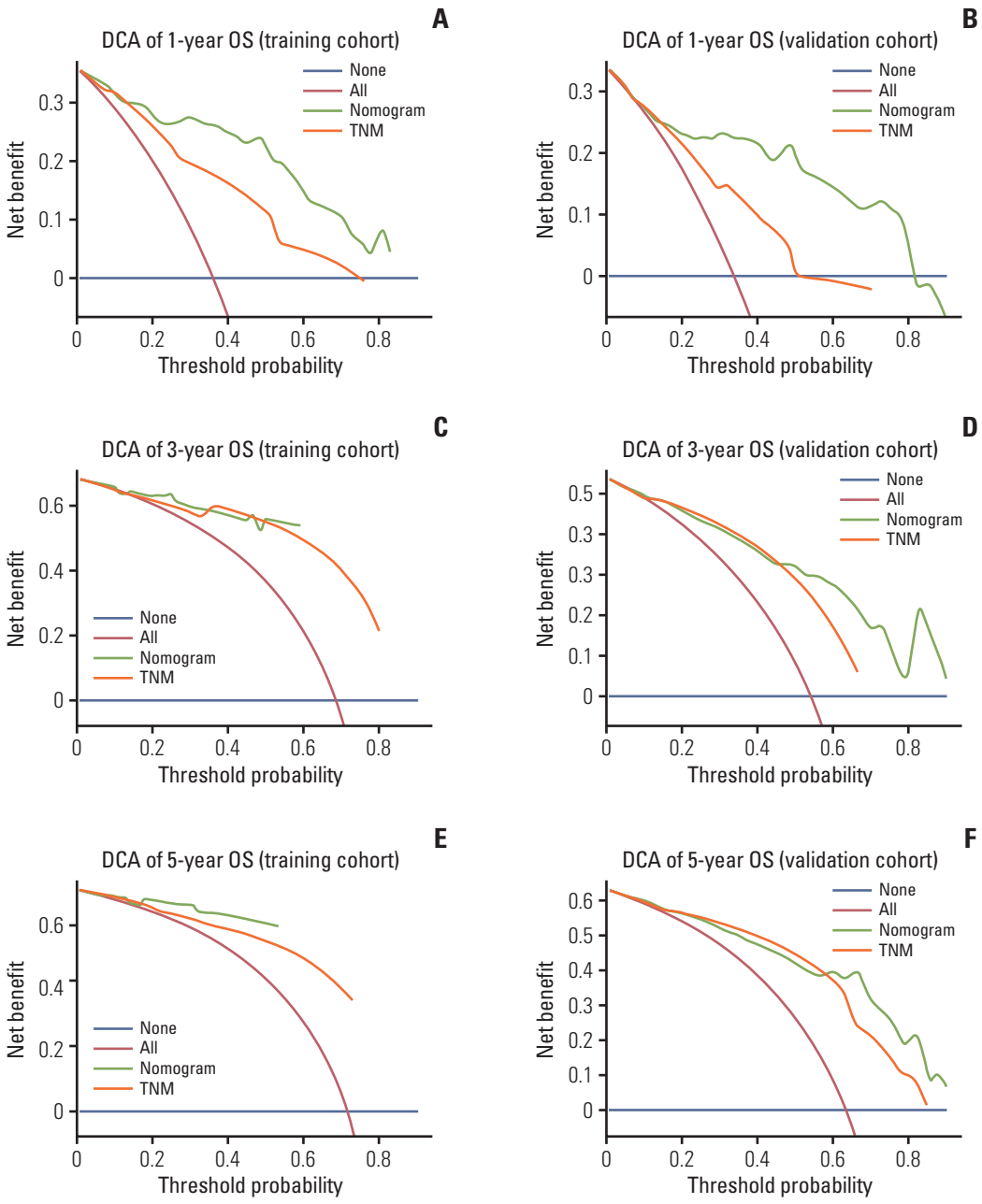

Fig. 6. Decision curve analysis (DCA) of the model and TNM staging system for 1- (A, B), 3- (C, D), and 5-year (E, F) overall survival (OS).

tem was 0.655 (95% CI, 0.592 to 0.718) in the training cohort and 0.649 (95% CI, 0.582 to 0.716) in the validation cohort, which was significantly lower than our prognostic model both in the training and the validation cohort.

Discussion

GBC is the most common malignancy in the biliary tract system [15,16]. Although surgical resection is a potentially curative therapy, over one-third of patients experience a recurrence [17]. Moreover, approximately 40% of cases are diagnosed at advanced stages [18,19]. All these factors contribute to its current poor prognosis situation, with only 10%-25% patients achieving 5-year survival [20]. Thus, the accuracy of prognosis prediction for different patients is crucial for physicians to make better clinical decisions. To date, the AJCC TNM staging system for both diagnosis and prognosis in GBC remains the gold standard; however, its own limitations in terms of its poor discrimination of the heterogeneity among patients at the same TNM stage are still unsolvable. To address this problem, we recognized the SIRI, a novel

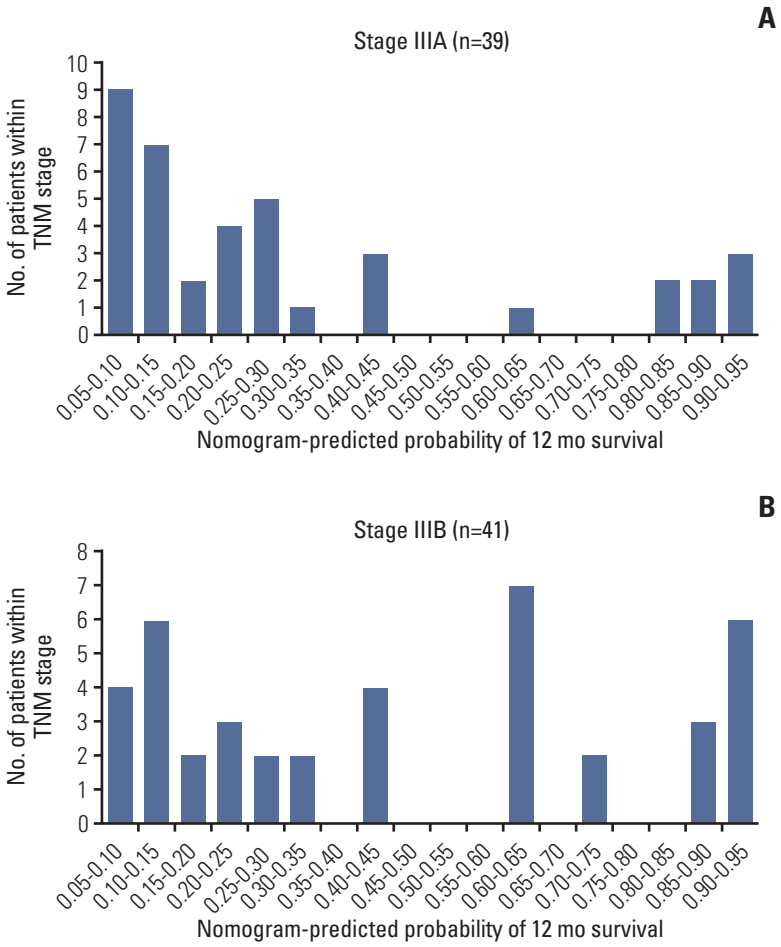

Fig. 7. Histograms of nomogram-predicted probability of 12-month survival according to the different American Joint Committee on Cancer TNM stage groupings.

inflammation-based index, as an independent significant prognostic indicator and developed a novel prediction model combining the SIRI and other clinicopathological factors that has a much better predictive ability compared with the TNM staging system.

As Hanahan and Weinberg [21] proposed, cancer-related inflammation is one of the hallmarks of cancer, and plays a vital role in carcinogenesis and tumor progression. Based on this theory, some indices using peripheral immune and inflammatory cells, such as PLR, MLR, and NLR, have been developed and their utility in survival prediction has been proven [22-24]. In 2016, Qi et al. [8] described a new inflammation-based index, the SIRI, which showed good prognostic value in patients with pancreatic cancer. In our study, we found that a high SIRI correlated to poor prognosis in respect of OS. Previous research has shown similar results in other solid tumors including gastric, esophageal, and nasopharyngeal cancer [9-11]. However, the SIRI's optimal cutoff differed among studies, at 1.8 in pancreatic cancer and at 1.2 in esophageal cancer [8,10]. We adopted 0.89 as the optimal cutoff to stratify our groups of patients, but whether it is applicable to all GBC patients requires further validation. Additionally, our results showed that the SIRI can also predict patients' surgical outcome such as length of stay in hospital and hemorrhage during surgery. To be more specific, patients in the high SIRI group may indicate the procedure's higher difficulty, which sheds new light on the SIRI regarding its potential in the assessment of surgical difficulty and therefore enabling individual peri-operative care decisions.

The specific mechanisms as to why a high SIRI indicates a poor outcome in GBC patients remain unclear; however, previous studies have revealed that lymphocytes have a vital function in anti-tumor defense in their role as infiltrating tumor cells, inducing cancer cell apoptosis [25]. Furthermore, the peripheral monocyte count has association with the level of tumor-associated macrophages, which facilitate tumor cell development and suppress the immune system against them [26,27]. Similarly, several studies suggested that peripheral neutrophils have a role in providing a favorable microenvironment for tumor growth, invasion, and metasta-

sis by means of secreting different types of cytokines including intercellular adhesion molecule 1 [28]. Taken together, either increasing neutrophils and monocytes or decreasing lymphocytes will cause an elevation in the SIRI, which will lead to a rather worse prognosis for patients with cancer. Finally, since the SIRI is easily calculated from the results of complete blood count tests, it is applicable to test the SIRI frequently during follow-up. Both the SIRI's value and dynamic changes may have the potential to serve as a marker to evaluate the efficacy of adjuvant chemoradiotherapy, to select appropriate patients to receive specific targeted therapy and immune therapy, and also to monitor for possible recurrence, although further investigations are needed.

In the present study, we took advantage of the user-friendly graphical interfaces of the nomogram to demonstrate our prediction model based on the SIRI and other clinicopathological factors including BMI, weight loss, CA19-9, radical surgery, and TNM stage. Among these factors, CA19-9 and TNM stage have also been utilized in other prognostic models of GBC [29,30]. BMI and weight loss are also easily acquired information, demonstrating our model's convenience. Though jaundice is significant in univariate analysis, it is not significant in multivariate analysis. Further studies should investigate the prognostic role of jaundice in larger cohorts. Compared with the traditional TNM staging system, our prediction model had better discriminatory ability, consistency, and clinical utility, as shown in the C-index, calibration plot, and decision curve analysis. Therefore, this prognostic model is appropriate for predicting GBC patient prognosis after surgery, which will be useful in helping clinicians with clinical counseling, decision-making, and follow-up planning. To the best of our knowledge, this is the first report to create a nomogram combining inflammatory indices including the SIRI and other indicators to predict OS probability in GBC patients.

Our study has several limitations. First, it was based on a retrospective cohort from a single center, which may cause potential selection bias. Second, the number of patients included in this study is relatively small; thus, further external validation is required before our results can be applied in other institutions. Third, this study only focused on the SIRI and other clinicopathological factors, and other inflammation-related indexes such as C-reactive protein, liver function test results, and coagulation were not investigated.

In conclusion, this is the first study to show that the SIRI is an independent predictor of OS in GBC patients. Our prediction model combining the SIRI and other clinicopathological indicators performed well in predicting patient's survival probability, surpassing the traditional TNM staging system regarding its predictive accuracy. It has the potential to serve as a practical clinical tool for individualized prognostication.

Conflicts of Interest

Conflict of interest relevant to this article was not reported.

Acknowledgments

This work was supported by grants from CAMS Innovation Fund for Medical Sciences (CIFMS) (No.2016-I2M-1-001) and Tsinghua University-Peking Union Medical College Hospital Cooperation Project (PTQH201904552).

References

1. de Aretxabala X. Biliary spillage a new prognostic factor in gallbladder cancer? Hepatobiliary Surg Nutr. 2019;8:537-8.
2. Buettner S, Margonis GA, Kim Y, Gani F, Ethun CG, Poultsides GA, et al. Changing odds of survival over time among patients undergoing surgical resection of gallbladder carcinoma. Ann Surg Oncol. 2016;23:4401-9.
3. Wi Y, Woo H, Won YJ, Jang JY, Shin A. Trends in gallbladder cancer incidence and survival in Korea. Cancer Res Treat. 2018;50:1444-51.
4. Fortner JG, Pack GT. Clinical aspects of primary carcinoma of the gallbladder. AMA Arch Surg. 1958;77:742-50.
5. Sung YN, Song M, Lee JH, Song KB, Hwang DW, Ahn CS, et al. Validation of the 8th edition of the American Joint Committee on Cancer staging system for gallbladder cancer and implications for the follow-up of patients without node dissection. Cancer Res Treat. 2020;52:455-68.
6. Diakos CI, Charles KA, McMillan DC, Clarke SJ. Cancer-related inflammation and treatment effectiveness. Lancet Oncol. 2014;15:e493-503.
7. Cho KM, Park H, Oh DY, Kim TY, Lee KH, Han SW, et al. Neutrophil-to-lymphocyte ratio, platelet-to-lymphocyte ratio, and their dynamic changes during chemotherapy is useful to predict a more accurate prognosis of advanced biliary tract cancer. Oncotarget. 2017;8:2329-41.
8. Qi Q, Zhuang L, Shen Y, Geng Y, Yu S, Chen H, et al. A novel systemic inflammation response index (SIRI) for predicting the survival of patients with pancreatic cancer after chemotherapy. Cancer. 2016;122:2158-67.
9. Li S, Lan X, Gao H, Li Z, Chen L, Wang W, et al. Systemic Inflammation Response Index (SIRI), cancer stem cells and survival of localised gastric adenocarcinoma after curative resection. J Cancer Res Clin Oncol. 2017;143:2455-68.
10. Geng Y, Zhu D, Wu C, Wu J, Wang Q, Li R, et al. A novel systemic inflammation response index (SIRI) for predicting postoperative survival of patients with esophageal squamous cell carcinoma. Int Immunopharmacol. 2018;65:503-10.
11. Chen Y, Jiang W, Xi D, Chen J, Xu G, Yin W, et al. Development and validation of nomogram based on SIRI for predicting the clinical outcome in patients with nasopharyngeal carcinomas. J Investig Med. 2019;67:691-8.

12. Amin MB, Greene FL, Edge SB, Compton CC, Gershenwald JE, Brookland RK, et al. The eighth edition AJCC cancer staging manual: continuing to build a bridge from a population-based to a more "personalized" approach to cancer staging. CA Cancer J Clin. 2017;67:93-9.
13. Vickers AJ, Elkin EB. Decision curve analysis: a novel method for evaluating prediction models. Med Decis Making. 2006;26:565-74.
14. General Assembly of the World Medical Association. World Medical Association Declaration of Helsinki: ethical principles for medical research involving human subjects. J Am Coll Dent. 2014;81:14-8.
15. Narayan RR, Creasy JM, Goldman DA, Gonen M, Kandoth C, Kundra R, et al. Regional differences in gallbladder cancer pathogenesis: insights from a multi-institutional comparison of tumor mutations. Cancer. 2019;125:575-85.
16. Siegel RL, Miller KD, Jemal A. Cancer statistics, 2019. CA Cancer J Clin. 2019;69:7-34.
17. Margonis GA, Gani F, Buettner S, Amini N, Sasaki K, Andreatos N, et al. Rates and patterns of recurrence after curative intent resection for gallbladder cancer: a multi-institution analysis from the US Extra-hepatic Biliary Malignancy Consortium. HPB (Oxford). 2016;18:872-8.
18. Li M, Liu F, Zhang F, Zhou W, Jiang X, Yang Y, et al. Genomic ERBB2/ERBB3 mutations promote PD-L1-mediated immune escape in gallbladder cancer: a whole-exome sequencing analysis. Gut. 2019;68:1024-33.
19. Yang P, Javle M, Pang F, Zhao W, Abdel-Wahab R, Chen X, et al. Somatic genetic aberrations in gallbladder cancer: comparison between Chinese and US patients. Hepatobiliary Surg Nutr. 2019;8:604-14.
20. Primrose JN, Fox RP, Palmer DH, Malik HZ, Prasad R, Mirza D, et al. Capecitabine compared with observation in resected biliary tract cancer (BILCAP): a randomised, controlled, multicentre, phase 3 study. Lancet Oncol. 2019;20:663-73.
21. Hanahan D, Weinberg RA. Hallmarks of cancer: the next generation. Cell. 2011;144:646-74.
22. Chen YM, Lai CH, Chang HC, Chao TY, Tseng CC, Fang WF, et al. Baseline and trend of lymphocyte-to-monocyte ratio as prognostic factors in epidermal growth factor receptor mutant non-small cell lung cancer patients treated with first-line epidermal growth factor receptor tyrosine kinase inhibitors. PLoS One. 2015;10:e0136252.
23. Cheng H, Luo G, Lu Y, Jin K, Guo M, Xu J, et al. The combination of systemic inflammation-based marker NLR and circulating regulatory T cells predicts the prognosis of resectable pancreatic cancer patients. Pancreatology. 2016;16:1080-4.
24. Diem S, Schmid S, Krapf M, Flatz L, Born D, Jochum W, et al. Neutrophil-to-lymphocyte ratio (NLR) and platelet-to-Lymphocyte ratio (PLR) as prognostic markers in patients with non-small cell lung cancer (NSCLC) treated with nivolumab. Lung Cancer. 2017;111:176-81.
25. Rosenberg SA. Progress in human tumour immunology and immunotherapy. Nature. 2001;411:380-4.
26. Shibutani M, Maeda K, Nagahara H, Fukuoka T, Nakao S, Matsutani S, et al. The peripheral monocyte count is associated with the density of tumor-associated macrophages in the tumor microenvironment of colorectal cancer: a retrospective study. BMC Cancer. 2017;17:404.
27. Franklin RA, Liao W, Sarkar A, Kim MV, Bivona MR, Liu K, et al. The cellular and molecular origin of tumor-associated macrophages. Science. 2014;344:921-5.
28. Liu S, Li N, Yu X, Xiao X, Cheng K, Hu J, et al. Expression of intercellular adhesion molecule 1 by hepatocellular carcinoma stem cells and circulating tumor cells. Gastroenterology. 2013;144:1031-41.
29. Bai Y, Liu ZS, Xiong JP, Xu WY, Lin JZ, Long JY, et al. Nomogram to predict overall survival after gallbladder cancer resection in China. World J Gastroenterol. 2018;24:5167-78.
30. Chen M, Lin J, Cao J, Zhu H, Zhang B, Wu A, et al. Development and validation of a nomogram for survival benefit of lymphadenectomy in resected gallbladder cancer. Hepatobiliary Surg Nutr. 2019;8:480-9.

pISSN 1598-2998, eISSN 2005-9256

Cancer Res Treat. 2020;52(4):1211-1218

https://doi.org/10.4143/crt.2019.506

Original Article

Open Access

Early Assessment of Response to Neoadjuvant Chemotherapy with ^{18}F-FDG-PET/CT in Patients with Advanced-Stage Ovarian Cancer

Young Shin Chung, MD[1]
Hyun-Soo Kim, MD, PhD[2]
Jung-Yun Lee, MD, PhD[1]
Won Jun Kang, MD, PhD[3]
Eun Ji Nam, MD, PhD[1]
Sunghoon Kim, MD, PhD[1]
Sang Wun Kim, MD, PhD[1]
Young Tae Kim, MD, PhD[1]

[1]*Department of Obstetrics and Gynecology, Institute of Women's Life Medical Science, Yonsei University College of Medicine, Seoul,* [2]*Department of Pathology and Translational Genomics, Samsung Medical Center, Sungkyunkwan University School of Medicine, Seoul,* [3]*Department of Nuclear Medicine, Yonsei University College of Medicine, Seoul, Korea*

Correspondence: Jung-Yun Lee, MD, PhD
Department of Obstetrics and Gynecology, Institution of Women's Medical Life Science, Yonsei University College of Medicine, 50-1 Yonsei-ro, Seodaemun-gu, Seoul 03722, Korea
Tel: 82-2-2228-2237
Fax: 82-2-313-8357
E-mail: jungyunlee@yuhs.ac

Co-correspondence: Won Jun Kang, MD, PhD
Department of Nuclear Medicine, Yonsei University College of Medicine, 50-1 Yonsei-ro, Seodaemun-gu, Seoul 03722, Korea
Tel: 82-2-2228-2391
Fax: 82-2-312-0578
E-mail: MDKWJ@yuhs.ac

Received September 3, 2019
Accepted April 27, 2020
Published Online April 28, 2020

Purpose

The aim of this study was to evaluate the ability of sequential ^{18}F-fluorodeoxyglucose positron emission tomography/computed tomography (^{18}F-FDG-PET/CT) after one cycle of neoadjuvant chemotherapy (NAC) to predict chemotherapy response before interval debulking surgery (IDS) in advanced-stage ovarian cancer patients.

Materials and Methods

Forty consecutive patients underwent ^{18}F-FDG-PET/CT at baseline and after one cycle of NAC. Metabolic responses were assessed by quantitative decrease in the maximum standardized uptake value (SUV_{max}) with PET/CT. Decreases in SUV_{max} were compared with cancer antigen 125 (CA-125) level before IDS, response rate by Response Evaluation Criteria in Solid Tumors criteria before IDS, residual tumor at IDS, and I chemotherapy response score (CRS) at IDS.

Results

A 40% cut-off for the decrease in SUV_{max} provided the best performance to predict CRS 3 (compete or near-complete pathologic response), with sensitivity, specificity, and accuracy of 81.8%, 72.4%, and 72.4%, respectively. According to this 40% cut-off, there were 17 (42.5%) metabolic responders (≥ 40%) and 23 (57.5%) metabolic non-responders (< 40%). Metabolic responders had higher rate of CRS 3 (52.9% vs. 8.7%, p=0.003), CA-125 normalization (< 35 U/mL) before IDS (76.5% vs. 39.1%, p=0.019), and no residual tumor at IDS (70.6% vs. 31.8%, p=0.025) compared with metabolic non-responders. There were significant associations with progression-free survival (p=0.021) between metabolic responders and non-responders, but not overall survival (p=0.335).

Conclusion

Early assessment with ^{18}F-FDG-PET/CT after one cycle of NAC can be useful to predic response to chemotherapy before IDS in patients with advanced-stage ovarian cancer.

Key words

Ovarian neoplasms, Neoadjuvant therapy, Positron emission tomography computed tomography, Treatment outcome

Introduction

Neoadjuvant chemotherapy (NAC) followed by interval debulking surgery (IDS) can be an alternative to primary debulking surgery for treating advanced-stage ovarian cancer when optimal cytoreduction cannot be achieved [1,2]. Chemotherapy sensitivity has been a well-known prognostic factor for survival, and evaluation of NAC response is mostly based on computed tomography (CT) imaging after three to four cycles of NAC. Earlier evaluation of NAC response would

allow for avoidance of unnecessary surgical complications and toxicity due to ineffective treatment.

Recently, several studies have shown that ^{18}F-fluorodeoxyglucose positron emission tomography/computed tomography (^{18}F-FDG-PET/CT) may be useful for predicting early response to NAC in other malignancies [3-9]. However, there are only a few studies on the use of PET/CT for evaluation of response to NAC in ovarian cancer [10-13]. Avril et al. [10] showed that the sequential ^{18}F-FDG-PET/CT after one cycle of NAC predicted patient's outcome. Other than the result of this study [10], there is no data on the use of PET/CT after one cycle of NAC to predict chemotherapy response before IDS.

Histopathological changes seen at IDS reflect direct NAC response [14-17]. However, there is no consensus regarding the prognostic value of the pathologic grading system to assess NAC response at IDS. Recently, Böhm et al. proposed the 3-tier chemotherapy response score (CRS) system for ovarian cancer, and our group performed an external validation of this system confirming a high reproducibility and prognostic value [18,19]. As pathologic response could be a surrogate endpoint, we evaluated how the early tumor metabolic change during NAC correlated with histopathological response observed at IDS. The aim of this study was to investigate the ability of PET parameters after one cycle of chemotherapy to predict NAC response in advanced-stage ovarian cancer patients.

Materials and Methods

1. Patients

From 2016 to 2018, 40 consecutive patients diagnosed with International Federation of Gynecology and Obstetrics stage IIIC or IV high-grade serous ovarian cancer underwent baseline ^{18}F-FDG-PET/CT before starting NAC. Thirty-eight of 40 patients underwent diagnostic laparoscopy showing Fagotti score ≥ 8 [20] before NAC, while two patients received NAC after histologically confirmed by cytologic evaluation of ascites without diagnostic laparoscopy. All of them underwent a second ^{18}F-FDG-PET/CT examination after one cycle of NAC. After the completion of NAC, 39 patients underwent IDS (Fig. 1). One patient did not receive IDS because she refused surgery and follow-up loss after four cycles of NAC.

2. Protocol-based treatment

Diagnostic work-up included contrast-enhanced CT scan of the chest/pelvis as well as FDG-PET/CT were obtained for all patients at baseline to determine the tumor burden.

In our institution, NAC was performed as the primary treatment strategy, when one of the following three selection criteria was met [21]: (1) pulmonary and/or hepatic parenchymal metastases observed on initial imaging work-up, (2) patients with poor performance status and high operative risk due to medical comorbidities, or (3) optimal debulking surgery (i.e., ≤ 1 cm of residual disease at debulking surgery) was unsuitable due to high tumor burden (Fagotti score ≥ 8). During diagnostic laparoscopy, the degree of tumor burden was described by Fagotti score.

All patients, preferably, are recommended to receive three cycles of NAC and IDS, as well as three cycles of postoperative adjuvant chemotherapy (POAC). For NAC and POAC, all patients received platinum-based combination chemotherapy (paclitaxel [175 mg/m^2]+carboplatin [area under the curve of 5 to 6]).

All patients underwent surgery with the intent to achieve complete cytoreduction (no gross residual disease) and followed the same routine, beginning with complete omentectomy, hysterectomy, bilateral salpingo-oophorectomy, and removal of all macroscopically detectable lesions using surgical resection. Furthermore, 29 patients underwent IDS following hyperthermic intraperitoneal chemotherapy.

3. ^{18}F-FDG-PET/CT imaging and imaging analysis

All subjects were requested to fast for over 8 hours before PET acquisition. Blood glucose concentrations were confirmed to be < 140 mg/dL at the time of FDG injection.

Intravenously, 5.5 MBq of ^{18}F-FDG per kg body weight

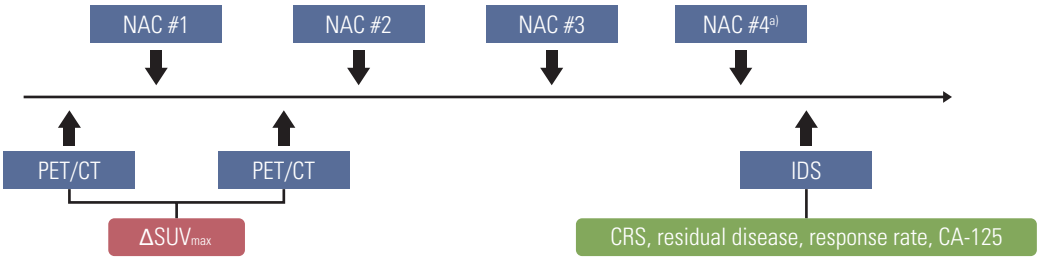

Fig. 1. Overall flow chart of positron emission tomography/computed tomography (PET/CT), neoadjuvant chemotherapy (NAC), and interval debulking surgery (IDS). SUV_{max}, maximum standardized uptake value; CRS, chemotherapy response score; CA-125, cancer antigen 125. [a]Two patients received four cycles of NAC.

were injected. After 60 minutes, integrated FDG-PET/CT was performed using a dedicated PET/CT scanner (Discovery STE, GE Healthcare, Milwaukee, WI). Whole body spiral CT scan was performed from the vertex of the skull to the mid-thigh using the following parameters: 120 kVp, 30 mA, 0.8-second rotation time, 3.75 mm helical thickness, 27 mm per rotation (speed), 2.5 mm scan reconstruction, with a reconstruction index of 1.25 mm, 15.7 cm field of view, and a 512×512 matrix. PET scan was acquired from the cerebellum to the proximal thigh, and acquisition time was 3 minutes per bed position using the 3D-mode. Attenuation corrected PET data were reconstructed iteratively using an ordered-subset expectation maximization algorithm.

4. PET parameter

All ^{18}F-FDG-PET/CT images were reviewed blinded to the clinical outcome by two nuclear medicine physicians. Each region with a higher FDG uptake than the background was considered significant. The maximum standardized uptake values (SUV_{max}) were measured by drawing a circular region of interest (ROI) at the site of the maximum ^{18}F-FDG uptake on the transaxial PET images. The SUV of the ROI was calculated as follows: (decay-corrected activity [MBq] per tissue volume [mL])/(injected ^{18}F-FDG dose [MBq] per body mass [g]).

Seven tumor lesions (right upper quadrant, left upper quadrant, sub-hepatic area, mesentery, pelvis, right ovary, and left ovary) per patients were identified; and SUV_{max} at each examination were calculated. The SUV_{max} after one cycle of NAC was compared with that of the baseline study. Multiple metastatic tumors observed by ^{18}F-FDG-PET/CT were found in all patients. Therefore, we used the lesion with the lowest change in ^{18}F-FDG uptake for the study analysis based on the rationale that the metastatic tumor with the worst response would determine survival. The change in SUV_{max} after one cycle of chemotherapy was expressed as ΔSUV_{max} (%)=100×(1st cycle SUV_{max}–baseline SUV_{max})/baseline SUV_{max}.

5. Assessment of response to NAC

1) Cancer antigen 125 normalization

Cancer antigen 125 (CA-125) levels were determined before diagnostic laparoscopy, before each NAC cycle, and before IDS. CA-125 response criterion was a complete normalization of CA-125 levels before IDS (< 35 U/mL).

2) Imaging response (CT) by Response Evaluation Criteria in Solid Tumors

Patients' radiological responses to NAC were generally estimated with contrast-enhanced CT before IDS and classified according to the Response Evaluation Criteria in Solid Tumors (RECIST) as complete response (CR), partial response (PR), stable disease, and progressive disease [22].

3) Residual tumor after IDS

During IDS, we collected information on the maximal diameter of the residual lesion for evaluation of the residual disease. Residual disease was reported using the following criteria: from no gross (microscopic) residual disease, 0.0-0.5 cm, 0.5-1.0 cm, 1.0-2.0 cm, or residual disease > 2.0 cm in the largest diameter.

4) Histopathological response by CRS

For the assessment of NAC-induced histopathological changes, specimens were taken from each of these three sites (omentum, right adnexa, and left adnexa) during IDS. All available hematoxylin and eosin–stained slides were reviewed by an experienced gynecologic pathologist (H.-S.K.). As Bohm et al. [18] and Lee et al. [19] reported significant correlations between outcome and omental CRS, we analyzed the histo-pathological response to NAC with omental CRS.

Specimens with no or minimal tumor response, appreciable tumor response, and complete or near-CR were indicated as CRS 1, 2, and 3, respectively. Patients with CRS 1 or 2 were considered as histopathological non-responders, while patients with CRS 3 were considered as histopathological responders.

6. Statistical analysis

Correlations between CRS and PET parameter were examined with the Mann-Whitney U test. The predictive performance regarding the identification of CRS 3 was evaluated using the receiver operating characteristic (ROC) curve analysis.

Associations between metabolic response and NAC parameters were examined with the chi-square and Fisher's exact tests. Progression-free survival (PFS) and overall survival (OS) were analyzed by the Kaplan-Meier method, and the difference of survival rates between metabolic responders and non-responders were compared by the log-rank test. Statistical analyses were conducted using IBM SPSS ver. 25.0 for Windows (IBM Corp., Armonk, NY). All tests were two-sided and p-values less than 0.05 were considered to indicate statistical significance.

7. Ethical statement

This study was approved by the Institutional Review Board of Severance Hospital at Yonsei University College of Medicine (No. 4-2018-0518), and the requirement of written informed consent was waived due to the retrospective nature of the study.

Results

Eighty PET/CT scans were performed in 40 patients. The patients' clinical, surgical, and pathological characteristics at

Table 1. Patient characteristics

Variable	Value (n=40)
Age at diagnosis (yr)	60.5 (39-77)
CA-125 level at diagnosis (U/mL)	1,846.5 (236.5-14,838.2)
CA-125 level before IDS (U/mL)	24.4 (6.4-1,222.8)
FIGO stage	
IIIC	15 (37.5)
IV	25 (62.5)
Histologic subtype	
HGSC	40 (100)
Method of IDS	
Laparotomy	7 (17.5)
Laparotomy+HIPEC	22 (55.0)
Laparoscopy	3 (7.5)
Laparoscopy+HIPEC	7 (17.5)
Not available	1 (2.5)
Residual disease after IDS	
NGR	20 (50.0)
≤ 0.5 cm	17 (42.5)
≤ 1 cm	1 (2.5)
≤ 2 cm	1 (2.5)
> 2 cm	1 (2.5)
Not available	1 (2.5)
Fagotti score	
8	13 (32.5)
10	18 (45.0)
12	5 (12.5)
14	2 (5.0)
Not available	2 (5.0)
Response rate before IDS[a]	
CR	3 (7.5)
PR	37 (92.5)
SD	0
PD	0
CRS	
1	1 (2.5)
2	28 (70.0)
3	11 (27.5)
NAC regimen	
Paclitaxel+carboplatin	40 (100)
No. of NAC cycles	
3	38 (95.0)
4	2 (5.0)

Values are presented as median (range) or number (%). CA-125, cancer antigen-125; IDS, interval debulking surgery; FIGO, Federation of Gynecology and Obstetrics; HGSC, high-grade serous carcinoma; HIPEC, hyperthermic intraperitoneal chemotherapy; NGR, no gross residual disease; CR, complete response; PR, partial response; SD, stable disease; PD, progressive disease; CRS, chemotherapy response score; NAC, neoadjuvant chemotherapy. [a]According to the Response Evaluation Criteria in Solid Tumors [22].

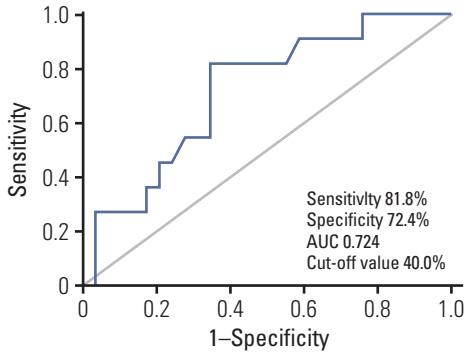

Fig. 2. Receiver operating characteristic analysis of ΔSUV_{max} (maximum standardized uptake value) for the identification of chemotherapy response score 3 after one cycle of neoadjuvant chemotherapy. AUC, area under the curve.

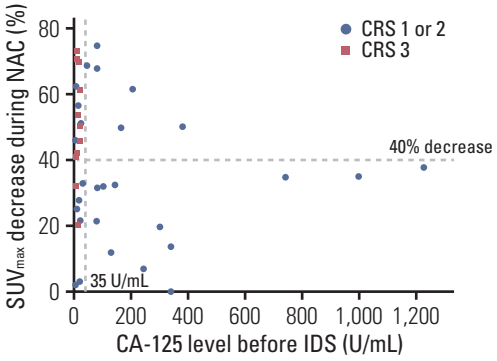

Fig. 3. Scatter plots showing the decrease in maximum standardized uptake value (SUV_{max}) and cancer antigen 125 (CA-125) level before interval debulking surgery (IDS). Chemotherapy response score (CRS) 1 or 2 are indicated by blue circles, CRS 3 by red triangles. NAC, neoadjuvant chemotherapy.

baseline are summarized in Table 1.

The baseline ^{18}F-FDG-PET/CT was performed before initiation of NAC at a median interval of 4.5 days (range, 1 to 17 days). The median time interval between the first cycle of NAC and the second (after the first cycle of NAC) ^{18}F-FDG-PET/CT was 19 days (range, 7 to 24 days). Median decrease in SUV_{max} between the baseline and after one cycle of NAC was 36.7% (range, –6.8% to 74.4%). One patient showed an increase in SUV after one cycle of NAC, and she was a metabolic non-responder. Of 39 patients who received IDS, we observed CRS 3 in 11 patients (27.5%) and no residual disease rate at IDS in 20 patients (50.0%). Median follow-up time was 19.7 months (range, 2.2 to 43.9 months). During this period, 18 patients experienced recurrence and eight of them died. Analysis of all 40 patients showed a median PFS of 21.0 months (95% confidence interval [CI], 17.8 to 24.3), and the median OS was not reached.

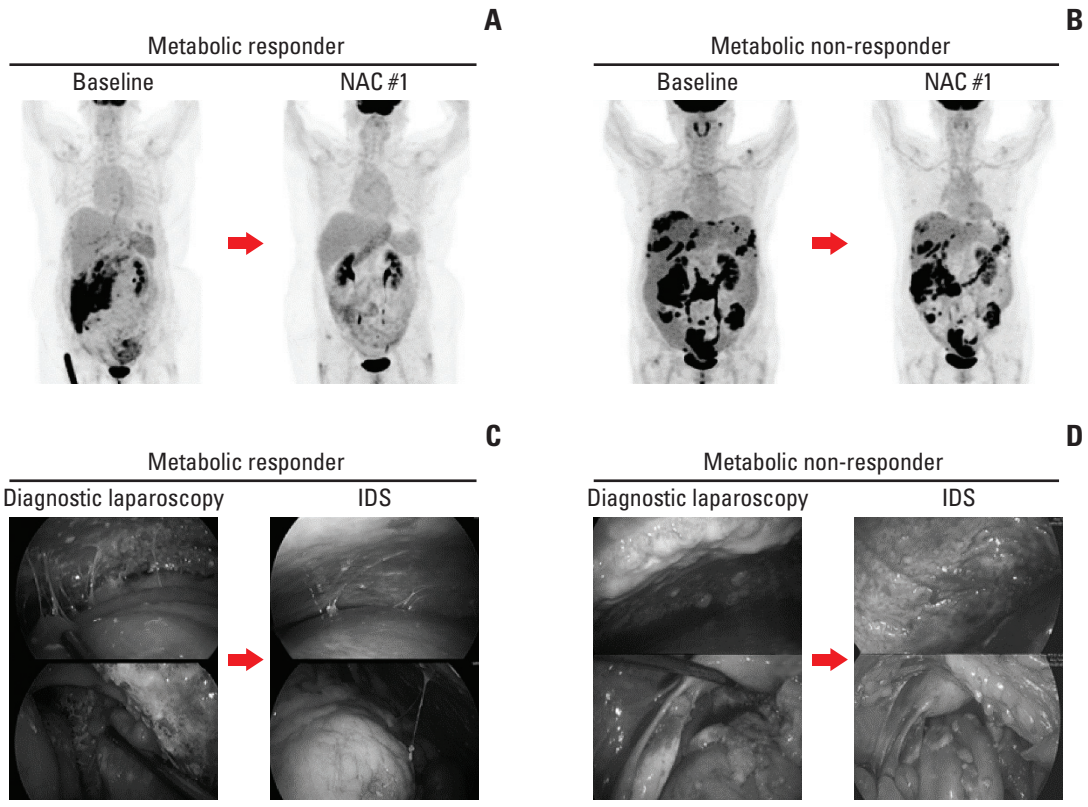

Fig. 4. Examples of metabolic responder and non-responder. [18]F-fluorodeoxyglucose positron emission tomography/computed tomography images, at baseline and after one cycle of neoadjuvant chemotherapy (NAC) in metabolic responder (A) and non-responder (B). Surgical findings of diagnostic laparoscopy and interval debulking surgery (IDS) in metabolic responder (C) and non-responder (D).

1. The ΔSUV_{max} threshold value and CRS (CRS 1 or 2 vs. CRS 3–metabolic response)

A cut-off of 40% of SUV_{max} decrease in metastatic sites offered the best accuracy in predicting CRS 3 (CR or near-CR) with a sensitivity of 81.8%, specificity of 72.4%, and area under the curve of 0.72. The ROC curve is presented in Fig. 2. We selected the 40% cut-off to define the metabolic response; there were 17 (42.5%) metabolic responders (≥ 40% decrease in SUV_{max}) with a median decrease in SUV_{max} of 53.5% (range, 40.7% to 74.4%) and 23 (57.5%) metabolic non-responders (< 40%) with a median decrease of 25.0% (range, –6.8% to 39.7%). After one cycle of NAC, a threshold of 40% decrease in SUV_{max} was found to differentiate between pathologic non-responders (CRS 1 or 2) and responders (CRS 3) (Fig. 3). Fig. 4 shows that examples of metabolic responder and non-responder observed in PET/CT and surgical findings before and after NAC.

2. Association between PET parameters and NAC parameters

There was a significant correlation between [18]F-FDG-PET/CT metabolic response and CRS. Metabolic responders had higher CRS 3 rate than metabolic non-responders (52.9% vs. 8.7%, p=0.003). Furthermore, there was a close relationship between [18]F-FDG-PET/CT metabolic response and CA-125 normalization (< 35 U/mL) before IDS (76.5% vs. 39.1%, p=0.019). No residual tumor rate at IDS was 70.6% within metabolic responders and 31.8% within non-responders; and a significant correlation was observed between [18]F-FDG-PET/ CT metabolic response and residual tumor at IDS (p= 0.025). Only CR or PR were found as radiological response rate before IDS, and there was no significant correlation radiological response rate before IDS between metabolic responder and non-responder (p=0.069) (Table 2).

3. Metabolic response and survival

There was a significant association between metabolic response in [18]F-FDG-PET/CT after one cycle of NAC and PFS (p=0.021), but not OS (p=0.335). Using defined 40% threshold for decrease in SUV_{max} from baseline after one cycle of NAC, median PFS was not reached in metabolic responders (n=17) compared with 18.5 months (95% CI, 13.9 to 23.0 months) in non-responders (n=23, p=0.021) (S1 Fig.).

Table 2. Associations between PET parameters and outcome of NAC

Characteristic	40% of ΔSUV_{max}		p-value
	Responder (n=17)	Non-responder (n=23)	
CA-125 level before IDS			
< 35 U/mL	13 (76.5)	9 (39.1)	0.019
≥ 35 U/mL	4 (23.5)	14 (60.9)	
Response rate before IDS[a]			
CR	3 (17.6)	0	0.069
PR	14 (82.4)	23 (100)	
Residual disease after IDS			
NGR	12 (70.6)	7 (31.8)	0.025
> 0 cm	5 (29.4)	15 (68.2)	
Unknown	0	1	
CRS			
1 or 2	8 (47.1)	21 (91.3)	0.003
3	9 (52.9)	2 (8.7)	

Values are presented as number (%). PET, positron emission tomography; NAC, neoadjuvant chemotherapy; SUV_{max}, maximum standardized uptake value; CA-125, cancer antigen-125; IDS, interval debulking surgery; CR, complete response; PR, partial response; NGR, no gross residual disease; CRS, chemotherapy response score. [a]According to the Response Evaluation Criteria in Solid Tumors [22].

Discussion

Our results demonstrated that tumor metabolic change after one cycle of NAC can be a valuable predictor of early response to chemotherapy, and potentially could identify metabolic responders and non-responders using a cut-off value of 40%.

In advanced-stage ovarian cancer, it is important to assess NAC response before IDS, as patients who do not respond to NAC seem to have less benefit from IDS. There is increasing need for sensitive and specific non-invasive imaging methods for evaluating chemotherapy response for proper decision making in the management of ovarian cancer patients. ^{18}F-FDG-PET/CT is a promising imaging method to evaluate NAC response and help to identify patients who response to treatment in ovarian cancer [10-13]. Avril et al. [10] showed that the sequential ^{18}F-FDG-PET/CT after one cycle of NAC predicted patient outcome. Nishiyama et al. [11] evaluated the ability of ^{18}F-FDG-PET/CT after five or six cycles of NAC to predict the response of NAC. Martoni et al. [12] reported the ability of ^{18}F-FDG-PET/CT after three cycles of NAC to identify patients who would obtain benefits from prolonged NAC. Vallius et al. [13] evaluated the usefulness of ^{18}F-FDG-PET/CT after three or four cycles of NAC for identifying patients who would not respond to NAC.

Furthermore, an early change of the treatment strategy could be considered to avoid delay of second-line chemotherapy and risk of unnecessary postoperative complications. Therefore, it would also be valuable for detecting metabolic responders and non-responders at an early time-point. In consistent with results of Park et al. [9], we demonstrated that early tumor metabolic change after one cycle of NAC could predict chemotherapy response before IDS. To date, other than the results of these two studies, there are no data on the use of PET/CT after one cycle of NAC to assess treatment response.

In this study, the optimal threshold of ΔSUV_{max} that discriminate between metabolic responders and non-responders after one cycle of NAC was 40%. Considering the kinetics of tumor cell kill and the relationship to ^{18}F-FDG-PET/CT, we hypothesized that early metabolic change would differentiate chemotherapy response. As the number of NAC cycles increases, the number of cancer cells that can be detected by ^{18}F-FDG-PET/CT decreases while the SUV_{max} value falls below the threshold that produced the difference in metabolic responder and non-responders; therefore, the metabolic difference between the two groups disappeared.

In 2009, Wahl et al. [23] proposed the PET response criteria in solid tumors (PERCIST) as a new standardized method by which the chemotherapy response was assessed by metabolic changes. The SUL (lean body mass corrected SUV) is determined for up to five measurable target lesions, typically the five hottest lesions. A metabolic response is considered more than a 30% decrease in SUL peak between the pre- and posttreatment scans, although not necessarily the same lesion. Moreover, our study shows that the metabolic response needed to be associated with a histopathologic response to NAC should be more than the SUVmax changes of the PERCIST criteria.

Since multiple metastatic tumors and sites were present in advanced-stage ovarian cancer, it is difficult to evaluate the metabolic response in only one lesion. In this study, we eval-

uated metabolic change regarding heterogeneous chemotherapy response according to metastatic sites. ^{18}F-FDG-PET/CT parameters such as the SUVmax of the right and left upper quadrant, sub-hepatic area, mesentery, pelvis, as well as the right and left ovary were assessed in all patients. Chemotherapy response is expected to vary depending on the location of primary and metastatic lesions due to intratumor heterogeneity in genomic profiles [24]. We mainly focused on the SUVmax values of the metastatic lesion with the lowest change in ^{18}F-FDG uptake, as the metastatic tumor with the worst response would determine survival.

There were several strengths in our study. First, we used CRS system to assess the pathologic response at IDS. We assessed the pathologic grading scale such as CRS system, which validated its prognostic significance, and high reproducibility [18,19]. Second, our study was the homogenous study cohort consisting of advanced-stage ovarian cancer patients who received protocol-based treatment at our institution [21]. Third, a definite value for SUVmax change that discriminates between metabolic responders and non-responders was presented using the ROC curve analysis in this study.

One of the limitations in our study was its retrospective design. Another was the small number of patients, and the short follow-up period. It may be a factor in which metabolic response did not reflected in OS. Interpretation of this study must be confined to short-term results, and further investigation with a prospective design and large population is needed.

In this study, using sequential ^{18}F-FDG-PET/CT and histo-pathological response evaluation with CRS system, we identified patients who did not respond to NAC and were not likely to benefit from IDS. It is important to identify poor metabolic response patients to avoid the risk of unnecessary surgical complications and toxicity due to ineffective treatment. In patients without metabolic response to NAC, the chemotherapy regimen may be changed to the second-line therapy or earlier oncologic surgery should be considered before the performance status gets worse. ^{18}F-FDG-PET/CT could provide initial information on tumor response in patients without clinical or radiologic progression on whether to continue the same NAC regimen, change to a different regimen, or to discontinue the regimen.

In conclusion, the change in SUV_{max} after one cycle of NAC offers powerful stratification of patient outcomes, early, during treatment. Therefore, ^{18}F-FDG-PET/CT can be useful in identifying patients who will not respond to NAC and metabolic non-responder might be candidates for second-line chemotherapy and clinical trials, instead of IDS.

Electronic Supplementary Material

Supplementary materials are available at Cancer Research and Treatment website (https://www.e-crt.org).

Conflicts of Interest

Conflicts of interest relevant to this article was not reported.

Acknowledgments

This research was supported by the Bio & Medical Technology Development Program of the National Research Foundation (NRF) funded by the Ministry of Science, ICT & Future Planning (2017-M3A9E8029714), and the Basic Science Research Program through the National Research Foundation of Korea (NRF), funded by the Ministry of Education (2016R1D1A1B03931916).

References

1. Kehoe S, Hook J, Nankivell M, Jayson GC, Kitchener H, Lopes T, et al. Primary chemotherapy versus primary surgery for newly diagnosed advanced ovarian cancer (CHORUS): an open-label, randomised, controlled, non-inferiority trial. Lancet. 2015;386:249-57.
2. Vergote I, Trope CG, Amant F, Kristensen GB, Ehlen T, Johnson N, et al. Neoadjuvant chemotherapy or primary surgery in stage IIIC or IV ovarian cancer. N Engl J Med. 2010;363:943-53.
3. Groheux D, Hindie E, Giacchetti S, Hamy AS, Berger F, Merlet P, et al. Early assessment with 18F-fluorodeoxyglucose positron emission tomography/computed tomography can help predict the outcome of neoadjuvant chemotherapy in triple negative breast cancer. Eur J Cancer. 2014;50:1864-71.
4. Lordick F, Ott K, Krause BJ, Weber WA, Becker K, Stein HJ, et al. PET to assess early metabolic response and to guide treatment of adenocarcinoma of the oesophagogastric junction: the MUNICON phase II trial. Lancet Oncol. 2007;8:797-805.
5. Evilevitch V, Weber WA, Tap WD, Allen-Auerbach M, Chow K, Nelson SD, et al. Reduction of glucose metabolic activity is more accurate than change in size at predicting histopathologic response to neoadjuvant therapy in high-grade soft-tissue sarcomas. Clin Cancer Res. 2008;14:715-20.
6. Kostakoglu L, Goldsmith SJ. PET in the assessment of therapy response in patients with carcinoma of the head and neck and of the esophagus. J Nucl Med. 2004;45:56-68.
7. MacManus MP, Seymour JF, Hicks RJ. Overview of early response assessment in lymphoma with FDG-PET. Cancer Imaging. 2007;7:10-8.
8. Burger IA, Schwarz EI, Samarin A, Breitenstein S, Weber A, Hany TF. Correlation between therapy response assessment using FDG PET/CT and histopathologic tumor regression grade in hepatic metastasis of colorectal carcinoma after neoadjuvant therapy. Ann Nucl Med. 2013;27:177-83.
9. Park JS, Choi JY, Moon SH, Ahn YC, Lee J, Kim D, et al. Response evaluation after neoadjuvant chemoradiation by

positron emission tomography-computed tomography for esophageal squamous cell carcinoma. Cancer Res Treat. 2013;45:22-30.
10. Avril N, Sassen S, Schmalfeldt B, Naehrig J, Rutke S, Weber WA, et al. Prediction of response to neoadjuvant chemotherapy by sequential F-18-fluorodeoxyglucose positron emission tomography in patients with advanced-stage ovarian cancer. J Clin Oncol. 2005;23:7445-53.
11. Nishiyama Y, Yamamoto Y, Kanenishi K, Ohno M, Hata T, Kushida Y, et al. Monitoring the neoadjuvant therapy response in gynecological cancer patients using FDG PET. Eur J Nucl Med Mol Imaging. 2008;35:287-95.
12. Martoni AA, Fanti S, Zamagni C, Rosati M, De Iaco P, D'Errico Grigioni A, et al. [18F]FDG-PET/CT monitoring early identifies advanced ovarian cancer patients who will benefit from prolonged neo-adjuvant chemotherapy. Q J Nucl Med Mol Imaging. 2011;55:81-90.
13. Vallius T, Peter A, Auranen A, Carpen O, Kemppainen J, Matomaki J, et al. 18F-FDG-PET/CT can identify histopathological non-responders to platinum-based neoadjuvant chemotherapy in advanced epithelial ovarian cancer. Gynecol Oncol. 2016;140:29-35.
14. Muraji M, Sudo T, Iwasaki S, Ueno S, Wakahashi S, Yamaguchi S, et al. Histopathology predicts clinical outcome in advanced epithelial ovarian cancer patients treated with neo-adjuvant chemotherapy and debulking surgery. Gynecol Oncol. 2013;131:531-4.
15. Petrillo M, Zannoni GF, Tortorella L, Pedone Anchora L, Salutari V, Ercoli A, et al. Prognostic role and predictors of complete pathologic response to neoadjuvant chemotherapy in primary unresectable ovarian cancer. Am J Obstet Gynecol. 2014;211:632.
16. Le T, Williams K, Senterman M, Hopkins L, Faught W, Fung-Kee-Fung M. Histopathologic assessment of chemotherapy effects in epithelial ovarian cancer patients treated with neoadjuvant chemotherapy and delayed primary surgical debulking. Gynecol Oncol. 2007;106:160-3.
17. Sassen S, Schmalfeldt B, Avril N, Kuhn W, Busch R, Hofler H, et al. Histopathologic assessment of tumor regression after neoadjuvant chemotherapy in advanced-stage ovarian cancer. Hum Pathol. 2007;38:926-34.
18. Bohm S, Faruqi A, Said I, Lockley M, Brockbank E, Jeyarajah A, et al. Chemotherapy response score: development and validation of a system to quantify histopathologic response to neoadjuvant chemotherapy in tubo-ovarian high-grade serous carcinoma. J Clin Oncol. 2015;33:2457-63.
19. Lee JY, Chung YS, Na K, Kim HM, Park CK, Nam EJ, et al. External validation of chemotherapy response score system for histopathological assessment of tumor regression after neoadjuvant chemotherapy in tubo-ovarian high-grade serous carcinoma. J Gynecol Oncol. 2017;28:e73.
20. Fagotti A, Ferrandina G, Fanfani F, Garganese G, Vizzielli G, Carone V, et al. Prospective validation of a laparoscopic predictive model for optimal cytoreduction in advanced ovarian carcinoma. Am J Obstet Gynecol. 2008;199:642.
21. Lee YJ, Lee JY, Cho MS, Nam EJ, Kim SW, Kim S, et al. Incorporation of paclitaxel-based hyperthermic intraperitoneal che-motherapy in patients with advanced-stage ovarian cancer treated with neoadjuvant chemotherapy followed by interval debulking surgery: a protocol-based pilot study. J Gynecol Oncol. 2019;30:e3.
22. Eisenhauer EA, Therasse P, Bogaerts J, Schwartz LH, Sargent D, Ford R, et al. New response evaluation criteria in solid tumours: revised RECIST guideline (version 1.1). Eur J Cancer. 2009;45:228-47.
23. Wahl RL, Jacene H, Kasamon Y, Lodge MA. From RECIST to PERCIST: evolving considerations for PET response criteria in solid tumors. J Nucl Med. 2009;50 Suppl 1:122S-50S.
24. Lee JY, Yoon JK, Kim B, Kim S, Kim MA, Lim H, et al. Tumor evolution and intratumor heterogeneity of an epithelial ovarian cancer investigated using next-generation sequencing. BMC Cancer. 2015;15:85.

pISSN 1598-2998, eISSN 2005-9256

Cancer Res Treat. 2020;52(4):1219-1228

https://doi.org/10.4143/crt.2019.688

Original Article

Open Access

Evaluation of Circulating Tumor DNA in Patients with Ovarian Cancer Harboring Somatic *PIK3CA* or *KRAS* Mutations

Aiko Ogasawara, MD[1]
Taro Hihara, PhD[2]
Daisuke Shintani, MD[1]
Akira Yabuno, MD[1]
Yuji Ikeda, MD, PhD[1]
Kenji Tai, MSc[2]
Keiichi Fujiwara, MD, PhD[1]
Keisuke Watanabe, BSc[2]
Kosei Hasegawa, MD, PhD[1]

[1]*Department of Gynecologic Oncology, Saitama Medical University International Medical Center, Hidaka,* [2]*Tsukuba Research Laboratories, Eisai Co., Ltd., Tsukuba, Japan*

Correspondence: Kosei Hasegawa, MD, PhD
Department of Gynecologic Oncology, Saitama Medical University International Medical Center, 1397-1 Yamane, Hidaka-shi, Saitama 350-1298, Japan
Tel: 81-42-984-4111
Fax: 81-42-984-4743
E-mail: koseih@saitama-med.ac.jp

Received November 10, 2019
Accepted May 1, 2020
Published Online May 6, 2020

Purpose

Circulating tumor DNA (ctDNA) is an attractive source for liquid biopsy to understand molecular phenotypes of a tumor non-invasively, which is also expected to be both a diagnostic and prognostic marker. *PIK3CA* and *KRAS* are among the most frequently mutated genes in epithelial ovarian cancer (EOC). In addition, their hotspot mutations have already been identified and are ready for a highly sensitive analysis. Our aim is to clarify the significance of *PIK3CA* and *KRAS* mutations in the plasma of EOC patients as tumor-informed ctDNA.

Materials and Methods

We screened 306 patients with ovarian tumors for somatic *PIK3CA* or *KRAS* mutations. A total of 85 EOC patients had somatic *PIK3CA* and/or *KRAS* mutations, and the corresponding mutations were subsequently analyzed using a droplet digital polymerase chain reaction in their plasma.

Results

The detection rates for ctDNA were 27% in EOC patients. Advanced stage and positive peritoneal cytology were associated with higher frequency of ctDNA detection. Preoperative ctDNA detection was found to be an indicator of outcomes, and multivariate analysis revealed that ctDNA remained an independent risk factor for recurrence (p=0.010). Moreover, we assessed the mutation frequency in matched plasma before surgery and at recurrence from 17 patients, and found six patients had higher mutation rates in cell-free DNA at recurrence compared to that at primary diagnosis.

Conclusion

The presence of ctDNA at diagnosis was an indicator for recurrence, which suggests potential tumor spread even when tumors were localized at the time of diagnosis.

Key words

Ovarian neoplasms, ctDNA, Biomarker, *KRAS*, *PIK3CA*

Introduction

With the recent advances in molecular biology and its surrounding technology, the approach to diagnosis and treatment of cancers has dramatically changed [1]. Major cancer therapeutics involve a combination of cytotoxic drugs, but current treatment options are shifting toward molecular targeted agents [2,3] and immuno-oncology agents. To determine the appropriate treatment for individual patients, identification of appropriate biomarkers such as specific mutations or expression patterns are necessary. The liquid biopsy technology such as cell-free DNA (cfDNA) is becoming an increasingly popular source of non-invasive biomarkers for diagnosis and disease monitoring in cancer patients [4]. The cell-free circulating tumor DNA (ctDNA) was first reported in 1948 [5]. ctDNA has been evaluated for assessing metastasis, prognosis or diagnosis in breast, colorectal, lung cancer and various other neoplasms [6-11].

Epithelial ovarian cancer (EOC) is one of the more common cancers in women with more than 238,000 new cases diagnosed in 2012 worldwide [12]. Its mortality rate is highest among gynecologic cancers. With advancements of new systemic therapies and surgical techniques, the survival rate is improving. However, the total disease control remains poor because of eventual resistance to chemotherapy or other targeted drugs [13]. Mutation and loss of *TP53* or

BRCA1/2 function, or activation *KRAS*, *BRAF*, *CTNNB1*, and *PIK3CA* have been reported as genetic abnormalities in EOC [13]. *KRAS* and *PIK3CA* mutations are seen in around 10% of EOC. Since the hotspots of *KRAS* and *PIK3CA* mutations are well defined, analysis of those mutations represents a potentially sensitive and solid approach to evaluate ctDNA in the blood of EOC patients.

Reports of ctDNA for EOC have been increasing in the last few years. Most of the reports investigated *TP53* mutation because it is the most frequently mutated gene in high-grade serous ovarian cancer (HGSC). *TP53* mutation monitoring in cfDNA of HGCS patients showed potential as a biomarker for treatment response [14]. ctDNA can be detected even in some of the cancers in the early stage including EOC [15]. Exploratory analysis of *PIK3CA* or *KRAS* mutations in cfDNA of 29 ovarian clear cell carcinoma (OCCC) patients showed shorter progression-free survival (PFS) in the patients with detectable ctDNA [16]. These reports encourage the use of ctDNA as a tool for diagnosis, monitoring disease progression and response to treatment in EOC patients [14-21]. However, tumor-informed ctDNA for *PIK3CA* or *KRAS* mutations of other ovarian histotypes were unclear, and the analysis as to whether it is prognostic, particularly in early stage EOC, has yet to be established.

Our aim in this study is to evaluate mutation rates of *KRAS* or *PIK3CA* in the plasma of patients with an ovarian tumor harboring *KRAS* or *PIK3CA* mutations using droplet digital polymerase chain reaction (ddPCR) in the largest cohort thus far, and to analyze if there is an association between ctDNA status and clinicopathological features or clinical outcomes in EOC. In addition, we compared mutation frequency in the matched plasma collected at the time of initial diagnosis and recurrence in those patients.

Materials and Methods

1. Patients and sample collection

Patients with ovarian tumor who were treated in Saitama Medical University International Medical Center between 2010 and 2016 were included in this study. The clinicopathological data was retrieved from medical records. Patients with non-epithelial ovarian tumors, synchronous cancer and ovarian metastasis from non-gynecological origin were excluded from this analysis. A total of 306 ovarian tumor patients were included in the analysis.

Tumor specimens were collected from each patient at the time of initial surgery and stored at –80°C until use. Frozen tumor specimens from 306 patients with ovarian tumors were used for extraction of genomic DNA. In 306 patients, 226 (73.9%), 15 (4.9%), 14 (4.6%), 43 (14.1), and eight (2.6%) patients had EOC, fallopian tube cancer, primary peritoneal cancer, borderline tumor and benign tumor, respectively (S1 Table). We collected plasma from these patients before the surgery and stored at –80°C until use. In addition, we collected the plasma of 17 patients who suffered a relapse at the time of recurrence.

2. Tumor genomic DNA and plasma cfDNA extraction

Genomic tumor DNA was extracted from approximately 25-50 mg of frozen tumor sample using the NucleoSpin Tissue kit (Macherey-Nagel, Duren, Germany) according to the manufacturer's instructions. Quantification of genomic DNA (gDNA) was performed using NanoDrop (Thermo Fisher Scientific, Waltham, MA). cfDNA was extracted from 0.5 mL of plasma (before surgery) and eluted in 60 μL of the supplied elution buffer using the QIAamp Circulating Nucleic Acid Kit (50) (Qiagen, Hilden, Germany) according to the manufacturer's instructions.

3. Droplet digital PCR

ddPCR was performed using the PrimePCR for ddPCR *PIK3CA* E542K, E545K, H1047R or *KRAS* screening multiplex kit (G12A, G12C, G12D, G12R, G12S, G12V, G13D) (Bio-Rad catalog No. 186-3131, 186-3132, 186-3133 or 186-3506, Hercules, CA). *KRAS* screening multiplex kit screens seven *KRAS* mutations in a single well simultaneously. This kit cannot determine each *KRAS* mutation separately. Reactions were carried out in a reaction volume of 20 μL on a QX200 AutoDG Droplet Digital PCR System (Bio-Rad). The 20 μL PCR mix was composed of 10 μL 2×ddPCR supermix for probes (no dUTP), 1 μL of each (target and reference) 20× amplification primer/probe mix (450 and 250 nmol/L, respectively), 3 μL distilled water, and 5 μL gDNA or cfDNA extracted. The cycling conditions were as follows; initial denaturation at 95°C for 10 minutes, followed by 40 repeated cycles of 94°C for 30 seconds and 55°C for 60 seconds, a step of 98°C for 10 minutes and finally samples were maintained at 4°C. Results were analyzed with Quatasoft v1.7.4 (Bio-Rad). All gDNA samples were first evaluated by ddPCR and confirmed by other PCR based methods. As for cfDNA, we repeated each experiment using ddPCR at least twice. If there was a discordance, we performed the third run for confirmation. We defined the mutation as positive when we saw more than one copy of mutation by ddPCR (S2 Fig.).

4. Statistical analysis

The statistical analysis was conducted using JMP version 10 and GraphPad Prism 6 (GraphPad Software Inc., San Diego, CA). Chi-square tests were used to estimate association between detection rate of mutation of ctDNA and clinicopathologial features. Survival analysis was performed by Kaplan-Meier methods and multivariate Cox regression models. Wilcoxon signed-rank test was performed to compare the level of cancer antigen 125 (CA125) and ctDNA at

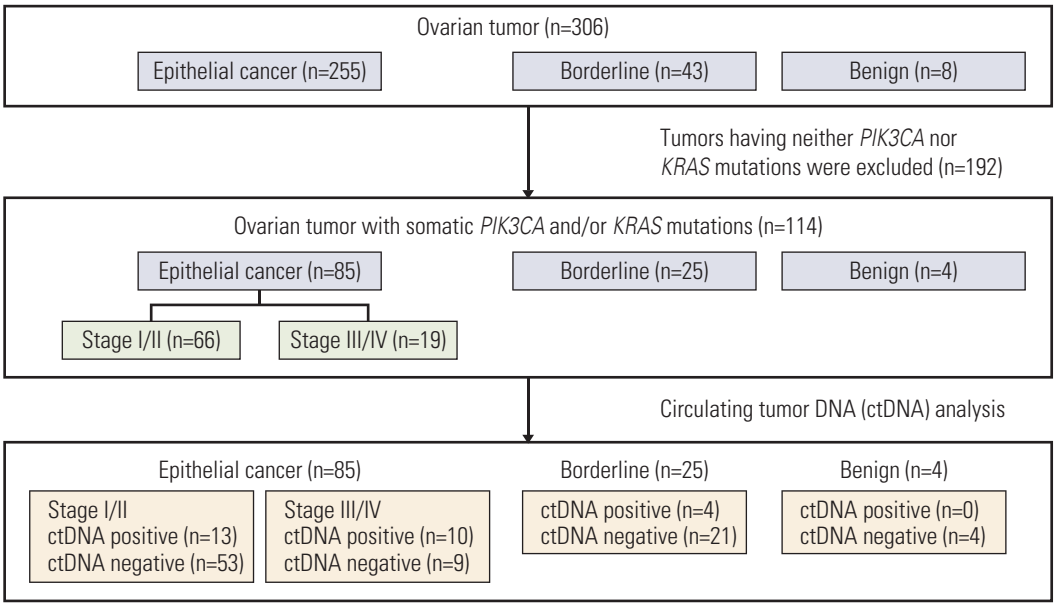

Fig. 1. Flow diagram. Numbers of patients who were included in the analyses.

the time of recurrence and before the primary operation.

5. Ethical statement

This study was approved by the Institutional Review Board of Saitama Medical University International Medical Center (#14-058). Informed consents including future research purposes were obtained from all patients in the previous studies (#10-078 and #12-096), and the Institutional Review Board approved to use the research materials in the current study.

Results

1. *PIK3CA* and/or *KRAS* mutations in ovarian tumors

A total of 306 patients who had ovarian tumors was screened for somatic *PIK3CA* and or *KRAS* mutations using their tumor specimens. A consort diagram of all patients in this study is shown in Fig. 1. Two hundred and fifty-five, 43 and eight patients had EOC, borderline ovarian tumor and benign ovarian tumor, respectively. Among EOC patients, 89 (34.9%), 82 (32.2%), 60 (23.5%), seven (2.7%), and 17 (6.7%) patients had clear cell carcinoma, high-grade serous carcinoma, endometrioid carcinoma, mucinous carcinoma and other histotypes, respectively.

We found that 114 patients out of 306 patients (37.3%) had tumors with somatic *PIK3CA* and/or *KRAS* mutations using ddPCR as described in the materials and methods section (Fig. 1). Those mutations were found in 85/255 (33.3%), 25/43 (58.1%), 4/8 (50.0%) of EOC, borderline, and benign tumor, respectively (Fig. 1). In 255 EOC patients, somatic *PIK3CA* mutations were observed in 40/255 patients (15.7%), and *KRAS* mutations were observed in 48/255 patients (18.8%) (Table 1). Three cases (1.2%) had both *PIK3CA* and *KRAS* mutations.

2. *PIK3CA* and/or *KRAS* mutations in plasma circulating tumor DNA

Next, cfDNA from the plasma of those 114 patients who had tumor *PIK3CA* and/or *KRAS* was tested for the corresponding mutations using ddPCR. We defined ctDNA detection to be positive when the corresponding mutations were detected in the plasma cfDNA. As shown in Table 1 and S3 Table, positive ctDNA was found in 27.1% (23/85), 16.0% (4/25), and 0% (0/4) of patients with EOC, borderline and benign tumor, respectively. Each *PIK3CA* or *KRAS* mutation was detected in 11/40 (27.5%) and 12/48 (25.0%) of cfDNA in EOC patients, respectively. Each *PIK3CA* or *KRAS* mutation was detected in 0/2 (0.0%) and 4/24 (16.7%) of cfDNA in borderline ovarian tumor patients, respectively. *KRAS* mutation was detected in 0/4 (0.0%) of cfDNA in benign ovarian tumor patients (Table 1).

3. Relationship between circulating tumor DNA and clinicopathological factors in EOC patients

We included only EOC patients in the subsequent analyses. We investigated the relationship between ctDNA status (positive or negative) and clinicopathological features in 85 EOC patients with *PIK3CA* and/or *KRAS* mutations (Table 2). High detection rate of ctDNA was associated with advanced stage and positive peritoneal cytology (p=0.008 and p=0.007, respectively), but not with other factors such as

Table 1. Detection rates for circulating tumor DNA (ctDNA)

	Positive/Cases with somatic mutations		
	ctDNA: *PIK3CA* and/or *KRAS*	ctDNA: *PIK3CA*	ctDNA: *KRAS*
Epithelial ovarian carcinoma			
Total	23/85 (27.1)	11/40 (27.5)	12/48 (25.0)
Stage I/II	13/66 (19.7)	7/32 (21.9)	6/37 (16.2)
Stage III/IV	10/19 (52.6)	4/ 8 (50.0)	6/11 (54.5)
Borderline tumor	4/25 (16.0)	0/2 (0.0)	4/24 (16.7)
Benign tumor	0/4 (0.0)	-	0/4 (0.0)

Values are presented as number (%).

Table 2. Relationship between ctDNA (*PIK3CA* and/or *KRAS*) detection and clinicopathological features in EOC patients

Characteristic	Positive/Cases with somatic mutations	p-value
Age (yr)		
> 57	10/40 (25.0)	0.808
≤ 57	13/45 (28.9)	
FIGO stage		
I/II	13/66 (19.7)	0.008
III/IV	10/19 (52.6)	
Histology		
Clear cell	12/36 (33.3)	0.833
Endometrioid	6/29 (20.7)	
Mucinous	2/7 (28.6)	
Serous	2/8 (25.0)	
Others	1/5 (20.0)	
Peritoneal cytology		
Positive	16/38 (42.1)	0.007
Negative	7/46 (15.2)	
Residual tumor at primary surgery		
No	15/57 (26.3)	0.206
Yes	7/15 (46.7)	

Values are presented as number (%). ctDNA, circulating tumor DNA; EOC, epithelial ovarian cancer; FIGO, International Federation of Gynecology and Obstetrics.

age, histologic type and status of residual tumor at primary surgery (Table 2).

4. Circulating tumor DNA and outcomes

Next, we examined a potential association between ctDNA status and patient outcomes. As shown in Fig. 2A and B, we observed that the ctDNA detection was associated with both shorter PFS and overall survival (OS) in EOC patients ($p < 0.001$ and $p=0.017$, respectively). Similar trends were observed when we separately analyzed the mutations for *PIK3CA* or *KRAS*. The PFS was significantly shorter in patients with *PIK3CA* or *KRAS* mutations in cfDNA ($p=0.008$ and $p=0.004$, respectively) (Fig. 2C and E). However, ctDNA mutations for *PIK3CA* or *KRAS* showed no significant difference for the OS ($p=0.118$ and $p=0.072$, respectively) (Fig. 2D and F).

Additionally, we performed cox univariate analyses to assess the prognostic factors in those patients. We found that the ctDNA detection, stage and residual tumor status at the time of primary surgery were significant prognostic factors for PFS ($p < 0.001$, $p < 0.001$, and $p < 0.001$, respectively) (Table 3). Those factors were also significant prognostic factors for OS ($p=0.012$, $p < 0.001$, and $p < 0.001$, respectively) (Table 3). We further examined the multivariate analyses including ctDNA status, stage, and residual tumor status at the time of primary surgery, and histology. As shown in Table 3, ctDNA status, stage, residual tumor status at the time of primary surgery, and age remained as independent prognostic factors for PFS ($p=0.010$, $p=0.001$, $p=0.006$, and $p=0.010$, respectively). However, only histology, stage

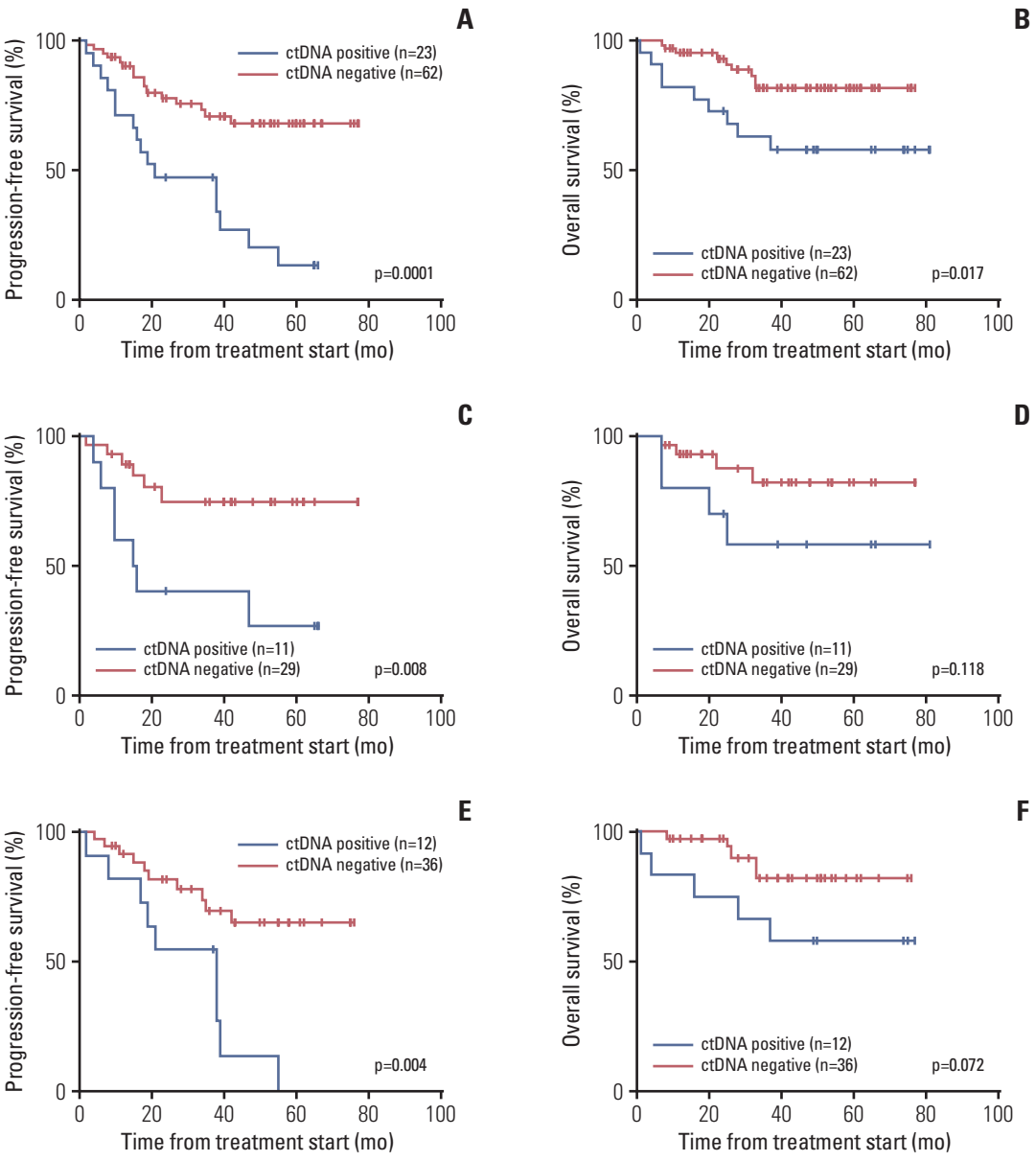

Fig. 2. Survival curves according to circulating tumor DNA (ctDNA) status, positive or negative. Progression-free survival (A) and overall survival (B) in all epithelial ovarian cancer (EOC) patients as to ctDNA status for *PIK3CA* and/or *KRAS* mutations (p=0.0001 and p=0.017, respectively). Progression-free survival (C) and overall survival (D) in all EOC patients as to ctDNA status for *PIK3CA* mutations (p=0.008 and p=0.118, respectively). Progression-free survival (E) and overall survival (F) in all EOC patients as to ctDNA status for *KRAS* mutations (p=0.004 and p=0.072, respectively). *(Continued to the next page)*

and age remained independent prognostic factors for OS (p=0.006, p < 0.0001, and p=0.041, respectively).

5. A subgroup analysis of ctDNA in early stage EOC

As shown in Table 2, more than 50% of the tumor *PIK3CA* and/or *KRAS* mutations were found in early stage EOC, and we think that ctDNA may reflect potential tumor spread even when the tumor is clinically localized. Therefore, we analyzed ctDNA status in a subgroup of early stage (stage I-II) EOC patients. We found that 13 of 66 EOC patients (19.7%) who had stage I-II tumor were positive for ctDNA (Table 1). We found no association between ctDNA detection and any clinicopathological features in early stage EOC patients (age, International Federation of Gynecology and Obstetrics stage, histological type, and peritoneal cytology) (S4 Table). As shown in Fig. 2G, detection of ctDNA was associated with shorter recurrence-free survival (RFS) in early stage EOC patients (p=0.010, log-rank test). *PIK3CA*-

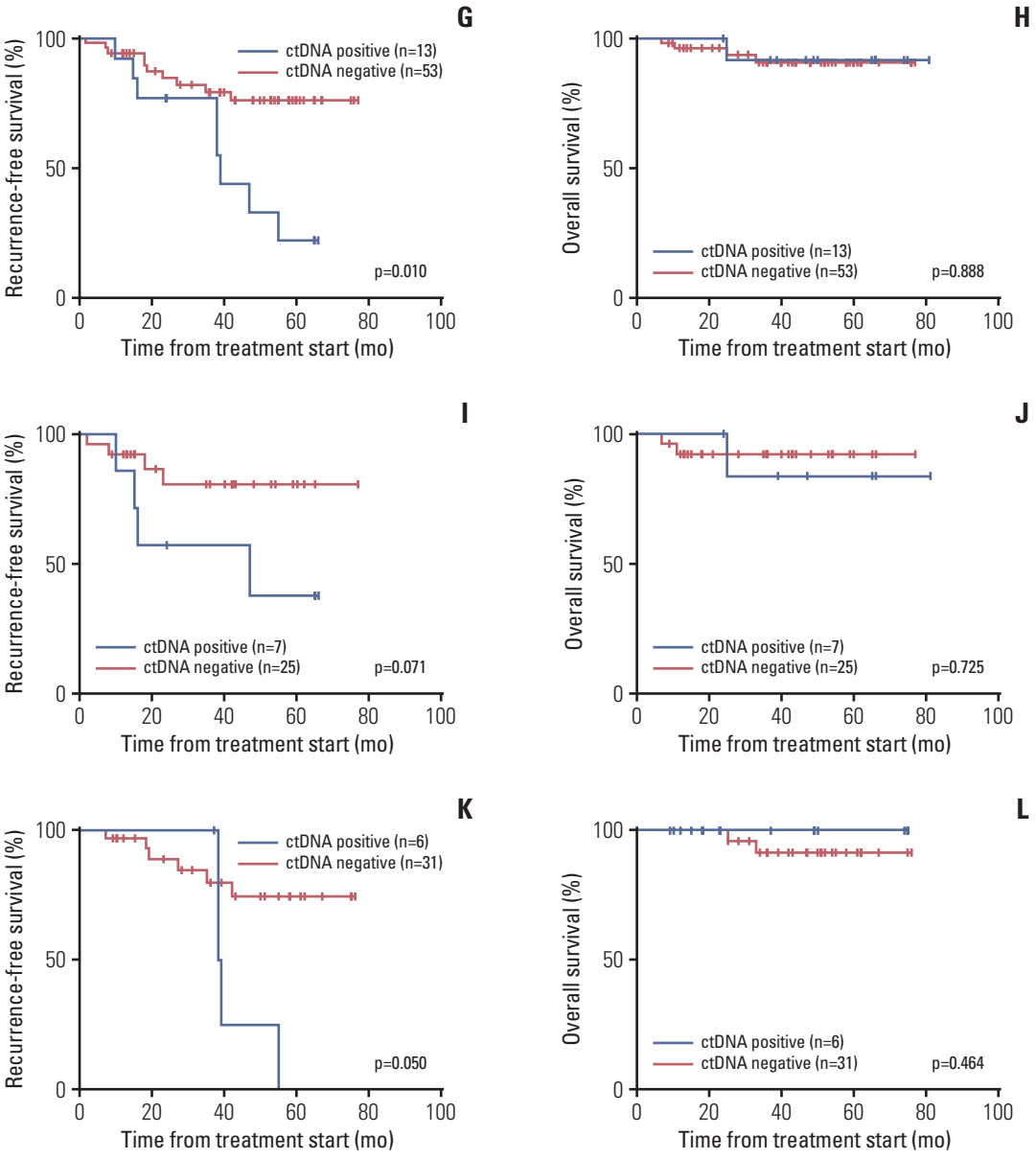

Fig. 2. *(Continued from the previous page)* Recurrence-free survival (G) and overall survival (H) in stage I/II EOC patients as to ctDNA status for *PIK3CA* and/or *KRAS* mutations (p=0.010 and p=0.888, respectively). Recurrence-free survival (I) and overall survival (J) in stage I/II EOC patients as to ctDNA status for *PIK3CA* mutations (p=0.071 and p=0.725, respectively). Recurrence-free survival (K) and overall survival (L) in stage I/II EOC patients as to ctDNA status for *KRAS* mutations (p=0.050 and p=0.464, respectively).

mutant and *KRAS*-mutant ctDNA in early stage EOC patients showed trends toward a shorter RFS (p=0.071 and p=0.050, respectively) (Fig. 2I and K). However, no statistical difference was found in OS (p=0.725 and p=0.464, respectively) (Fig. 2J and L). We performed Cox univariate analyses to assess the prognostic factors including ctDNA status, stage, peritoneal cytology at the time of primary surgery, age and histology in early stage EOC patients. We found that ctDNA detection, peritoneal cytology at the time of primary surgery and age were significant prognostic factors for RFS in univariate cox regression models (S5 Table). However, in early stage EOC patients, we found no specific prognostic factors for OS in univariate cox regression models (S5 Table) and for both RFS and OS in the multivariate cox regression analysis (S6 Table).

6. Comparing ctDNA in paired plasma samples at primary and recurrent diagnosis in EOC patients

Tumors may change their molecular status during a relapse, metastasis or following chemotherapy-induced selection

Table 3. Cox regression models for overall and progression-free survival in EOC patients

	Progression-free survival		Overall survival	
	HR (95% CI)	p-value	HR (95% CI)	p-value
Univariate				
ctDNA				
Positive	1	< 0.001	1	0.012
Negative	0.25 (0.13-0.50)		0.31 (0.12-0.77)	
Histology				
Clear cell	1	0.477	1	0.167
Others	0.78 (0.40-1.56)		0.25 (0.21-1.31)	
Stage				
I/II	1	< 0.001	1	< 0.001
III/IV	8.16 (3.93-16.93)		15.55 (5.89-48.53)	
Residual tumor				
No	1	< 0.001	1	< 0.001
Yes	6.64 (3.17-13.66)		6.96 (2.73-18.34)	
Age (yr)				
> 57	1	0.069	1	0.309
≤ 57	1.89 (0.95-3.84)		1.60 (0.65-4.17)	
Multivariate				
ctDNA				
Positive	1	0.010	1	0.410
Negative	0.38 (0.18-0.79)		0.65 (0.24-1.83)	
Histology				
Clear cell	1	0.137	1	0.006
Others	0.56 (0.27-1.20)		0.20 (0.059-0.64)	
Stage				
I/II	1	0.001	1	< 0.001
III/IV	5.26 (2.11-12.91)		20.41 (5.34-89.12)	
Residual tumor				
No	1	0.006	1	0.107
Yes	3.41 (1.43-7.90)		2.57 (0.81-8.16)	
Age (yr)				
> 57	1	0.010	1	0.041
≤ 57	2.61 (1.26-5.67)		2.97 (1.04-9.10)	

EOC, epithelial ovarian cancer; HR, hazard ratio; CI, confidence interval; ctDNA, circulating tumor DNA.

pressure. We compared ctDNA status in 17 paired plasma samples collected at the time of initial diagnosis and first recurrence. Detailed patient information and ctDNA status are described in S7 Table. Eight patients (47.1%) were ctDNA positive at the time of initial diagnosis, and seven of those eight patients (87.5%) remained ctDNA positive at the time of their first recurrence. We observed that one patient was ctDNA negative at the time of initial diagnosis but it became positive during recurrence. As shown in Fig. 3A, we did not observe any difference in the amount of cfDNA in the primary and recurrent tumor. The median total cfDNA (included mutation and wild-type) was 1,944 (range, 1,080 to 29,484 copies/mL) and 1,992 (range, 386 to 118,092 copies/mL) in patients with primary and recurrent tumors, respectively. When we examined the mutation rate in cfDNA, six of 17 patients (35.3%) had higher mutation rates in cfDNA at the time of recurrence compared to that at the time of primary diagnosis. However, no statically change was observed (Fig. 3B). In contrast, the levels of serum CA125 was lower and the tumor size was smaller when the patients had a recurrent tumor compared to that at the time of primary diagnosis ($p < 0.0001$) (Fig. 3C and D).

Discussion

In this study, we evaluated ctDNA status in EOC patients by investigating *PIK3CA* and *KRAS* mutations in the plasma cfDNA using ddPCR, and found ctDNA detection in 27.1% of EOC patients, 19.7% in early stage and 52.6% in advanced

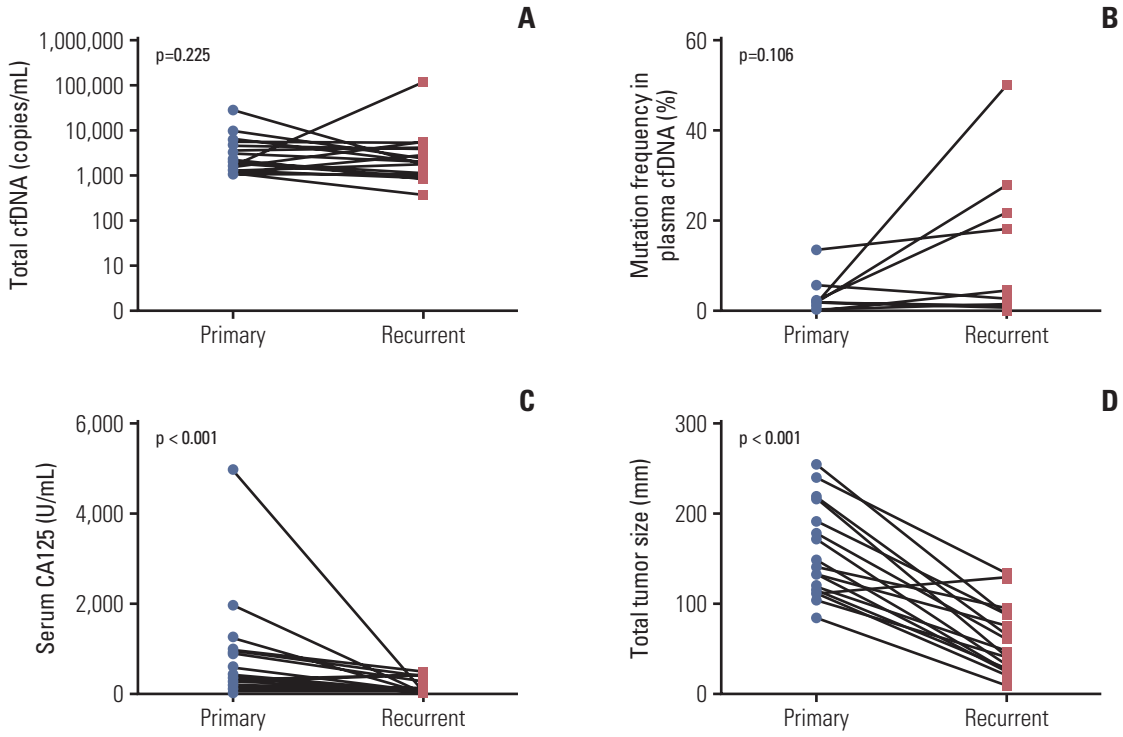

Fig. 3. Quantitative analysis of circulating tumor DNA (cfDNA) at the time of primary treatment and at recurrence. (A) Total mutation copies in plasma. (B) Mutation frequency in cell-free DNA (cfDNA) ([mutated copies/wild type copies]×100). (C) Levels of serum cancer antigen 125 (CA125). (D) Tumor size.

stage patients. The presence of ctDNA in the blood at the time of primary treatment was an independent prognostic factor for recurrence or relapse in EOC patients. In addition, increased mutation rates in cfDNA was observed in patients with recurrence compared with those at primary treatment.

There are some reports of tumor-informed mutations in cfDNA of EOC patients [14,16-20,22]. However, most of the studies have addressed a relatively small EOC patient cohort. Because of a high frequency of mutations in the *TP53* gene in HGSC patients, most of the reports for EOC previously examined *TP53* mutations in plasma cfDNA [14,17-20]. The first report of tumor-specific mutations in cfDNA for EOC evaluated *TP53* gene mutations, which were examined by fluorescence-based single-strand conformation polymorphism. Forty-four percent (12/27) of the patients with EOC were found to have a *TP53* mutation in the tumor, and 16.7% (2/12) of those patients had matched mutations in the plasma cfDNA [19]. Morikawa et al. [16] investigated *PIK3CA* and *KRAS* mutations in 29 cases of OCCC. Eight of 29 patients (27.6%) had *PIK3CA* and/or *KRAS* mutations, and they observed ctDNA in three of those (37.5%) patients by ddPCR [16]. *KRAS* and *PIK3CA* mutations in cfDNA were also evaluated in endometrial cancer by targeted sequencing, and 14% (2/14) and 33% (7/21) of the tumors had *KRAS* and *PIK3CA* mutations in cfDNA, respectively [23]. Our study demonstrated ctDNA detection in 27.1% of plasma cfDNA of EOC patients using ddPCR for *KRAS* and *PIK3CA* mutations. It is mostly in agreement with previous studies, and is the largest sample size assessing detection rate of plasma cfDNA in EOC patients.

We observed that ctDNA detection was associated with advanced stage and positive peritoneal cytology (p=0.008 and p=0.007, respectively). In 40 patients with HGSC, the levels of ctDNA (AC/mL) for *TP53* mutations correlated with tumor volume measured using 3D volume reconstructing from computed tomography (CT) images [20]. However, the other report for EOC showed no correlation between ctDNA status and other clinical and pathological factors in 69 EOC patients [17]. This discrepancy might be attributed to the fact that their study included only HGSC patients mostly in advanced stage disease, unlike our study that included all histotypes. When other types of cancers we examined, the clinical stage was reported to be the only clinical factor that affected the detection rate of ctDNA in colorectal cancer patients [24]. Higher performance status, presence of bone metastasis and metastasis in three or more organs were associated with high ctDNA detection rate in lung adenocarcinoma patients who had epidermal growth factor receptor (*EGFR*) driver mutations [25].

We demonstrated that presence of ctDNA in the blood at the time of initial treatment was found to be a prognostic factor for PFS and OS in EOC patients harboring *PIK3CA*

and/or *KRAS* somatic mutations. Our data are mostly in agreement with previous preliminary reports by other investigators. *TP53*, *PIK3CA*, or *KRAS* mutations in cfDNA were associated with poorer survival in ovarian cancer [16-18,20,21], but they included a limited sample size in those analyses. Previous reports have shown that not only in EOC, but also other cancer types including endometrial, breast, colon and pancreatic cancer positive for ctDNA, was also associated with worse prognosis [3,18,26,27]. Our study demonstrated for the first time that ctDNA detection in plasma at the time of initial treatment was an independent prognostic factor by multivariate cox analysis in EOC patients. However, ctDNA was not shown to be an independent prognostic factor for OS in this study. This might be in part due to the complex treatments for recurrent EOC patients or limited events for multivariate analysis on OS in this study. We also investigated the role of ctDNA in each histotype. We found both PFS and OS were decreased in patient with clear cell carcinoma who had ctDNA compared to those who did not (S8A and S8B Fig.). The PFS but not the OS was decreased in the patients with endometrioid carcinoma who had ctDNA compared to those who did not (S8C and S8D Fig.). In contrast, no difference was found in either PFS or OS for serous and mucinous carcinoma. However, the numbers of cases in those two histologic types were limited (S7E-S7H Fig.).

This is the first report comparing paired plasma samples at the time of primary surgery and recurrence for ctDNA evaluation. The levels of serum CA125 and the tumor size decreased at the time of relapse than those at the time of primary treatment. Interestingly, we found a higher mutation rate in plasma cfDNA at the time of recurrence compared with at the time of primary treatment though statistically not significant. This may be partly explained by the different molecular status between the primary and relapsed disease. *PIK3CA* or *KRAS* mutant clones may be enriched during the relapse, suggesting a more aggressive phenotype with *PIK3CA*/*KRAS* mutants. By monitoring plasma ctDNA, we may detect ovarian cancer relapse earlier. Other reports also showed that ctDNA was detected in six of 44 patients with ovarian or endometrial cancer, even when CT scanning was negative for those tumors [18]. A few cases of OCCC were shown to have increased ctDNA earlier than CA125 at the time of relapse [16].

Our study has several limitations. One is the retrospective design and the second is modest sample size and all cases arising from single institute, and specifically studying cases with *PIK3CA* and *KRAS* mutations without studying *TP53* mutations, which might affect the survivals in HGSC patients. The limited amount of plasma used in this study might affect the detection rate. Further studies using a large sample size or prospective design are warranted.

In conclusion, plasma ctDNA was detected in approximate 30% of EOC patients at the time of initial treatment in this study. The presence of ctDNA in the blood was shown to be an indicator for outcomes in EOC patients, suggesting that the presence of ctDNA could predict tumor spread even in cases of localized tumors.

Electronic Supplementary Material

Supplementary materials are available at Cancer Research and Treatment website (https://www.e-crt.org).

Conflict of Interest

This study was partially supported by the Grant from Hidaka Research Projects (28-D-1-03) at Saitama Medical University (AO) and a research grant from Eisai (KH).

Acknowledgments

We thank Drs. S. Nagao, N. Iwasa and T. Nishikawa for their support in sample collection during our study. We also thank Ms. A. Iwasa and S. Shimoyokkaichi for their excellent technical assistance.

References

1. Diehl F, Schmidt K, Choti MA, Romans K, Goodman S, Li M, et al. Circulating mutant DNA to assess tumor dynamics. Nat Med. 2008;14:985-90.
2. De Roock W, Claes B, Bernasconi D, De Schutter J, Biesmans B, Fountzilas G, et al. Effects of KRAS, BRAF, NRAS, and PIK3CA mutations on the efficacy of cetuximab plus chemotherapy in chemotherapy-refractory metastatic colorectal cancer: a retrospective consortium analysis. Lancet Oncol. 2010;11:753-62.
3. Tabernero J, Lenz HJ, Siena S, Sobrero A, Falcone A, Ychou M, et al. Analysis of circulating DNA and protein biomarkers to predict the clinical activity of regorafenib and assess prognosis in patients with metastatic colorectal cancer: a retrospective, exploratory analysis of the CORRECT trial. Lancet Oncol. 2015;16:937-48.
4. Haber DA, Velculescu VE. Blood-based analyses of cancer: circulating tumor cells and circulating tumor DNA. Cancer Discov. 2014;4:650-61.
5. Mandel P, Metais P. Article in undetermined language. C R Seances Soc Biol Fil. 1948;142:241-3.
6. Offin M, Chabon JJ, Razavi P, Isbell JM, Rudin CM, Diehn M, et al. Capturing genomic evolution of lung cancers through liquid biopsy for circulating tumor DNA. J Oncol. 2017;2017:4517834.

7. Dawson SJ, Tsui DW, Murtaza M, Biggs H, Rueda OM, Chin SF, et al. Analysis of circulating tumor DNA to monitor metastatic breast cancer. N Engl J Med. 2013;368:1199-209.
8. Cheuk IW, Shin VY, Kwong A. Detection of methylated circulating DNA as noninvasive biomarkers for breast cancer diagnosis. J Breast Cancer. 2017;20:12-9.
9. Beije N, Helmijr JC, Weerts MJA, Beaufort CM, Wiggin M, Marziali A, et al. Somatic mutation detection using various targeted detection assays in paired samples of circulating tumor DNA, primary tumor and metastases from patients undergoing resection of colorectal liver metastases. Mol Oncol. 2016;10:1575-84.
10. Przybyl J, Chabon JJ, Spans L, Ganjoo KN, Vennam S, Newman AM, et al. Combination approach for detecting different types of alterations in circulating tumor DNA in leiomyosarcoma. Clin Cancer Res. 2018;24:2688-99.
11. Huang A, Zhang X, Zhou SL, Cao Y, Huang XW, Fan J, et al. Detecting circulating tumor DNA in hepatocellular carcinoma patients using droplet digital PCR is feasible and reflects intratumoral heterogeneity. J Cancer. 2016;7:1907-14.
12. Torre LA, Bray F, Siegel RL, Ferlay J, Lortet-Tieulent J, Jemal A. Global cancer statistics, 2012. CA Cancer J Clin. 2015;65:87-108.
13. Bast RC Jr, Hennessy B, Mills GB. The biology of ovarian cancer: new opportunities for translation. Nat Rev Cancer. 2009;9:415-28.
14. Kim YM, Lee SW, Lee YJ, Lee HY, Lee JE, Choi EK. Prospective study of the efficacy and utility of TP53 mutations in circulating tumor DNA as a non-invasive biomarker of treatment response monitoring in patients with high-grade serous ovarian carcinoma. J Gynecol Oncol. 2019;30:e32.
15. Phallen J, Sausen M, Adleff V, Leal A, Hruban C, White J, et al. Direct detection of early-stage cancers using circulating tumor DNA. Sci Transl Med. 2017;9:eaan2415.
16. Morikawa A, Hayashi T, Shimizu N, Kobayashi M, Taniue K, Takahashi A, et al. PIK3CA and KRAS mutations in cell free circulating DNA are useful markers for monitoring ovarian clear cell carcinoma. Oncotarget. 2018;9:15266-74.
17. Swisher EM, Wollan M, Mahtani SM, Willner JB, Garcia R, Goff BA, et al. Tumor-specific p53 sequences in blood and peritoneal fluid of women with epithelial ovarian cancer. Am J Obstet Gynecol. 2005;193(3 Pt 1):662-7.
18. Pereira E, Camacho-Vanegas O, Anand S, Sebra R, Catalina Camacho S, Garnar-Wortzel L, et al. Personalized circulating tumor DNA biomarkers dynamically predict treatment response and survival in gynecologic cancers. PLoS One. 2015;10:e0145754.
19. Otsuka J, Okuda T, Sekizawa A, Amemiya S, Saito H, Okai T, et al. Detection of p53 mutations in the plasma DNA of patients with ovarian cancer. Int J Gynecol Cancer. 2004;14:459-64.
20. Parkinson CA, Gale D, Piskorz AM, Biggs H, Hodgkin C, Addley H, et al. Exploratory analysis of TP53 mutations in circulating tumour DNA as biomarkers of treatment response for patients with relapsed high-grade serous ovarian carcinoma: a retrospective study. PLoS Med. 2016;13:e1002198.
21. Zhuang R, Li S, Li Q, Guo X, Shen F, Sun H, et al. The prognostic value of KRAS mutation by cell-free DNA in cancer patients: a systematic review and meta-analysis. PLoS One. 2017;12:e0182562.
22. Barbosa A, Peixoto A, Pinto P, Pinheiro M, Teixeira MR. Potential clinical applications of circulating cell-free DNA in ovarian cancer patients. Expert Rev Mol Med. 2018;20:e6.
23. Bolivar AM, Luthra R, Mehrotra M, Chen W, Barkoh BA, Hu P, et al. Targeted next-generation sequencing of endometrial cancer and matched circulating tumor DNA: identification of plasma-based, tumor-associated mutations in early stage patients. Mod Pathol. 2019;32:405-14.
24. Scholer LV, Reinert T, Orntoft MW, Kassentoft CG, Arnadottir SS, Vang S, et al. Clinical implications of monitoring circulating tumor DNA in patients with colorectal cancer. Clin Cancer Res. 2017;23:5437-45.
25. Iwama E, Sakai K, Azuma K, Harada T, Harada D, Nosaki K, et al. Monitoring of somatic mutations in circulating cell-free DNA by digital PCR and next-generation sequencing during afatinib treatment in patients with lung adenocarcinoma positive for EGFR activating mutations. Ann Oncol. 2017;28:136-41.
26. Oshiro C, Kagara N, Naoi Y, Shimoda M, Shimomura A, Maruyama N, et al. PIK3CA mutations in serum DNA are predictive of recurrence in primary breast cancer patients. Breast Cancer Res Treat. 2015;150:299-307.
27. Pietrasz D, Pecuchet N, Garlan F, Didelot A, Dubreuil O, Doat S, et al. Plasma circulating tumor DNA in pancreatic cancer patients is a prognostic marker. Clin Cancer Res. 2017;23:116-23.

pISSN 1598-2998, eISSN 2005-9256

Cancer Res Treat. 2020;52(4):1229-1241

https://doi.org/10.4143/crt.2020.557

Original Article

Open Access

Germline and Somatic *BRCA1/2* Gene Mutational Status and Clinical Outcomes in Epithelial Peritoneal, Ovarian, and Fallopian Tube Cancer: Over a Decade of Experience in a Single Institution in Korea

Se Ik Kim, MD
Maria Lee, MD, PhD
Hee Seung Kim, MD, PhD
Hyun Hoon Chung, MD, PhD
Jae-Weon Kim, MD, PhD
Noh Hyun Park, MD, PhD
Yong-Sang Song, MD, PhD

Department of Obstetrics and Gynecology, Seoul National University College of Medicine, Seoul, Korea

Correspondence: Maria Lee, MD, PhD
Department of Obstetrics and Gynecology, Seoul National University College of Medicine, 101 Daehak-ro, Jongno-gu, Seoul 03080, Korea
Tel: 82-2-2072-2842
Fax: 82-2-762-3599
E-mail: marialeemd@gmail.com

Received June 8 2020
Accepted July 25, 2020
Published Online July 27, 2020

Purpose

This study aimed to present a single institutional experience with *BRCA1/2* gene tests and the effects of pathogenic mutations in epithelial peritoneal, ovarian, and fallopian tube cancer (POFTC) on survival outcomes.

Materials and Methods

We identified patients with epithelial POFTCs who underwent *BRCA1/2* gene testing by either germline or somatic methods between March 2007 and March 2020. Based on the *BRCA1/2* test results, patients were divided into *BRCA* mutation and wild-type groups, followed by comparisons of clinicopathologic characteristics and survival outcomes after primary treatment.

Results

The annual number of POFTC patients who received *BRCA1/2* gene tests increased gradually. In total, 511 patients were included and *BRCA1/2* mutations were observed in 143 (28.0%). Among 57 patients who received both germline and somatic tests, three (5.3%) showed discordant results from the two tests. Overall, no differences in progression-free survival (PFS; p=0.467) and overall survival (p=0.641) were observed between the *BRCA* mutation and wild-type groups; however, multivariate analyses identified *BRCA1/2* mutation as an independent favorable prognostic factor for PFS (adjusted hazard ratio [aHR], 0.765; 95% confidence interval [CI], 0.593 to 0.987; p=0.040). In 389 patients with International Federation of Gynecology and Obstetrics stage III-IV, different results were shown depending on primary treatment strategy: while *BRCA1/2* mutation significantly improved PFS in the subgroup of neoadjuvant chemotherapy (aHR, 0.619; 95% CI, 0.385 to 0.995; p=0.048), it did not affect patient PFS in the subgroup of primary debulking surgery (aHR, 0.759; 95% CI, 0.530 to 1.089; p=0.135).

Conclusion

BRCA1/2 mutations are frequently observed in patients with epithelial POFTCs, and such patients showed better PFS than did those harboring wild-type *BRCA1/2*.

Key words

Genital neoplasms, Female, Ovarian neoplasms, Germline test, Somatic test, *BRCA1/2* mutation, Clinical outcome, Survival outcome

Introduction

Ovarian cancer is the most lethal gynecologic malignancy and is estimated to account for 295,000 new cases and 185,000 cancer deaths annually worldwide [1]. Recent studies view epithelial peritoneal, ovarian, and fallopian tube cancers (POFTCs) as a single disease group that shares a common pathogenesis, diagnosis, and treatment [2]. Epithelial POFTCs tend to be diagnosed at an advanced-stage and show high recurrence and mortality rates, despite the standard primary treatment. Approximately 15% to 20% of patients with epithelial POFTCs present genetic predisposition or hereditary factors, with *BRCA1/2* identified as well-known causal genes [3,4].

Women harboring germline mutations in either *BRCA1/2* are at an excessive risk of developing both breast cancer (BC) and ovarian cancer [5,6]. Offspring of a germline *BRCA1/2*-mutation carrier have a 50% chance of inheriting the patho-

genic or likely pathogenic variant. Moreover, patients harboring germline or somatic *BRCA1/2* mutations with primary or platinum-sensitive relapsed POFTC experience positive survival outcomes from poly(ADP-ribose) polymerase (PARP) inhibitors based on their synthetic lethality [7-12]. Therefore, current guidelines from the Korean Society of Gynecologic Oncology recommend that patients with epithelial POFTC patients undergo *BRCA1/2* gene testing [13].

Previous studies have focused on the prognostic aspect of *BRCA1/2* mutations, frequently reporting that *BRCA1/2* mutations confer a survival advantage relative to wild-type *BRCA1/2* due to better response to platinum-based chemotherapy [14]. However, further analysis revealed that the study populations and designs, as well as the specific results, differ among studies. Although overall survival (OS) was improved in patients carrying *BRCA1/2* mutations [14,15], some studies identified advantages for only those harboring *BRCA2* mutations [16,17]. In our previous study that included patients with advanced-stage ovarian high-grade serous carcinoma (HGSC), longer progression-free survival (PFS) but not OS was associated with germline *BRCA1/2* mutations [18].

Therefore, additional scientific evidence concerning the effects of *BRCA1/2* mutations on POFTC prognosis according to the primary treatment strategy is necessary, especially in patients of Korean ethnicity. In this study, we investigated the impact of *BRCA1/2* mutational status on survival outcomes in patients with epithelial POFTC. Additionally, we present a single institutional experience with germline and somatic *BRCA1/2* gene testing not limited by initial International Federation of Gynecology and Obstetrics (FIGO) stage or histologic type.

Materials and Methods

1. Study population

Since starting germline *BRCA1/2* gene testing, our institution has conducted this test in patients with BC presenting a strong family history of BC or with family members harboring *BRCA1/2* mutations. In March 2007, patients with epithelial POFTC also began to receive germline *BRCA1/2* gene testing. In September 2017, our institutional hospital launched a targeted next-generation sequencing (NGS) cancer panel for clinical purposes, which enabled identification of somatic *BRCA1/2* mutational status in patients with epithelial POFTC.

To include all possible cases meeting the study purpose, we established the following inclusion criteria: (1) patients pathologically diagnosed with and treated for epithelial POFTC; and (2) patients who received either germline *BRCA1/2* gene testing or a somatic NGS cancer panel between March 2007 and March 2020, and thus whose germline or somatic *BRCA1/2* mutational status was verified. By contrast, we excluded patients with insufficient clinicopathologic data or those lost to follow-up during primary treatment.

We identified 563 patients from the Ovarian Cancer Cohort of the institution who met these criteria. For fair comparisons, we further excluded 52 patients who were enrolled in past or current clinical trials, during their primary treatment, which could affect survival outcomes.

2. Germline and somatic *BRCA1/2* gene test

Germline *BRCA1/2* gene testing methods at the Seoul National University Hospital (SNUH) were described in our previous study [18]. As of February 2016, the method has been changed from direct sequencing (Sanger sequencing) to NGS of *BRCA1/2* genes. Sequence variants found in NGS were confirmed by Sanger sequencing.

For somatic *BRCA1/2* gene testing, we used an NGS cancer panel named "SNUH FIRST-Cancer panel version 3.1" and performed DNA collection and profiling from archival formalin-fixed paraffin-embedded (FFPE) tumor tissues, as described previously [19]. Briefly, genomic DNA was extracted from FFPE tissues using the ReliaPrep FFPE gDNA miniprep system (Promega, Madison, WI), and a library was constructed using the SureSelectXT target enrichment protocol (Agilent Technologies, Carlsbad, CA) for Illumina paired-end sequencing (2×101 bp), which was performed on the Illumina Hiseq 2500 platform (Illumina, Carlsbad, CA). Details of the reporting algorithms used for single-nucleotide variants, copy number variants, and structural variants were also described previously [19]. The SNUH FIRST-Cancer panel version 3.1 provides information on all exons of 183 genes, specific introns of 23 fusion genes, the *TERT* promoter region, eight microsatellite-instability markers, and 45 drug-target lesions, covering a total length of approximately 1.949 Mbp. Of these, we focused on genomic alterations of *BRCA1/2* genes.

We referenced the detected *BRCA1/2* variants in two representative databases, the Breast Cancer Information Core (BIC) and the National Institutes of Health open-access database of clinically observed variants and their classification (ClinVar), and the literature. Sequence variants in *BRCA1* and *BRCA2* were classified into five categories according to the recommendation of the American College of Medical Genetics and Genomics and the Association for Molecular Pathology [20]. In the present study, we regarded patients with "pathogenic" and "likely pathogenic" variants as the *BRCA* mutation group (*BRCA*mut; study group) and the rest of the patients as the *BRCA* wild-type group (*BRCA*wt; control group).

3. Data collection

Review of medical records and pathologic reports allowed collection of the following clinicopathologic data: age at diagnosis, histologic type, FIGO stage, initial serum cancer anti-

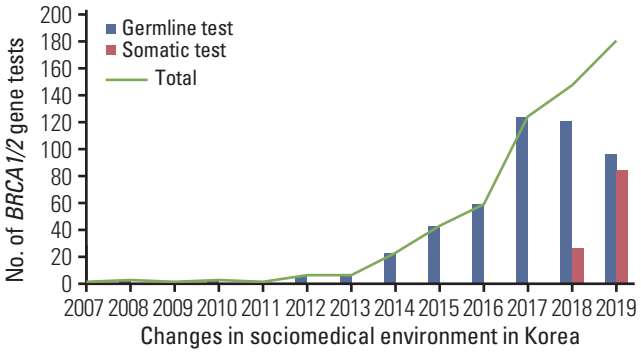

2012-04 NHIS covers *BRCA1/2* gene tests
2012-12 NHIS covers RRSO
2015-08 KFDA permits olaparib maintenance for *BRCA*mut, PSR, HGS POFTC (≥ 2 L)
2016-03 Positions statements on genetic test for POFTC, KSGO
2017-09 NHIS covers NGS cancer panel
2017-10 NHIS covers olaparib maintenance for *BRCA*mut, PSR, HGS POFTC (≥ 2 L)
2018-05 KFDA permits olaparib for *BRCA*mut, recurrent POFTC (≥ 4 L)
2019-03 KFDA permits niraparib maintenance for PSR, HGS POFTC (≥ 2 L)
2019-10 KFDA permits olaparib maintenance for PSR, HG POFTC (≥ 2 L)
2019-10 KFDA permits olaparib maintenance for *BRCA*mut, primary, HG POFTC (1 L)
2019-12 NHIS covers niraparib for germline *BRCA*mut, PSR, HGS POFTC (≥ 2 L)
2019-12 KFDA permits niraparib for *BRCA*mut or HRDpos, recurrent POFTC (≥ 4 L)

Fig. 1. Annual number of *BRCA1/2* gene tests among patients with peritoneal, ovarian, and fallopian tube cancers (POFTCs) and according to changes in sociomedical environment in Korea. NHIS, National Health Insurance Service; RRSO, risk reducing salpingo-oophorectomy; KFDA, Korea Food and Drug Administration; PSR, platinum-sensitive relapsed; HGS, high-grade serous; KSGO, Korean Society of Gynecologic Oncology; NGS, next-generation sequencing; HG, high-grade; HRDpos, homologous recombination deficiency-positive.

gen 125 levels, and primary treatment strategy. We considered optimal debulking to have occurred when the surgery resulted in the largest size of the residual tumor being < 1 cm. All patients received taxane- and platinum-based chemotherapy as part of their primary treatment unless they had low-grade IA/IB disease according to the 2014 FIGO staging system. Additionally, we retrieved personal and familial histories of cancer and the number of affected family members up to the second degree.

For survival analyses, PFS was defined as the time interval between the date of initial diagnosis and the date of disease progression confirmed by the Response Evaluation Criteria in Solid Tumours ver. 1.1 [21]. OS was defined as the time interval between the date of initial diagnosis to the date of cancer-related death or last visit.

4. Statistical analysis

Baseline clinicopathologic characteristics and survival outcomes were compared between the *BRCA*mut and *BRCA*wt groups. We used a Student's t or Mann-Whitney U test for comparisons of continuous variables, and Pearson's chi-squared or Fisher exact test for comparisons of categorical variables. For survival analyses, the Kaplan-Meier method with log-rank test and Cox proportional hazards regression models were used. We calculated the adjusted hazard ratio

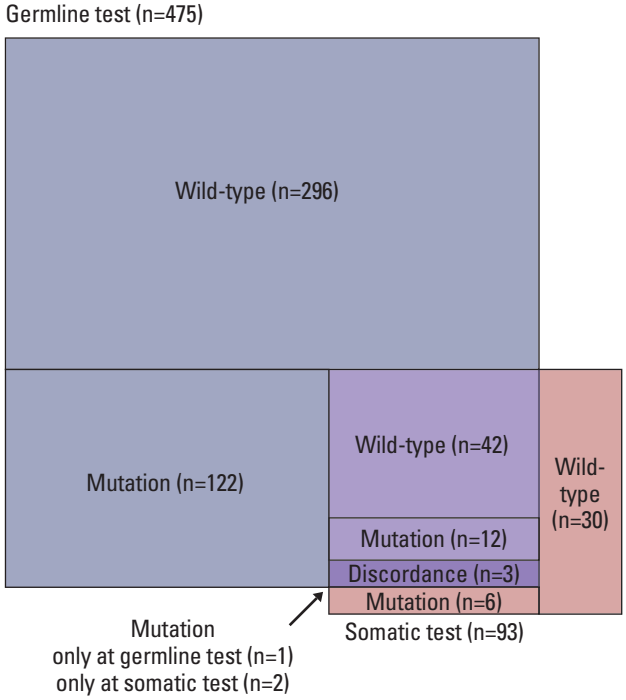

Fig. 2. Aerial chart depicting proportion of patients who underwent germline and somatic *BRCA1/2* gene tests along with the test results.

Table 1. Clinicopathologic characteristics of the study population

Characteristic	Total (n=511)	*BRCA* wild-type (n=368)	*BRCA* mutation (n=143)	p-value
Age (yr)	54.3±10.9	54.5±11.5	53.9±9.3	0.557
Parity	1.9±1.3	1.9±1.3	1.9±1.0	0.394
Origin				
Ovary	481 (94.1)	345 (93.8)	136 (95.1)	0.705
Fallopian tube	14 (2.7)	10 (2.7)	4 (2.8)	
Peritoneum	16 (3.1)	13 (3.5)	3 (2.1)	
Hx of BC	58 (11.4)	29 (7.9)	29 (20.3)	< 0.001
Hx of other cancers	28 (5.5)	18 (4.9)	10 (7.0)	0.349
Family Hx of POFTC	27 (5.3)	7 (1.9)	20 (14.0)	< 0.001
No. of relatives	0.1±0.2	0.0±0.1	0.2±0.4	< 0.001
Family Hx of BC	45 (8.8)	16 (4.3)	29 (20.3)	< 0.001
No. of relatives	0.1±0.4	0.1±0.2	0.3±0.6	< 0.001
Family Hx of other cancers	111 (21.7)	74 (20.1)	37 (25.9)	0.156
FIGO stage				
I	72 (14.1)	65 (17.7)	7 (4.9)	0.001
II	50 (9.8)	39 (10.6)	11 (7.7)	
III	259 (50.7)	177 (48.1)	82 (57.3)	
IV	130 (25.4)	87 (23.6)	43 (30.1)	
Histology				
High-grade serous	368 (72.0)	246 (66.8)	122 (85.3)	0.001
Low-grade serous	11 (2.2)	10 (2.7)	1 (0.7)	
Endometrioid	43 (8.4)	37 (10.1)	6 (4.2)	
Mucinous	16 (3.1)	13 (3.5)	3 (2.1)	
Clear cell	42 (8.2)	40 (10.9)	2 (1.4)	
Mixed	14 (2.7)	10 (2.7)	4 (2.8)	
Others	8 (1.6)	6 (1.6)	2 (1.4)	
Unknown	9 (1.8)	6 (1.6)	3 (2.1)	
Tumor grade				
1	30 (5.9)	27 (7.3)	3 (2.1)	0.027
2	28 (5.5)	23 (6.3)	5 (3.5)	
3	438 (85.7)	306 (83.2)	132 (92.3)	
Unknown	15 (2.9)	12 (3.3)	3 (2.1)	
CA-125 (IU/mL)	695.5 (3.4-17,313)	666.5 (3.4-15,700)	767.0 (5.1-17,313)	0.085
Primary treatment strategy				
PDS	379 (74.2)	278 (75.5)	101 (70.6)	0.255
NAC	132 (25.8)	90 (24.5)	42 (29.4)	
Residual tumor after PDS/IDS[a]				
No gross	374 (73.2)	278 (75.5)	96 (67.1)	0.224
< 1 cm	70 (13.7)	48 (13.0)	22 (15.4)	
1-2 cm	23 (4.5)	13 (3.5)	10 (7.0)	
≥ 2 cm	22 (4.3)	17 (4.6)	5 (3.5)	
Unknown	13 (2.5)	6 (1.6)	7 (4.9)	
Chemotherapy at primary treatment				
Bevacizumab- containing regimen	30 (5.9)	19 (5.2)	11 (7.7)	0.362
Non-bevacizumab regimen	464 (90.8)	335 (91.0)	129 (90.2)	
No chemotherapy	17 (3.3)	14 (3.8)	3 (2.1)	
Recurrence[b]	324 (63.4)	231 (62.8)	93 (65.0)	0.634
PSR[c]	238 (46.6)	156 (42.4)	82 (57.3)	0.001
PRR	78 (15.3)	67 (18.2)	11 (7.7)	

(Continued to the next page)

Table 1. Clinicopathologic characteristics of the study population

Characteristic	Total (n=511)	*BRCA* wild-type (n=368)	*BRCA* mutation (n=143)	p-value
Genetic test methods				
Germline only	418 (81.8)	296 (80.4)	122 (85.3)	0.264
Somatic only	36 (7.0)	30 (8.2)	6 (4.2)	
Both	57 (11.2)	42 (11.4)	15 (10.5)	
***BRCA1* mutational status**				
Wild-type	409 (80.0)	368 (100)	41 (28.7)	< 0.001
Mutation	102 (20.0)	0	102 (71.3)	
***BRCA2* mutational status**				
Wild-type	469 (91.8)	368 (100)	101 (70.6)	< 0.001
Mutation	42 (8.2)	0	42 (29.4)	

Values are presented as mean±SD, number (%), or median (range). Hx, history; BC, breast cancer; POFTC, peritoneal, ovarian, and fallopian tubal cancers; FIGO, International Federation of Gynecology and Obstetrics; CA-125, cancer antigen 125; PDS, primary debulking surgery; NAC, neoadjuvant chemotherapy; IDS, interval debulking surgery; PSR, platinum-sensitive recurrence; PRR, platinum-resistant recurrence; SD, standard deviation. [a]Nine patients did not receive debulking surgery, [b]Among the recurred, eight patients did not receive taxane- and platinum-based chemotherapy before, [c]PSR was defined as relapse ≥ 6 months after completion of taxane- and platinum-based chemotherapy, whereas PRR as relapse < 6 months.

(aHR) and 95% confidence interval (CI) for each variable. All statistical analyses were conducted by using SPSS software ver. 25.0 (IBM Corp., Armonk, NY), and a $p < 0.05$ was regarded as statistically significant.

5. Ethical statement

This retrospective cohort study was approved by the Institutional Review Board of SNUH (No. C-2005-042-1122) and performed in accordance with the principles of the Declaration of Helsinki. The requirement for informed consent was waived.

Results

1. *BRCA1/2* gene test results

The annual number of POFTC patients who received *BRCA1/2* gene tests increased gradually according to a series of sociomedical environment changes in Korea (Fig. 1). Of 511 patients who underwent *BRCA1/2* gene tests (418, 36, and 57 for germline test only, somatic test only, and both tests, respectively), *BRCA1/2* mutations were observed in 143 (28.0%), with 20.0% and 8.2% of patients harboring *BRCA1* and *BRCA2* mutations, respectively. One patient harbored mutations in both genes; however, germline testing identified only a *BRCA2* mutation (c.9097dupA), whereas somatic testing identified an additional *BRCA1* mutation (c.2206_2207delGA).

We observed differential *BRCA1/2* mutational status in patients with POFTC according to the presence of BC and/or other cancers, such as colorectal and gastric cancers (S1 Fig.). Although the prevalence of *BRCA1/2* mutations was lowest among patients presenting POFTC only (24.9%), it was highest among those presenting POFTC, BC, and another cancer (triple cancers; 75.0%). Of the 54 patients presenting both POFTC and BC, *BRCA1/2* mutations were identified in 26 (48.1%).

Among 57 patients who received both germline and somatic tests, three (5.3%) showed discordant results in their classification into the *BRCA*mut and *BRCA*wt groups (Fig. 2). Specifically, one patient harboring germline *BRCA1* mutation showed restoration of a wild-type *BRCA1* sequence according to somatic testing (true reversion), and the other two with germline *BRCA1/2* wild-type were identified as harboring somatic *BRCA1* mutation (acquired mutation). Details of *BRCA1/2* test results and clinical information of the 57 patients are presented in S2 Table.

2. Characteristics of the study population

Patient characteristics are shown in Table 1. Age at diagnosis of POFTC was similar between the *BRCA*mut and *BRCA*wt groups. However, patients with *BRCA* mutations displayed significantly higher personal and family histories of BC and a higher family history of POFTC relative to those without *BRCA* mutations. Initial disease presentation also differed between groups, with the *BRCA*mut group showing more advanced disease and more frequent HGSC histology. In terms of primary treatment, there were no differences in the proportion of neoadjuvant chemotherapy (NAC) cases and residual tumor after debulking surgery between groups. In this study, 5.9% (30/511) of the study population received be acizumab-containing chemotherapy during primary treatment, and the proportion of bevacizumab users was similar between the *BRCA*mut and *BRCA*wt groups. No patient received maintenance with a PARP inhibitor after primary treatment.

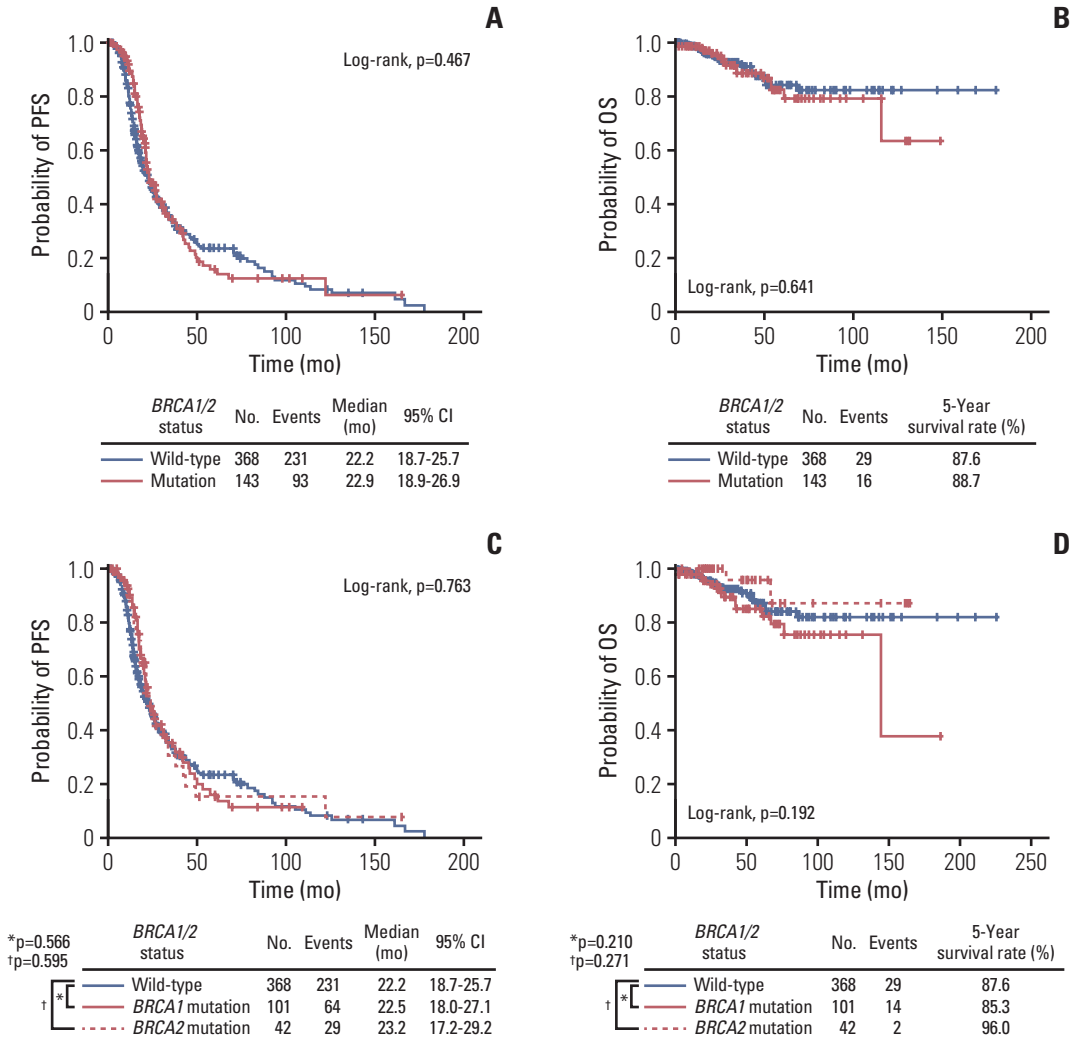

Fig. 3. Survival outcomes of the study population (A, B), and further comparisons according to the mutated *BRCA* gene (C, D). (A, C) Progression-free survival (PFS). (B, D) Overall survival (OS).

BRCA1/2 mutations were observed in 33.2% of patients with HGSC (n=368), a higher percentage than in the whole study population. As shown in S3 Table, patient characteristics were similar between the *BRCA*mut and *BRCA*wt groups, except for patient age, personal history of BC, and family history of BC and POFTC. In patients who had histologic types other than HGSC (non-HGSC, n=134), incidence of *BRCA1/2* mutation was 13.4%. As shown in S4 Table, patient characteristics, such as primary treatment strategy and residual tumor after debulking surgery, were similar between the two groups, whereas family history of BC and POFTC differed.

3. Clinical outcomes of all study populations

During the median observation period of 42.8 months, 93 patients (65.0%) in the *BRCA*mut group and 231 (62.8%) in the *BRCA*wt group experienced disease recurrence. Despite the higher proportion of platinum-sensitive recurrence in the *BRCA*mut group (p=0.001), which referred to recurrence within 6 months after completion of platinum-based primary treatment, the two groups showed similar PFS (median, 22.9 vs. 22.2 months; p=0.467) (Fig. 3A). However, multivariate analyses adjusting for age, FIGO stage, histologic type, primary treatment strategy, and residual tumor after debulking surgery revealed *BRCA1/2* mutation as an independent favorable prognostic factor for PFS (aHR, 0.765; 95% CI, 0.593 to 0.987; p=0.040) (Table 2). Both *BRCA*mut and *BRCA*wt groups showed similar OS (5-year survival rate, 88.7% vs. 87.6%; p=0.641) (Fig. 3B), and multivariate analyses revealed that presence of *BRCA1/2* mutations did not affect patient OS (Table 2). Use of bevacizumab in primary treatment did not improve patient PFS and OS in univariate and multivariate analyses.

Regarding the specific genes with mutations, we subdivided the *BRCA*mut group into the *BRCA1*mut (n=101) and

Table 2. Factors associated with survival outcomes

Characteristic	Progression-free survival						Overall survival					
	Univariate analysis			Multivariate analysis			Univariate analysis			Multivariate analysis		
	HR	95% CI	p-value	aHR	95% CI	p-value	HR	95% CI	p-value	aHR	95% CI	p-value
Age (yr)												
< 55	1			1			1			1		
≥ 55	1.590	1.273-1.985	< 0.001	1.325	1.043-1.683	0.021	2.237	1.218-4.107	0.009	1.704	0.904-3.211	0.099
FIGO stage												
I-II	1			1			1			1		
III	2.435	1.746-3.397	< 0.001	2.296	1.563-3.371	< 0.001	1.502	0.613-3.678	0.374	1.078	0.378-3.079	0.888
IV	3.568	2.478-5.139	< 0.001	2.637	1.681-4.138	< 0.001	2.768	1.068-7.176	0.036	1.490	0.465-4.775	0.502
Histology												
High-grade serous	1			1			1			1		
Non–high-grade serous	0.620	0.472-0.813	0.001	1.085	0.795-1.483	0.607	0.803	0.396-1.625	0.541	1.219	0.545-2.724	0.630
Primary treatment strategy												
PDS	1			1			1			1		
NAC	2.103	1.657-2.670	< 0.001	1.511	1.131-2.019	0.005	2.071	1.117-3.837	0.021	2.003	0.969-4.142	0.061
Residual tumor after PDS/IDS												
< 1 cm	1			1			1			1		
≥ 1 cm	1.738	1.229-2.457	0.002	1.310	0.894-1.918	0.166	2.729	1.381-5.395	0.004	2.676	1.261-5.678	0.010
***BRCA* mutational status**												
Wild-type	1			1			1			1		
Mutation	0.914	0.718-1.164	0.467	0.765	0.593-0.987	0.040	1.156	0.627-2.131	0.642	1.163	0.623-2.171	0.636

HR, hazard ratio; CI, confidence interval; aHR, adjusted hazard ratio; FIGO, International Federation of Gynecology and Obstetrics; PDS, primary debulking surgery; NAC, neoadjuvant chemotherapy; IDS, interval debulking surgery.

Table 3. Factors associated with survival outcomes in patients with FIGO stage III to IV disease

Characteristic	Progression-free survival						Overall survival					
	Univariate analysis			Multivariate analysis			Univariate analysis			Multivariate analysis		
	HR	95% CI	p-value	aHR	95% CI	p-value	HR	95% CI	p-value	aHR	95% CI	p-value
Age (yr)												
< 55	1			1			1			1		
≥ 55	1.431	1.127-1.815	0.003	1.406	1.076-1.837	0.013	2.261	1.160-4.405	0.017	1.650	0.831-3.276	0.152
FIGO stage												
III	1			1			1			1		
V	1.476	1.148-1.897	0.002	1.184	0.872-1.607	0.279	1.894	0.979-3.665	0.058	1.294	0.625-2.681	0.487
Histology												
High-grade serous	1			1			1			1		
Non–high-grade serous	1.068	0.764-1.492	0.701	1.345	0.931-1.942	0.114	1.029	0.430-2.463	0.949	1.250	0.466-3.355	0.658
Initial serum CA-125 (IU/mL)												
< 900	1			1			1			1		
≥ 900	1.294	1.006-1.666	0.045	1.163	0.887-1.525	0.275	1.842	0.952-3.566	0.070	1.456	0.723-2.933	0.293
Primary treatment strategy												
PDS	1			1			1			1		
NAC	1.683	1.315-2.153	< 0.001	1.502	1.093-2.066	0.012	1.918	1.005-3.664	0.048	2.105	0.963-4.604	0.062
Residual tumor after PDS/IDS												
< 1 cm	1			1			1			1		
≥ 1 cm	1.435	1.010-2.038	0.044	1.596	1.078-2.364	0.020	2.438	1.210-4.913	0.013	2.769	1.258-6.095	0.011
***BRCA* mutational status**												
Wild-type	1			1			1			1		
Mutation	0.828	0.642-1.068	0.147	0.722	0.546-0.956	0.023	0.986	0.512-1.899	0.967	1.066	0.547-2.078	0.851

FIGO, International Federation of Gynecology and Obstetrics; HR, hazard ratio; CI, confidence interval; aHR, adjusted hazard ratio; CA-125, cancer antigen 125; PDS, primary debulking surgery; NAC, neoadjuvant chemotherapy; IDS, interval debulking surgery.

Table 4. Factors associated with progression-free survival in patient with FIGO stage III to IV disease according to primary treatment strategy

Characteristic	Primary debulking surgery						Neoadjuvant chemotherapy					
	Univariate analysis			Multivariate analysis			Univariate analysis			Multivariate analysis		
	HR	95% CI	p-value	aHR	95% CI	p-value	HR	95% CI	p-value	aHR	95% CI	p-value
Age (yr)												
< 55	1			1			1			1		
≥ 55	1.286	0.952-1.737	0.101	1.491	1.060-2.097	0.022	1.543	1.020-2.333	0.040	1.508	0.948-2.401	0.083
FIGO stage												
III	1			1			1			1		
IV	1.587	1.107-2.275	0.012	1.873	1.263-2.777	0.002	0.895	0.604-1.327	0.581	0.691	0.439-1.088	0.111
Histology												
High-grade serous	1			1			1			1		
Non–high-grade serous	1.203	0.815-1.775	0.352	1.658	1.085-2.533	0.019	0.856	0.423-1.736	0.667	1.076	0.458-2.529	0.866
Initial serum CA-125 (IU/mL)												
< 900	1			1			1			1		
≥ 900	1.201	0.871-1.658	0.264	1.189	0.848-1.668	0.316	1.219	0.787-1.889	0.374	1.256	0.786-2.007	0.341
Residual tumor after PDS/IDS												
< 1 cm	1			1			1			1		
≥ 1 cm	1.471	0.975-2.218	0.066	1.340	0.857-2.096	0.200	1.887	0.943-3.775	0.073	3.200	1.357-7.544	0.008
***BRCA* mutational status**												
Wild-type	1			1			1			1		
Mutation	0.940	0.682-1.295	0.705	0.759	0.530-1.089	0.135	0.659	0.431-1.008	0.054	0.619	0.385-0.995	0.048

FIGO, International Federation of Gynecology and Obstetrics; HR, hazard ratio; CI, confidence interval; aHR, adjusted hazard ratio; CA-125, cancer antigen 125; PDS, primary debulking surgery; IDS, interval debulking surgery.

*BRCA2*mut (n=42) groups. The one patient harboring mutations in both genes was placed into the *BRCA2*mut group for statistical purposes. The *BRCA1*mut and *BRCA2*mut groups showed similar PFS and OS relative to the *BRCA*wt group (Fig. 3C and D). In multivariate analyses, *BRCA1* mutation rather than *BRCA1/2* wild-type was not a prognostic factor for improved PFS (aHR, 0.773; 95% CI, 0.575 to 1.040; p=0.089) and OS (aHR, 1.689; 95% CI, 0.870 to 3.280; p=0.121). Additionally, *BRCA2* mutation did not affect patient PFS (aHR, 0.780; 95% CI, 0.522 to 1.166; p=0.226) and OS (aHR, 0.403; 95% CI, 0.095 to 1.703; p=0.216), compared to *BRCA1/2* wild-type.

4. Subgroup analysis according to histologic type

We performed subgroup analyses of patients in order to investigate the effect of *BRCA1/2* mutations on survival outcomes according to the histologic type. Among patients with HGSC (n=368), no differences in PFS (p=0.576) and OS (p=0.980) were observed between the *BRCA*mut and *BRCA*wt groups (S5A and S5B Fig.). In multivariate analyses, *BRCA1/2* mutation was not associated with patient PFS (aHR, 0.785; 95% CI, 0.586 to 1.051; p=0.104) (S6 Table).

Among patients with non-HGSC (n=134), the *BRCA*mut and *BRCA*wt groups showed similar PFS (p=0.321) and OS (p=0.450) (S5C and S5D Fig.). Multivariate analyses revealed that presence of *BRCA1/2* mutations did not affect patient PFS (aHR, 0.530; 95% CI, 0.252 to 1.115; p=0.094) (S6 Table).

5. Subgroup analysis according to primary treatment strategy

We then performed subgroup analyses of only patients with stage III to IV disease (n=389) in order to determine differences in the effect of *BRCA1/2* mutations on survival outcomes according to the primary treatment strategy. Overall, the *BRCA*mut and *BRCA*wt groups showed similar PFS (p=0.146) and OS (p=0.967) (S7A-S7C Fig.). However, multivariate analyses identified *BRCA1/2* mutation as an independent favorable prognostic factor for PFS (aHR, 0.722; 95% CI, 0.546 to 0.956; p=0.023), although not for OS (aHR, 1.066; 95% CI, 0.547 to 2.078; p=0.851) (Table 3).

Among patients with stage III to IV disease who underwent primary debulking surgery (n=257), we observed no differences in PFS (p=0.705) or OS (p=0.768) between the *BRCA*mut and *BRCA*wt groups and no difference in PFS according to specific gene mutation (S7D-S7F Fig.). Multivariate analyses revealed that *BRCA1/2* mutation did not affect patient PFS (aHR, 0.759; 95% CI, 0.530-1.089; p=0.135) (Table 4).

Among patients with stage III to IV disease who underwent NAC (n=132), the *BRCA*mut group showed better PFS with marginal significance than did the *BRCA*wt group (p=0.052), whereas a similar OS was observed between the two groups (p=0.619) (S7G-S7I Fig.). Additionally, multivariate analyses identified *BRCA1/2* mutation as an independent favorable factor for improved PFS (aHR, 0.619; 95% CI, 0.385 to 0.995; p=0.048) (Table 4).

Discussion

In this single-institution, retrospective cohort study, we presented the *BRCA1/2* mutational status of patients with epithelial POFTC and evaluated its effect on survival outcomes. We found a high incidence (28.0%) of *BRCA1/2* mutation and that germline or somatic *BRCA1/2* mutations were associated with better PFS than were wild-type *BRCA* genes.

Identification of patients with *BRCA1/2* mutations and evaluation of their clinical outcomes are important issues in POFTC. Individuals with POFTC confirmed as harboring germline *BRCA1/2* mutations have an opportunity to undergo treatment with PARP inhibitors. At the same time, they should undergo cancer surveillance for BC or other *BRCA*-related cancers. Additionally, their family members might benefit from *BRCA1/2* gene testing in aspect of cancer prevention.

The incidence of *BRCA1/2* mutation in patients with POFTCs varies among different histologic types, with HGSC being the most common type and showing the highest mutation incidence (20%-25%) [22-24]. Consistently with previous studies, we found that the incidence of *BRCA1/2* mutations was higher in patients with HGSC (33.2%) and lower in non-HGSC patients (13.4%) relative to the overall study population (28.0%). Specifically, incidences of *BRCA1/2* mutations in endometrioid and clear cell carcinomas were 14.0% (6/43) and 4.8% (2/42), respectively. In Canadian and Australian populations, previous studies have reported that germline *BRCA1/2* mutations were found in approximately 7% to 8% of patients with ovarian endometrioid and clear cell carcinoma [15,25]. Although our study included a substantial number of Korean patients with non-HGSC POFTC (n=134), the sample size for each histologic type was so small that proper comparisons were difficult between our study results and those from previous studies. Considering that ovarian clear cell carcinoma is more common in East Asian populations than in Western populations [26], *BRCA1/2* test results from East Asians might differ from those from other regions. Therefore, an East Asian collaborative research is necessary to ascertain the exact incidences of *BRCA1/2* mutations in specific histologic types of epithelial POFTC.

Regarding survival outcomes, we identified *BRCA1/2* mutation as a favorable prognostic factor for PFS in the entire study population in consistence with previous studies reporting associations between *BRCA1/2* mutation and improved PFS [14,15,18,27]. We also observed similar results in patients with stage III to IV disease, especially in those who underwent NAC. This improved PFS in patients with POFTC har-

boring *BRCA1/2* mutations is likely due to a high response rate to platinum-based chemotherapy mediated by vulnerability to DNA double-strand breaks [28,29]. However, *BRCA1/2* mutational status did not affect patient PFS in the subgroup of primary debulking surgery, which might be explained by our institution's high optimal debulking rate (85.8%; 211/246), possibly offsetting *BRCA*-related favorable chemotherapy response.

Despite the elongated PFS in patients with *BRCA1/2* mutations, we did not observe differences in patient OS according to *BRCA1/2* mutational status, which differs from previous studies [15,30,31]. This deviation might originate from our study population not being limited by a specific stage or histologic type of epithelial POFTCs. In addition, as *BRCA* mutated tumor gains resistance through the sequential chemotherapy, it is likely that the initial high response to chemotherapy does not lead to improved OS. Although the mechanisms of acquired chemoresistance are heterogeneous, researchers have commonly reported secondary mutations in *BRCA1/2* genes, or reversion mutations, that restores homologous recombination repair functions [32,33]. Sokolenko et al. [34] also reported rapid selection of pre-existing *BRCA1*-proficient tumor clones during chemotherapy in ovarian cancer patients who had germline *BRCA1* mutations. Development of individualized, novel treatment strategies reflecting each patient's specific mechanisms underlying chemoresistance are highly warranted to improve patient OS.

The advent of treatment strategies involving the two PARP inhibitors olaparib and niraparib for POFTC has increased the demand for *BRCA1/2* gene testing in Korea. Based on the findings that tumors with somatically acquired *BRCA1* or *BRCA2* pathogenic mutations respond to PARP inhibitors [10-12], physicians at our institution are recommending somatic testing to patients harboring wild-type *BRCA1/2* according to germline test results and vice versa in order to expand candidate options for PARP inhibitors. As a result, 57 patients from the study population received both germline and somatic tests. The results of both tests within the same patient can be inconsistent due to differences in both the methods and specimens used. In the present study, among 13 patients with both germline and somatic *BRCA1/2* mutations, two (15.4%) showed different variations of *BRCA1/2* mutations, which is similar to a previous study from another institution in Korea [35]. However, a difference in patient classification represents an important issue. Classification of patients into *BRCA*mut and *BRCA*wt groups resulted in a 5.3% (3/57) discordance rate. Of the 57 patients receiving both germline and somatic tests, solitary germline testing failed to identify two patients harboring somatic *BRCA1/2* mutations (3.5%), and solitary somatic testing failed to identify one patient harboring germline *BRCA1/2* mutations (1.8%). Therefore, this suggests an advantage to conducting both germline and somatic testing in order to identify single *BRCA1/2* mutations. However, clinicians need to consider the accuracy of each test, as well as testing cost-effectiveness and available resources.

Although the Korea Food and Drug Administration (KFDA) recently permitted olaparib maintenance for newly diagnosed, high-grade POFTC involving *BRCA1/2* mutation in October 2019, few patients at our institution have actually received olaparib in this setting due to its high price; in the current study, none of the patients received maintenance with olaparib after primary treatment. Additionally, the use of niraparib for first-line maintenance has not yet been permitted by the KFDA. Therefore, we could not observe the substantial survival benefit from PARP inhibitors reported in the phase 3 SOLO-1 [7] or PRIMA [8] trials in this study. It is expected that more patients will use PARP inhibitors in a primary setting if the price of the drugs is lowered or if changes in the sociomedical environment encourage the use of such drugs. However, as PARP inhibitors continue to increase in popularity, further investigation of the exclusive effect of *BRCA1/2* mutations on survival outcomes will be increasingly difficult to conduct.

This study has several limitations. First, selection bias or survival bias might exist due to the retrospective study design. Especially, in terms of baseline characteristics, FIGO stage differed significantly between the *BRCA* mutation and wild-type groups. Second, initial tumor load and disease patterns were not examined. Third, despite collecting cases of *BRCA1/2* gene tests over a considerable time period (e.g., > 10 years for the germline test), some might argue that the sample size was small, especially for further comparisons according to the mutated *BRCA* gene types. Fourth, we only investigated details of the primary treatment. Nevertheless, because very small portion (5.9%) of the study population received bevacizumab during primary treatment, we could not assess survival benefit from bevacizumab exactly in relation with the *BRCA1/2* mutational status. Finally, although we recognize that somatic testing conducted using an NGS cancer panel reports variants of genes other than *BRCA1/2*, we only considered and collected *BRCA1/2* results for study purposes. Currently, we are planning further studies to investigate associations between deficiency in homologous recombination repair genes other than *BRCA1/2* and POFTC patient survival outcomes. Nevertheless, we attempted to organize the experiences of our institution regarding *BRCA1/2* gene testing and present them with systematic survival analyses.

In conclusion, we found that *BRCA1/2* mutations were frequently observed in patients with epithelial POFTCs. This study demonstrated that patients harboring pathogenic *BRCA1/2* mutations showed a better prognosis with longer PFS than did those harboring wild-type *BRCA1/2*. These findings might have important implications for real-world practice and clinical trial design.

Electronic Supplementary Material

Supplementary materials are available at Cancer Research and Treatment website (https://www.e-crt.org).

Conflicts of Interest

Conflicts of interest relevant to this article was not reported.

Acknowledgments

This work was supported by grants from the Seoul National University Hospital Research Fund (No. 0320190260) and the National Research Foundation of Korea (NRF) funded by the Ministry of Science and ICT (No. 2020R1G1A1005711).

References

1. Bray F, Ferlay J, Soerjomataram I, Siegel RL, Torre LA, Jemal A. Global cancer statistics 2018: GLOBOCAN estimates of incidence and mortality worldwide for 36 cancers in 185 countries. CA Cancer J Clin. 2018;68:394-424.
2. Kurman RJ, Shih IM. The origin and pathogenesis of epithelial ovarian cancer: a proposed unifying theory. Am J Surg Pathol. 2010;34:433-43.
3. Levine DA, Argenta PA, Yee CJ, Marshall DS, Olvera N, Bogomolniy F, et al. Fallopian tube and primary peritoneal carcinomas associated with BRCA mutations. J Clin Oncol. 2003;21:4222-7.
4. Norquist BM, Harrell MI, Brady MF, Walsh T, Lee MK, Gulsuner S, et al. Inherited mutations in women with ovarian carcinoma. JAMA Oncol. 2016;2:482-90.
5. Mavaddat N, Peock S, Frost D, Ellis S, Platte R, Fineberg E, et al. Cancer risks for BRCA1 and BRCA2 mutation carriers: results from prospective analysis of EMBRACE. J Natl Cancer Inst. 2013;105:812-22.
6. Kuchenbaecker KB, Hopper JL, Barnes DR, Phillips KA, Mooij TM, Roos-Blom MJ, et al. Risks of breast, ovarian, and contralateral breast cancer for BRCA1 and BRCA2 mutation Carriers. JAMA. 2017;317:2402-16.
7. Moore K, Colombo N, Scambia G, Kim BG, Oaknin A, Friedlander M, et al. Maintenance olaparib in patients with newly diagnosed advanced ovarian cancer. N Engl J Med. 2018;379:2495-505.
8. Gonzalez-Martin A, Pothuri B, Vergote I, DePont Christensen R, Graybill W, Mirza MR, et al. Niraparib in patients with newly diagnosed advanced ovarian cancer. N Engl J Med. 2019;381:2391-402.
9. Pujade-Lauraine E, Ledermann JA, Selle F, Gebski V, Penson RT, Oza AM, et al. Olaparib tablets as maintenance therapy in patients with platinum-sensitive, relapsed ovarian cancer and a BRCA1/2 mutation (SOLO2/ENGOT-Ov21): a double-blind, randomised, placebo-controlled, phase 3 trial. Lancet Oncol. 2017;18:1274-84.
10. Del Campo JM, Matulonis UA, Malander S, Provencher D, Mahner S, Follana P, et al. Niraparib maintenance therapy in patients with recurrent ovarian cancer after a partial response to the last platinum-based chemotherapy in the ENGOT-OV16/NOVA trial. J Clin Oncol. 2019;37:2968-73.
11. Ledermann J, Harter P, Gourley C, Friedlander M, Vergote I, Rustin G, et al. Olaparib maintenance therapy in patients with platinum-sensitive relapsed serous ovarian cancer: a preplanned retrospective analysis of outcomes by BRCA status in a randomised phase 2 trial. Lancet Oncol. 2014;15:852-61.
12. Coleman RL, Oza AM, Lorusso D, Aghajanian C, Oaknin A, Dean A, et al. Rucaparib maintenance treatment for recurrent ovarian carcinoma after response to platinum therapy (ARIEL3): a randomised, double-blind, placebo-controlled, phase 3 trial. Lancet. 2017;390:1949-61.
13. Choi MC, Lim MC, Suh DH, Song YJ, Kim TJ, Chang SJ, et al. Position statements on genetic test for peritoneal, ovarian, and fallopian tubal cancers: Korean Society of Gynecologic Oncology (KSGO). J Gynecol Oncol. 2016;27:e36.
14. Tan DS, Rothermundt C, Thomas K, Bancroft E, Eeles R, Shanley S, et al. "BRCAness" syndrome in ovarian cancer: a case-control study describing the clinical features and outcome of patients with epithelial ovarian cancer associated with BRCA1 and BRCA2 mutations. J Clin Oncol. 2008;26:5530-6.
15. Alsop K, Fereday S, Meldrum C, deFazio A, Emmanuel C, George J, et al. BRCA mutation frequency and patterns of treatment response in BRCA mutation-positive women with ovarian cancer: a report from the Australian Ovarian Cancer Study Group. J Clin Oncol. 2012;30:2654-63.
16. Hyman DM, Zhou Q, Iasonos A, Grisham RN, Arnold AG, Phillips MF, et al. Improved survival for BRCA2-associated serous ovarian cancer compared with both BRCA-negative and BRCA1-associated serous ovarian cancer. Cancer. 2012;118:3703-9.
17. Yang D, Khan S, Sun Y, Hess K, Shmulevich I, Sood AK, et al. Association of BRCA1 and BRCA2 mutations with survival, chemotherapy sensitivity, and gene mutator phenotype in patients with ovarian cancer. JAMA. 2011;306:1557-65.
18. Kim SI, Lee M, Kim HS, Chung HH, Kim JW, Park NH, et al. Effect of BRCA mutational status on survival outcome in advanced-stage high-grade serous ovarian cancer. J Ovarian Res. 2019;12:40.
19. Park C, Kim M, Kim MJ, Kim H, Ock CY, Keam B, et al. Clinical application of next-generation sequencing-based panel to BRAF wild-type advanced melanoma identifies key oncogenic alterations and therapeutic strategies. Mol Cancer Ther. 2020;19:937-44.
20. Richards S, Aziz N, Bale S, Bick D, Das S, Gastier-Foster J, et al. Standards and guidelines for the interpretation of sequence variants: a joint consensus recommendation of the American College of Medical Genetics and Genomics and the Association for Molecular Pathology. Genet Med. 2015;17:405-24.
21. Eisenhauer EA, Therasse P, Bogaerts J, Schwartz LH, Sargent D, Ford R, et al. New response evaluation criteria in solid tumours: revised RECIST guideline (version 1.1). Eur J Cancer. 2009;45:228-47.

22. Cancer Genome Atlas Research Network. Integrated genomic analyses of ovarian carcinoma. Nature. 2011;474:609-15.
23. Pennington KP, Walsh T, Harrell MI, Lee MK, Pennil CC, Rendi MH, et al. Germline and somatic mutations in homologous recombination genes predict platinum response and survival in ovarian, fallopian tube, and peritoneal carcinomas. Clin Cancer Res. 2014;20:764-75.
24. Hennessy BT, Timms KM, Carey MS, Gutin A, Meyer LA, Flake DD 2nd, et al. Somatic mutations in BRCA1 and BRCA2 could expand the number of patients that benefit from poly (ADP ribose) polymerase inhibitors in ovarian cancer. J Clin Oncol. 2010;28:3570-6.
25. Hanley GE, McAlpine JN, Miller D, Huntsman D, Schrader KA, Blake Gilks C, et al. A population-based analysis of germline BRCA1 and BRCA2 testing among ovarian cancer patients in an era of histotype-specific approaches to ovarian cancer prevention. BMC Cancer. 2018;18:254.
26. Kim SI, Lim MC, Lim J, Won YJ, Seo SS, Kang S, et al. Incidence of epithelial ovarian cancer according to histologic subtypes in Korea, 1999 to 2012. J Gynecol Oncol. 2016;27:e5.
27. Norquist BM, Brady MF, Harrell MI, Walsh T, Lee MK, Gulsuner S, et al. Mutations in homologous recombination genes and outcomes in ovarian carcinoma patients in GOG 218: an NRG Oncology/Gynecologic Oncology Group study. Clin Cancer Res. 2018;24:777-83.
28. Liu Y, West SC. Distinct functions of BRCA1 and BRCA2 in double-strand break repair. Breast Cancer Res. 2002;4:9-13.
29. Gorodnova TV, Sokolenko AP, Ivantsov AO, Iyevleva AG, Suspitsin EN, Aleksakhina SN, et al. High response rates to neoadjuvant platinum-based therapy in ovarian cancer patients carrying germ-line BRCA mutation. Cancer Lett. 2015;369:363-7.
30. Dong F, Davineni PK, Howitt BE, Beck AH. A BRCA1/2 mutational signature and survival in ovarian high-grade serous carcinoma. Cancer Epidemiol Biomarkers Prev. 2016;25:1511-6.
31. Bolton KL, Chenevix-Trench G, Goh C, Sadetzki S, Ramus SJ, Karlan BY, et al. Association between BRCA1 and BRCA2 mutations and survival in women with invasive epithelial ovarian cancer. JAMA. 2012;307:382-90.
32. Lheureux S, Bruce JP, Burnier JV, Karakasis K, Shaw PA, Clarke BA, et al. Somatic BRCA1/2 recovery as a resistance mechanism after exceptional response to poly (ADP-ribose) polymerase inhibition. J Clin Oncol. 2017;35:1240-9.
33. Norquist B, Wurz KA, Pennil CC, Garcia R, Gross J, Sakai W, et al. Secondary somatic mutations restoring BRCA1/2 predict chemotherapy resistance in hereditary ovarian carcinomas. J Clin Oncol. 2011;29:3008-15.
34. Sokolenko AP, Savonevich EL, Ivantsov AO, Raskin GA, Kuligina ES, Gorodnova TV, et al. Rapid selection of BRCA1-proficient tumor cells during neoadjuvant therapy for ovarian cancer in BRCA1 mutation carriers. Cancer Lett. 2017;397:127-32.
35. Eoh KJ, Kim HM, Lee JY, Kim S, Kim SW, Kim YT, et al. Mutation landscape of germline and somatic BRCA1/2 in patients with high-grade serous ovarian cancer. BMC Cancer. 2020;20:204.

pISSN 1598-2998, eISSN 2005-9256

Cancer Res Treat. 2020;52(4):1242-1250

https://doi.org/10.4143/crt.2020.286

Original Article

Open Access

Cause of Mortality after Radical Prostatectomy and the Impact of Comorbidity in Men with Prostate Cancer: A Multi-institutional Study in Korea

Sahyun Pak, MD[1]
Dalsan You, MD, PhD[2]
In Gab Jeong, MD, PhD[2]
Dong-Eun Lee, MSc[3]
Sung Han Kim, MD, PhD[1]
Jae Young Joung, MD, PhD[1]
Kang-Hyun Lee, MD, PhD[1]
Jun Hyuk Hong, MD, PhD[2]
Choung-Soo Kim, MD, PhD[2]
Hanjong Ahn, MD, PhD[2]

[1]*Department of Urology, Center for Urologic Cancer, National Cancer Center, Goyang,* [2]*Department of Urology, Asan Medical Center, University of Ulsan College of Medicine, Seoul,* [3]*Biostatistics Collaboration Team, Research Core Center, Research Institute and Hospital, National Cancer Center, Goyang, Korea*

Correspondence: Hanjong Ahn, MD, PhD
Department of Urology, Asan Medical Center, University of Ulsan College of Medicine, 88 Olympic-ro 43-gil, Songpa-gu, Seoul 05505, Korea
Tel: 82-2-3010-3733
Fax: 82-2-477-8928
E-mail: hjahn@amc.seoul.kr

Co-correspondence: Jae Young Joung, MD, PhD
Department of Urology and Center for Urologic Cancer, Research Institute and Hospital of National Cancer Center, 323 Ilsan-ro, Ilsandong-gu, Goyang 10408, Korea
Tel: 82-31-920-1740
Fax: 82-31-920-2799
E-mail: urojy@ncc.re.kr

Received April 7, 2020
Accepted July 1, 2020
Published Online July 3, 2020

Purpose

This study aimed to examine the causes of death in Korean patients who underwent radical prostatectomy for prostate cancer and investigate the relationship between comorbidity and mortality.

Materials and Methods

We conducted a retrospective multicenter cohort study including 4,064 consecutive patients who had prostate cancer and underwent radical prostatectomy between January 1998 and June 2013. The primary endpoint of this study was all-cause mortality, and the secondary endpoints were cancer-specific mortality (CSM) and other-cause mortality (OCM). Charlson comorbidity index (CCI) was calculated to assess the comorbidities of each patient.

Results

Of 4,064 patients, 446 (11.0%) died during follow-up. The cause of death was prostate cancer in 132 patients (29.6%), other cancers in 121 patients (27.1%), and vascular disease in 57 patients (12.8%) in our cohort. The overall 10-year CSM rate was lower than the OCM rate (4.6% vs. 10.5%). The 10-year CSM rate was lower than the OCM rate in low- to intermediate-risk group patients (1.2% vs. 10.6%), whereas they were similar in high-risk group patients (11.8% vs. 10.1%). In the multivariable analysis, CCI was independently associated with all-cause mortality after radical prostatectomy, regardless of age and pathologic features.

Conclusion

Death from prostate cancer was rare in Korean men who underwent radical prostatectomy. Clinicians should be aware of the possibility of overtreatment of low-risk prostate cancer in men with significant comorbidity. Our findings may help to facilitate counseling and plan management in this patient group.

Key words

Prostatic neoplasms, Survival, Comorbidity

Introduction

Prostate cancer remains the most commonly diagnosed cancer in men worldwide [1]. Men with prostate cancer are generally considered to have favorable survival outcomes [2,3]. Many studies have reported low prostate cancer-specific mortality (CSM) rates in men with non-metastatic prostate cancer, thus highlighting the importance of other causes of death. A recent study reported that surgical treatment was not associated with significantly lower 20-year overall mor-

tality or CSM than that in men with localized prostate cancer who are assigned to observation [4]. However, despite the emergence of conservative treatment, men with prostate cancer are most likely to be treated with radical prostatectomy [5].

Medical comorbidity is common among the aging population with cancer, and this affects treatment efficacy [6]. Comorbidities have a particularly profound impact on the overall survival in men with prostate cancer as prostate CSM is low. In men with prostate cancer, the assessment of long-term other-cause mortality (OCM) is important for the selection of patients who have a high probability of experiencing survival benefit from aggressive radical treatment. Administering radical treatment for prostate cancer in men with low life expectancy due to other comorbidities may lead to overtreatment [7]. One study pointed out that men with significant comorbidity were often over-treated for low-risk prostate cancer [8]. Although several studies have reported on the causes of death after radical prostatectomy in Western populations [9,10], these results may not be generalizable due to geographic and ethnic variations in prostate cancer characteristics and the prevalence of comorbidities.

In this multicenter study, we aimed to evaluate the causes of death after radical prostatectomy for prostate cancer in a Korean cohort. We also assessed the impact of comorbidity on mortality after radical prostatectomy.

Materials and Methods

1. Study design

To focus on survival outcomes after radical prostatectomy, patients who had received neoadjuvant or adjuvant therapy, had not achieved undetectable prostate-specific antigen (PSA) after surgery, or had inadequate clinical information were excluded from the analysis. The records of 4,064 men with prostate cancer who underwent radical prostatectomy (3,210 patients in Asan Medical Center and 854 patients in the National Cancer Center) between January 1998 and June 2013 were reviewed. Patient data, including demographic and clinical characteristics, treatment-related variables, and survival outcomes, were evaluated retrospectively. For the assessment of comorbidities among the enrolled patients, the Charlson comorbidity index (CCI) and age-adjusted CCI of each patient were calculated [11].

The levels of PSA were followed up postoperatively at 3-month intervals for the first 2 years, 6-month intervals for the third and fourth years, and annually thereafter. Biochemical recurrence was defined as two consecutive rises in the PSA level of ≥ 0.2 ng/mL after radical prostatectomy. The decision on secondary treatment modalities after biochemical recurrence, including salvage radiotherapy, androgen deprivation therapy, or surveillance, was based on patient's or physician's discretion. Abdominopelvic computed tomography and bone scanning were routinely performed at the time of biochemical relapse after radical prostatectomy and biochemical progression after secondary treatment. Radiographic progression was evaluated using computed tomography or magnetic resonance imaging for soft-tissue disease and bone scanning for bone disease. Survival was measured from the date of radical prostatectomy until the date

Table 1. Clinical and pathological characteristics of patients

	Total (n=4,064)
Age, mean (yr)	65.1
< 50	74 (1.8)
50-60	763 (18.8)
60-70	2,055 (50.6)
70-80	1,154 (28.4)
≥ 80	18 (0.4)
Body mass index, mean (kg/m²)	24.7
Comorbidity	
Hypertension	1,759 (43.3)
Diabetes mellitus	638 (15.7)
Other malignancy	141 (3.5)
Heart disease	190 (4.7)
Cerebrovascular disease	113 (2.8)
Liver cirrhosis	50 (1.2)
End-stage renal disease	6 (0.1)
Chronic obstructive pulmonary disease	112 (2.7)
Charlson comorbidity index	
0	2,993 (73.6)
1	380 (9.4)
2	543 (13.4)
≥ 3	148 (3.6)
Prostate-specific antigen, mean (ng/mL)	13.0
NCCN risk group	
Low	1,280 (31.5)
Favorable intermediate	1,041 (25.6)
Unfavorable intermediate	483 (11.9)
High	1,260 (31.0)
Pathologic Gleason score	
Unknown	129 (3.2)
6	909 (22.4)
3+4	1,368 (33.6)
4+3	857 (21.1)
8	343 (8.4)
9-10	458 (11.3)
Pathologic T category	
T2	2,573 (63.4)
T3a	989 (24.3)
T3b-T4	502 (12.3)
Positive lymph nodes	224 (5.5)
Positive surgical margins	1,309 (32.2)

Values are presented as number (%) unless otherwise indicated.
NCCN, National Comprehensive Cancer Network.

Table 2. Causes of death after radical prostatectomy

Cause of death	Total (n=446)
Prostate cancer	132 (29.6)
Non-prostate cancer	219 (49.1)
Other malignancy	121 (27.1)
Lung	25 (5.6)
Liver	11 (2.5)
Colon, rectum, and anus	8 (1.8)
Stomach	19 (4.2)
Biliary tract and pancreas	29 (6.5)
Hematopoietic malignancy	12 (2.7)
Bladder	7 (1.6)
Others	10 (2.2)
Vascular disease	57 (12.8)
Coronary heart disease	31 (7.0)
Cerebrovascular disease	26 (5.8)
Chronic pulmonary disease	22 (4.9)
Chronic liver disease	5 (1.1)
Other causes	14 (3.1)
Unknown	95 (21.3)

Values are presented as number (%).

of death. The cause of death was determined according to medical records.

Four-tier National Comprehensive Cancer Network (NCCN) risk groups defined by the guidelines were as follows: low risk: stage T1-T2a, Gleason score (GS) ≤ 6, and PSA < 10 ng/mL; favorable intermediate risk: one intermediate-risk factor (IRF, that is, stage T2b-T2c or GS 7 or PSA 10-20 ng/mL), GS 6 or 3+4, and < 50% biopsy cores positive; unfavorable intermediate risk: two or three IRFs, GS 4+3, and ≥ 50% biopsy cores positive; high risk: stage T3a or GS 8–10 or PSA > 20 ng/mL [12]. Cancer of the Prostate Risk Assessment Postsurgical (CAPRA-S) score was also calculated based on preoperative PSA, pathologic GS, positive surgical margin, presence of extracapsular extension, seminal vesicle invasion, and lymph node involvement [13].

Clinical and pathological data were expressed as frequencies and means. Survival outcomes were determined using the Kaplan-Meier method and compared with log-rank tests. Significant prognostic factors for survival were assessed by multivariate analysis using the Cox proportional hazard model with stepwise backward elimination approach. Competing risk regression was performed to test the association of predictor variables after accounting for prostate CSM and OCM. All statistical tests were two-tailed, with a significance level of 0.05. All statistical analyses were performed using SAS ver. 9.4 (SAS Institute Inc., Cary, NC) and R ver. 3.5.2 (R Foundation for Statistical Computing, Vienna, Austria).

2. Ethical statement

The study protocol was approved by the institutional review board of Asan Medical Center and National Cancer Center, Korea (AMC 2017-1036 and NCC 2018-0123). Informed consent was waived.

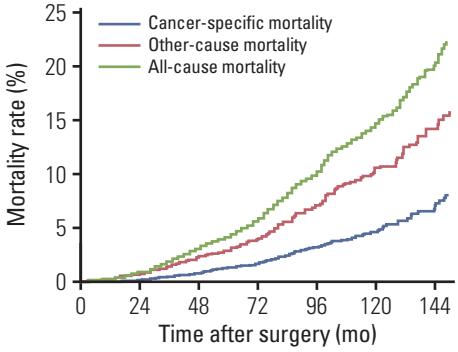

Fig. 1. Survival outcomes of the overall population.

Results

The clinical and pathological characteristics of the 4,064 men with prostate cancer who underwent radical prostatectomy in the two study centers, along with the baseline comorbidities, are summarized in Table 1. The median follow-up duration for enrolled patients was 92.6 months. Approximately 26.4% of the patients had CCI ≥ 1. During follow-up, 446 patients died at a median of 74.7 months after radical prostatectomy. The cause of death was prostate cancer in 132 patients (29.6%), other causes in 219 patients (49.1%), and unknown in 95 patients (21.3%) (Table 2).

The 10-year all-cause mortality rate was 15.5% in the overall population (Fig. 1). The 10-year CSM rate was lower than the OCM rate (4.6% vs. 10.5%) (Fig. 1). Comparisons between CSM and OCM stratified by preoperative risk groups are shown in Fig. 2A. The 10-year CSM rate was lower than the OCM rate in low- to intermediate-risk group patients (1.2% vs. 10.6%), but both were similar in high-risk group patients (11.8% vs. 10.1%).

The 10-year CSM rate was lower than the OCM rate in patients with pT2 (1.0% vs. 10.6%) and pT3a (5.4% vs. 10.2%) cancers. However, in patients with pT3b cancers, the 10-year CSM rate was higher than the OCM rate (20.1% vs. 10.4%). The 10-year CSM rate was lower than the OCM rate in patients with pathologic GS of ≤ 7 (1.5% vs. 10.3%). In patients with pathologic GS of 8-10, there was a trend toward having a higher 10-year CSM rate than OCM rate (14.8% vs. 11.3%). A comparison between CSM and OCM according to the preoperative NCCN risk groups and age-adjusted CCI is shown in Fig. 3. The 10-year CSM rate was higher than the OCM rate only in NCCN high-risk patients with age-adjusted CCI of < 3.

In the multivariable analyses, CCI was significantly asso-

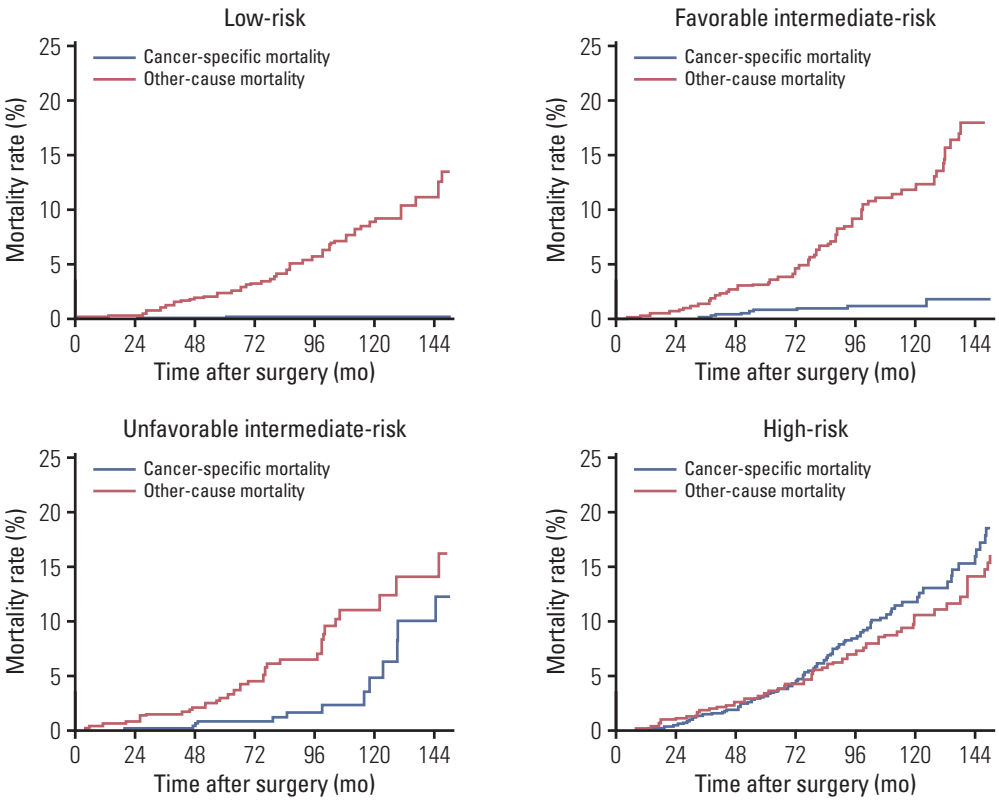

Fig. 2. Survival outcomes according to the preoperative National Comprehensive Cancer Network risk group.

ciated with overall mortality after radical prostatectomy, regardless of age and pathologic features (Table 3). Competing risks regression analysis showed that CCI was associated with OCM, but not with CSM (Table 4).

Discussion

Treatment decisions for men with non-metastatic prostate cancer are mostly influenced by age and clinical cancer characteristics [14,15]. Several previous studies have reported that men with prostate cancer were more likely to die from other causes, not prostate cancer [16,17]. In this study cohort, the overall OCM rate was significantly higher than the prostate CSM rate, which is consistent with most previous studies. In a European study, the survival benefit of radical prostatectomy ranged from 4.5% to 17.2% for low- to high-risk patients, in terms of risk reduction of CSM [18]. In a U.S. study that used the Surveillance, Epidemiology, and End Results database, the 10-year CSM rate of patients who underwent radical prostatectomy was 2.8% compared to 5.8% in patients assigned to observation [19]. These previous reports indicate that the appropriate selection of patients who will benefit from radical prostatectomy is important because the survival benefit may not be significant in a substantial portion of the patient population. Another important aspect to be taken into consideration in the treatment decision for men with non-metastatic prostate cancer is individual medical comorbidity. Comorbidities are frequent in men diagnosed with prostate cancer and have been associated with mortality after radical treatment [20].

The number of prostate cancer survivors is expected to increase continuously because of demographic changes and advances in treatment methods. Considering the heterogeneity of prostate cancer characteristics and comorbidities according to different geographical and ethnic populations [21,22], in this study, we investigated the cause of death after radical prostatectomy in a Korean cohort. We found that mortality from prostate cancer accounted for only a fraction of the overall mortality in men who underwent radical prostatectomy. Overall, the 10-year prostate CSM and OCM rates after radical prostatectomy in Korean men were similar to those recorded in the United States and European data [16,19,23,24]. The difference between the prostate CSM and OCM rates also varied according to medical comorbidities. Many studies have evaluated the impact of comorbidities on mortality in men with prostate cancer [7,14,16,19,25,26]. Consistent with previous findings, our findings showed that comorbidity was independently associated with overall mortality, regardless of age and pathologic features. Our data showed that the rate of mortality from prostate cancer was higher than mortality rate from other causes only in patients with

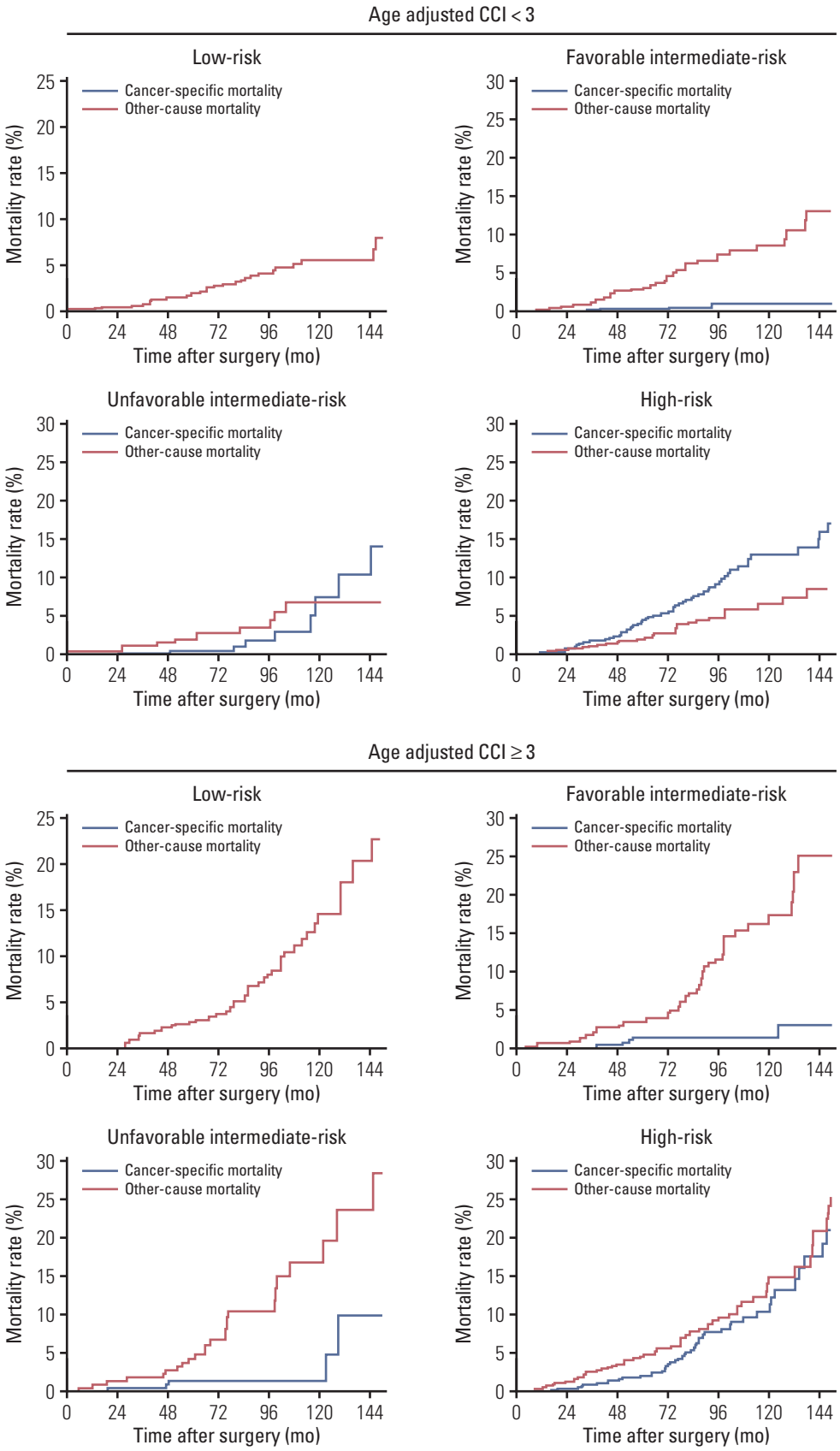

Fig. 3. Survival outcomes according to comorbidities and preoperative National Comprehensive Cancer Network risk group. CCI, Charlson comorbidity index.

Table 3. Multivariable Cox regression analyses for evaluating the risk of overall mortality

Variable	No. (event)	Univariable		Multivariable[a)]	
		HR (95% CI)	p-value	HR (95% CI)	p-value
Age	4,064 (447)	1.087 (1.070-1.105)	< 0.001	1.081 (1.063-1.098)	< 0.001
Body mass index	4,064 (447)	0.945 (0.912-0.978)	0.002	-	-
Charlson comorbidity index					
0-1	3,803 (370)	1 (reference)		1 (reference)	
≥ 2	261 (77)	3.236 (2.531-4.138)	< 0.001	2.964 (2.292-3.834)	< 0.001
Prostate-specific antigen	4,064 (447)	1.007 (1.005-1.010)	< 0.001	1.004 (1.000-1.008)	0.048
Pathologic stage					
T2	2,499 (206)	1 (reference)	< 0.001	1 (reference)	< 0.001
T3a	942 (105)	1.372 (1.085-1.736)	0.008	1.102 (0.860-1.412)	0.444
T3b-N1	623 (136)	2.750 (2.214-3.415)	< 0.001	2.194 (1.706-2.821)	<0.001
Pathologic Gleason score	Missing=129				
≤ 3+4	2,277 (186)	1 (reference)	< 0.001	1 (reference)	< 0.001
4+3	857 (77)	1.196 (0.916-1.560)	0.188	1.003 (0.766-1.314)	0.982
8-10	801 (165)	2.447 (1.984-3.018)	< 0.001	1.546 (1.222-1.957)	< 0.001
Surgical margins					
Negative	2,755 (267)	1 (reference)		-	
Positive	1,309 (180)	1.405 (1.163-1.698)	< 0.001	-	-

HR, hazard ratio; CI, confidence interval. [a)]Covariates were chosen based on backward selection.

NCCN high-risk disease and low age-adjusted CCI (< 3). In this study, we chose the four-tier NCCN risk groups because they have been widely used in current clinical practice. Additionally, we analyzed survival outcomes according to the CAPRA-S scores, and this yielded similar results (S1 Fig.). In patients who had CAPRA-S score < 9, the 10-year CSM rate was higher than the OCM rate only in those with a CAPRA-S score of 6–8 and age-adjusted CCI of < 3. The 10-year CSM rate was higher than the OCM rate in patients with CAPRA-S score ≥ 9, regardless of age-adjusted CCI.

In 2018, the mortality rates of the two top causes of death per 100,000 people in Korea were 154.3 for malignant neoplasms and 122.7 for circulatory system diseases [27]. As expected, in this study, we found that other cancers and circulatory system diseases accounted for the majority of non-prostate cancer deaths. In the overall population, the 10-year probability rates of mortality due to other cancers and circulatory system diseases after radical prostatectomy were 4.2% and 2.2%, respectively. The prostate CSM rate was higher than the mortality rates of other cancers and circulatory system diseases only in high-risk patients (S2 Fig.). In low-risk patients, the mortality rates of other cancers and circulatory system diseases were higher than the prostate CSM rate.

The over-diagnosis and overtreatment of non-metastatic prostate cancer have become a major health care issue [28]. Radical prostatectomy is associated with significant costs and complications. Moreover, common adverse events after surgery, such as incontinence and erectile dysfunction, may have a profound effect on the quality of life of patients. Daskivich et al. [8] reported that men with CCI ≥ 3 were treated aggressively in 54% of cases, indicating that men with low-risk prostate cancer were often over-treated despite significant comorbidities. Although active surveillance has been widely considered as a standard management modality for low-risk prostate cancer, it has been underutilized, particularly in Asian countries [29,30]. Among the patients who underwent radical prostatectomy in this study cohort, 547 (13.5%) had low-risk prostate cancer and significant comorbidity (age-adjusted CCI ≥ 3). In addition, 297 patients (7.3%) were eligible for active surveillance (based on the Prostate Cancer Research International Active Surveillance criteria) and had significant comorbidities. These data indicate that a substantial portion of the Korean male population with low-risk prostate cancer and significant comorbidity underwent radical prostatectomy, which may have led to overtreatment.

We acknowledge several limitations to this study. First, this study was retrospective in nature and could not eliminate the biases inherent to observational studies. Moreover, the lack of prospective standardized protocols for primary and salvage treatment may have introduced biases. Second, the study population may not be representative of all Korean men who undergo radical prostatectomy. Thus, the generalizability of our data from referral centers may be limited. Third, incomplete data on the statistics of the cause of death is another main limitation. These data on the cause of death solely depend on medical records; because of loss to follow-up, the causes of death in 95 patients (21.3%) were unknown. Few patients had evidence of prostate cancer recurrence until the last follow-up (biochemical recurrence: 17/95 [17.9%] and distant metastasis: 0/95 [0%]), suggesting that there may

Table 4. Cause-specific hazard model for prostate cancer-specific mortality and other-cause mortality

Variable	Prostate cancer-specific mortality					Other-cause mortality				
	No. (event)	Univariable		Multivariable[a]		No. (event)	Univariable		Multivariable[a]	
		HR (95% CI)	p-value	HR (95% CI)	p-value		HR (95% CI)	p-value	HR (95% CI)	p-value
Age	4,064 (133)	1.030 (1.003-1.058)	0.028	1.018 (0.990-1.047)	0.208	4,064 (314)	1.116 (1.094-1.139)	< 0.001	1.112 (1.090-1.135)	< 0.001
Body mass index	4,064 (133)	0.974 (0.915-1.038)	0.421	-	-	4,064 (314)	0.932 (0.894-0.972)	0.001	-	-
Charlson comorbidity index										
0-1	3,803 (124)	1 (reference)		1 (reference)		3,803 (246)	1 (reference)		1 (reference)	
≥ 2	261 (9)	1.127 (0.573-2.218)	0.729	1.265 (0.614-2.605)	0.524	261 (68)	4.303 (3.288-5.630)	< 0.001	3.832 (2.928-5.016)	< 0.001
Prostate-specific antigen	4,064 (133)	1.013 (1.010-1.015)	< 0.001	1.006 (1.002-1.010)	0.002	4,064 (314)	0.997 (0.990-1.004)	0.371	-	-
Pathologic stage										
T2	2,499 (17)	1 (reference)	< 0.001	1 (reference)	< 0.001	2,499 (189)	1 (reference)	0.783	-	-
T3a	942 (28)	4.430 (2.425-8.094)	< 0.001	2.383 (1.268-4.479)	0.007	942 (77)	1.097 (0.841-1.430)	0.494	-	-
T3b-N1	623 (88)	21.818 (12.979-36.676)	< 0.001	7.554 (4.264-13.382)	< 0.001	623 (48)	1.051 (0.765-1.443)	0.760	-	-
Pathologic Gleason score										
≤ 3+4	2,277 (9)	1 (reference)	< 0.001	1 (reference)	< 0.001	2,277 (177)	1 (reference)	0.593	-	-
4+3	857 (21)	6.723 (3.079-14.681)	< 0.001	4.282 (1.938-9.458)	< 0.001	857 (56)	0.915 (0.677-1.236)	0.563	-	-
8-10	801 (94)	29.26 (14.765-57.987)	< 0.001	11.627 (5.675-23.825)	< 0.001	801 (71)	1.098 (0.833-1.446)	0.507	-	-
Surgical margins										
Negative	2,755 (53)	1 (reference)		-		2,755 (214)	1 (reference)		-	-
Positive	1,309 (80)	3.168 (2.239-4.483)	< 0.001	-	-	1,309 (100)	0.970 (0.765-1.231)	0.805	-	-

HR, hazard ratio; CI, confidence interval. [a]Covariates were chosen based on backward selection included age and Charlson comorbidity index at treatment.

be a larger number of patients who died from other causes than the present data have shown. Fourth, we could not conduct comprehensive geriatric assessment (CGA) in this retrospective study. While CCI provides a quantitative approach to enumerate comorbid conditions, CGA is a multidisciplinary and comprehensive tool for evaluating elderly patients, which may be more appropriate for predicting survival and radical treatment selection. Lastly, the duration and severity of each comorbidity were not taken into consideration.

In conclusion, we have demonstrated that mortality from prostate cancer was rare in Korean men who underwent radical prostatectomy. Physicians should be aware of the possibility of overtreatment for low-risk prostate cancer in men with significant comorbidity. These findings may help to facilitate counseling and plan management in this patient group.

Electronic Supplementary Material

Supplementary materials are available at Cancer Research and Treatment website (https://www.e-crt.org).

Conflicts of Interest

Conflicts of interest relevant to this article was not reported.

Acknowledgments

This work was supported by a career development award (NCC-CDA2019-06) from the National Cancer Center, Korea.

References

1. Miller KD, Nogueira L, Mariotto AB, Rowland JH, Yabroff KR, Alfano CM, et al. Cancer treatment and survivorship statistics, 2019. CA Cancer J Clin. 2019;69:363-85.
2. ICECaP Working Group; Sweeney C, Nakabayashi M, Regan M, Xie W, Hayes J, et al. The Development of Intermediate Clinical Endpoints in Cancer of the Prostate (ICECaP). J Natl Cancer Inst. 2015;107:djv261.
3. Tosoian JJ, Carter HB, Lepor A, Loeb S. Active surveillance for prostate cancer: current evidence and contemporary state of practice. Nat Rev Urol. 2016;13:205-15.
4. Wilt TJ, Jones KM, Barry MJ, Andriole GL, Culkin D, Wheeler T, et al. Follow-up of prostatectomy versus observation for early prostate cancer. N Engl J Med. 2017;377:132-42.
5. Mahmood U, Levy LB, Nguyen PL, Lee AK, Kuban DA, Hoffman KE. Current clinical presentation and treatment of localized prostate cancer in the United States. J Urol. 2014;192:1650-6.
6. Sarfati D, Koczwara B, Jackson C. The impact of comorbidity on cancer and its treatment. CA Cancer J Clin. 2016;66:337-50.
7. Daskivich TJ, Kwan L, Dash A, Saigal C, Litwin MS. An age adjusted comorbidity index to predict long-term, other cause mortality in men with prostate cancer. J Urol. 2015;194:73-8.
8. Daskivich TJ, Chamie K, Kwan L, Labo J, Palvolgyi R, Dash A, et al. Overtreatment of men with low-risk prostate cancer and significant comorbidity. Cancer. 2011;117:2058-66.
9. Roder MA, Brasso K, Christensen IJ, Johansen J, Langkilde NC, Hvarness H, et al. Survival after radical prostatectomy for clinically localised prostate cancer: a population-based study. BJU Int. 2014;113:541-7.
10. Satariano WA, Ragland KE, Van Den Eeden SK. Cause of death in men diagnosed with prostate carcinoma. Cancer. 1998;83:1180-8.
11. Charlson M, Szatrowski TP, Peterson J, Gold J. Validation of a combined comorbidity index. J Clin Epidemiol. 1994;47:1245-51.
12. Mohler JL, Antonarakis ES, Armstrong AJ, D'Amico AV, Davis BJ, Dorff T, et al. Prostate cancer, version 2.2019, NCCN clinical practice guidelines in oncology. J Natl Compr Canc Netw. 2019;17:479-505.
13. Cooperberg MR, Hilton JF, Carroll PR. The CAPRA-S score: A straightforward tool for improved prediction of outcomes after radical prostatectomy. Cancer. 2011;117:5039-46.
14. Matthes KL, Limam M, Pestoni G, Held L, Korol D, Rohrmann S. Impact of comorbidities at diagnosis on prostate cancer treatment and survival. J Cancer Res Clin Oncol. 2018;144:707-15.
15. Boehm K, Larcher A, Tian Z, Mandel P, Schiffmann J, Karakiewicz PI, et al. Low other cause mortality rates reflect good patient selection in patients with prostate cancer treated with radical prostatectomy. J Urol. 2016;196:82-8.
16. Briganti A, Spahn M, Joniau S, Gontero P, Bianchi M, Kneitz B, et al. Impact of age and comorbidities on long-term survival of patients with high-risk prostate cancer treated with radical prostatectomy: a multi-institutional competing-risks analysis. Eur Urol. 2013;63:693-701.
17. Matthes KL, Pestoni G, Korol D, Van Hemelrijck M, Rohrmann S. The risk of prostate cancer mortality and cardiovascular mortality of nonmetastatic prostate cancer patients: a population-based retrospective cohort study. Urol Oncol. 2018;36:309.
18. Vickers A, Bennette C, Steineck G, Adami HO, Johansson JE, Bill-Axelson A, et al. Individualized estimation of the benefit of radical prostatectomy from the Scandinavian Prostate Cancer Group randomized trial. Eur Urol. 2012;62:204-9.
19. Abdollah F, Sun M, Schmitges J, Thuret R, Bianchi M, Shariat SF, et al. Survival benefit of radical prostatectomy in patients with localized prostate cancer: estimations of the number needed to treat according to tumor and patient characteristics. J Urol. 2012;188:73-83.
20. Ketchandji M, Kuo YF, Shahinian VB, Goodwin JS. Cause of death in older men after the diagnosis of prostate cancer. J Am Geriatr Soc. 2009;57:24-30.
21. Boyd LK, Mao X, Lu YJ. The complexity of prostate cancer: genomic alterations and heterogeneity. Nat Rev Urol. 2012;9:652-64.
22. Jeong IG, Dajani D, Verghese M, Hwang J, Cho YM, Hong JH, et al. Differences in the aggressiveness of prostate cancer

among Korean, Caucasian, and African American men: a retrospective cohort study of radical prostatectomy. Urol Oncol. 2016;34:3.
23. Eggener SE, Scardino PT, Walsh PC, Han M, Partin AW, Trock BJ, et al. Predicting 15-year prostate cancer specific mortality after radical prostatectomy. J Urol. 2011;185:869-75.
24. Bolton DM, Papa N, Ta AD, Millar J, Davidson AJ, Pedersen J, et al. Predictors of prostate cancer specific mortality after radical prostatectomy: 10 year oncologic outcomes from the Victorian Radical Prostatectomy Registry. BJU Int. 2015;116 Suppl 3:66-72.
25. Daskivich TJ, Fan KH, Koyama T, Albertsen PC, Goodman M, Hamilton AS, et al. Prediction of long-term other-cause mortality in men with early-stage prostate cancer: results from the Prostate Cancer Outcomes Study. Urology. 2015;85:92-100.
26. Rajan P, Sooriakumaran P, Nyberg T, Akre O, Carlsson S, Egevad L, et al. Effect of comorbidity on prostate cancer-specific mortality: a prospective observational study. J Clin Oncol. 2017;35:3566-74.
27. Vital Statistics Division, Statistics Korea, Shin HY, Lee JY, Kim JE, Lee S, Youn H, et al. Cause-of-death statistics in 2016 in the Republic of Korea. J Korean Med Assoc. 2018;61:573-84.
28. Etzioni R, Mucci L, Chen S, Johansson JE, Fall K, Adami HO. Increasing use of radical prostatectomy for nonlethal prostate cancer in Sweden. Clin Cancer Res. 2012;18:6742-7.
29. Jeong IG, Yoo S, Lee C, Kim M, You D, Song C, et al. Obesity as a risk factor for unfavorable disease in men with low risk prostate cancer and its relationship with anatomical location of tumor. J Urol. 2017;198:71-8.
30. Loppenberg B, Friedlander DF, Krasnova A, Tam A, Leow JJ, Nguyen PL, et al. Variation in the use of active surveillance for low-risk prostate cancer. Cancer. 2018;124:55-64.

pISSN 1598-2998, eISSN 2005-9256

Cancer Res Treat. 2020;52(4):1251-1261 https://doi.org/10.4143/crt.2020.140

Original Article Open Access

Genome-Wide Association Study for the Identification of Novel Genetic Variants Associated with the Risk of Neuroblastoma in Korean Children

Joon Seol Bae, PhD[1]
Ji Won Lee, MD, PhD[2]
Jung Eun Yoo, MD[3]
Je-Gun Joung, PhD[4]
Keon Hee Yoo, MD, PhD[2]
Hong Hoe Koo, MD, PhD[2]
Yun-Mi Song, MD, PhD[3]
Ki Woong Sung, MD, PhD[2]

[1]*Research Institute for Future Medicine, Departments of* [2]*Pediatrics and* [3]*Family Medicine,* [4]*Samsung Genome Institute, Samsung Medical Center, Sungkyunkwan University School of Medicine, Seoul, Korea*

Correspondence: Ki Woong Sung, MD, PhD
Department of Pediatrics, Samsung Medical Center, Sungkyunkwan University School of Medicine, 81 Irwon-ro, Gangnam-gu, Seoul 06351, Korea
Tel: 82-2-3410-3529
Fax: 82-2-3410-0043
E-mail: kwsped@skku.edu

Received February 24 2020
Accepted June 29, 2020
Published Online June 30, 2020

*Joon Seol Bae and Ji Won Lee contributed equally to this work.

Purpose
Neuroblastoma (NB) is the most common extracranial solid tumor found in children. To identify significant genetic factors for the risk of NB, several genetic studies was conducted mainly for Caucasians and Europeans. However, considering racial differences, there is a possibility that genetic predispositions that contribute to the development of NB are different, and genome-wide association study has not yet been conducted on Korean NB patients.

Materials and Methods
To identify the genetic variations associated with the risk of pediatric NB in Korean children, we performed a genome-wide association analysis with 296 NB patients and 1,000 unaffected controls (total n=1,296) after data cleaning and filtering as well as imputation of non-genotyped single nucleotide polymorphisms (SNPs) using IMPUTE v2.3.2.

Results
After adjusting for multiple comparisons, we found 21 statistically significant SNPs associated with the risk of NB ($p^{corr} < 0.05$) within 12 genes (*RPTN*, *MRPS18B*, *LRRC45*, *KANSL1L*, *ARHGEF40*, *IL15RA*, *L1TD1*, *ANO7*, *LAMA5*, *OR7G2*, *SALL4*, and *NEUROG2*). Interestingly, out of these, 12 markers were nonsynonymous SNPs. The SNP rs76015112 was most significantly associated with the risk of NB (p=8.1E-23, p^{corr}=2.3E-17) and was located in the *RPTN* gene. In addition, significant nonsynonymous SNPs in *ADGRE1* were found in patients with *MYCN* amplification (rs7256147, p=2.6E-05). In high-risk group, rs7256147 was observed as a significant SNP (p=5.9E-06).

Conclusion
Our findings might facilitate improved understanding of the mechanism of pediatric NB pathogenesis. However, functional evaluation and replication of these results in other populations are still needed.

Key words
Neuroblastoma, Genetic variation, Genome-wide association study, *MYCN* amplification, High risk, Korean children

Introduction

Neuroblastoma (NB) is the most common extracranial solid tumor accounting for up to 6%-10% of all childhood cancers and it is one of the leading cause of cancer mortality in children [1]. NB arises from the precursor cells of the sympathetic nervous system or the adrenal medulla. Since NB is widely heterogeneous in its clinical phenotypes and treatment outcomes, current treatment protocols are based on risk stratification of NB. High-risk group is currently defined as *MYCN*-amplified tumors at any age or metastatic tumors in patients older than 18 months according to the International Neuroblastoma Risk Group (INRG) classification system [2]. The patients in the high-risk group show poor prognosis despite modern intensive multimodal treatment. N-myc proto-oncogene protein, also known as N-Myc, is encoded by the *MYCN* gene in humans. Since *MYCN* amplification was found to be a highly predictive marker of poor outcome in the NB patients by the INRG cohort, the *MYCN* status is used for risk stratification [3]. Based on this, approximately 40% of NB patients have been classified as high-risk [2,4]. In a previous study regarding familial NB, *PHOX2A, ALK, KIF1Bβ,* and *RAS*

mutations were reported as causal mutations [5]. However, while only 1%-2% of NB cases were familial, further genetic association studies are required to identify the predisposing genetic factors. In 2008, the first genome-wide association study (GWAS) was performed for Europeans in a case of sporadic NB [6]. They reported three variants of chromosome 6p22, which have been mapped to the genes *CASC-15* and *NBAT-1*. Several candidate genes such as *LMO1*, *BARD1*, *HACE1*, and *LIN28B* have been reported by subsequent GWAS [5]. Capasso et al. [7] investigated the genetic factor for the NB patients who developed high-risk tumors and they found that the locus in 6p22 was enriched. Additionally, they found several novel risk-related single nucleotide polymorphisms (SNPs) including intronic variant in *BARD1* gene [7]. Although previous GWAS and candidate genetic studies have provided considerable information about the genetics and understanding for NB, most of these studies were performed on Caucasian and African Americans. To expand the genetic studies for other various populations such as Asians, it is necessary to explain the genetic aspects of NB.

Due to the remarkable phenotypic heterogeneity of NB, the mild to moderate effects on the risk of NB development are still unclear. In this study, we have performed GWAS using NB to discover genetic variants in Korean children. To our knowledge, this is the first GWAS study in Korean NB patients.

Materials and Methods

1. Study subjects

We screened patients who were diagnosed with NB between February 1998 and March 2017. After screening, 296 NB patients whose peripheral blood samples were already cryopreserved at Samsung Medical Center Biobank were enrolled in this study. The 77,472 exome chip genotypes of the healthy controls (n=1,000), without any history of tumor, were obtained from the National Biobank of Korea (No. 2018-019). Medical records were reviewed for obtaining detailed clinical and biological data such as the clinical features presented during diagnosis, tumor biology including *MYCN* amplification status and tumor histology by International Neuroblastoma Pathology Classification (INPC). During the study period, the patients were classified into high-risk group and non–high-risk group according to their age during diagnosis, tumor stage based on the International Neuroblastoma Staging System (INSS), and *MYCN* amplification status. In brief, stage 4 tumors in patients older than 1.5 years or with *MYCN*-amplified tumors were included in the high-risk group.

2. Genome-wide genotyping

Genomic DNA was extracted from the peripheral blood lymphocytes of the patients using the Wizard Genomic DNA Purification Kit (Promega, Madison, WI), according to the manufacturer's protocol. Approximately 200 ng of genomic DNA was used to genotype each sample using the Illumina's Global Screening Array (GSA) BeadChip (Illumina, San Diego, CA). The samples were then processed according to the Illumina Infinium assay manual. Each sample was whole-genome amplified, fragmented, precipitated, and resuspended into an appropriate hybridization buffer. The denatured samples were then hybridized on a prepared GSA BeadChip for a minimum of 16 hours at 48°C. Following hybridization, the BeadChips were processed for the single-base extension reaction, staining, and imaging on an Illumina iScan system. The normalized bead intensity data obtained for each sample were uploaded onto the GenomeStudio software (Illumina) which converted the fluorescent intensities into SNP genotypes. The quality of sample was checked by sample call rate (> 95%). The quality of cluster for marker was measured by GenTrain scores, and then high-quality markers used this study (> 0.7).

3. Imputation and statistical analysis

The clinical variables were summarized using mean±standard deviation or median (range), as appropriate (Table 1). We performed imputation consisting of 1,296 samples. The prephasing of genotypes was conducted with SHAPEIT.v2.r837. We then imputed variants from the 1000 Genomes Project phase 3 references using IMPUTE v2.3.2. Markers with low imputation quality as call rate (< 98%), minor allele frequency (MAF < 1%), p-value of Hardy-Weinberg equilibrium (HWE; < 1E-5), duplicated markers, and ambiguous strand markers were excluded from the association analysis. In addition, low-quality samples (call rate < 95%) were applied for quality control. For genome-wide association analysis, genotype distributions were compared using logistic regression analyses with the HelixTree software (Golden Helix Inc., Bozeman, MT). To predict a protein damaging score for each nonsynonymous SNP, PolyPhen-2 program [8] was used (http://genetics.bwh.harvard.edu/pph2/index.shtml) according to the manual. Gene pathway analysis for significantly associated SNPs with the risk of NB was performed using the Database for Annotation, Visualization, and Integrated Discovery (DAVID) functional annotation tool (https://david.ncifcrf.gov/). In addition, biological network analysis was performed by GluGo, Cytoscape plug-in that visualizes non-redundant biological terms for large clusters of genes in a functionally grouped network (https://cytoscape.org/).

4. Ethical statement

This study was approved by the Institutional Review Board of Samsung Medical Center (IRB No. SMC 2015-06-068-006) and written informed consent was obtained from the parents or their guardians.

Table 1. Characteristics of the study subjects

Variable	Neuroblastoma	Healthy control
Total No. of subjects	296	1,000
Sex (male:female)	164:132	500:500
Age, median (min-max, yr)	2.1 (0.0-19.3)	61.4 (47-78)
***MYCN* amplification**	56 (18.9)	-
High-risk group	142 (48.0)	-
Clinical stage		
I	27 (9.1)	-
II	47 (15.9)	-
III	54 (18.2)	-
IV	160 (54.1)	-
IV-S	6 (2.0)	-
NA	2 (0.7)	-
Site of origin		
Retroperitoneum	221 (74.7)	-
Mediastinum	71 (24.0)	-
Other regions	4 (1.4)	-

Values are presented as number (%) unless otherwise indicated.

Results

1. Clinical characteristics

A total of 296 NB patients were recruited for the current study. In addition, genotypes of 1,000 normal healthy controls were obtained from the National Biobank of Korea. The average age of the NB patients was 2.1 years (range, 0.0 to 19.3 years). Among the 296 patients, 142 patients were stratified into high-risk group and *MYCN* amplification was seen in 56 patients. Table 1 shows the characteristics of the patients and healthy controls.

2. Association analysis and identification of novel susceptibility loci

A quantile-quantile plot for the association test between NB and healthy controls showed a significant deviation of measures at the tail (S1 Fig.) indicating potentially true associations between the SNPs and NB. A total of 281K markers were imputed from 535K genotypes of patients and 76K genotypes of healthy controls using strict quality control parameters (MAF > 1%, missing rate < 1%, or p for HWE < 1×10^{-5}). First, we tested the association between NB patients and healthy controls using logistic regression analysis. A total of 21 markers showed significant association with the risk of NB after adjusting for multiple comparisons (p^{corr} < 0.05) (Fig. 1A). The significant markers for the risk of NB are summarized in Table 2. The markers were located in *RPTN*, *MRPS18B*, *LRRC45*, *KANSL1L*, *ARHGEF40*, *IL15RA*, *L1TD1*, *ANO7*, *LAMA5*, *OR7G2*, *SALL4*, and *NEUROG2* genes. In addition, *PARP8*, *EPB41L3*, and *MAP4K1* genes were found to be the nearby genes for the markers such as rs7717033, rs1375128, rs10737958, rs2594708, rs2463796, rs35296988, rs3864235, rs32396, rs9964022, rs17847695, rs117910631, rs147260795, rs146801912, rs17847686, rs200216392, rs77270842, rs149013375, and rs74990833 (Table 2). Among all the markers, 12 markers were distributed in the coding region. Most of the nonsynonymous SNPs showed low MAF except of rs76015112 (MAF < 0.010). In rs76015112, the MAF of NB was lower than healthy controls (0.125 vs. 0.332) as shown in Table 2. However, the other markers in the coding region showed a high MAF in NB compared to the controls (Table 2). We analyzed the regional association of 400 kb around *RPTN* on chromosome 1q21.3 (Fig. 1B) and observed that the rs76015112 marker showed relatively robust association signal (p^{corr}=2.3E-17) (Table 2). The results of linkage disequilibrium (LD) analysis showed that the marker was unlikely to be in LD with the nearby genes (Fig. 1B).

3. Association analysis of NB subgroups

The NB patients were classified as either with *MYCN* amplification or without. Table 3 shows the significant SNPs after genome-wide association analysis between *MYCN*-amplified NB patients and the other NB patients. Interestingly, many SNPs within *ADGRE1* (synonyms: *EMR1*) gene showed significant associations (S2A Fig.). Among them, rs725614 and rs457857 had nonsynonymous SNPs as V589I (NM_001256253) and I424V (NM_001256253) (Table 3). In the regional association analysis of 200 kb around *ADGRE1* (synonyms: *EMR1*), we found that 32 SNPs were in tight LD (S2B Fig.). In addition, three significantly associated SNPs were found to be located in the intron region of *C2CD6* gene (rs143074421, rs77468686, and rs117943473).

In the following analysis, GWAS was performed with NB patients in high-risk group and non–high-risk group. The

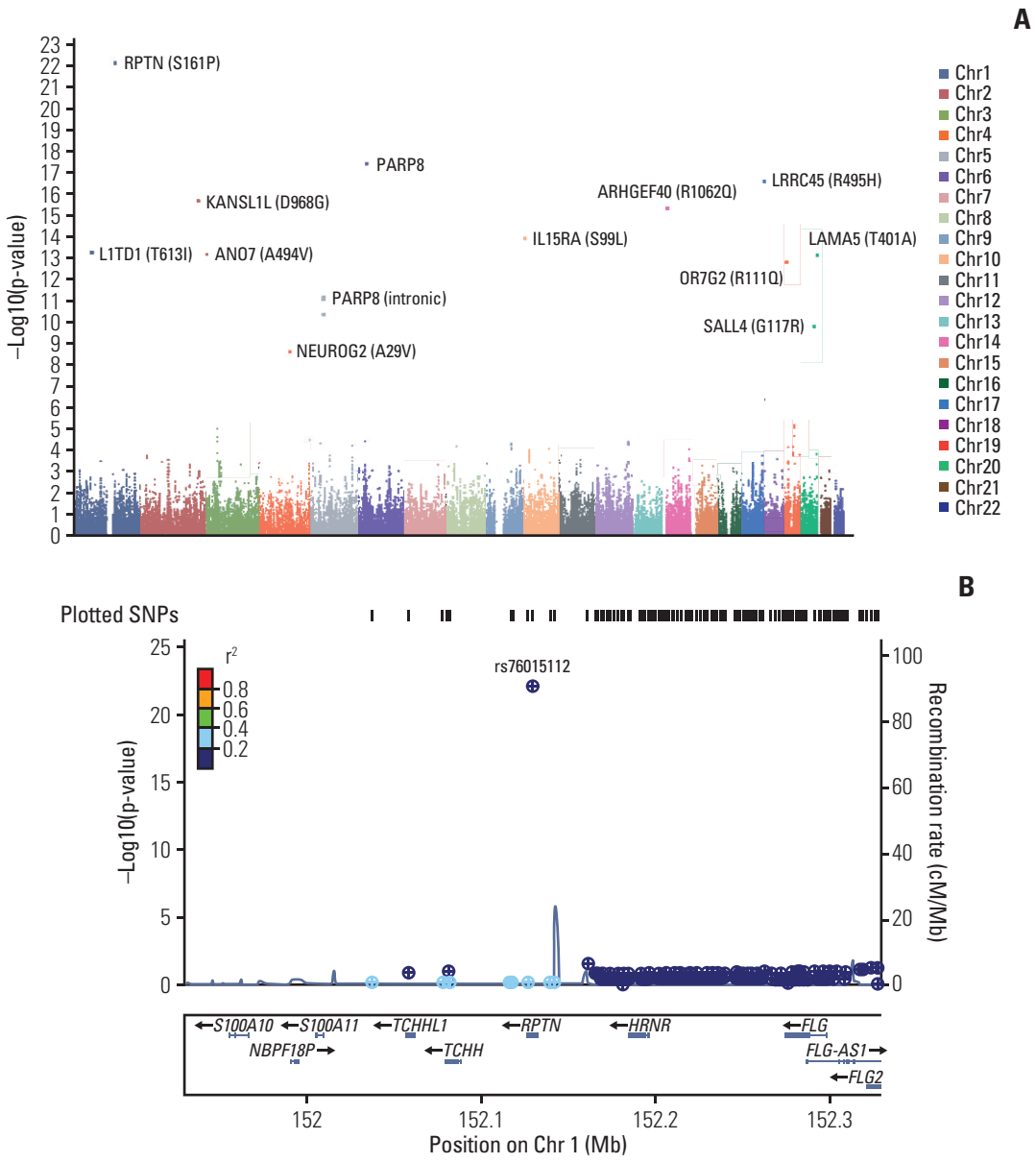

Fig. 1. (A) The p-values of genome-wide association study. The Manhattan plot shows the p-values for the risk of neuroblastoma using logistic regression analysis. x-axis represents the single nucleotide polymorphism (SNP) markers on each chromosome. The highest p-value (p=8.1E-23, p^{corr}=2.3E-17) was observed in rs76015112 on 1q21.3. (B) Regional association plots at the *RPTN*. Regional association plots including both genotyped and SNPs for the *RPTN* was generated by LocusZoom within 400 kb. The significance of association (−log10-transformed p-values) and the recombination rate are plotted. SNPs are colored to reflect pairwise linkage disequilibrium (r^2) with the most significantly associated genotyped SNP in the 1000 Genomes Project Phase 1 interim release Asian (ASN) population genotypes. The most significant genotyped SNPs are labeled and shown in purple.

top 30 significant SNPs are listed in Table 4. As a result, rs62296061 located intron region in *FGFGL1* gene was found to be highly associated with the high-risk group. Many SNPs within *ADGRE1* gene showed significant associations (S3A Fig.). In the rs725614 and rs457857 located in coding region, the MAF in high-risk group was lower than other groups (0.080 vs. 0.217 in rs725614, 0.109 vs. 0.233 in rs457857). In the regional association analysis of 200 kb around *ADGRE1*, 32 SNPs were found to be in tight LD (S3B Fig.). In Table 4, we have shown that *PON1* and *PON2* genes were located near seven markers such as rs11981667, rs17166829, rs73422040, rs11980347, rs17884252, rs17883750, and rs149643570.

Table 2. Significant SNP loci associated with neuroblastoma on the GWAS

Marker	Chromosome	Position	Transcript(s)	Gene (nearby)	In-exon	Mutation(s)	Alleles	MAF	MAF (case)	MAF (control)	OR (95% CI)	p-value	p^{corr}	Protein damaging prediction (score)
rs76015112	1	152,129,094	NM_001122965	*RPTN*	Exon	Missense_S161P	A>G	0.284	0.125	0.332	0.3 (0.2-0.4)	8.1E-23	2.3E-17	Benign (0.01)
rs148828689	6	30,593,528	NM_014046	*MRPS18B*	Exon	Missense_A244V	C>T	0.030	0.093	0.012	7.8 (4.7-12.9)	4.0E-18	5.7E-13	Benign (0.00)
rs117249618	17	79,987,501	NM_144999	*LRRC45*	Exon	Missense_R495H	G>A	0.029	0.088	0.011	7.8 (4.7-13.1)	2.6E-17	2.5E-12	Probably damaging (1.00)
rs117674897	2	210,887,734	NM_152519	*KANSL1L*	Exon	Missense_D968G	T>C	0.034	0.096	0.015	6.1 (3.9-9.7)	2.2E-16	1.5E-11	Probably damaging (0.88)
rs114591848	14	21,550,212	NM_018071	*ARHGEF40*	Exon	Missense_R1062Q	G>A	0.029	0.086	0.012	7.0 (4.2-11.6)	4.7E-16	2.6E-11	Probably damaging (0.99)
rs77226427	10	6,002,518	NR_046362, NM_001243539, NM_001256765, NM_002189, NM_172200	*IL15RA*	Exon	Silent, Missense_S96L, Missense_S218L, Missense_S132L, Missense_S99L	G>A	0.055	0.130	0.033	3.7 (2.6-5.1)	1.2E-14	5.7E-10	Benign (0.01)
rs2886644	1	62,676,284	NM_001164835, NM_019079	*L1TD1*	Exon	Missense_T613I, Missense_T613I	C>T	0.054	0.128	0.032	3.5 (2.5-4.8)	5.9E-14	2.4E-09	Benign (0.14)
rs57677160	2	242,149,010	NM_001001891	*ANO7*	Exon	Missense_A494V	C>T	0.030	0.081	0.015	6.0 (3.7-9.7)	6.8E-14	2.4E-09	Benign (0.00)
rs4925229	20	60,921,643	NM_005560	*LAMA5*	Exon	Missense_T401A	C>T	0.045	0.113	0.026	3.9 (2.7-5.6)	8.0E-14	2.5E-09	Benign (0.40)
rs62621389	19	9,213,651	NM_001005193	*OR7G2*	Exon	Missense_R111Q	C>T	0.033	0.086	0.017	5.3 (3.4-8.4)	1.6E-13	4.4E-09	Benign (0.00)
rs7717033	5	49,982,726	-	*(PARP8)*	-	-	A>T	0.316	0.429	0.282	2.0 (1.6-2.5)	7.4E-12	1.4E-07	-
rs1375128	5	50,014,674	-	*(PARP8)*	-	-	G>A	0.316	0.429	0.282	2.0 (1.6-2.5)	7.4E-12	1.4E-07	-
rs10737958	5	50,023,374	-	*(PARP8)*	-	-	A>C	0.316	0.429	0.282	2.0 (1.6-2.5)	7.4E-12	1.4E-07	-
rs2594708	5	50,024,668	-	*(PARP8)*	-	-	G>A	0.316	0.429	0.282	2.0 (1.6-2.5)	7.4E-12	1.4E-07	-
rs2463796	5	50,025,690	-	*(PARP8)*	-	-	C>G	0.316	0.429	0.282	2.0 (1.6-2.5)	7.4E-12	1.4E-07	-
rs35296988	5	50,046,753	-	*(PARP8)*	-	-	GA>G	0.315	0.429	0.282	2.0 (1.6-2.5)	8.7E-12	1.5E-07	-
rs3864235	5	49,945,474	-	*(PARP8)*	-	-	T>C	0.316	0.429	0.282	2.0 (1.6-2.5)	8.8E-12	1.5E-07	-
rs32396	5	50,106,439	-	*(PARP8)*	-	-	G>A	0.314	0.423	0.282	2.0 (1.6-2.4)	4.5E-11	7.0E-07	-
rs77538589	20	50,408,673	NM_020436	*SALL4*	Exon	Missense_G117R	C>T	0.046	0.103	0.030	3.3 (2.3-4.7)	1.4E-10	2.1E-06	Benign (0.00)
exm419398	4	113,436,546	NM_024019	*NEUROG2*	Exon	Missense_A29V	G>A	0.097	0.162	0.078	2.5 (1.8-3.3)	2.3E-09	3.2E-05	Benign (0.01)

SNP, single nucleotide polymorphism; GWAS, genome-wide association study; MAF, minor allele frequency; OR, odds ratio; CI, confidence interval.

Table 3. Logistic analysis of neuroblastoma with *MYCN* amplification

Marker	Chromosome	Position	Transcript(s)	Gene (nearby)	In-exon	Mutation(s)	Alleles	MAF	MAF (with *MYCN*)	MAF (without *MYCN*)	OR (95% CI)	p-value
rs143074421	2	202,378,651	-	*C2CD6*	-	-	A>G	0.014	0.063	0.002	32.7 (3.9-272.0)	2.3E-05
rs77468686	2	202,318,941	-	*C2CD6*	-	-	C>A	0.014	0.063	0.002	32.4 (3.9-269.6)	2.4E-05
rs117943473	2	202,256,710	-	*C2CD6*	-	-	A>G	0.014	0.063	0.002	32.3 (3.9-268.4)	2.5E-05
rs7256147	19	6,921,868	NM_001256253, NM_001974, NM_001256252, NM_001256255, NM_001256254	*ADGRE1*[a]	Exon	Missense_V589I, Missense_V589I, Missense_V537I, Missense_V412I, Missense_V448I	G>A	0.152	0.036	0.180	0.2 (0.1-0.5)	2.6E-05
rs1917448	11	103,498,150	-	LOC105369463	-	-	G>A	0.458	0.634	0.413	2.5 (1.6-3.8)	3.0E-05
rs62123078	19	6,913,435	-	*ADGRE1*	-	-	A>C	0.179	0.054	0.206	0.2 (0.1-0.5)	3.3E-05
rs62123079	19	6,913,436	-	*ADGRE1*	-	-	A>C	0.179	0.054	0.206	0.2 (0.1-0.5)	3.3E-05
rs62123080	19	6,913,437	-	*ADGRE1*	-	-	G>C	0.179	0.054	0.206	0.2 (0.1-0.5)	3.3E-05
rs62123081	19	6,913,438	-	*ADGRE1*	-	-	T>A	0.179	0.054	0.206	0.2 (0.1-0.5)	3.3E-05
rs466649	19	6,913,310	-	*ADGRE1*	-	-	T>C	0.177	0.054	0.203	0.2 (0.1-0.5)	3.5E-05
rs465642	19	6,913,350	-	*ADGRE1*	-	-	T>C	0.177	0.054	0.203	0.2 (0.1-0.5)	3.5E-05
rs461352	19	6,913,398	-	*ADGRE1*	-	-	C>T	0.177	0.054	0.203	0.2 (0.1-0.5)	3.5E-05
rs457857	19	6,913,811	NM_001256253, NM_001974, NM_001256252, NM_001256255, NM_001256254	*ADGRE1*	Exon	Missense_I424V, Missense_I424V, Missense_I372V, Missense_I247V, Missense_I283V	G>A	0.177	0.054	0.203	0.2 (0.1-0.5)	3.5E-05
rs462913	19	6,913,878	-	*ADGRE1*	-	-	T>G	0.177	0.054	0.203	0.2 (0.1-0.5)	3.5E-05
rs455476	19	6,914,099	-	*ADGRE1*	-	-	T>C	0.177	0.054	0.203	0.2 (0.1-0.5)	3.5E-05
rs460955	19	6,914,933	-	*ADGRE1*	-	-	G>A	0.177	0.054	0.203	0.2 (0.1-0.5)	3.5E-05
rs677767	19	6,915,230	-	*ADGRE1*	-	-	A>G	0.177	0.054	0.203	0.2 (0.1-0.5)	3.5E-05
rs34406206	19	6,922,014	-	ADGRE1	-	-	C>T	0.147	0.036	0.175	0.2 (0.1-0.5)	3.8E-05
rs72986353	19	6,922,093	-	ADGRE1	-	-	T>C	0.147	0.036	0.175	0.2 (0.1-0.5)	3.8E-05
rs12975999	19	6,922,418	-	ADGRE1	-	-	A>C	0.147	0.036	0.175	0.2 (0.1-0.5)	3.8E-05
rs11671182	19	6,922,504	-	*ADGRE1*	-	-	T>C	0.147	0.036	0.175	0.2 (0.1-0.5)	3.8E-05
rs11671186	19	6,922,574	-	*ADGRE1*	-	-	T>C	0.147	0.036	0.175	0.2 (0.1-0.5)	3.8E-05
rs7249799	19	6,922,815	-	*ADGRE1*	-	-	T>G	0.147	0.036	0.175	0.2 (0.1-0.5)	3.8E-05
rs3890539	19	6,923,073	-	*ADGRE1*	-	-	A>G	0.147	0.036	0.175	0.2 (0.1-0.5)	3.8E-05
rs35615093	19	6,923,498	-	*ADGRE1*	-	-	T>C	0.147	0.036	0.175	0.2 (0.1-0.5)	3.8E-05
rs67011688	19	6,923,667	-	*ADGRE1*	-	-	A>G	0.147	0.036	0.175	0.2 (0.1-0.5)	3.8E-05
rs57675929	19	6,924,125	-	*ADGRE1*	-	-	G>C	0.147	0.036	0.175	0.2 (0.1-0.5)	3.8E-05

(Continued to the next page)

Table 3. Continued

Marker	Chromosome	Position	Transcript(s)	Gene (nearby)	In-exon	Mutation(s)	Alleles	MAF	MAF (with *MYCN*)	MAF (without *MYCN*)	OR (95% CI)	p-value
rs10421295	19	6,912,894	-	*ADGRE1*	-	-	A>G	0.176	0.054	0.202	0.2 (0.1-0.5)	4.1E-05
rs11669085	19	6,915,052	-	*ADGRE1*	-	-	T>C	0.175	0.054	0.201	0.2 (0.1-0.5)	4.7E-05
rs35090409	19	6,915,887	-	*ADGRE1*	-	-	G>A	0.172	0.054	0.198	0.2 (0.1-0.6)	6.4E-05

MAF, minor allele frequency; OR, odds ratio; CI, confidence interval. [a]Synonyms: EMR1.

4. Assessment of gene functional annotation and biological network analyses

The result of Gene Ontology (GO) analysis was listed in S4 Table. A total of 37 significant GO terms were identified. Among them, 10 biological pathways such as lipid transporter activity, kidney morphogenesis, regulation of macrophage derived foam cell differentiation, positive regulation of macrophage derived foam cell differentiation, sensory perception of taste, negative regulation of cell division, foam cell differentiation, macrophage derived foam cell differentiation, dicarboxylic acid catabolic process, and synaptic membrane adhesion was maintained the signals after multiple correction ($p^{corr} < 0.05$). S5 Fig. shows the result of biological network related to other biological functions. In the regulation of macrophage derived foam cell differentiation, it was closely linked to positive regulation of macrophage derived foam cell differentiation. To examine the biological function, we performed GO analysis using the DAVID. We have shown the result of GO analysis for the identified significant SNPs using the risk of NB using DAVID in S4 Table. Ten GO terms were observed have significantly corrected p-value (< 0.05). These were lipid transporter activity, kidney morphogenesis, regulation of macrophage derived foam cell differentiation, positive regulation of macrophage derived foam cell differentiation, sensory perception of taste, negative regulation of cell division, foam cell differentiation, macrophage derived foam cell differentiation, dicarboxylic acid catabolic process, and synaptic membrane adhesion.

Discussion

In the current study, we investigated novel genetic susceptibility markers for the risk of NB and its subgroups such as *MYCN* amplification group and high-risk group. We used the imputed markers from the genotypes of Illumina's GSA BeadChip through strict quality control. The Illumina GSA BeadChip, which was recently launched, contains highly optimized multi-ethnic clinical markers from well-defined databases of known diseases such as ClinVar, the Pharmacogenomics Knowledgebase (PharmGKB), and the National Human Genome Research Institute (NHGRI)-EBI database.

According to the INRG, four categories (very low-risk, low-risk, intermediate-risk, and high-risk) could be classified by seven clinical and biological factors [4]. Over the past 10 years, several genetic studies have been performed to identify somatic and germline variants affecting the onset and survival rate of NB. In the first GWAS, *CASC-15* and *NBAT-1* genes found on chromosome 6p22 were identified as the susceptible genes. Interestingly, we identified significant markers in cases with high-risk or *MYCN*-amplified NB. Subsequently, it was found that rs6939340 was most significantly associated with the risk of sporadic NB [6]. In the next GWAS, several novel risk SNPs

Table 4. Logistic analysis of neuroblastoma with high-risk grade

Marker	Chromosome	Position	Transcript(s)	Gene(s)	In-exon	Mutation(s)	Alleles	MAF	MAF (high risk)	MAF (no high risk)	OR (95% CI)	p-value
rs62296061	4	1,014,172	-	*FGFRL1*	-	-	G>A	0.039	0.078	0.007	13.6 (3.1-59.3)	2.8E-06
rs11981667	7	94,963,270	-	(PON1, PON3)	-	-	C>G	0.039	0.004	0.067	-	5.2E-06
rs17166829	7	94,966,716	-	(PON1, PON3)	-	-	G>T	0.039	0.004	0.067	-	5.2E-06
rs73422040	7	94,972,055	-	(PON1, PON3)	-	-	A>G	0.039	0.004	0.067	-	5.2E-06
rs11980347	7	94,977,637	-	(PON1, PON3)	-	-	G>A	0.039	0.004	0.067	-	5.2E-06
rs17884252	7	94,985,267	-	(PON1, PON3)	-	-	C>A	0.039	0.004	0.067	-	5.2E-06
rs17883750	7	94,995,345	-	(PON1, PON3)	-	-	A>G	0.039	0.004	0.067	-	5.2E-06
rs149643570	7	95,012,509	-	(PON1, PON3)	-	-	A>G	0.039	0.004	0.067	-	5.2E-06
rs7256147	19	6,921,868	NM_001256253, NM_001974, NM_001256252, NM_001256255, NM_001256254	*ADGRE1*	Exon	Missense_V589I, Missense_V589I, Missense_V412I, Missense_V448I	G>A	0.152	0.080	0.217	0.3 (0.2-0.6)	5.9E-06
rs34406206	19	6,922,014	-	*ADGRE1*	-	-	C>T	0.147	0.080	0.209	0.3 (0.2-0.6)	1.4E-05
rs72986353	19	6,922,093	-	*ADGRE1*	-	-	T>C	0.147	0.080	0.209	0.3 (0.2-0.6)	1.4E-05
rs12975999	19	6,922,418	-	*ADGRE1*	-	-	A>C	0.147	0.080	0.209	0.3 (0.2-0.6)	1.4E-05
rs11671182	19	6,922,504	-	*ADGRE1*	-	-	T>C	0.147	0.080	0.209	0.3 (0.2-0.6)	1.4E-05
rs11671186	19	6,922,574	-	*ADGRE1*	-	-	T>C	0.147	0.080	0.209	0.3 (0.2-0.6)	1.4E-05
rs7249799	19	6,922,815	-	*ADGRE1*	-	-	T>G	0.147	0.080	0.209	0.3 (0.2-0.6)	1.4E-05
rs3890539	19	6,923,073	-	*ADGRE1*	-	-	A>G	0.147	0.080	0.209	0.3 (0.2-0.6)	1.4E-05
rs35615093	19	6,923,498	-	*ADGRE1*	-	-	T>C	0.147	0.080	0.209	0.3 (0.2-0.6)	1.4E-05
rs67011688	19	6,923,667	-	*ADGRE1*	-	-	A>G	0.147	0.080	0.209	0.3 (0.2-0.6)	1.4E-05
rs57675929	19	6,924,125	-	*ADGRE1*	-	-	G>C	0.147	0.080	0.209	0.3 (0.2-0.6)	1.4E-05
rs466649	19	6,913,310	-	*ADGRE1*	-	-	T>C	0.177	0.109	0.233	0.4 (0.3-0.6)	7.4E-05
rs465642	19	6,913,350	-	*ADGRE1*	-	-	T>C	0.177	0.109	0.233	0.4 (0.3-0.6)	7.4E-05
rs461352	19	6,913,398	-	*ADGRE1*	-	-	C>T	0.177	0.109	0.233	0.4 (0.3-0.6)	7.4E-05
rs457857	19	6,913,811	NM_001256253, NM_001974, NM_001256252, NM_001256255, NM_001256254	*ADGRE1*	Exon	Missense_I424V, Missense_I424V, Missense_I372V, Missense_I247V, Missense_I283V	G>A	0.177	0.109	0.233	0.4 (0.3-0.6)	7.4E-05
rs462913	19	6,913,878	-	*ADGRE1*	-	-	T>G	0.177	0.109	0.233	0.4 (0.3-0.6)	7.4E-05
rs455476	19	6,914,099	-	*ADGRE1*	-	-	T>C	0.177	0.109	0.233	0.4 (0.3-0.6)	7.4E-05
rs460955	19	6,914,933	-	*ADGRE1*	-	-	G>A	0.177	0.109	0.233	0.4 (0.3-0.6)	7.4E-05
rs677767	19	6,915,230	-	*ADGRE1*	-	-	A>G	0.177	0.109	0.233	0.4 (0.3-0.6)	7.4E-05

(Continued to the next page)

Table 4. Continued

Marker	Chromosome	Position	Transcript(s)	Gene(s)	In-exon	Mutation(s)	Alleles	MAF	MAF (high risk)	MAF (no high risk)	OR (95% CI)	p-value
rs10216960	8	82,939,088	-	(SNX16, LOC105375929)	-	-	T>C	0.466	0.380	0.543	0.5 (0.4-0.7)	7.4E-05
rs116876380	20	61,444,523	NM_007346	*OGFR*	EXON	Missense_S519L	C>T	0.030	0.004	0.053	0.1 (0.0-0.5)	8.3E-05
rs10421295	19	6,912,894	-	-	-	-	A>G	0.176	0.109	0.232	0.4 (0.3-0.7)	9.6E-05

MAF, minor allele frequency; OR, odds ratio; CI, confidence interval.

including *BARD1* gene on chromosome 2q35 were identified [7]. Other GWAS conducted using in familial and sporadic cases of NB have reported novel additional risk SNPs in candidate genes such as *DUSP12*, *HSD17B12*, *DDX4*, *IL31RA*, *LMO1*, *HACE1*, *LIN28B*, *SPAG16*, *NEFL*, *TP53*, *CPZ*, *MLFL*, *CDKN1B*, *KIF15*, and *MMP20* [9-19]. Among them, SNPs in *BARD1* and *LMO1* candidate genes were replicated in other cohorts due to its association by large cohort study [19,20]. In the current study, we also identified significant associations between the genes and the risk of NB (p=0.001, rs3768716, rs2070094 in *BARD1* gene; p=0.0002, rs110419 in *LMO1* gene).

However, as the previous GWAS studies were performed mostly with Caucasian and Africans, there is a serious lack of GWAS studies for Asian populations. In the current study, we identified novel genetic markers for comparing the risk between children with NB and healthy controls with no tumor record in Korean population. Using high-quality markers and strict criteria, imputed markers were used. As a result, we found 21 statistically significant markers associated with the risk of NB ($p^{corr} < 0.05$) such as *RPTN*, *MRPS18B*, *LRRC45*, *KANSL1L*, *ARHGEF40*, *IL15RA*, *L1TD1*, *ANO7*, *LAMA5*, *OR7-G2*, *SALL4*, and *NEUROG2*. Interestingly, out of these 21 significant SNPs ($p^{corr} < 0.05$), 12 SNPs were nonsynonymous (average MAF=0.064). Except rs76015112, rs77226427, and rs2886644, most nonsynonymous SNPs showed rare MAF above 5%. The most significantly associated marker was found to be rs76015112 which was located on the *RPTN* gene (p=8.1E-23, p^{corr}=2.3E-17). The *RPTN* gene encodes for repetin, an extracellular epidermal matrix protein consisting of 784 amino acids. This protein is rich in glutamine with EF-hands of the S100 type and contributes to the formation of the cornified envelope [21]. However, this gene has not yet been reported to be associated with NB. Interestingly, three nonsynonymous SNPs (rs117249618, rs117674897, and rs114591848) in *LRRC45*, *KANSL1L*, and *ARHGEF40* genes showed high protein function damaging scores (1.00, 0.88, and 0.99). Moreover, the MAF of the SNPs was higher in NB than in controls (Table 2). This implies that the SNPs may be risk factors for the onset of NB. Candidate markers within *BAL1*, *LMO1*, *MLF1*, and *HACE1* previously reported to be related with the risk of NB in Caucasian and European were not replicated in this study. The reason is presumed to be due to ethnic difference and platform difference.

NB patients were further divided into two subgroups, *MYCN*-amplified group and high-risk group, and then logistic regression analysis was performed for each of the subgroups. In these two subgroups, we found that many significant SNPs were located in the *ADGRE1* gene. Interestingly, two nonsynonymous SNPs (rs7256147 and rs457857) were identified in the *ADGRE1* gene (Tables 3 and 4). The frequencies of the two nonsynonymous SNPs in *MYCN*-amplified or high-risk tumors were lower than those in *MYCN* non-amplified or non-high-risk tumors, respectively. This

implies that the SNPs might have a protective role against the risk of NB. *ADGRE1* gene has been renamed as *EMR1* gene, which encodes for epidermal growth factor–like module containing mucin-like hormone receptor 1. *ADGRE1* gene encodes for proteins belonging to a group of hormone receptor with seven transmembrane segments [22]. Therefore, the mutated product of the *ADGRE1* gene might act as a neurotransmitter and influence the biological function of the signal transduction. When calculated using the GAS Power Calculator (http://csg.sph.umich.edu/abecasis/cats/gas_power_calculator), the expected power was 0.449. This result suggests that this study used insufficient samples, and that further studies using a large number of samples through multi-center collaboration in Asia are needed to verify the significant markers found by GWAS analysis.

To our knowledge, this is the first GWAS study in Korean NB patients. We discovered novel susceptible SNPs for the risk of NB. Of them, 12 nonsynonymous SNPs were identified. When the protein damaging prediction was performed by PolyPhen-2 algorithm, three SNPs showed high protein activity damaging scores (> 0.8). Additionally, we performed GWAS for two subgroups, *MYCN*-amplified group and the high-risk group, and identified the significantly associated SNPs in the *ADGRE1* gene. The identified variations may helpful to investigate the potential function for the onset of NB by functional assay. Our study may provide a new direction in the formulation of medication for the risk of NB in Korean population.

Electronic Supplementary Material

Supplementary materials are available at Cancer Research and Treatment website (https://www.e-crt.org).

Conflicts of Interest

Conflicts of interest relevant to this article was not reported.

Acknowledgments

This work was supported by the National Research Foundation of Korea (NRF) grant funded by the Korea government (NRF-2016R1A2B1012908) and by grants from the National R&D Program for Cancer Control, Ministry of Health & Welfare, Republic of Korea (No. 1520210 and No. 1720270). This study was conducted with bioresources from National Biobank of Korea, the Centers for Disease Control and Prevention, Republic of Korea (2018-019).

References

1. Latimer E, Anderson G, Sebire NJ. Ultrastructural features of neuroblastic tumors in relation to morphological, and molecular findings; a retrospective review study. BMC Clin Pathol. 2014;14:13.
2. Cohn SL, Pearson AD, London WB, Monclair T, Ambros PF, Brodeur GM, et al. The International Neuroblastoma Risk Group (INRG) classification system: an INRG Task Force report. J Clin Oncol. 2009;27:289-97.
3. Lee JW, Son MH, Cho HW, Ma YE, Yoo KH, Sung KW, et al. Clinical significance of MYCN amplification in patients with high-risk neuroblastoma. Pediatr Blood Cancer. 2018;65:e27257.
4. Pinto NR, Applebaum MA, Volchenboum SL, Matthay KK, London WB, Ambros PF, et al. Advances in risk classification and treatment strategies for neuroblastoma. J Clin Oncol. 2015;33:3008-17.
5. Barr EK, Applebaum MA. Genetic predisposition to neuroblastoma. Children (Basel). 2018;5:119.
6. Maris JM, Mosse YP, Bradfield JP, Hou C, Monni S, Scott RH, et al. Chromosome 6p22 locus associated with clinically aggressive neuroblastoma. N Engl J Med. 2008;358:2585-93.
7. Capasso M, Devoto M, Hou C, Asgharzadeh S, Glessner JT, Attiyeh EF, et al. Common variations in BARD1 influence susceptibility to high-risk neuroblastoma. Nat Genet. 2009;41:718-23.
8. Adzhubei IA, Schmidt S, Peshkin L, Ramensky VE, Gerasimova A, Bork P, et al. A method and server for predicting damaging missense mutations. Nat Methods. 2010;7:248-9.
9. Chang X, Zhao Y, Hou C, Glessner J, McDaniel L, Diamond MA, et al. Common variants in MMP20 at 11q22.2 predispose to 11q deletion and neuroblastoma risk. Nat Commun. 2017;8:569.
10. Hungate EA, Applebaum MA, Skol AD, Vaksman Z, Diamond M, McDaniel L, et al. Evaluation of genetic predisposition for MYCN-amplified neuroblastoma. J Natl Cancer Inst. 2017;109:djx093.
11. Capasso M, McDaniel LD, Cimmino F, Cirino A, Formicola D, Russell MR, et al. The functional variant rs34330 of CDKN1B is associated with risk of neuroblastoma. J Cell Mol Med. 2017;21:3224-30.
12. McDaniel LD, Conkrite KL, Chang X, Capasso M, Vaksman Z, Oldridge DA, et al. Common variants upstream of MLF1 at 3q25 and within CPZ at 4p16 associated with neuroblastoma. PLoS Genet. 2017;13:e1006787.
13. Diskin SJ, Capasso M, Diamond M, Oldridge DA, Conkrite K, Bosse KR, et al. Rare variants in TP53 and susceptibility to neuroblastoma. J Natl Cancer Inst. 2014;106:dju047.
14. Capasso M, Diskin S, Cimmino F, Acierno G, Totaro F, Petrosino G, et al. Common genetic variants in NEFL influence gene expression and neuroblastoma risk. Cancer Res. 2014;74:6913-24.
15. Latorre V, Diskin SJ, Diamond MA, Zhang H, Hakonarson H, Maris JM, et al. Replication of neuroblastoma SNP association at the BARD1 locus in African-Americans. Cancer Epidemiol Biomarkers Prev. 2012;21:658-63.
16. Diskin SJ, Capasso M, Schnepp RW, Cole KA, Attiyeh EF, Hou C, et al. Common variation at 6q16 within HACE1 and LIN28B influences susceptibility to neuroblastoma. Nat Gen-

et. 2012;44:1126-30.
17. Nguyen le B, Diskin SJ, Capasso M, Wang K, Diamond MA, Glessner J, et al. Phenotype restricted genome-wide association study using a gene-centric approach identifies three low-risk neuroblastoma susceptibility loci. PLoS Genet. 2011; 7:e1002026.
18. Matthews JM, Lester K, Joseph S, Curtis DJ. LIM-domain-only proteins in cancer. Nat Rev Cancer. 2013;13:111-22.
19. Wang K, Diskin SJ, Zhang H, Attiyeh EF, Winter C, Hou C, et al. Integrative genomics identifies LMO1 as a neuroblastoma oncogene. Nature. 2011;469:216-20.
20. Capasso M, Diskin SJ, Totaro F, Longo L, De Mariano M, Russo R, et al. Replication of GWAS-identified neuroblastoma risk loci strengthens the role of BARD1 and affirms the cumulative effect of genetic variations on disease susceptibility. Carcinogenesis. 2013;34:605-11.
21. Huber M, Siegenthaler G, Mirancea N, Marenholz I, Nizetic D, Breitkreutz D, et al. Isolation and characterization of human repetin, a member of the fused gene family of the epidermal differentiation complex. J Invest Dermatol. 2005;124:998-1007.
22. Baud V, Chissoe SL, Viegas-Pequignot E, Diriong S, N'Guyen VC, Roe BA, et al. EMR1, an unusual member in the family of hormone receptors with seven transmembrane segments. Genomics. 1995;26:334-44.

pISSN 1598-2998, eISSN 2005-9256

Cancer Res Treat. 2020;52(4):1262-1272 https://doi.org/10.4143/crt.2020.089

Original Article Open Access

Increasing Incidence of B-Cell Non-Hodgkin Lymphoma and Occurrence of Second Primary Malignancies in South Korea: 10-Year Follow-up Using the Korean National Health Information Database

Jin Seok Kim, MD, PhD[1]
Yanfang Liu, MD, MPH[2]
Kyoung Hwa Ha, PhD[3]
Hong Qiu, MD, PhD[4]
Lee Anne Rothwell, PhD[5]
Hyeon Chang Kim, MD, PhD[6]

[1]*Department of Internal Medicine, Severance Hospital, Yonsei University College of Medicine, Seoul, Korea,* [2]*Janssen Research & Development, Global Epidemiology, Singapore,* [3]*Department of Endocrinology and Metabolism, Ajou University School of Medicine, Suwon, Korea,* [4]*Janssen Research & Development, Global Epidemiology, Titusville, NJ, USA,* [5]*Janssen Medical Affairs, Macquarie Park, Australia,* [6]*Department of Preventative Medicine, Yonsei University College of Medicine, Seoul, Korea*

Correspondence: Jin Seok Kim, MD, PhD
Department of Internal Medicine, Severence Hospital, Yonsei University College of Medicine, 50-1 Yonsei-ro, Seodaemun-gu, Seoul 03722, Korea
Tel: 82-2-2228-1972
Fax: 82-2-393-6884
E-mail: hemakim@yuhs.ac

Co-correspondence: Hyeon Chang Kim, MD, PhD
Department of Preventative Medicine, Yonsei University College of Medicine, 50-1 Yonsei-ro, Seodaemun-gu, Seoul 03722, Korea
Tel: 82-2-2228-1873
Fax: 82-2-392-8133
E-mail: hckim@yuhs.ac

Received February 7, 2020
Accepted April 30, 2020
Published Online May 4, 2020

Purpose
The epidemiology of B-cell non-Hodgkin lymphoma (BNHL) in Asia is not well described, and rates of second primary malignancies (SPM) in these patients are not known. We aimed to describe temporal changes in BNHL epidemiology and SPM incidence in Korea.

Materials and Methods
A retrospective cohort study used claims data from the National Health Insurance Service that provides universal healthcare coverage in Korea. Newly diagnosed patients aged at least 19 years with a confirmed diagnosis of one of six BNHL subtypes (diffuse large cell B-cell lymphoma [DLBCL], small lymphocytic and chronic lymphocytic [CLL/SLL], follicular lymphoma [FL], mantle cell lymphoma [MCL], marginal zone lymphoma [MZL], and lymphoplasmacytic lymphoma/Waldenström's macroglobulinemia [WM]) during the period 2006-2015 were enrolled and followed up until death, dis-enrolment, or study end, whichever occurred first. Patients with pre-existing primary cancers prior to the diagnosis of BNHL were excluded.

Results
A total of 19,500 patients with newly diagnosed BNHL were identified out of 27,866 with non-Hodgkin lymphoma (NHL). DLBCL was the most frequently diagnosed subtype (41.9%-48.4% of NHL patients annually, 2011-2015). Standardized incidence of the six subtypes studied per 100,000 population increased from 5.74 in 2011 to 6.96 in 2015, with most increases in DLBCL, FL, and MZL. The incidence (95% confidence interval) of SPM per 100 person-years was 2.74 (2.26-3.29) for CLL/SLL, 2.43 (1.57-3.58) for MCL, 2.41 (2.10-2.76) for MZL, 2.23 (2.07-2.40) for DLBCL, 1.97 (1.61-2.38) for FL, and 1.41 (0.69-2.59) for WM.

Conclusion
BNHL has been increasingly diagnosed in Korea. High rates of SPM highlight the need for continued close monitoring to ensure early diagnosis and treatment.

Key words
Non-Hodgkin lymphoma, Prevalence, Incidence, Korea, Second primary neoplasms

Introduction

B-cell non-Hodgkin lymphoma (BNHL) comprises a heterogeneous group of lymphoid malignancies that differ in their clinical presentation and progression [1]. The most common type of mature BNHL in adults is diffuse large B-cell lymphoma (DLBCL), which comprises approximately 46% of mature BNHL in Korea [2]. Other subtypes include follicular lymphoma (FL), mantle cell lymphoma (MCL), marginal zone lymphoma (MZL, including mucosa-associated lymphoid tis-

sue [MALT] lymphoma), chronic lymphocytic and small lymphocytic lymphoma (CLL/SLL), and Waldenström's macroglobulinemia (WM or lymphoplasmacytic lymphoma). BNHL subtypes vary in their ethnic and regional distribution, possibly influenced by genetic, lifestyle, and environmental factors [1,3].

The prognosis of BNHL has improved in the last decade, attributed primarily to the addition of rituximab to standard chemotherapy regimens [4]. Depending on subtype, some patients will be cured with treatment and others will survive for longer than a decade [1]. Prolonged survival is associated with its own complications, such as the development of second primary malignancies (SPM). A meta-analysis of 23 studies reported that SPM occur in patients with non-Hodg-kin's lymphoma significantly more frequently than primary malignancies in the general population, with a relative risk estimated at 1.88 (95% confidence interval [CI], 1.58 to 2.22) [5]. However, most of the data came from North American and European populations, and only two Japanese studies were included from the Asian region. Exposure to chemotherapy, autologous stem cell transplant, total body irradiation, and younger age at diagnosis have all been implicated as risk factors in the development of SPM [5,6].

The incidence of BNHL is reportedly lower in Asian than in Western countries and the distribution of BNHL subtypes is also different [1,2]. Compared to Western countries, a higher proportion of patients in Asia with BNHL have MZL, and lower proportions have FL and CLL/SLL [7-9]. Some of these differences likely reflect known variations in genetic susceptibility to BNHL between Asian and Western populations [10,11]. However, for some subtypes, other mechanisms, such as different molecular pathways or etiologic factors are thought to contribute to regional differences in incidence rates. For example, while the incidence of FL is lower in Asian than in Western populations, the occurrence of the characteristic bcl-2 translocation found in FL is similar in healthy populations in both regions, suggesting that the development of FL may be triggered differently in Asia than in Western countries [12].

The Republic of Korea is a high-income, industrialized country that lies to the East of the Asian mainland, with a population of approximately 52 million. The Korean government began national health insurance programs in 1976, expanded their coverage to all citizens in 1989, and created a single-payer system (Korean National Health Insurance System, NHIS) from 2000 [13]. Those insured pay contributions and receive medical services from their healthcare providers. The National Health Information Database (NHID) is maintained by the NHIS and contains all medical and prescription drug claim records for the Korean population, and is a rich repository of information for health research [14].

Between 1999 and 2012, the age-standardized incidence of mature BNHL increased annually by 5.6% [2]. The rate of SPM among patients with BNHL in Korea is not known. To address this knowledge gap, we conducted a retrospective cohort study using claims data from the NHID to describe temporal changes in the incidence and prevalence of BNHL in Korea up until 2015, and to evaluate the incidence of SPM in patients with BNHL.

Materials and Methods

1. Data source

The NHID holds comprehensive information on health care utilization, demographic characteristics, and mortality for the whole population of South Korea [13,14]. The NHID was built in 2012 to perform NHIS activities using information from medical treatment and health screening records, and socio-demographic data from an existing database system [14]. Inpatient and outpatient visits including diagnoses recorded in International Classification of Diseases, 10th revision (ICD-10) format, length of stay, treatment costs, procedures, and prescriptions are recorded [13,14].

2. Study population

All patients who were newly diagnosed with one of six BNHL subtypes (ICD-10 codes C83.3 DLBCL, C91.1 CLL/SLL, C82 FL, C83.1 MCL, C88.4 MALT lymphoma and C83.0 MZL, or C88.0 WM) between 01 January 2006 and 31 December 2015 were identified in the NHID. Nodal and extra-nodal MZL were included under one category because they are unable to be differentiated under C83.0. Patients were defined as newly diagnosed if they had no previous record of diagnosis or treatment of BNHL for at least 1 year. The diagnosis of BNHL was confirmed if the patient had at least three outpatient visits, and/or one hospital admission with the specific ICD-10 code after the diagnosis index date.

Patients were included in the study cohort if they were at least 19 years of age and if they had been in the database for at least 12 months prior to the BNHL diagnosis index date. Patients were excluded if they had any cancer other than BNHL prior to the diagnosis index date.

SPM were defined as new malignant tumors diagnosed more than 180 days after the BNHL index date to reduce the risk of including pre-existing undiagnosed malignancies in the analysis [15], SPM were identified in the NHID. Patients were followed up for SPM from the diagnosis index date until death, end of the study period, or dis-enrolment, whichever occurred first. All kinds of solid tumors were considered as SPM. For hematologic malignancies as SPM, we included acute myeloid leukemia (C92), monocytic leukemia (C93), myelodysplastic syndrome (D46), and myeloproliferative neoplasms (D47), but excluded acute leukemia of unspecified cell type (C95), multiple myeloma (C90) and all subtypes of lymphoma.

Since there have been changes in the diagnostic codes for

BNHL subtypes in the NHIS over time, the study period was divided into two parts: years 2006 to 2010 and years 2011 to 2015. The cohort analysis of incidence and prevalence was conducted using data from 2011-2015, whereas the full dataset from 2006 to 2015 was used to estimate the incidence of SPM.

3. Statistical analysis

The incidence of BNHL for each study year was calculated as the number of newly diagnosed patients with BNHL divided by the total Korean population in each calendar year. Prevalence included all patients with existing and incident BNHL divided by the total Korean population in each calendar year. Mortality rates for BNHL and its six subtypes were calculated as the number of patient deaths due to any cause divided by the total Korean population in each calendar year. Age-standardized rates were calculated by the direct standardization method, using the age distribution of the Korean population in 2011 as the standard population. Overall survival (OS) was calculated using Kaplan-Meier methods.

The number of patients with at least one SPM was determined and the incidence calculated using the number of patients divided by the sum of the total follow-up period (per 100 person-years). Kaplan-Meier survival curves for SPM used the first SPM event for the time-to-event analysis. Cochran-Armitage tests were used to describe trends in the data over time. All analyses were performed using SAS ver. 9.4 (SAS Institute Inc., Cary, NC).

4. Ethical statement

All personally identifiable information was encrypted to protect patient privacy. The study protocol was reviewed and received approval from the Institutional Review Board of Yonsei University Health System, Severance Hospital with a waiver of informed consent (4-2016-0824), and the National Health Information Data Request Review Committee of the NHIS (REQ0000006774).

Results

A total of 19,500 patients with BNHL in the NHID had a diagnosis index date between 2006 and 2015 out of 27,866 with NHL (Table 1). Of these, 13,671 were diagnosed between 2011-2015 and were included in the cohort analysis. The mean age of patients diagnosed between 2011 and 2015 was 59.5 years, 60.0% (n=8,202) of patients were 19-64 years of age and 54.0% (n=7,389) were male.

The total number of BNHL cases diagnosed increased annually from 2,298 in year 2011 up to 3,128 in year 2015. DLBCL was the most common diagnosis in each study year (Table 1), although the relative proportion of DLBCL tended to decrease over time from 43.0% of all NHL diagnoses in

Table 1. New diagnoses of non-Hodgkin B-cell lymphomas in patient over the 2006 to 2015 study period

	Study period 1					Study period 2				
	2006	2007	2008	2009	2010	2011	2012	2013	2014	2015
DLBCL (C83.3)	657 (36.6)	792 (41.5)	847 (42.3)	971 (42.4)	1,134 (46.8)	1,348 (43.0)	1,387 (41.9)	1,501 (42.6)	1,639 (43.4)	1,791 (48.4)
CLL/SLL (C91.1)	119 (6.6)	110 (5.8)	100 (5.0)	113 (4.9)	111 (4.6)	143 (4.6)	144 (4.3)	142 (4.0)	165 (4.4)	138 (3.7)
FL (C82)	100 (5.6)	89 (4.7)	89 (4.4)	94 (4.1)	110 (4.5)	199 (6.4)	197 (5.9)	267 (7.6)	293 (7.8)	288 (7.8)
MCL (C83.1)	4 (0.2)	6 (0.3)	12 (0.6)	4 (0.2)	32 (1.3)	65 (2.1)	74 (2.2)	78 (2.2)	83 (2.2)	81 (2.2)
MZL (C83.0, C88.4)	23 (1.3)	19 (1.0)	24 (1.2)	29 (1.3)	152 (6.3)	521 (16.6)	602 (18.2)	707 (20.1)	878 (23.3)	802 (21.7)
WM (C88.0)	14 (0.8)	17 (0.9)	19 (0.9)	19 (0.8)	19 (0.8)	22 (0.7)	32 (1.0)	27 (0.8)	29 (0.8)	28 (0.8)
Total BNHL	917	1,033	1,091	1,230	1,558	2,298	2,436	2,722	3,087	3,128
Other	880 (49.0)	876 (45.9)	913 (45.6)	1,060 (46.3)	866 (35.7)	834 (26.6)	878 (26.5)	799 (22.7)	689 (18.2)	571 (15.4)
Total NHL	1,797	1,909	2,004	2,290	2,424	3,132	3,314	3,521	3,776	3,699

Values are presented as number (%). DLBCL, diffuse large B-cell lymphoma; CLL/SLL, small lymphocytic lymphoma and chronic lymphocytic; FL, follicular lymphoma; MCL, mantle cell lymphoma; MZL, marginal zone lymphoma; WM, Waldenström's macroglobulinemia or lymphoplasmacytic lymphoma; BNHL, B-cell non-Hodgkin lymphoma; NHL, non-Hodgkin lymphoma. %=percentage of all NHL

Table 2. Crude and age-standardized incidence, prevalence and all-cause mortality rates of BNHL in the Korean population

Year	No. of cases	Incidence (95% CI) per 100,000		Prevalence (95% CI) per 100,000		Mortality (95% CI) per 100,000	
		Crude	Age-standardized[a)]	Crude	Age-standardized[a)]	Crude	Age-standardized[a)]
2011	2,298	5.74 (5.51-5.98)	5.74 (5.51-5.98)	10.62 (10.28-10.92)	10.62 (10.28-10.92)	1.33 (1.22-1.44)	1.33 (1.22-1.44)
2012	2,436	6.00 (5.77-6.25)	5.90 (5.67-6.13)	14.82 (14.45-15.20)	14.56 (14.19-14.93)	1.62 (1.50-1.75)	1.55 (1.43-1.67)
2013	2,722	6.62 (6.37-6.87)	6.39 (6.15-6.63)	18.93 (18.52-19.36)	18.31 (17.90-18.72)	1.80 (1.67-1.93)	1.65 (1.52-1.77)
2014	3,087	7.39 (7.14-7.66)	7.06 (6.81-7.31)	23.41 (22.95-23.87)	22.35 (21.91-22.79)	2.07 (1.94-2.21)	1.82 (1.69-1.95)
2015	3,128	7.39 (7.13-7.65)	6.96 (6.72-7.20)	28.32 (27.82-28.83)	26.69 (26.21-27.17)	2.24 (2.10-2.39)	1.89 (1.76-2.02)

BNHL, B-cell non-Hodgkin lymphoma; CI, confidence interval. [a)]Standardized to the 2011 Korean population structure.

2011 to 43.4% in 2014 (but increasing to 48.4% in 2015). The proportion of CLL/SLL decreased during the study, from 4.6% of NHL in 2011 to 3.7% in 2015. By contrast, the proportion of FL and MZL increased between 2011 and 2015 (6.4% to 7.8% for FL and MZL 16.6% to 21.7% for MZL). There was little change in the proportion of patients diagnosed with NHL with MCL or WM over time.

1. Incidence, prevalence, and all-cause mortality rates in patients with BNHL

The age-standardized incidence of BNHL increased over time from 5.74 (95% CI, 5.51 to 5.98) per 100,000 population in 2011 to 6.96 (95% CI, 6.72 to 7.20) per 100,000 population in 2015 (Table 2). Age-standardized incidence rates of DLBCL, MZL, and FL increased significantly ($p < 0.001$ for all), with similar increases observed in men and women (Fig. 1). Between 2011 and 2015, the incidence of DLBCL increased by 11%, the incidence of MZL increased by 32%, and the incidence of FL increased by 25%. Age-standardized incidence rates of MCL and WM remained steady between 2011 and 2015, although there was some annual variation in the incidence in women versus men for WM. A decrease in the incidence of CLL/SLL appeared in 2015 (Fig. 1).

Crude and age-standardized BNHL prevalence increased steadily each year and were approximately 2.5-fold higher in 2015 than in 2011 (Table 2). Prevalence rates of each BNHL subtype also increased (Fig. 2). The age-adjusted prevalence of DLBCL increased by 1.8-fold, CLL/SLL by 1.7-fold, FL by 2.6-fold, MCL by 4.0-fold, MZL by 11.3-fold and WM by 1.6-fold ($p < 0.001$ for all six subtypes). Increases appeared to be similar in women and men for all BNHL subtypes.

Crude and age-standardized BNHL mortality rates increased over time. Age-standardized mortality increased by 42%, from 1.33 (95% CI, 1.22 to 1.44) per 100,000 population in 2011 to 1.89 (95% CI, 1.76 to 2.02) per 100,000 population in 2015 (Table 2). Age-standardized mortality increased among men and women for all BNHL subtypes; except for women with WM in whom the mortality rate remained rather constant (Fig. 3). The increase in age-standardized mortality was statistically significant for DLBCL ($p=0.010$), and CLL/SLL, MCL, MZL ($p < 0.001$). Between 2011 and 2015, all-cause mortality rates increased by 35% in patients with for DLBCL, 49% in patients with CLL/SLL, 31% in patients with FL, 172% in MCL, 77% in MZL and 121% in WM.

2. Overall survival

Five-year OS was highest in patents with MZL (88%) followed by FL (79%), CLL/SLL (62%), DLBCL (60%), WM (54%), and MCL (53%) (Table 3, Fig. 4). Up to three years after diagnosis, DLBCL patients had the lowest survival rate. However, when followed for a longer duration, MCL and WM subtypes showed lower survival rates than DLBCL.

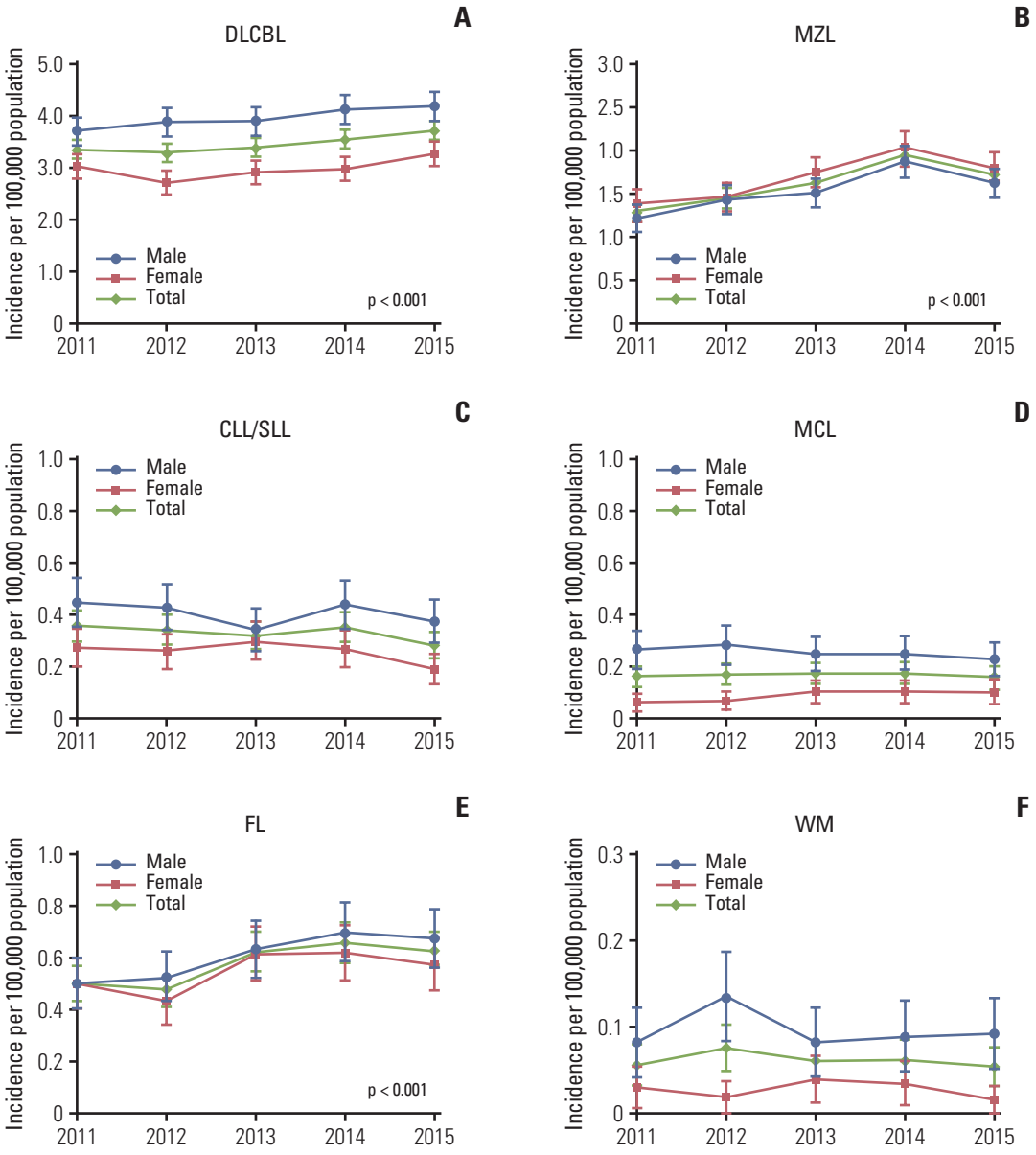

Fig. 1. Age-standardized incidence rates (95% confidence intervals) of B-cell non-Hodgkin lymphoma subtypes in South Korea, 2011-2015. Age-standardized rates were calculated by direct standardization method, using the 2011 Korean population as the reference. p-values for trend: DLBCL $p < 0.001$ (A), MZL $p < 0.001$ (B), CLL/SLL $p=0.489$ (C), MCL $p=0.077$ (D), FL $p < 0.001$ (E), WM $p=0.661$ (F). DLBCL, diffuse large B-cell lymphoma; MZL, marginal zone lymphoma; CLL/SLL, small lymphocytic lymphoma and chronic lymphocytic; MCL, mantle cell lymphoma; FL, follicular lymphoma; WM, Waldenström's macroglobulinemia or lymphoplasmacytic lymphoma.

3. Occurrence of SPM

Of the 19,500 patients diagnosed with BNHL in 2006-2015, 1,183 patients (6.1%) developed a total of 1,203 SPMs. The incidence of the first SPM was highest in patients with CLL/SLL (2.74 per 100 person-years), followed by MCL (2.43 per 100 person-years), MZL (2.41 per 100 person-years), DLBCL (2.23 per 100 person-years), FL (1.97 per 100 person-years), and WM (1.41 per 100 person-years) (Table 4).

The incidence of solid SPM was highest in patients with MCL (2.32 per 100 person-years) (Table 4). The most frequent solid malignancies were prostate cancer in 190 patients (0.64 per 100 person-years; 95% CI, 0.55 to 0.73), liver cancer in 234 patients (incidence rate 0.43 per 100 person-years; 95% CI, 0.38 to 0.49), stomach cancer in 174 patients (0.32 per 100 person-years; 95% CI, 0.28 to 0.37), colorectal cancer in 167 patients (0.31 per 100 person-years; 95% CI, 0.26 to 0.36), lung cancer in 139 patients (0.26 per 100 person-years; 95% CI, 0.22 to 0.30), brain cancer in 88 patients (0.16 per 100 person-

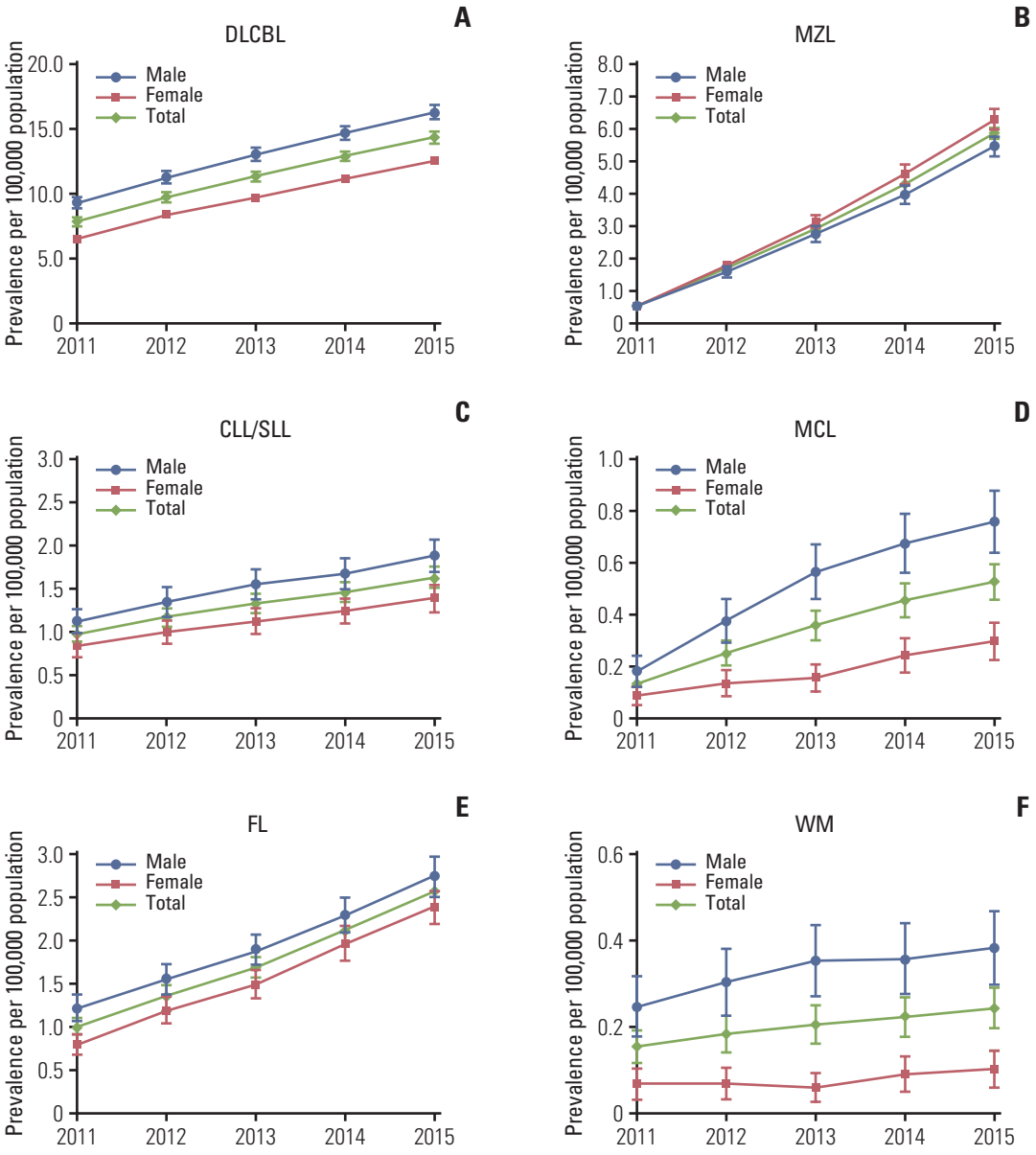

Fig. 2. Age-standardized prevalence (95% confidence intervals) of B-cell non-Hodgkin lymphoma subtypes in South Korea, 2011-2015. Age-standardized rates were calculated by direct standardization method, using the 2011 Korean population as the reference. p-values for trend: DLBCL $p < 0.001$ (A), MZL $p < 0.001$ (B), CLL/SLL $p < 0.001$ (C), MCL $p < 0.001$ (D), FL $p < 0.001$ (E), WM $p < 0.001$ (F). DLBCL, diffuse large B-cell lymphoma; MZL, marginal zone lymphoma; CLL/SLL, small lymphocytic lymphoma and chronic lymphocytic; MCL, mantle cell lymphoma; FL, follicular lymphoma; WM, Waldenström's macroglobulinemia or lymphoplasmacytic lymphoma.

years; 95% CI, 0.13 to 0.20), pancreatic cancer in 84 patients (0.15 per 100 person-years; 95% CI, 0.12 to 0.19), ovarian cancer in 37 patients (0.15 per 100 person-years; 95% CI, 0.11 to 0.21), breast cancer in 33 patients (0.13 per 100 person-years; 95% CI, 0.09 to 0.19), and head and neck cancer in 59 patients (0.11 per 100 person-years; 95% CI, 0.08 to 0.14).The cumulative incidence at 5 years for developing the first SPM was 15% for CLL/SLL, 12% for MCL and MZL, 11% for DLBCL, 9% for FL, and 7% for WM (Table 5).

A sensitivity analysis conducted in which the SPM analysis was restricted to 2011-2015 after implementation of changes in the diagnostic codes for BNHL subtypes showed similar results compared to the entire study period from 2006-2015 (data not shown).

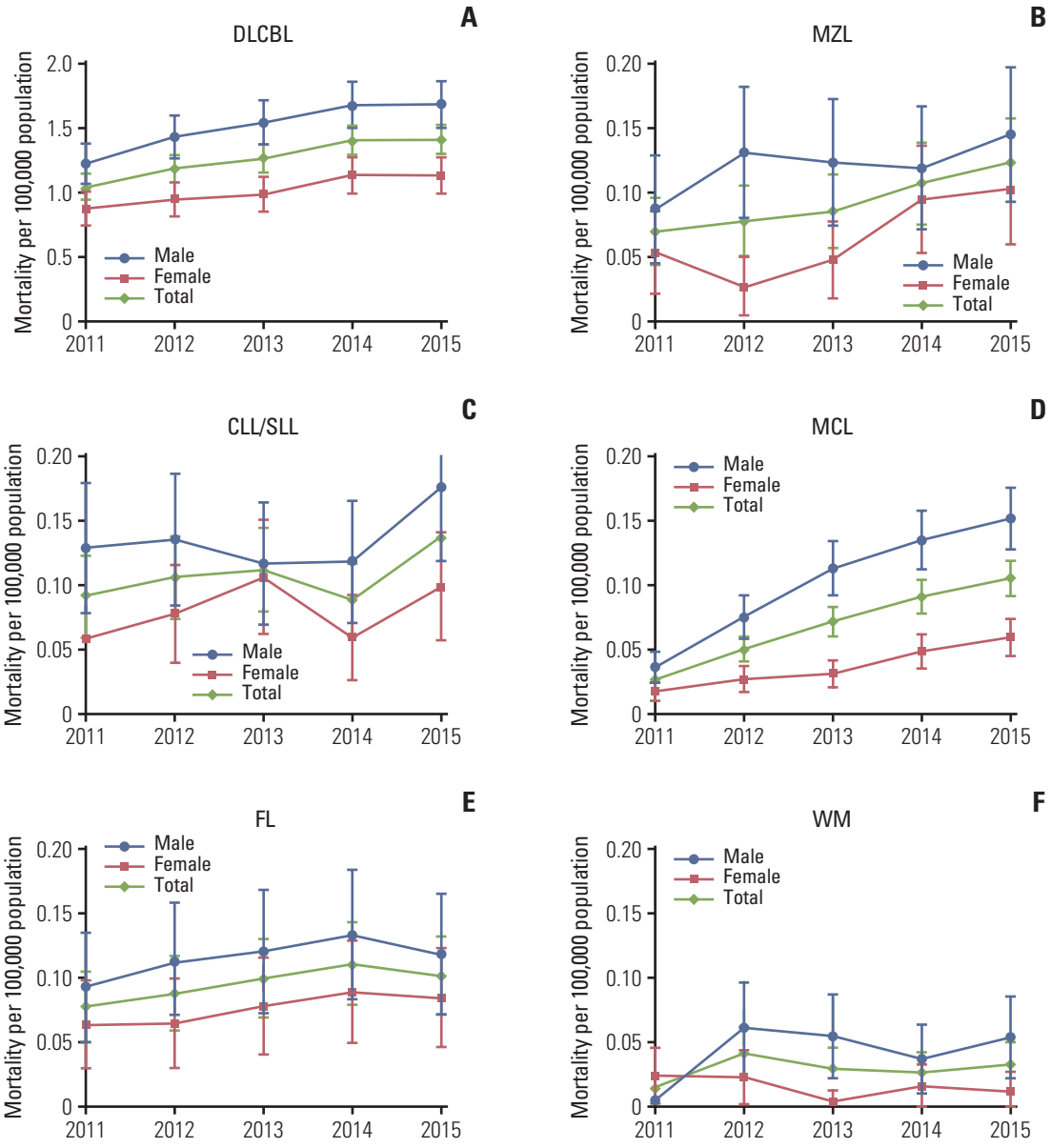

Fig. 3. Age-standardized all-cause mortality rates (95% confidence intervals) in patients with B-cell non-Hodgkin lymphoma subtypes in the Korean population, 2011-2015. Age-standardized rates were calculated by direct standardization method, using the 2011 Korean population as the reference. p-values for trend: DLBCL $p < 0.010$ (A), MZL $p < 0.001$ (B), CLL/SLL $p < 0.001$ (C), MCL $p < 0.001$ (D), FL $p=0.937$ (E), WM $p=0.923$ (F). DLBCL, diffuse large B-cell lymphoma; MZL, marginal zone lymphoma; CLL/SLL, small lymphocytic lymphoma and chronic lymphocytic; MCL, mantle cell lymphoma; FL, follicular lymphoma; WM, Waldenström's macroglobulinemia or lymphoplasmacytic lymphoma.

Discussion

To our knowledge, this is the first analysis of the incidence of SPM in Korean patients with BNHL. By analyzing virtually all cases of BNHL in the Korean health system, we found a high rate of progression to SPM, with a 5-year cumulative incidence of 7% to 15% depending on subtype after the BNHL diagnosis, and evidence of progression to SPM that continued past the 9-year follow-up period of our study. This contrasts with 5-year cumulative incidence of approximately 3% for patients with early stage Hodgkin's lymphoma [16], and 6% for patients with multiple myeloma [17].

Our estimates of the cumulative incidence of SPM are somewhat higher than reported elsewhere. Studies in the United States using the Surveillance, Epidemiology, and End Results (SEER) database report 5- and 10-year cumulative

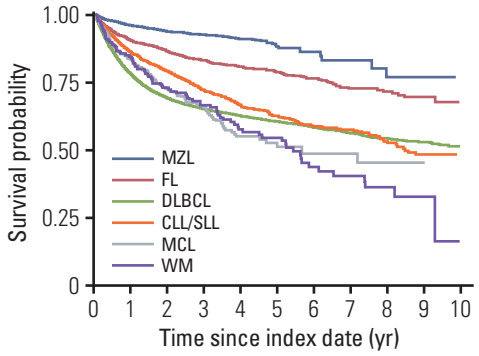

Fig. 4. Overall survival after B-cell non-Hodgkin lymphoma diagnosis index date: follow-up of all patients enrolled from 2006-2015 and death from any cause. MZL, marginal zone lymphoma; FL, follicular lymphoma; DLBCL, diffuse large B-cell lymphoma; CLL/SLL, small lymphocytic lymphoma and chronic lymphocytic; MCL, mantle cell lymphoma; WM, Waldenström's macroglobulinemia or lymphoplasmacytic lymphoma.

incidence of SPM of 5.68% and 11.06%, respectively for patients with FL, and 9.5% and 16.1% for patients with WM [18,19]. Another SEER study reported that 8.2% of patients with MCL developed a SPM, although the median follow-up was only 31 months [20]. The 5- and 10-year cumulative incidences of SPM in patients with DLBCL was 5.41% and 10.47% in California in the post-rituximab era, which was higher than in the years prior to rituximab introduction [21]. At this time, we have no clear view of why SPM may be more frequent in Korean patients with BNHL than elsewhere, although different follow-up periods, study populations, methodologies and possibly treatment regimens are likely to have contributed. Similar data on SPM rates in patients with BNHL from Asian countries are limited, and we cannot confirm whether the rates of SPM observed in our study are reflective of trends present across Asia. Corroborative data from other parts of Asia as well as studies investigating the genetic predispositions associated with BNHL in Asia populations could help inform these findings. In 2015 the age-standardized cancer incidence rate in Korea was 258.9 per 100,000 population, and the lifetime cumulative risk of developing cancer was 35.3% [22]. However, the cumulative lifetime risk of cancer is expected to increase as because the average lifespan of Koreans continues to increase [23].

Consistent with previous reports, the age-standardized incidence rate of BNHL in Korea was substantially lower than those observed in Western countries, although direct comparisons should be made cautiously given that the data were not standardized using the same reference population [2,24]. The incidence of DLBCL was an exception. In Europe, the age-standardized incidence of DLBCL in 2000-2002 was 3.13 per 100,000, which is lower than our 2015 estimate of 3.67 per 100,000 population, the highest incidence yet recorded in

Table 3. Overall survival in patients with different BNHL subtypes (2006-2015)

	1 Year			3 Years			5 Years		
	No. at risk	No. of events	Survival (95% CI)	No. at risk	No. of events	Survival (95% CI)	No. at risk	No. of events	Survival (95% CI)
DLBCL	7,994	2,474	0.78 (0.77-0.79)	4,631	328	0.65 (0.64-0.66)	2,649	110	0.60 (0.59-0.61)
CLL/SLL	984	170	0.86 (0.84-0.88)	588	63	0.72 (0.69-0.75)	324	24	0.62 (0.59-0.66)
FL	1,296	155	0.90 (0.89-0.92)	713	37	0.83 (0.81-0.85)	364	11	0.79 (0.76-0.81)
MCL	302	68	0.83 (0.80-0.87)	132	16	0.66 (0.61-0.71)	35	2	0.53 (0.46-0.60)
MZL	2,821	144	0.96 (0.95-0.97)	1,231	23	0.92 (0.91-0.93)	177	8	0.88 (0.86-0.90)
WM	164	34	0.84 (0.80-0.89)	94	10	0.66 (0.60-0.74)	48	3	0.54 (0.47-0.63)

BNHL, B-cell non-Hodgkin lymphoma; CI, confidence interval; DLBCL, diffuse large B-cell lymphoma; CLL/SLL, chronic lymphocytic and small lymphocytic lymphoma; FL, follicular lymphoma; MCL, mantle cell lymphoma; MZL, marginal zone lymphoma; WM, Waldenström's macroglobulinemia or lymphoplasmacytic lymphoma.

Table 4. Incidence rate of second primary malignancies by BNHL subtype

	Total	Person-years	No. of patients			Incidence rate per 100 person-years (95% CI)		
			At least 1 SPM	Solid tumor	Hematologic malignancy	Total	Solid tumor	Hematologic malignancy[a]
DLBCL	12,067	32,970	736	681	65	2.23 (2.07-2.40)	2.06 (1.91-2.22)	0.19 (0.15-0.24)
CLL/SLL	1,285	4,016	110	73	45	2.74 (2.26-3.29)	1.77 (1.40-2.22)	1.08 (0.80-1.44)
FL	1,726	5,137	101	91	12	1.97 (1.61-2.38)	1.77 (1.43-2.16)	0.23 (0.12-0.38)
MCL	439	948	23	22	1	2.43 (1.57-3.58)	2.32 (1.49-3.45)	0.10 (0.01-0.51)
MZL	3,757	8,458	204	195	9	2.41 (2.10-2.76)	2.30 (2.00-2.64)	0.10 (0.05-0.19)
WM	226	637	9	7	2	1.41 (0.69-2.59)	1.09 (0.47-2.15)	0.31 (0.05-1.01)
Total	19,500	52,166	1,183	1,069	134	2.27 (2.14-2.40)	2.04 (1.92-2.16)	0.25 (0.21-0.29)

BNHL, B-cell non-Hodgkin lymphoma; CI, confidence interval; SPM, second primary malignancy; DLBCL, diffuse large B-cell lymphoma; CLL/SLL, chronic lymphocytic and small lymphocytic lymphoma; FL, follicular lymphoma; MCL, mantle cell lymphoma; MZL, marginal zone lymphoma; WM, Waldenström's macroglobulinemia or lymphoplasmacytic lymphoma. [a]Acute myeloid leukemia (C92), monocytic leukemia (C93), myelodysplastic syndrome (D46), or myeloproliferative neoplasms (D47).

Korea [24]. The European age-standardized incidence was 3.79 per 100,000 for CLL/SLL, and 1.92 per 100,000 for FL, compared with 2015 estimates of 0.27 and 0.63 per 100,000 respectively in Korea. In Canada, the incidence of mature BNHL was 54.0 per 100,000 population in men, and 38.5 per 100,000 in women between 2010-2013 [25], compared to an overall rate of < 7 per 100,000 population during the same years in Korea.

The age-adjusted incidence of BNHL increased by 17% from 2011 to 2015. The increase in incidence was driven by changes in DLBCL, MZL, and FL, which increased by 17%, 40%, and 36%, respectively, over the study period. In parallel, there was a 16% decrease in the incidence of CLL/SLL. The changes in disease incidence appeared to be similar in men and women. Our observations compliment and extend those reported by Lee et al. [2] using data from the Korean Central Cancer Registry and confirm the steady increase in the age-standardized incidence of DLBCL, MZL, and FL in Korea over the last 16 years (Fig. 5). While we cannot exclude that some of the observed increases may be due to improved surveillance or diagnostic methods, marked increases in the incidence of DLBCL and FL have been observed previously in other countries including Canada and the United States [25,26]. Age-standardized mortality rates in patients with BNHL increased in the Korean population over the study period reflecting increases in incidence and prevalence.

The distribution of BNHL subtypes in our study was somewhat different to that reported previously by Yoon et al. [8] from a single large institution in Korea using data from 1989 to 2008. Compared to Yoon et al. [8], we observed higher proportions of patients with CLL/SLL (4.4% to 6.2% vs. 3.7%), FL (8.1% to 9.8% vs. 3.4%) and WM (0.9% to 1.3% vs. 0.5%). Estimates for the other subtypes were within the same range. Differences for some subtypes could reflect the case definition used by Yoon et al. [8] which was laboratory-based with exclusion of patients without pathological material available for review, in contrast to our study that used ICD-10 codes arising from claims data. Additionally, our study covered a later period, from 2006 to 2015, allowing us to include more patients from recent years.

Lee et al. [2], explored the epidemiology of lymphoid malignancies in Korea using data from the Korean Central Cancer Registry between 1999 and 2012. The age-standardized incidence rate of mature BNHL increased significantly (5.6% annually) during the study and was 6.60 per 100,000 in 2012. Significant increases were also observed for MCL (7.1% annual increase), FL (5.1% annual increase), DLBCL (4.0% annual increase), and MZL (18.4% annual increase).

Strengths of our study include the use of a national health insurance database which ensured we captured essentially all cases of BNHL and SPMs diagnosed in Korea during the study years. The 10-year study duration was important for detecting SPM in view of the long latency between BNHL

Table 5. Cumulative incidence (95% CI) for developing a SPM among patients with BNHL subtypes

Year	DLBCL	CLL/SLL	FL	MCL	MZL	WM
1	0.02 (0.02-0.02)	0.02 (0.01-0.03)	0.01 (0.01-0.02)	0.02 (0.00-0.03)	0.02 (0.02-0.02)	0.01 (0.00-0.02)
3	0.08 (0.07-0.08)	0.08 (0.06-0.10)	0.06 (0.04-0.07)	0.10 (0.05-0.14)	0.07 (0.06-0.08)	0.06 (0.01-0.10)
5	0.11 (0.10-0.12)	0.15 (0.12-0.18)	0.09 (0.07-0.11)	0.12 (0.06-0.17)	0.12 (0.10-0.14)	0.07 (0.02-0.13)

CI, confidence interval; SPM, second primary malignancy; BNHL, B-cell non-Hodgkin lymphoma; DLBCL, diffuse large B-cell lymphoma; CLL/SLL, chronic lymphocytic and small lymphocytic lymphoma; FL, follicular lymphoma; MCL, mantle cell lymphoma; MZL, marginal zone lymphoma; WM, Waldenström's macroglobulinemia or lymphoplasmacytic lymphoma.

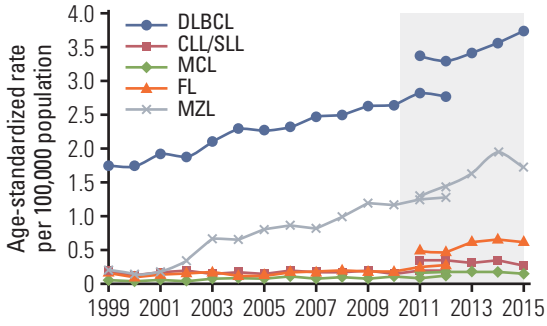

Fig. 5. Age-standardized incidence of B-cell non-Hodgkin lymphoma subtypes as reported fan Central Cancer Registry from 1999-2012 [2] and the National Health Information database from 2011-2015 (shaded). DLBCL, diffuse large B-cell lymphoma; CLL/SLL, small lymphocytic lymphoma and chronic lymphocytic; MCL, mantle cell lymphoma; FL, follicular lymphoma; MZL, marginal zone lymphoma.

diagnosis and the development of SPM. Median latency periods from diagnosis until the development of SPM are approximately 4 years [18,20].

Potential study limitations included the lower accuracy of coding information in the years 2006-2010, which meant that we restricted the cohort analysis of incidence and prevalence to 5 years from 2011. In addition, patients who achieved a cure after appropriate treatment might be included in the calculation of prevalence in this study because we were not able to identify the exact disease status. Therefore, prevalence might be overestimated. The Korean health insurance database does not differentiate between malignancies that are primary or metastatic. By excluding patients with a previous cancer diagnosis, solid tumors diagnosed more than 180 days after the BNHL index date were likely to be SPM. For hematological malignancies it was not possible to distinguish between disease progression/transformation and a new primary hematological cancer. We excluded unspecified acute leukemia, multiple myeloma, and all subtypes of lymphoma to reduce the risk of over-estimating hematological SPM. However, potential overestimation of the incidence of SPM cannot be ruled out. Nevertheless, in view of the different epidemiology of BNHL in Asia compared to Western countries, our findings potentially reflect an important trend of increased SPM in Asia that warrants further investigation.

In conclusion, the incidence of BNHL in Korea continues to increase, driven by increases in MZL, FL, as well as DLBCL. Our findings present new challenges for clinicians managing BNHL. High incidences of SPM in patients with BNHL warrant careful ongoing review of these patients to ensure early diagnosis and treatment. BNHL and the long-term complications associated with survival remain important unmet medical needs in South Korea.

Conflict of Interest

YL, HQ, and LAR are employees of Janssen Research & Development LLC. YL, HQ, and LAR report stock ownership in Johnson & Johnson Pte Ltd. HCK, KHH, and JSK declare no conflicts of interest. Writing assistance was provided by Joanne Wolter (independent on behalf of Johnson & Johnson Pte Ltd). The work was supported by Janssen Research & Development LLC (Titusville, New Jersey, United States).

References

1. Armitage JO, Gascoyne RD, Lunning MA, Cavalli F. Non-Hodgkin lymphoma. Lancet. 2017;390:298-310.
2. Lee H, Park HJ, Park EH, Ju HY, Oh CM, Kong HJ, et al. Nationwide statistical analysis of lymphoid malignancies in Korea. Cancer Res Treat. 2018;50:222-38.
3. Morton LM, Slager SL, Cerhan JR, Wang SS, Vajdic CM, Skibola CF, et al. Etiologic heterogeneity among non-Hodgkin lymphoma subtypes: the InterLymph Non-Hodgkin Lymphoma Subtypes Project. J Natl Cancer Inst Monogr. 2014; 2014:130-44.
4. Feugier P. A review of rituximab, the first anti-CD20 monoclonal antibody used in the treatment of B non-Hodgkin's lymphomas. Future Oncol. 2015;11:1327-42.
5. Pirani M, Marcheselli R, Marcheselli L, Bari A, Federico M,

Sacchi S. Risk for second malignancies in non-Hodgkin's lymphoma survivors: a meta-analysis. Ann Oncol. 2011;22:1845-58.
6. Tward JD, Wendland MM, Shrieve DC, Szabo A, Gaffney DK. The risk of secondary malignancies over 30 years after the treatment of non-Hodgkin lymphoma. Cancer. 2006;107:108-15.
7. Perry AM, Diebold J, Nathwani BN, MacLennan KA, Muller-Hermelink HK, Bast M, et al. Non-Hodgkin lymphoma in the developing world: review of 4539 cases from the International Non-Hodgkin Lymphoma Classification Project. Haematologica. 2016;101:1244-50.
8. Yoon SO, Suh C, Lee DH, Chi HS, Park CJ, Jang SS, et al. Distribution of lymphoid neoplasms in the Republic of Korea: analysis of 5318 cases according to the World Health Organization classification. Am J Hematol. 2010;85:760-4.
9. Chuang SS, Chen SW, Chang ST, Kuo YT. Lymphoma in Taiwan: review of 1347 neoplasms from a single institution according to the 2016 Revision of the World Health Organization Classification. J Formos Med Assoc. 2017;116:620-5.
10. Bassig BA, Cerhan JR, Au WY, Kim HN, Sangrajrang S, Hu W, et al. Genetic susceptibility to diffuse large B-cell lymphoma in a pooled study of three Eastern Asian populations. Eur J Haematol. 2015;95:442-8.
11. Cerhan JR, Slager SL. Familial predisposition and genetic risk factors for lymphoma. Blood. 2015;126:2265-73.
12. Biagi JJ, Seymour JF. Insights into the molecular pathogenesis of follicular lymphoma arising from analysis of geographic variation. Blood. 2002;99:4265-75.
13. Kim JA, Yoon S, Kim LY, Kim DS. Towards actualizing the value potential of Korea Health Insurance Review and Assessment (HIRA) data as a resource for health research: strengths, limitations, applications, and strategies for optimal use of HIRA data. J Korean Med Sci. 2017;32:718-28.
14. Seong SC, Kim YY, Khang YH, Heon Park J, Kang HJ, Lee H, et al. Data resource profile: the National Health Information Database of the National Health Insurance Service in South Korea. Int J Epidemiol. 2017;46:799-800.
15. Moertel CG, Dockerty MB, Baggenstoss AH. Multiple primary malignant neoplasms. I. Introduction and presentation of data. Cancer. 1961;14:221-30.
16. LeMieux MH, Solanki AA, Mahmood U, Chmura SJ, Koshy M. Risk of second malignancies in patients with early-stage classical Hodgkin's lymphoma treated in a modern era. Cancer Med. 2015;4:513-8.
17. Engelhardt M, Ihorst G, Landgren O, Pantic M, Reinhardt H, Waldschmidt J, et al. Large registry analysis to accurately define second malignancy rates and risks in a well-characterized cohort of 744 consecutive multiple myeloma patients followed-up for 25 years. Haematologica. 2015;100:1340-9.
18. Castillo JJ, Gertz MA. Secondary malignancies in patients with multiple myeloma, Waldenstrom macroglobulinemia and monoclonal gammopathy of undetermined significance. Leuk Lymphoma. 2017;58:773-80.
19. Giri S, Bhatt VR, Verma V, Pathak R, Bociek RG, Vose JM, et al. Risk of second primary malignancies in patients with follicular lymphoma: a United States population-based study. Clin Lymphoma Myeloma Leuk. 2017;17:569-74.
20. Shah BK, Khanal A. Second primary malignancies in mantle cell lymphoma: a US population-based study. Anticancer Res. 2015;35:3437-40.
21. Tao L, Clarke CA, Rosenberg AS, Advani RH, Jonas BA, Flowers CR, et al. Subsequent primary malignancies after diffuse large B-cell lymphoma in the modern treatment era. Br J Haematol. 2017;178:72-80.
22. Jung KW, Won YJ, Kong HJ, Lee ES; Community of Population-Based Regional Cancer Registries. Cancer statistics in Korea: incidence, mortality, survival, and prevalence in 2015. Cancer Res Treat. 2018;50:303-16.
23. IACR International Association of Cancer Registries. Korea Central Cancer Registry profile page [Internet]. Lyon: IACR Official Website; 2020 [cited 2018 Nov 1]. Available from: http://www.iacr.com.fr/index.php?option=com_comprofiler&task=userprofile&user=973&Itemid=498.
24. Sant M, Allemani C, Tereanu C, De Angelis R, Capocaccia R, Visser O, et al. Incidence of hematologic malignancies in Europe by morphologic subtype: results of the HAEMACARE project. Blood. 2010;116:3724-34.
25. Ye X, Mahmud S, Skrabek P, Lix L, Johnston JB. Long-term time trends in incidence, survival and mortality of lymphomas by subtype among adults in Manitoba, Canada: a population-based study using cancer registry data. BMJ Open. 2017;7: e015106.
26. Morton LM, Wang SS, Devesa SS, Hartge P, Weisenburger DD, Linet MS. Lymphoma incidence patterns by WHO subtype in the United States, 1992-2001. Blood. 2006;107:265-76.

pISSN 1598-2998, eISSN 2005-9256

Cancer Res Treat. 2020;52(4):1273-1282

https://doi.org/10.4143/crt.2020.032

Original Article

Open Access

Forkhead Box C1 (FOXC1) Expression in Stromal Cells within the Microenvironment of T and NK Cell Lymphomas: Association with Tumor Dormancy and Activation

Ji Hae Nahm, MD, PhD
Woo Ick Yang, MD, PhD
Sun Och Yoon, MD, PhD

Department of Pathology, Severance Hospital, Yonsei University College of Medicine, Seoul, Korea

Correspondence: Sun Och Yoon, MD, PhD
Department of Pathology, Severance Hospital, Yonsei University College of Medicine, 50-1 Yonsei-ro, Seodaemun-gu, Seoul 03722, Korea
Tel: 82-2-2228-1763
Fax: 82-2-362-0860
E-mail: soyoon@yuhs.ac

Received January 13, 2020
Accepted July 3, 2020
Published Online July 3, 2020

Purpose

Forkhead box C1 (FOXC1) is critical for maintaining bone marrow microenvironments during hematopoiesis, but its role in hematological malignancies remains obscure. Here, we investigated whether FOXC1 regulates tumor dormancy and activation in the microenvironments of T and natural killer (NK) cell lymphomas.

Materials and Methods

One hundred and twenty cases of T and NK cell lymphomas were included; the immunohistochemical expression of FOXC1 was investigated in stromal cells, and numbers of FOXC1$^+$ stromal cells were counted. Furthermore, the expression of phosphorylated p38 (p-p38) and phosphorylated ERK1/2 (p-ERK1/2) in tumor cells was investigated using immunohistochemistry.

Results

FOXC1 was variably expressed in C-X-C motif chemokine 12–associated reticular stromal cells, histiocytes, (myo)fibroblasts, and endothelial cells. The phenotypes of cases were categorized as dormant (high p-p38/low p-ERK1/2; n=30, 25.0%), active (high p-ERK1/2/low p-p38; n=25, 20.8%), or intermediate (others; n=65, 54.2%). Lower FOXC1+ stromal cell infiltration was associated with the dormant phenotype, the precursor T lymphoblastic leukemia/lymphoma subtype, and inferior overall survival rates, whereas higher FOXC1$^+$ stromal cell infiltration was associated with the active phenotype and favorable patient prognosis ($p < 0.05$ for all).

Conclusion

These results suggested that FOXC1$^+$ stromal cells within the microenvironments of T and NK cell lymphomas might be related to tumor phenotypes.

Key words

FOXC1, T and NK cell lymphomas, Tumor microenvironment, Stromal cells, Dormancy, p38, ERK

Introduction

The tumor microenvironment plays an important role in tumorigenesis and tumor progression by fostering a cross-talk among tumor cells and several types of stromal cells via various signaling pathways [1]. Recent studies have shown that the tumor microenvironment is involved in regulating tumor dormancy and activation [2,3]. *FOX* genes, encoding transcription factors of a family characterized by the presence of a forkhead box (Fox) DNA-binding domain, play key roles in developmental processes during embryogenesis and tissue differentiation [4,5]. The gene encoding forkhead box C1 (*FOXC1*), located at 6p25, is involved in the pathogenesis of Hodgkin lymphoma, via the deregulation of B-cell differentiation [6]. FOXC1 expression has been studied in epithelial tumor cells, such as those of nasopharyngeal carcinoma, breast cancer, prostate cancer, and melanoma, and it plays a regulatory role in the biological behavior of these tumors [7,8]. A recent study revealed that FOXC1 is preferentially expressed in C-X-C motif chemokine 12 (CXCL12)–associated reticular cells (CAR cells), and might promote CAR cell development, upregulating CXCL12 and stem cell factor expression [9]. CAR cells play essential roles in the tumor microenvironment and are involved in the regulation of hematopoietic stem cells and disseminated tumor cells within the bone marrow, affecting retention in the bone marrow, quiescence, and repopulation [10,11]. This connection between CAR cells and FOXC1 indicates that FOXC1 expression in the tumor micro-

environment is critical and specific for hematopoietic stem cell niche formation and maintenance [12]. Although FOXC1 has a potential role in stromal cells in regulating cell dormancy and activation within the tumor microenvironment, similar to CAR cells, studies on FOXC1 expression in stromal cells within tumor microenvironments of hematological malignancies are limited.

The imbalance in activation of the p38 mitogen-activated protein kinase (MAPK) pathways and extracellular signal regulated kinase (ERK) MAPK pathways plays a key role in the establishment of tumor dormancy and activation. In dormant tumors, phosphorylated p38 MAPK is generally more active than phosphorylated ERK MAPK, and vice versa with respect to tumor activation [2,3]. Studies also show that the p38 and ERK MAPK pathways are involved in normal immature T cell differentiation. Increased p38 MAPK activation blocks T cell differentiation, whereas increased ERK1/ERK2 activation is required for T cell differentiation [13,14].

Here, we hypothesized that FOXC1 might be involved in regulating tumor dormancy and activation within the tumor microenvironments of T cell and natural killer (NK) cell lymphomas, which occur frequently at various extramedullary sites, disseminate regularly into the bone marrow, and are clinically aggressive [15]. In the present study, we investigated the implications of FOXC1 expression in the tumor microenvironments of T and NK cell lymphomas, focusing on tumor dormancy and activation with respect to the p38 MAPK and ERK MAPK pathways.

Materials and Methods

1. Case selection and clinicopathological analysis

In total, 120 cases of T and NK cell lymphomas diagnosed at the Severance Hospital from 1999 to 2013 were selected. Consecutive patients with pathological diagnoses of T and NK cell lymphomas based on biopsied or excised specimens were included in this study. Patients with remaining tissue inadequate to construct tissue microarrays (TMAs) or perform immunohistochemical staining were excluded. The included subtypes were 35 cases of peripheral T cell lymphoma, not otherwise specified (PTCL, NOS), 39 cases of extranodal natural killer/T cell lymphoma (NKTL), 12 cases of angioimmunoblastic T cell lymphoma (AITL), 20 cases of anaplastic large-cell lymphoma (ALCL), anaplastic lymphoma kinase (ALK)-positive, or ALK-negative (ALCL, ALK+, n=10; ALCL, ALK−, n=10) disease, 11 cases of T lymphoblastic leukemia/lymphoma (T-LBL), and three cases of other types. The extramedullary sites were the primary epicenter of all cases. All cases were reviewed and reclassified based on the 2008 and 2017 World Health Organization classification [16,17].

Clinical data including age, sex, primary site, Ann-Arbor stage, International Prognostic Index (IPI) risk score, lactate dehydrogenase (LDH) level, bone marrow involvement, and follow-up data were obtained from electronic medical records, and prognostic implications were analyzed for 120 patients with available clinical data. The mean follow-up period after diagnosis was 14 months (range, 1 to 184 months). The clinicopathological features of the patients are summarized in S1 Table.

2. TMA construction and immunohistochemical evaluation

TMA construction and immunohistochemical staining of TMA blocks were performed following a standard protocol using a Ventana automatic immunostainer (Ventana, Benchmark, Tuscan, AZ) as previously described [18]. The following primary antibodies were used: FOXC1 (1:50, Abcam, Cambridge, UK), CXCL12 (1:50, CXCL12/SDF1, R&D Systems, Minneapolis, MN), phosphorylated p38 (p-p38; 1:100, phospho T180+Y182, Abcam), phosphorylated ERK1 and ERK2 (p-ERK1/2; 1:100, Erk1 [pT202/pY204]+Erk2 [pT185/pY187], Abcam), CD163 (1:100, clone MRQ-26, Cell Marque, Rocklin, CA), CD68 (1:150, clone PG-M1, Dako, Glostrup, Denmark), CD34 (1:50, clone QBEnd 10, Dako), S100 (1:2,000, Dako), and α-smooth muscle actin (1:500, clone 1A4, Dako).

To identify $FOXC1^+$ and $CXCL12^+$ stromal cells, the number of spindled reticular cells with positive immunoexpression in the cytoplasm was counted in at least five fields of the captured microscopic photographs at 400× magnification and the average cell number was obtained. The cutoff for high $FOXC1^+$ stromal cell infiltration was defined as the number of $FOXC1^+$ stromal cells that surpassed the median value of the 120 tested cases. To evaluate p-p38 and p-ERK1/2 immunoexpression in tumor cells, moderate to strongly stained nuclei of tumor cells were counted and divided by the total cell count of the same field. These markers were also counted in at least five high-power fields using photographs and the average proportion was obtained. Protein expression was divided into high and low using median values.

3. Genetic analyses using acute myeloid leukemia cases based on the Cancer Genome Atlas Network data

The mRNA expression levels of *FOXC1*, *p38 MAPKs* (*MAPK11*, *MAPK14*, *MAPK12*, and *MAPK13*), *ERK MAPKs* (*MAPK1/ERK2* and *MAPK3/ERK1*), and *DUSP1* (MAPK phosphatase 1, MKP-1; the regulator of MAPK phosphorylation) were compared using the data on acute myeloid leukemia (AML) in The Cancer Genome Atlas Network (TCGA; https://cancergenome.nih.gov). Comprehensive genetic analyses were performed using cBioPortal; mRNA expression z-scores were calculated relative to diploid samples as select genomic profiles and to *FOXC1*, *MAPK14*, *MAPK11*, *MAPK12*, *MAPK13*, *MAPK1*, *MAPK3*, and *DUSP1* as enter genes (TCGA, PanCancer Atlas; n=165; http://www.cbioportal.

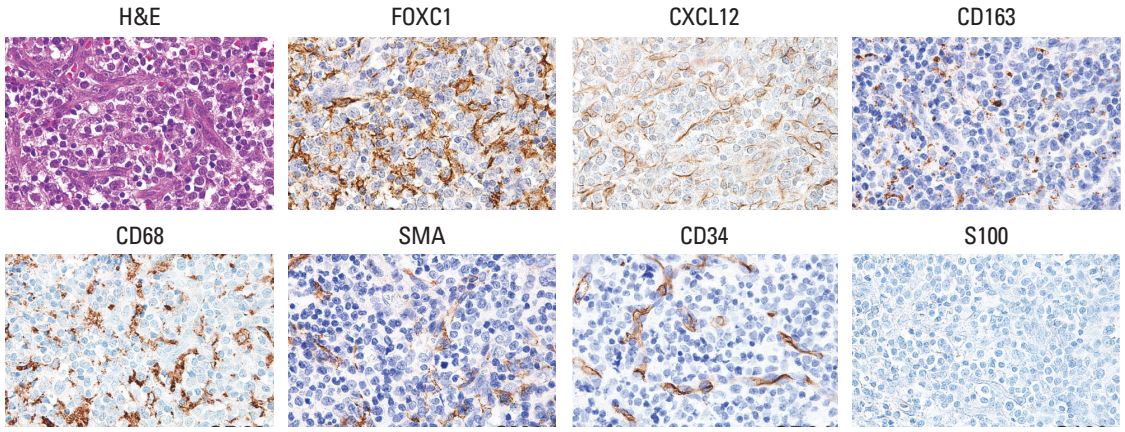

Fig. 1. Representative features of the microenvironments of T and NK cell lymphomas (×400). Hematoxylin and eosin staining, and immunostaining for FOXC1, CXCL12, CD163, CD68 (PG-M1), SMA, CD34, and S100. FOXC1 was expressed in stromal cells, which were morphologically compatible with reticular spindle cells, histiocytes, activated macrophages, (myo)fibroblasts, and endothelial cells. NK, natural killer; FOXC1, forkhead box C1; SMA, smooth muscle actin.

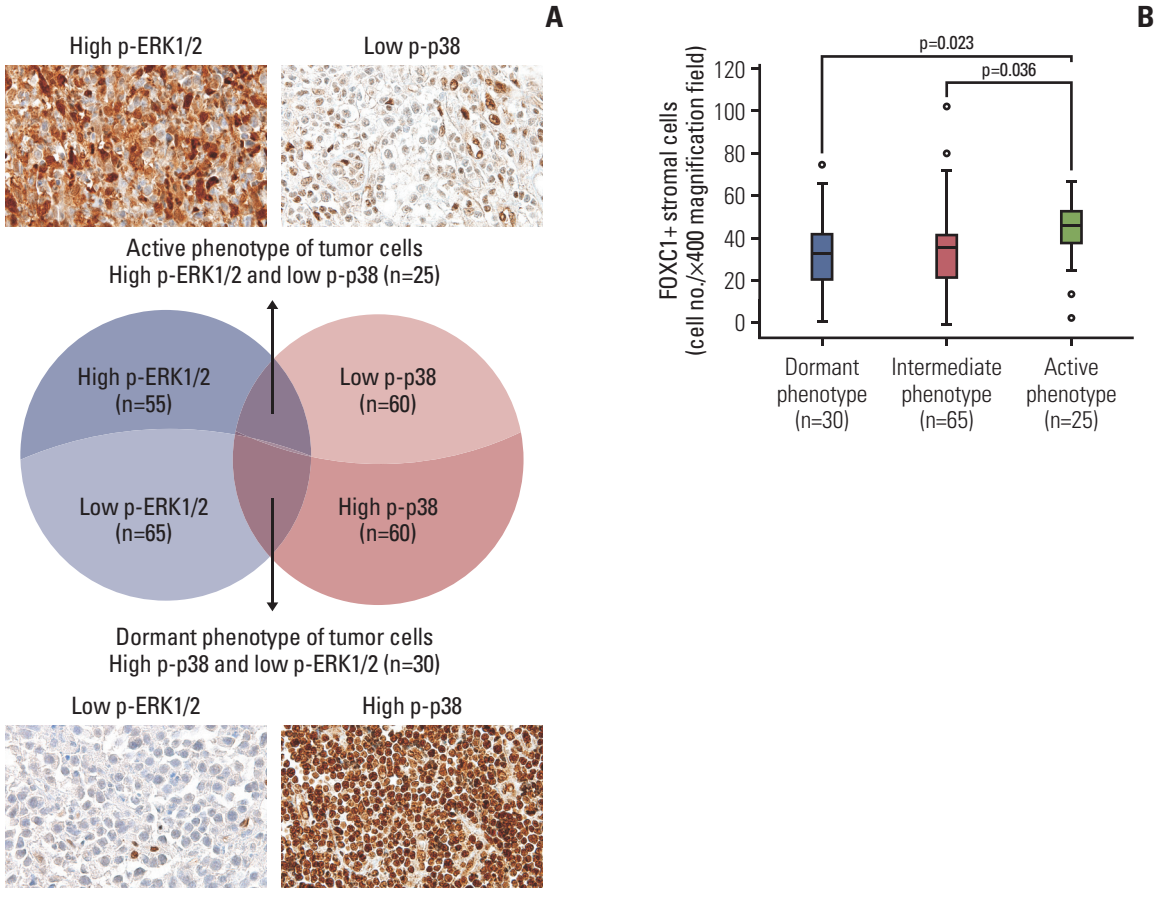

Fig. 2. Phenotypes of tumor cells based on p-p38 and p-ERK1/2 expression. (A) Tumor cells with high p-ERK1/2 and low p-p38 were grouped into an active phenotype (n=25), those with high p-p38 and low p-ERK1/2 were grouped into a dormant phenotype (n=30), and the remaining cases were defined as an intermediate phenotype (n=65). (B) The active phenotype showed significantly higher FOXC1^{+} stromal cell infiltration into the tumor microenvironments than the dormant or intermediate phenotypes. p-p38, phosphorylated p38; p-ERK1/2, phosphorylated ERK1/2; FOXC1, forkhead box C1.

Table 1. Clinicopathological characteristics according to FOXC1+ stromal cell infiltration into the microenvironments of T and NK cell lymphomas (n=120)

Clinical feature	No. (%)	FOXC1+ stromal cell infiltration (number)		FOXC1+ stromal cell infiltration (low and high)		
		Mean±SD	p-value	Low (n=95)	High (n=25)	p-value
Age (yr)						
< 60	78 (65.0)	37.59±19.40	0.354	59 (62.1)	19 (76.0)	0.195
≥ 60	42 (35.0)	34.38±15.09		36 (37.9)	6 (24.0)	
Sex						
Male	86 (71.7)	34.08±16.50	0.020*	71 (74.7)	15 (60.0)	0.146
Female	34 (28.3)	42.50±20.39		24 (25.3)	10 (40.0)	
Subtype						
PTCL, NOS	35 (29.2)	35.17±12.06	0.003*	32 (33.7)	3 (12.0)	0.008*
NKTL	39 (32.5)	42.23±22.53		24 (25.3)	15 (60.0)	
AITL	12 (10.0)	40.42±7.84		10 (10.5)	2 (8.0)	
ALCL, ALK+	10 (8.3)	37.00±20.97		6 (6.3)	4 (16.0)	
ALCL, ALK-	10 (8.3)	35.50±15.53		9 (9.5)	1 (4.0)	
T-LBL	11 (9.2)	16.00±11.82		11 (11.6)	0	
Others	3 (2.5)	37.33±2.31		3 (3.2)	0	
Primary site						
Lymph node	63 (52.5)	34.97±13.18	0.018*	56 (58.9)	7 (28.0)	0.001*
Head and neck	31 (25.8)	45.07±25.12		16 (16.8)	15 (60.0)	
GI tract	8 (6.7)	33.13±9.43		7 (7.4)	1 (4.0)	
Soft tissue and bone	11 (9.2)	27.00±16.32		10 (10.5)	1 (4.0)	
Others	7 (5.8)	30.57±17.60		6 (6.3)	1 (4.0)	
LDH level[a)]						
Normal	33 (39.3)	29.85±15.64	0.013*	28 (42.4)	5 (27.8)	0.259
Elevated	51 (60.7)	40.00±19.08		38 (57.6)	13 (72.2)	
BM involvement[a)]						
Absent	67 (69.8)	36.93±19.27	0.495	53 (66.2)	14 (87.5)	0.136
Present	29 (30.2)	34.17±14.87		27 (33.8)	2 (12.5)	
Ann-Arbor stage[a)]						
I-II	24 (26.7)	32.54±22.87	0.275	18 (25.4)	6 (31.6)	0.586
III-IV	66 (73.3)	37.38±16.63		53 (74.6)	13 (68.4)	
IPI score[a)]						
0-2	55 (60.4)	32.07±19.63	0.016*	44 (61.1)	11 (57.9)	0.799
3-5	36 (39.6)	41.53±15.06		28 (38.9)	8 (42.1)	

Values are presented as number (%) unless otherwise indicated. FOXC1, forkhead box C1; NK, natural killer; SD, standard deviation; PTCL, NOS, peripheral T cell lymphoma, not otherwise specified; NKTL, extranodal natural killer/T cell lymphoma; AITL, angioimmunoblastic T cell lymphoma; ALCL, anaplastic large-cell lymphoma; ALK, anaplastic lymphoma kinase; T-LBL, precursor T lymphoblastic leukemia/lymphoma; GI, gastrointestinal; LDH, lactate dehydrogenase; BM, bone marrow; IPI, International Prognostic Index. *p < 0.05. [a)]For some cases, data were unavailable for the clinicopathological variables. The differences between variables were compared and analyzed for cases for which clinicopathological data were available.

org). These genes were selected based on the information in UniProtKB (https://www.uniprot.org).

4. Statistical analysis

Statistical analyses were performed using SPSS software, ver. 23.0 for Windows (IBM Corp., Armonk, NY). Pearson's chi-square test or Fisher exact test was used to compare differences between variables, and the Spearman coefficient was used for correlation analysis. Patient survival with variables was analyzed using univariate and multivariate Cox proportional hazard models. Overall survival curves were plotted using the Kaplan-Meier method and compared using the log-rank test. All p-values < 0.05 were considered statistically significant.

5. Ethical statement

This study was approved by the Institutional Review Board of Severance Hospital (Seoul, Korea) and the need for

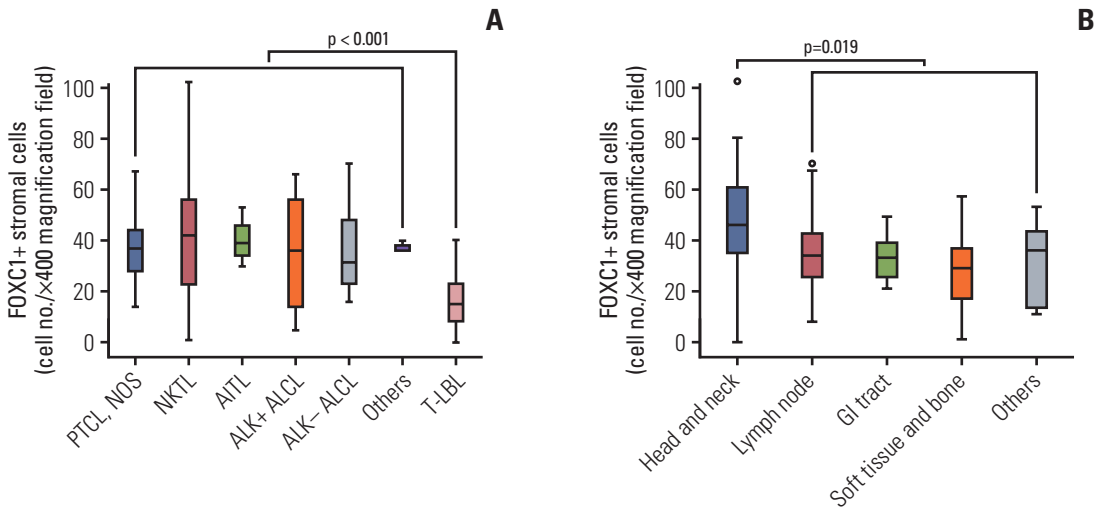

Fig. 3. Number of FOXC1⁺ stromal cells based on T and NK cell tumor subtype and anatomic site/organ of the tumors. (A) Precursor T lymphoblastic leukemia/lymphoma samples had significantly lower numbers of FOXC1⁺ stromal cells than mature T or NK cell lymphoma samples. (B) Head and neck sites were associated with higher FOXC1⁺ stromal cell infiltration than did other sites/organs. FOXC1, forkhead box C1; NK, natural killer; PTCL, NOS, peripheral T cell lymphoma, not otherwise specified; NKTL, extranodal natural killer/T cell lymphoma; AITL, angioimmunoblastic T cell lymphoma; ALK, anaplastic lymphoma kinase; ALCL, anaplastic large-cell lymphoma; T-LBL, precursor T lymphoblastic leukemia/lymphoma; GI, gastrointestinal.

patient consent was waived (4-2015-0954).

Results

1. Association of FOXC1⁺ stromal cells in the tumor microenvironment with tumor dormancy and activation

FOXC1⁺ stromal cells variably expressed CXCL12 (Fig. 1). FOXC1 and CXCL12 expression was not significantly concordant in reticular stromal cells within the microenvironments of T and NK cell lymphomas (r=−0.053, p=0.565) (S2 Fig.). FOXC1 was also expressed in other types of stromal cells, most of which were morphologically similar to reticular spindle cells, histiocytes, activated macrophages, (myo) fibroblasts, and endothelial cells, which express CD163, CD68, α-smooth muscle actin, and CD34. However, only a portion of each cell type expressed FOXC1, and some of these cells did not express FOXC1 (Fig. 1).

Nuclear expression of p-p38 and p-ERK1/2 in tumor cells was individually grouped into high and low based on a cutoff of the median value of the tested lymphoma cases. Tumors were defined as having a dormant phenotype (high p-p38 and low p-ERK1/2; n=30, 25.0%), active phenotype (high p-ERK1/2 and low p-p38; n=25, 20.8%), or intermediate type (both high p-p38 and p-ERK1/2 or both low p-p38 and p-ERK1/2; n=65, 54.2%) (Fig. 2A). Cases with an active phenotype of tumor cells showed significantly more infiltrating FOXC1⁺ stromal cells within the tumor microenvironment than those with dormant or intermediate phenotypes (p=0.023 and p=0.036, respectively) (Fig. 2B).

2. Status of FOXC1⁺ stromal cells in the tumor microenvironment with respect to clinicopathological variables

The status of FOXC1⁺ stromal cell infiltration in the tumor microenvironment according to clinicopathological variables is summarized in Table 1 and Fig. 3. The number of FOXC1⁺ stromal cells that infiltrated into the tumor microenvironment differed significantly according to the T and NK cell tumor subtype (p=0.003) (Table 1). Precursor T-LBL was characterized by significantly low numbers of FOXC1⁺ stromal cells as compared to that in mature T or NK cell lymphomas (p < 0.001) (Fig. 3A). The number of FOXC1⁺ stromal cells also differed significantly according to the anatomic site/organ of the tumors; head and neck sites contained relatively higher numbers of FOXC1⁺ stromal cells than did the remaining sites (p=0.019) (Table 1, Fig. 3B). Increased LDH levels and higher IPI scores (score ≥ 3) were significantly associated with increased numbers of counted FOXC1⁺ stromal cells (p < 0.05 for both); however, such association was not noted when cases were divided into two groups of low and high FOXC1⁺ stromal cell infiltration (Table 1). Bone marrow involvement, Ann-Arbor stage, or age did not correlate significantly with FOXC1⁺ stromal cells within the tumor microenvironment (Table 1).

The clinicopathological features did not show any significant correlation with the dormant, intermediate, or active phenotypes of tumor cells (S3 Table). Although statistical significance was not observed, the active phenotype was rela-

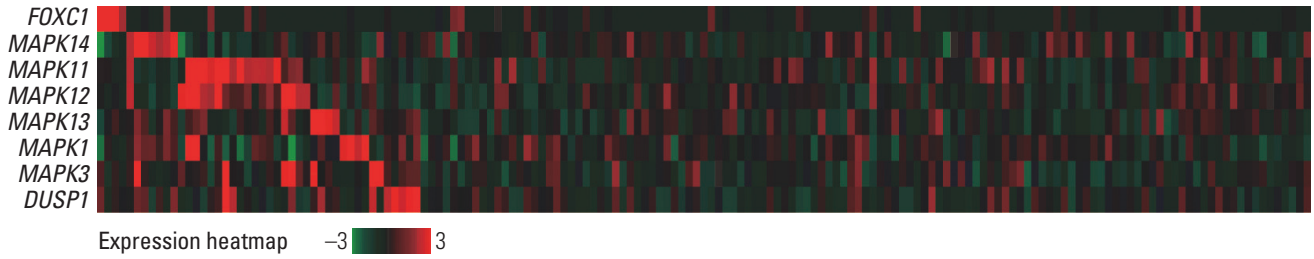

Fig. 4. Comparison of the mRNA levels of *FOXC1*, *p38 MAPKs* (*MAPK11*, *MAPK14*, *MAPK12*, and *MAPK13*), *ERK MAPKs* (*MAPK1*/*ERK2* and *MAPK3*/*ERK1*), and *DUSP1* (MAPK phosphatase 1, MKP-1; regulator of MAPK phosphorylation) in acute myeloid leukemia (The Cancer Genome Atlas Network, PanCancer Atlas; n=165). Note that the expression of p38 MAPKs was not high in cases showing high FOXC1 expression. FOXC1, forkhead box C1; MAPK, mitogen-activated protein kinase.

Table 2. Univariate and multivariate Cox analyses for overall survival of patients with T and NK cell lymphomas

Variable	Univariate analysis			Multivariate analysis		
	HR	95% CI	p-value	HR	95% CI	p-value
Age (≥ 60 yr vs. < 60 yr)	1.8	1.2-2.8	0.007*	-	-	-
Sex (female vs. male)	1.5	0.9-2.3	0.102	-	-	-
Subtype (vs. PTCL, NOS)						
NKTL	0.7	0.4-1.2	0.180	-	-	-
AITL	1.2	0.6-2.4	0.665	-	-	-
ALK+ ALCL	0.1	0.03-0.6	0.008*	-	-	-
ALK– ALCL	2.0	1.0-4.2	0.064	-	-	-
T-LBL	0.9	0.4-1.9	0.754	-	-	-
Others	0.3	0.04-2.4	0.267	-	-	-
Tumor sites (vs. lymph node)						
Head and neck	0.5	0.3-0.9	0.029*	-	-	-
GI tract	1.3	0.6-2.9	0.509	-	-	-
Soft tissue and bone	0.3	0.1-0.8	0.021*	-	-	-
Others	0.8	0.3-2.0	0.633	-	-	-
LDH[a] (elevated vs. normal)	1.3	0.7-2.2	0.375	-	-	-
BM involvement[a] (present vs. absent)	1.1	0.7-1.9	0.646	-	-	-
Ann-Arbor stage[a] (III-IV vs. I-II)	1.9	1.0-3.6	0.049*	-	-	-
IPI score[a] (3-5 vs. 1-2)	3.4	2.0-5.6	< 0.001*	3.5[b]	2.1-6.0	< 0.001*
Phenotype (vs. active phenotype)						
Dormant phenotype	1.1	0.6-2.0	0.812	-	-	-
Intermediate phenotype	0.8	0.4-1.3	0.331	-	-	-
FOXC1$^+$ stromal cells (low vs. high)	2.1	1.1-3.9	0.014*	1.9	1.0-3.8	0.059

NK, natural killer; HR, hazard ratio; CI, confidence interval; PTCL, NOS, peripheral T cell lymphoma, not otherwise specified; NKTL, extranodal natural killer/T cell lymphoma; AITL, angioimmunoblastic T cell lymphoma; ALK, anaplastic lymphoma kinase; ALCL, anaplastic large-cell lymphoma; T-LBL, precursor T lymphoblastic leukemia/lymphoma; GI, gastrointestinal; LDH, lactate dehydrogenase; BM, bone marrow; IPI, International Prognostic Index; FoxC1, forkhead box C1. *p < 0.05. [a]Survival analyses were performed for cases with available survival data and clinicopathological data, [b]In multivariate analysis, age, Ann-Arbor stage, and extranodal tumor sites were not included, as these factors are included in IPI risk scoring.

tively rare in cases of precursor T-LBL (9.1%, 1/11). However, the dormant phenotype was relatively more frequent (45.5%, 5/11) than other subtypes (S3 Table, S4 Fig.).

3. Comparison of *FOXC1*, *p38 MAPK*, and *ERK MAPK* mRNA expression levels in AML cases

Cases with high *FOXC1* mRNA expression were not matched with those with high *p38 MAPKs* (*MAPK11*, *MAPK14*, *MAPK12*, and *MAPK13*) mRNA, *ERK MAPKs* (*MAPK1*/*ERK2*, *MAPK3*/*ERK1*) mRNA or *DUSP1* mRNA expression. The expression of *p38 MAPKs* was not high in cases showing high *FOXC1* expression (Fig. 4).

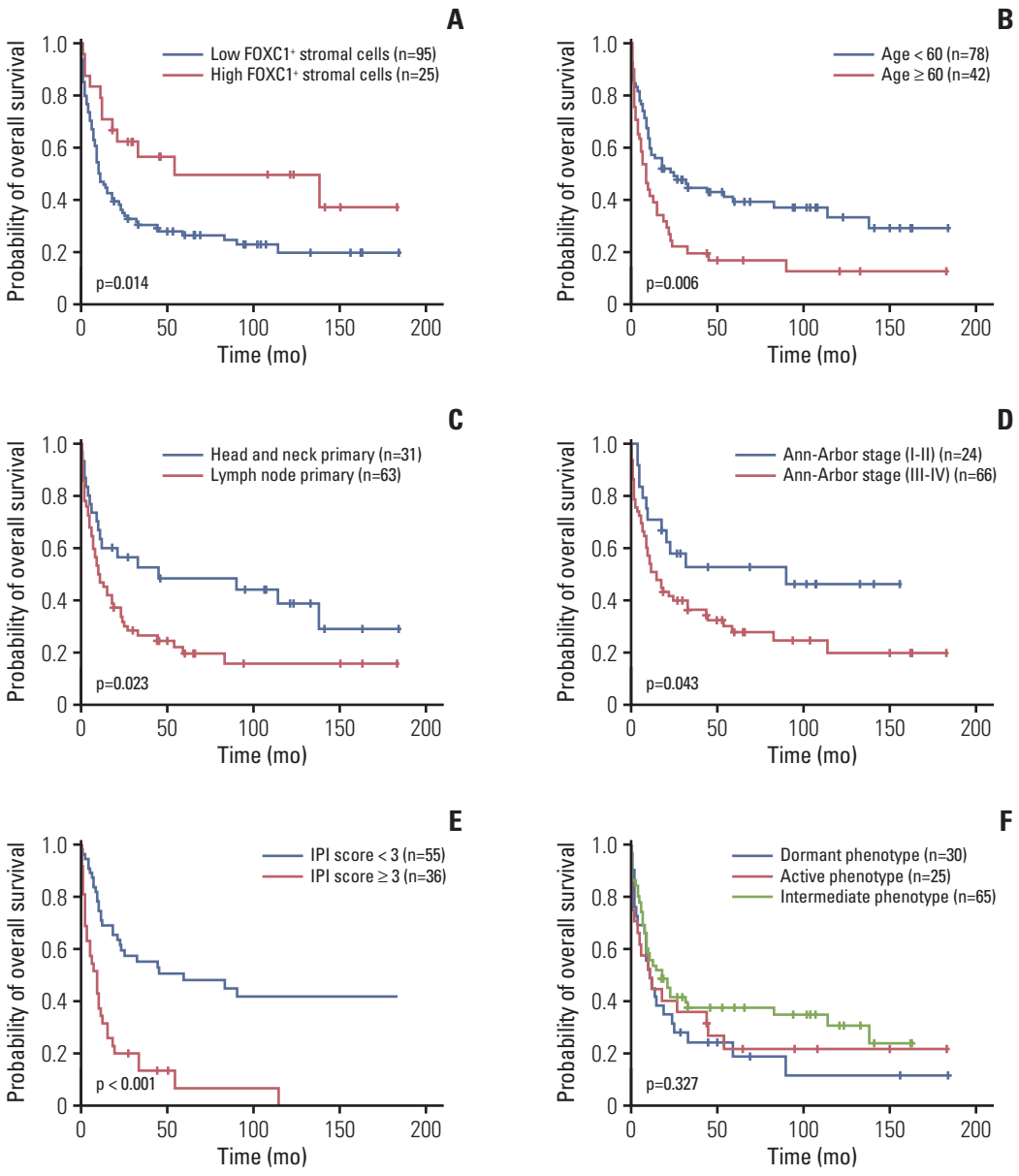

Fig. 5. Kaplan-Meier analyses for overall survival of T and NK cell lymphoma patients. Lower FOXC1+ stromal cell infiltration (A), age > 60 years (B), lymph nodes as the primary tumor site (C), higher Ann-Arbor stage (≥ III) (D), and higher IPI score (≥ 3) (E) were significantly related to poor overall survival. (F) Dormant, active, or intermediate tumor phenotypes showed no significant association with overall survival. Survival analyses were performed for cases with available survival and clinicopathological data. NK, natural killer; FOXC1, forkhead box C1; IPI, International Prognostic Index.

4. Prognostic implications of FOXC1+ stromal cells within the T or NK cell lymphoma microenvironments

The overall survival rates of patients according to the status of FOXC1+ stromal cells, as well as other clinicopathological variables, were evaluated using univariate and multivariate analyses and are summarized in Table 2 and Fig. 5. Low FOXC1+ stromal cell infiltration correlated significantly with a worse overall survival rate (p=0.014) (Table 2, Fig. 5A). In addition, age > 60 years, lymph nodes as tumor sites (vs. head and neck sites), higher Ann-Arbor stage (≥ III), and higher IPI scores (≥ 3) were significantly related to poor overall survival based on univariate analysis (p < 0.05 for all) (Table 2, Fig. 5B-E). However, the tumor phenotypes (dormant, active, or intermediate) were not related to overall survival rates (p=0.327) (Table 2, Fig. 5F). In multivariate analysis, higher IPI scores (≥ 3) were independent prognostic factors for overall survival (p < 0.001) (Table 2). Although not statistically significant, low FOXC1+ stromal cell status

tended to be marginally yet independently related to poor overall survival (p=0.059) (Table 2).

Survival analyses for high and low FOXC1$^+$ infiltrated tumors were performed according to each subtype, PTCL and AITL cases (known to be associated with poor prognosis), and NKTL and ALK+ ALCL cases (with good prognosis) (S5 Fig.). There was no statistically significant association in each subtype. Survival analysis for high and low FOXC1$^+$ stromal cells in all cases except those with tumors arising in the head and neck was performed; low FOXC1$^+$ stromal cell-infiltrated tumors showed significantly poorer survival (p=0.020) (S6 Fig.). According to the primary site, tumors with low FOXC1$^+$ stromal cell infiltration arising in lymph nodes were associated with significantly lower survival (p=0.025) (S7 Fig.). In NKTL cases, tumors arising in lymph nodes were associated with a worse prognosis than those arising in the head and neck ($p < 0.001$) (S8 Fig.). In the univariate and multivariate analyses of subtypes and primary sites, ALK+ ALCL showed a significantly better prognosis (S9 Table).

Discussion

Although the microenvironments of extramedullary hematopoietic disorders have not been studied extensively, the contribution of the tumor microenvironment to the pathogenesis of lymphoid malignancies is being increasingly recognized [19,20]. Based on a recent study showing that FOXC1 is critical for maintaining the bone marrow microenvironment associated with hematopoietic stem cell regulation [9], we hypothesized that it might be involved in the regulation of tumor dormancy and activation in the microenvironments of T and NK cell lymphomas. Here, we investigated the infiltration of FOXC1$^+$ stromal cells within the tumor microenvironment, along with p-ERK1/2 and p-p38 expression in tumor cells.

Unlike previous results showing that FOXC1 expression is the highest in CAR cells within the normal bone marrow microenvironment compared to that in other bone marrow non-hematopoietic cells (with very low levels) [9], various lineages of stromal cells were found to express FOXC1 in this study. We observed that FOXC1 was expressed in stromal cells, most of which were morphologically compatible with reticular spindle cells, fibroblasts, and histiocytes. Some FOXC1$^+$ stromal cells expressed CXCL12, whereas the others did not. This difference might be caused by variations in the microenvironments; extramedullary sites, which are sites of lymphomagenesis, instead of the normal bone marrow microenvironment, were investigated in this study.

To assess the putative role of FOXC1$^+$ stromal cells in regulating tumor dormancy and activation within the tumor microenvironment, we divided tumor phenotypes into active or dormant phenotypes based on phosphorylated p38 and ERK1/2 expression in accordance with previous reports [2,3]. The number of infiltrating FOXC1$^+$ stromal cells was significantly lower in the dormant tumor cells than in active phenotype tumor cells within the microenvironments of T and NK cell lymphomas. This observation was not concordant with the results of a previous study [9]. In that study, FOXC1 was found to be essential for the maintenance of mesenchymal niches for hematopoietic stem cells and progenitor cells within the normal bone marrow [9]. Although our study focused on tumors of T and NK cell lineages in extra-bone marrow sites, these conflicting results require further in-depth investigations.

Evidence supporting either observation is limited as studies on the role of FOXC1 in hematological malignancies are rare. Although recent comprehensive genetic analyses on AML based on TCGA data have not focused on T and NK cell lymphomas or their microenvironments, they might support our observations. We also compared the mRNA expression levels of *FOXC1*, *p38 MAPKs* (*MAPK11*, *MAPK14*, *MAPK12*, and *MAPK13*), *ERK MAPKs* (*MAPK1*/*ERK2*, and *MAPK3*/*ERK1*), and *DUSP1* using the AML data. We noted that the expression of *p38 MAPKs* was not high in cases showing high *FOXC1* expression. A comparison of the mRNA levels of a limited number of genes cannot be used to delineate the overall signaling cascade involving the phosphorylation and activation of the p38 MAPK and ERK MAPK pathways. However, this finding suggests that FOXC1 activation occurs predominantly in non-dormant hematological malignancies.

In addition, patients with precursor T-LBL had fewer FOXC1$^+$ stromal cells than those with mature T and NK cell lymphomas. Moreover, in the precursor T lymphoblastic lymphoma, the active phenotype was relatively rare, whereas the dormant phenotype was relatively more common than other subtypes. Another study showed that imbalances between p38 MAPK and ERK MAPK pathways were associated with the dormancy of acute T lymphoblastic leukemia, the leukemic counterpart of precursor T lymphoblastic lymphoma [21]. Taken together, these observations suggested that the number of FOXC1$^+$ stromal cells might be associated with the tumor status, i.e., an active or dormant phenotype. Further in-depth study is required to understand the mechanisms through which FOXC1 is downregulated in the stromal cells of dormant tumors. Studies show that crosstalk between tumor cells and their microenvironments controls the switch between proliferating and dormant tumor cells, and various signals are involved in this switch [22]. FOXC1 activation or suppression in the tumor microenvironment might be one of the signals involved in the regulation of tumor dormancy or activation, along with the p38 MAPK and ERK MAPK pathway cascades.

In the present study, low infiltration of FOXC1$^+$ stromal cells were associated with a dormant phenotype and poor

outcome for patients with T and NK cell lymphomas. The dormant phenotype is generally considered to be associated with therapy resistance, resulting in treatment failure and disease progression [2,3]. However, this phenotype was not specifically associated with patient prognosis in our series. The reduced infiltration of FOXC1$^+$ stromal cells into the tumor microenvironment appears to be related to the aggressive clinical behavior of T and NK cell lymphomas. Survival could be affected by the behavior of each subtype, but the tendency of low FOXC1$^+$ stromal cell-infiltrated tumors to show poor prognosis was maintained according to the subtypes. This tendency was also maintained according to the primary site, except the head and neck, which included similar numbers of cases of NKTL in both the FOXC1$^+$ low and high groups. NKTL is known to be associated with a good prognosis among T and NK cell lymphomas, but NKTLs arising in the lymph node have a poorer prognosis than those arising in the head and neck, and NKTLs with low FOXC1$^+$ stromal cell-infiltrated tumors showed a similar tendency of poor prognosis. Overall, patient outcome appears to be ultimately determined by a combination of intrinsic factors, such as the dormant or activated status of tumor cells, and extrinsic factors, such as the tumor microenvironment [23]. For T and NK cell lymphomas, FOXC1$^+$ stromal cells in the tumor microenvironment might be an important extrinsic factor determining the biological phenotypes of tumor cells and the clinical risk of patient outcome.

Our study has certain limitations. FOXC1 is a transcription factor, and recent studies have revealed that its expression is preferentially nuclear [9]. In addition, in several studies on carcinomas of epithelial origin, upregulated nuclear expression of FOXC1 was found to be related to proliferation, epithelial-mesenchymal transition, angioinvasion, and poor patient prognosis for basal-like breast carcinoma [24,25], gastric carcinoma [26], non-small cell lung cancer [27], and oral squamous cell carcinoma [28]. However, in our study on T and NK cell lymphoma tissues, FOXC1 was generally expressed in the cytoplasm of stromal cells within the tumor microenvironment, and a reduction in the number of FOXC1$^+$ stromal cells was related to unfavorable patient prognosis. Some studies have shown that FOXC1 is phosphorylated and activated by the ERK1/2 MAPK pathways and that phosphorylated FOXC1 localizes to the nuclei, while the unphosphorylated form remains in the cytosol [29,30]. Although the results of these *in vitro* analyses do not completely support our observations, they might partially explain our results regarding the association between increased FOXC1 expression and the active phenotype characterized by high p-ERK1/2 levels. FOXC1 in the cytosol of stromal cells might be unphosphorylated and could act as a substrate for activated ERK MAPK. The suppression of ERK MAPK in dormant tumors might not necessarily lead to an increase in the levels of unphosphorylated FOXC1 in the cytosol. Actually, a recent study on ovarian serous tumors showed that cytoplasmic FOXC1 expression decreases with higher histological tumor grade, which suggests that cytoplasmic FOXC1 might be unphosphorylated [31]. Our observations cannot explain the function of cytoplasmic FOXC1 in stromal cells within the microenvironments of T and NK cell lymphomas. However, the FOXC1 status in the tumor microenvironment might be indicative of the molecular crosstalk between tumor cells and stromal cells during the regulation of tumor dormancy or activation.

In summary, a decrease in the number of FOXC1$^+$ stromal cells within the microenvironments of T and NK cell lymphomas was found to be associated with the dormant phenotype of tumor cells and poor patient outcome. To the best of our knowledge, this is the first study to provide evidence regarding a putative relationship between FOXC1$^+$ stromal cells and tumor phenotype (dormant or active) in T and NK cell lymphomas. Further investigations are required to elucidate how FOXC1$^+$ stromal cells regulate tumor dormancy or activation within the tumor microenvironment. The modulation of FOXC1 expression in stromal cells within the tumor microenvironment could be utilized as a possible therapeutic strategy to treat aggressive T and NK cell lymphomas, especially with respect to the regulation of tumor dormancy and activation.

Electronic Supplementary Material

Supplementary materials are available at Cancer Research and Treatment website (https://www.e-crt.org).

Conflicts of Interest

Conflicts of interest relevant to this article was not reported.

Acknowledgments

This work was supported by the National Research Foundation of Korea (NRF) grant funded by the Korea government (Ministry of Science and ICT) (No. NRF-2019R1A2C1002370).

References

1. Quail DF, Joyce JA. Microenvironmental regulation of tumor progression and metastasis. Nat Med. 2013;19:1423-37.
2. Yumoto K, Eber MR, Berry JE, Taichman RS, Shiozawa Y. Molecular pathways: niches in metastatic dormancy. Clin Cancer Res. 2014;20:3384-9.
3. Sosa MS, Bragado P, Aguirre-Ghiso JA. Mechanisms of disseminated cancer cell dormancy: an awakening field. Nat Rev Cancer. 2014;14:611-22.

4. Lehmann OJ, Sowden JC, Carlsson P, Jordan T, Bhattacharya SS. Fox's in development and disease. Trends Genet. 2003;19:339-44.
5. Hannenhalli S, Kaestner KH. The evolution of Fox genes and their role in development and disease. Nat Rev Genet. 2009;10:233-40.
6. Nagel S, Meyer C, Kaufmann M, Drexler HG, MacLeod RA. Deregulated FOX genes in Hodgkin lymphoma. Genes Chromosomes Cancer. 2014;53:917-33.
7. Liu J, Shen L, Yao J, Li Y, Wang Y, Chen H, et al. Forkhead box C1 promoter upstream transcript, a novel long non-coding RNA, regulates proliferation and migration in basal-like breast cancer. Mol Med Rep. 2015;11:3155-9.
8. Wang J, Li L, Liu S, Zhao Y, Wang L, Du G. FOXC1 promotes melanoma by activating MST1R/PI3K/AKT. Oncotarget. 2016;7:84375-87.
9. Omatsu Y, Seike M, Sugiyama T, Kume T, Nagasawa T. Foxc1 is a critical regulator of haematopoietic stem/progenitor cell niche formation. Nature. 2014;508:536-40.
10. Sugiyama T, Kohara H, Noda M, Nagasawa T. Maintenance of the hematopoietic stem cell pool by CXCL12-CXCR4 chemokine signaling in bone marrow stromal cell niches. Immunity. 2006;25:977-88.
11. Greenbaum A, Hsu YM, Day RB, Schuettpelz LG, Christopher MJ, Borgerding JN, et al. CXCL12 in early mesenchymal progenitors is required for haematopoietic stem-cell maintenance. Nature. 2013;495:227-30.
12. Omatsu Y, Nagasawa T. The critical and specific transcriptional regulator of the microenvironmental niche for hematopoietic stem and progenitor cells. Curr Opin Hematol. 2015;22:330-6.
13. Diehl NL, Enslen H, Fortner KA, Merritt C, Stetson N, Charland C, et al. Activation of the p38 mitogen-activated protein kinase pathway arrests cell cycle progression and differentiation of immature thymocytes in vivo. J Exp Med. 2000;191:321-34.
14. Crompton T, Gilmour KC, Owen MJ. The MAP kinase pathway controls differentiation from double-negative to double-positive thymocyte. Cell. 1996;86:243-51.
15. Vose J, Armitage J, Weisenburger; International T-Cell Lymphoma Project. International peripheral T-cell and natural killer/T-cell lymphoma study: pathology findings and clinical outcomes. J Clin Oncol. 2008;26:4124-30.
16. Swerdlow SH, Campo E, Harris NL, Jaffe ES, Pileri SA, Stein H, et al. WHO classification of tumours of haematopoietic and lymphoid tissues. 4th ed. Lyon: International Agency for Research on Cancer; 2008.
17. Swerdlow SH, Campo E, Harris NL, Jaffe ES, Pileri SA, Stein H, et al. WHO classification of tumours of haematopoietic and lymphoid tissues. Revised 4th ed. Lyon: International Agency for Research on Cancer; 2017.
18. Kim SH, Yang WI, Min YH, Ko YH, Yoon SO. The role of the polycomb repressive complex pathway in T and NK cell lymphoma: biological and prognostic implications. Tumour Biol. 2016;37:2037-47.
19. Dave SS, Wright G, Tan B, Rosenwald A, Gascoyne RD, Chan WC, et al. Prediction of survival in follicular lymphoma based on molecular features of tumor-infiltrating immune cells. N Engl J Med. 2004;351:2159-69.
20. Lenz G, Wright G, Dave SS, Xiao W, Powell J, Zhao H, et al. Stromal gene signatures in large-B-cell lymphomas. N Engl J Med. 2008;359:2313-23.
21. Masiero M, Minuzzo S, Pusceddu I, Moserle L, Persano L, Agnusdei V, et al. Notch3-mediated regulation of MKP-1 levels promotes survival of T acute lymphoblastic leukemia cells. Leukemia. 2011;25:588-98.
22. Aguirre-Ghiso JA. Models, mechanisms and clinical evidence for cancer dormancy. Nat Rev Cancer. 2007;7:834-46.
23. Kumar V, Abbas AK, Aster JC. Robbins and Cotran pathologic basis of disease. 9th ed. Philadelphia, PA: Elsevier/Saunders; 2015.
24. Ray PS, Bagaria SP, Wang J, Shamonki JM, Ye X, Sim MS, et al. Basal-like breast cancer defined by FOXC1 expression offers superior prognostic value: a retrospective immunohistochemical study. Ann Surg Oncol. 2011;18:3839-47.
25. Yamaguchi H, Hung MC. Regulation and role of EZH2 in cancer. Cancer Res Treat. 2014;46:209-22.
26. Xu Y, Shao QS, Yao HB, Jin Y, Ma YY, Jia LH. Overexpression of FOXC1 correlates with poor prognosis in gastric cancer patients. Histopathology. 2014;64:963-70.
27. Wei LX, Zhou RS, Xu HF, Wang JY, Yuan MH. High expression of FOXC1 is associated with poor clinical outcome in non-small cell lung cancer patients. Tumour Biol. 2013;34:941-6.
28. Liu Z, Xu S, Chu H, Lu Y, Yuan P, Zeng X. Silencing FOXC1 inhibits growth and migration of human oral squamous cell carcinoma cells. Exp Ther Med. 2018;16:3369-76.
29. Berry FB, Saleem RA, Walter MA. FOXC1 transcriptional regulation is mediated by N- and C-terminal activation domains and contains a phosphorylated transcriptional inhibitory domain. J Biol Chem. 2002;277:10292-7.
30. Berry FB, Mirzayans F, Walter MA. Regulation of FOXC1 stability and transcriptional activity by an epidermal growth factor-activated mitogen-activated protein kinase signaling cascade. J Biol Chem. 2006;281:10098-104.
31. Wang LY, Li LS, Yang Z. Correlation of FOXC1 protein with clinicopathological features in serous ovarian tumors. Oncol Lett. 2016;11:933-8.

pISSN 1598-2998, eISSN 2005-9256

Cancer Res Treat. 2020;52(4):1283-1287 https://doi.org/10.4143/crt.2020.002

Case Report Open Access

Seminal Vesicle Involvement by Carcinoma *In Situ* of the Bladder: Clonal Analysis Using Next-Generation Sequencing to Elucidate the Mechanism of Tumor Spread

Hyun Sik Park, MD[1]
Hyun Bin Shin, MD[1]
Myung-Shin Lee, MD, PhD[2]
Joo Heon Kim, MD, PhD[3]
Seon-Young Kim, PhD[4]
Jinsung Park, MD, PhD[1]

[1]*Department of Urology, Eulji University Hospital, Eulji University School of Medicine, Daejeon, Departments of* [2]*Microbiology and Immunology and* [3]*Pathology, Eulji University School of Medicine, Daejeon,* [4]*Personalized Genomic Medicine Research Center, Korea Research Institute of Bioscience & Biotechnology, Daejeon, Korea*

Correspondence: Jinsung Park, MD, PhD
Department of Urology, Eulji University Hospital, Eulji University School of Medicine, 95 Dunsanseo-ro, Seo-gu, Daejeon 35233, Korea
Tel: 82-42-611-3533
Fax: 82-42-259-1111
E-mail: jspark.uro@gmail.com

Received January 2, 2020
Accepted March 17, 2020
Published Online March 19, 2020

We present a rare case of urothelial carcinoma *in situ* (CIS), which invades the prostate and seminal vesicle (SV). A 70-year-old man underwent transurethral resection of bladder (TURB), and the pathologic examination revealed multiple CIS. Although the patient received intravesical bacillus Calmette-Guerin (BCG) therapy following TURB, recurrence of CIS was confirmed in the bladder and left distal ureter at 3 months following BCG. Radical cystectomy was performed due to BCG-refractory CIS. Microscopically, CIS was found throughout the mucosa of the bladder, left ureter, prostatic duct, and both SVs. Next-generation sequencing revealed significant differences in tumor clonality between bladder and SV CIS cells. Among 101 (bladder CIS) and 95 (SV CIS) somatic mutations, only two were shared, and only one gene (*ARHGAP23*) was common exon coding region gene. In conclusion, multicentric genetic changes, in line with the field-cancerization effect, may result in SV involvement by CIS of the bladder.

Key words
Urinary bladder neoplasms, Seminal vesicle involvement, Carcinoma-*in-situ*, High-throughput nucleotide sequencing, Clonality

Introduction

Bladder cancer (BC) is the second most common cancer of the genitourinary tract worldwide [1]. Approximately 75% of patients with BC present with non-muscle invasive BC which is either confined to the mucosa (stage Ta and carcinoma *in situ* [CIS]) or the submucosa (stage T1) [2]. Non-muscle invasive BC is characterized by frequent recurrence, and muscle-invasive BC often metastasizes to regional or distant lymph nodes and distant sites such as the bone, lung, and liver. However, the seminal vesicle (SV) involvement of urothelial carcinoma is uncommon [3-5]. Hypothetically, two distinct patterns have been suggested to explain how primary BC extends to the SVs: One is direct invasion through the bladder wall and perivesical fat, which occurs in most cases, while the other pattern is pagetoid mucosal spread of urothelial carcinoma, which is uncommon [5,6].

Specifically, CIS of the SVs has been previously reported by few studies [5-8], always in association with multifocal CIS of the bladder, prostate, and ureter. Although several possibilities including pagetoid mucosal spread, tumor cell implantation, and *de novo* development of urothelial carcinoma [5,6] have been suggested with regard to the mechanism of the SV involvement by CIS, clonal analysis of the tumor cells has not been analyzed yet. Clonal analysis of the bladder and SV CIS cells may be helpful to elucidate the mechanism by which CIS invades the SV. Next-generation sequencing (NGS) is a technology of DNA sequencing for genomic research, and new knowledge may be obtained by employing NGS in the field of BC [9]. In this study, we present a very rare case of bladder CIS, which did not respond to bacillus Calmette-Guerin (BCG) therapy and invaded the prostatic duct and SV. For the first time, we also report results of tumor clonal analysis from CIS cells of bladder and SV using NGS.

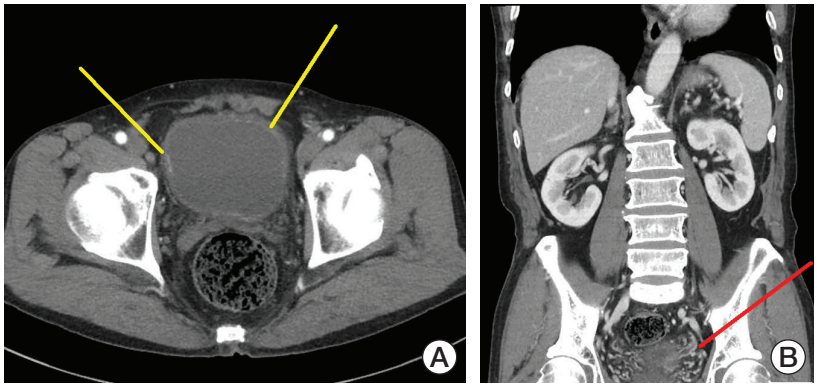

Fig. 1. Computed tomography scan shows multiple enhancing lesion at bladder mucosa (yellow lines) (A) and segmental enhancement of the left distal ureter (red line) (B).

Case Report

1. Case

A 70-year-old man visited the Eulji University Hospital with gross hematuria, with no specific medical history. As diagnostic work-ups for hematuria, cystoscopy showed a wide spread of velvety lesions on posterior bladder wall. The computed tomography (CT) scan revealed focal enhancing lesion at the right lateral and left anterolateral wall of the bladder and segmental enhancement of the left distal ureter (Fig. 1). For pathologic diagnosis of the lesions on bladder and left distal ureter, retrograde-pyelography (RGP), diagnostic ureteroscopy (URS), and transurethral resection of bladder (TURB) were performed. The RGP showed ureterovesical junction narrowing and proximal ureter kinking. No definite mass was observed in the left distal ureter, in diagnostic URS. Therefore, random biopsies were performed in left distal ureter, where segmental enhancement was observed on CT scan. All velvety lesions in the bladder were resected using a bipolar resectoscope. The pathologic findings depicted multifocal urothelial CIS in the bladder and left distal ureter. At postoperative 2 weeks, the patient was treated with 6 weeks of intravesical BCG. At 3 months after TURB, follow-up CT showed enhancing lesions at multiple bladder mucosa and left distal ureter again. The patient underwent diagnostic URS and TURB again. Diagnostic URS showed left distal ureter obstruction with a mass-like lesion, and multiple biopsies of ureter lesion were performed, while TURB was also performed for the newly developed multiple velvety lesions in the bladder. The pathologic findings showed multiple urothelial CIS in the bladder, but no malignancy of ureter. Since the tumor was considered to be BCG-refractory CIS of bladder, the patient underwent robot-assisted radical cystectomy with ileal neobladder. After radical cystectomy, the patient recovered without any specific complications and did not undergo adjuvant chemotherapy. Up to 24 months after cystectomy, there was no evidence of recurrence in follow-up CT scans and urine cytology examinations.

The microscopic findings of cystectomy specimens showed urothelial CIS throughout the mucosa of the bladder, left ureter, prostatic urethra with prostatic ductal extension and multifocal stromal invasion, ejaculatory ducts, and SV (Fig. 2). Tumor cells revealed distinct nuclear membranes and relatively abundant eosinophilic cytoplasm. The nuclei of tumor cells were large, hyperchromatic, markedly pleomorphic and angular with irregular contours, coarse chromatin, prominent nucleoli, and frequent mitoses. The tumor cells showed pagetoid spread into the prostatic acini and ducts, neighboring ejaculatory ducts and the mucosa of the SV. These pagetoid spread were mainly observed between the intact overlying epithelium and underlying basement membrane of prostatic ducts and/or acini and SV, thereby resulting in complete replacement of ducts and acini by tumor cells. In immunohistochemical staining, the tumor cells in the urinary bladder as well as the prostatic ducts and SV were seen to be positive for cytokeratin 20 and p53, but negative for CD44 and prostate-specific antigen.

Whole exome sequencing was performed to analyze the genomic differences between CIS cells of the bladder and SVs. A total amount of 1.0 μg genomic DNA per sample was used as an input material for the DNA library preparation using formalin-fixed, paraffin-embedded samples obtained from bladder and SV lesions under light microscopy by an experienced uro-pathologist (J.H.K.). Blood sample was used as a normal reference for the two tumor samples. Sequencing libraries were generated using the Agilent SureSelect Human All Exon V7 kit (Agilent Technologies, Santa Clara, CA), following the manufacturer's recommendations, and index codes were added to each sample. The average depths for each sequenced data were 109.33 (blood), 136.06 (bladder CIS), and 117.50 (SV CIS), respectively. We used the MuTect [10] to detect somatic single nucleotide variants (SNVs), and the Strelka to detect somatic small insertions and deletions (InDels), and copy number variations (CNVs) in the tumor

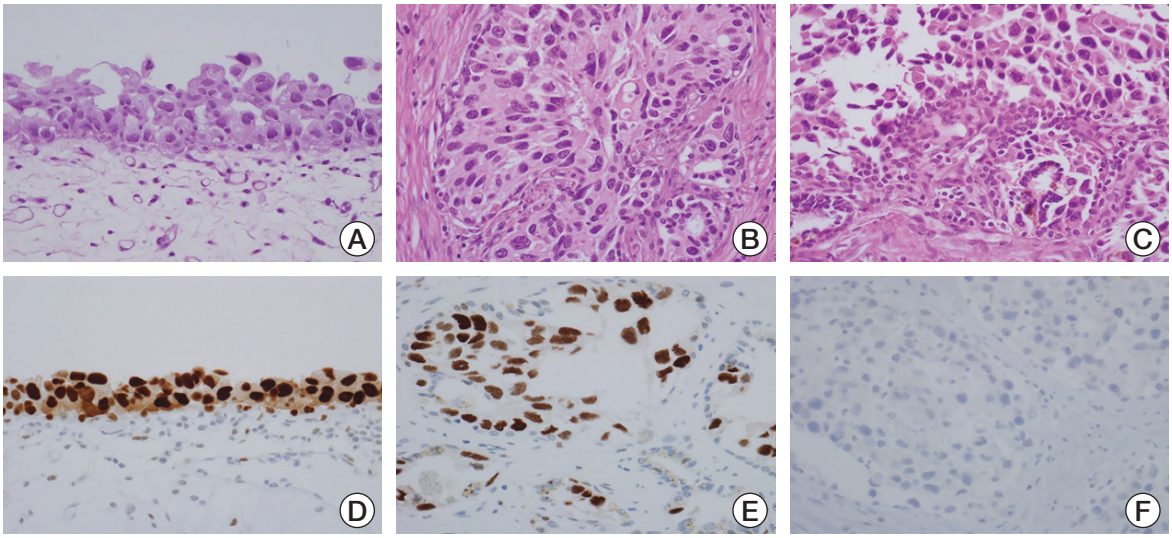

Fig. 2. Microscopic findings of radical cystectomy specimen. (A) Urothelial carcinoma *in situ* (CIS) is observed in the urinary bladder, in which mucosal epithelium is covered by the highly anaplastic tumor cells (H&E staining, ×400). (B) The prostatic acini and ducts are also involved by neoplastic urothelial cells (H&E staining, ×400). (C) The mucosa of the seminal vesicle shows pagetoid spread of the tumor cells (H&E staining, ×400). (D) In the urothelial CIS of the bladder, p53 was highly expressed on the nuclei of tumor cells (×400). (E) p53 was highly expressed in pagetoid spreading tumor cells of the seminal vesicle (×400). (F) Prostate-specific antigen was not expressed in the tumor cells in the ducts of prostate (×400).

Table 1. Common somatic single nucleotide variants which were shared by the bladder and seminal vesicle carcinoma *in situ* lesions

Chromosome	Startp	Endp	Ref_ allele	Var_ allele	VAF of bladder	VAF of seminal vesicle	Category	Gene
11	68549472	68549472	C	T	0.448	0.273	Intronic	CPT1A
17	36636008	36636008	C	T	0.250	0.278	Exonic	ARHGAP23

VAF, variant allele frequency.

samples. SNVs and InDels with variant allele frequency (≥ 0.1) and sequencing read (≥ 10) were used for further analysis. Mutations were defined as genes with a frequency of less than 1% in three human genomic databases such as 1000 Genomes, Exome Aggregation Consortium (ExAC) and exome sequencing project. We also excluded SNVs frequently observed in Korean population by using KRGDB of 1,722 samples (http://coda.nih.go.kr/coda/KRGDB/index.jsp). We found only two common SNVs among 101 SNVs of bladder CIS and 95 SNVs of SV CIS lesions (Table 1). Among the two SNVs which were shared by the bladder and SV tumor cells, only one gene (Rho GTPase activating protein 23 [*ARHGAP23*]) lie in exonic coding region. Notably, we found significant differences in the genomic changes between bladder and SV tumor cells, including the SNVs (S1 and S2 Tables), the InDels (S3 and S4 Tables), and the CNVs (S5 and S6 Tables).

2. Ethical statement

The study protocol was approved by the Institutional Review Board of the Eulji University Hospital (No. 2019-12-011). Written informed consent was obtained from our patient after explaining the present study.

Discussion

Multifocality is an important feature of urothelial carcinoma, frequently occurring in the BC, renal pelvis, and ureter tumors [11]. The concept of "field change" and "a monoclonal origin" has been proposed with regard to the multifocal nature [12,13]. The monoclonal theory suggests that multiple tumors occur from an intraluminal seeding or intra-epithelial migration of single malignant transformed urothelial cells [14]. In contrast, the field change theory describes that exposure of carcinogens may lead to independent genetic change at different sites of the urinary tract [15]. Many previous studies [12-15] were carried out to analyze the clonality of multifocal urothelial carcinoma, but at present there is no consensus whether multifocal lesions have a monoclonal ori-

gin or an independent origin.

Meanwhile, the incidence of SV involvement by urothelial carcinoma is reported to be approximately 3% in radical cystectomy cases [4-6]. However, SV involvement by CIS is very rare [5-8]. Notably, no prior study analyzed the mechanism of the SV involvement, but some previous studies [5-8] have suggested that bladder CIS cells of monoclonal origin spread to SV. For example, two U.S. studies have hypothetically suggested the implantation or intramucosal metastasis of monoclonal tumor cells [5] or intraepithelial (pagetoid) spread of bladder CIS to SV [6] as a mechanism of the SV involvement. Similarly, a Korean study suggested CIS involvement of SV by the pagetoid spread of bladder CIS rather than the de novo development of separate SV CIS, based on microscopic features [8].

In line with the hypothetical mechanism, our pathological findings and immunohistochemical staining results support the notion of pagetoid mucosal extension of bladder CIS to prostatic ducts and SV. However, of note, our whole exome sequencing analyses results indicate that CIS cells of SV were quite distinct from bladder CIS cells in terms of clonality. For example, among somatic SNVs frequently detected in BC, *TP53* (one of tumor suppressor genes) and *KDM6A* (one of most commonly mutated, chromatin-modifying genes in BC) mutations were present in bladder CIS, but absent in SV CIS (S1 and S2 Tables). Meanwhile, *ZDHHC21*, *PGGHG*, and *USP7* mutations, which were reported to be associated with BC, were present in SV CIS only, not in bladder CIS. Notably, only one gene (*ARHGAP23*) was common exon coding region gene, supporting our findings. Thus, in contrast to the circumstantial evidence suggested by previous studies [5,6,8], our results based on direct clonal analysis indicate that multiclonal oncogene activation or loss of tumor suppressor genes may be responsible for the formation of separate CIS lesions in SVs with more or less malignant behavior, depending on the type of genetic change [13]. Interestingly, our NGS analysis showed that majority of somatic variants are non-coding mutations (such as intronic, ncRNA_exonic, ncRNA_intronic, etc.) while clinical significance of those mutations is largely unknown (S1 and S2 Tables). Thus, clinical significance of those mutations needs further investigation with more samples, although SV involvement by CIS of the bladder is extremely rare. Integrating our results, we believe that SV involvement by CIS may not occur by hypothetical pagetoid spread of bladder CIS cells, but independent tumor progression in SVs through field-cancerization effect.

The prognostic significance of the SV involvement by bladder CIS remains unclear due to its infrequency [8]. Although several studies have noted that mucosal spread to SV should be a separate subcategory owing to its better prognosis compared to direct SV invasion [4,5], more cases are needed to define the prognosis of patients with SV involvement by CIS. Meanwhile, a prior study raised the possibility of inadequate pathological sampling as a reason of the uncommon occurrence of SV involvement by BC in surgical pathology laboratories [6]. Thus, the adequate evaluation of SV involvement in radical cystectomy specimens is needed. Importantly, because all reported cases including our study had multifocal CIS in urinary tract (bladder, ureter, prostatic duct, and SV) and our data support multicentric genetic changes in urinary tract, we need to carefully monitor synchronous CIS development in remnant urinary tracts with regular CT scan and urine cytology.

To our knowledge, our study is the first report to analyze the tumor clonality between bladder and SV CIS using NGS to elucidate the mechanism of tumor spread into the SV. Integrating our results, we believe that multicentric genetic changes, in line with the field-cancerization effect, may result in SV involvement by CIS of the bladder. Although, the pagetoid spread of CIS in SV is uncommon, the clinician must be aware of the possibility of SV involvement by CIS, specifically in patients with multifocal CIS lesions. Further studies are needed to determine clinical implications of SV involvement by CIS.

Electronic Supplementary Material

Supplementary materials are available at Cancer Research and Treatment website (https://www.e-crt.org).

Conflicts of Interest

Conflict of interest relevant to this article was not reported.

Acknowledgments

This research was supported by the Basic Science Research Program through the National Research Foundation of Korea (NRF), funded by the Ministry of Education (2019R1I1A3A01060913).

References

1. Global Burden of Disease Cancer Collaboration; Fitzmaurice C, Allen C, Barber RM, Barregard L, Bhutta ZA, et al. Global, regional, and national cancer incidence, mortality, years of life lost, years lived with disability, and disability-adjusted life-years for 32 cancer groups, 1990 to 2015: a systematic analysis for the global burden of disease study. JAMA Oncol. 2017;3: 524-48.
2. Babjuk M, Bohle A, Burger M, Capoun O, Cohen D, Comperat

EM, et al. EAU guidelines on non-muscle-invasive urothelial carcinoma of the bladder: update 2016. Eur Urol. 2017;71:447-61.
3. Daneshmand S, Stein JP, Lesser T, Quek ML, Nichols PW, Miranda G, et al. Prognosis of seminal vesicle involvement by transitional cell carcinoma of the bladder. J Urol. 2004;172:81-4.
4. Volkmer BG, Kufer R, Maier S, Bartsch G Jr, Bach D, Hautmann R, et al. Outcome in patients with seminal vesicle invasion after radical cystectomy. J Urol. 2003;169:1299-302.
5. Montie JE, Wojno K, Klein E, Pearsall C, Levin H. Transitional cell carcinoma in situ of the seminal vesicles: 8 cases with discussion of pathogenesis, and clinical and biological implications. J Urol. 1997;158:1895-8.
6. Ro JY, Ayala AG, el-Naggar A, Wishnow KI. Seminal vesicle involvement by in situ and invasive transitional cell carcinoma of the bladder. Am J Surg Pathol. 1987;11:951-8.
7. Jakse G, Putz A, Hofstadter F. Carcinoma in situ of the bladder extending into the seminal vesicles. J Urol. 1987;137:44-5.
8. Choi SY, Lee HC, Song HG, Kim WJ, Lee OJ. Seminal vesicle involvement by urothelial carcinoma in situ of the bladder with mucosal spread pattern: a case report. Korean J Urol. 2012;53:368-70.
9. Pietzak EJ, Bagrodia A, Cha EK, Drill EN, Iyer G, Isharwal S, et al. Next-generation sequencing of nonmuscle invasive bladder cancer reveals potential biomarkers and rational therapeutic targets. Eur Urol. 2017;72:952-9.
10. Cibulskis K, Lawrence MS, Carter SL, Sivachenko A, Jaffe D, Sougnez C, et al. Sensitive detection of somatic point mutations in impure and heterogeneous cancer samples. Nat Biotechnol. 2013;31:213-9.
11. Kiemeney LA, Witjes JA, Heijbroek RP, Verbeek AL, Debruyne FM. Predictability of recurrent and progressive disease in individual patients with primary superficial bladder cancer. J Urol. 1993;150:60-4.
12. Sidransky D, Frost P, Von Eschenbach A, Oyasu R, Preisinger AC, Vogelstein B. Clonal origin of bladder cancer. N Engl J Med. 1992;326:737-40.
13. Harris AL, Neal DE. Bladder cancer: field versus clonal origin. N Engl J Med. 1992;326:759-61.
14. Habuchi T, Takahashi R, Yamada H, Kakehi Y, Sugiyama T, Yoshida O. Metachronous multifocal development of urothelial cancers by intraluminal seeding. Lancet. 1993;342:1087-8.
15. Jones TD, Wang M, Eble JN, MacLennan GT, Lopez-Beltran A, Zhang S, et al. Molecular evidence supporting field effect in urothelial carcinogenesis. Clin Cancer Res. 2005;11:6512-9.

pISSN 1598-2998, eISSN 2005-9256

Cancer Res Treat. 2020;52(4):1288-1290 https://doi.org/10.4143/crt.2020.278

Case Report Open Access

EGFR C797S as a Resistance Mechanism of Lazertinib in Non-small Cell Lung Cancer with *EGFR* T790M Mutation

Sehhoon Park, MD[1]
Bo Mi Ku, PhD[2]
Hyun Ae Jung, MD, PhD[1]
Jong-Mu Sun, MD, PhD[1]
Jin Seok Ahn, MD, PhD[1]
Se-Hoon Lee, MD, PhD[1]
Keunchil Park, MD, PhD[1]
Myung-Ju Ahn, MD, PhD[1]

[1]*Division of Hematology-Oncology, Department of Medicine,*
[2]*Samsung Biomedical Research Institute, Samsung Medical Center, Sungkyunkwan University School of Medicine, Seoul, Korea*

Correspondence: Myung-Ju Ahn, MD, PhD
Division of Hematology-Oncology, Department of Medicine, Samsung Medical Center, Sungkyunkwan University School of Medicine, 81 Irwon-ro, Gangnam-gu, Seoul 06351, Korea
Tel: 82-2-3410-3438
Fax: 82-2-3410-1754
Email: silkahn@skku.edu

Received April 5, 2020
Accepted June 19, 2020
Published Online June 22, 2020

The non-small cell lung cancer with activating epidermal growth factor receptor (*EGFR*) mutation eventually acquires resistant to either first or second-generation EGFR tyrosine kinase inhibitor (TKI). As the following option, targeting *EGFR* T790M with third-generation EGFR TKI is now established as a standard treatment option. In this study, we are reporting the first case of resistance mechanism to the novel third-generation EGFR TKI, lazertinib, which showed promising clinical efficacy in phase 1-2 study. The patients showed resistance to the treatment by acquiring the additional *EGFR* C797S mutation in cis which is also confirmed from the patient-derived cell lines.

Key words
Non-small cell lung cancer, Lazertinib, Third-generation EGFR tyrosine kinase inhibitor, ErbB receptors

Introduction

Non-small cell lung cancer (NSCLC) with activating epidermal growth factor receptor (*EGFR*) mutation treated with either a first- or second-generation tyrosine kinase inhibitor (TKI) can experience treatment failure, most commonly by acquiring an additional genomic alteration in *EGFR* T790M [1]. Lazertinib (YH25448) is a potent irreversible third-generation EGFR TKI that targets both T790M and activating *EGFR* mutation with high penetration to the blood-brain barrier. Lazertinib showed promising anti-tumor efficacy with a 57% overall response rate and 9.7-month median progression-free survival in *EGFR* T790M-positive patients [2]. However, there is no previous report showing the mechanism of tumor resistance acquisition to lazertinib. In this case report, we conducted deep-targeted sequencing of resistant tumor samples and established patient-derived cell lines (PDC) from a patient treated with lazertinib to elucidate the underlying genomic alteration associated with resistance.

Case Report

A 38-year-old current male smoker presented with stage 4, cT1bN3M1b, NSCLC adenocarcinoma. Informed consent was received under supervision of institutional review board (SMC 2011-10-054-034). The patient was shown to harbor an *EGFR* exon 19 deletion using real-time polymerase chain

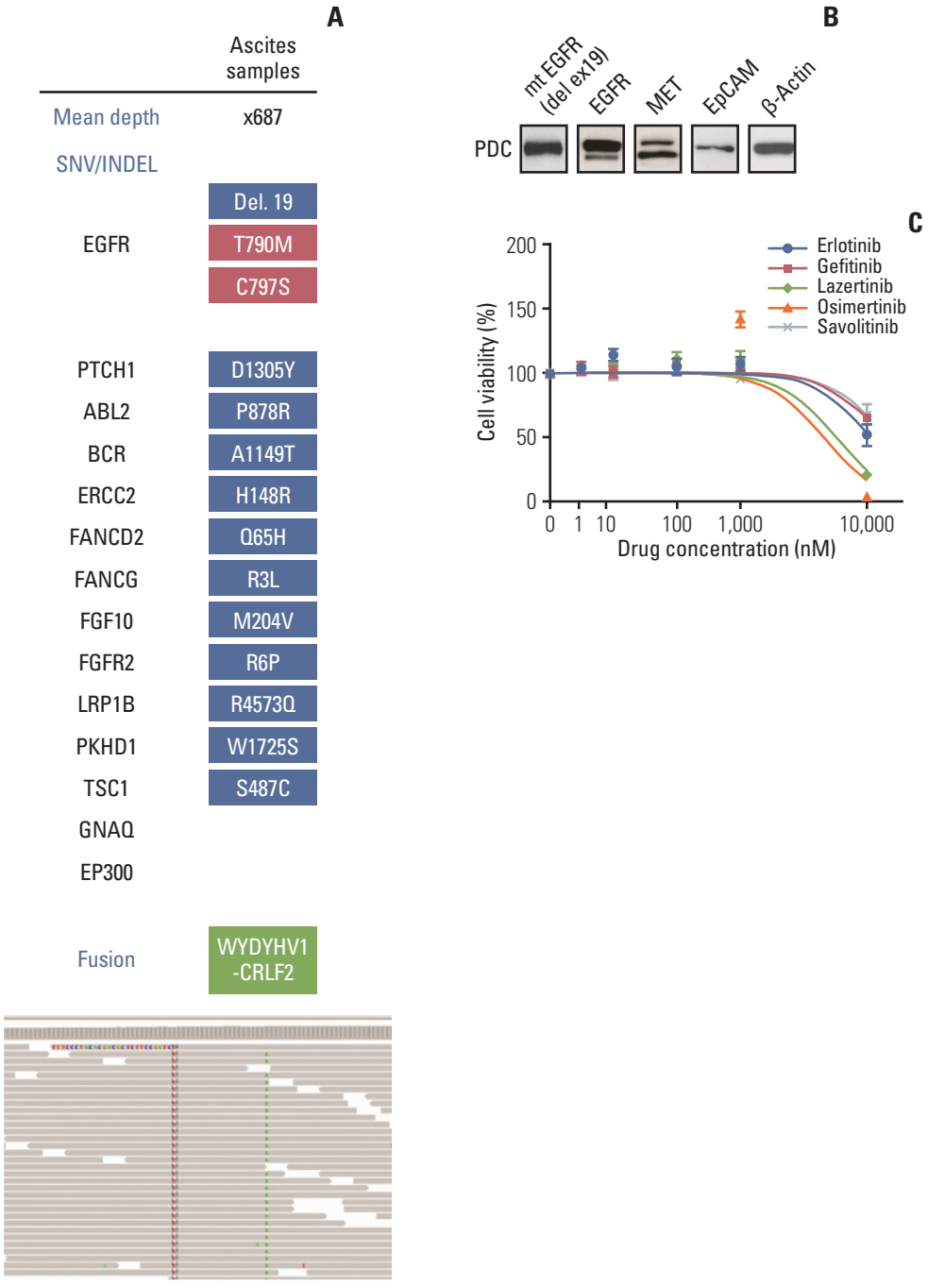

Fig. 1. (A) Target sequencing in samples from lazertinib-resistant malignant ascites. Integrative genomic viewer of sample showing additional epidermal growth factor receptor (*EGFR*) C797S cis mutation. (B) Western blot of patient-derived cell line (PDC) samples. (C) Cell viability analyses conducted in samples after exposure to tyrosine kinase inhibitor for 72 hours. SNV, single nucleotide variant; INDEL, insertion/deletion; EpCAM, epithelial cell adhesion molecule.

reaction from the initial biopsy sample obtained from the mediastinal lymph node. Afatinib was administered as a first-line treatment and showed very good partial response with 7.1 months of progression-free survival. After first-line EGFR TKI failure, a second biopsy from the newly progressed metastatic lymph node showed acquired *EGFR* T790M mutation. As a subsequent treatment, the patient received lazertinib as a part of a clinical trial (NCT03046992, YH25448-201). However, after 6.2 months of partial response to lazertinib, the patient developed malignant ascites, suggesting peritoneal seeding due to resistance.

Deep-targeted sequencing (CancerSCAN [3]) of ascites

samples demonstrated acquired *EGFR* C797S mutation *in cis*, variant allele frequency (VAF) of 9.4%, *EGFR* T790M (VAF of 3.5%), and *EGFR* exon 19 deletion (VAF 9.2%) (Fig. 1A). PDCs established from the same ascites sample showed *EGFR* exon 19 deletion (Fig. 1B). Cell viability of PDCs showed resistance to first- and third-generation EGFR TKIs including erlotinib, gefitinib, lazertinib, and osimertinib or the c-Met inhibitor savolitinib (Fig. 1C).

Discussion

Diverse resistance mechanisms to third-generation EGFR TKI have been reported including loss of T790M, acquisition of *EGFR* C797S mutation, c-Met amplification, activation of other bypass tract, or small cell lung cancer transformation. Among them, *EGFR* C797S/T790M mutation is the most frequently observed, accounting for 20%-30% of cases. It is of note that tumors acquiring an additional mutation of *EGFR* C797X maintain the original *EGFR* T790M mutation [4]. In this report, we present the first clinical case of new *EGFR* C797S/T790M mutation in a patient who failed lazertinib. Further validation with a large number of patients and new treatment strategies to overcome this resistance mutation are warranted.

Conflicts of Interest

Conflict of interest relevant to this article was not reported.

References

1. Sequist LV, Waltman BA, Dias-Santagata D, Digumarthy S, Turke AB, Fidias P, et al. Genotypic and histological evolution of lung cancers acquiring resistance to EGFR inhibitors. Sci Transl Med. 2011;3:75ra26.
2. Ahn MJ, Han JY, Lee KH, Kim SW, Kim DW, Lee YG, et al. Lazertinib in patients with EGFR mutation-positive advanced non-small-cell lung cancer: results from the dose escalation and dose expansion parts of a first-in-human, open-label, multicentre, phase 1-2 study. Lancet Oncol. 2019;20:1681-90.
3. Shin HT, Choi YL, Yun JW, Kim NK, Kim SY, Jeon HJ, et al. Prevalence and detection of low-allele-fraction variants in clinical cancer samples. Nat Commun. 2017;8:1377.
4. Oxnard GR, Hu Y, Mileham KF, Husain H, Costa DB, Tracy P, et al. Assessment of resistance mechanisms and clinical implications in patients with EGFR T790M-positive lung cancer and acquired resistance to osimertinib. JAMA Oncol. 2018;4:1527-34.

pISSN 1598-2998, eISSN 2005-9256

Cancer Res Treat. 2020;52(4):1291-1295 https://doi.org/10.4143/crt.2020.406

Case Report Open Access

Crohn's Disease Following Rituximab Treatment for Follicular Lymphoma in a Patient with Synchronous Gastric Signet Ring Cells Carcinoma: A Case Report and Literature Review

Elisabetta Cavalcanti, PhD[1]
Raffaele Armentano, MD[1]
Ivan Lolli, MD[2]

[1]*Histopathology Unit of National Institute of Gastroenterology "S. de Bellis" and* [2]*Oncology Unit of National Institute of Gastroenterology "S. de Bellis", Research Hospital, Castellana Grotte, Bari, Italy*

Correspondence: Elisabetta Cavalcanti, PhD
Histopathology Unit of National Institute of Gastroenterology "S. de Bellis," Research Hospital, Via Turi 27, 70013 Castellana Grotte (Ba), Italy
Tel: 39-0804994111
Fax: 39-0804994340
E-mail: elisabetta.cavalcanti@irccsdebellis.it

Received April 30, 2020
Accepted July 10, 2020
Published Online July 13, 2020

Recently, there have been a few reports of rituximab (RTX)-induced Crohn's disease, but there is no literature available on successful long-term treatment and the clinical outcome of this condition. We retrospectively analyzed the clinical data of a rare case of Crohn's disease induced by RTX administered as induction and prolonged maintenance therapy of a follicular lymphoma, diagnosed synchronously with a gastric signet ring cells carcinoma, treated at our hospital.

Key words
Rituximab, Crohn's disease, Lymphoma, Gastric signet ring cells carcinoma

Introduction

Crohn's disease is an inflammatory bowel disease (IBD) inducing abdominal pain, severe diarrhea, fatigue, weight loss, and malnutrition. Signs and symptoms of Crohn's disease range from mild to severe, with periods of disease remission. The most common areas affected by Crohn's disease are the last part of the small intestine and the colon but any segment of the gastrointestinal tract may be affected. The pathogenesis is complex, stemming from genetic susceptibility and mucosal immunity dysfunction as a result of B-cell depletion with a regulatory function to control inflammation [1].

Rituximab (RTX) is an IgG1, anti-CD20 chimeric monoclonal antibody that induces a selective transient depletion of peripheral CD20-positive B cells [2]. RTX is part of the standard treatment of patients with B-cell non-Hodgkin's lymphoma (NHL), including follicular lymphoma (FL). The mechanisms of action are not fully clarified. A number of antitumor effects have been suggested, including antibody-dependent cellular cytotoxicity, complement-dependent cytotoxicity, the induction of apoptosis and sensitization of B cells to chemotherapy [3]. RTX is usually well-tolerated but that adverse events can occur, such as severe mucocutaneous reactions, infusional reactions, progressive multifocal leukoencephalopathy, acute respiratory distress syndrome and cardiovascular events. Recently, RTX has also been associated with adverse gastrointestinal effects, including diarrhea and bowel perforation, and recent reports have associated RTX with the development of de novo IBD [4,5].

Gastrointestinal toxicities are uncommon, indeed, only two reports of RTX-induced Crohn's disease have been published in the literature [6,7]. FL is an indolent B-cell lymphoproliferative disorder of transformed follicular center B cells. It is the second most common subtype of NHL diagnosed in Western countries. The neoplastic cells consist of a mixture of centrocytes (small to medium-sized cells) and centroblasts (large cells). The clinical aggressiveness of the tumor increases with increasing numbers of centroblasts [8]. Gastric signet

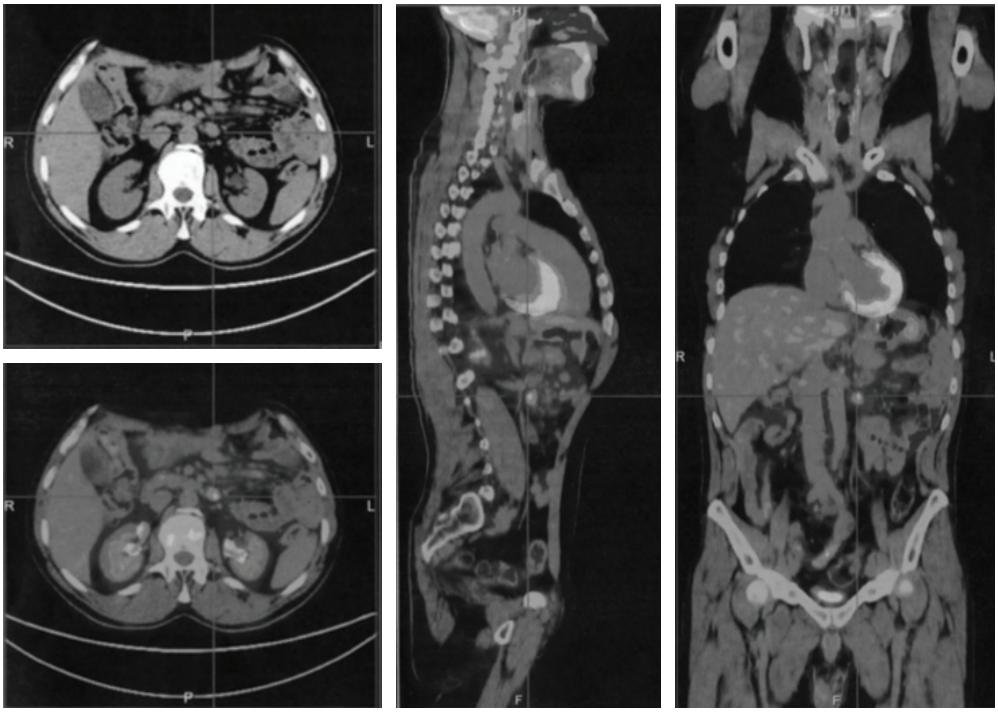

Fig. 1. Positron emission tomography scan showing massive ^{18}F-fluorodeoxyglucose uptake (maximum standardized uptake value, 7) and mesenteric lymph nodes enlargement.

ring cells carcinoma (SRCC) is defined as an adenocarcinoma in which the majority of cells (> 50%) consists of isolated or small groups of malignant non-cohesive cells containing intracytoplasmic mucin. Surgical resection with lymphadenectomy is the treatment of choice for gastric signet ring cell (SRC). To date, there has been no evaluation of the sensitivity of gastric SRCC toward chemotherapeutic drugs [9]. Synchronous FL and gastric SRC adenocarcinoma are extremely rare. Here, we present a case of prolonged RTX maintenance treatment-induced Crohn's disease in a patient with synchronous FL and gastric SRC adenocarcinoma.

Case Report

A 48-year-old male was admitted to our hospital in July 2009 due to upper abdominal pain, nausea, vomiting, and weight loss lasting 4 weeks. The patient had no personal or family medical history of a malignant neoplasm. Gastroscopy revealed an antropyloric neoformation, 3 cm in diameter, and biopsy of the gastric lesion was positive for gastric SRC carcinoma. Computed tomography scan confirmed the gastric tumor and showed a coexistent massive mesenteric abdominal mass, with enlarged para-aortic, aorto-caval, and coeliac axis lymph nodes. A subtotal gastrectomy with D2 lympho-adenectomy and an excisional mesenteric node biopsy were performed. Histologic examination was consistent with two synchronous malignancies: a poorly differentiated intramucosal gastric SRC adenocarcinoma with embolic micrometastases in 2+/19 nodes of the stomach greater curvature (pT1, N1, M0, stage IB), and a follicular NHL (FL), grade 3a (> 15 centroblasts/high-power field and centrocytes present in the sample). Immunohistochemical staining of B FL cells revealed the co-expression of CD20, BCL6, BCL2, and CD79a within the B neoplastic follicles and a Ki-67 index > 20%. Bone marrow biopsy showed sporadic interstitial aggregates of small lymphoid CD20 and CD3 positive elements. After surgery, the patient showed a good recovery and was discharged on postoperative day 9. The surgical procedure was considered appropriate for early-stage I-B gastric cancer so no adjuvant chemotherapy was administered. However, a systemic chemotherapeutic regimen was selected for the FL bulky disease. The patient received seven cycles of a chemotherapy regimen including, on day 1: cyclophosphamide 750 mg/m^2, doxorubicin 50 mg/m^2, and vincristine 1.4 mg/m^2, and on days 1-5: prednisone 100 mg (CHOP regimen).The treatment was well-tolerated and induced a complete response. Two years later, a positron emission tomography (PET) scan showed disease recurrence, with mesenteric lymph nodes enlargement and increased ^{18}F-fluorodeoxyglucose uptake (maximum standardized uptake value, 7) (Fig. 1). The patient was treated with eight cycles of R-CNOP (day 1: RTX 375 mg/m^2; day 2: cyclophosphamide 750 mg/m^2, mitoxantrone 10 mg/m^2, vincristine 2 mg; days 2-6: pre-

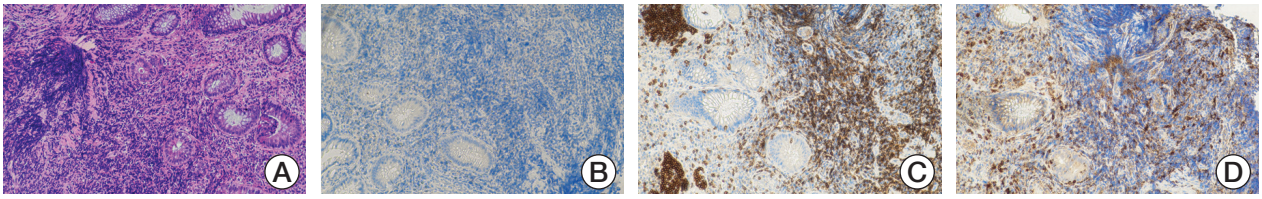

Fig. 2. (A) Active-chronic inflammation with ulceration, crypt abscess formation and goblet cell depletion (H&E staining, ×5), (B) After rituximab therapy, CD20 cells staining was negative. (C) Immunohistochemistry with an anti-CD3 antibody demonstrated numerous intraepithelial mucosal T cells after therapy. (D) High tonaca propria and intraepithelial infiltration of macrophages ($CD68^+$) (B-D, ×10).

dnisone 100 mg). He achieved complete remission and in February 2013 he began maintenance therapy with RTX (MR), at a dose of 375 mg/m^2 every 3 months. After eight MR cycles the patient suffered a 2-month period of watery diarrhea with a frequency of 3-4 times a day, of mushy stool that occasionally contained mucus, together with periumbilical and right abdominal pain. A surveillance PET scan, performed at that time, showed an increased activity in the terminal ilium (TI) and mesenteric lymphadenopathy. An ileo-colonoscopy revealed no significant abnormality in the colon mucosa, but macroscopic inflammatory changes in the TI including an erythematous mucosa and aphthous erosions covered with fibrin. Biopsy demonstrated active non-specific ileitis. Treatment with 5-aminosalicylates (5-ASA) induced a prompt relief of symptoms. He was treated with another six cycles of RTX for a presumed recurrence of the lymphoma. A follow-up computed tomography enterography, performed 6 months later, showed resolution of the mesenteric adenopathy but the presence of a modest hyperenhanced bowel wall thickening in the terminal ileum. In September 2017, two months after the last cycle of RTX, the patient's clinical conditions worsened. He developed bloody diarrhea, cramping abdominal pain, anemia and weight loss. Endoscopic evaluation showed a transmural involvement of the TI by an inflammatory process, with mucosal damage, deep ulceration, and edema. Histological examination revealed goblet cell depletion and active-chronic inflammation with crypt abscess formation (Fig. 2A); the lamina propria was occupied by granulation tissue with dilated, inflamed capillaries. Immunohistochemistry analysis showed a total depletion of the CD20 positive B cells in the ileal mucosa (Fig. 2B), an increased cellularity of $CD3^+$ T lymphocytes in the tonaca propria and intraepithelial mucosa (Fig. 2C) and moderate excess of enlarged macrophages ($CD68^+$), exclusively in the lamina propria (Fig. 2D), suggesting exacerbation of the Crohn's disease. Pathological features were in keeping with active Crohn's disease.

RTX therapy was interrupted. He was treated with budesonide and 5-ASA, and responded well. After 10 weeks the patient was asymptomatic and an endoscopic control showed slight signs of inflammation of the TI. A follow-up PET scan was negative for activity in the TI. He has remained in remission for 30 months without any adverse events. At present he is taking 5-ASA as maintenance therapy and the clinical conditions have clearly improved.

Written informed consent was obtained from the patient prior to publication of this case report and all procedures performed were in accordance with the ethical standards of the institutional research committee (IRCCS Giovanni Paolo II, Bari, Italy).

Discussion

Synchronous gastric SRC and abdominal FL is rare and there is no standard treatment strategy for patient management. A number of factors such as age, performance status, pathological features and tumor staging must be taken into consideration during decision making, in terms of which cancer to treat first and what is the optimal therapy. In our case, the patient underwent a combination of treatments, including surgical excision and chemotherapy. Subtotal gastrectomy with D2 lymphadenectomy was considered appropriate for the early-stage I-B gastric SRC treatment, while a systemic chemotherapeutic regimen was selected based on the FL bulky disease. FL is the second most common form of NHL [10]. Management is characterized by a risk-adapted therapy based on the stage of the disease and the patient's symptoms. For patients with a high tumor burden, the standard treatment option is immuno-chemotherapy. The addition of the anti-CD20 monoclonal antibody RTX to chemotherapy has yielded a higher rate of complete remission and improved survival. In addition, RTX as maintenance therapy after the induction regimen improves progression-free survival in high-tumor burden patients [11]. The use of B-cell depletion therapy with RTX has shown some success in the treatment of autoimmune diseases such as rheumatoid arthritis, by reducing the adaptive immune response against self. The elimination of B cells to treat autoimmunity also has a disadvantageous side, as it results in the depletion of regulatory B cells (B-regs) that suppress inflammation [12]. Some adverse events have been reported after RTX therapy, such as cutaneous reactions, cardiomyopathies, interstitial pneumonia, infections, and progressive multifocal leukoencephalopathy.

Table 1. Review of cases of RTX and Crohn's disease

Study	Year	No. of cases	Age (yr)	Sex	Type of colitis	Indication for RTX	Presenting gastrointestinal symptoms	Treatment with RTX (mo)
Varma et al. [6]	2017	2	80 74	F M	Crohn's disease	Lymphoma	Diarrhea, abdominal pain, weight loss, fever	Three-monthly maintenance rituximab over 2-year period
Morita et al. [7]	2019	1	15	M	Crohn's disease	Refractory nephrotic syndrome	Abdominal pain, localized in the area of the umbilicus watery stools	Over a 2-year period, the patient received four doses of RTX
Present case	2020	1	59	M	Crohn's disease	Follicular B-cell non-Hodgkin lymphoma	Watery diarrhea, abdominal pain, anemia, weight loss and dilated cardiomyopathy	Three-monthly maintenance rituximab over 4 and half years period

RTX, rituximab.

Recently, Eckmann et al. [13] described patients with RTX-associated *de novo* colitis, raising the hypothesis that B cells may play a protective role of the intestinal mucosa. There are only a few reports in the literature of the induction or exacerbation of IBD by RTX. In a patient with refractory ulcerative colitis (UC), Goetz et al. [14] reported that RTX exacerbated the disease by locking interleukin 10 (IL-10) producing B cells, suggesting an important anti-inflammatory rather than proinflammatory role of B cells in UC. To our knowledge, only three case of RTX-induced Crohn's disease have been previously reported in the literature (Table 1): two cases in elderly patients treated with 3-month MR over a 2-year period and one case of a 15-year-old boy with refractory nephrotic syndrome receiving 4 doses of RTX over a 2-year period. Compared with the cases reported previously, our patient was treated with a three-monthly MR for a longer period, fourteen doses in four and half years. At the time, the increased uptake at the mesenteric lymph nodes and at TI level, detected by the PET scan performed after eight MR cycles, suggested lymphoma recurrence and the incorrect assessment induced to continue treatment with RTX whereas, most likely, the finding was correlated with a Crohn's disease in initial phase, a rare and unexpecteted complicance. In particular this case demonstrates the importance of being alert to the possibility of Crohn's disease in presence of abdominal pain, weight loss, and diarrhea during RTX treatment. In the present report, the histopathological and immunohistochemical analysis suggests that exacerbation of Crohn's disease may be related to the total depletion of CD20 positive B cells in the intestinal mucosa and high tonaca propria and intraepithelial infiltration of the T cells ($CD3^+$) and macrophages ($CD68^+$). B and T cells have been involved in the pathogenesis of IBD. It has been suggested that B cells may not have a proinflammatory role in IBD; indeed, they may have a protective effect, reducing inflammation by producing the anti-inflammatory cytokine IL-10. Most studies performed in IBD experimental models suggest that B-regs suppress mucosal inflammation, either by secreting cytokines such as IL-10 or by interacting with T cells. Inhibition of B–T cell interaction caused by B-cell depletion may lead to T-regulatory cell dysfunction, and the subsequent activation of Th1 and Th17 cells. As a consequence, Crohn's disease could develop due to a dysregulated mucosal immune response [15]. This immune dysregulation of the gastrointestinal tract may potentially lead to Crohn's disease as a secondary complication in susceptible RTX patients. Nevertheless, the fact remains that RTX is an effective treatment for B-cell lymphoma.

In this case, we propose that Crohn's disease was caused by an abnormal dysfunction of mucosal immunity that resulted in a disturbed intestinal balance secondary to the use of RTX. Therefore, inflammatory bowel disease should be considered if severe abdominal symptoms with weight

loss are observed following RTX administration.

Conflicts of Interest

Conflict of interest relevant to this article was not reported.

Acknowledgments

This study has been supported by Ricerca corrente 2019.

References

1. Torres J, Mehandru S, Colombel JF, Peyrin-Biroulet L. Crohn's disease. Lancet. 2017;389:1741-55.
2. Edwards JC, Cambridge G. Sustained improvement in rheumatoid arthritis following a protocol designed to deplete B lymphocytes. Rheumatology (Oxford). 2001;40:205-11.
3. Pierpont TM, Limper CB, Richards KL. Past, present, and future of rituximab: the world's first oncology monoclonal antibody therapy. Front Oncol. 2018;8:163.
4. Barreiro Alonso E, Alvarez Alvarez A, Tojo Gonzalez R, de la Coba Ortiz C. Rituximab-associated colitis. Gastroenterol Hepatol. 2019;42:251-2.
5. Mallepally N, Abu-Sbeih H, Ahmed O, Chen E, Shafi MA, Neelapu SS, et al. Clinical features of rituximab-associated gastrointestinal toxicities. Am J Clin Oncol. 2019;42:539-45.
6. Varma P, Falconer J, Aga A, Prince HM, Pianko S. Rituximab-induced Crohn's disease. Scand J Gastroenterol. 2017;52:606-8.
7. Morita K, Shibano T, Maekawa K, Hattori M, Hida N, Nakamura S, et al. Crohn's disease following rituximab treatment in a patient with refractory nephrotic syndrome. CEN Case Rep. 2019;8:55-60.
8. Swerdlow SH, Campo E, Pileri SA, Harris NL, Stein H, Siebert R, et al. The 2016 revision of the World Health Organization classification of lymphoid neoplasms. Blood. 2016;127:2375-90.
9. Machlowska J, Puculek M, Sitarz M, Terlecki P, Maciejewski R, Sitarz R. State of the art for gastric signet ring cell carcinoma: from classification, prognosis, and genomic characteristics to specified treatments. Cancer Manag Res. 2019;11:2151-61.
10. Dada R. Diagnosis and management of follicular lymphoma: a comprehensive review. Eur J Haematol. 2019;103:152-63.
11. Buske C, Hutchings M, Ladetto M, Goede V, Mey U, Soubeyran P, et al. ESMO Consensus Conference on malignant lymphoma: general perspectives and recommendations for the clinical management of the elderly patient with malignant lymphoma. Ann Oncol. 2018;29:544-62.
12. Mauri C, Menon M. Human regulatory B cells in health and disease: therapeutic potential. J Clin Invest. 2017;127:772-9.
13. Eckmann JD, Chedid V, Quinn KP, Bonthu N, Nehra V, Raffals LE. De novo colitis associated with rituximab in 21 patients at a tertiary center. Clin Gastroenterol Hepatol. 2020;18:252-3.
14. Goetz M, Atreya R, Ghalibafian M, Galle PR, Neurath MF. Exacerbation of ulcerative colitis after rituximab salvage therapy. Inflamm Bowel Dis. 2007;13:1365-8.
15. Xu XR, Liu CQ, Feng BS, Liu ZJ. Dysregulation of mucosal immune response in pathogenesis of inflammatory bowel disease. World J Gastroenterol. 2014;20:3255-64.

Tables of Contents

(Vol. 52, No. 1~4, 2020)

Volume 52, Number 1, January 2020

Original Articles

Retraction

Volume 52, Number 2, April 2020

Special Articles

Original Articles

Volume 52, Number 3, July 2020

Special Article

Original Articles

Case Report

Volume 52, Number 4, October 2020

Original Articles

Acknowledgment of Reviewers (2020)

We, the editors of Cancer Research Treatment (CRT), have strived toward the goal to make CRT a high quality journal. It could not be achieved without the peer reviewers' unselfish contribution of their valueless time and effort. Their thorough insights and constructive critiques have helped to maintain high standard of research articles published in CRT.

We owe a lot to the following peer reviewers during 2019 and 2020 and acknowledge their enormous contribution with our most heartfelt appreciation.

Ahn, G-One	*Seoul National Univ. College of Veterinary Medicine, Korea*
Ahn, Hee Kyung	*Gachon Univ. Gil Medical Center, Korea*
Ahn, Hyong Gin	*Korea Univ. College of Medicine, Korea*
Ahn, Joong-Bae	*Yonsei Univ. College of Medicine, Korea*
Ahn, Myung Ju	*Sungkyunkwan Univ. School of Medicine, Korea*
Ahn, Soomin	*Seoul National Univ. Bundang Hospital, Korea*
Ahn, Soyeon	*Seoul National Univ. Bundang Hospital, Korea*
Ahn, Yong Chan	*Sungkyunkwan Univ. School of Medicine, Korea*
Bae, Jeong Mo	*Seoul National Univ. College of Medicine, Korea*
Bae, Jong-Myon	*Jeju National Univ. College of Medicine, Korea*
Baek, Sun Kyung	*Kyung Hee Univ. Medical Center, Korea*
Beom, Seung-Hoon	*Yonsei Univ. College of Medicine, Korea*
Chang, Heung Moon	*Univ. of Ulsan College of Medicine, Korea*
Chang, Hyun	*Catholic Kwandong Univ. Int'l St. Mary Hospital, Korea*
Cheong, Jae Ho	*Yonsei Univ. College of Medicine, Korea*
Cheuh, Heewon	*Dong-A Univ. College of Medicine, Korea*
Chie, Eui Kyu	*Seoul National Univ. College of Medicine, Korea*
Cho, Deog-Gon	*The Catholic Univ. of Korea, College of Medicine, Korea*
Cho, Jae Yong	*Yonsei Univ. College of Medicine, Korea*
Cho, Jae-Young	*Seoul National Univ. Bundang Hospital, Korea*
Cho, Sang Hee	*Chonnam National Univ. Medical School, Korea*
Cho, Soo Youn	*Sungkyunkwan Univ. School of Medicine, Korea*
Cho, Yong Mee	*Univ. of Ulsan College of Medicine, Korea*
Choi, Chul Won	*Korea Univ. College of Medicine, Korea*
Choi, Hyoung Soo	*Seoul National Univ. Bundang Hospital, Korea*
Choi, Jin Hyuk	*Ajou Univ. School of Medicine, Korea*
Choi, Jin Young	*Yonsei Univ. College of Medicine, Korea*
Choi, Ji-Yeob	*Seoul National Univ. College of Medicine, Korea*
Choi, Joon Hyuk	*Yeungnam Univ. Medical Center, Korea*
Choi, Joon Young	*Sungkyunkwan Univ. School of Medicine, Korea*
Choi, Kui Son	*National Cancer Center, Korea*
Choi, Yoon Ji	*Korea Univ. College of Medicine, Korea*
Choi, Yoon-La	*Sungkyunkwan Univ. School of Medicine, Korea*
Choi, Young Rok	*Seoul National Univ. Bundang Hospital, Korea*
Choi, Yunhee	*Seoul National Univ. Hospital, Korea*
Chon, Hongjae	*CHA Univ., Korea*
Chun, Mi Son	*Ajou Univ. School of Medicine, Korea*
Chung, Byung Ha	*Yonsei Univ. College of Medicine, Korea*
Chung, Hyun Hoon	*Seoul National Univ. College of Medicine, Korea*
Chung, Man Ki	*Sungkyunkwan Univ. School of Medicine, Korea*
Cohn, David Elliot	*The Ohio State Univ. College of Medicine, USA*
Eom, Hyeon Seok	*National Cancer Center, Korea*
Eom, Keun-Yong	*Seoul National Univ. Bundang Hospital, Korea*
Eom, Ki-Seong	*The Catholic Univ. of Korea, College of Medicine, Korea*
Goo, Jin Mo	*Seoul National Univ. College of Medicine, Korea*
Ha, Sang Yun	*Sungkyunkwan Univ. School of Medicine, Korea*
Han, Boo-Kyung	*Sungkyunkwan Univ. School of Medicine, Korea*
Han, Ho-Seong	*Seoul National Univ. Bundang Hospital, Korea*
Han, Hye Sook	*Chungbuk National Univ. College of Medicine, Korea*
Han, Ilkyu	*Seoul National Univ. College of Medicine, Korea*
Han, Ji-Youn	*National Cancer Center, Korea*
Han, Sae-Won	*Seoul National Univ. College of Medicine, Korea*
Han, Wonshik	*Seoul National Univ. College of Medicine, Korea*
He, Jing	*Guangzhou Women and Children, China*
Heo, Dae Seog	*Seoul National Univ. College of Medicine, Korea*
Hong, Jin Hwa	*Korea Univ. College of Medicine, Korea*
Hong, Se Mie	*Konkuk Univ. Medical Center, Korea*
Hong, Sook-hee	*The Catholic Univ. of Korea, College of Medicine, Korea*
Hong, Yong Sang	*Univ. of Ulsan College of Medicine, Korea*
Hur, Sooyoung	*The Catholic Univ. of Korea, College of Medicine, Korea*
Hwang, In Gyu	*Chung-Ang Univ. College of Medicine, Korea*
Hwang, Kihwan	*Seoul National Univ. Bundang Hospital, Korea*
Jang, Bo Gun	*Jeju National Univ. College of Medicine, Korea*

Jang, Jin-Young	*Seoul National Univ. College of Medicine, Korea*
Jang, Joung Soon	*Chung-Ang Univ. College of Medicine, Korea*
Jeon, Yoon Kyung	*Seoul National Univ. College of Medicine, Korea*
Jeong, Hansin	*Sungkyunkwan Univ. School of Medicine, Korea*
Jeong, Joon	*Yonsei Univ. College of Medicine, Korea*
Jeung, Hei-Cheul	*Yonsei Univ. College of Medicine, Korea*
Jo, Dong Hyun	*Seoul National Univ. College of Medicine, Korea*
Jung, Chan Kwon	*The Catholic Univ. of Korea, College of Medicine, Korea*
Jung, Hye Lim	*Sungkyunkwan Univ. School of Medicine, Korea*
Jung, Hyun Ae	*Sungkyunkwan Univ. School of Medicine, Korea*
Jung, Joo Young	*Hallym Univ. Medical Center, Korea*
Jung, Kyung Hae	*Univ. of Ulsan College of Medicine, Korea*
Jung, Minkyu	*Yonsei Univ. College of Medicine, Korea*
Kang, Eun Joo	*Korea Univ. College of Medicine, Korea*
Kang, Haeyoun	*CHA Univ., Korea*
Kang, Hyoung Jin	*Seoul National Univ. College of Medicine, Korea*
Kang, Hyun-Cheol	*Seoul National Univ. College of Medicine, Korea*
Kang, Hyunseok	*Univ. of San Francisco, USA*
Kang, Jeonghyun	*Yonsei Univ. College of Medicine, Korea*
Kang, Jung Hun	*Gyeongsang National Univ. School of Medicine, Korea*
Kang, Seok Yun	*Ajou Univ. School of Medicine, Korea*
Kang, Seok-Gu	*Yonsei Univ. College of Medicine, Korea*
Kang, Won Kyung	*The Catholic Univ. of Korea, College of Medicine, Korea*
Kang, Yu Na	*Kyungpook National Univ. School of Medicine, Korea*
Kang, Yun Kyung	*Inje Univ. College of Medicine, Korea*
Keam, Bhumsuk	*Seoul National Univ. College of Medicine, Korea*
Kim, Chang Wook	*The Catholic Univ. of Korea, College of Medicine, Korea*
Kim, Chungyeul	*Korea Univ. College of Medicine, Korea*
Kim, Dae-Young	*IBM, Korea*
Kim, Do Young	*Yonsei Univ. College of Medicine, Korea*
Kim, Dong-Wan	*Seoul National Univ. College of Medicine, Korea*
Kim, Eunsoo	*Pusan National Univ. School of Medicine, Korea*
Kim, Haeryoung	*Seoul National Univ. College of Medicine, Korea*
Kim, Hak Jae	*Seoul National Univ. College of Medicine, Korea*
Kim, Hee Jun	*Chung-Ang Univ. College of Medicine, Korea*
Kim, Hee Seung	*Seoul National Univ. College of Medicine, Korea*
Kim, Hee Sung	*Chung-Ang Univ. College of Medicine, Korea*
Kim, Hyeong Rok	*Chonnam National Univ. Medical School, Korea*
Kim, Hyery	*Univ. of Ulsan College of Medicine, Korea*
Kim, Hyojin	*Seoul National Univ. College of Medicine, Korea*
Kim, Hyoung-Il	*Yonsei Univ. College of Medicine, Korea*
Kim, Hyunki	*Yonsei Univ. College of Medicine, Korea*
Kim, In Ah	*Seoul National Univ. College of Medicine, Korea*
Kim, In-Ho	*The Catholic Univ. of Korea, College of Medicine, Korea*
Kim, Insuk	*Pusan National Univ. School of Medicine, Korea*
Kim, Jeongseon	*National Cancer Center, Korea*
Kim, Ji Hun	*Univ. of Ulsan College of Medicine, Korea*
Kim, Jin Hyoung	*Univ. of Ulsan College of Medicine, Korea*
Kim, Jin Seok	*Yonsei Univ. College of Medicine, Korea*
Kim, Jin Won	*Seoul National Univ. Bundang Hospital, Korea*
Kim, Jin Young	*Keimyung Univ. School of Medicine, Korea*
Kim, Jinho	*Seoul National Univ. College of Medicine, Korea*
Kim, Jinsung	*Yonsei Univ. College of Medicine, Korea*
Kim, Jong Gwang	*Kyungpook National Univ. School of Medicine, Korea*
Kim, Jong Hoon	*Univ. of Ulsan College of Medicine, Korea*
Kim, Jung Bae	*Korea Univ., Korea*
Kim, Jung Ho	*SNU Boramae Medical Center, Korea*
Kim, Kidong	*Seoul National Univ. Bundang Hospital, Korea*
Kim, Ku Sang	*Ulsan City Hospital, Korea*
Kim, Kyo-pyo	*Univ. of Ulsan College of Medicine, Korea*
Kim, Kyoung Mee	*Sungkyunkwan Univ. School of Medicine, Korea*
Kim, Kyubo	*Ewha Womans Univ. School of Medicine, Korea*
Kim, Min Hwan	*Yonsei Univ. College of Medicine, Korea*
Kim, Miso	*Seoul National Univ. College of Medicine, Korea*
Kim, Nam Kyu	*Yonsei Univ. College of Medicine, Korea*
Kim, Sang We	*Univ. of Ulsan College of Medicine, Korea*
Kim, Se Hyun	*Seoul National Univ. Bundang Hospital, Korea*
Kim, Se Hyung	*Seoul National Univ. College of Medicine, Korea*
Kim, Seok Jin	*Sungkyunkwan Univ. School of Medicine, Korea*
Kim, Songyee	*Yonsei Univ. College of Medicine, Korea*
Kim, Su Ssan	*Univ. of Ulsan College of Medicine, Korea*
Kim, Suk-Il	*The Catholic Univ. of Korea, College of Medicine, Korea*
Kim, Sun Young	*Univ. of Ulsan College of Medicine, Korea*
Kim, Sung Hwan	*The Catholic Univ. of Korea, College of Medicine, Korea*
Kim, Tae Hyun	*National Cancer Center, Korea*
Kim, Tae Min	*Seoul National Univ. College of Medicine, Korea*
Kim, Wan Seop	*Konkuk Univ. Medical Center, Korea*
Kim, Won Dong	*Chungbuk National Univ. College of Medicine, Korea*

Noh, Jae Myoung	*Sungkyunkwan Univ. School of Medicine, Korea*
Oh, Dongryul	*Sungkyunkwan Univ. School of Medicine, Korea*
Oh, In-Jae	*Chonnam National Univ. Medical School, Korea*
Oh, Jin-Kyoung	*National Cancer Center, Korea*
Oh, Sung Yong	*Dong-A Univ. College of Medicine, Korea*
Paek, Jiheum	*Ajou Univ. School of Medicine, Korea*
Paik, Jin Ho	*Seoul National Univ. Bundang Hospital, Korea*
Pak, Kyoungjune	*Pusan National Univ. School of Medicine, Korea*
Park, Boram	*National Cancer Center, Korea*
Park, Boyoung	*Hanyang Univ. College of Medicine, Korea*
Park, Chul-Kee	*Seoul National Univ. College of Medicine, Korea*
Park, Eun Young	*National Cancer Center, Korea*
Park, Hee Chul	*Sungkyunkwan Univ. School of Medicine, Korea*
Park, Hyun Woo	*Yonsei Univ. Korea*
Park, In Hae	*Korea Univ. College of Medicine, Korea*
Park, In Kyu	*Seoul National Univ. College of Medicine, Korea*
Park, Jae Young	*Korea Univ. College of Medicine, Korea*
Park, Ji Soo	*Yonsei Univ. College of Medicine, Korea*
Park, Ji-Kyoung	*Inje Univ. College of Medicine, Korea*
Park, Joon Seong	*Yonsei Univ. College of Medicine, Korea*
Park, Keon Uk	*Keimyung Univ. School of Medicine, Korea*
Park, Kwonoh	*Pusan National Univ. School of Medicine, Korea*
Park, Kyong Hwa	*Korea Univ. College of Medicine, Korea*
Park, Sung Taek	*Hallym Univ. Medical Center, Korea*
Park, Sung-Hye	*Seoul National Univ. College of Medicine, Korea*
Park, Won	*Sungkyunkwan Univ. School of Medicine, Korea*
Park, Woong-Yang	*Sungkyunkwan Univ. School of Medicine, Korea*
Park, Yeon Hee	*Sungkyunkwan Univ. School of Medicine, Korea*
Park, Yoon	*KIST, Korea*
Park, Young Soo	*Univ. of Ulsan College of Medicine, Korea*
Roh, Byung-Yoon	*National Forensic Service, Korea*
Roh, Mi Ryung	*Yonsei Univ. College of Medicine, Korea*
Ryu, Ji Kon	*Seoul National Univ. College of Medicine, Korea*
Seo, An Na	*Kyungpook National Univ. School of Medicine, Korea*
Seo, Ji Hye	*Keimyung Univ. School of Medicine, Korea*
Shim, Hyo Sup	*Yonsei Univ. College of Medicine, Korea*
Shin, Aesun	*Seoul National Univ. College of Medicine, Korea*
Shin, Cheol Min	*Seoul National Univ. Bundang Hospital, Korea*
Shin, Dong Wook	*Sungkyunkwan Univ. School of Medicine, Korea*
Shin, Eui-Cheol	*KAIST, Korea*
Shin, Hee Young	*Seoul National Univ. College of Medicine, Korea*
Shin, Kyung Hwan	*Seoul National Univ. College of Medicine, Korea*
Shin, Sang Joon	*Yonsei Univ. College of Medicine, Korea*
Shin, Sang Won	*Korea Univ. College of Medicine, Korea*
Shin, Seong Hoon	*Kosin Univ. College of Medicine, Korea*
Shin, Young Kee	*Seoul National Univ. College of Medicine, Korea*
Sim, Sung Eun	*The Catholic Univ. of Korea, College of Medicine, Korea*
Song, Changhoon	*Seoul National Univ. Bundang Hospital, Korea*
Song, Eun-Kee	*Jeonbuk National Univ. Medical School, Korea*
Suh, Chang Ok	*CHA Univ., Korea*
Suh, Koung Jin	*Seoul National Univ. College of Medicine, Korea*
Suh, Yang-Gun	*National Cancer Center, Korea*
Suh, Young Jin	*The Catholic Univ. of Korea, College of Medicine, Korea*
Suh, Yun-Suhk	*Seoul National Univ. College of Medicine, Korea*
Sun, Jong-Mu	*Sungkyunkwan Univ. School of Medicine, Korea*
Sung, Chang Ohk	*Univ. of Ulsan College of Medicine, Korea*
Sung, Joohon	*Seoul National Univ. College of Medicine, Korea*
Sung, Ki Woong	*Sungkyunkwan Univ. School of Medicine, Korea*
Tae, Kyung	*Hanyang Univ. College of Medicine, Korea*
Whang, Young Mi	*Seoul National Univ. Hospital Biomecical Research Institute, Korea*
Won, Jong Ho	*Soonchunhyang Univ. College of Medicine, Korea*
Won, Young-Joo	*National Cancer Center, Korea*
Won, Young-Woong	*Hanyang Univ. College of Medicine, Korea*
Woo, Sang Uk	*Korea Univ. College of Medicine, Korea*
Wu, Hong-Gyun	*Seoul National Univ. College of Medicine, Korea*
Yang, Seoung-Oh	*Dongnam Inst. of Radiological & Medical Sciences, Korea*
Yi, Eunsang	*Korea Univ. College of Medicine, Korea*
Yoo, Changhoon	*Univ. of Ulsan College of Medicine, Korea*
Yoon, Dok Hyun	*Univ. of Ulsan College of Medicine, Korea*
Yoon, Kyong-Ah	*Konkuk Univ. Medical Center, Korea*
Yoon, Sang Min	*Univ. of Ulsan College of Medicine, Korea*
Yu, Jeong Il	*Sungkyunkwan Univ. School of Medicine, Korea*
Yuh, Young Jin	*Inje Univ. College of Medicine, Korea*
Yun, Ik Jin	*Konkuk Univ. Medical Center, Korea*
Yun, Sook-Jung	*Chonnam National Univ. Medical School, Korea*
Yun, Sumi	*Samkwang Medical Laboratories, Korea*

유한이 가야 하는 길.

국민이 사랑하고, 국민과 함께 자란 기업 유한양행
지난 90여년 동안 이어진 정직과 성실의 기업문화와
기업의 사회적 책임에 대한 확고한 신념이 지금의 유한을 만들었습니다.

지금껏 걸어온 길을 돌아보며, 앞으로 가야 할 길을 생각합니다.
혁신적 신약개발을 통한 글로벌 제약사로의 도약, 대한민국을 넘어
모든 인류가 건강하고 행복한 길을 걸어가려 합니다.

다가올 100년에는 창업자 유일한 박사의 숭고한 정신을 바탕으로
미래를 향한 도약과 발전의 역사를 써나가겠습니다.

우리의 도전은 이미 시작되었습니다.

유한양행

ZALTRAP®
aflibercept

Think
More & Change

The Multiple Angiogenic Factor Trap[1] - ZALTRAP®

다중 혈관신생인자 억제제[1] 잘트랩®은
전이성 직결장암 환자에서 FOLFIRI와 병용시
OS, PFS, ORR 모두를 유의하게 연장시킨 2차 치료제입니다.[2]

More blockage of angiogenic factors[2]

More treatment **options**[3]

More heterogeneous **population**[2]*

*VELOUR 임상에는 Adjuvant early relapse<6개월인 환자가 포함됨

References 1. ZALTRAP® Summary of Product Characteristics (Last updated date : 2019.11.12). Available from: https://www.ema.europa.eu/en/documents/product-information/zaltrap-epar-product-information_en.pdf **2.** Van Cutsem E et al. Addition of Aflibercept to Fluorouracil, Leucovorin, and Irinotecan Improves Survival in a Phase III Randomized Trial in Patients With Metastatic Colorectal Cancer Previously Treated With an Oxaliplatin-Based Regimen. *J Clin Oncol.* 2012;30:3499-3506. **3.** Clinical Practice Guidelines in Oncology (NCCN Guidelines) Colon Cancer. Version 4. November 8, 2019.

Product Information

잘트랩®주25mg/mL(애플리버셉트) [원료약품 및 그 분량] 이 약 1바이알(4mL) 중(주성분) 애플리버셉트(별규) 100 mg 이 약 1바이알(8mL) 중(주성분) 애플리버셉트(별규)200 mg **[효능·효과]** 이리노테칸 및 5-FU를 기본으로 하는 화학요법(FOLFIRI)과 병용하여, 옥살리플라틴을 포함하는 화학요법 치료에 저항성이거나 이후 진행된 전이성 결장직장암의 치료 **[용법.용량]** 매 2주마다 이 약 4 mg/kg를 FOLFIRI요법(5-플루오로우라실(fluorouracil, 5-FU), 류코보린, 이리노테칸) 시작이전에 1시간동안 정맥주입한다. 질병이 진행되거나 허용되지 않는 독성이 발생할 때까지 투여를 지속한다. **[사용상 주의사항]** ■ 금기 1) 이 약의 주성분 또는 부형제에 대해 과민반응이 있는 것으로 알려진 환자에게 투여해서는 안된다. 2) 이 약은 고삼투압 용액이므로 안과용/유리체내주사용으로 투여해서는 안된다. 3) FOLFIRI요법 구성 약물(이리노테칸, 5-FU, 류코보린)의 투여금기는 해당 약물의 허가사항을 참고한다. ■ 신중투여 1) 출혈 2) 위장관계 천공 3) 누공 4) 고혈압 5) 혈전색전증 6) 단백뇨 7) 호중구감소증 및 호중구감소성 합병증 8) 설사 및 탈수 9) 과민반응 10) 상처치유관련 합병증 11) 후두부 가역적 뇌병증 증후군(posterior reversible encephalopathy syndrome, PRES) 12) 활동도(performance status) 및 동반질환 13) 심부전 및 박출률 감소 ■ 이상반응 이전에 치료받은 적이 있는 전이성 결장직장암 환자를 대상으로 한, 매 2주마다 이 약 4 mg/kg을 FOLFIRI요법과 병용투여 받은 611명과 위약과 FOLFIRI요법을 병용투여 받은 605명에 대한 3상 임상시험에서, 이 약과 FOLFIRI요법의 병용투여(이 약/FOLFIRI요법)시 안전성을 평가하였다. 이 약/FOLFIRI요법 투여군에서 위약/FOLFIRI요법 투여군과 비교하여 최소 2 % 이상 발생한, 가장 흔하게 보고된 이상반응(모든 등급, 20% 이상에서 발생, 발생빈도 내림차순)은 백혈구감소증, 설사, 호중구감소증, 단백뇨, AST 증가, 구내염, 피로, 혈소판감소증, ALT 증가, 고혈압, 체중 감소, 식욕부진, 비출혈, 복통, 발성장애, 혈청 크레아티닌 증가 및 두통이었다. 이 약/FOLFIRI요법 투여군에서 위약/FOLFIRI요법군과 비교하여 최소 2 % 이상 발생한, 가장 흔하게 보고된 3-4등급 이상반응(5 % 이상에서 발생, 발생빈도 내림차순)은 호중구감소증, 설사, 고혈압, 백혈구감소증, 구내염, 피로, 단백뇨 및 무력증이었다. 이 약/FOLFIRI요법 투여군의 1 % 이상에서 영구적 투약중단으로 이어진 가장 흔한 이상반응은 고혈압(2.3 %)을 포함하는 혈관계 장애(3.8 %), 감염(3.4 %), 무력증/피로(1.6 %/2.1 %), 설사(2.3 %), 탈수(1 %), 구내염(1.1 %), 호중구감소증(1.1 %), 단백뇨(1.5 %), 그리고 폐색전(1.1 %)이었다. 시판 후 경험을 통해 다음의 이상반응이 보고되었다: 심장 이상(심부전, 박출률 감소), 근골격계 및 연결조직 이상(턱뼈 괴사)
최종문안개정연월일: 2019.10. 28

*자세한 사항은 제품설명서 또는 회사 홈페이지(www.sanofi.co.kr)를 참조해주십시오.

SAKRAFL.19.10.1515(1)[19.11]

㈜사노피 아벤티스 코리아 서울특별시 서초구 반포대로 235 10층(반포동, 반포오피스빌딩1)
Tel: 02)2136-9000 / Fax: 02)2136-9399

SANOFI GENZYME